Some spectroscopic studies related to atmospheric chemistry and the thermal decomposition of organic azides

A thesis submitted to the University of Southampton
for the degree of Doctor of Philosophy

Giacomo Levita

School of Chemistry
University of Southampton

April 2005

UNIVERSITY OF SOUTHAMPTON

ABSTRACT

Faculty of Science
School of Chemistry

Doctor of Philosophy

Some spectroscopic studies related to atmospheric chemistry and the thermal decomposition of organic azides

by Giacomo Levita

The work described in this thesis is a study of the thermal decomposition of some aliphatic azides and of the atmospherically relevant reaction between dimethyl sulphide (DMS) and molecular chlorine. The aim of the work was to describe the mechanisms with which these reactions take place, and to identify the most important parameters influencing the reactions, such as decomposition temperature or reaction time.

UV-photoelectron spectroscopy (PES) and infrared matrix isolation spectroscopy have been used to monitor the extent of the reaction and to detect intermediates and products, and *ab initio* calculations have been used to facilitate spectral assignments and to provide information on the electronic structure and the thermochemistry of the reactions studied.

In the DMS + Cl_2 reaction, evidence of formation of an unstable $(CH_3)_2SCl_2$ species was found; for the first time structural and spectroscopic information have been described for this reaction intermediate.

The pyrolysis of ten aliphatic azides has been studied: two general modes of thermal decomposition were observed which were interpreted in terms of two types of reaction mechanism. In some cases the reaction involved formation of reaction intermediates: two of them have been observed and characterized for the first time.

MEMORANDUM

This thesis is an account of original research performed by the author in the School of Chemistry of the University of Southampton between October 2001 and September 2004. Where findings of other work have been used, due reference has been given.

Acknowledgements

This page is going to be very dense: not only because of my being wordy, but because I really have to thank so many people.
First I would like to acknowledge Prof. John Dyke who dared to make me work with him: he always supported my activity with a competence and an enthusiasm that never had a moment of hesitation throughout all these three years.
I thank Dr. Alan Morris for his amazing help in dealing with the "scary" spectrometer he designed, and his ability to individuate the solution for any problem even before I had finished explaining what the problem was.
Dr. Steve Ogden always supported my data with his IR matrix isolation results that helped all the interpretations: I thank him for his constant disposition in checking my intuitions, no matter how wrong they were.
Dr. Ed Lee offered his invaluable experience on *ab initio* calculations with such a patience and dedication that made my initial and uncertain first steps into the world of molecular orbitals become an enthusiastic activity.
Dr. Mariana Ghosh was my indispensable partner in our Rutherford campaign: we raided laboratories, pubs and B&Bs in Chilton with our gipsy attitude that at the end- I think- had its own good results.
Dr. Manuel "Joub" Goubet has been an unparalleled mate: especially in the DMS research, but also in our trips throughout the UK and Europe.
When I thank Fabrizio Innocenti I should refer to him as "doctor", which sounds almost as funny as "doctor Giacomo Levita"; what was not funny- but crucial- was his decisive help in making my PC and printer behave even when the one using them was the 19th century man sometimes I think I am.
Unfortunately I spent only one year with the company of Santi de Frutos: I hope the reason why he couldn't stay for longer in Soton was not just my awkward singing in the lab.
Dr. Manuel Algarra was great in leaving me free of trying strange attempts in my first approaches to the azides: thank you for this trust!
Prof. Maria Lourdes Costa and Antonio Dias have made my two months in Lisbon one of my best periods, both for the work and the atmosphere they created: what I don't thank them for is the *saudade* I feel whenever I think back at that period.
In these three years Paulinha Rodrigues punctuated my life so many times- in Soton and in Lisbon- that it looks so strange the idea that I will have much less chances to appreciate her competence and vitality from now on.
I have to thank Dr. David Kinnison- the safety officer-, Dr. Jeremy Hinks from the organic teaching lab, Dr. Colin Flowers from the physical chemistry teaching lab, Dr. Joan Street and Dr. Neil Wells from the NMR group, Dr. Julie Herniman from the mass-spec group, Bob, David and John from the mechanical workshop, Melanie from the glass workshop and Carl from the stores: if my needs in their fields have always been satisfied quickly and efficiently, this is because of their kindness.
Dr. Lucia Zuin... well, she didn't really help me in my work: this is why she is the one I thank probably more than anyone else.

Finally- beyond the strict working activity of this thesis- all my friends in Soton, from all the parts of the world you came. It will be unfair to make a list, because the names will sound equal and undistinguished, and this will not correspond to what my feelings are. You all know who you are, what each one of you gave and what each one of you took. Thanks once again; and- as usual- Forza Pisa.

INDEX

Chapter 1- Introduction

Chapter 2- Experimental section

Chapter 3- Theoretical methods

Chapter 4- A spectroscopic study of the atmospherically relevant reaction of dimethyl sulphide with molecular chlorine

Chapter 5- A spectroscopic study of the thermal decomposition of aliphatic azides

CHAPTER 1

INTRODUCTION

The objective of this work is to study the reaction of dimethyl sulphide with molecular chlorine and the thermal decomposition of aliphatic azides using spectroscopic methods.

The first reason for the choice of these reactions was the possibility- suggested by some results in the literature [1,2]- that they could proceed via formation of reactive intermediates: the study of short-lived species has in fact been a long-established field of research in the Southampton PES group.

In addition to this, the chemistry of dimethyl sulphide and of organic azides has been object of increasing investigations, due to the importance of dimethyl sulphide as an atmospheric agent- especially in the air above the oceans- and the new applications found for organic azides especially for their capability of releasing energy when heated.

These studies were carried out by means of ultraviolet photoelectron spectroscopy and infrared matrix isolation spectroscopy, with the support of *ab initio* electronic structure calculations.

The dimethyl sulphide-molecular chlorine reaction was studied in the gas-phase in Southampton using UV-photoelectron spectroscopy and using the high resolution FT-IR and FT-UV spectroscopic facility at the Rutherford laboratory.

The study of the thermal decomposition of selected aliphatic azides is a continuation of joint research between the PES groups of the Universities of Southampton and Lisbon.

This chapter will describe the importance and main applications of dimethyl sulphide and aliphatic azides; it will also discuss why photoelectron spectroscopy and infrared matrix isolation spectroscopy have been chosen to monitor these reactions. A more detailed description of the experimental and underlying principles of these spectroscopic techniques will be given in Chapters 2 and 3. Chapter 3 will outline in detail the basic principles of the *ab initio* electronic structure calculations used, and the reason why their use was of central importance in the outcome of the work.

1.1 DIMETHYL SULPHIDE

Dimethyl sulphide (DMS), CH_3SCH_3, is considered the main source of sulphur in the Earth's atmosphere [3-7], contributing roughly 25% of the total atmospheric sulphur, and almost 50% of the biogenic flux. It is mainly produced by biodegradation of algae in oceanic environments, but is also produced from anthropogenic activities such as paper mills or fishmeal production [8].

In the atmosphere DMS is consumed by different oxidizing agents leading to the formation of aerosols containing sulphur dioxide, sulphuric acid or methanesulfonic acid. These compounds play a crucial role in climate regulation [9], as they contribute to the formation of cloud condensation nuclei (CCN) above the oceans [4, 10] and to the acidity of rain. In fact, the contribution from marine salt particles is not enough to reach the observed amount of CCNs at cloud height. Around these nuclei, liquid droplets form providing suitable conditions for cloud formation and subsequent reduction of solar radiation reaching the Earth's surface.

The cooling effect produced by the DMS in the atmosphere is therefore of great importance. Also the fact that a lower temperature above the oceans inhibits biological degradation of organo-sulphur compounds, which is the main source of the DMS presence in the atmosphere, should be considered. The mechanism of DMS formation → cloud formation → lowering temperature- is therefore a cyclic mechanism, that can be represented as in Figure 1.1. An increase in DMS production by algae degradation is reflected by a decrease of temperature which reduces algae degradation; on the other hand, when the amount of DMS- and then of CCNs- is reduced, the solar irradiation causes an increased biological activity of the sulphur containing algae and then an increase of DMS production.

Such an equilibrium is very delicate, and it is subject to fluctuations due for example to the actual degree of production of CCNs from DMS oxidation. The main oxidising agents responsible for DMS degradation above the oceans are OH and NO_3 radicals, acting respectively at daytime and at night-time [11-13]. The observed removal of DMS from the atmosphere cannot, however, be completely explained by just these reactions: other sink processes have been proposed involving halogen or halogenated radicals such as Br, Cl or BrO [14, 15]. Considering the role played by halogens, particular importance must be given to the fact that high amounts of chlorine have been observed in coastal air, either as HCl produced by sea salt particles, from algae decomposition or from anthropogenic activities [14, 16].

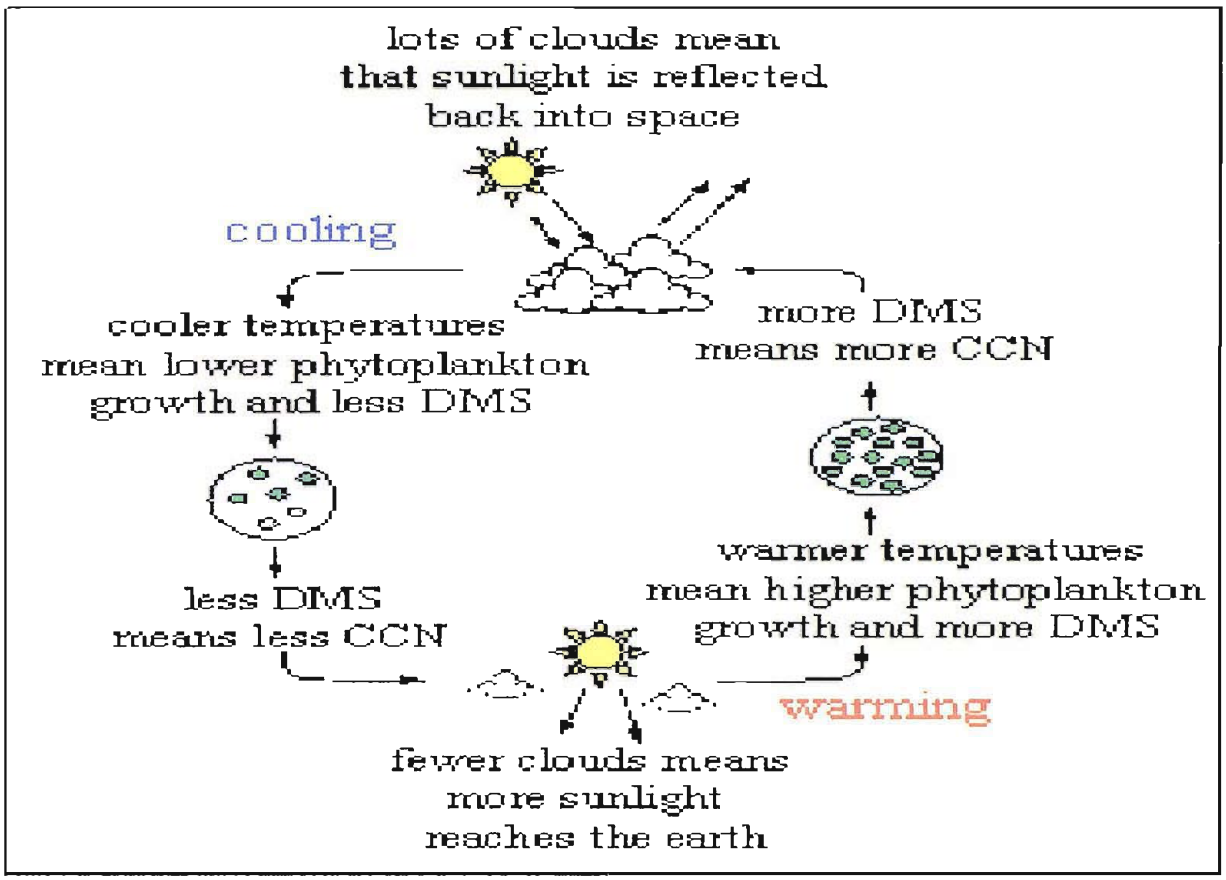

Figure 1.1- The cyclic CLAW mechanism [5] for the role of DMS in climate control

An investigation of the reaction between Cl_2 and DMS is therefore important in order to provide a full representation of the atmospheric degradation of DMS and thus of its effect on the solar radiation reaching the Earth. Moreover, the early morning photolysis of molecular chlorine leads to the production of atomic chlorine, which is also a possible oxidiser of DMS.

An initial PES study was made on the DMS+Cl_2 reaction at the University of Southampton [17], indicating that a reaction intermediate is formed in the first step of the reaction, before decomposition occurs to CH_3SCH_2Cl + HCl.

1.2 ALIPHATIC AZIDES

The main characteristic of organic azides, characterized by the presence of a terminal $-N_3$ chain, is the easy release of nitrogen [18, 19] following the overall reaction

$$R_2(R')CN_3 \xrightarrow{\Delta} N_2 + R_2C = NR'$$

The reaction can occur with considerable explosive potential, due to the favourable nature of nitrogen as a leaving group. Azides must therefore be handled with care, and this has set a limitation in the study of their reactivity.

However, this characteristic represents also the most useful aspect of azides, because of the high energy storage role they can play in different fields. They are in fact used both in organic synthesis [20], for example for preparing heterocycles [21] and for biochemical applications [22], and in inorganic synthesis [23], where they are used in low-temperature preparations of single crystals of gallium and silicon nitrides on semiconductors substrates. They also find use in industrial applications, for example in pharmaceutical processes [24], or as propellants [25], as seismic explosives [26], as photoresistors [27] and as sources of gases for air-bags [28]. Such a variety of applications indicates that the nature of the azide greatly affects its reactivity: this is an important way to control the potential dangers of azides in order to make use of their characteristic of energy release.

The study of the decomposition of such class of compounds is therefore of interest, especially considering that their intrinsic instability has often represented an obstacle for measurement of their characteristics and for the practical use that can be made from them. Moreover, the first step in the decomposition path offers an interesting challenge for electronic structure calculations, because it is not certain if organic azides release nitrogen to form an imine directly via a 1,2-alkyl (or hydrogen) shift or if first a nitrene is formed, which subsequently decomposes to the imine, as represented by

$$R_2(R')CN_3 \xrightarrow{\Delta} N_2 + R_2(R')CN^* \rightarrow R_2C = NR'$$

Pioneered by the works of Bock and Dammel [29], the study of organic azides has recently been developed from both the theoretical and experimental points of view. Experimental work by Dianxun *at al.* [30] suggested that, under particular conditions, surface effects can lead to the formation of the nitrene intermediate, whose presence was expected from theoretical calculations [31]. In recent years joint work [32] between the Universities of Southampton and Lisbon have focused on gas-phase

thermal decomposition of some organic azides, studied by photoelectron spectroscopy and infrared matrix isolation.

The aim of the present work is to move forward in the understanding of the behaviour of this class of compounds, in order to increase the number of aliphatic azides for which the major features of the thermal decomposition reaction (reaction products, decomposition temperatures, reaction pathways and, if possible, reaction intermediates) are known.

1.3 THE CHOICE OF PES AND IR MATRIX ISOLATION AS SPECTROSCOPIC TECHNIQUES FOR THE STUDY OF REACTIVE INTERMEDIATES

Photoelectron spectroscopy (PES) provides a direct link to one of the crucial characteristics of the molecule under study, the ionization energies from valence region orbitals (see Chapters 2 and 3 for a more detailed treatment of the technique). It is one of the most useful experimental methods to provide information on the electronic structure of a molecule, and it is a useful analytical tool for the detection of compounds in gas-phase. For these reasons, the first studies on simple azide decompositions [29] were conducted with PES: moreover, PES has the great advantage that it requires sample gas-phase pressures in the region 10^{-4} –10^{-6} mbar, so that the risk of explosions for such unstable compounds is minimized. However, PE spectra of organic azides are generally characterized by broad bands, often overlapping with each other in the high ionization energy region: this limits the ability of PES to study decomposition of azides and means that a complementing monitoring technique is required.

Infrared spectroscopy offers a valuable alternative "fingerprint" characterization of a molecule. The fact that PES can give information on the vibrational frequencies of the ion- if the experimental resolution is sufficient- creates a bridge between the two techniques, and the combination of PES and IR measurements offers an immediate link with results of quantum chemistry calculations. The number of molecules for which IR spectra are known is very large, and this facilitates assignments when thermal decomposition products are produced from aliphatic azides. The development of the matrix isolation technique has opened a further possibility for IR spectroscopy, as most thermal excitations are quenched at the low temperature of the matrix and the bands are more resolved and their energy value better defined than in the corresponding room temperature gas-phase spectrum. The possibility of accumulating sample molecules condensed with an inert gas on a detection window (see Chapter 2), and the fact that the matrix is sufficiently rigid to successfully isolate molecules that would otherwise react with each other, allows the detection of substances in very low concentration, such as short-lived

molecules [33]. Also, the possibility of isotopic substitutions on C, H, N and O atoms provides the possibility of unambiguous assignments for bands associated with any reaction intermediate observed and this should enable proposals to be made on the decomposition paths, once the experimental results are combined with results of electronic structure calculations.

The combination of these factors has led to the fact that PES and IR matrix isolation are among the most used characterization techniques for reaction intermediates. Their possibilities are fully exploited if calculations are performed in order to determine valence ionization energies and vibrational frequencies for molecules, in order to facilitate the assignments of the experimental spectra. They can also allow a detailed description of the reaction path, by evaluating the relative energy values for reagents, products, intermediates and transition states for a particular azide decomposition.

In this work all the reactions have been studied by UV-photoelectron spectroscopy and infrared matrix isolation spectroscopy, and *ab initio* electronic structure calculations have been performed on reactant, products and intermediates at different degrees of sophistication to support the experimental work.

REFERENCES

[1] H. Bock, R. Dammel, *Angew. Chem. Int. Ed. Engl.*, **26**, 1987, 504

[2] N.P. Machara, B.S. Ault, *J. Phys. Chem.*, 91, *1987*, 2046

[3] J.E. Lovelock, R.J. Maggs, R.A. Rasmussen, *Nature*, **237**, *1972*, 452

[4] a) R.A. Cox, *Phil. Trans. R. Soc. Lond. B*, **352**, *1997*, 251

b) J. Lelieveld, G.J. Roelofs, L. Ganzeveld, J. Feichter, H. Rodhe, *Phil. Trans. R. Soc. Lond.* B, **352**, *1997*, 149

c) P.S. Liss, A.D. Hatton, G. Malin, P.D. Nightingale, S.M. Turner, *Phil. Trans. R. Soc. Lond. B*, **352**, *1997*, 159

[5] R.J. Charlson, J.E. Lovelock, M.O. Andreae, S.G. Warren, *Nature*, **326**, *1987*, 655

[6] S.F. Watts, *Atmosph. Envir.*, **34**, *2000*, 761

[7] D. Smythe-Wright, S.M. Boswell, Climatically active halogenated gases in the ocean; their measurement and distribution SOC Research and Consultancy Report **53**, *2001*, 64

[8] R.P. Wayne, *Chemistry of the atmospheres, 2nd edition*, Clarendon press, Oxford, *1991*

[9] J. Wallington, Ellerman and J. Nielsen, *J. Phys. Chem.*, **97**, *1993*, 8442

[10] G.P. Ayers, J.M. Caney, R.W. Gillett, J.P. Ivey, *Phil. Trans. R. Soc. Lond. B*, **352**, *1997*, 203

[11] A.R. Ravishankara, Y. Rudich, R. Talukdar, S.B. Barone, *Phil. Trans. R. Soc. Lond. B*, **352**, *1997*, 171

[12] J.B. Nowak, D.D. Davis, G. Chen, F.L. Eisele, R.L. Mauldin, D.J. Tanner, C. Cantrall, E. Kosciuch, A. Bandy, D. Thornton, A. Clarke, *Geophys. Res. Letters*, **28**, *2001*, 2201

[13] N. I. Butokovskaia, G. Poulet and G Le Bras, J. *Phys. Chem.*, **99**, *1995*, 4536

[14] M.O. Andreae, P.J. Cutzen, *Science*, **276**, *1997*, 1052

[15] R. Vogt, P.J. Crutzen, R. Sander, *Nature*, **383**, *1996*, 327

[16] C.W. Spicer, E.G. Chapman, B.J. Finlatson-Pitts, R.A. Plastridge, J.M. Hubbe, J.D. Fast, C.M. Berkowitz, *Nature*, **394**, *1998*, 353

[17] S. De Frutos, *M.Sc. thesis*, University of Southampton, *2002*

[18] P.A.S. Smith, *Open-chain nitrogen compounds*, Vol. 1, Benjamin, Reading, *1961*

[19] E.V.F Scriven, *Azides and Nitrenes*, Academic press, New York, *1984*

[20] a) S. Patai, *The chemistry of the azide group*, Interscience, New York, *1971*

b) E.F.V. Scriven, K. Turnbull, *Chem. Rev.*, **88**, *1988*, 298

c) F. Zaragoza, S.V. Petersen, *Tetrahedron*, **52**, *1996*, 10823

[21] V. Vantinh, W. Stadlbauer, *J. Heterocycl. Chem.*, **33**, *1996*, 1025

[22] a) K. Marumoto, H. Kamiya, *Agric. Biol. Chem.*, **52**, *1988*, 547

b) B.M. Joensson, K. Hakanson, A. Lijlas, *FEBS Lett.*, **322**, *1993*, 186

[23] a) A. Bridges, R. Greef, N.B. Jonathan, A. Morris, G. Parker, *Surf. Rev. Lett.* **1**, *1994*, 573

b) R. Ishihara, H. Kanoh, O. Suguira, M. Matsumara, *Japan J. Appl. Phys.*, **31**, *1992*, L74

d) Y. Bu, J.C.S. Chu, M.C. Lin, *Surface Sci. Lett.*, **264**, *1992*, L15111

e) C. Tindall, J. Hemminger, *Surf. Sci.*, **330**, *1995*, 67

[24] a) R. Maurus, R. Bogumil, N. Nguyen, A. Mauk, G. Brayer, *Biochem. J.*, **332**, *1998*, 67

b) G.B. Schuster, M.S. Platz, *Adv. Photochem.*, **17**, *1992*, 69

c) Y. Matsumara, T. Shiozawa, H. Matsuhita, Y. Terao, *Biol. Pharm. Bull.*, **18**, *1995*, 1805

[25] N.J. Kubota, *Propul. Power*, **11**, *1995*, 677

[26] M. Badri, H.M. Mooney, *Geophysics*, **52**, 1987, 772

[27] H. Ban, A. Tanaka, Y. Kawai, K. Degushi, *Japan J. Appl. Phys.* Part 2, **10**, *1989*, 1863P

[28] Y.L. Liu, G.H. Hsuie, Y.S. Chiu, *J. Appl. Polymer Sci.*, **58**, *1995*, 578

[29] a) H. Bock, R. Dammel, L. Horner, *Chem. Ber.*, **114**, *1981*, 220

b) H. Bock, R. Dammel, S.J. Aygen, *J. Amer. Chem. Soc.*, **105**, *1983*, 7681

c) R. Dammel, *Reaktive Moleküle mit N-Mehrfachbindungen: azide, imine, nitrile*, Inaugural-Dissertation, Univeristy of Frankfurt am Main (*1985*)

d) H. Bock, R. Dammel, *J. Amer. Chem. Soc.*, **110**, *1988*, 5261

[30] a) W. Jing, S. Zheng, Z. Xinjiang, Y. Xiaojun, G. Maofa, W. Dianxun, *Angew. Chem. Int. Ed.*, **40**, n° 16, *2001*, 3055

b) W. Dianxun *et al.*, unpublished work (*2001*)

[31] J.F. Arenas, J.I. Marcos, J.C. Otero, A. Sanchez-Galvez, J. Soto, *J. Chem. Phys.*, **111**, n° 2, *1999*, 551

[32] a) J.M. Dyke, A.P. Groves, A. Morris, J.S. Ogden, A.A. Dias, A.M. Oliveira, M.L. Costa, M.T. Barros, M.H. Cabral, A.M. Moutinho, *J. Am. Chem. Soc.*, **119**, *1997*, 6883.

b) J.M. Dyke, A.P. Groves, A. Morris, J.S. Ogden, M.I Catarino, A.A. Dias, A.M. Oliveira M.L. Costa, M.T. Barros, M.H. Cabral, A.M. Moutinho, *J. Phys. Chem. A*, **103**, *1999*, 8239.

c) N. Hooper, L.J. Beeching, J.M. Dyke, A. Morris, J.S. Ogden, A.A. Dias, M.L. Costa, M.T. Barros, M.H. Cabral, A.M.H. Moutinho, *J. Phys. Chem.A*, **106**, *2002*, 9968

[33] M.E. Jacox, *Chem. Soc. Rev.*, **31**, *2002*, 108

CHAPTER 2

EXPERIMENTAL SECTION

This chapter presents the most important experimental aspects of the two spectroscopic techniques used in this work- photoelectron spectroscopy and infrared matrix isolation spectroscopy- notably the apparatus and the spectral acquisition procedures. A general introduction to the basic features of the methods used is given in this Chapter, with the underlying principles being described in Chapter 3.
The experimental apparatus used for Fourier Transform (FT) infrared and ultraviolet spectroscopy are described in Chapter 4, as it has been used only in the study of the reaction between DMS and Cl_2.

2.1 UV-PHOTOELECTRON SPECTROSCOPY

2.1.1 Basics of the technique [1]

Photoelectron spectroscopy is a technique aimed at determining the ionization energy of a molecule. It can provide information not only on the first ionization energy, but on all possible higher ionization energies obtained by removing one electron from any of the occupied molecular orbitals; according to the nature of the photon source used in the process, the technique is given the name of *UV-photoelectron spectroscopy* (UPS, or more simply PES) or *X-ray-photoelectron spectroscopy* (XPS). PES considers ionizations from valence molecular orbitals and is mainly used for gas-phase studies, while XPS investigates ionizations from core and valence orbitals and is mostly used to investigate solid compounds; as the name suggests, the discrimination is based on which kind of radiation source is used to ionize the molecule, vacuum ultraviolet radiation or X-rays.
The most valuable aspect of photoelectron spectroscopy (hereafter "photoelectron spectroscopy" will be referred to as PES) is the possibility of using the results from this method to build up orbital energy level diagrams for the molecules studied, as the ionization energy- the energy to remove an electron from a molecular orbital- can be linked to the negative of the orbital energy for a closed shell molecule. Apart from the importance of the information itself, a valuable link to theoretical calculations can be immediately established, as the orbital energy is one of the most readily available pieces of information available from such calculations (see Chapter 3).

Photoelectron spectroscopy is not a resonance technique: it is not based on the absorption of a photon with the same energy as the energy difference of two electronic states between which the molecule moves as a consequence of the interaction with the photon.

Instead, it is a scattering technique; it occurs because the photon is energetic enough to directly ionize the molecule by extracting an electron (called the *photoelectron*) from the molecule, as consequence of the impact of the photon beam on the sample

$$A + h\nu \rightarrow A^+ + e^- \qquad (2.1)$$

The energy and angular distribution of the photoelectrons are characteristic of the orbital they were ejected from; the technique gives information therefore about the electronic structure of the molecule under observation.

It will be assumed that A is a molecule possessing some rotational and vibrational energy. Given the fact that- due to the great difference in mass between the photoelectron e^- and the nucleus A^+- virtually all the excess energy associated with photoionization will be associated with the electron, then the energy conservation law for the process of extracting an electron from the molecular orbital j of molecule A means that the photon energy ($h\nu$) can be written as follows:

$$h\nu = IE_j + KE_{el} + \Delta E_{vib} + \Delta E_{rot} \qquad (2.2)$$

where IE_j is the j^{th} ionization energy of A, KE_{el} the kinetic energy of the photoelectron produced and ΔE_{vib} and ΔE_{rot} are the changes in vibrational and rotational energy between the molecule and ion on photoionization. In practice, the experimental resolution in conventional PES can be reduced to around 200 cm^{-1}, a value that usually allows vibrational changes to be resolved but not rotational changes: the change in rotational energy between A and A^+ will therefore be averaged and included in IE_j'. The energy conservation expression becomes then

$$h\nu = IE_j' + KE_{el} + \Delta E_{vib} \qquad (2.2a)$$

If a monochromatic source of radiation is used and the kinetic energies of the photoelectrons are measured, it is possible to obtain $IE_j' + \Delta E_{vib}$ for all the ionizations.

An observed spectral band does not therefore give just the ionization energy, it also provides information on the change in vibrational state between the neutral and the cation: given the fact that the energy scale for such a change is around 1/100 of the ionization energy, vibrational energy changes will just cause sub-structure- or a broadening- of the band. Further details of the possible band shapes arising from a photoionization process will be given in Chapter 3. At this time, it will just be stated that

at room temperature most molecules are in the ground vibrational state, as the separation of the lowest and the first excited vibrational state is usually much higher than kT, i.e. at room temperature the Boltzmann population of vibrational levels means that the lowest vibrational level is the most populated. Therefore, all the changes in vibrational energy in the photoionization process can be seen in the PE spectrum as ionizations from a v''=0 state of the neutral A to a v'=0, 1…k state of the cation A^+. If structure in the experimental band is observed, it will give information on the vibrational spacing of the levels in the cation and not in the neutral.

In photoelectron spectroscopy only two selection rules apply [1]:

- only one electron ionizations are possible (one-electron selection rule)
- no change in the total spin between the initial and final (cation plus free electron) states must be introduced in the ionization process. To clarify this rule, it must be noted that the photoelectron is obviously produced with s= ½ so that to respect the $\Delta S = 0$ rule, the cation and the neutral molecule must differ in spin quantum number by ½. This means that from a neutral molecule in a singlet spin multiplicity state only a doublet cation can be formed, and from a doublet neutral only a triplet or a singlet cation will be formed.

Despite the fact that often no vibrational structure is observed in the photoelectron bands, the spectra are nevertheless suitable for easy identification of the molecule studied, if a high enough number of ionization bands is considered. This makes PES a valuable analytical technique, and a valuable source of information about the electronic structure of the molecules examined.

Due to the very low pressures of operation, only a very limited amount of sample is required to record a PE spectrum of a sample.

As already mentioned, for a photoelectron band, transitions to a number of vibrational states of an ionic state are possible, and this could lead to a relatively broad band. The limitations on the ability to resolve such contributions have different sources [2], and the most important will be listed below.

- The most crucial factor is instrumental resolution. For this, the characteristics of the analyzer of the spectrometer must be discussed. The photoelectrons pass through a pair of slits, and then into a hemispherical analyzer chamber; with a procedure that will be presented in further detail in Section 2.1.2, the photoelectrons are directed towards another set of slits which focus them on the detector. A schematic diagram of the hemispherical analyzer chamber of the PE spectrometers used in this work is presented in Figure 2.1. The radius of the inner hemisphere is R1 and the radius of the outer

sphere is R2. The electrons travel between the entrance and the exit slits with a trajectory of radius R, between R1 and R2.

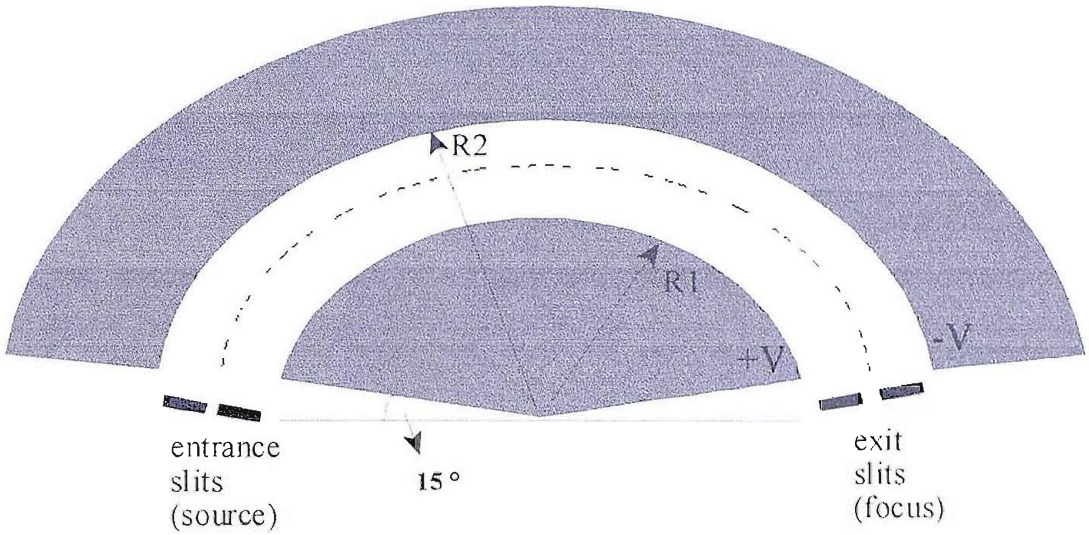

Figure 2.1- Section of the hemispherical analyser chamber of the photoelectron spectrometers used in the Southampton PES group.

Instrumental broadening depends on the analyser geometry, notably the slit width and the radius of the hemispheres. The instrumental resolution [2] can in fact be expressed by $\Delta E = E \cdot (S/2R)$, where S is the total slit width (the combined width of the entrance slits and the exit slits) and R the mean electron orbit radius, and E is the energy of the photoelectron. Clearly, narrower slits will improve the resolution but lower the intensity of the signal: a compromise between the two factors must be found according to the particular experimental requirement. A longer radius of the analyser hemispheres leads to improvement of the resolution; for this, in the Southampton PES group a spectrometer with R= 20 cm has been designed and built, and used in this project as well as one with mean radius of 10 cm. Finally, it must be noted that the resolution ΔE is directly proportional to E, which is the kinetic energy of the electrons: therefore, ionizations from the highest molecular orbitals will have higher kinetic energy and then broader bands than those arising from deeper orbitals and lower kinetic energy [3, 4]. For example, in O_2 HeI (21.22 eV) photoelectron spectrum, the bands at ~12 eV ionization energy are broader than those at ~18 eV ionization energy.

Instrumental broadening can contribute up to 15 meV for an analyser chamber with mean radius of 10 cm.

However, other factors can also contribute:

- the electron energy changes according to the velocity of the originating molecule, due to its thermal motion (Doppler effect [1, 5]). The expression for this energy spread is $\Delta E = 2(E \cdot k_b T \cdot m_{el}/M_{mol})^{1/2}$

For example, in atomic argon (which is the sample normally used to test the resolution), this leads to an energy spread of 5.6 meV at room temperature. Moreover, it can be seen that the resolution worsens at increasing temperatures

- the ionizing radiation is subject to broadening. This is due for example to its lifetime, to Doppler broadening (the radiating molecules are moving) and to self-reversal broadening (unexcited He atoms absorb the He(I) radiation especially in the central part of the lamp: this increases the intensity of the "sides" and causes broadening of the photon source). Of these, the last contribution is the most relevant, causing broadening in the PE bands by about 1-2 meV

Further contributions to the broadening (due to assuming that the photoelectron does not take all the angular momentum in the ionization process, or to the effect connected to the lifetime of the cation) are generally small; a much more important factor is the presence of stray fields, charge accumulation or contact potentials in the analyser chamber. In order to avoid any charge accumulation which could distort the photoelectron free path, and therefore affect the quality of the spectra, the internal walls of the spectrometer are all made of aluminium alloy (*dural*) and are coated with a conductive layer of graphite [6]. To eliminate distortions of the photoelectron paths due to the Earth's magnetic field, the spectrometer is placed inside a cage of three pairs of mutually perpendicular coils (Helmholtz coils). Current is passed through each pair of coils to generate a magnetic field equal and opposite to the Earth's field in that direction. By tuning the three values of the currents, this local field can be changed so that the characteristics of the spectrum (intensity, resolution and transmission) are optimized.

A careful choice of the magnetic fields produced by the Helmholtz coils to balance the Earth's field, and a good quality of the graphite layer in the ionization chamber and analyzer region is crucial: for example, dirty or badly spread graphite can increase the resolution by at least 10 meV.

For all these factors, the overall expression [2] for the resolution can be written as

$$\Delta E = (\sum_i \Delta E_i^2)^{1/2} \qquad (2.3)$$

where $\sum_i \Delta E_i^2$ is the sum of the square of all the contributions to the band width.

In practice even the most carefully assembled photoelectron spectrometer will give an overall resolution of not less than 20 meV, as measured for the $(3p)^{-1}$ ionization of argon with good intensity of this band ($3 \cdot 10^4$ counts/s).

2.1.2 Experimental apparatus

A schematic of the photoelectron spectrometer [6-8] used in this work is shown in Figure 2.2. Further details of each single component will be given in the following paragraphs.

Sample vapours are ionized by a monochromatic vacuum ultraviolet photon beam in the ionization region of the spectrometer. The photoelectrons generated pass through a pair of slits (entrance slits) placed at 90° with respect to the photon beam, and from the slits they pass into a hemispherical analyser chamber; by applying a uniformly changing potential between the two hemispheres, the electrons can be focused onto the electron detector according to their kinetic energy. The detector is placed after another set of slits (the exit slits).

The mean free path of an electron is inversely proportional to the pressure in the apparatus, and as a result, in order that photoelectrons will not undergo any inelastic collisions, the analyser chamber, the ionization chamber and the detector regions are evacuated to a pressure of at least 10^{-5} mbar. To avoid contamination of the hemispheres, differential pumping is used; this involves the ionization chamber and analyser region being pumped separately by diffusion pumps, each backed by rotary pumps.

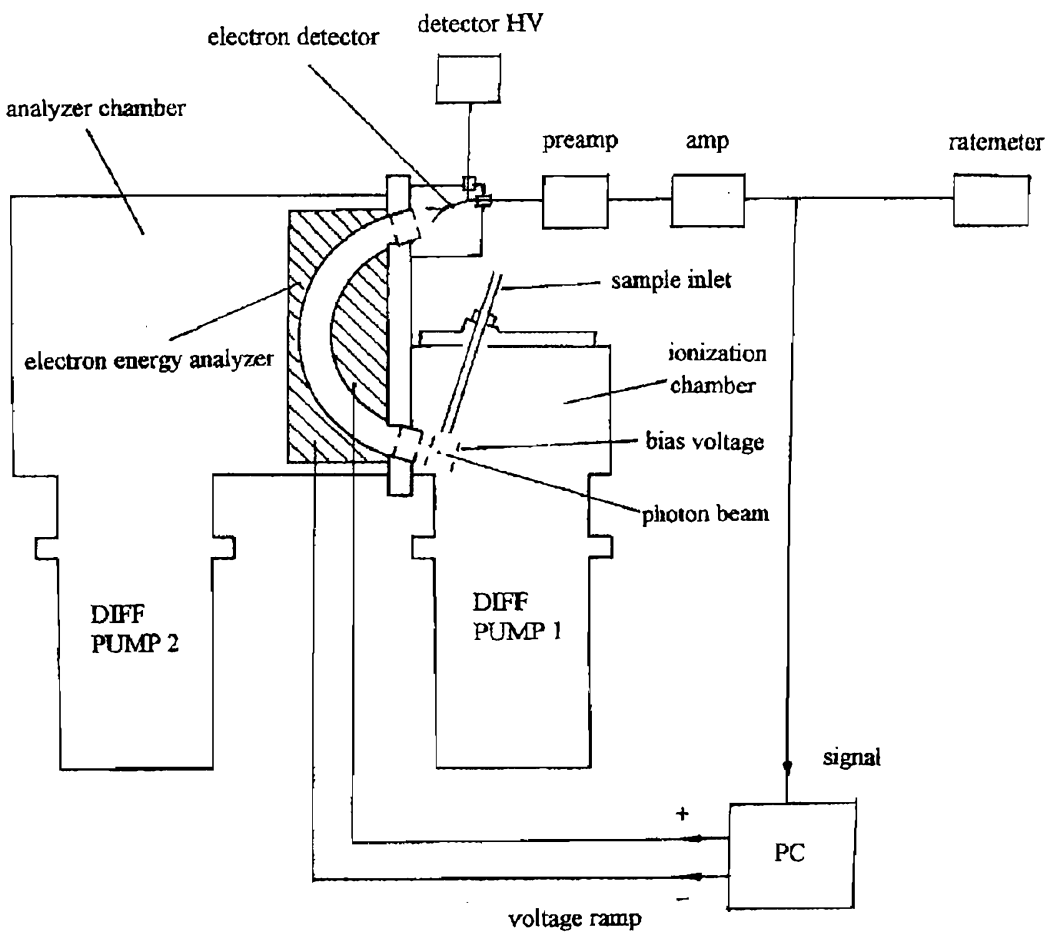

Figure 2.2- Main components of the PE spectrometer used in this work for the study of gas-phase samples

The monochromatic UV source

As can be seen in the formula of energy conservation (equation 2.2a), a strictly monochromatic photon source is needed if precise determinations of ionization energies are to be obtained and radiation energetic enough to ionize electrons from the deepest valence orbitals is required. Therefore vacuum-UV radiation is needed.

A widely used source is the one obtained by means of a d.c. discharge in helium. The process causes emission of numerous wavelengths, in the visible region (they are not able to cause ionizations, but are a useful test to check the functioning of the lamp) and in the vacuum-UV region. Of these, the predominant radiation is the one corresponding to the transition ^1P ($1s2p$) → ^1S ($1s^2$). Its wavelength is 58.43 nm, corresponding to an energy of 21.22 eV; it is also called He(I)- or He(I)α- radiation because it refers to the transition between the first electronic excited state of the neutral molecule and the neutral ground state (if it is a transition in the cation, the label would be He(II)). There are other ^1P states obtainable from the $1s$ np configuration if n = 3, 4...; in this case the emitted radiations are labelled He(I)β, He(I)γ, etc [9]. The most intense, He(I)β, is however only 1.3/100 the intensity of the He(I) α emission: in a PE spectrum this will be reflected by the fact that each band due to He(I) α radiation has a "shadow" band 1.87 eV higher in electron kinetic energy (that is, lower in apparent ionization energy), with intensity around 2% of the He(I) α band intensity.

A schematic representation of the helium discharge lamp used in this work is shown in Figure 2.3.

The differential pumping system (shown at "Gas out" in Figure 2.3) is necessary to prevent helium being introduced into the ionization region and hence increasing the pressure there [10]: it is in fact impossible to isolate the lamp from the ionization region, as no suitable window materials are available for radiation below 100 nm. Usually, a helium pressure of about 0.2 mbar is used, and the discharge current is set at about 65 mA. Under these conditions, the heat generated by the lamp must also be dissipated: this is why the body of the lamp is water cooled.

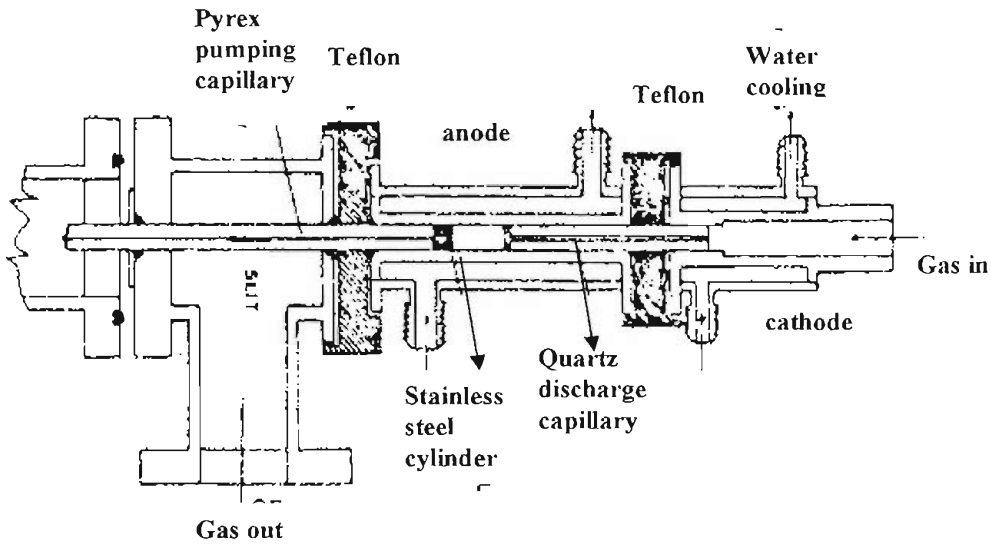

Figure 2.3- Schematic of the Helium discharge lamp used in the UV-PES experiments in this work

The ionization chamber and the reaction cell

He(I) radiation passes from the lamp into a cell- called the *reaction cell*- where vapour from the sample is introduced from above. Photoelectrons produced travel in all directions; perpendicular to both the radiation and the sample gas flow there is a pair of slits that selects some of the electrons and allows them to pass into the electron analyzer. A schematic diagram of the reaction cell is presented in Figure 2.4.

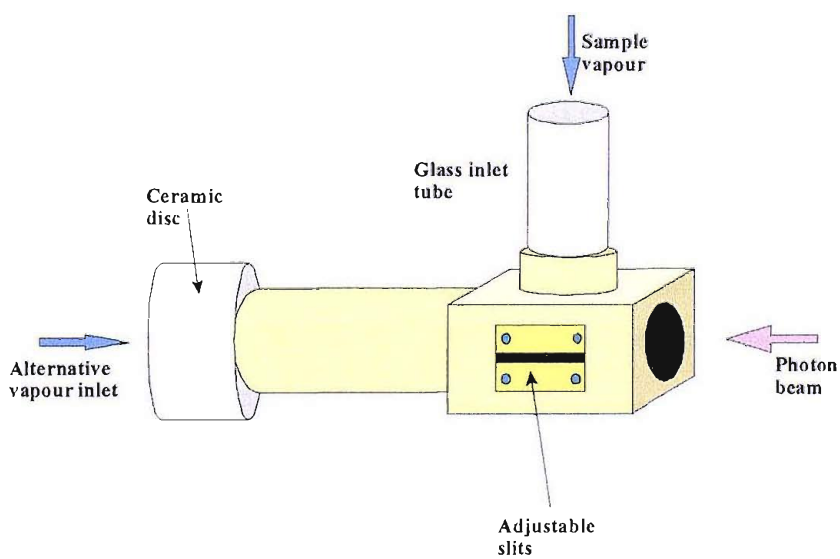

Figure 2.4- Schematic of the reaction cell of the UV-photoelectron spectrometer used in this work

After passing through these slits, photoelectrons pass through another double set of slits, the *entrance slits* of the spectrometer analyser: in this way only a small sample of electrons enters the analyser region. All the surfaces of the reaction cell, the slits, and the walls of the ionization chamber are coated with a layer of graphite in order to minimize distortions in the trajectories of the photoelectrons.

To avoid inelastic scattering of photoelectrons, the ionization chamber and analyser region are kept under vacuum by means of two diffusion pumps (see Figure 2.2) which- in absence of sample vapours- produce a pressure of less than 10^{-5} mbar in both regions. To obtain photoelectron spectra of acceptable signal-to-noise, the total pressure in the ionization chamber after the introduction of the sample vapours must be less than 10^{-4} mbar.

The analyser chamber

Once the photoelectrons are sampled by the entrance slits, they enter a 150° hemispherical sector region created by two concentric hemispheres [11, 12], one with radius R_1 and another with radius R_2, covered in graphite; a schematic of the analyzer chamber has already been shown in Figure 2.1.

By applying an equal and opposite potential to the hemispheres, an electrostatic field is created in the gap region where the photoelectrons move. Recalling that photoelectrons have a range of different kinetic energies, it is possible to select a certain energy of photoelectrons to reach the detector by selecting the voltage on the analysing hemispheres. From the characteristics of a hemispherical condenser [13], it is found that by applying a +V potential to the inner sphere and a -V potential to the outer sphere, the only electrons that can reach the detector are those with kinetic energy equal to

$$KE = \tfrac{1}{2} \cdot V \cdot [(R_1+R_2) / (R_2-R_1)] \qquad (2.4)$$

A hemispherical analyser is chosen because of its the *double focussing* property, that is the possibility of an electron travelling from the entrance to the exit slits on numerous trajectories around the gap between the spheres. In this way more electrons can reach the detector region, and then a stronger signal-to-noise ratio is achieved: this is especially important for "slow" photoelectrons.

The exit slits are needed to focus the arriving photoelectrons onto the detector, in the same way as the entrance slits focus them into the analyser region.

By linearly sweeping the voltage on the hemispheres (by means of a ramp generator), it is possible to record the relative number of photoelectrons reaching the detector as a function of their kinetic energy. A photoelectron spectrum can be therefore be recorded by acquiring the photoelectron signal while

linearly increasing the voltage on the hemispheres. It is possible to pre-select the speed of the linear voltage sweep: a slower acquisition will lead to more intense and better resolved spectra.

Given the fact that the parameter to be changed to record a spectrum is the potential applied to the hemispheres, and as equation 2.4 cannot be used because of local charging effects, no direct determination of the electron kinetic energies can be obtained from the voltages used: for this, calibration is needed. This is usually achieved by introducing into the ionization chamber a standard gas whose photoelectron bands are sharp and well established in ionization energy, and which does not interact with the molecules under study; methyl iodide and argon are among the most commonly used calibrants, because of their sharp, intense bands [14].

To minimize collisions and to maximize the electron mean free path, the pressure inside the analysing chamber must be kept to less 10^{-5} mbar: this can be achieved with a diffusion pump which pumps on the analyser chamber, to ensure a pressure lower than in the ionization chamber. The presence of the entrance slits is also a way to achieve this pressure difference between the two chambers.

The electron detector

The detector used is a spirally shaped channel electron multiplier. The front cone is earthed and the far end has a voltage of +2.5 kV applied to it. This causes the electrons which impact on the cone to be amplified by a series of cascade processes in the detector.

The signal is then passed to a pre-amplifier and then an amplifier. It is then transmitted to a rate-meter (equipped with signal discriminator to minimize the noise) which is connected either to a PC or to a chart recorder.

2.2 HEATING SYSTEMS USED IN PES EXPERIMENTS

PES can be successfully used for pyrolysis studies, and the technique is a powerful tool to detect short-lived molecules generated in thermal decompositions [15, 16]. In order to study solid or liquid compounds having too low vapour pressure at room temperature to enable PE spectra to be obtained, heating methods were used in this work to facilitate evaporation and increase the vapour pressure. In addition to this, pyrolysis was frequently carried out: often the evaporation and pyrolysis region had to be separated in order to avoid too fast or uncontrolled evaporations. According to the different characteristics of the substance under investigation, different heating arrangements and/or heating methods were used.

After an introduction of the fundamental principles on which the different heating methods used are based, a detailed description of the heating apparatus used in this project will be reported.

2.2.1 General description of heating methods [17]

Different methods to evaporate solid samples for PES studies have been used by other workers and they include resistive heating, laser heating or electron bombardment.

Laser radiation heating produces very localized heating, and no electrons and electromagnetic fields are produced [18-20]. The problem is that few materials absorb at typical laser wavelengths; also, extremely localized heating can produce rapid and uneven evaporations that give rise to a photoelectron signal which is not constant with time.

Electron bombardment is another form of heating which could be used, but is not really suitable when photoelectrons are to be detected [21-24].

The most suitable technique for use with PES for studying materials with very low vapour pressures is undoubtedly resistive heating [25-28]. However, if temperatures above 700° C are required, radiofrequency (RF) induction heating is the best choice.

When resistive heating was used in this work, an inlet system consisting of two coaxial quartz tubes was used (Figure 2.5). A spiral of molybdenum wire is positioned on the final 12 centimetres of the inner tube (which has an external diameter of 5 mm): it is connected to an external Variac voltage supply via two metal feedthroughs placed in the Pyrex piece connecting the coaxial tubes (see Figure 2.5). The applied DC voltage causes a heating of the molybdenum wire proportional to the square of the current circulating in it. A current through the helical winding of the wire produces magnetic fields that could disturb the path of photoelectrons produced in the ionization region: to avoid this, the wire is

wrapped around the inner tube in a non-inductive way, that is by having the wire wound back on itself so that the fields from both windings cancel each other [29]. Inside the outer quartz tube a K-type thermocouple is positioned, protected by an alumina sleeve and connected to a temperature reading unit (voltmeter) via a second set of feedthroughs. The photon beam was approximately 1 cm below the opening of the inlet tube, which allows an estimate of ca. 1 ms for the flight time of the sample vapours from the pyrolysis region to the photon beam [30]: in this way the distance between the high temperature region and the photon beam is reduced to minimize the possibility of re-deposition of the molecules in a colder region and to maximize the flux in the photon beam. With this arrangement it was possible to reach a temperature of 550 °C without any major loss of resolution of the UV-PES spectrometer signal (around 30 meV, measured on the $(3p)^{-1}$ Ar^{+} $^{2}P_{3/2}$ ← Ar $^{1}S_{0}$ photoelectron signal). The top of the inner tube can be closed in different ways according to the type of substance studied. If a low vapour-pressure compound is to be studied, it is possible to place the sample in two small glass vials held by some glass wool at roughly 2 centimetres above the region heated by the molybdenum wire (see Figure 2.5): in this way the sample is in an intermediate temperature zone, therefore helping the vaporization process and allowing some pyrolysis, but the time available for the acquisition of spectra is relatively low compared to that for a high vapour pressure sample. The other possibility is in studies of substances with quite high vapour pressure: in this case the inner tube is directly connected to a needle valve and from this to a flask containing the sample to be pyrolysed. The vapour from the sample is then continuously flushed through the hot region, and a longer acquisition time is obtained. Resistive heating was used for all azides studied in this project, except for azidoacetamide, where radiofrequency induction heating was used.

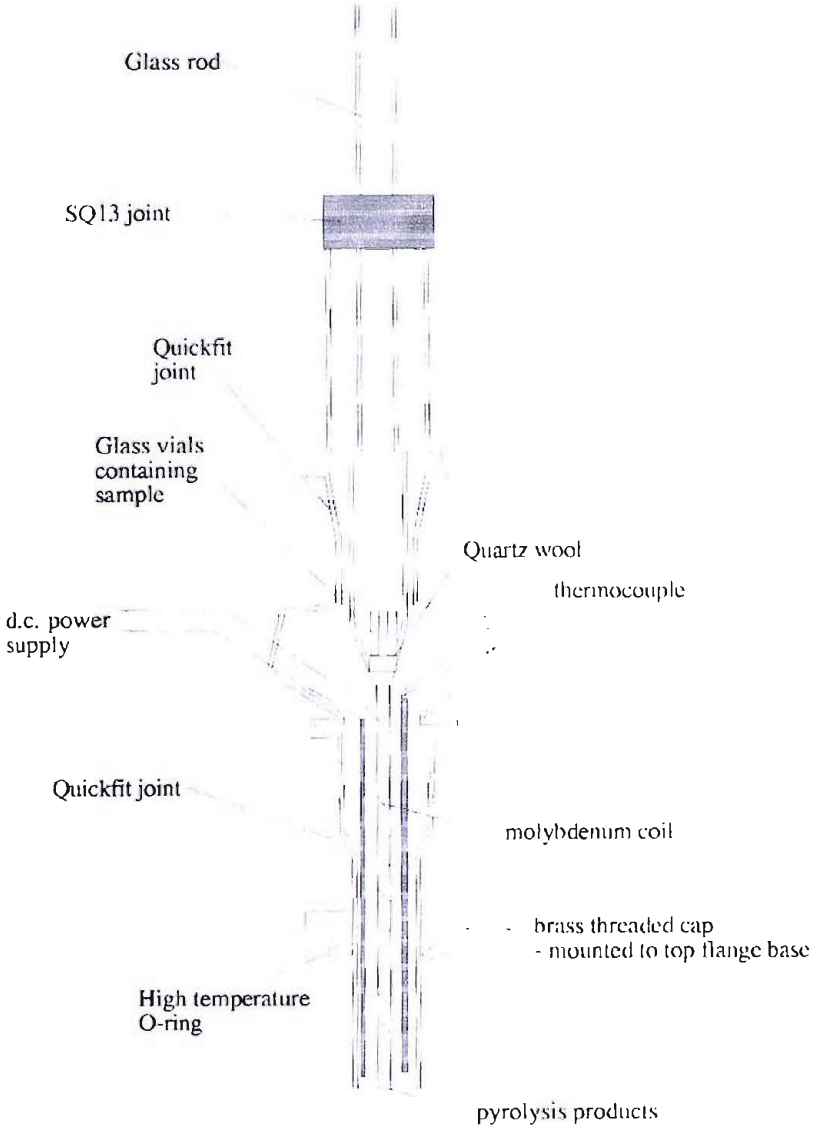

Figure 2.5- A schematic of the resistive heating inlet system used in this work; this shows the arrangement with the sample held in glass vials

The radiofrequency induction heating method used can be described as follows.

When pyrolysis temperatures above 600 °C are required, a water cooled brass shield is placed around the heating region in order to minimize heat losses, to collimate the vapour produced and to shield the reaction cell and the ionization region from the hot furnace; this is particularly important because, to have the highest concentration of sample vapour in the ionization region, the pyrolysis region must be positioned as close as possible to the reaction cell in which photoionization occurs. The pyrolysis region is characterized by a circular exit aperture with a very narrow diameter a: in fact, in this case the mean free path of an electron (inversely proportional to the pressure, that in this apparatus is very low)

is greater than the diameter of the tube. This condition- enhanced if the length of the tube, L, is much longer than its diameter a- makes the vapour flow highly directional, and both the PE signal intensity and the flow rate are proportional to the pressure in the vapour source. This is also known as *molecular effusive* flow [31].

Alternating radiofrequency radiation (1 MHz), generated by an external supply, is passed through water cooled copper coils which are wound in a spiral around a susceptor, which is the material to be heated (see Figure 2.7). The current generates a fluctuating magnetic field (directed along the axis of the coils), whose flux density is maximum near the coils. Because of this, the susceptor is placed as close as possible to the coils ("tight coupling condition"). This field induces eddy currents on the surface of the susceptor, which is directly proportional to the rate of change of the magnetic field, $\overline{B}$.

$$i = \frac{d\overline{B}}{dt} \qquad (2.5)$$

These eddy currents produce [32] a resistive heating effect in the susceptor which is proportional to the square of the current. The heat generated, Q, is given by:

$$Q = i^2 \cdot R = i^2 \cdot \rho(T) \cdot \frac{l}{A} \qquad (2.6)$$

Eddy currents are especially strong on the susceptor surface. They penetrate the susceptor but their value falls to $1/e$ of their value at the outer surface when they reach the *skin depth*.

This is given by

$$\delta = \sqrt{\frac{2\rho}{\mu\omega}} \qquad (2.7)$$

In this equation, μ is the permeability of the material, ρ is its resisivity and ω is the angular frequency of the radiofrequency (RF) current in the coils. 86% of the power is dissipated in the skin depth. To avoid parts of the susceptor being heated only by conduction, the susceptor thickness should be equal or close to the skin depth, δ. The susceptor is positioned immediately adjacent to the coils in order to maximize the heating [33]; it must not, however, be in contact with the coils, otherwise conduction losses would arise and shorting between the coils would occur.

Radiative heat losses are minimized by surrounding the susceptor with a strip of carbon felt [32], which is a material with low thermal conductivity and low RF pick-up because of its fibrous nature.

To avoid a short circuit between the furnace or the carbon felt, and the RF coils, a ceramic cylinder is placed around the carbon felt. This must be electrically insulating, refractory, have permanent shape, high melting point and good resistance to thermal shock: usually Al_2O_3 and BN ceramics have been

used, the latter being more suitable for higher temperatures (>1500 °C), at which alumina can react with the carbon felt [34]. However, in this work only alumina was used for the ceramic [35].

The furnace is the component in which the sample is held and heated; it is not necessarily the same as the susceptor. The furnace need not be the same as the susceptor, if particular conditions of evaporation have to be used (such as when the evaporation temperature of the sample must be different from the pyrolysis temperature, see following paragraphs). Wherever the furnace is placed, however, it is held by a ceramic rod by means of a tungsten pin (see Figure 2.7); this rod can be moved along its axis to get the optimum position of the furnace inside the RF coils. An O-ring makes the vacuum seal between the rod and the top flange.

Graphite is usually the best option as a furnace material [17, 35], if the sample does not react with it, because it has a quite high resistivity, is a good refractory, relatively inexpensive, machinable to give thin walls and it has a large skin depth. Alternatively, a stainless steel furnace can be used. Because of possible reactions of graphite with the organic azides studied in this work, a stainless steel furnace was used to acquire the azide PE spectra. The furnace used was closed at the top and had a capillary opening towards the photon beam to collimate the sample vapours produced into the photon beam (see Figure 2.7). Once the evaporation temperature of the compounds had been reached (usually around 120 °C), good quality PE spectra were recorded.

In the top flange and in the RF coils there is a cooling system (water passes through copper coils) to keep their temperature as low as possible.

To avoid RF interference in the detection of photoelectrons, the RF supply is pulsed at a frequency of 50 Hz, and a gating unit allows a detection window 180° out-of-phase with the RF pulses, so that the photoelectron signal is not affected by RF interference (Figure 2.6), i.e. photoelectrons are detected when the RF is off.

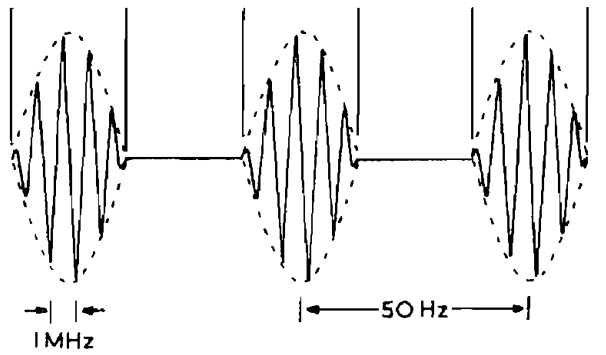

Figure 2.6- Representation of the gating and pulsing of the RF used to avoid interference with the detection of photoelectrons

Chloroacetamide and dimethyl-chloroacetamide studies

In the simplest arrangement the furnace corresponds to the susceptor, and it is placed inside the RF coils (Figure 2.7): this configuration was used to record PE spectra of chloroacetamide and dimethyl-chloroacetamide, which are the synthetic precursors of azidoacetamide and dimethyl-azidoacetamide respectively. It must be noted that these compounds could have also been studied by heating them with the resistive method, as they did not need to be pyrolysed.

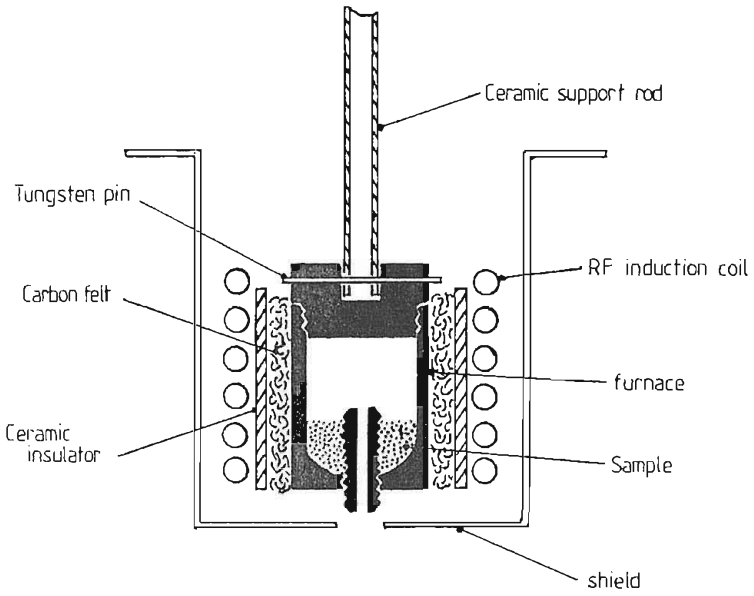

Figure 2.7- Diagram of the furnace arrangement used to record the PE spectra of chloroacetamide and dimethylchloroacetamide

Azidoacetamide and dimethylazidoacetamide studies

When azidoacetamide and dimethylazidoacetamide were studied, it was found that with a simple RF heating arrangement like the one described in Figure 2.7, these two azides, which at room temperature are respectively a solid and a viscous liquid, would start to evaporate at temperatures at which little decomposition occurred. If the temperature of the furnace was raised to values at which high degrees of pyrolysis were expected, fast total evaporation of the sample occurred, thus leading to a short spectral acquisition time. It was therefore necessary to separate the region in which the sample evaporated from the region in which it was pyrolysed. A simple conductively heated furnace, in which the furnace holding the sample to be evaporated is in contact with the susceptor (or radiator) placed a few centimetres below (in the pyrolysis region) has the disadvantage that the pyrolysis region has a fixed temperature difference from the furnace region. This does not allow full control on the evaporation

process. For example conduction is so efficient that under these conditions the sample in the furnace begins to evaporate when the temperature in the lower pyrolysis region is too low to achieve a high degree of decomposition. On the other hand, when the temperature of the susceptor is set to the correct value for a high degree of pyrolysis, then uneven and fast evaporations occur.

In this case, the heating region has been divided into two completely separate regions: the upper part is where the sample is vaporized, and the lower part is where that vapour is pyrolysed (see Figure 2.8).

In the upper part, the furnace which holds the sample has been changed from the simple stainless steel furnace to a stainless steel furnace wrapped with non-inductive wound molybdenum wire connected to an external voltage supply via tungsten feedthroughs; the furnace was resistively heated by applying a voltage from an external supply.

In the lower part, due to the difficulty in getting a high degree of pyrolysis in the RF heated region, the residence time of the vapour in the pyrolysis region was increased by using as the susceptor a cylinder with only a very small opening (1 mm diameter) at the bottom near the photon beam and a long capillary inside it (Figure 2.8). The volume inside the susceptor (or radiator) has also been filled with small tantalum pieces to increase the residence time of the vapour inside the pyrolysis region. The vapour then reaches the lower pyrolysis region, whose temperature is regulated by the RF supply. This system has permitted the recording of a series of spectra of azidoacetamide from zero to total decomposition. Recording of the spectra of the unpyrolysed and pyrolysed parent azide has been achieved by setting the temperature of the upper furnace approximately equal to 90 °C, while the temperature of the lower region was increased from 0 °C up to 900 °C, so that the vapours produced from the upper region could be increasingly pyrolysed.

With this system, the temperatures of evaporation and pyrolysis regions could be independently controlled.

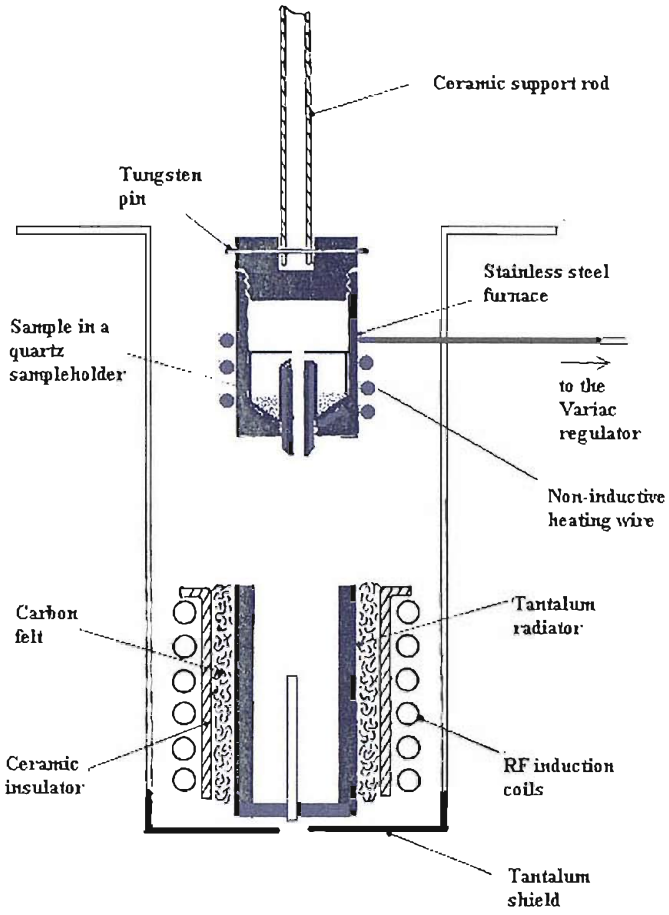

Figure 2.8- Furnace arrangement used for PES acquisitions on azidoacetamide and dimethylazidoacetamide

2.3 EXPERIMENTAL PROCEDURE FOR PHOTOELECTRON SPECTRAL ACQUISITION

In the vaporization and pyrolysis experiments carried out in this work, the temperature calibration of the pyrolysis region as a function of the applied voltage was achieved with a K-type thermocouple placed very close to the heating wires (or to the susceptor) for each different heating configuration used. In all configurations used the photon beam was only roughly 1 centimetre below the opening of the heated region, or the mixing region for the DMS+Cl_2 experiments.

Spectra of pure compounds (such as the aliphatic azides or DMS, or pure products on which precise calibration was needed such as methyl formate) were usually calibrated by first calibrating their first band with methyl iodide added to the sample in the ionization region of the spectrometer: CH_3I has two characteristic strong and sharp bands at 9.538 and 10.165 eV [36]. Then full spectra of the compounds

under study were acquired with argon added to the ionization region and the vertical ionization energies (VIEs) of all bands were measured using the VIE of the first band and the known ionization energy of argon (the $Ar^+ {}^2P_{3/2} \leftarrow Ar\ {}^1S_0\ (3p)^{-1}$ ionization at 15.759 eV) [36].

In the azide studies, spectra of their precursors (chloro- or bromo-compounds) have been recorded and calibrated in order to verify the absence of these precursors in the samples studied. Actually, all parent azide spectra were free of any significant trace of the precursors used in the preparations. In azides of high volatility, some solvent was sometimes present in the sample: the solvent was eliminated by pumping on the sample connected to the inlet of the ionization chamber and exploiting the higher volatility of the solvent with respect to the azide: after some minutes the intensity of the solvent PE bands reduced to zero and the azide was then considered as virtually pure.

In the DMS+Cl_2 studies the reactants needed no purification, but to passivate the internal surfaces of the inlet system it was necessary to eliminate HCl formed when Cl_2 was initially introduced into the inlet system and reacted with water on the walls. Also in this case, after some minutes in which all the system was kept under vacuum, hydrochloric acid was considerably reduced.

Photoelectron spectra were recorded in real-time while increasing the temperature of the pyrolysis region (see Chapter 5) or changing the mixing distance of DMS and molecular chlorine above the photon beam (see Chapter 4). In the case of the azides, the onset of pyrolysis was marked by the appearance of characteristic N_2 bands, an associated lowering of the parent azide bands and an increase of bands associated with the pyrolysis products; the extent of the DMS+Cl_2 reaction was marked by the increase of intensity of the HCl bands, and a decrease of the reactant bands.

When the pyrolysis or reaction had started, the formation of products with clearly identifiable photoelectron bands was exploited as internal calibrants, avoiding any introduction of further compounds into the reaction cell.

Calibration of spectra obtained on pyrolysis of azides was normally achieved using the bands associated with the first vertical ionization energy (VIE) of nitrogen (15.579 eV, [36]), of H_2O, whose traces were sometimes found on the inlet systems, (VIE 12.616 eV, [36]) or of HCN (VIE 13.60 eV, [36]). In DMS+Cl_2, the bands used were the first VIEs of DMS (VIE 8.72 eV, [37]), Cl_2 (VIE 11.82 eV, [37]) and HCl (VIE 12.75 eV, [37]).

2.4 INFRARED MATRIX ISOLATION SPECTROSCOPY

2.4.1 Basics of the infrared technique

Infrared spectroscopy is- in contrast with photoelectron spectroscopy- a resonance technique.

Infrared photons absorbed by a molecule induce a transition from a low vibrational level to the next vibrational level, their energy difference being the same as the photon energy.

Normally, at room temperature the separation between the lowest vibrational energy levels is much higher than the average molecular thermal energy k_bT, so only the ground vibrational state will be occupied before the infrared absorption.

The *first selection rule* for vibrational spectroscopy is that only transitions between adjacent levels are possible or- in other words- that only transitions between states with vibrational quantum numbers differing by ±1 are allowed. Vibrational spectroscopy can then be seen as the absorption of photons with energy corresponding to the energy gap between the ground and the first excited vibrational levels for each possible vibration within the molecule under study.

In a molecule containing N atoms, there are $3N$-6 vibrations (*vibrational modes*) in non-linear molecules and $3N$-5 vibrations in linear molecules; the remaining 6 (or 5) modes are associated with the translational and rotational modes. However, not all of these vibrational modes are active in infrared spectroscopy: the *second selection rule* states that only vibrations involving a change in the dipole moment of the molecule on vibration are infrared active: if the internal co-ordinates are labelled Q, this means that only transitions with $\partial\mu / \partial Q \neq 0$ are active. A more comprehensive expression for this selection rule [38] is that a vibration is infrared active if it has the same symmetry as one of the cartesian displacement co-ordinates x, y or z.

For a diatomic molecule the potential energy curve plotted against the internuclear distance will look like that shown in Figure 2.9.

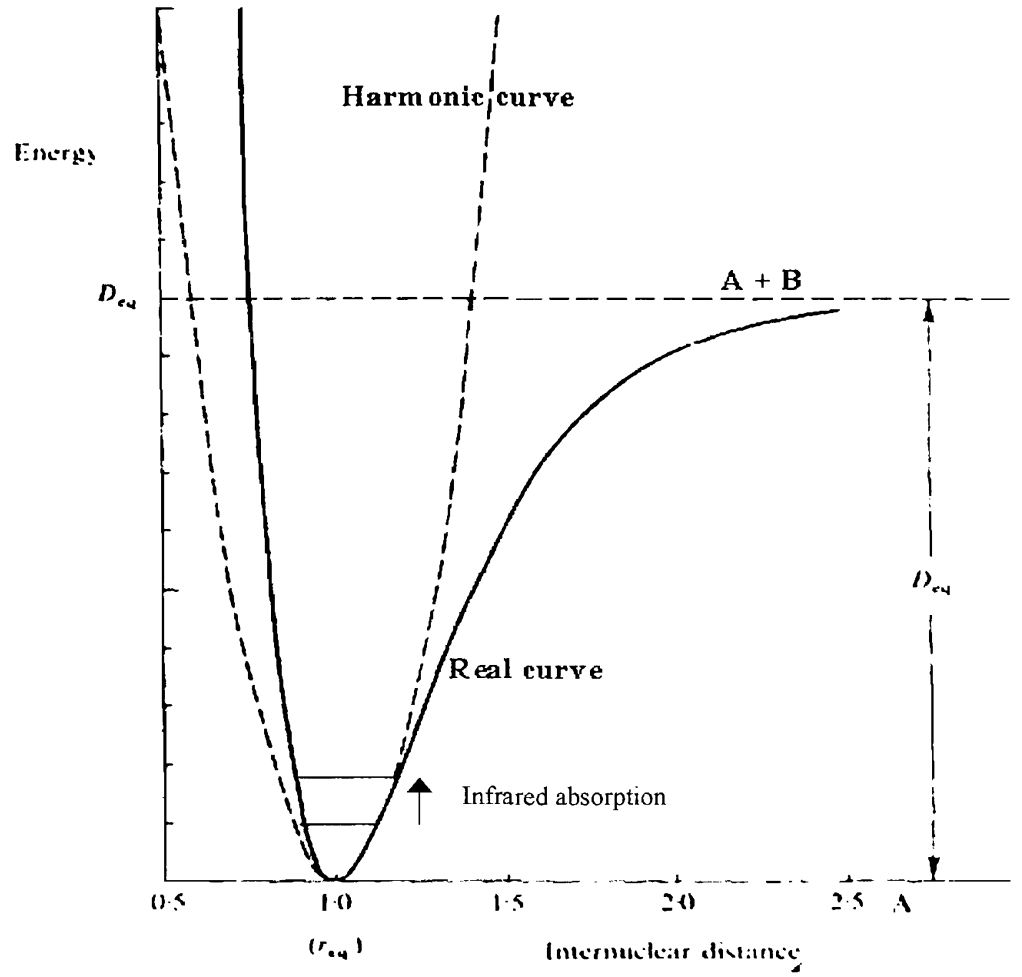

Figure 2.9- The schematic vibrational potential energy curve compared with the curve from the harmonic approximation

2.4.2 IR matrix isolation

The matrix isolation technique has been developed to allow trapping of molecules, and infrared spectroscopy has been used to study molecules trapped in the matrix. In this method, an effusive beam of sample gas from a cell is dispersed in a large excess (nearly 1000:1) of an inert carrier gas (the "matrix" gas), usually nitrogen or argon. The mixture is then frozen on a cold surface; a transparent window is placed opposite the cryostat to allow spectroscopic investigation of the deposited sample in the desired spectral region. The temperature of the cell from which the gas is introduced into the chamber can be varied by an induction heater, so that vapour beams with different composition or characteristics according to the temperature of the heater can be deposited. The material of the cell can be changed, so that the interactions between the sample and the walls of the cell can be minimized. The inert gas plays the role of isolating the sample molecules in the matrix. Elimination of interactions

between molecules in the matrix, and the cooling of the sample, leads to IR spectra with much narrower bands than the ones obtained in a high temperature vapour spectrum. As the molecules are trapped at low temperature, the contribution of "hot bands", background radiation and rotational-vibrational structure is almost eliminated. Moreover, matrix isolation of the vapours eliminates the requirement of having a suitable high vapour pressure of a sample for a short period of time, as a matrix sample can be built over several hours of deposition. The only effect that must be taken into account is the possible shift of the bands from their gas-phase values due to interactions with the matrix.

In the present work, an instrument equipped with a CsI deposition window, transparent to IR radiation, has been used [39]. As in the azide experiments nitrogen was one of the decomposition products, the matrix gas was chosen to be nitrogen, in order to achieve a more uniform deposition of the species on the cold window, which was kept at 10 K. Spectra were acquired at increasing temperatures of the furnace. In the DMS+Cl_2 experiments, both nitrogen and argon have been used as matrix gases.
A schematic diagram of the matrix isolation infrared spectroscopy apparatus used in this work is shown in Figure 2.10, while Figure 2.11 shows in greater detail the detection region of the matrix isolation instrument. Sample vapours are introduced into the system by means of a needle valve, usually made of PTFE. From this they pass into a 15 cm long silica tube (with internal diameter 5 mm) which can be heated up to 1000 K by means of an RF heated furnace surrounding the tube. On leaving the tube, the sample vapours are co-deposited with the matrix gas on the CsI window cooled at 10 K.
Cryogenic cooling is provided by an Air Products CSW-202 water cooled 'Displex' closed-cycle unit, which uses helium as the refrigerant. The unit consists of two parts, a compressor and an expander module which are connected by flexible, high pressure hoses. The expander is mounted in a high vacuum chamber using a double 'o'-ring seal. A CsI window is mounted at the base of the expander unit to provide a cold deposition surface. The window frames and the connections to the expander module are copper with indium gaskets to ensure good thermal conductivity. The copper radiation shield ensures that the minimum temperatures are attained and this also protects the expander from contamination by the sample.
The lower section of the vacuum shroud has two CsI windows to permit the passage of the infrared beam. The beam is perpendicular to the direction of the vapours, so the windows are rotated by 90° after a suitable amount of sample has been deposited on the window: in this way, IR spectra can be obtained. The matrix gas inlet pipe and a brass fitting for mounting samples are also situated in this part of the apparatus.

The vacuum chamber is maintained at low pressure, ca. $1x10^{-6}$ mbar, using an Edwards 'Diffstak' unit comprising oil diffusion and rotary pumps and a liquid nitrogen cold trap. These vacuum conditions are essential to prevent the condensation of atmospheric gases on the cold window during the course of an experiment. High purity argon and nitrogen are used as matrix gases, the deposition rate being controlled by a needle valve and monitored via the overall increase in system pressure due to incomplete condensation.

The vacuum shroud and the cryostat are mounted in the sample cell of a Perkin Elmer 983G (5000-180 cm^{-1}) infrared spectrometer. The instrument is fitted with a Perkin Elmer CD 3 purger unit in order to improve spectral quality in the lower wavenumber region. The spectrometer is interfaced to a Perkin Elmer 3600 data station to allow manipulation and storage of experimental data.

In the study of azides, usually a series of IR spectra of the parent azide were recorded first by switching off the heating unit and adjusting the flow rate. Subsequently the heating temperature was increased, and spectra were recorded after allowing a suitable deposition time of the vapours on the window (typically 30 to 90 minutes). IR spectra of pure samples of the species produced in the azide decompositions were recorded- where available- in order to have a better proof for the assignment and to confirm the frequencies of the bands from the literature. Spectra of the precursors of the azides were also recorded to check if some precursor was still present in the azide sample.

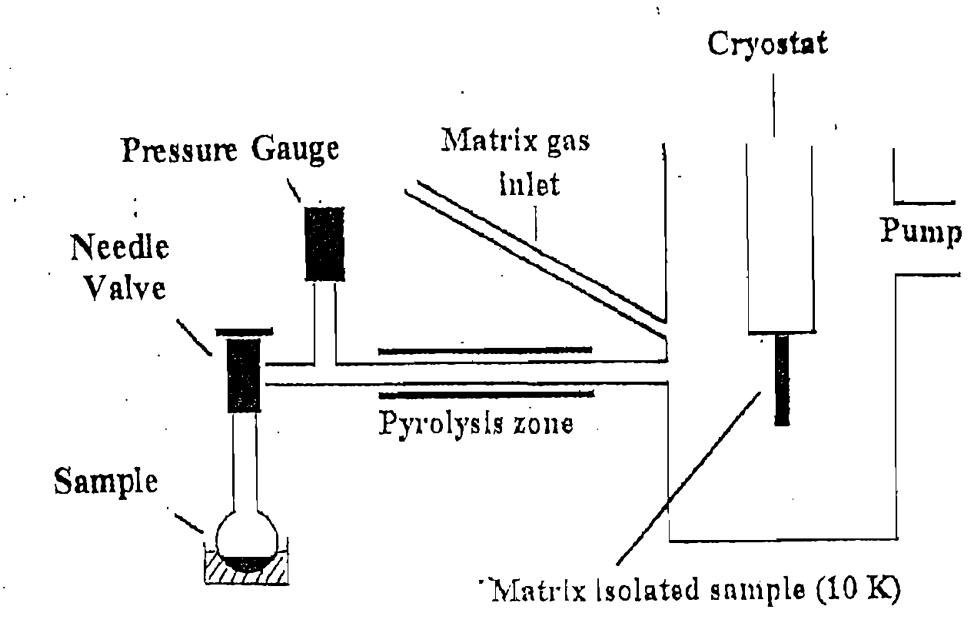

Figure 2.10- Schematic representation of the different sections of the infrared matrix isolation spectrometer used in this work

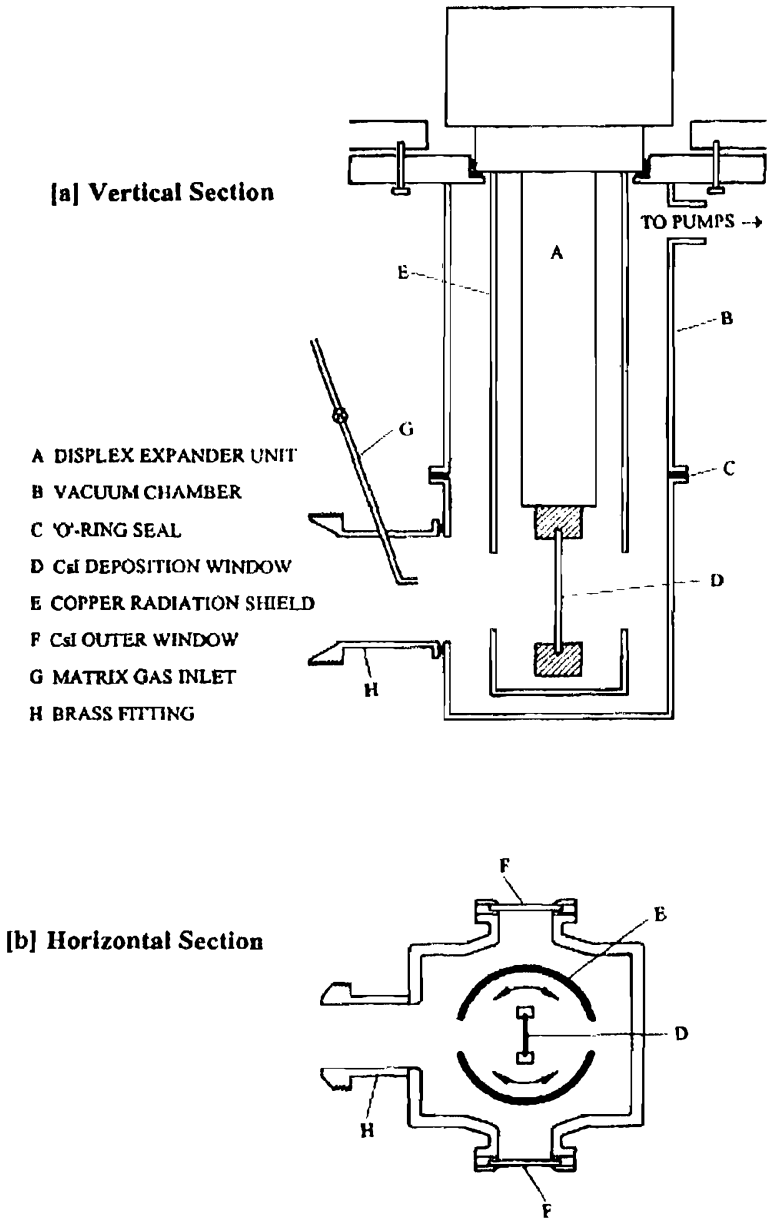

Figure 2.11- Detailed scheme of the "Displex" cryogenic cooling unit of the IR matrix isolation spectrometer used in this work

CONCLUSIONS

In this work, UV-photoelectron spectroscopy (PES) and IR matrix isolation spectroscopy have been used in both the studies on azides and on DMS+Cl_2. This Chapter described only the spectrometers used for these studies: the FT-IR and FT-UV instrumentation used only for the DMS+Cl_2 study will be presented in Chapter 4.

In PES, two different spectrometers have been used: their difference consisted in the mean radius of the hemispheres of the analyser region. Because the study was focused on the thermal decomposition of the azides, radiofrequency induction heating and resistive heating were used to vaporize and pyrolyze the samples. The different experimental arrangements- choice of the furnaces, the heating arrangements, positioning of the sample, temperatures reached - for these heating methods have been described.

In IR matrix isolation spectroscopy, the same apparatus has been used for all the studies: the fundamentals of infrared spectroscopy and the experimental set-up used for the deposition of a sample in the cold matrix have been presented.

For both techniques, the procedure for spectral acquisitions that was usually performed in this work has also been described.

REFERENCES

[1] J.H.D. Eland, *Photoelectron spectroscopy*, Butterworths, *1984*

[2] A. Morris, *Handouts on photoelectron spectroscopy*, University of Southampton, *1980*

[3] I.R. Trickle, *Ph.D. thesis*, University of Southampton, *1980*

[4] J.C.H. Stevens, *Ph.D. thesis*, University of Southampton, *1987*

[5] J.W. Rabalais, *Principles of Ultraviolet photoelectron spectroscopy*, Wiley Interscience, *1977*

[6]: D. Bulgin, J.M. Dyke, F. Goodfellow, N.B.H. Jonathan, E. Lee, A. Morris, *A. J. Electron Spectrosc. Relat. Phenom.*, **12**, *1977*, 67

[7] J.M. Dyke, N. Jonathan, A. Morris, *Electron spectroscopy* Vol. 3, ed. C.R. Brundle and A.D. Baker, Academic Press, London, *1979*

[8] J.M. Dyke, N. Jonathan, A. Morris, *Int. Rev. Phys. Chem.*, **2**, *1982*, 3

[9] J.A.R. Samson, *Techniques of vacuum ultraviolet photoelectron spectroscopy*, Wiley, New York, *1967*

[10] J.A.R. Samson, *Rev. Sci. Inst.*, **40**, *1969*, 1174

[11] E.M. Purcell, *Phys. Rev.*, **54**, *1938*, 818

[12] C.E. Kuyatt, J.A. Simpson, *Rev. Sci. Inst.*, **38**, *1967*, 103

[13] K. Siegbahn *et al.*, ESCA: atomic, molecular and solid state structure studied by means of electron spectroscopy, Almqvist & Wiksells, Uppsala, Sweden, *1967*

[14] D.R. Lloyd, *J. Physics E, scient. Instrum.*, **3**, *1970*, 629

[15] J.L. Beauchamp, F.A. Houle, *J. Amer. Chem. Soc.*, **101**, *1979*, 4067

[16] A. Morris, J.M. Dyke, G.D. Josland, M.P. Hastings, P.D. Francis, *High temp. Sci.*, **22**, *1986*, 95

[17] K.J. Ross, B. Sonntag, *Rev. Sci. Instrum.*, **66** (9), *Sept. 1995*

[18] J.D. Allen, G.W. Boggess, T.D. Goodman, A.S. Wachtel, G.K. Schweitzer, *J. Elec. Spec. and rel. Phen.*, **2**, *1973*, 289

[19] G.K. Schweitzer, W.E. Bull, F.A. Grimm, *Technical report*, Air force materials Laboratory, Wright-Patterson AFB, Ohio, *1973*

[20] D.G. Streets, J. Berkowitz, *J. Elec. Spec. and rel. Phen.*, **9**, *1976*, 269

[21] S. Elbel, H.T. Dieck, H. Walther, J. Krizek, *Inorg. Chim. Acta*, **53**, *1981*, L101

[22] B. Solouki, H. Bock, R. Appel, A. Westerhaus, G. Becker, G. Uhl, *Chem. Ber.*, **115**, *1982*, 3747

[23] T. Prescher, M. Richter, B. Sonntag, H.E. Wetzel, *Nucl. Instrum. Meth. Phys. Res.*, **A254**, *1987*, 627

[24] L. Wang, B. Nui, Y.T Lee, D.A. Shirley, *Chem. Phys. Lett.*, **158**, *1989*, 297

[25] S. Suezer, M.S. Banna, D.A. Shirley, *J. Chem. Phys.*, **63**, *1975*, 3473

[26] E.P.F. Lee, A.W. Potts, J.E. Bloor, *Proc. Roy. Soc. Lond.*, **A381**, *1982*, 373

[27] E.P.F. Lee, A.W. Potts, *Proc. Roy. Soc. Lond.*, **A365**, *1979*, 395

[28] E. Schmidt, H. Schroeder, B. Sonntag, H. Voss and H.E. Wetzel, *J. Phys. B*, **16**, *1983*, 2961

[29] J. Berkowitz, C.H. Batson, G.L. Goodman, *J. Chem. Phys.*, **71**, *1979*, 2624

[30] A.M. Ellis, *Ph.D. Thesis*, University of Southampton, *1989*

[31]: C.B. Lucas, *Vacuum*, **23**, *1972*, 395

[32]: C.A. Adams, J.C. Hodge, M.H. Mackusik, *Elec. Eng.* **53**, *1934*, 194

[33]: *A first guide to induction heating*, INTERTHERM, Blenheim Gardens, London

[34]: R.A. Lewis, *Ph.D. Thesis*, University of Southampton, *1984*

[35] P.D: Zavitsanos, G.A. Carlson, *J. Chem. Phys.*, **59**, *1973*, 2966

[36]: D.W. Turner, C. Baker, A.D. Baker, C. Brundle, *Molecular Photoelectron Spectroscopy*, Wiley Interscience, London, *1970*

[37]: K. Kimura, S. Katsumata, Y. Achiba, T. Yamaszaki, S. Iwata, *Handbook of HeI Photoelectron Spectra*, Japan Scientific Press, Tokyo, *1981*

[38]: J.S. Ogden, Introduction to Molecular Symmetry, *Oxford University Press*, Oxford, *2001*

[39]: J.S. Ogden, R.S. Wyatt, *J. Chem. Soc. Dalton Trans.*, *1987*, 859

CHAPTER 3

THEORETICAL METHODS

3.1 INTRODUCTION

The DMS+Cl_2 reaction and the decompositions of organic azides have been studied by UV-photoelectron spectroscopy and infrared matrix isolation spectroscopy. Both spectroscopic methods can provide very important information about the molecule under investigation: PES gives information on the electronic structure, IR spectroscopy gives information on the vibrational modes of the molecule.

IR is a resonance technique: a molecule absorbs photons having the exact energy corresponding to the excitation energy of the different vibrational modes in the molecule. Experimentally, the intensities of the IR radiation before and after it has passed through the sample under study are measured: when the intensity of the radiation transmitted through the sample is lower than the intensity of the incident radiation, absorption has occurred. By comparing the intensities of the incident and the transmitted radiations at different wavelengths, it is possible to obtain the IR spectrum of a molecule. Therefore, in IR spectroscopy the energy and the intensity of the absorbed radiation are the essential parameters.

On the other hand, PES is not a resonance technique: in this method molecules are irradiated with high energy photons. They do not induce a transition between electronic states, but they cause photoionization to take place, that is the ejection of an electron from the molecule and the production of a positive ion. Experimentally the intensity of electrons is measured as a function of electron kinetic energy. The difference between the energy of the photon and the measured electron kinetic energy gives the sum of the ionization energy and the vibrational energy change between the molecule and the ion (see Chapter 1). In photoelectron spectroscopy the intensity and energy of the bands are not the only important spectral parameters: the different type of molecular orbitals from which the electron is extracted and the presence of vibrational excitation on ionization lead to different shapes and appearances between PE bands.

The basics of the technique have already been described in Chapter 1, while the experimental apparatus used in this work has been described in Chapter 2; this chapter will deal with the possibility of linking the information obtained from these spectroscopic techniques- notably the measured ionization

energies and vibrational frequencies- with the intrinsic properties of the molecule studied. The relationship between experimental spectroscopic measurements and molecular properties is established via a suitable theoretical method.

Such theoretical methods are crucial for spectral interpretation, as in a lot of cases this is not straightforward: notably in PES, the impossibility of resolving the vibrational structure of the bands of large molecules- such as the azides or DMS- reduces the chances of a reliable assignment. This inconvenience is particularly important for reaction intermediates, and more generally for molecules for which no spectroscopic data are available from the literature. A correct assignment of spectral bands is crucial for analytical purposes- indicating for example which products are formed on decomposing a starting material.

In addition to this, it is possible to describe the potential energy surface for the molecule with an electronic structure method: this allows the determination of the molecular geometry, which corresponds to the minimum energy position. The method is not restricted to equilibrium geometries, but can also be extended to determine a reaction co-ordinate: this allows the location of transition states for a reaction, helping in understanding the mechanism of the reaction and providing important indications on the thermodynamic values of the reaction (heats of formation, activation energies).

In this work all the experiments have been supported by electronic structure calculations; however, only limited use of relative band intensities has been made, so in the description of the calculations only the problem of spectral assignments will be discussed and no mention will be made of theoretical treatment or use of experimental band intensities.

The electron distribution of a molecule is the crucial factor to determine all its relevant characteristics. Calculations aimed at determining the equilibrium geometry of a molecule, its vibrational frequencies, the ionization energies and all the other molecular properties obtainable quantitatively from experimental spectroscopic data must describe the molecular electron distribution first, which comes from the molecular orbital wavefunction. This leads to these theoretical calculations being termed as *molecular orbital calculations.*

The starting point of the theoretical description of the molecular electronic structure is that it can be expressed in terms of the electronic structure of the constituent atoms. Molecular orbital calculations can be based either on first principles- basically the Coulomb interactions between negatively charged electrons and positively charged nuclei- without any consideration of the chemical characteristics of the molecule studied, or they can use theoretical expressions depending on the nature of the atom, with the introduction of parametric expressions in which the parameters change according to the chemical

properties of the molecule. In the first case, the calculations are defined as *ab initio* calculations, and are mostly based on the Hartree-Fock method [1-3]; in the second, they are defined as *semi-empirical* calculations. As a bridging technique between these two categories, *Density Functional Theory* (DFT) uses empirical functionals but is closer to *ab initio* methods in the principles on which it is based: it is therefore considered as a *semi-ab initio* method [4-7].

Ab initio methods have the great advantage of being universal; they can be used on both open- and closed-shell molecules and fast methods to optimize the molecular geometries and harmonic vibrational frequencies are available. While in DFT calculations if a mathematical expression of a quantity, called the density functional, does not give acceptable results, it must be changed by a new expression to be found and tested empirically, in *ab initio* calculations the degree of sophistication in the approximations used in the molecular orbital expressions is defined without any reliance on parametrizations. Moreover, modern computation power rapidly increases the feasibility of *ab initio* calculations for large systems: the *ab initio* method is therefore the most important class of theoretical calculations. The DFT method is nevertheless a widely used method, because of its rapidity: it has been found in particular that transition metal systems are quickly and accurately described by this method.

In this project, only *ab initio* molecular orbital calculations have been performed to support the experimental spectroscopic results: it will therefore be the only method described. The programs used were Gaussian98 or Gaussian03 [8] for geometry optimizations, vibrational frequency and ionization energy determinations at the MP2 level; when CCSD(T) energies were calculated, the MOLPRO 5.0 program was used [9].

3.2 SCHROEDINGER EQUATION AND BORN-OPPENHEIMER APPROXIMATION

When a molecule in its ground electronic state X and ground vibrational state $v''=0$ is irradiated with vacuum-UV radiation or X-rays, it can be ionized to a cation in the generic electronic state X, A, B, C... and vibrational state v' following the scheme

$$A\,(X;\, v''=0) + h\nu \rightarrow A^{+}\,(X, A, B\ldots;\, v') + e^{-} \qquad (3.1)$$

This process is the basis of *photoelectron spectroscopy*. In general, spectroscopic techniques are based on perturbation of the molecular stationary state by radiation: the consequence of this perturbation is a change in the probability of finding the molecule in the initial state.

In quantum mechanics [10] the state of a molecular system is described by a *wavefunction* Ψ. The product of the wavefunction with its complex conjugate (Ψ^*) with a volume element dV gives the probability of finding an electron in that volume element. When stationary states of the molecule are considered, Ψ must obey the *time independent Schroedinger equation*

$$H\Psi = E\cdot\Psi \qquad (3.2)$$

where E is the energy of the system and H is the *Hamiltonian operator*. The Hamiltonian contains the kinetic energy of the N electrons and M nuclei within the molecule, plus the Coulomb interactions between all of these M+N particles. The nucleus *a*- nucleus *b* repulsive energy is expressed by $+Z_aZ_be^2/R_{ab}$ in which Z is the charge of the nucleus and R is the internuclear distance, while the nucleus *a*- electron *j* attractive energy is expressed by $-Z_ae^2/R_{aj}$ and the electron *i*- electron *j* interaction is expressed is expressed by e^2/r_{ij}.

Because of this latter term, it is only possible to solve the Schroedinger equation exactly for a system with only two particles [11], such as the hydrogen atom-like system (H, He^+, Li^{2+}, etc). To extend its application to all the other possible systems such as many electron atoms or molecules, it is therefore necessary to introduce approximations in the terms considered in equation (3.2).

The fundamental approximation made in molecular orbital theory is to consider that the time scale of the nuclear motions is much longer than the electronic motions, due to the great difference in mass of these particles: this allows the motions of electrons and nuclei to be separated. This is commonly referred as the *Born-Oppenheimer approximation* [12]. Such an approach gives rise to a partitioning in the total wavefunction expression. This can be written as

$$\Psi(\mathbf{r}, \mathbf{R}) = \psi_{nucl}(\mathbf{R})\cdot\psi_{elec}(\mathbf{r}, \mathbf{R}) \qquad (3.3)$$

-where **r** and **R** are the electron and nuclear coordinates respectively- for each electronic state of the molecule. Assuming that the translational and rotational modes are fully separable from the internal molecular motions, the molecular Hamiltonian can be separated into a term operating only on the nuclear co-ordinates and one operating only on the electronic co-ordinates. This means that

$$H = H_{nucl} + H_{elec} \qquad (3.4)$$

It is then possible to solve an electronic Schroedinger equation for the electronic state *k*,

$$H_{elec}\psi_{elec}(\mathbf{r},\mathbf{R}) = E_{elec\,k}\cdot\psi_{elec}(\mathbf{r},\mathbf{R}) \qquad (3.5)$$

with the nuclei kept in fixed **R** positions. It must be noted that $\psi_{elec}(\mathbf{r},\mathbf{R})$ is related only to the possibility of locating the electrons in **r** after fixing the nuclei in **R**, and not to the possibility of locating the nuclei in **R**.

Having obtained $E_{elec\,k}(\mathbf{R})$ at different values of **R** by solving equation (3.5), it is possible to solve the nuclear- or vibrational- Schroedinger equation

$$H_{nucl}\psi_{nucl}(\mathbf{R}) = E_{nucl\,k}\cdot\psi_{nucl}(\mathbf{R}) \qquad (3.6)$$

$E_{elec\,k}(\mathbf{R})$ in fact in the nuclear Hamiltonian plays the role of a potential energy affecting the relative positions of the nuclei, and can be therefore labelled $U_k(\mathbf{R})$. The index *k* is reported because the nuclear wavefunctions will be different according to the electronic state: in fact there is a potential energy surface for each electronic state.

Once the electronic state has been found, it is possible to write one equation $H_{nucl}\psi_{nucl}(\mathbf{R}) = E_{nucl\,k}\cdot\psi_{nucl}(\mathbf{R})$ for each electronic state *k*. The eigenvalue for a single equation is the sum of the electronic and vibrational energy for the electronic state *k* and vibrational state *u*.

Then, in the Born-Oppenheimer approach the $\psi_{nucl}(\mathbf{R})$ functions are the solutions for the vibrational Schroedinger equations in which the kinetic energies are those of the nuclei and the potential energy is the electronic energy of the state *k*.

A different formulation for the Born-Oppenheimer approximation, called the *adiabatic* approximation, is that $\psi_{nucl}(\mathbf{R})\cdot\psi_{elec}(\mathbf{r},\mathbf{R})$ is a good solution of the molecular Hamiltonian if no couplings between different electronic states are considered. Given the fact that such couplings are possible, corrections must be introduced into the adiabatic wavefunctions: usually this is done as perturbative contributions to the adiabatic term, which are then called *non-adiabatic* corrections. If the non-adiabatic perturbation couples a state *k*, *u* (*k* refers to the electronic state, *u* to the vibrational one) with a state *l*, *v* then this correction is usually negligible when the ground electronic state (k=0) is involved; for a highly distorted molecular geometry- that is, a highly excited vibrational state- the non-adiabatic contribution is however more important, and the Born-Oppenheimer approximation is consequently less accurate. For excited electronic states, it is more probable that the non-adiabatic interaction couples such a state with a lower electronic state but high vibrational excitation: this means that the energy can be transformed from electronic to vibrational in an *internal conversion* (IC) process which is associated with a non-radiative transition between the two states involved.

3.2.1 Potential energy surfaces and vibrational motions

The nuclei make small oscillations around the equilibrium positions- with energy $U_{min}(\mathbf{R})$-, the minima of $U_k(\mathbf{R})$ determining the molecular geometry for the electronic state k. When two minima on this potential energy surface are connected so as to follow the path with minimal energy, the *reaction co-ordinate* is located. The highest point in energy on this path is a saddle point whose $U_k^*(\mathbf{R})$ energy defines the *activation energy* of the process, defined by $E_k^* = U_k^*(\mathbf{R}) - U_{min}(\mathbf{R})$. When the vibrational energy E_{ku} is higher than E_k^* the system can move from one minimum to another minimum (reactant → product). The process needs first a vibrational excitation from a low to a high u value: this can happen in a thermal reaction, as a consequence of collisions with other molecules which can efficiently convert translational energy into rotational or vibrational energy. The reaction can be a simple isomerization if the two minima of the surface are separated by a low energy barrier.

For every specific vibrational motion, however, if the vibrational excitation is raised above a certain value it can become higher than $U_r(\infty)$, which is the energy towards which the potential curve tends asymptotically at an infinite distance between the vibrating nuclei: this means that at energies above $U_r(\infty)$ the two nuclei are not bound anymore and the molecule can dissociate. In this case the reaction co-ordinate passes from a vibrational co-ordinate within the molecule to a translational co-ordinate between the two new fragments and the state is defined as *dissociative*.

A first approximation to express the molecular vibrations would be to consider the vibration of a diatomic molecule as that arising from a spring of force constant k, equilibrium distance r_{eq} and mass equal to the reduced mass of the system, μ: this approximation is called the *harmonic approximation*, and leads to the potential between the nuclei being expressed by a parabola, $V = \frac{1}{2} \cdot k(r-r_{eq})^2$ and it assumes that on displacement the restoring force is proportional to the displacement. Substitution of this expression into the vibrational Schroedinger equation leads to an expression for the vibrational energy levels given by $E_{vib} = h\omega(v+ \frac{1}{2})$, in which h is the Planck constant, v the vibrational quantum number and ω the frequency of that vibration.

In this model, the vibrational levels are equally spaced by an energy amount of $h\omega$, and the lowest state is characterized by a *zero point energy* (ZPE) of $\frac{1}{2} h\omega$.

In a molecule containing N atoms, there are $3N$-6 vibrations (*vibrational modes*) in non-linear molecules and $3N$-5 vibrations in linear molecules. $U_k(\mathbf{R})$ can be expanded in Taylor series around one of its minima, U_{min}. If the expansion is truncated at the second-order term (*harmonic approximation*), the co-ordinates can be chosen so to that the potential expression for a molecule is given by $3N$-6 terms depending on a single co-ordinate,

$$U_k(\mathbf{X}) = U_{min} + \tfrac{1}{2}\sum_r \omega_r^2 \mathbf{X}_r^2 \qquad (3.7)$$

At the same time, the vibrational wavefunction $\psi_{ku}(\mathbf{R})$ can be expanded as a product of $3N$-6 terms

$$\psi_u(\mathbf{X}) = \prod_r \psi_r(\mathbf{X}_r) \qquad (3.8)$$

so that every ψ_r is solution of a mono-dimensional Schroedinger equation. In the harmonic approximation, the eigenvalues given by the Schroedinger equation for each of these co-ordinates are equidistant in energy and the gap represents the vibrational frequency on that co-ordinate.

The total vibrational energy is given by

$$E_{vibr} = h/2\pi \sum_r (u_r + \tfrac{1}{2}) \cdot \omega_r \qquad (3.9)$$

where u_r is the vibrational quantum number for the harmonic vibration on the co-ordinate $\mathbf{X}_r$ (and assumes integer values 0, 1, 2...) and ω_r is the frequency of that vibration. For high quantum numbers u_r the vibration has larger excursions along the nuclear co-ordinate and the system can be in a broader $\mathbf{X}_r$ range: the harmonic approximation is therefore not accurate at high vibrational excitations.

The harmonic approximation is satisfied only near the equilibrium: a better approximation for the potential energy curve is given by the *Morse equation* [13], which express the potential as

$$V = D_e \cdot (1 - e^{-\alpha \cdot (r - r_{eq})})^2 \qquad (3.10)$$

The equation, though good at equilibrium (where is approximates a parabolic potential) and at dissociation distances, does not describe correctly the curve for $r \rightarrow 0$; nevertheless, its properties are overall much better suited for a description of the potential curve than the harmonic potential.

D_e is the depth of the potential curve- as can be seen by setting r as infinite- but the dissociation energy, D_0, is given by considering zero point energy, i.e. $D_0 = D_e - ZPE$. α is a constant related to the second derivative of the curve at equilibrium distance, i.e. the force constant.

By substituting the Morse potential into the vibrational Schroedinger equation and solving, the expression of the vibrational levels of a diatomic molecule becomes [14]

$$E_{vib} = h\omega(v + \tfrac{1}{2}) \cdot [1 - x_a(v + \tfrac{1}{2})] \qquad (3.11)$$

where x_a is a constant known as the *anharmonicity constant*- related to α- which takes into account the deviation from a parabolic potential; with this contribution the vibrational levels are not equally spaced, but their energy gap becomes narrower with increasing quantum number. Near the dissociation limit, the distribution becomes virtually a continuum.

When anharmonicity is considered, the expression of the vibrational energy of a polyatomic molecule is given by

$$E_{vibr} = \sum_i \omega_i(v_i + \tfrac{1}{2})\cdot[1 - \sum_{j\geq i} \chi_i(v_j + \tfrac{1}{2})] \qquad (3.12)$$

Using this expression [14], in some cases it is possible to obtain the values of both ω and χ_a in an ionic state from the vibrational spacings within a photoelectron band; hence, D_e and α can be calculated.

Consideration of anharmonicity implies that the potential curve increases more slowly than in the harmonic approximation, where a parabolic curve describes the potential, and the energy levels become more dense at higher quantum number, that is their energy separation decreases. Moreover, if the harmonic approximation is not followed, it is not possible to completely separate the vibrational motions of different normal co-ordinates: this means that the ψ_r in $\psi_u(\mathbf{X}) = \prod_r \psi_r(\mathbf{X}_r)$ are no longer correct stationary states but just approximations.

Another consequence of anharmonicity- and of the not strict separation of the vibrational motions- is that it can couple bound states to dissociative ones when the energy E_{vibr} is higher than $U_r(\infty)$. With this coupling it is possible that bound states in which the excitation quanta are all below the $U_r(\infty)$ limit can evolve to one in which all the excitation quanta are concentrated on a single bond, so that under the effect of a constant perturbation, such an infrared absorption, a vibrational dissociation is possible.

3.3 SELECTION RULES IN PHOTOELECTRON SPECTROSCOPY

By irradiating a molecule in its initial state Ψ'', a perturbation V is introduced in the unperturbed Hamiltonian so that

$$H' = H'' + V \qquad (3.13)$$

and therefore the molecular state becomes expressed by Ψ'. The transition between the two states can be possible if the integral that describes the coupling between the initial and the final state is non-zero. This is expressed by

$$\int \Psi'^* \, V \, \Psi'' \, d\tau \neq 0 \qquad (3.14)$$

where $d\tau$ spans on all spatial and spin co-ordinates.

In case of a photoionization process the expression becomes

$$\int \Psi'^* \sum_{\alpha i} \mu \, \Psi'' \, d\tau \qquad (3.15)$$

μ is the electric dipole moment operator, and the sum runs on all nuclei α and electrons *i*. The integral is named the *transition moment integral*.

As consequence of the Born-Oppenheimer approximation, the dipole moment can be separated into an electronic and a nuclear part, μ_e and μ_n. This separation and the fact that electronic wavefunctions of different electronic states are orthogonal lead to a simplified expression of the transition moment integral, given by

$$\int \Psi_v'(\mathbf{R})^* \, \Psi_v''(\mathbf{R}) \, d\mathbf{R} \cdot \int \Psi_e'(\mathbf{r},\mathbf{R})^* \sum_i \mu_e \, \Psi_e''(\mathbf{r},\mathbf{R}) \, d\mathbf{r} \qquad (3.16)$$

The photoionization probability is given by the squared modulus of the integral,

$$P = \left| \int \Psi_v'(\mathbf{R})^* \, \Psi_v''(\mathbf{R}) \, d\mathbf{R} \cdot \int \Psi_e'(\mathbf{r},\mathbf{R})^* \sum_i \mu_e \, \Psi_e''(\mathbf{r},\mathbf{R}) \, d\mathbf{r} \right|^2 \qquad (3.17)$$

The process has therefore the capability of coupling the two states Ψ' and Ψ'' only if both the integrals

$$\int \Psi_v'(\mathbf{R})^* \, \Psi_v''(\mathbf{R}) \, d\mathbf{R} \qquad (3.18)$$

and

$$\int \Psi_e'(\mathbf{r},\mathbf{R})^* \sum_i \mu_e \, \Psi_e''(\mathbf{r},\mathbf{R}) \, d\mathbf{r} \qquad (3.19)$$

are not zero. This sets the basis for the *photoionization selection rules* [14, 15].

3.3.1 Electronic selection rules

It can be demonstrated that the electronic integral $\int \Psi_e'^*(\mathbf{r},\mathbf{R}) \sum_i \mu_e \, \Psi_e''(\mathbf{r},\mathbf{R}) \, d\mathbf{r}$ does not vanish only if there is no change in the overall spin of the system. The photoelectron is obviously liberated with s= ½, so to respect the $\Delta S = 0$ rule between the neutral and final (ion plus free electron) states the cation and the neutral molecule must differ in spin by ½. This means that from a neutral molecule in a singlet spin multiplicity state only a doublet cation can be formed, and from a doublet neutral only a triplet or a singlet ion can be formed, and so on. This is the *first photoionization selection rule*.

In addition to this, it is possible to show that the integral vanishes if excitations or ionizations other than one-electron ionizations are considered; this is the *second photoionization selection rule*.

3.3.2 Vibrational selection rules

For the vibrational integral $\int \Psi_v'(\mathbf{R})^* \, \Psi_v''(\mathbf{R}) \, d\mathbf{R}$ to be non-zero, the direct product of the irreducible representations of the initial and final wavefunctions Ψ_v' and Ψ_v'' must be equal to the totally symmetric representation of the molecular point group. Given the fact that at room temperature $k_B T$ is around 209 cm^{-1} (0.60 $kcal.mol^{-1}$), a value usually much lower than the typical energy separation between vibrational states, for the great majority of the molecules at room temperature only the totally

symmetric vibration ground level with $v''=0$ is populated. This means that only transitions leading to totally symmetric ionic vibrational levels are allowed. In practice, the fact that the product of $\Psi_v'(\mathbf{R})$ and $\Psi_v''(\mathbf{R})$ must be totally symmetric, with $\Psi_v''(\mathbf{R})$ totally symmetric for the ground state, leads to vibrational selection rules in PES of polyatomic molecules.

When the ionization involves a geometry change between the neutral molecule and the ion, the selection rules apply only to the symmetry elements common to the point groups of the molecule and the ion. If the geometry change can be associated to a particular vibration within the molecule, this vibration is the one most likely to be excited in the photoionization process.

3.4 PHOTOELECTRON SPECTRA

Probably the most important piece of information obtainable from a photoelectron spectrum are the ionization energies associated with each band and their relative intensities. Each photoelectron band is associated with the energy necessary to produce an ion in a particular electronic state: the first band is associated with the ionization to the ground ionic level, the second band to the first excited ionic state, and so on. PES is not usually able to resolve rotational structure in a band, but it is often possible to resolve the different vibrational transitions associated with the ionization process associated with the PE band; in this case, the band is resolved into different vibrational components. The lowest in energy of these components is defined as the *adiabatic ionization energy* (AIE), while the most intense component is called *vertical ionization energy* (VIE).

The adiabatic ionization energy of a band is the energy necessary to ionize a molecule in its ground electronic and vibrational state to the lowest vibrational state of the ionic electronic state related to that particular PE band. In other words, both the molecule and the ion are in their $v=0$ vibrational level; the adiabatic transition is also referred as the 0-0 transition. The vertical transition is the transition for which the overlap of the vibrational wavefunctions of the molecule and the ion, given by $\int\Psi_v'(\mathbf{R})^* \Psi_v''(\mathbf{R})\, d\mathbf{R}$, is a maximum. The relative intensities of the vibrational components of a photoelectron band is expressed by the *Franck-Condon factor* (FCF), which is proportional to the squared modulus of this integral.

$$FCF \propto \left| \int\Psi_v'(\mathbf{R})^* \Psi_v''(\mathbf{R})\, d\mathbf{R} \right|^2$$

The most probable vibrational transition in an ionization process is related to the strongest component of a PE band, and the vertical transition is the one for which the FCF is maximum. The VIE and AIE

coincide only if the most intense component of the band is the lowest in energy, or in other words if the ionic vibrational wavefunction that produces the highest overlap with the $v''=0$ vibrational wavefunction of the neutral molecule is $v'=0$. In general, however, $v''=0$ and $v' \neq 0$ for the most intense component.

Considering that at room temperature the neutral molecule would be in its ground vibrational level, the spacings observable in a PE band are associated with the vibrational spacings of the ionic electronic state reached with the ionization associated with that particular PE band.

Along with the AIEs, the VIEs and the energy separation between vibrational components, the other important information obtainable from a PE spectrum is the shape of the band: if this shows resolved vibrational structure, the relative intensities between these components can provide useful information. It is important to emphasize that the vibrational structure of a photoelectron band reflects the vibrational spacings of the ion produced, and not of the neutral molecule: in fact, the vibrational intensities are due to the different relative probabilities of reaching different vibrational states of the ion, as in the molecule the starting vibrational state is almost always the ground state ($v''=0$).

Supposing that photoionization from the neutral to the ion involves also a vibrational excitation along a normal co-ordinate separable from all the others in both the states, and that the initial state is in the ground vibrational state ($v''=0$), then the intensity of the transition depends on the relative positions of the minima of the potential curves of the neutral and ionic states along the co-ordinate axis. In practice, the most intense transition to a vibrational state of the ionic configuration is the one in which the states are connected by a vertical line on the potential energy diagram: this explains the definition of *vertical* given to the most intense component in the band.

If vibrational structure is present, then different types of photoelectron spectra are possible according to the nature of the electronic states involved in the transition. Figure 3.1 helps in illustrating these cases.

The first possibility (reported as A in Figure 3.1) is that the neutral and ionic potentials have their minimum at around the same co-ordinate $\mathbf{X}_r$: this often happens in large molecules. Such a situation implies that by tracing a vertical line corresponding to the equilibrium geometry for the neutral state, this line will also connect the maxima of the wavefunctions $\psi_{v''}$ and $\psi_{v'}$. In this case the largest Franck-Condon factor is the one related to the lowest vibrational states, $\psi_{v''}$ and $\psi_{v'}$, where all the others involving higher vibrational states of the ionic state are increasingly weaker. The result is that the spectrum displays a strong band corresponding to the $v''=0 \rightarrow v'=0$ energy (the adiabatic transition) and much less intense bands at higher energies, related to the $v''=0 \rightarrow v'=1$, $v''=0 \rightarrow v'=2$ etc. transitions. The vertical transition is here coincident with the adiabatic transition: the vibrational spacing observed is expected to be very similar to the vibrational frequency of the neutral molecule, and the ionization

involved is from a non-bonding orbital in the neutral. This is the case, for example, with the first photoelectron band of water.

The second possibility (marked as B in Figure 3.1) is that the two potential curves have minima which are displaced along the co-ordinate $\mathbf{X}_r$. In this case the maxima of the vibrational wavefunctions for $v''=0$ and $v'=0$ are shifted, so the overlap between the wavefunctions for $v''=0$ and v' is greater when a higher v' state is reached in the photoionization process. In particular, the Franck-Condon factor is a maximum for a *vertical transition* corresponding to keeping the nuclei fixed to the initial co-ordinate $\mathbf{X}_r^{eq}$. The adiabatic absorption $v''=0 \rightarrow v'=0$ in this case is not the most intense, and the spectrum will be given by a series of bands increasing in intensity until the vertical transition energy, obtained for a state with a certain v' value. The intensities of the bands related to transitions to states with higher v' decrease, so the overall intensity pattern after the vertical transition will be a decrease.
This distribution pattern reflects an ionization involving a bonding molecular orbital. The vibrational spacing will be smaller than that of the neutral molecule.

Finally, the possibility that the ionization produces an electronically dissociative state must also be considered: in this case a continuous absorption band will be observed, as only translational levels will be accessed, which are very closely spaced. Even if a dissociative state is accessed, the maximum of the absorption will still be given by the transition with highest Franck-Condon factor, that is the vertical transition.

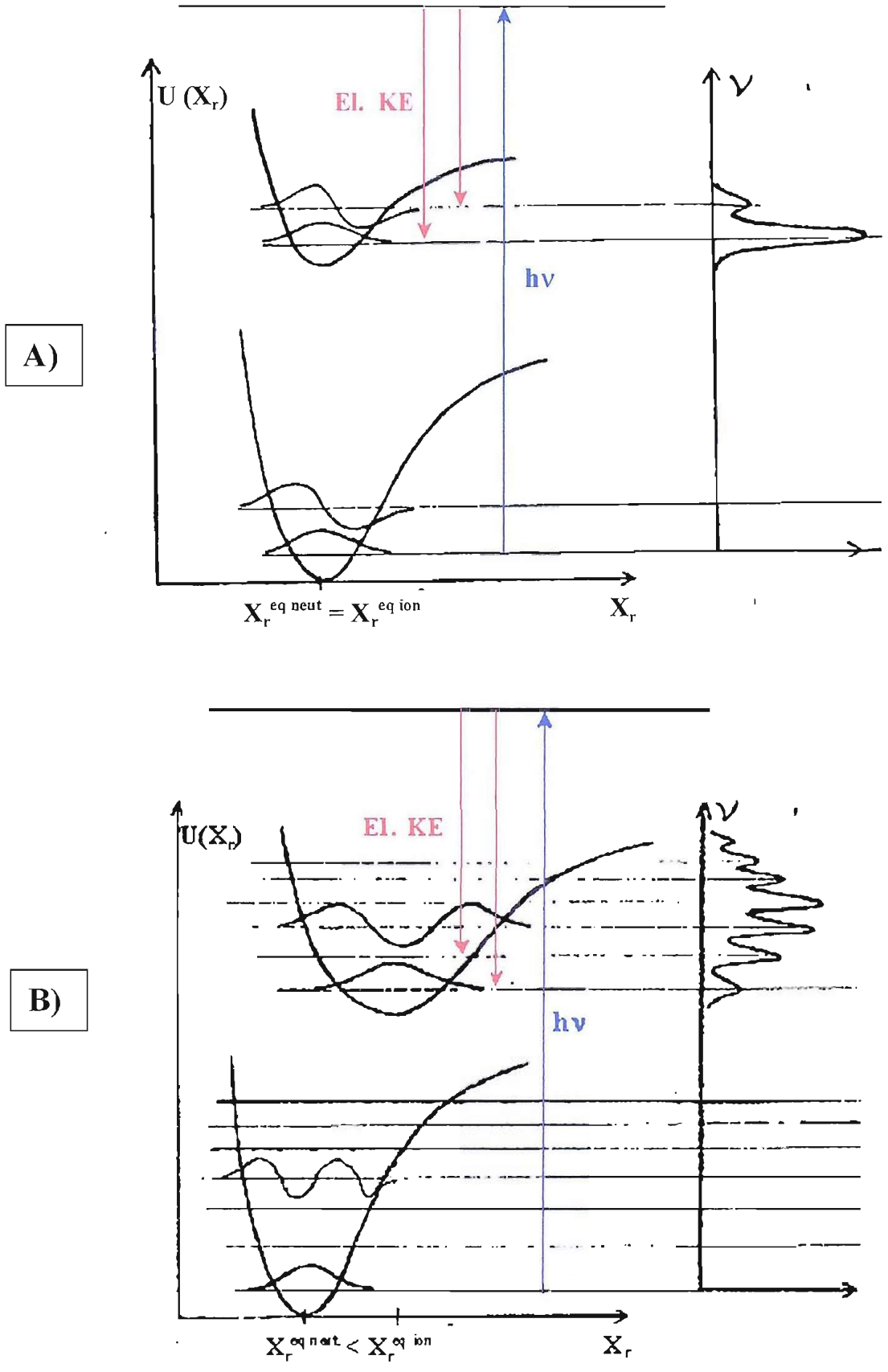

Figure 3.1- The different probabilities of PE bands according to the relative positions of the minima of the potential energy curves of the neutral and the ion produced by photoionization; the PE band is reported on the right hand side

3.5 THE HARTREE-FOCK METHOD

As it was stated in Section 2.2, the Schroedinger equation $H\Psi = E\cdot\Psi$ cannot be solved analytically for atoms with more electrons than hydrogen-like atoms and molecules with more electrons than H_2^+. As stated earlier, the Born-Oppenheimer approximation [12] leads to the partition of the total electronic wavefunction as follows:

$$\Psi(\mathbf{r},\mathbf{R}) = \Psi_{vib}(\mathbf{R})\cdot \Psi_{elec}(\mathbf{r},\mathbf{R}) \qquad (3.20)$$

and the Schroedinger equation can be separated into an electronic equation for the state k

$$H_{elec}\Psi_k(\mathbf{r},\mathbf{R}) = E_{elec\,k}(\mathbf{R})\cdot \Psi_k(\mathbf{r},\mathbf{R}) \qquad (3.21)$$

and into a nuclear (or vibrational) equation for each vibrational state u associated with the electronic state k

$$H_{vibr}\Psi_{ku}(\mathbf{R}) = E_{nucl\,ku}\cdot\Psi_{ku}(\mathbf{R}) \qquad (3.22)$$

The notation has been slightly changed from the one used in Section 3.2 in order to simplify the expression of the two partial Schroedinger equations.

In order to obtain a method to describe the molecular electronic distribution, the electronic Schroedinger equation plays the central role. To handle this task, another approximation is needed, that is to describe the motion of each electron by just a one-electron function. Such a function is called a *spin-orbital*, and this approximation is labelled the *one-electron approximation*. For each spin-orbital-indicated with λ- it is possible to separate the spatial term from that associated with the spin wavefunction of the electron. In the case of a single electron, the wavefunction can be factorized as

$$\lambda(\mathbf{r},s) = \phi(\mathbf{r})\cdot\sigma(s) \qquad (3.23)$$

The $\phi(\mathbf{r})$ spatial factor is called a *space orbital* and is associated with the volume of space where there exists a probability of finding the electron, while the $\sigma(s)$ factor is called a *spin* factor. The spin variable s represents the component of the electron spin along a certain axis and can assume only two values, $+\frac{1}{2}$ and $-\frac{1}{2}$, denoted as α and β.

The total electronic wavefunction Ψ_{elec} is approximated by an antisymmetrized product of spin-orbitals, in order to satisfy the Pauli exclusion principle [16] which states that the total wavefunction must be antisymmetric on interchange of electrons (or that no two electrons can have the same set of quantum

numbers). To satisfy this condition, the electronic wavefunction of a system with n electrons is expressed by an antisymmetrized determinant:

$$\Phi_{elec} = 1/\sqrt{n!} \cdot \begin{vmatrix} \lambda_1(1)\ \lambda_2(1) \ldots \lambda_n(1) \\ \lambda_2(1)\ \lambda_2(2) \ldots \lambda_n(2) \\ \ldots\ldots\ldots\ldots \\ \lambda_1(n)\ \lambda_2(n) \ldots \lambda_n(n) \end{vmatrix} \qquad (3.24)$$

λ_i are the spin-orbitals, and the determinant in the above expression is called the *Slater determinant* [3, 11]. In a more compact expression, the wavefunction can be written as

$$\Phi(1, 2 \ldots n) = (n!)^{-1/2} \sum (-1)^p \lambda_1(k_1)\ \lambda_2(k_2) \ldots \lambda_n(k_n) \qquad (3.25)$$

where p is the number of electron exchanges to obtain a two-electron permutation (a system with n electrons allows $n!$ possible permutations: $k_1, k_2 \ldots k_n$).

3.5.1 The Variational theorem [11]

The total energy of a system associated with a wavefunction Ψ is given by the *Rayleigh-Schroedinger ratio*

$$E = \frac{\langle \Psi | H | \Psi \rangle}{\langle \Psi | \Psi \rangle} \qquad (3.26)$$

According to the variational theorem (11), if a trial wavefunction is used this ratio always gives a value higher than the true total energy for the ground state. In other words, if Ψ_0 is the true solution of the Schroedinger equation for the ground state of the molecule, its eigenvalue E_0 can then be seen as the lower limit of the Rayleigh-Schroedinger ratio. For any other trial wavefunction Ψ_{trial} giving a total energy E_{trial}, it can be shown that

$$E_{trial} = \frac{\langle \Psi_{trial} | H | \Psi_{trial} \rangle}{\langle \Psi_{trial} | \Psi_{trial} \rangle} \geq \frac{\langle \Psi_0 | H | \Psi_0 \rangle}{\langle \Psi_0 | \Psi_0 \rangle} = E_0 \qquad (3.27)$$

In fact, if the trial wavefunction is expressed as a linear combination of the true solutions of the system

$$\Psi_{trial} = \sum_i a_i \cdot \Psi_i \qquad (3.28)$$

then the total energy difference between the system described by this trial wavefunction and by the true ground state wavefunction can be written as

$$E_{trial} - E_0 = \frac{\sum_i a_i^* a_i \cdot (E_i - E_0)}{\sum_i a_i^* a_i} \qquad (3.29)$$

With E_0 being the total energy of the ground state, $E_i \geq E_0$ and also $a_i^* a_i \geq 0$, therefore, $E_{trial} \geq E_0$.
The immediate conclusion of the variational theorem is that the best trial wavefunction describing the system is the one producing the lowest total energy. Usually, the search for the "best" wavefunction is carried out by minimizing the ground state energy of the system by varying the parameters a while keeping the Ψ_i fixed. An accurate choice of Ψ_i is therefore crucial for the success of the method.
An advantage of the variational principle is that- despite being valid only for the lowest state of a given symmetry- it gives solutions also for excited states. It is important to remark that the theorem is valid only for the total energy of the system, and not for other properties.

3.5.2 The Hartree-Fock equations |17|

As already mentioned in Section 2.2., applying the Born-Oppenheimer approximation the electronic Schroedinger equation can be written as $H_{el}\Psi_{el} = E_{el} \cdot \Psi_{el}$, in which the molecular Hamiltonian is given by

$$H_{el} = -\tfrac{1}{2} \sum_i \nabla_i^2 - \sum_\alpha \sum_i Z_\alpha e^2 / R_{\alpha i} + \sum_i \sum_j e^2 / r_{ij} \qquad (3.30)$$

The first term is the kinetic energy of the electrons, while the following two terms are respectively the electron-nucleus attractions and the electron-electron interactions. The kinetic energy of the nuclei is assumed as negligible compared to the kinetic energy of the electrons, and the nuclei-nuclei repulsion is initially omitted and only subsequently added to E_{el}.
With the definition of H_{el} given above, and the Φ_{el} expressed by the Slater determinant, it is possible to obtain E_{el} with the variational method [17, 18]; in the case of a closed-shell molecule the expression for the total energy, E_0, is given by

$$E_{el} = \sum_i I'_i + \sum_i \sum_j (J'_{ij} - K'_{ij}) \qquad (3.31)$$

in which the energy integral I'_i, the Coulomb integral J'_{ij} and the exchange integral K'_{ij} are respectively defined as

$$I'_i = \int \lambda_i^*(1) \left[-\tfrac{1}{2}\nabla_i^2(1) - \sum_\alpha Z_\alpha / r_{i\alpha}\right] \lambda_i(1)\, d\tau \qquad (3.32)$$

$$J'_{ij} = \int \lambda_i^*(1)\lambda_j^*(2) \left[1/r_{ij}\right] \lambda_i(1)\lambda_j(2)\, d\tau \qquad (3.33)$$

$$K'_{ij} = \int \lambda_i^*(1)\lambda_j^*(2) \left[1/r_{ij}\right] \lambda_j(1)\lambda_i(2)\, d\tau \qquad (3.34)$$

In these formulae, the integration involves both spatial and spin co-ordinates.

If integration is carried out on the spin components, the expressions of the operators depend on ϕ_i rather than on λ_i, i.e.:

$$I_i = \int \phi_i^*(1) \left[-\tfrac{1}{2}\nabla_i^2(1) - \sum_\alpha Z_\alpha / r_{i\alpha}\right] \phi_i(1)\, \mathbf{dr} \qquad (3.35)$$

$$J_{ij} = \int \phi_i^*(1)\phi_j^*(2) \left[1/r_{ij}\right] \phi_i(1)\phi_j(2)\, \mathbf{dr} \qquad (3.36)$$

$$K_{ij} = \int \phi_i^*(1)\phi_j^*(2) \left[1/r_{ij}\right] \phi_j(1)\phi_i(2)\, \mathbf{dr} \qquad (3.37)$$

and the total energy of the system is given by

$$E_{el} = 2 \cdot \sum_i I_i + \sum_i \sum_j (J_{ij} - K_{ij}) \qquad (3.38)$$

These equations are called *Hartree-Fock* equations [17]: the sum runs over all the occupied molecular orbitals. E_{el} includes the electronic kinetic energies and the Coulomb electron-nuclei attraction in the term I- which can therefore be seen as the sum of the energies of each electron moving in the orbital *i* under the effect of the potential of the nuclei. The electrostatic interactions between electrons in orbitals *i* and *j* are taken into account in the term J, which is referred as the *Coulomb operator*. K, which has no straightforward physical analogue, it is called the *exchange operator*, as it swaps spin-orbitals with the same spin function: it vanishes for pairs of electrons having opposite spin.

An alternative- and simpler- expression for the operators is to express them in terms of one-electron integrals

$$J_i(1)\, \phi_j(1) = \left[\int \phi_i^*(2)\, (1/r_{ij})\, \phi_i(2)\, \mathbf{dr}\right] \phi_j(1) \qquad (3.39)$$

$$K_i(1)\, \phi_j(1) = \left[\int \phi_i^*(2)\, (1/r_{ij})\, \phi_j(2)\, \mathbf{dr}\right] \phi_i(1) \qquad (3.40)$$

In this way J_{ij} and K_{ij} assume the form

$$J_{ij} = \langle \phi_i(1) | J_j(1) | \phi_i(1) \rangle = \langle \phi_j(2) | J_i(2) | \phi_j(2) \rangle \qquad (3.41)$$

$$K_{ij} = \langle \phi_i(1) | K_j(1) | \phi_i(1) \rangle = \langle \phi_j(2) | K_i(2) | \phi_j(2) \rangle \qquad (3.42)$$

From them, it is possible to obtain a diagonalized form of the $n \times n$ Hartree-Fock matrix: in this way the final expression for the Hartree-Fock equations is given by

$$\mathbf{F}\phi_i = \varepsilon_i \cdot \phi_i \qquad (3.43)$$

in which **F** is called Fock operator, defined as $\mathbf{F}(1) = \mathbf{H}_i(1) + \sum_j (2J_j(1) - K_j(1))$ where the sum runs over all the occupied spin-orbitals. **H** is itself the one-electron equivalent of the I_i operator (defined as $-\frac{1}{2}\nabla_i^2 - \sum_\alpha Z_\alpha / r_{i\alpha}$), and ε_i is the energy of one of the n occupied molecular orbitals. Its full expression is therefore given by

$$\varepsilon_i = I_i + \sum_j (2J_{ij} - K_{ij}) \qquad (3.44)$$

Both the J and K expressions contain the wavefunctions to be calculated. Therefore the Hartree-Fock equations are a so called *pseudo-eigenvalue problem* and they have to be solved iteratively.

A way to start the search of accurate wavefunctions for the system is to choose an initial set of orbitals ϕ_i: from this a mean Coulombic potential can be derived for each electron. If this Coulomb potential is added to the kinetic energy of all the electrons, a Fock operator can be built, and used to solve the electronic Hartree-Fock equation $\mathbf{F}\phi_i = \varepsilon_i \cdot \phi_i$. In this way, more accurate orbitals are found and used to re-calculate the mean Coulomb potential for the electrons in the system. The procedure is iterated until no difference in the molecular orbitals (or in the total energy) can be found as consequence of an additional optimization cycle: this condition of self-consistency has led to the name of the method as the *self consistent field* (SCF) method.

3.5.3 The Hartree-Fock-Roothan method [17]

A powerful tool for the solution of the Hartree-Fock equations is to expand the molecular orbitals ϕ_i as a linear combination of basis functions

$$\phi_i = \sum_k c_{ik} \cdot \chi_k \qquad (3.45)$$

If the functions χ_k are chosen as atomic orbital functions, the method of expressing the molecular orbitals is therefore called *LCAO* (linear combination of atomic orbitals).

The Hartree-Fock equations are then written as

$$\sum_k c_{ik} \cdot \mathbf{F}\chi_k = \varepsilon_i \cdot \sum_k c_{ik} \cdot \chi_k \qquad (3.46)$$

and finally- after multiplication by χ_k^* and integration- the *Hartree-Fock-Roothan* (HFR) expression is obtained

$$\sum_k c_{ik} \cdot (\mathbf{F}_{pq} - \varepsilon_i \cdot S_{pq}) = 0 \qquad (3.47)$$

In this expression, S_{pq} is defined as the overlap integral

$$S_{pq} = \int \chi_p^* \chi_q \, d\mathbf{r} \qquad (3.48)$$

and $\mathbf{F}_{pq}$ as

$$\mathbf{F}_{pq} = \int \chi_p^* \mathbf{F} \chi_q \, d\mathbf{r} = I_{pq} + \sum_j [2 \cdot \iint \chi_p^*(1)\chi_q(1)\,(1/r_{12})\,\chi_j^*(2)\chi_j(2)\,d\mathbf{r} - \iint \chi_p^*(1)\chi_j(1)\,(1/r_{12})\,\chi_j^*(2)\chi_q(2)\,d\mathbf{r}]$$

The method is equivalent to the Hartree-Fock method: it is based on minimization of the energy by changing the coefficients c_{ik} keeping fixed the atomic orbitals χ_k, and is a pseudo-eigenvalue method that can be only solved iteratively. First the coefficients c_{ik} are estimated, and from them initial $\mathbf{F}_{pq}$ and S_{pq} integrals are calculated. From them, ε_i are obtained by solving the equation

$$\det | \mathbf{F}_{pq} - \varepsilon_i \cdot S_{pq} | = 0 \qquad (3.49)$$

and a new set of c_{ik} is re-calculated for each ε from $\sum_k c_{ik} \cdot (\mathbf{F}_{pq} - \varepsilon_i \cdot S_{pq}) = 0$ until self-consistency is reached.

The method- used for closed-shell molecules- is usually referred as LCAO-SCF; when the expansion of the molecular orbitals ϕ_i is as an infinite set of χ_k the result is the same as in the HF-SCF procedure. For practical reasons is nevertheless necessary to make use of a finite number of basis functions χ_k: when a very large number of functions is used, and the total energy does not change with a further increase of the number of functions- this is defined as the *Hartree-Fock limit*. The accuracy of this set (commonly named as *basis set*) is a factor of the greatest importance to give results of good quality. This aspect will be discussed in more detail in Section 3.5.6.

3.5.4 Koopmans' theorem and ΔSCF method

Ionization energies are probably the most important pieces of information obtainable in a photoelectron spectrum: it is therefore necessary to be able to calculate them (and assigning the molecular and ionic states associated with such ionizations) independently from the experimental results. If the ionization is thought as leaving unaltered the molecular geometry (vertical ionization), and if the Hartree-Fock spin-orbitals are considered to apply both to the neutral and the ionized molecule, then *Koopmans' theorem* [19] states that the energy necessary to ionize a closed-shell molecule by extracting an electron from the spin-orbital λ_k is equal and opposite to the energy of the spin-orbital λ_k itself calculated at the Hartree-Fock limit.

$$IE = E_N - E_{N-1} = -\varepsilon_k \qquad (3.50)$$

where IE is the vertical ionization energy.

Koopmans' theorem is based on a number of approximations: the single determinant in the Hartree-Fock equations, the neglect of electron correlation change between the molecule (a more detailed discussion on the electron correlation problem will be given in Section 3.6) and the ion, and the neglect of orbital relaxation (the change of the spin-orbitals when passing from the neutral to the cation). Because of these approximations, it sometimes fails to correctly reproduce the correct order of the ionic states, as happens for example in molecular nitrogen.
In fact, the "true" VIE is related to the VIE predicted by Koopmans' theorem by the relation

$$VIE = VIE_{KT} - R + C \qquad (3.51)$$

where R is the term considering orbital relaxation and C the term considering correlation energy change between the molecule and ion. The electron correlation change on ionization and the orbital reorganization often tend to compensate each other, so Koopmans' theorem sometimes obtains fortuitously the experimental VIEs with a good approximation [20]. The fact that very often Koopmans' theorem overestimates the true VIE implies that $R > C$.

An alternative approach to calculate vertical ionization energies (VIEs) is to calculate the energy of the cation at the neutral equilibrium geometry and to subtract from this energy the energy of the neutral molecule: this is called the ΔSCF method [21], and it takes into account the effect of orbital relaxation. As the cation has one electron less than the neutral, the ΔSCF method often leads to calculated vertical ionization energies which are too low as no allowance has been made for electron correlation in each state. Normally ΔSCF VIEs are lower than the experimental ones, while Koopmans' values are higher.

3.5.5 The unrestricted Hartree-Fock method (UHF) [22]

It must be kept in mind that the HF-SCF and HFR-SCF methods described above are valid only for closed-shell molecules: in those cases the calculations are referred as spin-restricted, as they assign the same spatial function to the α and β electrons paired within the same molecular orbital. If wavefunctions of open-shell molecules- in which at least one of the spatial orbitals ϕ is singly occupied- are studied, the initial estimate Φ can be made by a Slater determinant with a different number of spin-orbitals $\lambda(\alpha)$ and spin-orbitals $\lambda(\beta)$: the α and β electrons do not experience the same Coulomb or exchange potential and so the two sets will have different energies and spatial distribution. This aspect is exploited in the theoretical treatment of open-shell molecules because it does not

introduce any restriction on the spatial distribution of the molecular orbitals to be obtained: the method [22] is then called *unrestricted Hartree-Fock* (UHF) in contrast to the restricted method (RHF) used for closed-shell molecules.

For a molecular system of n electrons in α-type molecular orbitals and m ($\neq n$) electrons in β-type molecular orbitals, the expression for the two sets of molecular orbitals can be written as

$$\phi_i^{\alpha} = \sum_p c^{\alpha}_{pi} \cdot \chi_p \qquad \text{and} \qquad \phi_i^{\beta} = \sum_p c^{\beta}_{pi} \cdot \chi_p \qquad (3.52)$$

Two separate SCF calculations must be carried on the two sets, using the same procedure described for the spin-restricted methods.

The UHF method has the advantage of providing a lower total energy with respect to RHF methods; however, the problem in UHF calculations is the fact that the different spatial nature of the spin-orbitals introduces spin impurities in the resulting wavefunction. For example, doublet states can be contaminated with quartet states. This arises from the fact that a single open shell configuration can fail in being an eigenfunction of the spin operator, S^2: the S^2 value obtained at the end of the calculation must always be checked in order to estimate if the spin contamination is acceptable.

In this work, UHF calculations have been carried out on the ions needed for ΔSCF calculations: in these cases, the S^2 value will be reported along with the total energies obtained of the ions.

3.5.6 Basis sets

In the choice of the basis set with which the molecular orbitals are expressed, two important factors must be considered. A larger basis sets usually decreases the total energy of the system, then- as stated by the variational principle- it describes better the system; there is a lower energy limit, called the *Hartree-Fock limit*, beyond which an increase of basis functions does not cause any energy lowering. The Hartree-Fock limit is defined as the "true" total SCF energy of the system in the specific symmetry. Therefore, on one side the results given by the basis set must be as close as possible to those obtained at the Hartree-Fock limit; to reach this degree of accuracy, a large set of basis functions must be used. On the other side, the computational time needed for a calculation with a very large basis set can be prohibitive: the number of two-electron integrals- the most demanding calculational effort- rises as n^4 where n is the number of basis functions.

Two main types of basis functions have been commonly used to describe atomic orbitals, Gaussian-type orbitals (GTO) and Slater-type orbitals (STO).

STOs [23] are represented as

$$\chi(r,\theta,\phi) = N \cdot Y_{lm}(\theta,\phi) \cdot r^{n-1} \cdot e^{-\zeta \cdot r} \qquad (3.53)$$

in which N is a normalization factor, n, l, and m are the principal, azimuthal and magnetic quantum numbers respectively, and $Y_{lm}(\theta,\phi)$ is a spherical harmonic. ζ is an orbital exponential factor depending on the nature of the atom and on its state, and can be chosen so that each atomic orbital is expressed by a single STO; the ζ value is usually obtained via independent calculations and left unaltered in the molecular orbital calculations. STOs reproduce satisfactorily the whole "real" electronic distribution, including the cusp shape of the electronic density near the nuclei. However, the two-electrons integrals they produce cannot be solved analytically but only numerically, with a high computational effort.

The GTO [24] expression is given by

$$\chi(r,\theta,\phi) = N' \cdot x^a y^b z^c \cdot exp(-\alpha r^2) \qquad (3.54)$$

a, b, c are here integers whose sum is equal to the azimuthal quantum number *l*. The absence of any dependence on the principal quantum number *n* implies that the shape of single *s*, *p*, *d*... orbitals produced by GTOs is the same whichever their *n* value. GTOs cannot satisfactorily reproduce the proper electronic distribution both near the nuclei and at large *r*, but two-electrons integrals involving GTOs can be evaluated analytically, because a product of Gaussian functions centred on different points can be expressed by an equivalent single Gaussian centred on a third point. Considering the numerous and complicated integrals in the Roothan-Hartree-Fock equations, GTOs have a formidable advantage over STOs, and they are widely used in LCAO-MO *ab initio* calculations. The problem of their inadequate physical description of real AOs near the nuclei and at large *r* is solved by combining some of them together [10], to produce what is called a *contracted Gaussian-type orbital* (CGTO); the coefficients for such a combination are not optimized in the LCAO-MO procedure but are initially chosen and kept fixed. In this way [25], a much larger basis set necessary to obtain the same quality of calculation as the Slater-type orbitals can be used without losing too much computational time.

The basis set choice is very important, and the development of accurate basis sets is one of the most crucial fields in quantum chemistry. An ideal basis set should be able to afford accurate orbital energies in a reasonable computational time, and be applicable to a particular atom no matter its environment or charge. Within the basis set, different functions are included to take into account different aspects of the electronic distribution of the specific molecular state. Care must also be taken about the

computational time required by large basis sets, especially when electron correlation (see later) must be treated in cases where a high number of spin-orbital configurations are used.

The basis set must firstly correctly reproduce the core and valence electronic distribution: for this purpose, a basis with the same number of CGTOs (or STOs) as the core+valence atomic orbitals (*minimal basis*) is usually not accurate enough. A double or triple number of CGTOs with respect to the number of formally occupied atomic orbitals should be used: in these cases, the basis sets are labelled double-zeta (DZ) or triple-zeta (TZ). Zeta refers to the exponential term ζ in the STO and GTO expressions: double-zeta means that that two CGTOs (or STOs) are used to represent a single atomic orbital, triple-zeta means that three CGTOs are used, and so on.

A type of basis set widely used is the split-valence K-LM G basis set [26, 27], in which each core orbital is described by one CGTO resulting from contraction of K GTOs and the valence space is represented by a double-zeta basis in which the first (or inner region) CGTO per valence function comes from a contraction of L GTOs and the second (or outer region) by M GTOs; the advantage of this basis sets is the balance between relative time economy and the flexibility for different atomic states.

The valence space can be also described at the TZ level: for example, in the 6-311G basis set, the third CGTO of the valence space is a simple GTO.

The electron density produced in this way needs to be augmented to take into account more angular electronic distribution: this is useful to express the distortion in electron density arising from bond formation, and is particularly important when the molecular geometry requires (such as in strained rings or when double or triple bonds are present) flexibility in the electron density to cover the region where the bonds must be formed. This is achieved by adding *polarization functions* to the core+valence functions of the single atom: these functions have usually an angular momentum one unit higher than the valence orbital of the atom but with the same radial size. For example, for carbon the polarization functions will be *d*-type orbitals. In the K-LM G basis sets, the presence of polarization functions of this type is indicated by the presence of an asterisk (e.g. 6-31G*); if these polarization functions are introduced also on the hydrogen atoms a double asterisk, as in 6-31G**, is used.

Finally, for light elements or weakly interacting systems an additional contribution is given by *diffuse functions*, in order to increase the radial distribution: diffuse functions are characterized by a lower angular momentum quantum number than the valence functions. Their presence in a K-LM G basis set is indicated by the presence of a + sign, as in 6-311+G**. Again, a double + indicates that diffuse functions centred on the hydrogen atoms have been included.

All these different contributions must be balanced in a reasonable way in the basis set expression: for example, a very large polarization function on a reduced valence region size would lead to unreliable results.

Numerous types of basis sets exist, and are constantly improved while new ones are developed: large basis set libraries are available [28-31] , allowing the choice of those more suited for the study of the system under observation.

Apart from the K-LM G type, a widely used type of basis sets was recently developed by Dunning [32-34] and found very valuable in electron correlation calculations, due to their balance and their relatively low computational time cost. They are made by contracted GTOs, and they have been developed up to the quadruple-Z or quintuple-Z level. Moreover, for this class of basis set an extrapolation of the total energy values obtained with the number of basis functions (DZ, TZ, QZ, etc.) can be carried out in order to obtain the complete basis set (CBS) limit, which indicates the "true" energy of the system. For their reliability in considering electron correlation, they have been labelled as *correlation consistent* (cc) basis sets, and they are labelled as cc-VXZ, where X reflects the number of basis functions used for each formally occupied atomic orbital (cc-VDZ, cc-VTZ, etc.).

They can be used with polarization functions; it was found that the degree of accuracy improves when polarization functions of more than one unit higher *l* number than the valence functions are included (for example, for first row elements also *d* and *f* functions can be included). In correlation consistent basis sets, the presence of polarization function is indicated by a *p* prefix (e.g. cc-p-VDZ): this corresponds roughly to the polarization functions presence marked as ** in the K-LM G basis set type. For second-row elements, the presence of two maxima in the radial electron distribution of the *3p* orbital requires the introduction of an additional *d* polarization function to take into account also the inner maximum; the presence of this additional function, defined as a *tight polarization function*, is reported in the basis set labelling in the exponential part, as for example in cc-pV(T+d)Z.

The presence of diffuse functions is in this case represented by the *aug* prefix, as in aug-cc-pVDZ.

3.6 ELECTRON CORRELATION

The greatest limitation of the SCF methods described so far is that with the SCF method electron-electron interaction is treated as an average Coulomb potential felt by an electron as well as an exchange term between electrons of parallel spin; this is different from the instantaneous spatial interaction experienced by electrons in a real system. As electrons are not properly correlated in the

SCF method, this problem is called *electron correlation*. A consequence of this can be immediately seen in the case of molecular hydrogen, when the Hartree-Fock treatment- without considering the correlation between the two electrons- predicts that at dissociation an equal amount of ions and atoms are formed, while in reality the dissociation produces only atoms.

Two types of electron correlation can be distinguished: *dynamic electron correlation* [35] is a short-range effect depending on the instantaneous motions of the single electrons, and a *non-dynamic electron correlation* [36], which arises from the fact that a wavefunction based on a single configuration is inadequate to describe particular systems where near-degeneracies in the electronic configuration are possible. Non-dynamic correlation varies with the internuclear distance, and its effect is particularly relevant at the dissociation limit.

These two factors constitute the general electron correlation effect; only by adding correlation energy to the Hartree-Fock energy it is possible to obtain the "true" total energy of the system under examination. Even if the net correlation energy is a small fraction of the Hartree-Fock energy, it assumes particular importance when energy differences (such as in ΔSCF calculations of ionization energies) are to be evaluated. In particular, as well as at equilibrium (where it also causes a lowering in the total energy and an increase in band length), the effect of electron correlation is important at dissociation, where the energy calculated by the Hartree-Fock method is always greater than the true total energy. Moreover, electron correlation also affects other calculated properties, such as the frequencies of the vibrational modes of the molecule.

To reach a high chemical accuracy, effective ways to take into account electron correlation have to be considered. Different methods have been developed to tackle the electron correlation problem, and they find extensive application for *ab initio* calculations: the choice of method depends on the particular class of molecule to be studied, and to the degree of accuracy of the results required related to the computational time needed to perform the calculation. In this work, only two methods- Moeller-Plesset perturbation theory (MP) and the coupled cluster method (CC)- have been used: they will therefore be described in some detail.

In general, a single Slater determinant is not capable of satisfactorily representing a molecular wavefunction: this approximation is too crude to take into account electron correlation.

The wavefunction should be expressed instead as a combination of single-determinant HF wavefunctions of proper spin and angular symmetry obtained by single and higher excitations from a reference determinant, i.e.:

$$\Psi = \sum_j B_j \cdot \Psi^0_j \qquad (3.55)$$

All the possible configurations with the same total angular and spin momentum as the reference one can be used in this expression, considering also spatial orbitals that are usually considered vacant. In this case contributions from excited configurations are included into the wavefunction expression. The leads to the formation of new *polarized orbitals* [10] obtained by the combination of two spin-orbitals in Ψ^0_j: the amount of such a combination is given by the relative value of their coefficients, which itself depends on the coupling magnitude between the different configurations, $\langle \Psi^0_j | H | \Psi^0_k \rangle$, and on the energy difference between them.

Inserting the electrons into polarized orbitals allows a reduction of the electron Coulomb interaction because they are spatially different between each other. Polarized orbitals are not the same as hybrid orbitals, as each of them host only one electron (in hybrid orbitals there are two electrons) and they do not necessarily extend along a bond of the molecule, as happens for hybrid orbitals. The introduction of excited configurations allows dynamic electron correlation to be treated satisfactorily.

The real energy of the system is obtained by using a *complete active space* method (CAS-SCF) in which all the possible configurations arising from all the electron permutations in a selected group of molecular orbitals are included in the expansion; if also a complete basis set is used, the result is the exact solution of the Schroedinger equation. In practice it is necessary to truncate both the LCAO and the multiconfiguration expansions to a certain point, given the fact that otherwise millions of configurations would arise; considering that the computing time depends on the square or the cubic power of the number of configurations, CAS-SCF is usable only for small molecular systems.

The methods of incorporating electron correlation in the Hartree-Fock method can be broadly divided in two main categories [10]: those based on the variational theorem and those based on perturbation theory.

3.6.1 Variational methods

Two main variational-based methods are used in *ab initio* calculations, the *multiconfigurational self-consistent field* method (MC-SCF) and the *configuration interaction* method (CI). The advantages of the variational treatment is that it does not rely on one particular configuration, and that it can "bracket" the true energy of the system, so there will always be a true energy value between two calculated ones. The weakness lie mainly in the fact that they are usually very computationally time-consuming (often tens of thousands of configurations must be taken into account to afford good chemical accuracy) and they are not size-extensive, in the sense that for the variational approach two fragments at very long distance do not produce twice the energy of a single fragment.

The MC-SCF method [10] minimizes the Rayleigh-Schroedinger ratio by varying the LCAO coefficients c_i at the same time as the multiconfiguration coefficients B_j are varied; this method is particularly important to treat non-dynamic electron correlation, but it depends heavily on the quality of the choice of the configurations to be included in the procedure, and usually the number of excited configurations is not high enough to completely describe non-dynamic electron correlation.

The CI method [37, 38] first determines the LCAO coefficients by using a single-configuration spin-restricted SCF, then expands this configuration (*reference configuration*) with new ones arising from substituting occupied orbitals with virtual ones (*excited configurations*); the coefficients for this expansion are determined by applying the variational treatment to the Rayleigh-Schroedinger ratio. As the first step, the single-determinant Slater expression Φ_0 is used to solve the Hartree-Fock equations; the wavefunction is then re-formulated as a combination of single-determinant HF wavefunctions- of the same spin and angular symmetry- obtained by exciting one or more electrons from occupied MOs to virtual ones in the reference wavefunction. According to the number of electrons removed from occupied MOs, single, double, triple... excitation functions Φ_j will be formed (their number is m, while the number of electrons is n). The total wavefunction is then expressed as

$$\Phi = B_o\Phi_0 + \sum_j B_j \cdot \Phi_j \qquad (3.56)$$

Variational treatment leads, as in the HF-SCF method, to secular equations

$$\sum_j (H_{jr} - E_k \cdot \delta_{jr}) \cdot B_{jk} = 0 \qquad (3.57)$$

in which

$$H_{jr} = \int\int \Phi_j \mathbf{H} \Phi_r \, d\tau_1 \, d\tau_2 \ldots d\tau_n \qquad (3.58)$$

The most used option is the one using just single and double excitations, CISD: in this way an approximate contribution of just single and double excitations on the total correlation energy, ΔE_{CISD}, is obtained. A useful formula [39] to approximate the real energy correction due to electron correlation is given by

$$\Delta E_{el.\ corr.} = (1 - B_0^2) \cdot \Delta E_{CISD} \qquad (3.59)$$

where B_0 is the coefficient of the reference determinant in the multiconfiguration expansion. In this way part of the correlation energy is taken into account.

3.6.2 Perturbative methods [40]

The other important category is based on the perturbation approach; even if the coupled cluster method (CC) is not strictly a perturbation method, its results are quite similar to those produced by properly perturbation treatments like MP2 and it is therefore presented with them [41].

Perturbation methods are size-consistent, because the energy of two equal fragments at infinite distance is equal to twice the energy of the single fragment, and the equations for the two (or more) fragments are separable. The drawbacks of the MP2 and CC methods are the fact that the energies they give are not necessarily an upper limit of the correct energy: they can be lower than the true energy. Moreover, the results arise from corrections of an initial reference wavefunction: in cases of inadequacies in choosing this reference- or situations in which more than one reference wavefunction are necessary to describe the system, such as in interactions between electronic surfaces- the results are often unreliable, especially in open-shell molecules.

Moeller-Plesset perturbation theory (MPPT) is one of the most used molecular orbital *ab initio* methods [42]; it starts by assuming the sum of all the Fock operators for every electron within the molecule as the unperturbed Hamiltonian $\mathbf{H}_0$. A perturbation treatment is then applied by expressing the exact Hamiltonian **H** as:

$$\mathbf{H}_\lambda = \mathbf{H}_0 + \lambda\mathbf{V} \qquad (3.60)$$

where λ is a numerical parameter and **V** is the perturbative operator. From perturbation theory [40], the exact wavefunction is then formulated as

$$\Phi_\lambda = \sum_i \lambda^i \cdot \Phi^{(i)} \qquad (3.61)$$

in which the $\Phi^{(i)}$ are the i-th order contributions to the wavefunction. In the same way, the total energy is given by

$$E_\lambda = \sum_i \lambda^i \cdot E^{(i)} \qquad (3.62)$$

These expansions may be truncated at a certain order: according to where this truncation occurs, the perturbative series is defined as MP1, MP2... MPn.

Recalling that

$$\Phi^{(0)} = \Phi_0 \qquad \text{and} \qquad E^{(0)} = \sum_i \varepsilon_i \qquad (3.63)$$

it is possible to show that the MP1 energy $E^{(0)} + E^{(1)}$ is equal to the HF energy

$$E^{(0)} + E^{(1)} = \int\!\!\int \Phi_0 \mathbf{H} \Phi_0 \, d\tau_1 \, d\tau_2 \ldots d\tau_n \qquad (3.64)$$

The second order contribution is given by

$$E^{(2)} = -\sum_k (E_0 - E_k)^{-1} \cdot |V_{ko}|^2 \qquad (3.65)$$

The sum runs only over double substitutions. V_{ko} is expressed as

$$V_{ko} = \iint \chi_i^*(1)\chi_j^*(2)(1/r_{ij})[\chi_a(1)\chi_b(2) - \chi_b(1)\chi_a(2)]\, d\tau_1\, d\tau_2$$

Concerning the wavefunction expression, the first-order correction consists just of double excitations (two virtual spinorbitals replace two occupied ones), while in second order wavefunction corrections also single and triple excitations appear.

It is possible to consider higher order contributions to the total energy and the wavefunction; nevertheless, truncation at the second order (MP2) already takes into account between 50 and 80% of electron correlation, with a relatively small computational time. This is why MP2 is one of the most successful methods in quantum chemistry- and the more extensively used in this work: its main advantage is the relative economy in computational time, and the fact that after choosing the initial reference wavefunction no other assumptions must be made on the other configurations because they are directly determined in the method.

In the Moeller-Plesset method, the first and second derivatives of the energy are obtained analytically: this has an advantage for the location of stationary points and for the calculation of the harmonic vibrational frequencies, and this is why all the geometries and vibrational frequencies in this work have been calculated at the MP2 level. Not being a variational method, oscillations have been observed in the MP*n* energies for increasing *n*: the true energy of the system could be extrapolated from the asymptotic value for MP∞; the method has been observed to work better when a large basis set is used because in the perturbation approach a good description of the virtual spin-orbitals is particularly important. In this case, it has been calculated that in general around 75% of electron correlation has been taken into account already at the MP3 level.

The *coupled-cluster* method (CC) [41] adopts a different approach of expressing the correlation-corrected wavefunction not as a combination of single-determinant wavefunctions but by multiplying the SCF wavefunction by e^T, i.e.:

$$\Psi = e^T \Phi$$

where the operator T acts to introduce excitations on the single-determinant SCF wavefunction Φ.

Its analytical expression is given by

$$T = \sum_{i,m} t_i \cdot M^{+} + \sum_{i,m,j,n} t_{ij} \cdot M^{++} + \ldots$$

In this expression, M^{+} is the operator producing a virtual spin-orbital *m* from an occupied one *i*, while operator M^{++} causes a double excitation from spin-orbitals *i* and *j* to spin-orbitals *m* and *n*, and so on. The coefficients *t* are to be determined just as the coefficients C had to be determined in the other methods. The CC equations to be solved are quartic functions of the coefficients *t* and must be solved iteratively. This implies that a good choice of the initial approximate wavefunction is needed. If only the terms linear in *t* are considered and no coupling between doubly-excitation configurations are allowed, the coefficients become very similar to those of the MP wavefunction: these have been proved to be a good starting point, and offer a valuable link to the Moeller-Plesset method. The most used class within CC methods is the one considering only single and double excitations, plus triple excitations evaluated using perturbation theory, i.e. CCSD(T): this method has the limitation of being quite time-consuming with respect to MPn, but it is considered as the best single-reference method, as it can lead to good results even if the initial reference wavefunction may not be particularly accurate. However, the lack of an analytical expression for the energy gradient in CC calculations still makes MP2 the most suitable method to carry out the geometrical optimization for large molecules, as well as the calculation of their harmonic vibrational frequencies.

3.7 DETERMINATION OF MINIMUM ENERGY GEOMETRIES AND VIBRATIONAL FREQUENCIES

To calculate the minimum energy geometry of a molecule and its harmonic vibrational frequencies [43-48], it must be recalled that the nuclear energy of a molecule in a certain electronic state as a function of the internuclear co-ordinate can be seen as a multidimensional potential energy surface: in this case, a minimum has a zero first derivative of the energy on all the *n* internal co-ordinates, while all the n^2 second derivatives must be positive. In the case of a *transition state*, all the second derivatives are all positive but one, indicating a saddle point along that particular co-ordinate on which the second derivative is negative.

The first derivatives form a *n*-long column vector called a *gradient* and all the negative of its elements (that is, the negatives of the first derivatives) are called *forces*; the second derivatives form a $n \cdot n$ square matrix called a *Hessian matrix*, and its terms are defined as *force constants*.

For the location of a minimum on the potential energy hyper-surface, the *analytic gradient method* is normally used; in it, the first step is to formulate an initial approximate geometry. Then an expression for the Hessian matrix is estimated, allowing the Hartree-Fock energy to be calculated at the initial geometry, and from this an analytical expression of the gradient vector $\mathbf{g} = \partial E / \partial \mathbf{r}$ is obtained. At this point, the Hessian matrix can be obtained from numerical differentiation of the gradient vector or by being simply updated using available formulae such as the BFGS algorithm [49]. From the starting geometry, steps are moved in different directions and the one producing the lowest energy is followed as the direction to obtain the new geometry. The process is then reiterated until both the step size and the forces become lower than a value fixed at the beginning of the geometry optimization procedure.

Once the minimum energy geometry has been located, the forces are analytically derived and subsequently numerically differentiated to obtain the force constants H_{ij}. Considering that in the harmonic approximation [14] the energy near the minimum is given by

$$U_k(\mathbf{R}) = U_{min} + \tfrac{1}{2}\sum_{ij} H_{ij}\, \Delta\mathbf{R}_i\, \Delta\mathbf{R}_j$$

then it is possible to change variables so that it becomes

$$U_k(\mathbf{R}) = U_{min} + \tfrac{1}{2}\sum_r \omega_r^2 \mathbf{R}_r^2$$

The Hessian matrix can therefore be diagonalized and the harmonic vibrational frequencies obtained.

3.8 CONCLUSIONS

Calculations aimed at determining the molecular electronic distribution- and the most relevant characteristics of molecules, such as their minimum energy geometry, ionization energies, vibrational frequencies and total energy- can be divided in two major classes: *ab initio* calculations and density function calculations. For their general validity, systems without heavy atoms are usually preferably approached by means of *ab initio* calculations: with this category, the Roothan-Hartree-Fock method is the most commonly used. The method is based on the use of a Slater determinant description of the

molecular wavefunction, and the calculations are carried out by minimization of the total energy of the system, using the Variational theorem. This operation is conducted by optimization of the coefficients used to express the atomic orbitals as a linear combination of a pre-determined set of functions (the basis set). The approximation introduced by using a finite set of basis functions is compensated by the improvement of the basis functions quality, by including contributions from polarization and diffuse functions. The problem of electron correlation is tackled either by variational or by perturbative methods, and is based on the use of more than one Slater determinant to express the molecular wavefunction.

In this work, calculations were needed to facilitate the assignments of the experimental photoelectron and infrared spectra recorded for studies on the DMS+Cl_2 reaction (Chapter 4) and on organic azide decompositions (Chapter 5); moreover, they were needed to establish the mechanism for these reactions. Calculations at the MP2 level have been used in all the geometrical optimizations and the calculations of total energies, harmonic vibrational frequencies and vertical ionization energies (VIEs), both for the azides and their decomposition products and for the DMS+Cl_2 system. For the azide calculations only the 6-31G** basis set has been used, while the DMS+Cl_2 system has been described by means of different basis sets, which will be presented in Chapter 4. The total energies at fixed points on the DMS+Cl_2 potential surface have been determined also by means of single-point CCSD(T) calculations at geometries obtained at the MP2 level. Given the more accurate values provided by the CCSD(T) method with respect to the MP2 method, this was necessary because- in contrast with the azide systems- the formation of a reaction intermediate between DMS and chlorine was observed only by PES without the alternative fingerprint provided by IR matrix isolation spectroscopy. Also for CCSD(T) calculations different basis sets have been used, as will be reported in Chapter 4.

REFERENCES

[1] D.R. Hartree, *Proc. Camb. Phil. Soc.*, **24**, *1928*, 89

[2] V. Fock, *Z. Physik*, **61**, *1930*, 161

[3] D.R. Hartree, W. Hartree, B. Swirles, *Phil. Trans. Roy. Soc. A*, **238**, *1939*, 229

[4] J.C. Slater, *Adv. Quant. Chem.*, **6**, *1972*, 1

[5] W. Kohn, L.J. Sham, *Phys. Rev. A*, **140**, *1965*, 1133

[6] E.J. Baerends, D.E. Ellis, P. Ros, *Chem. Phys.*, **2**, *1973*, 41

[7] E.J. Baerends, P. Ros, *Chem. Phys.*, **2**, *1973*, 52

[8] Gaussian 03, Revision C.01, M. J. Frisch, G. W. Trucks, H. B. Schlegel, G. E. Scuseria, M. A. Robb, J. R. Cheeseman, J. A. Montgomery, Jr., T. Vreven, K. N. Kudin, J. C. Burant, J. M. Millam, S. S. Iyengar, J. Tomasi, V. Barone, B. Mennucci, M. Cossi, G. Scalmani, N. Rega, G. A. Petersson, H. Nakatsuji, M. Hada, M. Ehara, K. Toyota, R. Fukuda, J. Hasegawa, M. Ishida, T. Nakajima, Y. Honda, O. Kitao, H. Nakai, M. Klene, X. Li, J. E. Knox, H. P. Hratchian, J. B. Cross, C. Adamo, J. Jaramillo, R. Gomperts, R. E. Stratmann, O. Yazyev, A. J. Austin, R. Cammi, C. Pomelli, J. W. Ochterski, P. Y. Ayala, K. Morokuma, G. A. Voth, P. Salvador, J. J. Dannenberg, V. G. Zakrzewski, S. Dapprich, A. D. Daniels, M. C. Strain, O. Farkas, D. K. Malick, A. D. Rabuck, K. Raghavachari, J. B. Foresman, J. V. Ortiz, Q. Cui, A. G. Baboul, S. Clifford, J. Cioslowski, B. B. Stefanov, G. Liu, A. Liashenko, P. Piskorz, I. Komaromi, R. L. Martin, D. J. Fox, T. Keith, M. A. Al-Laham, C. Y. Peng, A. Nanayakkara, M. Challacombe, P. M. W. Gill, B. Johnson, W. Chen, M. W. Wong, C. Gonzalez, and J. A. Pople, Gaussian, Inc., Wallingford CT, 2004.

[9] MOLPRO- a package of *ab initio* programs, H.-J. Werner, P.J. Knowles, R. Lindh, M. Schutz, *et al*

[10] J. Simons, *J. Phys. Chem.*, **95**, *1991*, 1017, and references within it.

[11] P.W. Atkins, *Molecular quantum mechanics* 2nd ed., Oxford University press, Oxford, *1983*

[12] M. Born, R. Oppenheimer, *Ann. Phys.*, **84**, *1927*, 457

[13] P.M Morse, *Phys. Rev.*, **34**, *1927*, 57

[14] J.W. Rabalais, *Principles of ultraviolet photoelectron spectroscopy*, Wiley, New York, *1977*

[15] J.H. Eland, *Photoelectron spectroscopy*, Butterworths, London, *1984*

[16] W. Pauli, *Z. Physik*, **31**, *1925*, 265

[17] C.C.J. Roothan, *Rev. Mod. Phys.*, **23**, *1951*, 69

[18] R.G. Parr, *Quantum theory of molecular electronic structure*, W.A. Benjamin, New York, *1964*

[19] T. Koopmans, *Physica*, **1**, *1934*, 104

[20] W.G. Richards, *J. Mass Spectrom. Ion Phys.*, **2**, *1969*, 419

[21] M.F. Guest, V.R. Saunders, *Mol. Phys.*, **29**, *1975*, 873

[22] J.A. Pople, R.K. Nesbet, *J. Chem. Phys.*, **22**, *1954*, 571

[23] J.C. Slater, *Phys. Rev.*, **36**, *1930*, 57

[24] S.F. Boys, *Rev. Mod. Phys.*, **32**, *1960*, 306

[25] T.H. Dunning, *J. Chem. Phys.*, **53**, *1970*, 2823

[26] J.S. Binkley, J.A. Pople, W.J. Hehre, *J. Amer. Chem. Soc.*, **102**, *1980*, 939

[27] M.J. Frisch, J.A. Pople, J.S. Binkley, *J. Chem. Phys.*, **80**, *1984*, 3265

[28] T.H. Dunning, P.J. Hay, *Methods of electronic structure theory*, H.F. Schaefer III, Plenum, New York, *1977*

[29] R. Ahlrichs, P.R. Taylor, *J. Chem. Phys.*, **78**, *1981*, 315

[30] E.R. Davidson, D. Feller, *Chem. Rev.*, **86**, *1986*, 681

[31] S. Wilson, *Ab initio methods in quantum chemistry*, edited by K.P. Lawley, Wiley, London, *1987*

[32] T.H. Dunning, *J. Chem. Phys.*, **90**, *1989*, 1007

[33] D.E. Woon, T.H. Dunning, *J. Chem. Phys.*, **100**, *1994*, 2975

[34] T.H. Dunning, *J. Chem. Phys.*, **98**, *1993*, 1358

[35] O. Sinanoglu, *Adv. Chem. Phys.*, **6**, *1964*, 315

[36] O. Sinanoglu, D. Fu-Tai Tuan, *J. Chem. Phys.*, **38**, *1963*, 1740

[37] I. Shavitt, *Methods of electronic structure theory*, H.F. Schaefer III, Plenum, New York, *1977*

[38] W.J. Hehre, L. Radom, P.v.R. Schleyer, J.A. Pople, "*Ab initio molecular orbital theory*", Wiley Interscience, New York, *1986*

[39] S.R. Langhoff, E.R. Davidson, *Int. J. Quant. Chem.*, **8**, *1974*, 61

[40] I.N. Levine, *Quantum chemistry* 3rd ed., Allyn and Bacon, Boston, *1983*

[41] R.J. Bartlett, G.D. Purvis, *Int. Journ. Quantum Chem.*, **14**, *1978*, 561

[42] C. Moeller, M.S. Plesset, *Phys. Rev.*, **49**, *1934*, 618

[43] P. Pulay, *Mol. Phys*, **17**, *1969*, 197

[44] P. Pulay, *Application of electronic structure theory*, H.F. Schaefer III, Plenum, New York, *1977*

[45] *Geometrical derivatives of energy surfaces and molecular properties*, P. Joergensen and J. Simons, Reidel, Dordrecht, *1986*

[46] R.D. Amos, *Adv. Chem. Phys.*, **69**, *1987*, 99

[47] H.B. Schlegel, *Adv. Chem. Phys.*, **69**, *1987*, 249

[48] T. Helgaker, P. Joergensen, *Adv. Quant. Chem.*, **19**, *1988*, 183

[49] a) C.G. Broyden, *J. Inst. Math. Appl.*, **6**, *1970*, 76

b) R. Fletcher, *Comp. J.*, **13**, *1970*, 317

c) D. Goldfarb, *Math. Comput.*, **24**, *1970*, 23

d) D.F. Shanno, *Math. Comput.*, **24**, *1970*, 647

CHAPTER 4

A SPECTROSCOPIC STUDY OF THE ATMOSPHERICALLY RELEVANT REACTION OF DIMETHYL SULPHIDE WITH MOLECULAR CHLORINE

4.1 INTRODUCTION

While the reaction between DMS and Cl atoms has been subject of numerous experimental [1-3] and theoretical [4, 5] studies (recently, also PES experiments have been conducted at Southampton University, and the results are currently under analysis [6]), the reaction between DMS and Cl_2 has been less studied: spectroscopic studies have been conducted in the liquid phase [7], and in a matrix [8, 9], but questions on the actual reaction mechanism have been left unresolved.

When DMS and molecular chlorine were co-deposited in a matrix, in fact, evidence was found of a reaction intermediate [8]- which decomposed when irradiated by a mercury lamp- characterized by a strong vibrational band at around 360 cm^{-1}, but no assignment was given for the intermediate, and the overall reaction mechanism was not determined.

In the gas-phase, the reaction has been the subject of a study by photoelectron spectroscopy by the Southampton PES group: along with PE bands associated with the reagents and the products, monochloro-DMS + HCl, two unassigned bands with VIEs at approximately 9.6 and 10.5 eV were observed: the dependence of their intensities on the mixing distance of DMS and Cl_2 above the photon beam suggested they are associated with an intermediate of the reaction, but no convincing assignment has been given. Moreover, a more systematic investigation of the experimental conditions (mixing ratios and times, and partial pressures) was needed in order to fully characterize the compound associated with these bands.

The aim of this work was to give a deeper insight into this reaction, both from the mechanistic and the kinetics point of view. For this, it was decided to perform also FT-IR and FT-UV studies on the reaction in the gas-phase, in order to provide additional "fingerprints" for the monitoring of the reaction, and for the formation of highly chlorinated species. The work presented here will focus on the

mechanistic aspect, as a measurement of the rate constant of this reaction in the gas-phase at room temperature has been carried out by Dr. Ghosh in the Southampton PES group [10].

In the present work, the DMS + Cl_2 reaction was studied in Southampton by UV-photoelectron spectroscopy and by infrared matrix isolation spectroscopy, and at the Rutherford Appleton Laboratory by FT-infrared and ultraviolet spectroscopy. The most important difference between the experiments at Southampton and at the Rutherford Laboratory is the fact that in Rutherford the spectroscopic measurements were conducted in a static cell in which the gases were mixed, while in Southampton the UV-photoelectron spectrometer was equipped with an inlet system in which the gases were continuously flowing: this- and the possibility of changing the distance between the detection and the mixing point, see following section- meant that PES measurements could be performed at lower reaction times with respect to those in the FT-IR or UV experiments, where the closed cell led to the formation of reaction products under equilibrium conditions. In the matrix isolation experiments performed in Southampton, the gases were also pre-mixed prior to deposition in a matrix.

The data obtained from the different techniques provided evidence about how the reaction proceeds under different conditions.

Supporting the experimental work, *ab initio* calculations have been extensively used to interpret the PES results and to obtain a relative energy diagram and to elucidate the mechanism for the reaction, in particular for the first steps in the chlorination of DMS.

4.2 Experimental section

4.2.1 UV-photoelectron spectroscopy

The 10 cm analyser radius single detector photoelectron spectrometer- specifically built for the study of reaction intermediates [11]- was the same one as used in the azide project. This has been extensively described in Chapter 2.

The only change for the DMS+ Cl_2 study was the use of a gas-inlet system. A system of two concentric glass tubes was used, as represented in Figure 4.1.

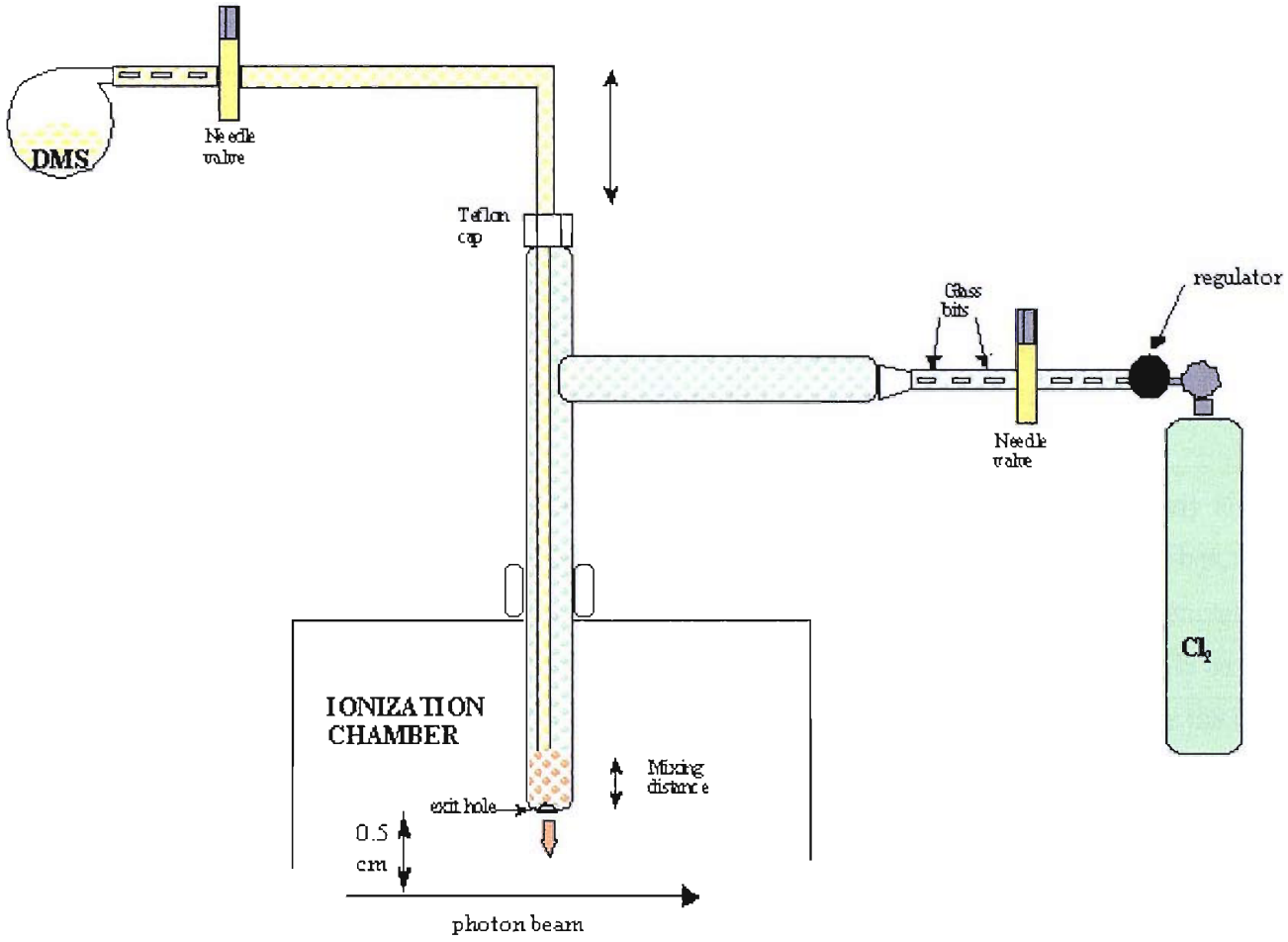

Figure 4.1- The inlet system used for the PE study of the DMS + Cl_2 reaction

In Figure 4.1 the external tube is T-shaped. One end fits into the top of the reaction cell inside the ionization chamber of the spectrometer, so that its opening lies 0.5 cm above the photon beam. The side-arm of the tube is connected to a needle valve via a short Teflon tube. The needle valve is connected to a chlorine cylinder via a regulator. The inner inlet tube is also connected to a needle valve, which in turn is connected to a flask holding a DMS sample via another short Teflon connection. In order to passivate the internal surface of the glass inlet and of the Teflon tubes, it was necessary to flush DMS through the system (DMS is a liquid of high enough volatility to allow a stable vapour flow by simply opening the needle valve to the vacuum of the ionization chamber) for some minutes. The surfaces were considered passivated once the photoelectron signal of DMS showed no trace of impurities, and when the pressure recorded in the chamber by the ion gauge showed no fluctuation leaving the needle valve setting unaltered. The distance of the inner tube relative to the end hole of the outer tube could be easily adjusted so that PE spectra can be recorded as a function of mixing distance (time). Different outer tubes have been used: they differed in the diameter of the exit hole. Tubes with

openings of 0.5, 1 and 2 mm have been used, along with an "open" one in which the opening was the maximum possible for fitting inside the reaction cell (approximately 1 cm). Different openings mean different mixing times, because as the exit hole gets smaller the longer the gases stay inside the mixing volume inside the outer tube. The open tube allows the molecules to be pumped efficiently towards the photon beam by means of the pumping provided by the diffusion pump below the reaction cell (see Figure 4.1); on the other hand, the 0.5 mm hole increased the probability of collisions between molecules inside the outer tube. In the case of such small openings, the situation approached that of a static cell, in which the gases are mixed. These were the conditions used in the FT-IR and UV experiments at the Rutherford laboratory.

The inner tube could be moved inside the outer one through a Teflon seal without allowing any air to enter the system. By varying the distance between the openings of the outer and inner tubes, the reaction times could be varied: when the two holes were together (0.5 cm above the photoionization point) the two gases had virtually no space to mix and therefore to react with each other, while as the inner tube was raised above the outer one, this space increased allowing a higher probability for the two gases to mix and react. A maximum mixing distance of 45 cm was used in these experiments.

In this way, two parameters were used to control the extent of the reaction: the outer tube opening and the distance between the ends of the two tubes. It was assumed that there was a direct relation between this distance and the contact time between the two gases: for an open outer tube, a distance of 1 cm corresponded- considering the pressure gradient between the ionization chamber and the inner inlet tube- to a contact time of roughly 0.5 ms [12]. From now on, the distance between the opening of the inner and outer tube will be therefore referred as the mixing distance, which is itself related to the reaction time.

Studies were conducted by varying the mixing distance for a fixed outer tube opening. For example, when the 1 mm hole for the outer tube was used, spectra at mixing distances varying from 0 to 45 cm (and vice-versa) were acquired, with usually four spectra being obtained at each distance; the same operation was then repeated for an outer tube with a different opening. The two extreme situations were a mixing distance of zero using the open outer tube (in this case the two gaseous substances had virtually no time to be in contact and react, even if the mixing distance is still 0.5 cm above the photon beam) and a mixing distance of 45 cm with the 0.5 mm outer tube, where a long volume of the outer tube was available as a mixing volume for the gases, and the small opening made the reaction time very high.

It was preferred to introduce Cl_2 along the inner tube. Chlorine was introduced by directly connecting a cylinder of the pure gas to a needle valve. Also in this case, it was necessary to flush chlorine through

the system for some minutes, in order to get rid of the hydrochloric acid produced by reaction with residual water. This operation was monitored by recording the first photoelectron band of HCl, which is an easily recognisable strong, sharp band with VIE at 12.75 eV [13]. The surfaces were considered as satisfactorily passivated when the intensity of this band was around a hundredth of the first band of Cl_2, which is a broader band with VIE at 11.69 eV [13].

The choice of the operating pressure was controlled by two main factors:

- the DMS partial pressure in the ionization chamber could not exceed $4 \cdot 10^{-5}$ mbar.
- DMS should always be in excess or approximately in equal molar concentration to Cl_2, in order to study the first chlorination mechanism and to avoid the presence of higher chlorinated DMS species.

Given the similar molecular weights (62 a.m.u. for DMS, 71 a.m.u. for Cl_2), it was assumed that the molar ratio between the gases was directly proportional to the ratio of their partial pressures, and that the total pressure increase read by the ion gauge in the ionization chamber was the sum of the partial pressures of the gases introduced. Typical experiments were performed with a base pressure of $1.0 \cdot 10^{-5}$ mbar; then DMS was introduced until a total pressure of $4.0 \cdot 10^{-5}$ mbar was reached. Chlorine was then introduced until a total pressure of around $7.0 \cdot 10^{-5}$ mbar was obtained. The stability of the pressure of chlorine in the system proved to be less easily reached than for DMS: routinely, the pressure of Cl_2 was periodically checked (and readjusted to the pre-set value) every few minutes by closing the valve of DMS and reading the pressure both on the ion gauge in the ionization chamber of the spectrometer and on the regulator on the chlorine cylinder.
Calibration of the spectra was usually performed using the well known VIEs for the reactants (DMS, first band with VIE at 8.72 eV; Cl_2, first band with VIE at 11.69 eV, second band with VIE at 14.40 eV), or for the HCl produced (first band, VIE at 12.75 eV) [13]. These bands were usually easily recognized, due to their intensity and shape, without major overlap with bands of reaction products.

4.2.2 Infrared matrix isolation spectroscopy

The apparatus used for infrared matrix isolation spectroscopy is the same as used for the azide project, and has been described in Chapter 2.
Nitrogen was used as the matrix gas. DMS and Cl_2 were mixed in a cell with usually a 1:2 molar ratio, as evaluated by their partial pressures. The total pressure was typically set at 10 mbar.

Deposition times of the condensed mixture ranged between 30 and 90 minutes: no major changes were observed in the spectra between these times, indicating that the reaction is fast enough to reach an advanced stage after 30 minutes after the mixing of DMS and Cl_2 in the cell.

The DMS/Cl_2 molar ratio and the long deposition times made the IR matrix isolation experimental conditions more similar to those of the FT-IR and UV measurements in the Rutherford laboratory rather than those of PES experiments: while the PES measurements were more focused on the early stage of the DMS + Cl_2 reaction leading to the production of mono-chlorinated DMS, the matrix isolation and the Fourier Transform IR and UV studies were more focused on the subsequent steps, which lead to the formation of highly chlorinated DMS species.

4.2.3 Gas-phase FT-IR and UV spectroscopy

These experiments were conducted at the Molecular Spectroscopy Facility at the Rutherford Appleton Laboratory.

The pure reactants were introduced into a mixing cell via a vacuum line, which is shown schematically in Figure 4.2.

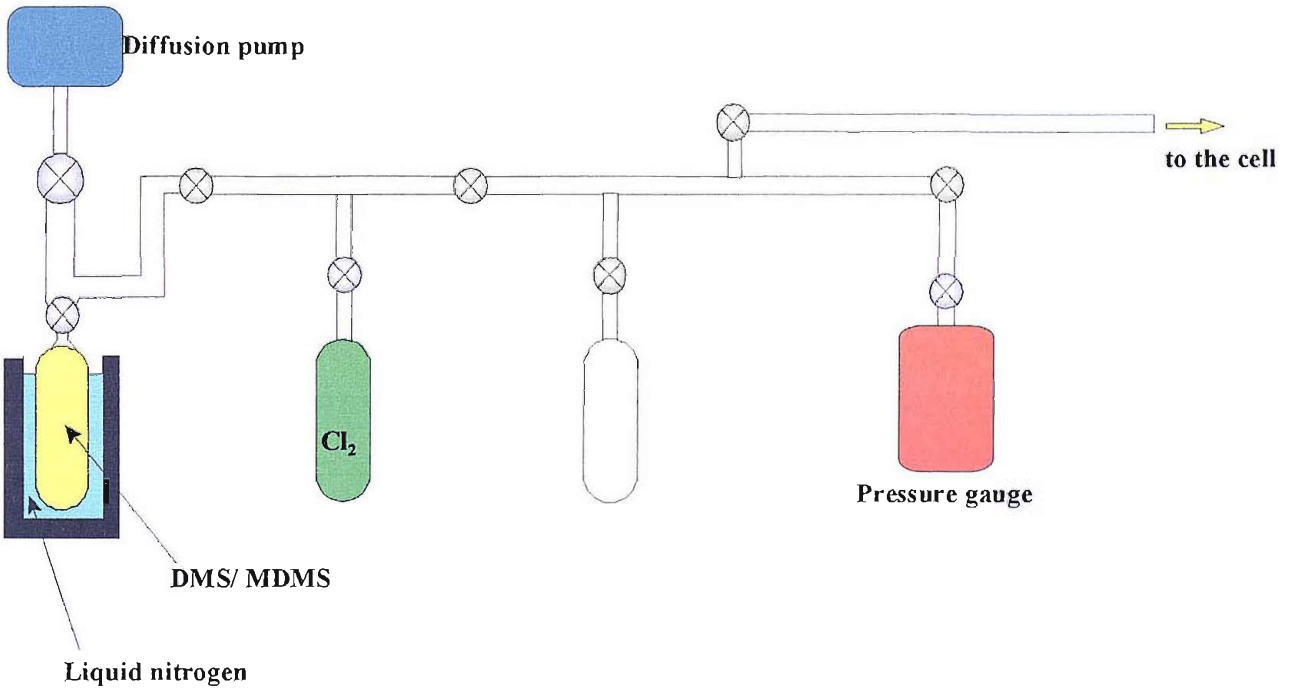

Figure 4.2- Schematic diagram of the vacuum line used to introduce DMS and Cl_2 into the FT-IR/UV spectrometer

The mixing cell was a glass cylinder 22.85 centimetres long- measured between the internal surfaces of the circular windows, which had a diameter of 5 centimetres. The windows used were made of KBr, when radiation between 400 and 40,000 cm^{-1} wavenumbers was used, while for radiation between

40,000 and 50,000 cm^{-1} windows of CaF_2 were used. Each window had a wedge shape in order to minimize fringes in the radiation transmitted. The outer surface of the cell was covered with aluminium foil to minimize external effects of temperature or radiation on the cell, and ethanol was flowed in a jacket around the cell to avoid heating.

The mixing cell was connected to a Bruker IFS 66V/S Fourier Transform Spectrometer, which provided a spectral coverage from 370 to 50,000 cm^{-1} with a resolution of 0.12 cm^{-1}. An overall representation of the spectrometer is given in Figure 4.3.

Radiation was produced in the UV region by a Xenon lamp, while in the IR region it was produced by a glowing filament of silicon carbide; the beam was collimated to a gold-coated paraboloid mirror which reflected it towards the cell. After passing through the cell, the radiation enters the detection chamber.

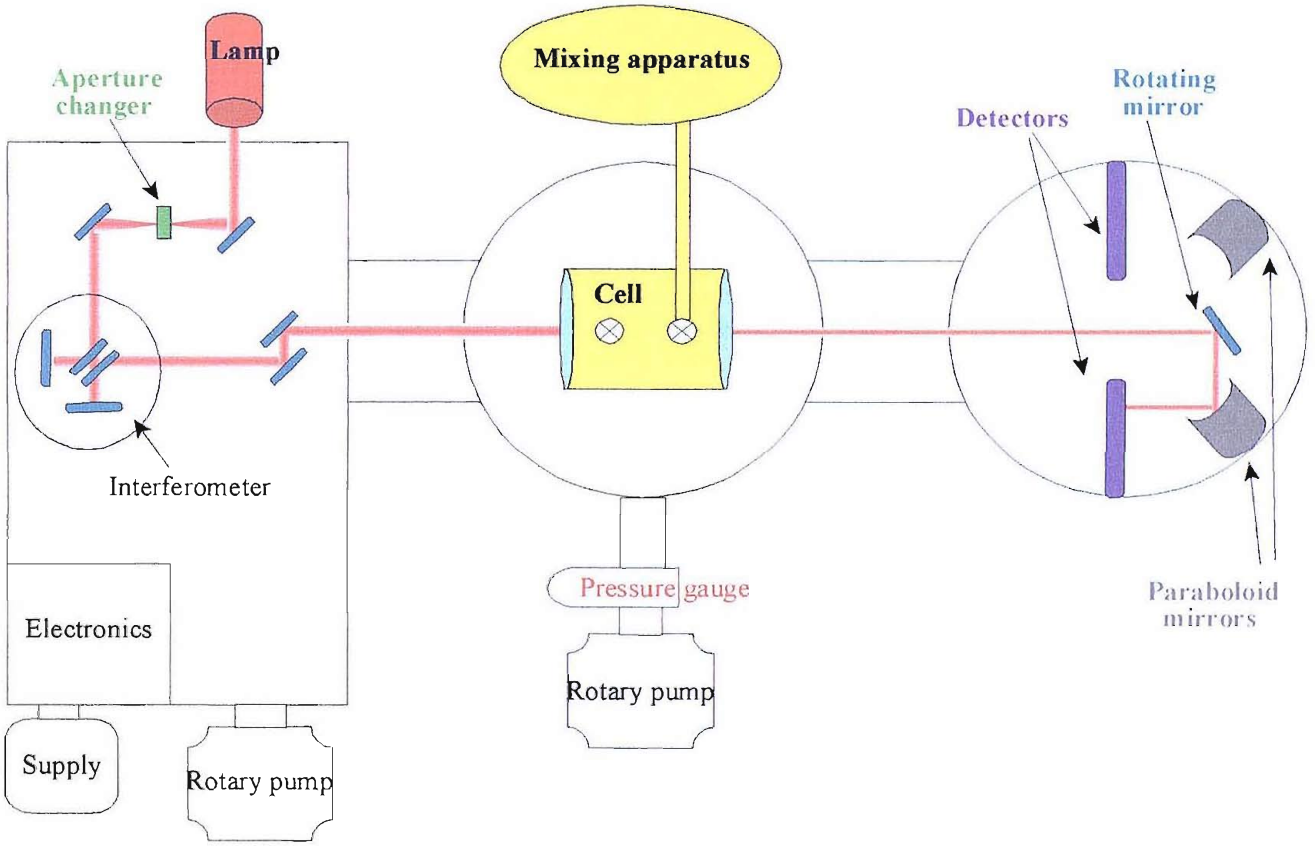

Figure 4.3- Schematic diagram of the FT-IR/UV spectrometer used in the study of the DMS+Cl_2 reaction

The beam can be oriented towards different detectors by adjusting the mirror positioned at the entrance of the chamber; once oriented, the radiation beam is collimated towards a specific detector by another gold-coated paraboloid mirror.

For IR radiation, an indium antimonite (InSb) detector was used for the 1800-6000 cm^{-1} region, while a mercury cadmium telluride (MCT) detector was chosen for the 500-8000 cm^{-1} region. For the UV region, the detectors were either a silicon photodiode (between 9,000 and 25,000 cm^{-1}) or a Gallium phosphide detector (between 25,000 and 52,000 cm^{-1}).
All the volume where the radiation passes (except for the mixing cell) was kept at low pressure- at around 10^{-3} mbar- by means of pumps connected to different sections of a stainless steel cell which comprises all the radiation path.

DMS was first frozen by lowering the flask holding the sample into liquid nitrogen and pumping away any residual air or impurities by opening the flask to a vacuum line. A freeze-pump-thaw procedure was repeated several times, chlorine was directly connected from the cylinder, but the section between the cylinder and the vacuum line was first evacuated to eliminate air or other volatile impurities.
The experiments were conducted by first filling the cell with a certain pressure of one of the reactants, then evacuating the rest of the vacuum line after having closed the connection to the cell. The vacuum line was then filled with the second reactant and the connection to the mixing cell was opened, letting the two gases mix and react.
The pressure of the first gas introduced in the cell is known with certainty, because it is the one read by the ion gauge connected to the vacuum line; concerning the second gas, no direct measurements of its partial pressure were possible. The facts that had to be considered were

- the initial pressure of the second gas read by the ion gauge refers to the one in the vacuum line *before* the opening of the connection to the mixing cell
- the final total pressure is affected by the expansion of the first gas initially contained in the cell
- as consequence of the reaction, new products can be formed which alter the molar ratio in the gaseous mixture in the cell

Therefore, an ideal behaviour of the reacting gases was assumed. After an initial measured pressure x of gas B was introduced in the vacuum line, by opening the connection between the vacuum line and the cell this pressure clearly drops to y: this is the therefore the pressure of gas B in the cell. From assumed ideal behaviour, the ratio y/x between the initial and final partial pressures is unaltered by the content of the cell, but is only due to the ratio between the initial and final volume available for the gas. This y/x ratio was determined by averaging several different measurements, and set as K. In practice, this was done for DMS and the ratio of the volume of the line to the volume of the cell was found to be 1:1.8. Supposing that a pressure Y of gas A is already present in the cell when the connection to the vacuum line is opened to introduce gas B, the partial pressures of A and B in the cell can be calculated

knowing the ratio of the volume of the line to the volume of the cell. So for gas A initially in the cell at a pressure P_A, the final pressure is $P_A \cdot (1.8/ 2.8)$. For B, introduced into the line with the valve to the cell closed, the initial pressure P_B gives a final pressure in the cell of $P_B \cdot (1/ 2.8)$.

The intensity of the lamp emission was subject to considerable fluctuations, especially in the first hours after it had been switched on. It was therefore necessary to record background spectra on the empty cell before and after every mixing, then to average these background spectra and subtract them from the one obtained for the reaction.

Typical acquisition times before obtaining the spectral results were set as 30 seconds: longer times provide better quality spectra, but the speed of the reaction required faster scans to monitor the actual increases or decreases of bands with time as consequence of the mixing and reaction of Cl_2 and DMS.

4.2.4 Chemicals used in the experiments

In all the experiments, commercially available compounds were used without any further purification. The commercial samples were

- DMS: 99+ %, Aldrich
- Cl_2: 99.9 %, Air products
- CH_3SCH_2Cl (monochloro DMS): 95 %, Aldrich, hereafter referred as MDMS
- CH_3SCHCl_2 (1,1-dichloro DMS): 95 %, Aldrich, hereafter referred as DDMS

1,1,1-trichloro DMS (CH_3SCCl_3) was prepared following a method in the literature [14], that is mixing DMS with SO_2Cl_2 at room temperature with a molar ratio roughly 1:3.5, and subsequently degassing the yellow liquid obtained for few hours. Characterization by mass spectrometry showed that the mixture obtained is mostly composed of 1,1,1-trichloro DMS (hereafter referred as TDMS), with a small amount of DDMS. Infrared and UV-photoelectron spectra will be presented in Section 4.4.

1,1,1,1'-tetrachloro DMS ($ClCH_2SCl_3$) was prepared by mixing DMS with SO_2Cl_2 at room temperature with a molar ratio around 1:4.5. The orange coloured liquid obtained was characterized by mass spectrometry and showed that it consists mostly of 1,1,1,1'-tetrachloro DMS (hereafter referred as TrDMS), but not negligible amounts of TDMS were still present. IR and PE spectra will be presented in Section 4.4.

4.3 Spectroscopic characterization of DMS and stable chlorinated DMS compounds

4.3.1 DMS

Dimethyl sulphide infrared, ultraviolet and photoelectron spectra are well known in literature [14-16]; nevertheless, for the sake of compatibility between the experiments, IR, UV and PE spectra were re-acquired and calibrated in this work.

FT-infrared spectroscopy

The Fourier transform infrared spectrum of gas-phase DMS is reported in Figure 4.4. Below 900 cm^{-1} and above 3100 cm^{-1} no significant bands were observed. The most significant bands experimentally observed are listed in Table 4.1, along with the normal mode with which they are associated (results taken from *ab initio* calculations on DMS, see Section 4.6).

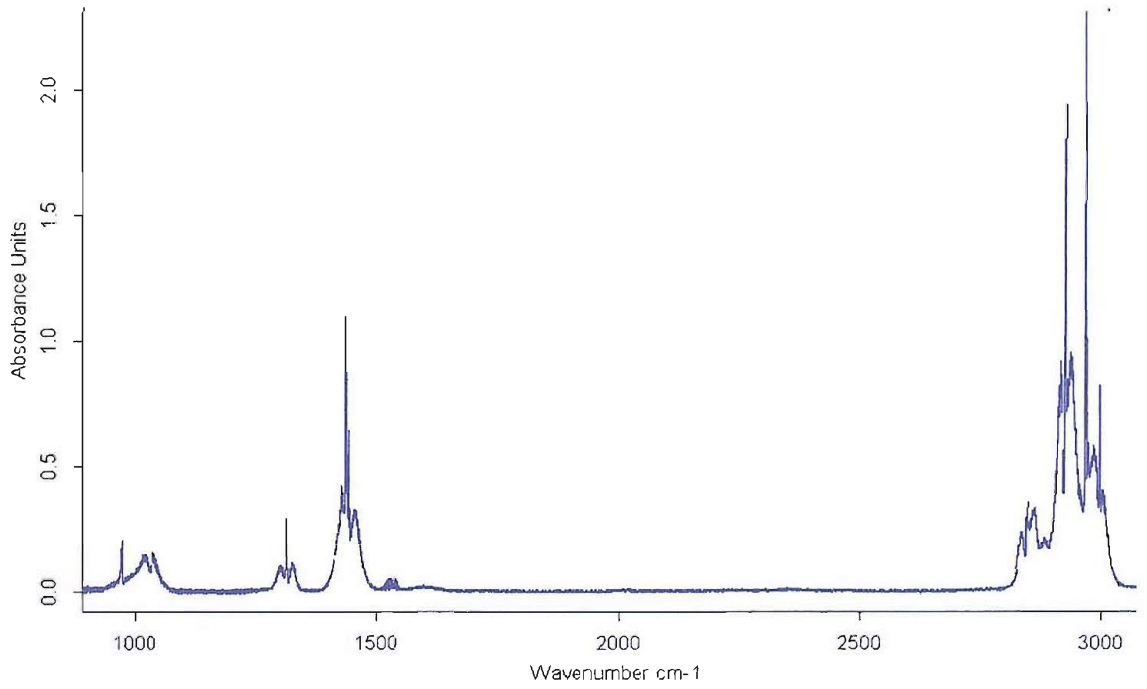

Figure 4.4- The FT-IR spectrum of DMS in the gas phase (approx. pressure 20 mbar)

Table 4.1- Vibrational frequencies measured for DMS with the associated normal mode

IR frequency (cm^{-1})	Normal modes
966	$C-H_3$ wagging
1016	
1039	
1314	$C-H_3$ scissoring
1428	
1437	
1457	
2926	$C-H_3$ stretching
2969	
2997	

FT-ultraviolet spectroscopy

The Fourier Transform UV spectrum of gas-phase DMS at different pressures is reported in Figure 4.5.

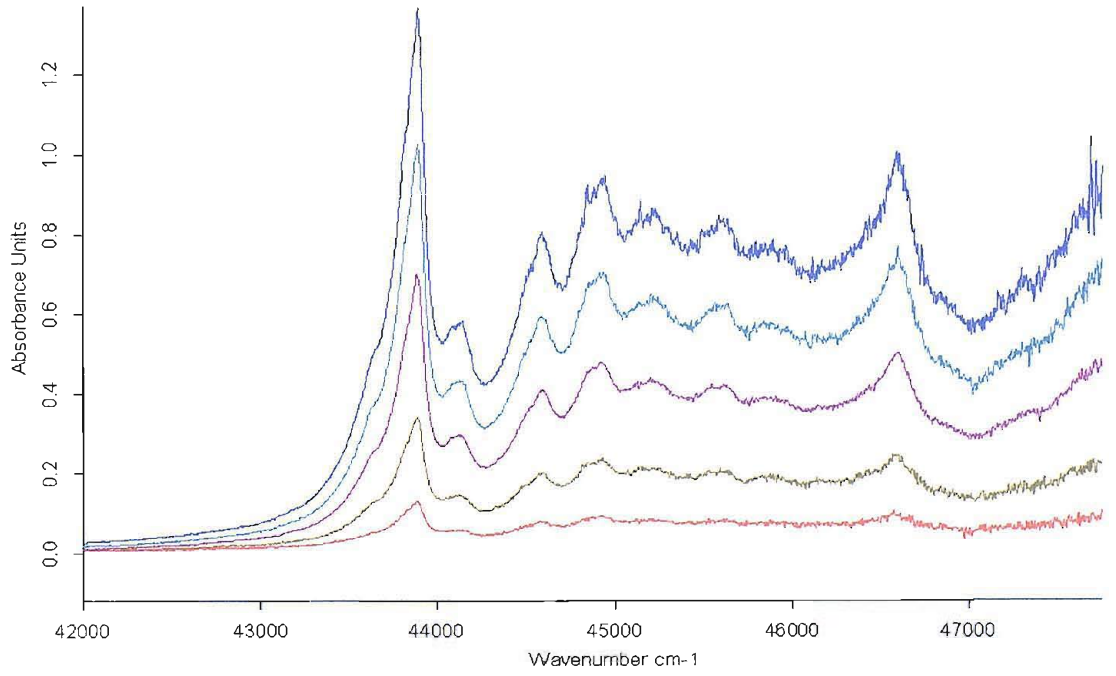

Figure 4.5- The FT-UV spectrum of DMS in gas phase at pressures of 0.2, 0.5, 1.0, 1.5 and 2.0 mbar

The spectrum is in good agreement with that reported in the literature: the most intense peaks in the UV spectrum recorded in this work are at 227.9 and 214.2 nm, compared with literature values [14] of 228 and 213 nm.

Photoelectron spectroscopy

The literature UV-PE spectrum of gas-phase DMS [16] is reported in Figure 4.6, while Table 4.2 lists the calibrated values for the vertical ionization energies (VIEs) of the bands, which are numbered in Figure 4.6.

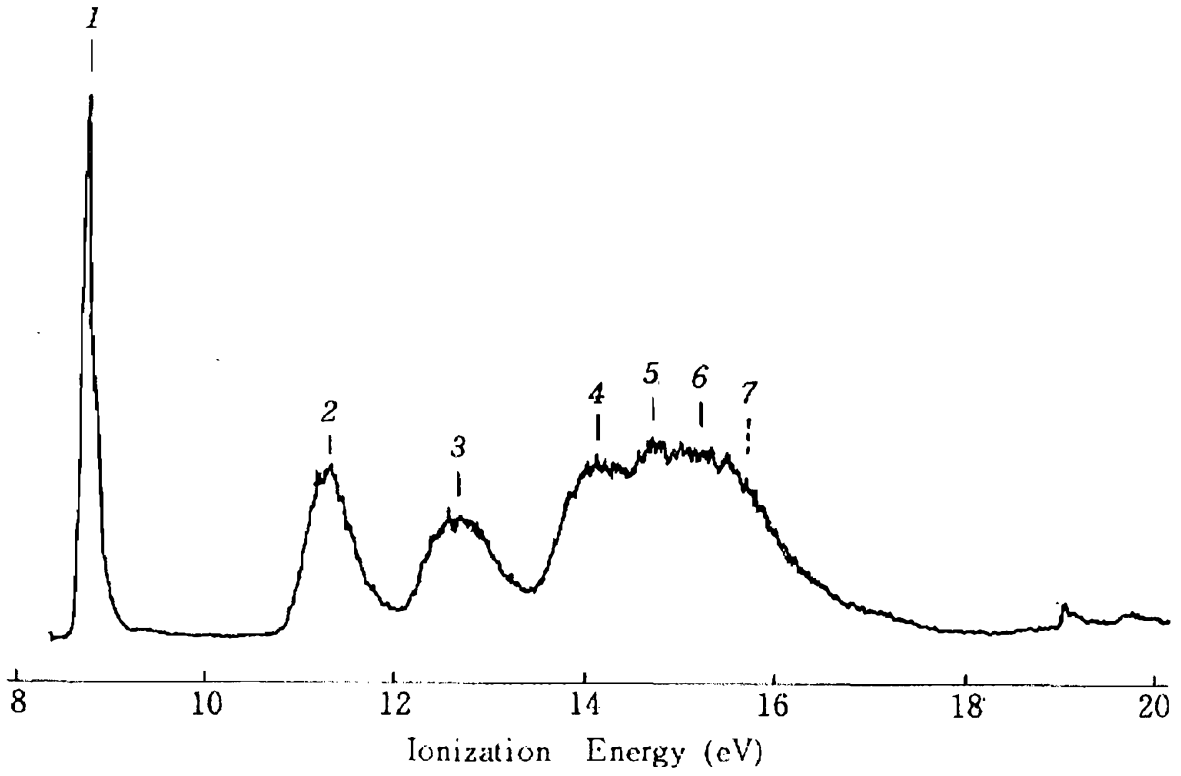

Figure 4.6- HeI-photoelectron spectrum of DMS with numbering of the bands

Table 4.2- VIEs of the PE bands of DMS reported in the literature (see Figure 4.6 for the numbering of the bands)

Band	1	2	3	4	5	6	7
VIE (± 0.02 eV)	8.72	11.30	12.68	14.07	14.73	15.25	15.70

4.3.2 MDMS (CH_3SCH_2Cl)

Monochloro DMS is a pale yellow liquid, for which no UV absorption spectra have been reported in the literature, and photoelectron spectra had been recorded only in the early studies of this project [17]. Infrared, ultraviolet and photoelectron spectra will be all summarized in the next pages.

FT-infrared spectroscopy

The Fourier Transform IR spectrum of gas-phase MDMS in the 600-3100 cm^{-1} range (no bands are present outside this range) is reported in Figure 4.7, and Table 4.3 lists the most significant vibrational frequencies, along with the normal modes derived from *ab initio* calculations (see Section 4.6). Clearly, the spectrum displays more bands than the DMS infrared spectrum (Figure 4.4), due to the C-Cl vibrations, visible in the 660-760 cm^{-1} region.

The IR spectrum acquired in the liquid phase is in good agreement with the gas phase spectrum; the two sets of vibrational frequencies are compared in Table 4.3.

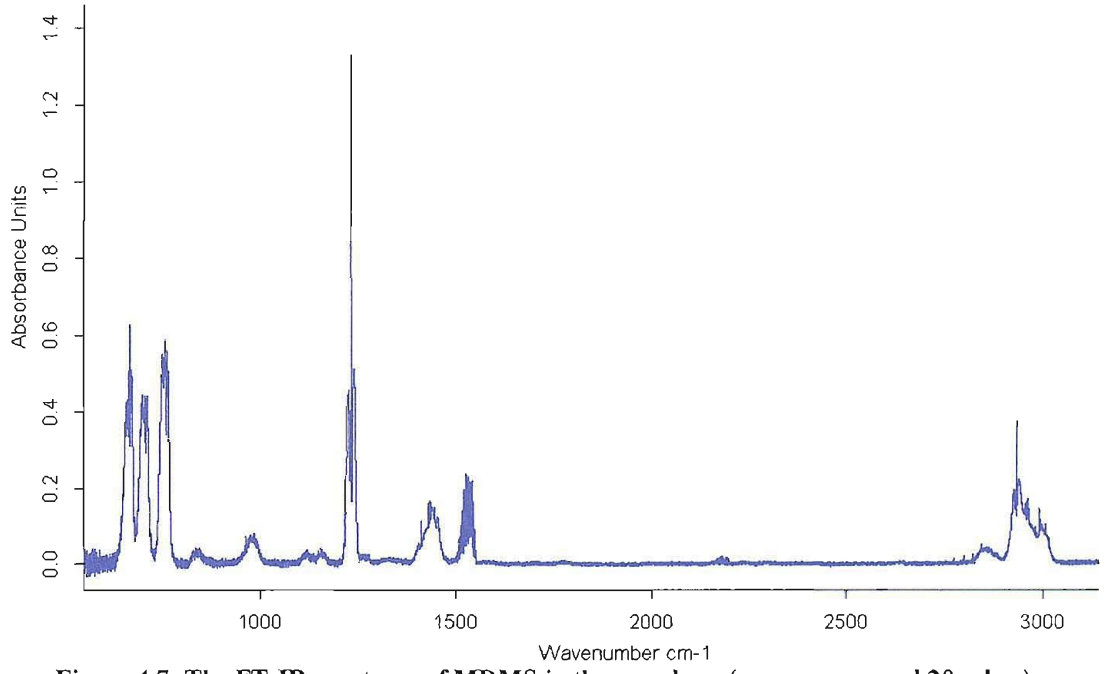

Figure 4.7- The FT-IR spectrum of MDMS in the gas phase (pressure around 20 mbar)

Table 4.3- Vibrational frequencies measured for MDMS with the associated normal mode

Liquid phase IR frequency (cm^{-1})	Gas phase IR frequency (cm^{-1})	Normal mode
646	666	S-C-Cl stretching
696	704	
749	757	
961	962	$C-H_3$ wagging
978	983	
	1117	$C-H_2$ wagging
1151	1155	
1226	1222	$C-H_2$ scissoring
	1229	
1421	1411	$C-H_3$ scissoring
1434	1436	
	2852	C-H stretching
	2933	
	2993	

FT-ultraviolet spectroscopy

The Fourier Transform UV spectrum of gas-phase MDMS at different pressures is shown in Figure 4.8.

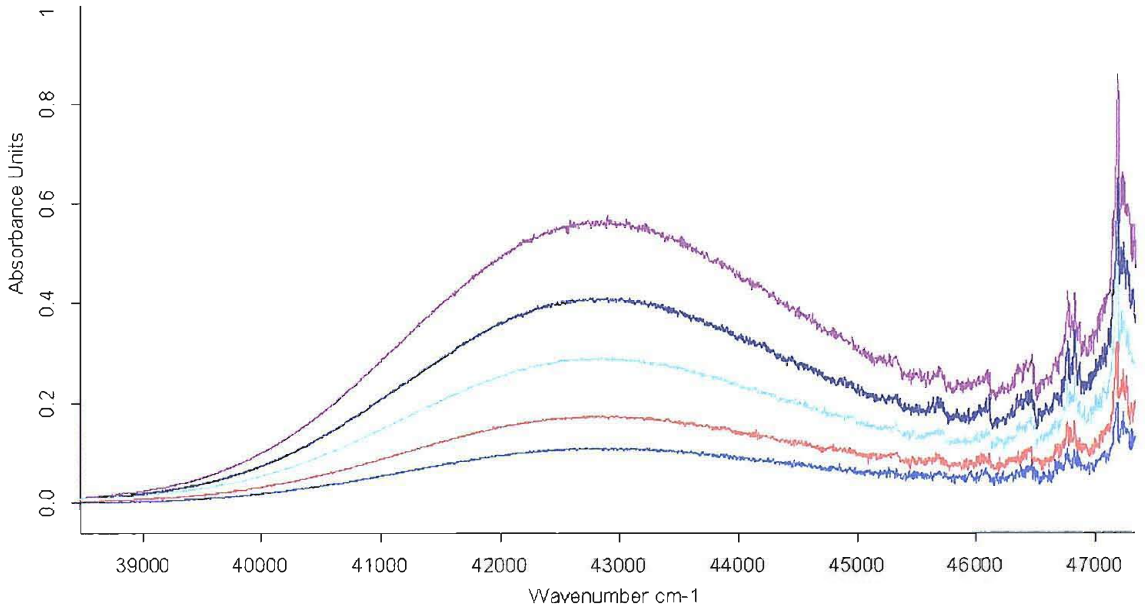

Figure 4.8- The FT-UV spectrum of MDMS in the gas phase at pressures of 0.5, 0.8, 1.25, 1.6 and 2.0 mbar

The introduction of a chlorine atom into the CH_3SCH_3 structure to give CH_3SCH_2Cl is reflected by the presence of the broad band in the 40,000-45,000 cm^{-1} region which has its maximum intensity at around 42,800 cm^{-1} (233.8 nm), while a series of sharper bands at higher wavenumbers are observed- more similar to the DMS spectrum, Figure 4.4- with the highest frequency being the one at 47,200 cm^{-1} (211.9 nm).

Photoelectron spectroscopy

The UV-PE spectrum of gas-phase MDMS is reported in Figure 4.9, while Table 4.4 lists the calibrated VIE values- obtained by averaging the VIE values from eight spectra- for the bands, labelled as in Figure 4.9.

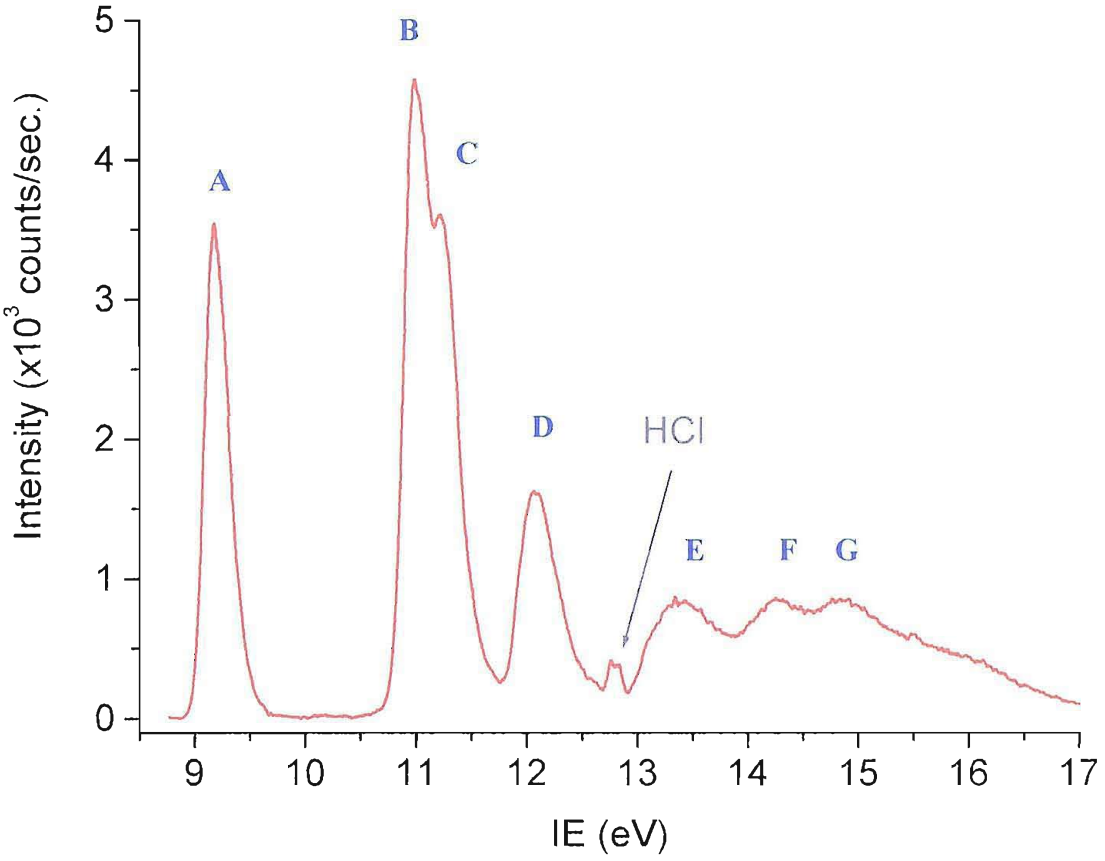

Figure 4.9- HeI-photoelectron spectrum of MDMS with labelling of the bands

Table 4.4- Calibrated VIEs of the PE bands of MDMS (see Figure 4.9 for the labelling of the bands)

Band	A	B	C	D	E	F	G
VIE (± 0.02 eV)	9.17	10.98	11.21	12.06	13.42	14.25	14.84

The main difference between this PE spectrum and the PE spectrum of DMS is the strong band with components at 10.98 and 11.21 eV: this is due to the contribution from the lone pair on the chlorine atom, as can be seen both from results from *ab initio* calculations and from comparison with other chlorinated alkanes, which all display [16] a band in the 10.5-12.0 eV region associated with a molecular orbital centred on the chlorine atom(s).

4.3.3 DDMS (CH_3SCHCl_2)

Dichloro DMS (DDMS) is a yellow liquid. For DDMS no UV or PES spectra have been reported in the literature. In the present work, infrared and photoelectron spectra have been recorded on a commercially obtained sample (95%, Aldrich). These results are summarized in the next pages.

Liquid phase infrared spectroscopy

Spectra have been acquired in the liquid phase; the main bands are shown in Figure 4.10. No major bands were displayed in the 1500-2500 cm^{-1} region.

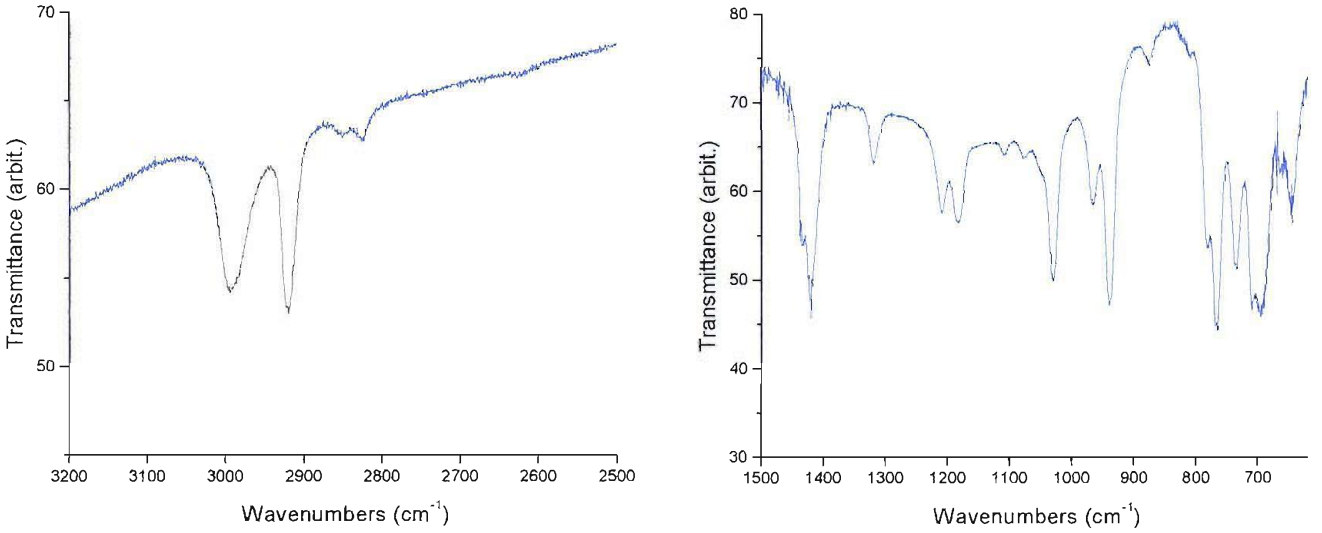

Figure 4.10- IR spectrum of liquid-phase DDMS, in the ranges 3200-2500 and 1500-600 cm^{-1}

The main vibrational frequencies are listed in Table 4.5.

Table 4.5- Vibrational frequencies measured for liquid phase DDMS

IR frequency (cm^{-1})	IR frequency (cm^{-1})	IR frequency (cm^{-1})
644	937	1319
695	967	1419
709	1030	2825
734	1182	2921
766	1208	2994

Photoelectron spectroscopy

The UV-PE spectrum of gas-phase DDMS is reported in Figure 4.11, and Table 4.6 lists the calibrated VIE values- obtained by averaging the values of seven spectra- for the vertical ionization energies (VIEs) of the bands, labelled as in Figure 4.11. The band at 12.63 eV in Figure 4.11 presents a double peak because of a small contribution from HCl.

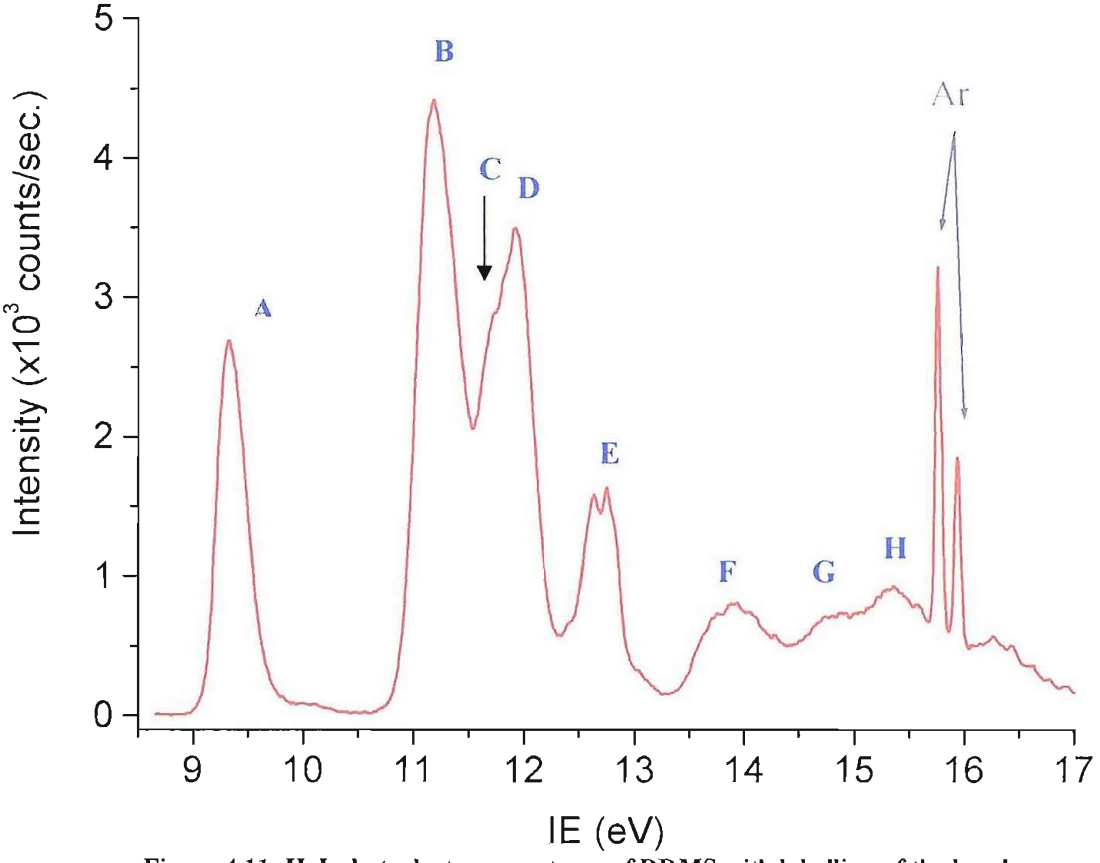

Figure 4.11- HeI-photoelectron spectrum of DDMS with labelling of the bands

Table 4.6- Calibrated VIEs of the PE bands of DDMS (see Figure 4.11 for the labelling of the bands)

Band	A	B	C	D	E	F	G	H
VIE (± 0.02 eV)	9.32	11.18	11.73	11.92	12.63	13.90	14.88	15.35

As well as changing the VIEs of the bands, the introduction of an extra chlorine atom in the molecule is reflected by an increased intensity of the bands in the 11.0-12.5 eV region; in particular, band D is much more intense than in MDMS (c.f. Figure 4.9), and band C overlaps with bands B and D and not just with band B as occurs in MDMS.

4.3.4 TDMS (CH_3SCCl_3) and TrDMS ($ClCH_2SCl_3$)

Trichloro-DMS and tetrachloro-DMS will be presented together because- not being commercially available products- they have been synthesized in this work: no complete separation between these different chlorinated products could be achieved, as shown mainly by mass spectrometry characterization (see Section 4.3). For these samples, IR and PES spectra will be presented (no UV spectral measurements were made on these compounds) with the assumption that contributions from higher or lower chlorinated DMS can be present, even if the dominant compound will be TDMS in the first case and TrDMS in the second.

The batch where TDMS was prepared showed initially, in PE spectra, traces of DMS and MDMS: the bands associated with these low chlorinated DMS species disappeared after degassing the sample for some minutes- also, the liquid turned to a darker tone of yellow. Such an operation was not conducted before IR spectra were acquired, so it is likely that the PE spectrum will be more representative of genuine TDMS than the IR spectrum, where contributions from lower chlorinated species can be more significant.

The IR spectrum of TDMS is shown in Figure 4.12, where it is compared with spectra of MDMS and DDMS in the two most significant regions of the infrared.

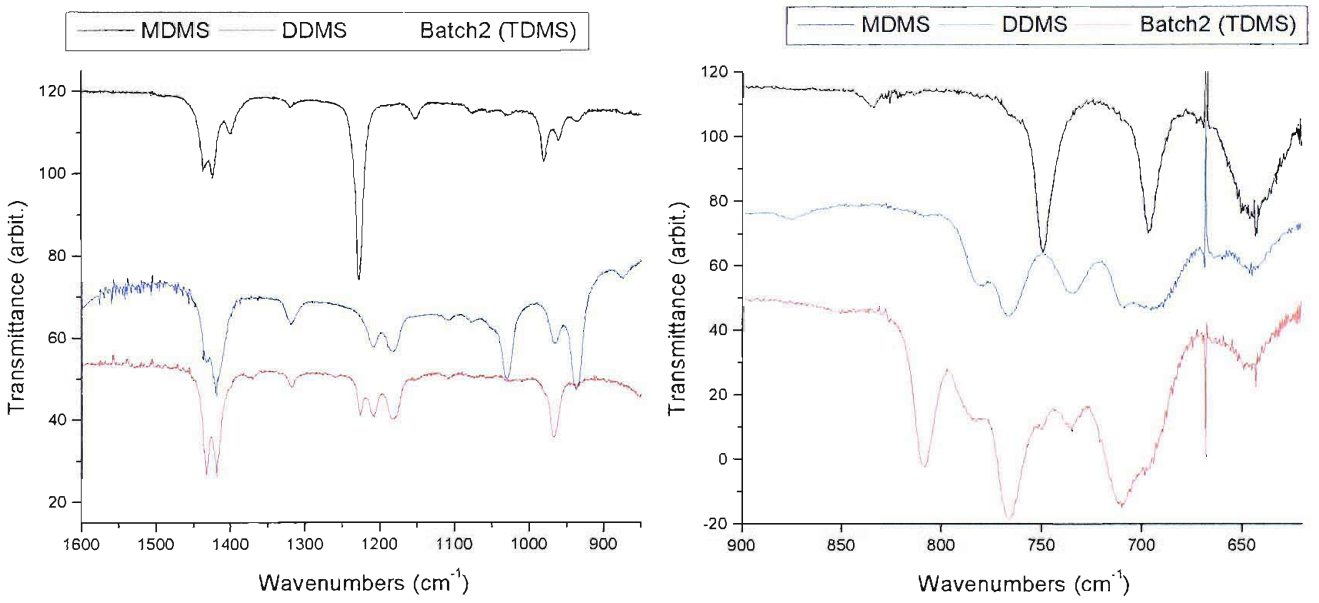

Figure 4.12- Comparison of the liquid phase IR spectra of MDMS (black line), DDMS (blue line) and the liquid obtained in Batch 2 (red line) which is mostly TDMS, in the 1600-850 and the 900-600 cm^{-1} regions

From a comparison of the spectra, it is evident that- even by taking into account the possible contributions from MDMS and DDMS, vibrational bands associated with TDMS should be those at 709, 766, 808, 967 and 1433 cm^{-1}.

The PES spectrum obtained after degassing the sample is reported in Figure 4.13.

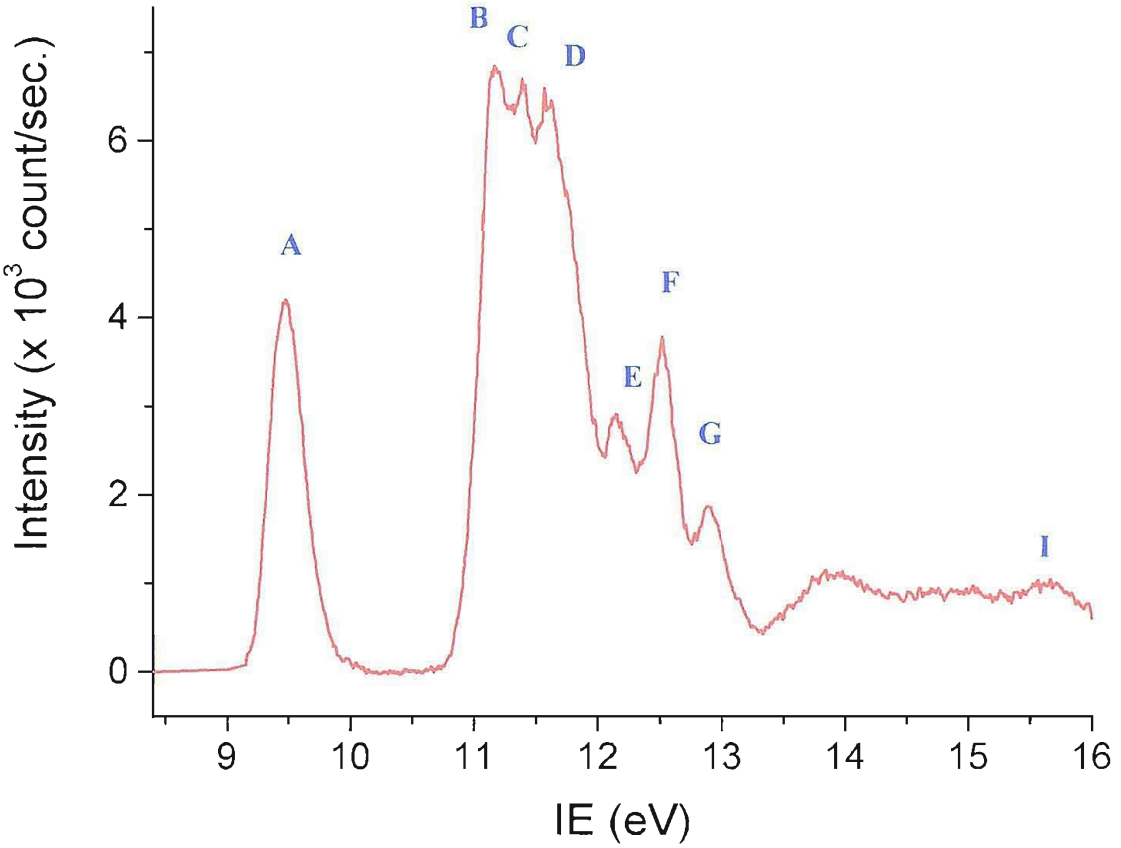

Figure 4.13- HeI photoelectron spectrum of TDMS obtained after degassing of the initial liquid product

The VIE values obtained after averaging the bands from seven different TDMS spectra are listed in Table 4.7

Table 4.7- Calibrated VIEs of the PE bands of TDMS (see Figure 4.13 for the labelling of the bands)

Band	A	B	C	D	E	F	G	H	I
VIE (± 0.02 eV)	9.47	11.17	11.39	11.59	12.13	12.49	12.87	13.90	15.63

Despite some similarities with the DDMS spectrum, the photoelectron spectrum of TDMS shows an increased complexity in the 11.0-13.0 eV region, where photoelectron bands associated with molecular orbitals centred on the halogen atoms are expected.

The orange liquid obtained when TrDMS was prepared proved- according to mass spectrometry data- to contain not negligible amounts of TDMS; in this case, no major changes were noticed in the PE spectra when the liquid was degassed. This is due to the fact that TDMS and TrDMS are expected to have relatively similar vapour pressures at room temperature.

Figure 4.14 compares the most significant region of the IR spectra of the liquids contained in Batch 2 (red line, mostly TDMS) and Batch 3 (dark yellow line, mostly TrDMS with some TDMS).

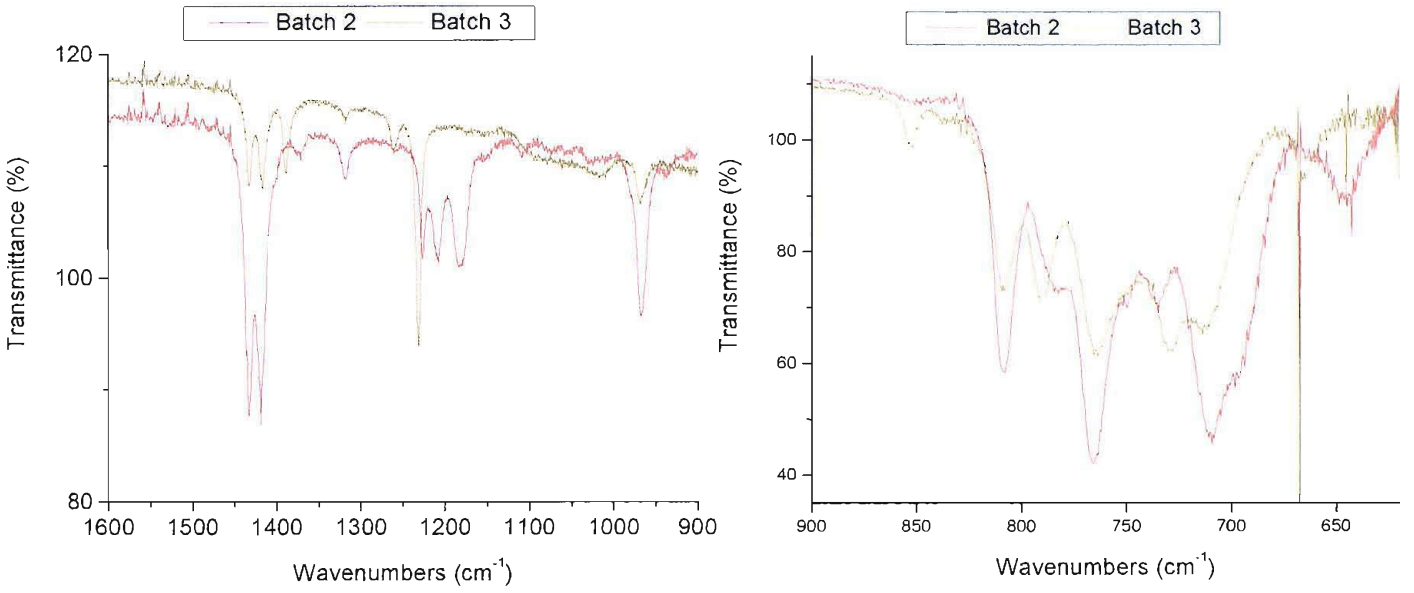

Figure 4.14- IR spectra of the liquids contained in Batch 2 (mostly TDMS) and Batch 3 (mostly TrDMS)

A comparison of the spectra of the two batches allows TrDMS bands to be identified at 666, 730, 790, 852, 1261 and 1388 cm^{-1}. Also the band at 1231 cm^{-1} should be associated with TrDMS, as it has no correspondent in the TDMS spectrum (red line in Figure 4.14) but it is possible that- because of its strong intensity- it could be due to a residual MDMS (which in the liquid phase displays a strong band at 1226 cm^{-1}).

The photoelectron spectrum obtained after degassing the TrDMS sample is reported in Figure 4.15 (no major changes were observed as a consequence of this operation, however), and the calibrated values of the VIEs of the bands (obtained by averaging 11 different spectra) are listed in Table 4.8.

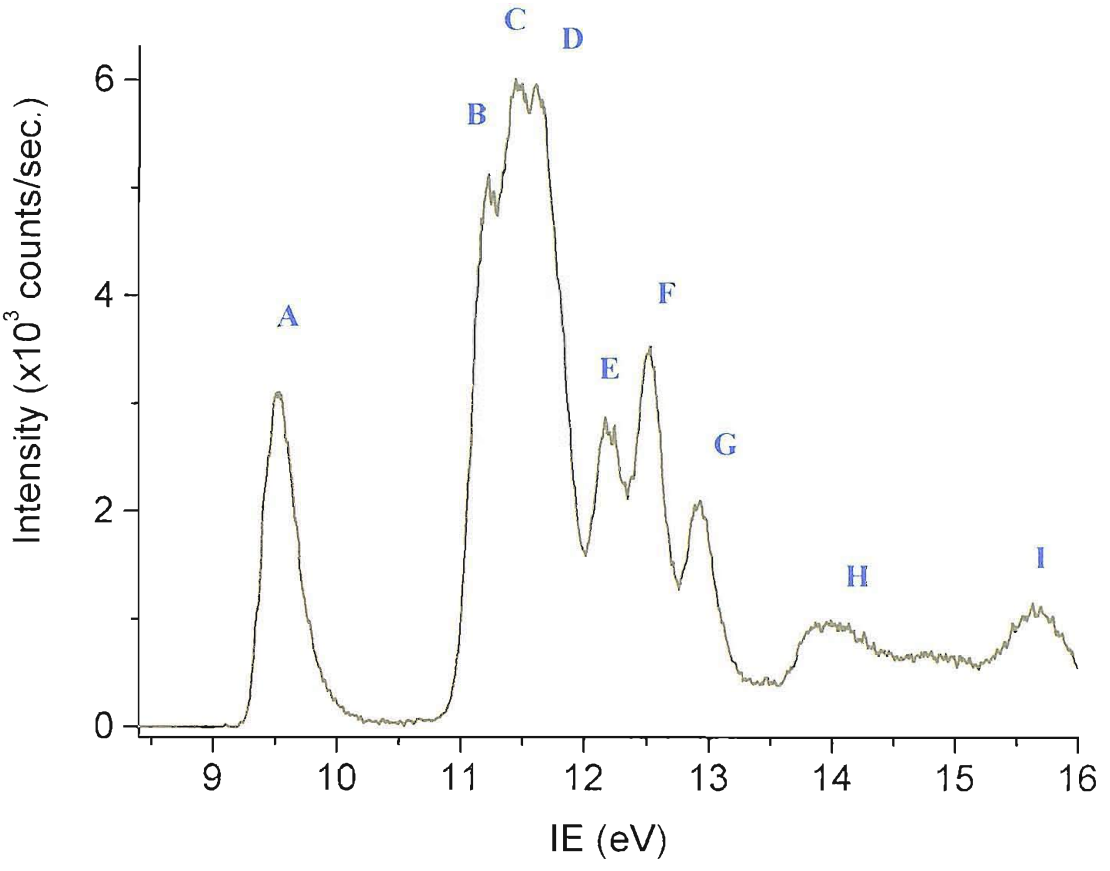

Figure 4.15- HeI photoelectron spectrum of Batch 3, containing mostly TrDMS

Table 4.8- Calibrated VIEs of the PE bands of TrDMS (see Figure 4.15 for the labelling of the bands)

Band	A	B	C	D	E	F	G	H	I
VIE (± 0.02 eV)	9.53	11.23	11.45	11.62	12.24	12.54	12.96	14.29	15.87

Also in this case, the difference with the photoelectron spectrum of the lower chlorinated DMS species (TDMS) is small: the bands appear in almost the same positions. The most immediate difference, as can be seen by comparing Figures 4.15 and 4.13, is the diminished intensity of band B (at 11.23 eV).

To visualize the changes in the HeI-photoelectron spectra of DMS at increasing level of chlorine substitution, the PE spectra of MDMS, DDMS, TDMS and TrDMS are reported in Figure 4.16. Apart from the already observed increase in the complexity of the 11.0-13.0 eV region, it must be noted that with the increase of chlorine atoms in the molecule, the first band moves slowly towards lower energies. To have an estimate of the relative intensity of the first bands of all the chlorinated DMS compounds, spectra have been acquired at the same pressure for all of them. The relative intensities of the first bands for DMS / MDMS / DDMS / TDMS / TrDMS were found as 1 / 3.11 / 2.81 / 1.05 / 0.91.

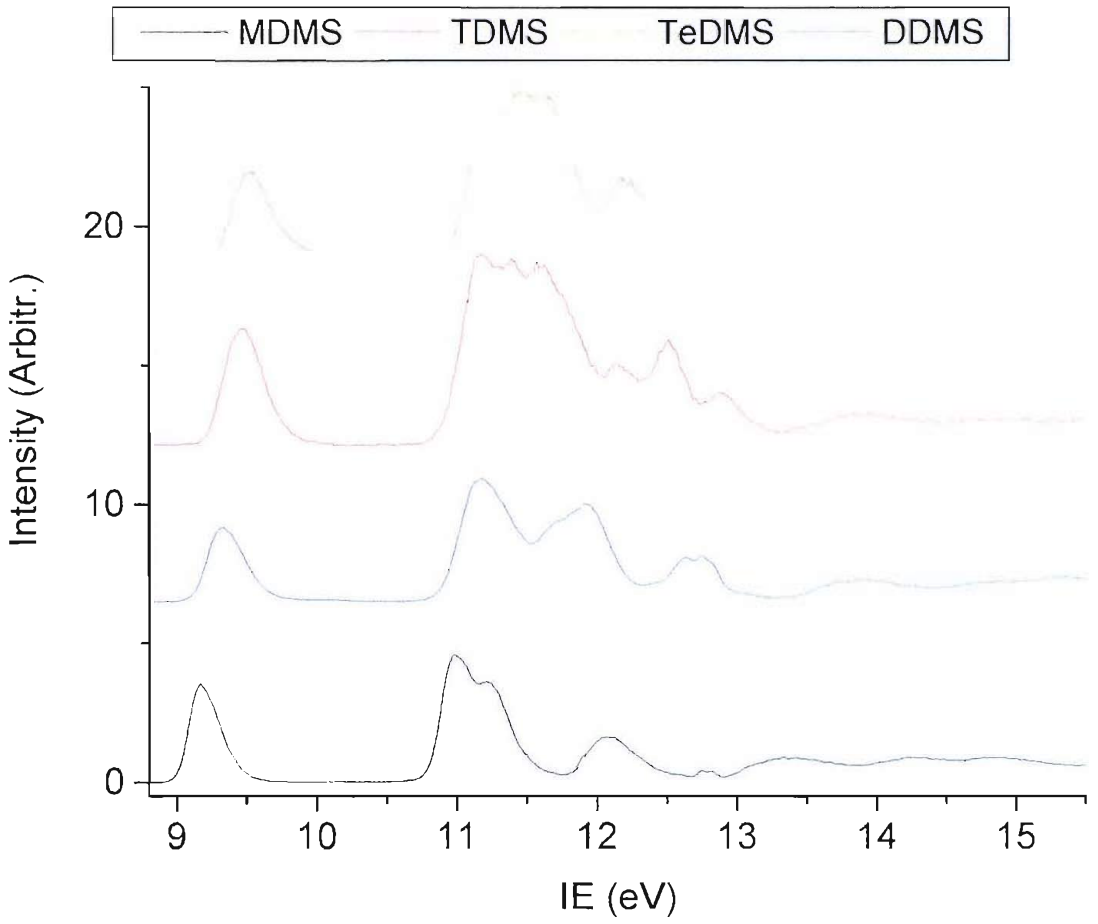

Figure 4.16- Comparison of the HeI-photoelectron spectra of increasingly chlorinated DMS: monochloro-DMS (black line), dichloro-DMS (blue line), trichloro-DMS (red line) and tetrachloro-DMS (dark yellow line)

One final observation must be reported. The IR spectroscopic characterization (liquid phase and matrix isolation studies) of samples obtained from the reaction between DMS and Cl_2 with different mixing ratios confirm what is reported in literature [7]- that chlorine substitution on DMS always occurs first on the same carbon atom. That is, when dichloro DMS is formed, the two chlorine atoms are attached to the same carbon atom. Subsequent chlorination still occurs on the same carbon atom, and the other methyl group is only attacked when all the protons from the first methyl group have been substituted, that is when 1,1,1-trichloro DMS is formed.

IR and PE spectra of commercially available bis-dichloro DMS ($ClCH_2SCH_2Cl$) have also been recorded and compared with those obtained for samples from Batches 2 and 3: although they are not reported here, the spectra are not the same as spectra of these liquid substances. It is then important to remark that the chlorination mechanism of DMS- at least in liquid phase- proceeds via a mechanism

$$CH_3SCH_3 \rightarrow CH_3SCH_2Cl \rightarrow CH_3SCHCl_2 \rightarrow CH_3SCCl_3 \rightarrow ClCH_2SCCl_3$$

and *not* via bis-dichloro DMS ($ClCH_2SCH_2Cl$).

4.4 SPECTROSCOPIC STUDY OF THE DMS + Cl_2 REACTION

The gas-phase reaction between dimethyl sulphide and molecular chlorine has been studied (1) by IR matrix isolation spectroscopy, (2) in a closed cell, monitored by FT-IR and UV spectroscopy, and (3) in a continuously flowing inlet system, monitored by PES.

As already mentioned, these different types of investigation allow study of different stages of the reaction, as- for a fixed mixing ratio- mixing the gases in a closed cell involves an equilibrium condition to be reached because of long contact times between reactants, while mixing the gases in a flowing system (with DMS:Cl_2 ratios with DMS in excess or equal to Cl_2) allows the study of the early stage of the reaction, that is the mechanism of the first chlorination of DMS.

The results will be presented in the above order, presenting for each type of spectroscopic investigation the different parameters chosen for the reactions, i.e. molar ratios, mixing distance or acquisition times.

4.4.1 FT-INFRARED (GAS PHASE) RESULTS

The DMS+Cl_2 reaction has been monitored by IR spectroscopy by varying the different experimental parameters that affect the extent of the reaction. It was found that of all the possible parameters (molar ratio, mixing order, total pressure, acquisition time), the most crucial one is the molar ratio. In the case of IR monitoring, it was found that total pressures around 20 mbar are the most suited for a clear detection of a noise-free spectrum, while the introduction order did not affect the quality of the spectra that much.

The results will therefore be presented considering the molar ratio as the most important parameter.

a) DMS in excess

The most significant regions of the IR spectrum obtained by mixing DMS and Cl_2 in a 1.8: 1 molar ratio and total pressure 20 mbar are reported in Figure 4.17, along with the IR spectra of pure MDMS and DMS shown to assist the assignment.

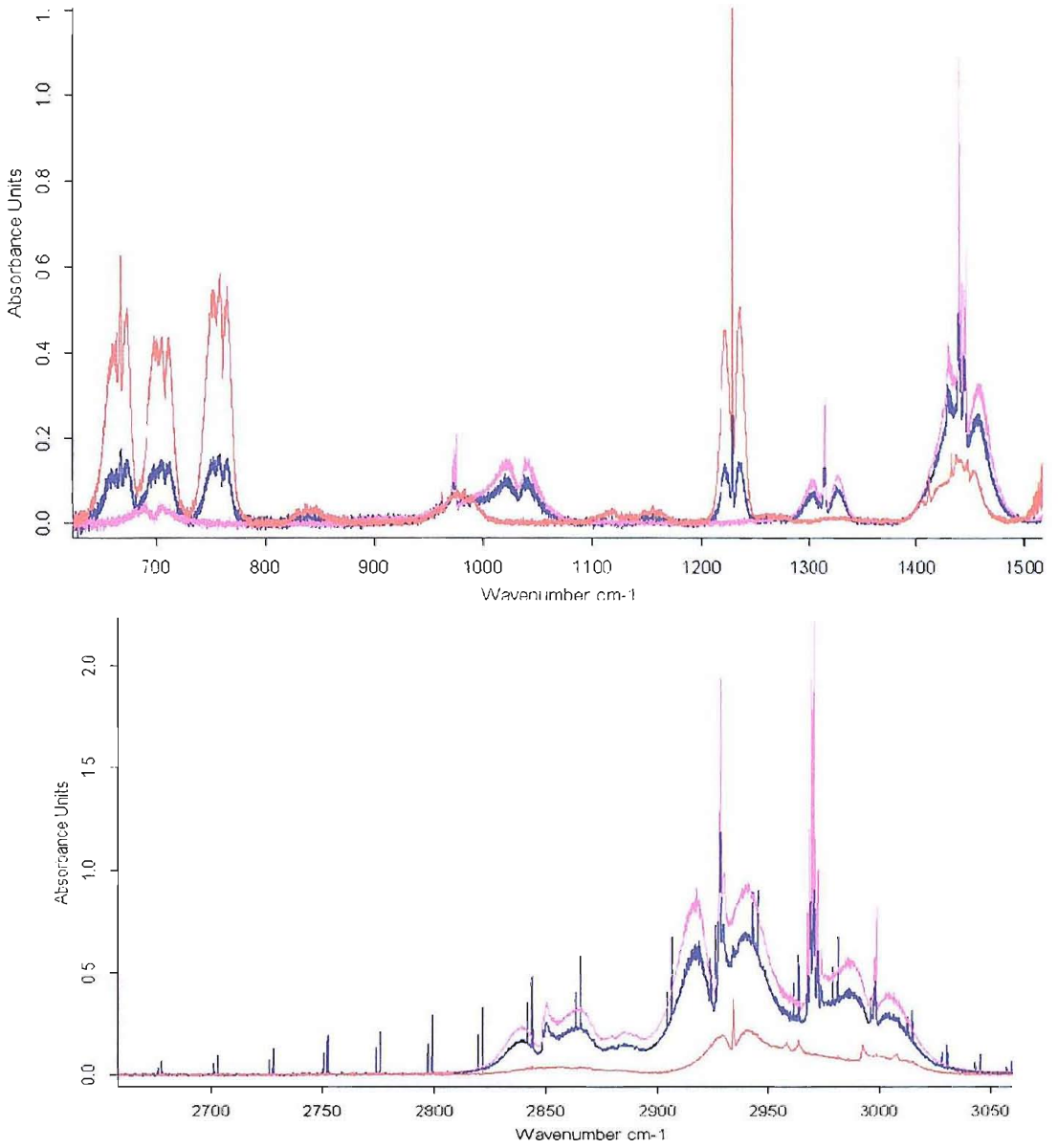

Figure 4.17- IR spectrum (blue line) of the DMS+Cl_2 reaction monitored starting with a 1.8: 1 molar ratio and total pressure 20 mbar. Spectra of DMS (pink line) and MDMS (red line) are shown for comparison

It is clear that the spectrum of the reaction consists of unreacted DMS plus MDMS initially formed (the bands at 1230 cm^{-1} and below 800 cm^{-1}). In the infrared spectra, bands associated with HCl can also be observed (the very sharp peaks in the 2650-3050 region, which show a P-branch between 2650 and 2875 cm^{-1} and a R-branch between 2900 and 3075 cm^{-1}).

IR data therefore indicate that in excess DMS, the first step of the reaction is the formation of MDMS and HCl following the reaction

$$CH_3SCH_3 + Cl_2 \rightarrow CH_3SCH_2Cl + HCl$$

b) DMS and Cl_2 in equal proportion

Figure 4.18 reports the most relevant region of the infrared spectrum obtained when mixing DMS and chlorine in 1:1 molar ratio, with a total pressure of 25.5 mbar; DMS was first introduced in the cell, and Cl_2 added later.

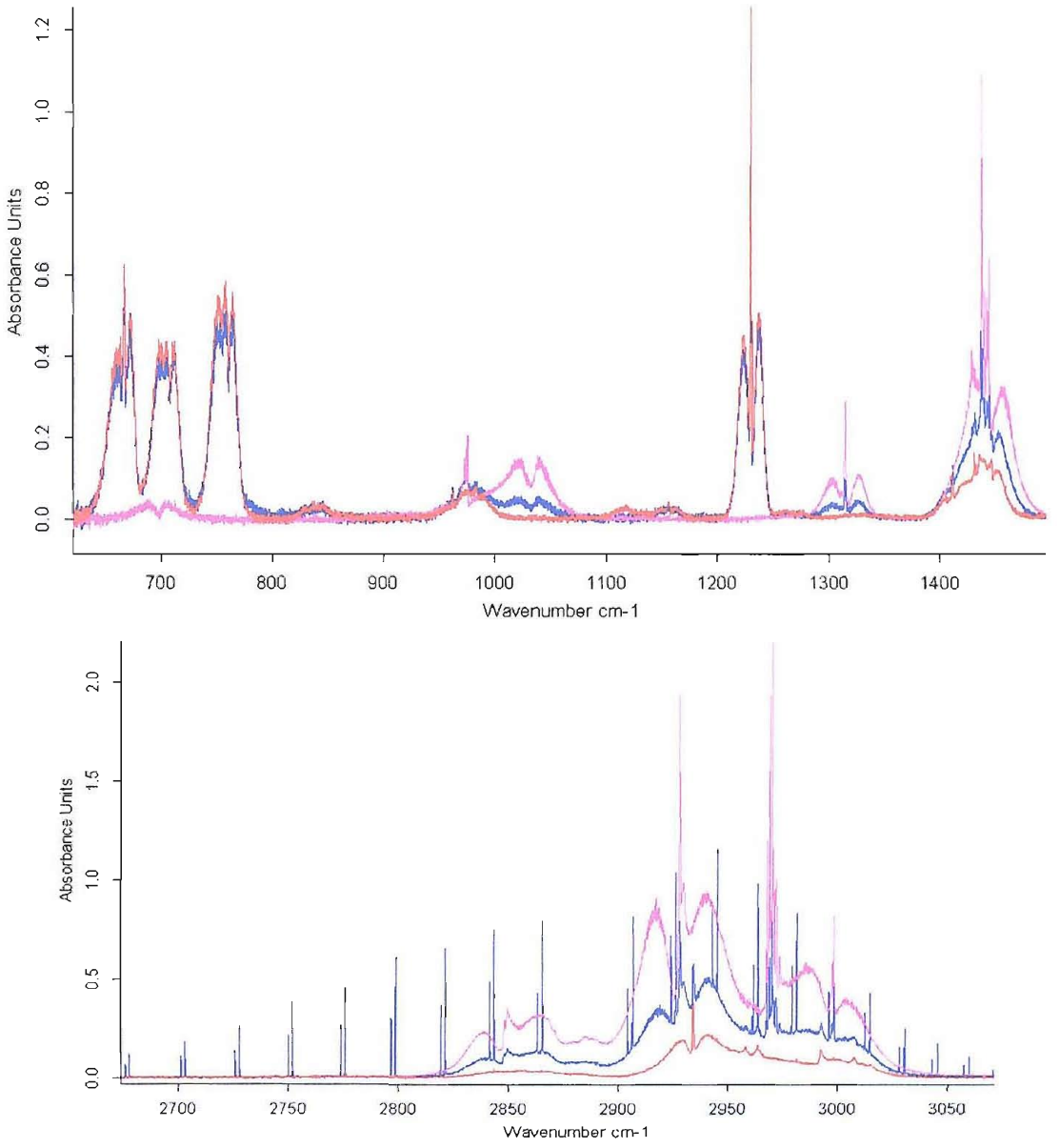

Figure 4.18- IR spectrum (blue line) of the reaction of DMS and Cl_2 mixed in equal proportion and total pressure 25.5 mbar. Spectra of DMS (pink line) and MDMS (red line) are reported for comparison

The pattern reflects the one obtained for the DMS in excess situation (Figure 4.22), but here the reaction is more advanced, as can be seen by the stronger intensity of the bands associated with HCl and MDMS and the corresponding lowering of the contributions from unreacted DMS.

c) Cl_2 in excess

The IR spectrum of the mixture obtained starting from chlorine and DMS in 1.8: 1 molar ratio (total pressure 20 mbar) is reported in Figure 4.19.

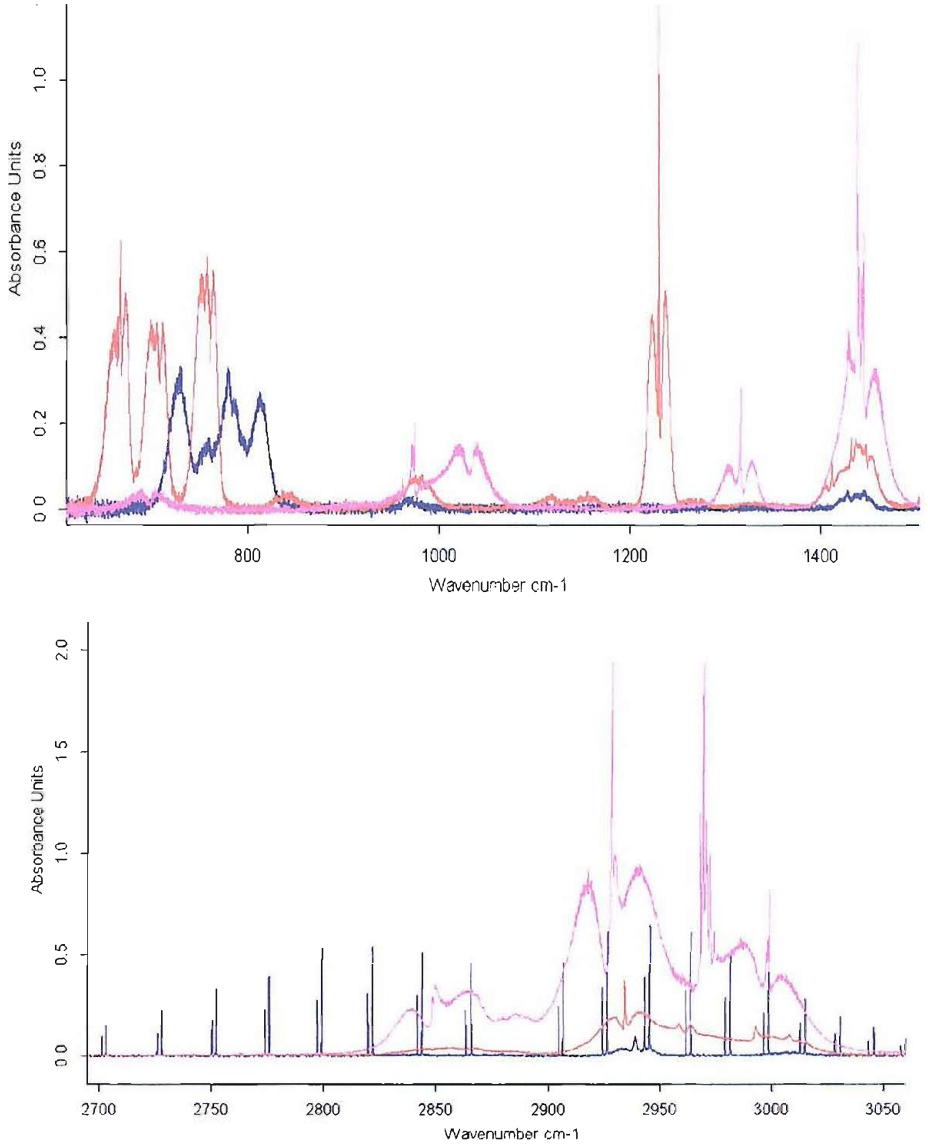

Figure 4.19- IR spectrum of the reaction DMS+Cl_2 (blue line) mixed in 1:1.8 molar ratio and total pressure 20 mbar. Spectra of DMS (pink line) and MDMS (red line) are shown for comparison

The spectrum radically changes when an excess of chlorine is the initial condition: in the 2800-3000 cm^{-1} region there are just very weak bands due to C-H stretching modes, compared with the strong signals due to HCl. The lower energy region of the spectrum clearly indicates that both DMS and MDMS are not present in the mixture (no signals are found at 1230 and 1440 cm^{-1} where MDMS and DMS have strong bands), and the pattern of bands between 700 and 850 cm^{-1} clearly indicates the formation of a new chlorinated form of DMS. The latter is the most significant feature to allow identification of the new species: a comparison with the spectra of DDMS, TDMS and TrDMS

(reported in Figures 4.12 and 4.14) strongly indicates TDMS as the obvious candidate for the assignment of the unknown bands. Both the positions and the relative intensities of the bands in the 850-700 cm^{-1} region reproduce well those obtained for the liquid contained in Batch 2, which was mostly TDMS. The small differences between the two spectra can in fact be due to the presence of residual MDMS- and maybe DDMS- in Batch 2: if all possible peaks due to MDMS (at 696 and 749 cm^{-1}) or DDMS (at 783 cm^{-1}) are eliminated from the spectrum of Batch 2 (Figure 4.12), an almost perfect match with the spectrum obtained for the DMS + Cl_2 reaction of Figure 4.19 is obtained.
It is noteworthy that the HCl bands are not stronger than in the 1:1 molar ratio situation (Figure 4.18): this seems to suggest that the formation of TDMS is not accompanied by an increased amount of HCl compared to the one formed together with MDMS. From this, an initial suggestion for the reaction path can be expressed as

$$DMS + Cl_2 \rightarrow HCl + MDMS$$

followed by $$MDMS + Cl_2 \rightarrow TDMS + H_2$$

instead of $$DMS + 3Cl_2 \rightarrow 3HCl + TDMS$$

If TDMS is the product observed, it is evident that an excess of chlorine on DMS largely favours formation of the tri-chlorinated compound compared to the di-chlorinated compound, whose presence cannot be confirmed among the reaction products. A further discussion of the experimental data and a proposal for the substitution mechanism will be given in Section 4.7.

4.4.2 INFRARED MATRIX ISOLATION RESULTS

Matrix isolation experiments were carried out at just two different mixing ratios, that is either equimolar DMS/Cl_2 mixtures, or a 2:1 molar ratio with chlorine in excess. The gases were pre-mixed before samples were trapped in a matrix for spectroscopic study. The two mixing ratios were studied with a different choice of the matrix gas: for the 2:1 ratio nitrogen was chosen, while for the 1:1 ratio the matrix gas was argon. Spectra of DMS and MDMS have also been recorded to facilitate the assignments and to provide reference spectra; for DDMS and TDMS assignments have been made by using the vibrational frequencies for the species trapped in matrix reported in the literature [18, 19].

a) DMS and Cl_2 in 1:2 molar ratio

Figure 4.20 reports the low wavenumber regions of the IR spectra of DMS, MDMS, DDMS and of the products obtained by mixing DMS and Cl_2, and MDMS and Cl_2 both in a 1:2 ratio. The high wavenumber regions of these spectra are presented in Figure 4.21.

Nitrogen was chosen as the matrix gas; the deposition time was 30 minutes for all the spectra.

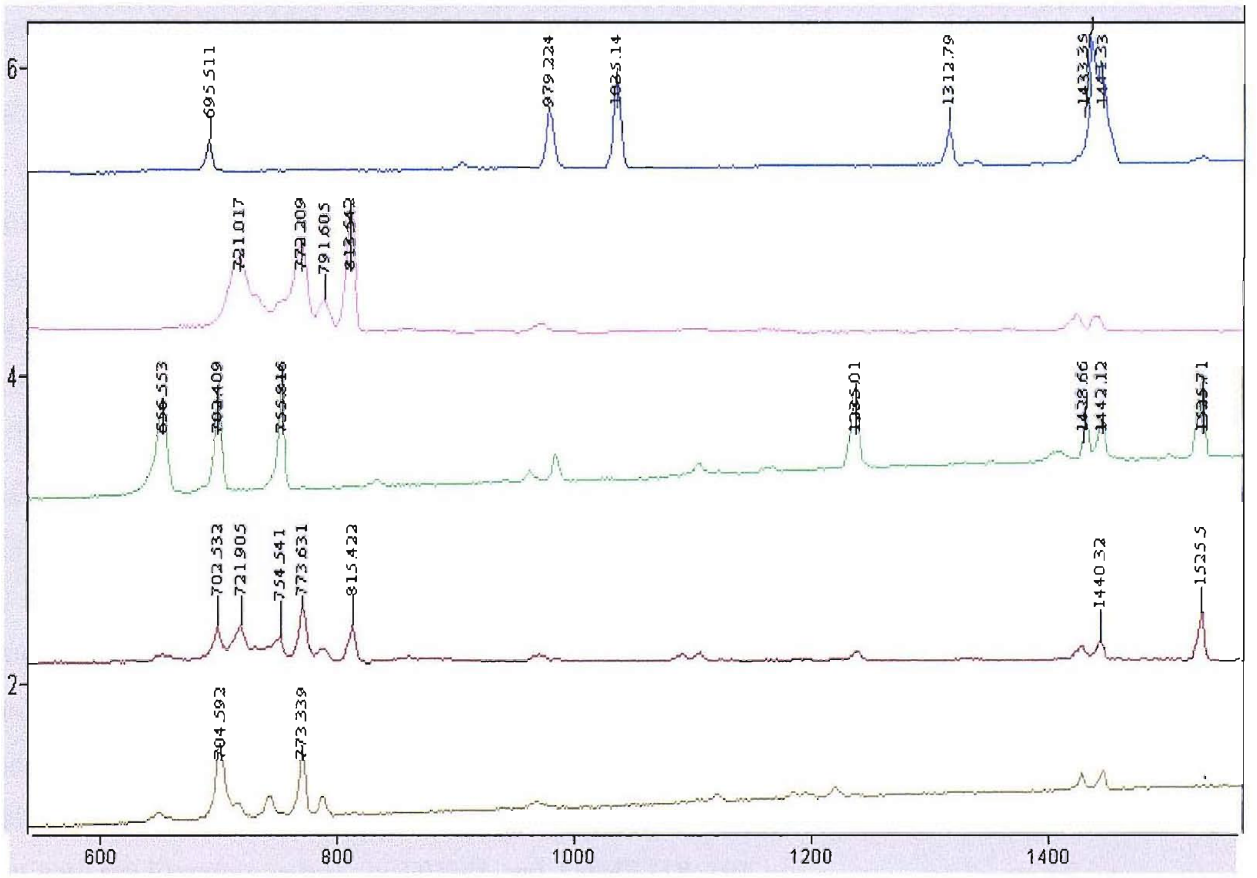

Figure 4.20- Low wavenumber IR spectra of DMS (blue line), MDMS (green line), DDMS (dark yellow line) and mixtures obtained from DMS:Cl_2 (pink line) and MDMS:Cl_2 (wine red line) in 1:2 molar ratio in a nitrogen matrix

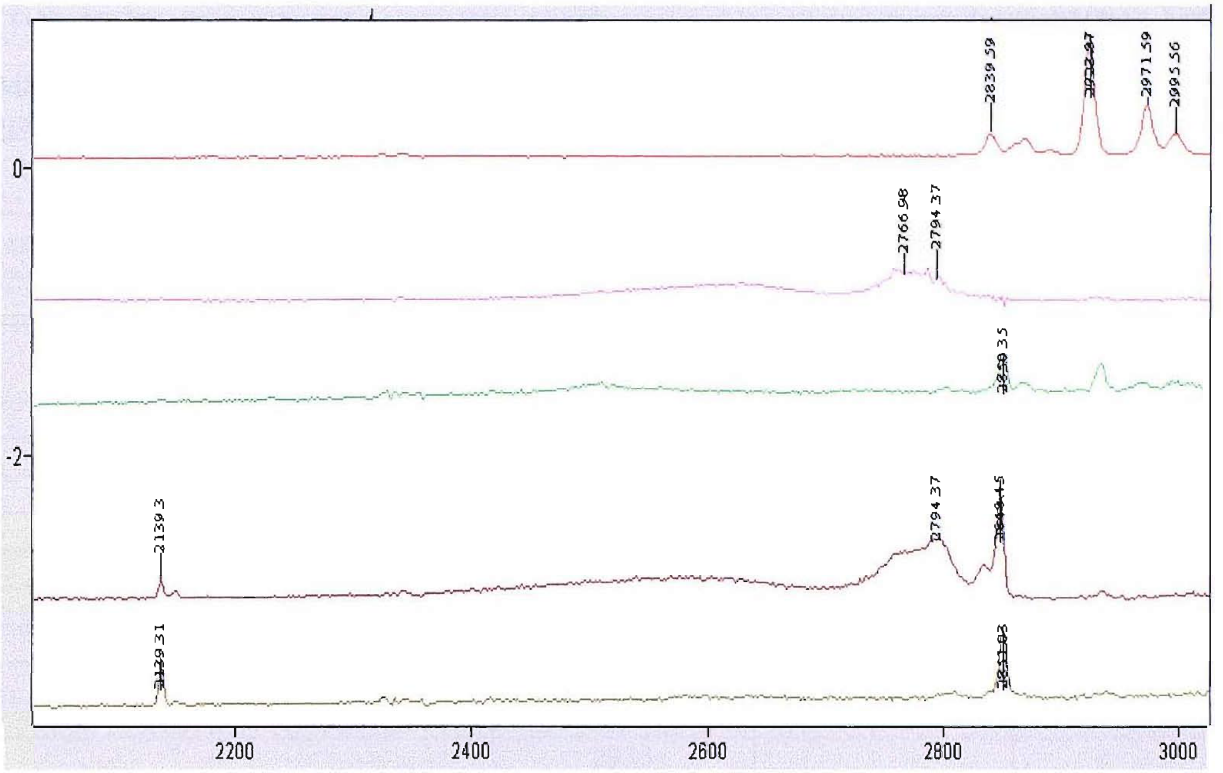

Figure 4.21- High wavenumber IR spectra of DMS (red line), MDMS (green line), DDMS (dark yellow line) and mixtures obtained from DMS:Cl_2 (pink line) and MDMS:Cl_2 (wine red line) in 1:2 molar ratio, isolated in a nitrogen matrix

The first important evidence is that the spectra obtained for the reaction between DMS with Cl_2 and for the reaction between MDMS with Cl_2 are different, consistent with different products being formed from the two reactions after the same amount of time. It would be reasonable to expect a higher concentration of highly chlorinated DMS species if MDMS is chosen as starting reactant instead of DMS. Despite this, an important spectral observation is that while the spectrum of DMS+Cl_2 bears no traces of residual DMS, the spectrum of MDMS+Cl_2 still shows bands associated with MDMS, such as, for example, those at 775 or at 14441 cm^{-1}. All the main MDMS bands can be traced in the MDMS+Cl_2 spectrum, even if with a much lower intensity. For the bands at 702, 1526 or 2850 cm^{-1}, MDMS contributes only partially- as can be seen from the intensity of other MDMS bands like those at 657 or 1235 cm^{-1}. Therefore, the bands observed from the MDMS + Cl_2 reaction whose wavenumber values have been reported in Figure 4.25 and 4.26 are due also to a reaction product being formed.

Finally, in the DMS+Cl_2 spectrum the contribution of DDMS is negligible, as can be seen by the absence of the bands at 705 and 2851 cm^{-1}.

Table 4.9 reports the most significant bands of the DMS+Cl_2 and the MDMS+Cl_2 spectra and compares them with the literature values for DDMS and TDMS [18, 19].

Table 4.9- Frequency values of the most intense bands measured in a nitrogen matrix for the DMS+Cl_2 and MDMS+Cl_2 reactions, compared with the MDMS, DDMS and TDMS frequencies

DMS+Cl_2 exper. frequencies (cm^{-1})	MDMS+Cl_2 exper. frequencies (cm^{-1})	MDMS exper. frequencies (cm^{-1})	DDMS exper. frequencies (cm^{-1})	TDMS literature frequencies (cm^{-1})
		655	653	
	702	702	704	
721	**721**			722
	754	756		
772	**773**		773	774
791				793
813	**815**			815
		983		
		1104		
		1235	1218	
1420		1429	1425	1420
1435	**1440**	1444	1442	1435
			1684	
	2139		2139	
			2326	
	2848	2851	2851	
		2933		

It is clear that all of the most intense bands observed in the spectrum of the DMS+Cl_2 reaction can be associated with TDMS. On the other hand, among the most intense bands observed from the MDMS+Cl_2 reaction, there are some bands attributable to DDMS and even some to unreacted MDMS: it is quite surprising to observe how the latter reaction seems to proceed more slowly to give TDMS than the DMS + Cl_2 reaction. However, as was pointed out earlier, the correspondence between the bands observed from the MDMS + Cl_2 reaction and the MDMS or DDMS bands does not mean that there are no new products being formed which share vibrational band positions with MDMS or DDMS. It is possible that highly chlorinated DMS species can present very similar IR patterns.

b) DMS and Cl_2 in equimolar ratio

The IR spectra recorded for MDMS and for DMS+Cl_2 when the reactants were initially in a 1:1 molar ratio are reported in Figures 4.22. In these experiments, argon was used as the matrix gas, and the deposition time was 30 minutes for both spectra.

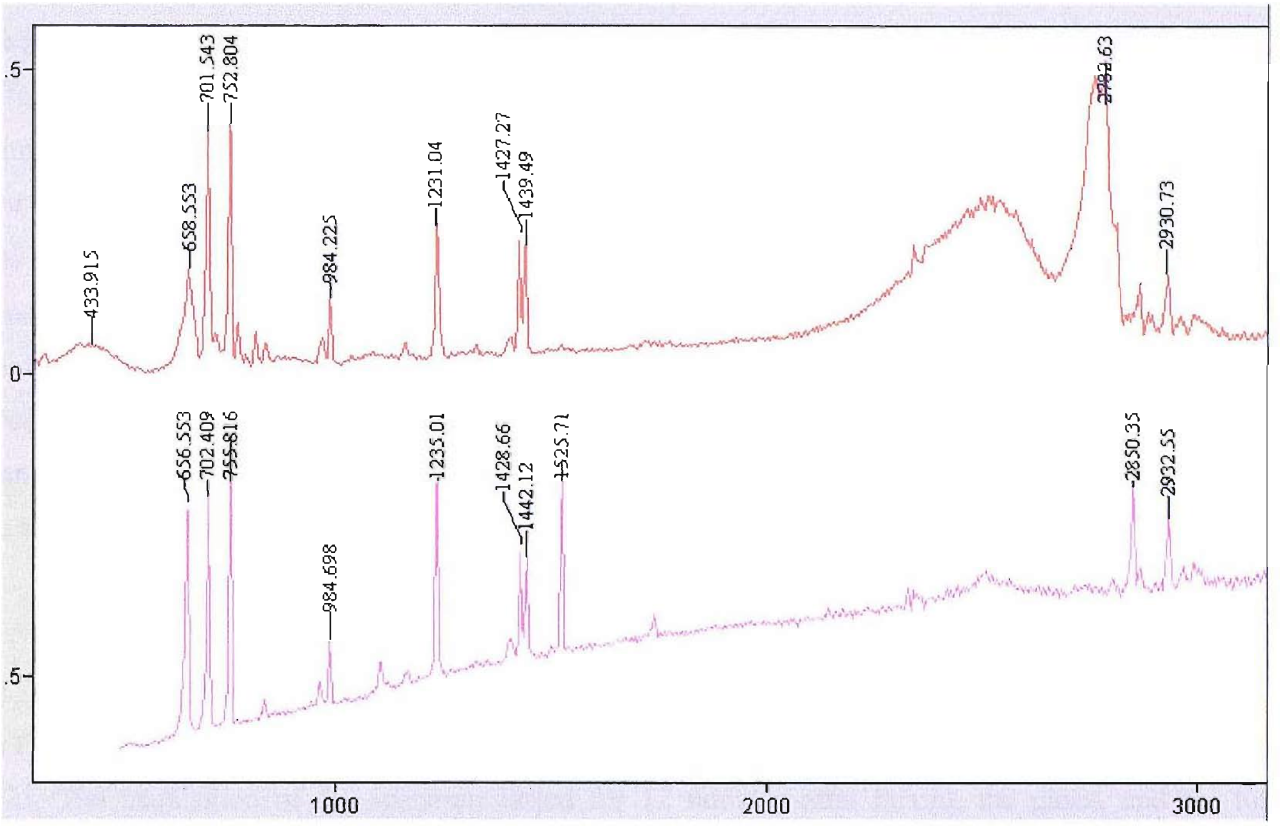

Figure 4.22- IR spectrum of the DMS+Cl_2 reaction starting from a 1:1 molar ratio (red line) compared with the spectrum of MDMS (pink line) recorded in an argon matrix after 30 minutes of deposition

As can be seen immediately, the results of the reaction between DMS and Cl_2 reproduce what was obtained in the gas phase, that is the formation of MDMS and HCl as the only reaction products. In the spectra, the only difference- apart from the absorptions due to water present in the MDMS sample (band at 1525 cm^{-1})- is the presence of two broad bands centred around 2600 and 2800 cm^{-1}, which could be attributed to HCl polymers [20].

For an equimolar ratio, DMS+Cl_2 leads therefore mostly to MDMS, as has already been found by FT-IR and UV measurements in the gas-phase (see Sections 4.5.1 and 4.5.2).

4.4.3 FT-ULTRAVIOLET RESULTS

The different parameters that can be chosen for this study are the molar DMS:Cl_2 ratio, the introduction order into the mixing cell, the total pressure and the time allowed before measuring a spectrum of the mixture.

The order of introduction is important mainly for spectra acquired at low mixing times: after that, the effect of the equilibrium makes mixtures in which DMS is introduced first almost indistinguishable from those where Cl_2 is introduced first, and only the molar ratio becomes important.

For a constant molar ratio, the total pressure affects mostly the intensity of the band associated with the gas in excess. It was found experimentally that total pressures above 20 mbar are less favourable than those between 10 and 20 mbar, because longer times were needed at the higher pressures to reach the same extent of the reaction: this created problems in the stability of the background, and therefore produced a spectrum affected by a higher level of noise.

For a chosen molar ratio and total pressure, spectra acquired at different times after the gas mixing will be reported to give an idea of the extent of the reaction.

a) DMS in slight excess

A FT-UV spectrum acquired when a DMS:Cl_2 ratio of about 1.4: 1 was studied is reported in Figure 4.23. The acquisition of the spectrum lasted for 12 minutes after mixing the gases, and the total pressure was set at around 3 mbar.

To facilitate the assignment, FT-UV spectra of DMS and MDMS have been added to the graph: they are reported respectively in pink and red line.

No significant bands were observed below 40,000 cm^{-1} or above 47,000 cm^{-1} (where the noise affecting the signal was very strong).

From the spectrum it is evident that under these conditions the mixture consists mostly of monochloro DMS, plus a small amount of unreacted DMS, as can be seen from the presence of the sharp band at around 43,800 cm^{-1}. Spectra acquired for shorter times after the mixing are not reported, as the signals of the products are weaker.

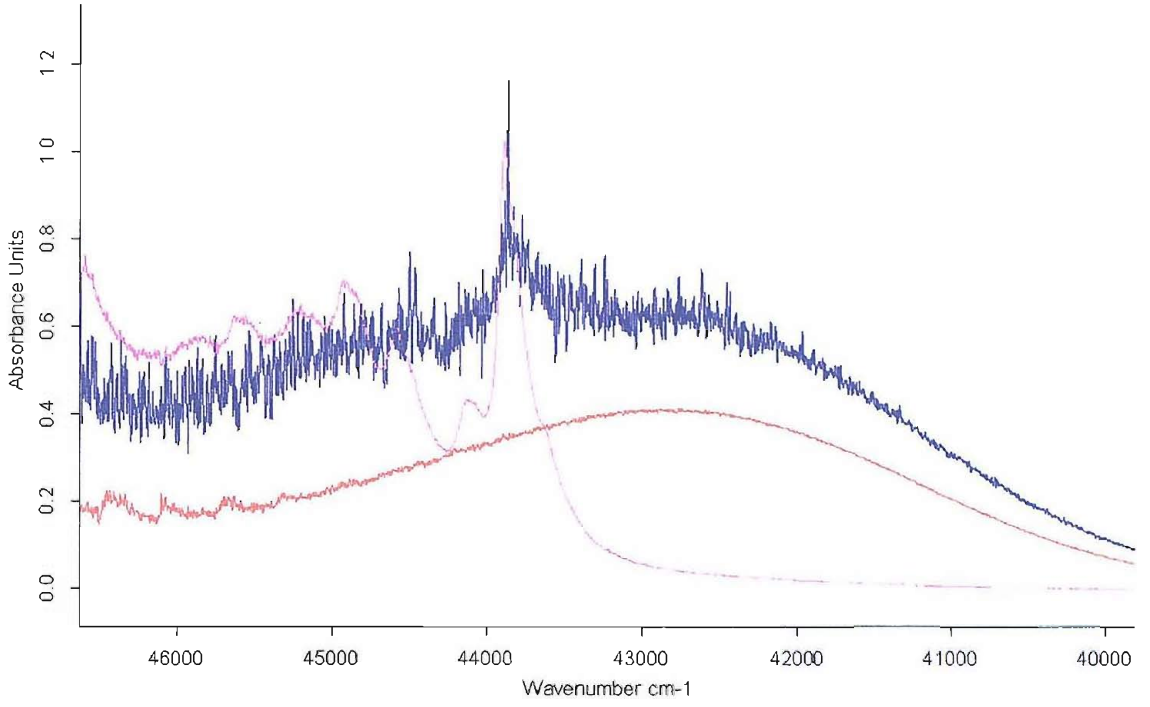

Figure 4.23- FT-UV spectrum of the DMS+Cl_2 reaction (blue line) acquired for a 1.4: 1 DMS/Cl_2 molar ratio, after a period of 12 minutes after the mixing of the gases. DMS and MDMS spectra are shown as pink and red traces respectively

b) Cl_2 in slight excess

A FT-UV spectrum acquired in the 29,000-47,000 cm^{-1} region for a mixture of Cl_2: DMS with a molar ratio approximately 1.4: 1 is reported in Figure 4.24. The total pressure was set at 3 mbar, and the acquisition lasted for 9 minutes after the mixing of the gases.

Also in this case, spectra of MDMS (red line) and DMS (pink line) have been added to the figure to facilitate the interpretation of the spectrum of the mixture (blue line). MDMS is still the predominant species, but a small amount of chlorine is still visible (the weak band at around 30,000 cm^{-1}); despite the high level of noise above 43,000 cm^{-1}, no bands associated with unreacted DMS can be clearly found. It can also be noted that the weak plateau between 36,000 and 38,000 cm^{-1} indicates an initial formation of a product of the reaction: evidence for the identity of this feature can be obtained at higher Cl_2:DMS ratios.

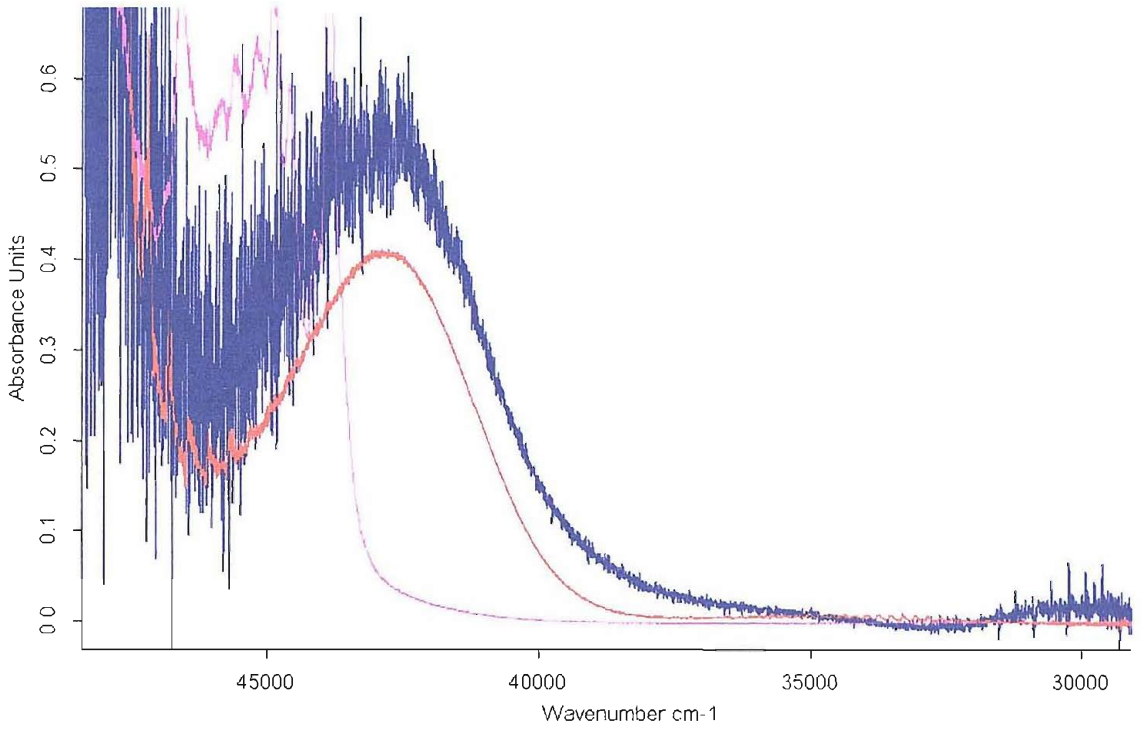

Figure 4.24- FT-UV spectrum of the DMS+Cl_2 reaction (blue line) acquired for a 1.4 Cl_2/DMS molar ratio, for a period of 9 minutes after the mixing of the gases. DMS and MDMS spectra are shown as pink and red traces respectively

c) Cl_2 in large excess

A FT-UV spectrum of a Cl_2:DMS mixture with molar ratio of about 1.8: 1 is reported in Figure 4.25.

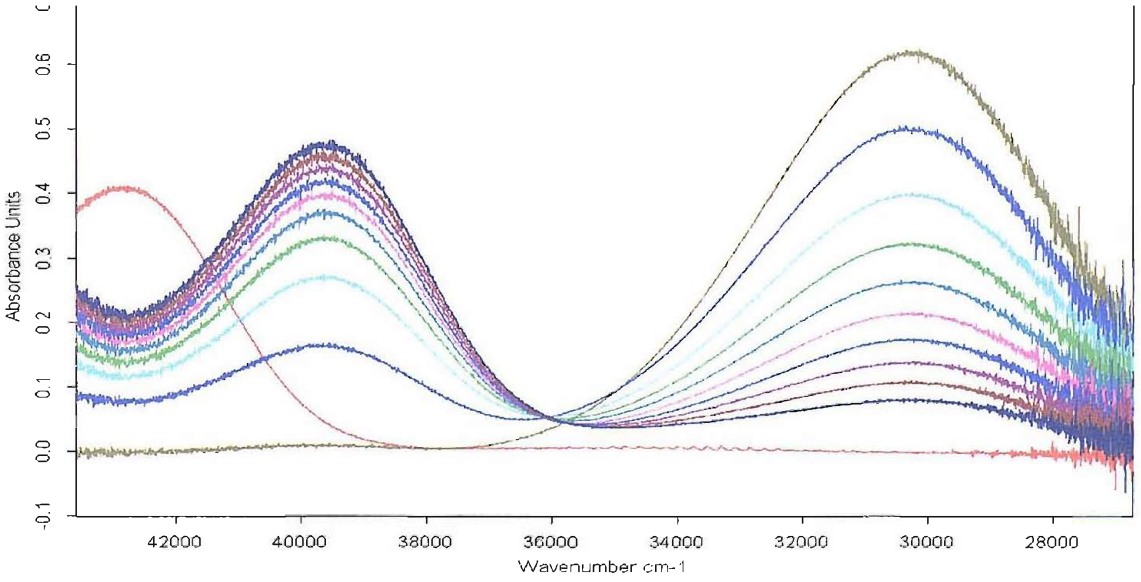

Figure 4.25- FT-UV spectra of a Cl_2/DMS mixture with initial molar ratio 1.8: 1 and total pressure 15 mbar acquired at increasing times (from 2 to 20 minutes) after the mixing. A spectrum of MDMS is reported for comparison (red trace)

The red line represents the spectrum of MDMS, inserted for comparison with the other bands. The dark yellow spectrum is the one acquired for the first two minutes immediately after mixing the gases, then all the other spectra were acquired successively every two minutes, until the dark blue spectrum, acquired 18 minutes after the mixing was obtained.

As can be seen from Figure 4.25, successive spectra show a marked decrease of the Cl_2 band at around 30,000 cm^{-1}, and in parallel there is a steady increase of the band centred at around 39,500 cm^{-1} which, from a comparison with the superimposed red spectrum, cannot be assigned to MDMS, or to DMS. The assignment of this latter band will be discussed later.

It is worth noticing that chlorine is still present as an unreacted molecule even 20 minutes after mixing it with DMS and that the band associated with the product slowly increases in intensity. This indicates that at the pressure used in this experiment (total pressure 15 mbar) chlorine consumption is unexpectedly slow. The reaction advances almost to completion in 14 minutes if a lower total pressure is investigated: Figure 4.26 represents the spectra obtained for the same Cl_2:DMS molar ratio (1.8: 1) but with a total pressure of just 8 mbar.

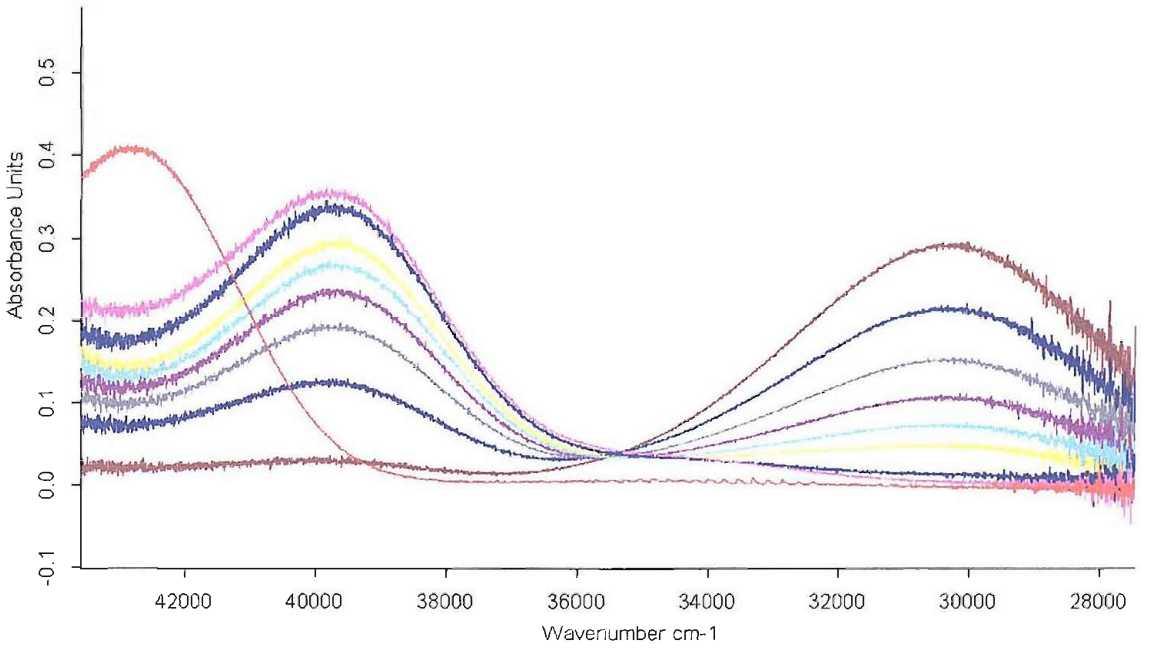

Figure 4.26- FT-UV spectra of a Cl_2/DMS mixture with initial molar ratio 1.8: 1 and total pressure 8 mbar acquired at increasing times (from 2 to 16 minutes) after the mixing. A spectrum of MDMS is reported for comparison (red line)

To definitely highlight the different nature of the product arising from the DMS+Cl_2 reaction from DMS and MDMS, Figure 4.27 compares the spectrum from the reaction with those of MDMS and DMS in the 46,000-38,000 cm^{-1} range.

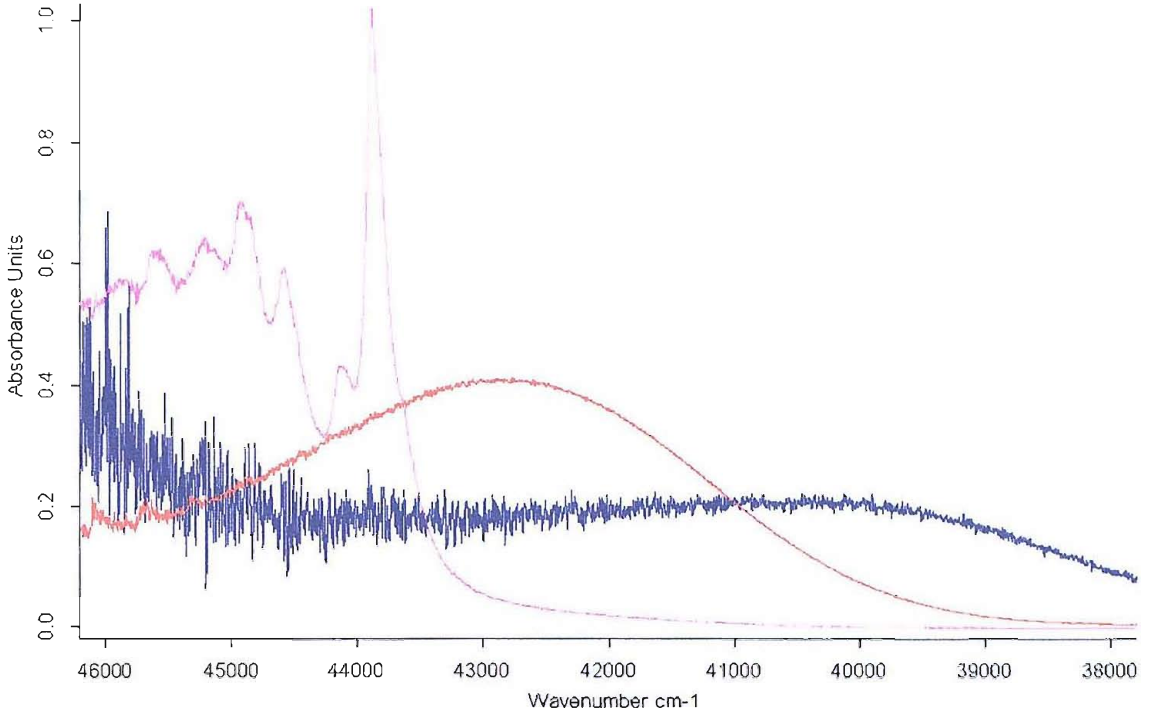

Figure 4.27- FT-UV spectrum of the DMS+Cl_2 reaction (blue line) acquired for a 1.8: 1 Cl_2/DMS molar ratio, for a total pressure of 4 mbar. DMS and MDMS spectra are shown as pink and red lines

In the absence of any direct UV spectral information on chlorinated DMS species with more than one chlorine atom, it is impossible to assign the band arising from the DMS+Cl_2 reaction to dichloro DMS, trichloro DMS or tetrachloro DMS. It might be expected, if a Cl_2:DMS molar ratio below 1.5 yields mostly MDMS, the next compound to be formed and detected should be DDMS, which then should be responsible for the observed broad band with maximum between 39,500 and 40,000 cm^{-1}. Nevertheless, IR data- see Sections 4.5.1 and 4.5.2- recorded for the reaction under the same experimental conditions seem to indicate that TDMS is the predominant species produced in a closed cell when DMS and chlorine are mixed, with Cl_2 in excess with a molar ratio close to 1: 2.

It is therefore concluded that the reaction proceeds to MDMS for molar ratios Cl_2: DMS below 1.5, while above this value TDMS is preferably formed.

4.4.4 PHOTOELECTRON SPECTROSCOPY RESULTS

The gas-phase PES experiments used a different inlet system and mixing arrangement: instead of mixing the gases in a static cell and then acquiring the spectrum of the mixture at different times, the gases were continuously flowed towards the photoionization point, and this situation, even when an inlet system with a small opening to connect the mixing volume and the photoionization region was used, allowed the study of the mixture under conditions in which the degree of the reaction was much lower because the detection occurred few milliseconds after the molecules were effectively mixed. It was assumed that in the pressure range used, a mixing distance of 1 cm corresponded roughly to a contact time of 0.5 ms with an open outer inlet tube.

Studies with PES have focused mostly on DMS+Cl_2 with a slight excess of DMS. Under these conditions, the first chlorination step, DMS+Cl_2 → MDMS+HCl, was studied.

The results will be presented first with a constant initial DMS:Cl_2 ratio, as determined by their partial pressures: this ratio was set at around 1.3 (1.0 for the 0.5 mm exit hole system), so as to have a slight excess of DMS in order not to go past the first chlorination step. The total pressure was set between 7 and $8 \cdot 10^{-5}$ mbar, as measured by the ion gauge on the side of the ionization chamber: even if the pressure in the reaction cell is expected to be in practice ca. $5 \cdot 10^{-4}$ mbar [21], this value is still several orders of magnitude lower than in the other gas phase spectroscopic measurements (Sections 4.5.1-4.5.2).

Each set of results is obtained with a particular exit hole aperture of the inlet system, with spectra acquired at different mixing distances superimposed in the same figure to observe clearly the changes in intensity of the PE bands.

a) 0.5 mm exit hole

This is the narrowest aperture for the inlet system used in this work; it is expected that the largest contact time of the gases can be achieved with this arrangement, especially for long mixing distances. A series of photoelectron spectra at different mixing distances is reported in Figure 4.28; for this inlet system, the initial DMS:Cl_2 ratio was set as approximately 1.0.

The first evidence is that under these conditions there is almost no change in the band intensities when the mixing distance is changed. The only change is the dropping to zero when the distance passes from 0 to 10 cm of the very weak bands with VIEs at 9.7 and 10.6 eV. This is an important result and the

behaviour of these bands will be clarified when spectra with larger exit holes are considered (see next paragraphs). All the other bands remained constant with changing distances.

The band at 8.72 eV is assigned to unreacted DMS, while the out-of-scale band centred at 12.70 eV is due to HCl being formed from the reaction.

The band with VIE at 9.36 has a shoulder at about 9.18 eV, while that with VIE at 11.20 eV has a shoulder at ca. 10.97 eV. Finally, the band with VIE at 11.96 displays a shoulder at around 11.71 eV.

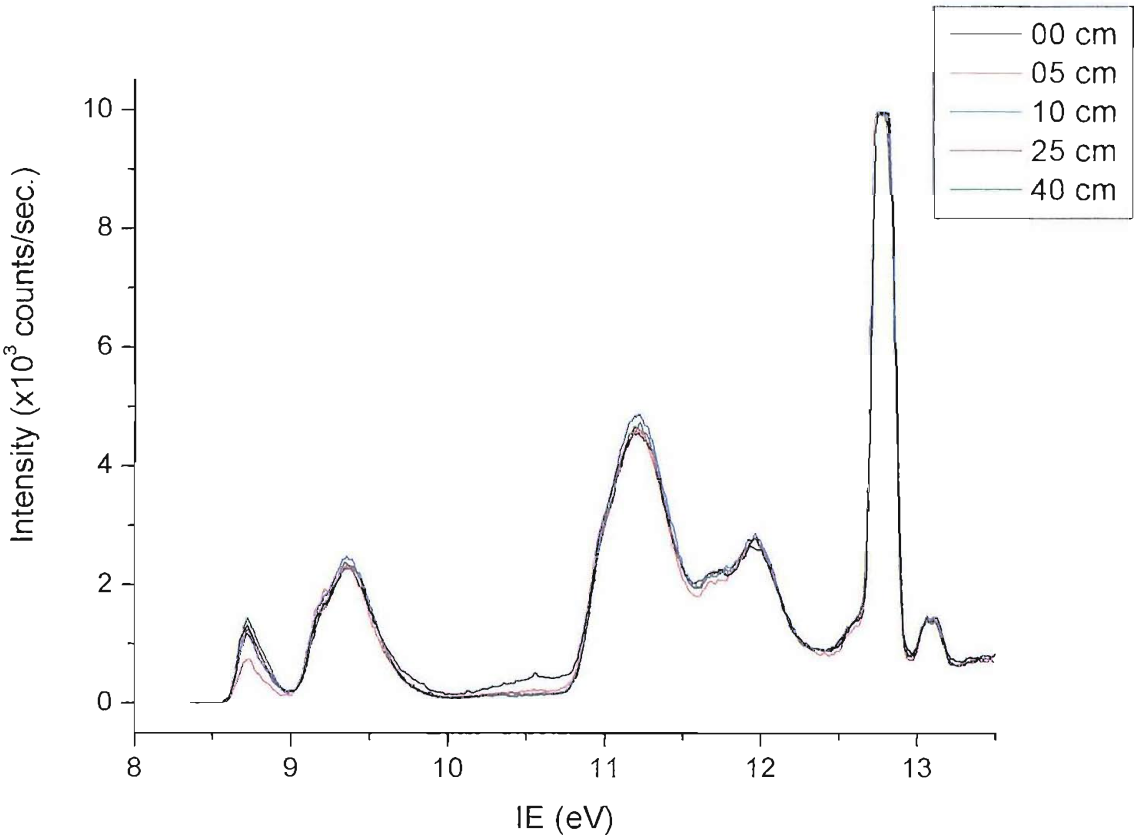

Figure 4.28- PE spectra of DMS+Cl_2 mixtures with a 0.5 mm exit inlet system at different mixing distances

All the observed PE bands can be assigned to MDMS and DDMS: comparing the spectra obtained (Figures 4.10, 4.12 and 4.17) and the values of the calibrated bands (Table 4.4 and 4.6), it can be seen that the spectra obtained for the 0.5 mm mixing distance can be seen as a superimposition of DDMS and MDMS. The band at 9.36 eV can be identified as the DDMS first band (VIE at 9.32 eV) with the shoulder at 9.18 eV corresponding to the MDMS first band (VIE at 9.17 eV); the band at 11.20 eV arises from an overlap of the DDMS second band (VIE at 11.21 eV) with the MDMS third band (VIE at 11.18 eV), while the shoulder at 10.97 eV is attributed to the MDMS second band (VIE at 10.98 eV). In the same way, the band at 11.96 eV is assigned to the DDMS fourth band (VIE at 10.92 eV), while

the shoulder at 11.71 eV can be attributed to the DDMS third band (VIE at 11.73 eV) as well as to some unreacted chlorine.

All the spectra can be then interpreted as composed of DDMS and MDMS, plus HCl and some unreacted DMS. For very short mixing distances, two additional weak bands at around 9.7 and 10.6 eV are observed.

b) Exit hole 1 mm

A series of spectra at different mixing distances recorded using a 1 mm exit inlet system is reported in Figure 4.29.

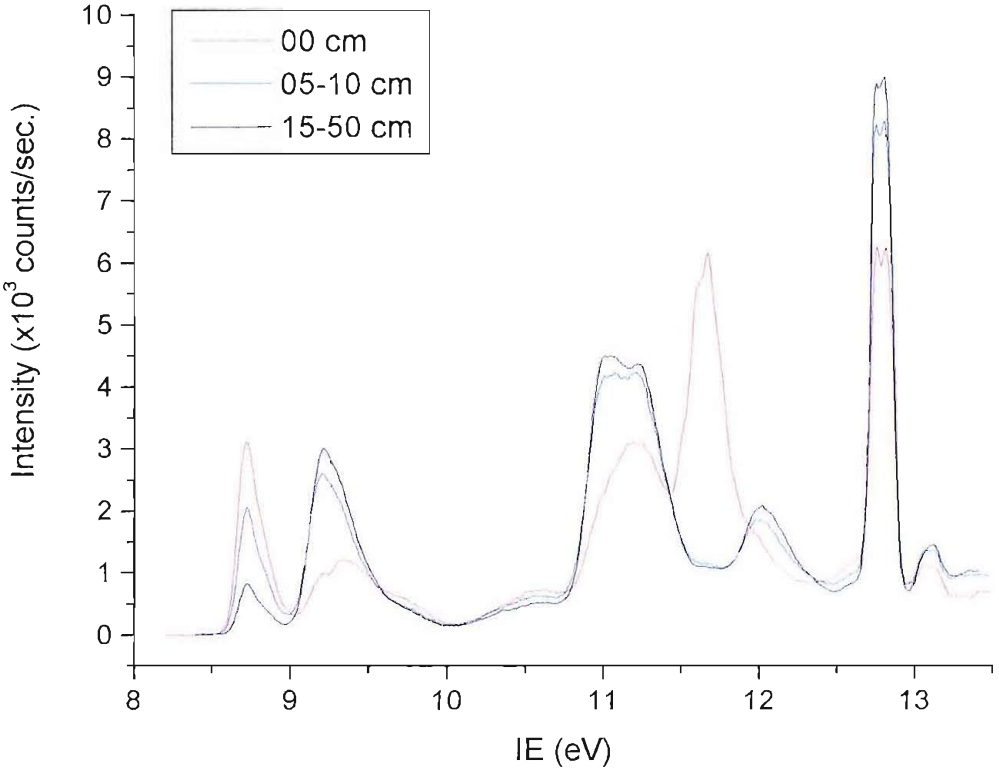

Figure 4.29- PE spectra of DMS+Cl_2 mixtures with a 1 mm exit inlet system at different mixing distances

In this situation the spectral changes are more evident when the mixing distance is changed between 0 and 20 cm; at mixing distances greater than 20 cm the spectra show no change. For this wider aperture in the inlet system, it is expected that the signals of the reagent gases will be seen at short distances: in fact the DMS signal (VIE at 8.72 eV) is strong at 0 cm and- though diminishing in intensity- is still present at long mixing distances. At 0 cm Cl_2 is also clearly visible (strong band with VIE at 11.69 eV): however its signal drops to almost zero already at a distance of 5 cm. This is not surprising, given the 1.3: 1 excess of DMS over chlorine.

The spectrum at 0 cm (red line) also displays the first HCl band (sharp doublet with VIE at 12.75 and 12.82 eV) and broad bands with VIEs around 9.40 eV (with a shoulder around 9.20 eV) and 11.20 eV. These bands can be attributed to a MDMS/DDMS mixture. Finally the bands centred at 9.70 and 10.60 eV are more intense than with the 0.5 mm exit hole arrangement. Their intensity decreases but does not vanish when the mixing distance is increased.

The spectra at longer distances (black and blue lines) show no Cl_2 contribution, while the bands associated with HCl increase regularly and those of DMS decrease regularly; also the unassigned bands at 9.70 and 10.60 eV decrease regularly. The bands centred at 9.40 and 11.20 eV, on the other hand, change their shape as they increase in intensity when the mixing distance is changed: at long mixing distance the first band has VIE at 9.18 eV with a shoulder around 9.36 eV, and the second is centred at 10.97 eV with a shoulder around 11.20 eV: this appearance is the reverse of that observed with the 0.5 mm exit tube.

The indication is that in this case MDMS is the predominant species, with a lower contribution from DDMS: the result is consistent with the fact that a wider aperture (and also a higher DMS:Cl_2 ratio) should lead to a lower extent of molecular reaction, therefore towards single chlorination of DMS.

A plot of the relative intensities of the bands with increasing mixing distance is reported in Figure 4.30. The plot has been obtained considering the areas of the bands: this was possible by simulating the bands with Gaussian profiles and measuring the integrals for such simulated bands. The simulation was conducted by first fitting the Gaussian functions for each component separately (DMS, MDMS, etc.): the operation involved choosing the number of functions, their centred position and their width. The fitting was carried out using the OPUS program. The error bars reported in the graph in Figure 4.30 were obtained by simply considering the variation of the integral values for the band intensities from the four spectra that were acquired for each condition (exit hole size and mixing distance).

The overall results for the 1 mm exit inlet system suggest that for these conditions the main product-with HCl- of the DMS+Cl_2 reaction is MDMS.

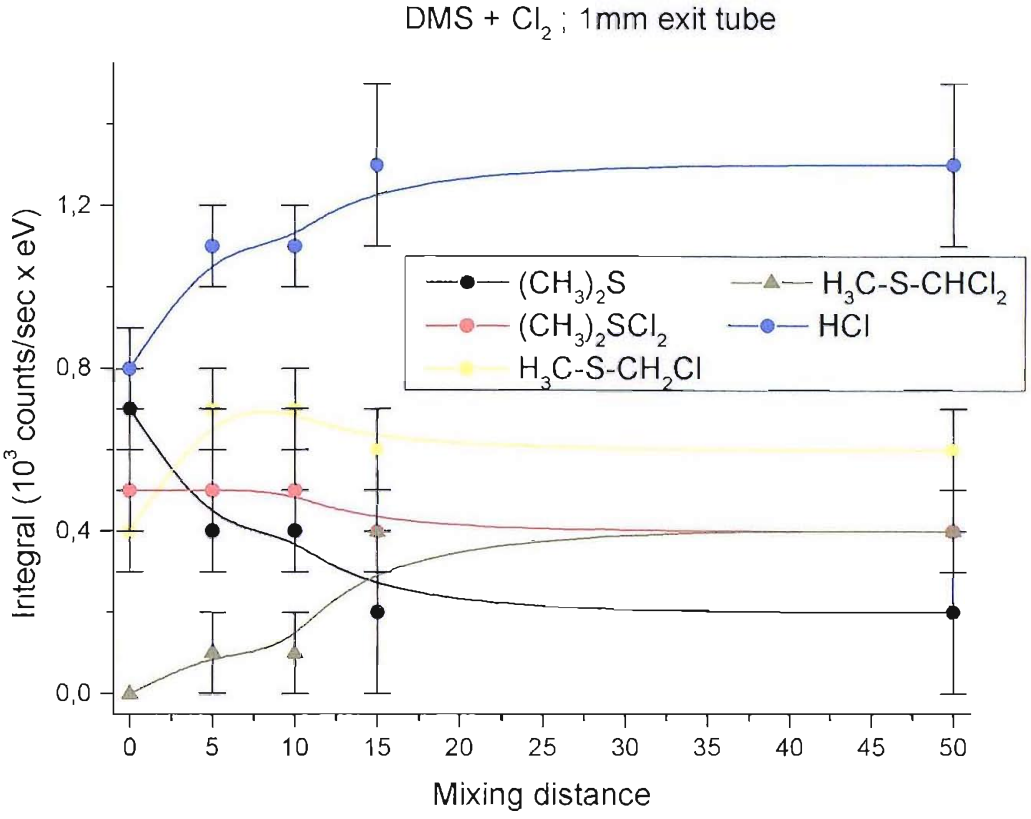

Figure 4.30- Plot of the relative areas for the bands of the species involved in the DMS+Cl_2 reaction studied by PES with a 1 mm exit size inlet system

c) Exit hole 2 mm

A series of spectra at different mixing distances recorded using a 2 mm exit inlet system is reported in Figure 4.31.

The results for the 2 mm inlet system are probably the most important, especially with respect to the unassigned bands: it can be seen that- in contrast to what happened with the 1 mm exit hole- these bands increase in intensity as the mixing distance increases from 0 to 25-30 cm, until they reach a maximum intensity. The calibration of these bands gives VIEs at 9.69 and 10.62 eV.

The other important evidence is that when the mixing distance increases from 0 to 25 cm, these bands are the only ones that increase in intensity, even more than the HCl first bands (the doublet at 10.75 and 10.83 eV), whose increase is much less pronounced. Considering the fact that the first band of HCl has a high photoionization cross section (by measuring spectra of the single compounds at the same pressure, it was found that HCl bands are three times more intense than MDMS bands), such a low signal suggests that HCl is formed in very limited amount for mixing distances shorter than 25 cm. On

the other hand, a constant decrease of the DMS and (not reported in Figure 4.31 due to the scale chosen) of Cl_2 signals are observed.

The clear indication is that for the early stages of the DMS + Cl_2 reaction, assured by the wide exit hole and by the short mixing distances, no HCl or MDMS are formed. The consumption of DMS and chlorine is then due to the formation of a DMS-Cl_2 reaction intermediate characterized by PE bands with VIEs at 9.69 and 10.62 eV.

This species is a reaction intermediate: in fact, its bands decrease for mixing distance above 25 cm. After this distance, bands of MDMS (VIEs at 9.18 and 10.97 eV) and HCl start to appear and grow in intensity- first rapidly then much slower- while the bands of DMS and Cl_2 decrease dramatically.

Still, the fact that the reaction intermediate is observed at very long mixing distances and in an open tube (see following section) shows that such an intermediate has a very long lifetime (tens of milliseconds, according to the 1cm=0.5 ms relation [12] for the conditions used); this tends to exclude that it is a weakly bound complex, such as DMS:Cl_2 as suggested in the literature from matrix isolation evidence [9].

A plot of the relative intensities of the bands with increasing mixing distance is reported in Figure 4.32. From Figure 4.32 it is evident the behaviour displayed by the bands associated with the DMS-Cl_2 species is consistent with a reaction intermediate, while bands of MDMS and HCl show a typical behaviour for stable reaction products (the slight decrease for the HCl integral at long distances is a statistical error due to the difficulty of fitting such a narrow, doublet-shaped band).

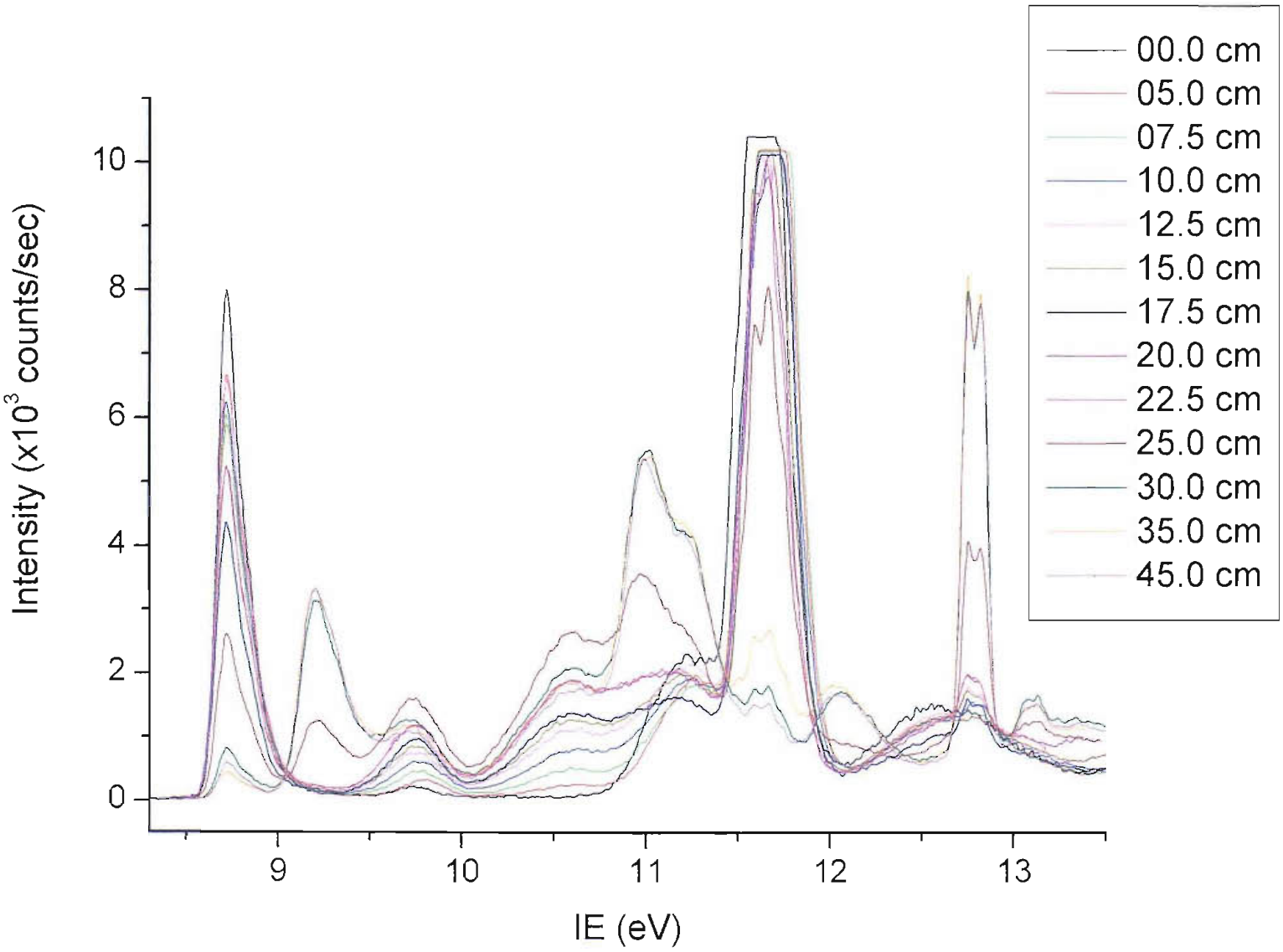

Figure 4.31- PE spectra of DMS+Cl_2 mixtures with a 2 mm exit inlet system at different mixing distances

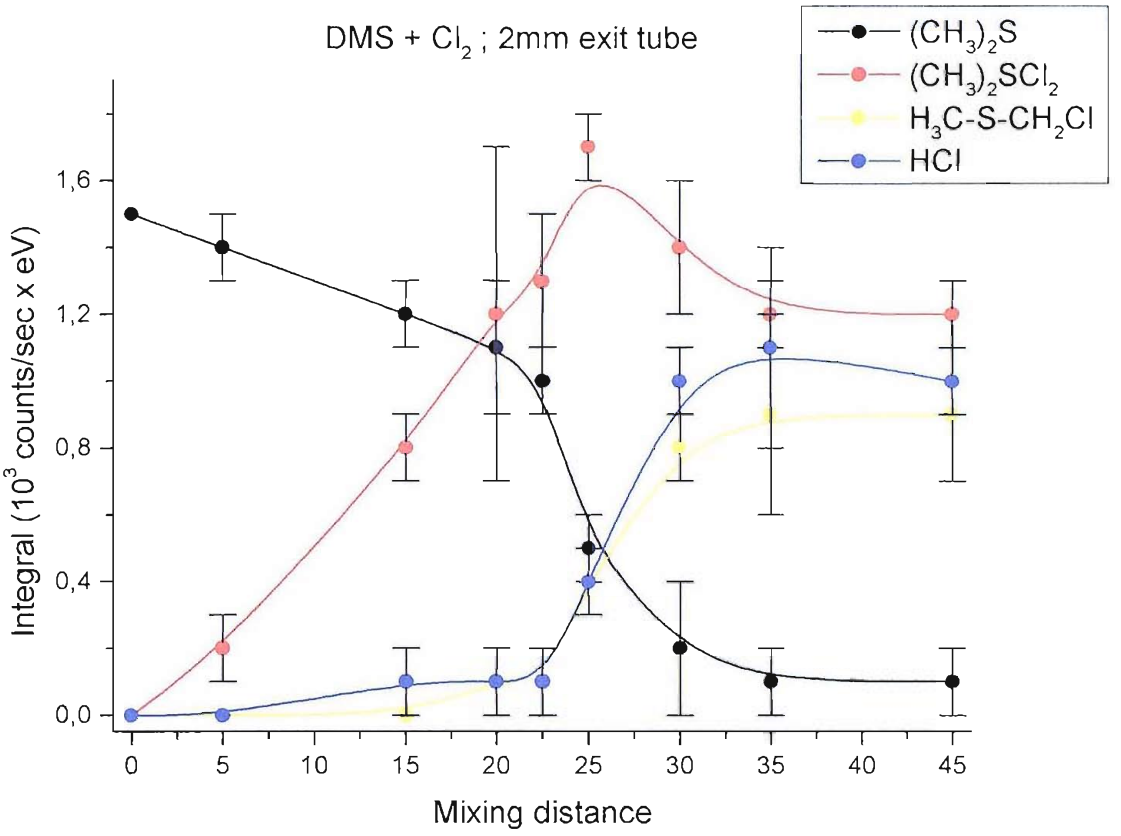

Figure 4.32- Plot of the relative areas for the bands of the species involved in the DMS+Cl_2 reaction studied by PES with a 2 mm exit size inlet system

The trends of the relative band intensities with mixing distances in Figure 4.32 matches the trends observed for the 1 mm exit tube: in that case it was seen that the bands associated with a reaction intermediate diminish at increasing distance while the MDMS and HCl bands increase. Empirically, it is possible to view the plot for the 1 mm exit hole as a continuation of the 2mm plot on the long distance side: if this assumption is made, it is possible to extrapolate the behaviour of the bands to very long mixing distances. In that case, the bands associated with a reaction intermediate will disappear while the MDMS bands will increase until they will decrease due to DDMS formation (as it was seen for the 0.5 mm exit hole). The HCl signal will keep on increasing until all the protons on the DMS structure have been removed.

Support for this hypothesis will be presented by the behaviour of the relative band intensities for a wider exit hole, that is for the low mixing distance side of the plot of Figure 4.32.

d) Open tube

To study the behaviour of this reaction at short reaction times, a tube with no restriction at its end was used: this was equivalent to a 1 cm opening. A sequence of spectra obtained with this open tube for increasing mixing distances is reported in Figure 4.33.

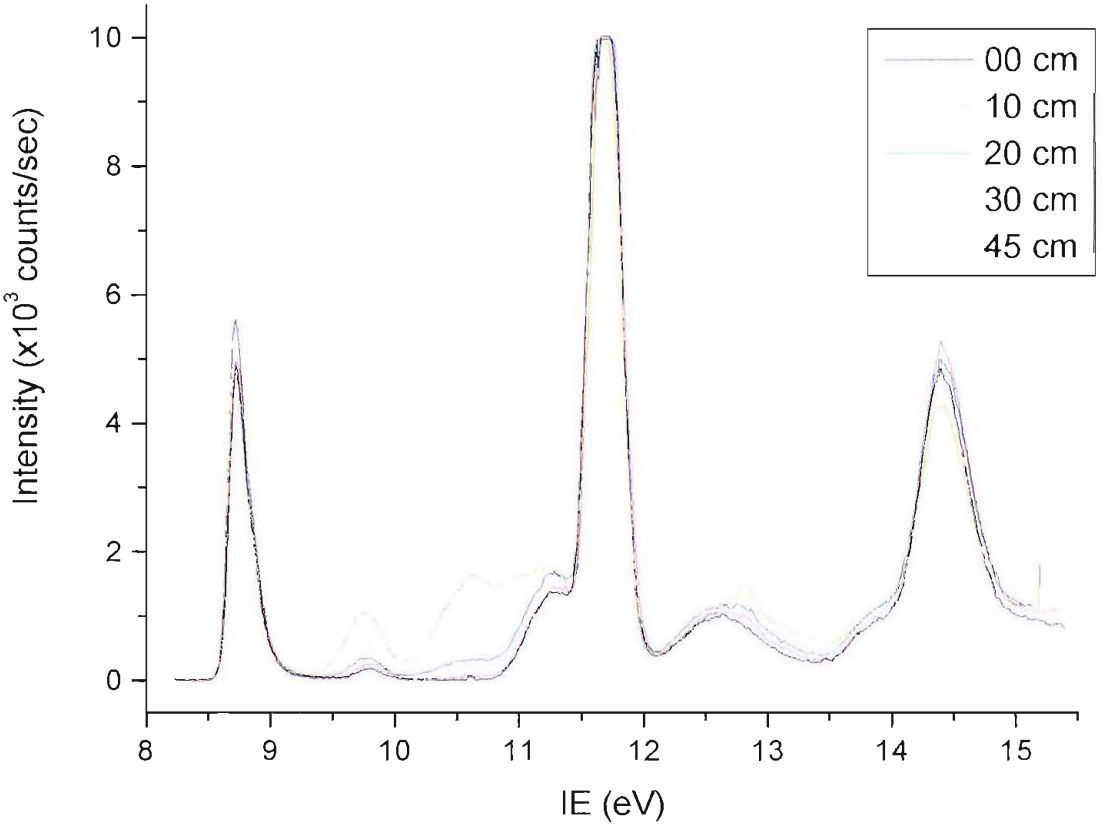

Figure 4.33- PE spectra of DMS+Cl_2 mixtures with a open exit inlet system at different mixing distances

The spectra show almost unchanged DMS bands (VIEs at 8.72, 11.29 and 12.66 eV), a moderate lowering of the second band of Cl_2 (VIE at 14.40 eV; the first band is the one out of scale one at VIE 11.69 eV), and a marked increase of the intensity of the intermediate bands at 9.69 and 10.62 eV occurs. Significantly, no bands of MDMS and HCl (apart from a small trace beyond 30 cm) can be found. This confirms that the first product of the reaction is not MDMS or HCl but a different molecule.

A plot of the relative areas of the bands as a function of the mixing distance is reported in Figure 4.34.

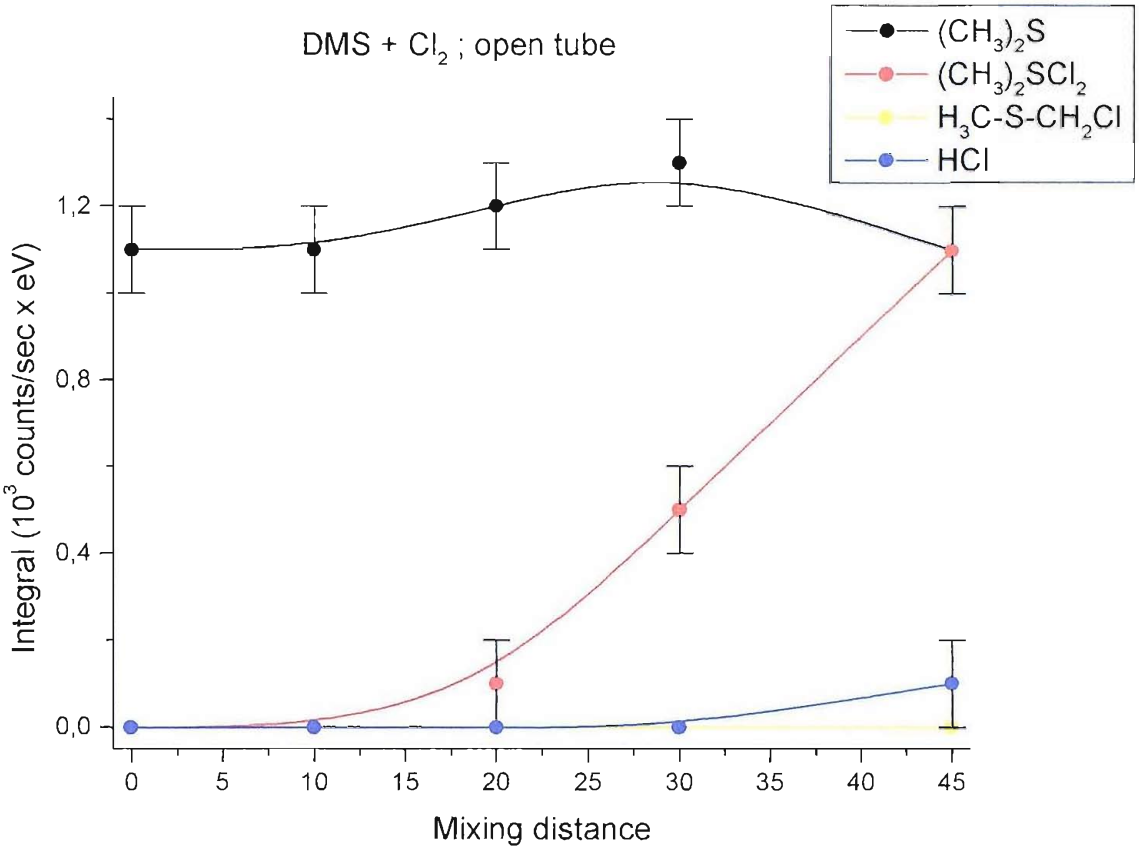

Figure 4.34- Plot of the relative band areas of the species involved in the DMS+Cl_2 reaction studied by PES with an open exit inlet system

The behaviour expected for the low distance side of the plot of the 1 mm exit hole (see Figure 4.32) is a slow decrease of the reactant bands (DMS and Cl_2), no formation of the stable products (HCl and MDMS) and a steady increase of the intermediate species. Considering the negligible the amount of HCl formed, the only unexpected part of the experimental plot is the stability of DMS signal (with a slight increasing fluctuation); nevertheless, this is not completely a genuine result, as for the open tube the control on the pressure of the reacting gases was more difficult. The plot therefore does not contradict the expected behaviour for DMS, that is a slow decrease as the reaction intermediate is formed.

e) Variable molar ratio and fixed mixing distance

Instead of keeping fixed the molar ratio and varying the mixing distance, an experiment was carried out by keeping the mixing distance fixed and altering the molar ratio: this was achieved by keeping the DMS pressure fixed and increasing (and subsequently decreasing, to check the reproducibility of the

results) the pressure of chlorine to cover a wide molar ratio range. The spectra- reported in Figure 4.35- were acquired with the 1 mm opening inlet tube, at a mixing distance of 25 cm.

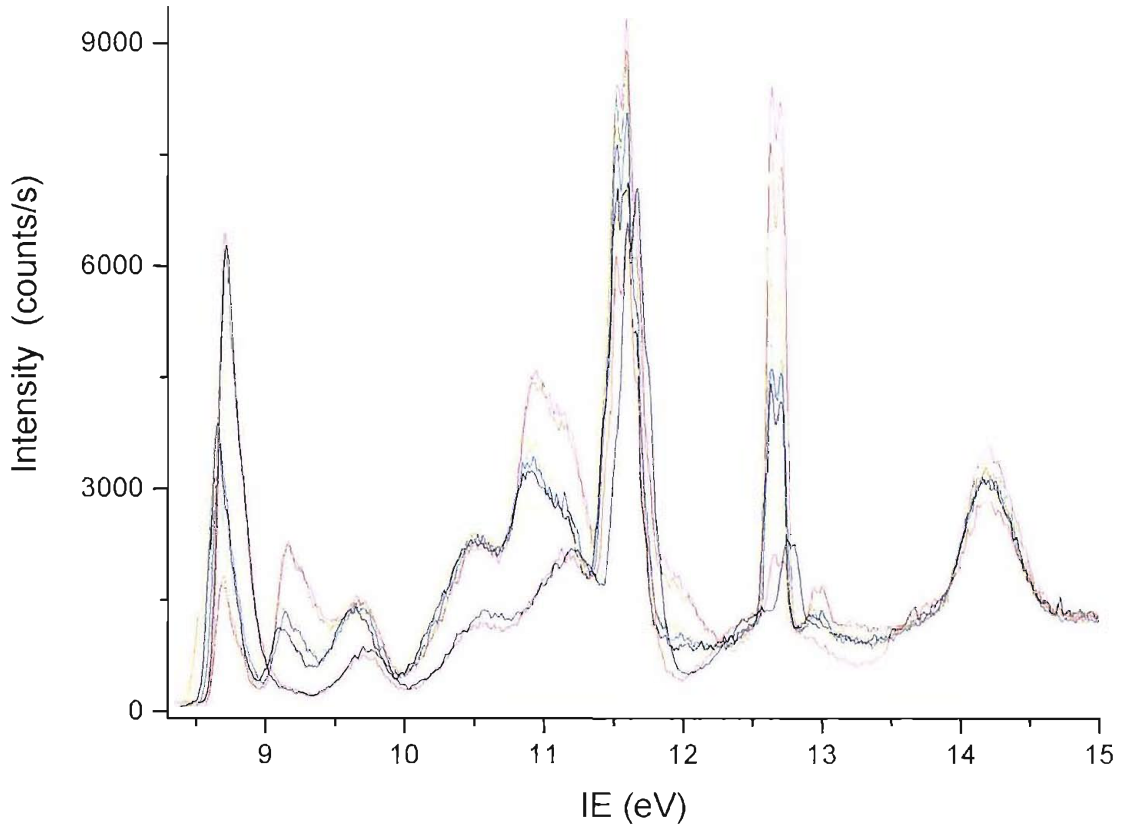

Figure 4.35- PE spectra of the DMS+Cl_2 reaction monitored- using a 1 mm exit hole system at a fixed mixing distance of 25 cm- by changing the Cl_2 pressure keeping fixed the DMS one

The results follow the expected behaviour: by increasing the chlorine pressure, the band of DMS (8.72 eV) decreases. The bands of Cl_2 (11.69 and 14.40 eV) slowly increase, because even if introducing more Cl_2 involves the start of the reaction, the additional Cl_2 introduced is not totally consumed. The initial slow decrease of the DMS bands is accompanied by the growth of the bands associated with the intermediate at 9.69 and 10.62 eV. This growth slows down markedly (and DMS decreases faster) when MDMS begins to be formed, as can be seen by the bands at 9.18 and 10.96 eV. For the highest values of the Cl_2:DMS pressure ratio, the bands of the intermediate show no increase in intensity, while MDMS signals are still growing.

No traces of DDMS can be seen: it is possible that the broadening of the first MDMS band can be due to the initial formation of DDMS (whose first band VIE is at 9.32 eV), but it must also be considered the overlap of this band with the low energy side of the first intermediate band: this can introduce an asymmetry in the MDMS first band by increasing its intensity on the high energy side.

4.4.5 SUMMARY OF THE EXPERIMENTAL RESULTS

By studying the reaction at different contact times and molar ratios, different stages of the DMS + Cl_2 reaction have been monitored in the gas-phase and in matrices with the UV, IR and PE spectroscopic methods.

For the gas mixed in a closed cell (i.e., a long contact time between DMS and Cl_2 before the detection), it was found that

- when DMS is in excess or when the two reactants are in equal ratio, monochloro DMS (MDMS) is the only reaction product clearly detected
- when Cl_2 is in excess, trichloro DMS (TDMS) is the main product of the reaction, while probably just a small amount of dichloro DMS (DDMS) is observed

In the PES studies, where a continuous flow of the reagent gases was used, earlier stages of the DMS+Cl_2 reaction are probed: this was always achieved by introducing DMS in a slight molar excess over chlorine. By varying the size of the exit hole of the inlet system and the distance between the mixing and the photoionization points, it was found that the reaction initially proceeds through an intermediate which is formed without any formation of MDMS or HCl. The bands associated with this intermediate (with VIEs at 9.69 and 10.62 eV) decrease just after HCl and MDMS begin to be formed and they are almost totally consumed when DDMS begins to be observed. From the experimental evidence, it seems that DDMS is preferentially formed from MDMS, and not from the intermediate, due to the fact that the major part of the intermediate is consumed when MDMS is the only species being formed. This suggest a stepwise mechanism

$$DMS + Cl_2 \rightarrow \text{intermediate} \rightarrow MDMS + HCl \rightarrow DDMS + HCl \rightarrow TDMS + HCl$$

Concerning the characterization of this intermediate, the absence of partner products suggests the formation of a structure of formula DMS_xCl_{2y}. This formula does not imply that a more rearranged structure is forbidden: it is possible that the intermediate can be due to a $MDMS_xHCl_{2y-x}$ structure. Given the fact that HCl + MDMS are observed as products, it is likely that the intermediate is due to a complex between the reactants (DMS:Cl_2) or between the products (MDMS:HCl), or to a product with the same overall formula.

The assignment of the unknown bands can be achieved only with the support of *ab initio* calculations on all these possible structures.

4.5 RESULTS OF THE AB INITIO CALCULATIONS ON THE REACTION INTERMEDIATE

The most obvious candidates for the reaction intermediate in the DMS + Cl_2 → MDMS + HCl reaction are

- a molecular complex between DMS and Cl_2, CH_3SCH_3:Cl_2 (a reactant-type complex)
- a molecular complex between MDMS and HCl, CH_3SCH_2Cl:HCl (a product-type complex)
- a sulphurane-like structure in which two chlorine atoms are co-ordinated on the sulphur centre, $(CH_3)_2SCl_2$.

In this work, geometry optimizations of these structures have been performed at the second order Moeller-Plesset perturbation (MP2) level of calculation [22], using different basis sets. While no problems arose for the optimization of the DMS:Cl_2 and MDMS:HCl structures, some basis sets used could not locate a stationary point with all real vibrational frequencies for the $(CH_3)_2SCl_2$ compound. When a suitable geometry was optimized, calculations with this optimized geometry with the coupled-cluster (CC) method [23]- at the CCSD(T) level- were performed in order to obtained more accurate determinations of the total energies; also in this case two different basis sets have been used. For a more complete description of the basis set characteristics, see Section 2.5.

All-real frequencies structures of $(CH_3)_2SCl_2$ have been obtained at the MP2 level using the basis sets

- 6-31G**: optimized in the C_1 point group
- 6-311++G**: optimized in the C_1 point group
- 6-31++G(2p,2d): optimized in the C_1 and C_{2v} point groups
- 6-311++G(2p,2d): optimized in the C_{2v} point group
- aug-cc-pVDZ optimized in the C_{2v} point group
- aug-cc-pVTZ optimized in the C_{2v} point group

The basis sets that were considered more suitable for the description of the potential energy surface of the DMS + Cl_2 reaction were 6-31++G(2p, 2d), aug-cc-pVDZ and aug-cc-pVTZ. In the section dealing with $(CH_3)_2SCl_2$ (Section 4.6.3), the differences in results obtained with these basis sets will be presented in more detail. In the sections dealing with DMS:Cl_2 and MDMS:HCl, the results will be given on the assumption that the "best" basis set is the aug-cc-pVDZ basis (because of the relative energy it gives for the intermediate compared to DMS+Cl_2), and equilibrium geometries, vibrational frequencies and ionization energies have been obtained with this basis set.

4.5.1 DMS:Cl_2

Two different structures were optimized at the MP2/aug-cc-pVDZ level for the complex between dimethyl sulphide and chlorine, which differ in the relative orientation of the two interacting molecules.

The first structure is characterized by a Cl-Cl bond perpendicular to the C-S-C plane, and oriented so that the chlorine atoms and the sulphur atom are almost collinear. Each chlorine atom is equidistant from the two carbon atoms, so the symmetry point group is C_S. The geometry of this structure, which is labelled α, is reported in Figure 4.36; Table 4.10 reports its most significant geometrical parameters.

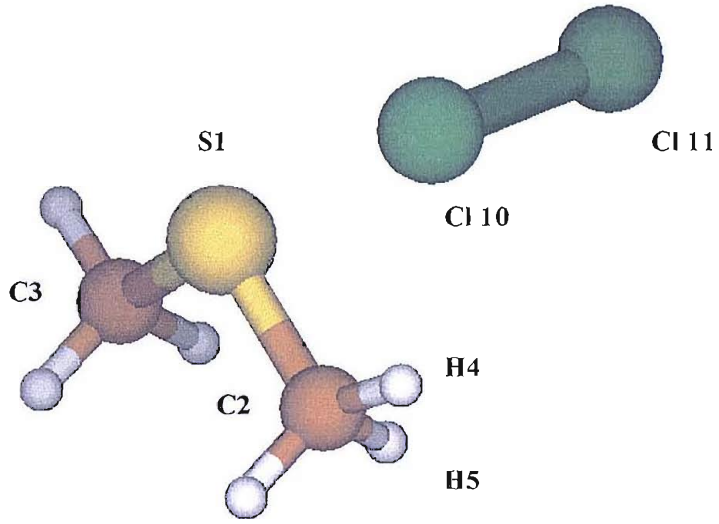

Figure 4.36- Optimized geometry of α-DMS:Cl_2 at the MP2/aug-cc-pVDZ level, with labelling of the atoms shown

Table 4.10- The most significant geometrical parameters for α-DMS:Cl_2 optimized at the MP2/aug-cc-pVDZ level

Bond	Distance (Å)	Angle	Value (°)
S1-C2	**1.820**	C2-S1-C3	**98.87**
C2-H4	**1.099**	H4-C2-S1	**107.17**
C2-H5	**1.100**	C2-S1-Cl10	**93.42**
Cl10-Cl11	**2.190**	C2-H4-Cl10	**68.31**
Cl10-S1	**2.552**	S1-Cl10-Cl11	**174.55**
Cl10-C2	**3.222**	H4-C2-S1-C3	**174.49**
Cl10-H4	**3.462**	H4-C2-S1-Cl10	**80.49**
Cl10-H5	**2.974**	C2-S1-Cl10-Cl11	**49.56**

The second structure optimized for DMS:Cl_2 is characterized by a Cl-Cl bond perpendicular to the direction it has in the structure α: this time the Cl-Cl bond is almost parallel to one of the C-S bonds and parallel also to the C-S-C plane. One chlorine atom is still equidistant from the two carbon atoms, while the second one is displaced along the same line of the C-S bond, but in the opposite direction: this means that- referring to Figure 4.37- if the chlorine molecule is projected on the plane of DMS then Cl 11 would overlay on S1 while Cl 10 will be at 180° with respect to C2. The overall structure lacks of any symmetry element, despite the fact that the DMS molecule retains C_S symmetry (and its geometrical parameters are almost unchanged from free DMS); therefore the point group of the complex is C_1. This structure, labelled β-DMS:Cl_2 is presented in Figure 4.37, while its most important geometrical parameters are listed in Table 4.11.

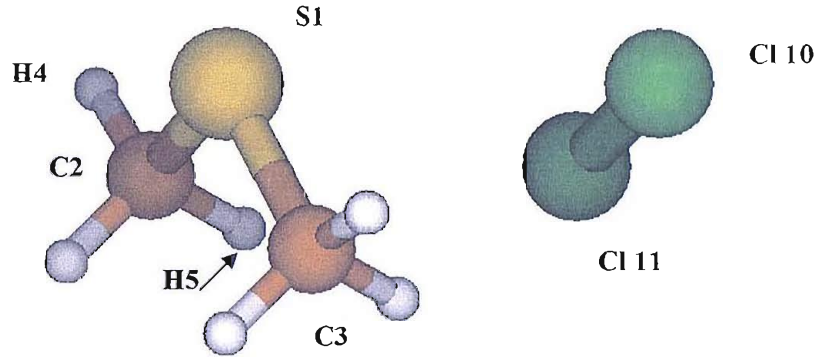

Figure 4.37- Optimized geometry of β-DMS:Cl_2 at the MP2/aug-cc-pVDZ level, with labelling of the atoms shown

Table 4.10- The most significant geometrical parameters for β-DMS:Cl_2 optimized at the MP2/aug-cc-pVDZ level

Bond	Distance (Å)	Angle	Value (°)
S1-C2	**1.821**	C2-S1-C3	**97.47**
C2-H4	**1.100**	H4-C2-S1	**107.74**
C2-H5	**1.101**	C2-S1-Cl10	**107.71**
Cl10-Cl11	**2.037**	H4-C2-Cl11	**109.63**
Cl10-S1	**3.781**	C2-H5-Cl11	**130.35**
Cl11-S1	**3.853**	S1-Cl10-Cl11	**72.59**
Cl11-C2	**3.585**	S1-C2-Cl11	**75.31**
Cl11-H5	**3.039**	H4-C2-S1-C3	**178.84**
		H4-C2-S1-Cl10	**-109.33**
		C2-S1-Cl10-Cl11	**5.74**

Structure β is a looser complex than structure α: this can be seen from the much larger distance between the chlorine atom closer to the DMS frame and the sulphur atom in this structure. Moreover, the Cl-Cl bond is shorter than in conformer α, where the proximity between Cl 10 and the sulphur atom allows an attractive interaction between these atoms, so that Cl 10 is attracted towards the sulphur atom increasing the Cl-Cl bond to 2.19 Å. This will have implications on the vibrational and electronic characteristics of the two complexes: therefore, the two different structures α- and β-DMS:Cl_2 should be considered as two different complexes.

The total energies of structure α- and structure β of DMS:Cl_2 have been calculated at the MP2/aug-cc-pVDZ level as respectively -1396.4914622 hartrees and as -1396.4816631 hartrees: α-DMS:Cl_2 is therefore more stable by 6.149 kcal/mol.

Harmonic vibrational frequencies at the MP2/aug-cc-pVDZ level have been calculated for the two structures: the vibrational frequencies which show the most intensities are reported in Table 4.11, while the two computed IR spectra are shown in Figure 4.38, assuming a Gaussian shape for the bands.

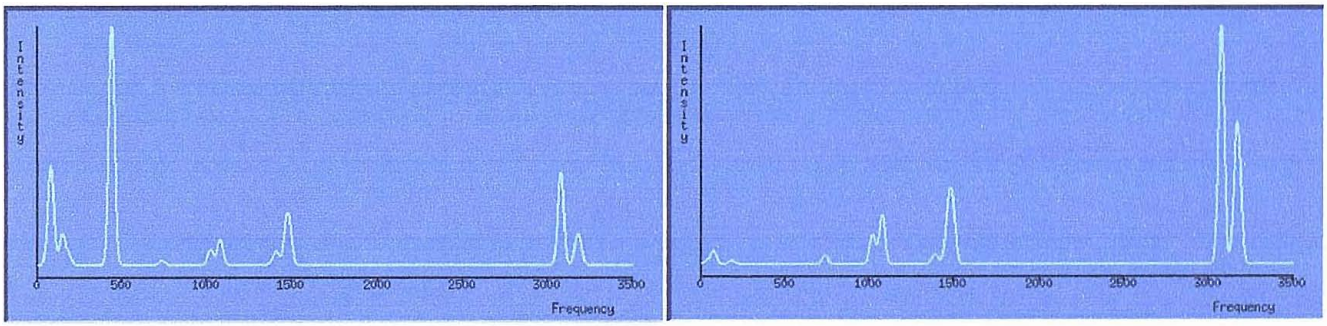

Figure 4.38- Calculated IR spectra for the α- (left) and β- (right) DMS:Cl_2 complexes at the MP2/aug-cc-pVDZ level

The IR frequencies are very similar between the two complexes. The only significant difference is the presence of a very strong band in structure α, which is due to the stretching of the Cl-Cl-S system, due to the proximity of the chlorine and the sulphur atoms: this mode is absent in structure β due to the different dispositions of the DMS and Cl_2 molecules.

However, the intensity pattern is very different for the two structures, α-DMS:Cl_2 being dominated by the Cl-S-Cl band at 440 cm^{-1} which is absent in β-DMS:Cl_2. The latter spectrum exhibits much stronger C-H stretching bands around 3000 cm^{-1}.

Table 4.11- Computed vibrational frequencies for the structures of DMS:Cl_2 optimized at the MP2/aug-cc-pVDZ level (intensities of the bands are reported in brackets)

α-DMS:Cl_2 frequencies (cm^{-1})	β-DMS:Cl_2 frequencies (cm^{-1})	Normal mode
440.7 (121.85)		Cl-Cl···S stretching
737.0 (2.48)	739.3 (2.33)	
1023.3 (7.88)	1020.1 (7.80)	
1079.8 (13.15)	1076.3 (12.69)	
1386.7 (1.37)	1385.0 (2.09)	C-H scissoring
1412.6 (6.68)		
1470.0 (17.00)	1468.5 (14.03)	
1487.5 (12.65)	1493.3 (10.96)	
1499.5 (2.06)	1504.2 (1.86)	
3076.1 (28.81)	3071.7 (34.92)	C-H stretching
3079.8 (19.53)	3075.1 (28.00)	
3171.4 (9.95)	3161.0 (29.12)	
3189.0 (7.00)	3182.4 (10.55)	
3189.9 (1.53)	3183.5 (4.24)	

These results are particularly important, because in the literature [9] experiments involving co-deposition of DMS and Cl_2 in a matrix have shown the presence of a strong band around 360 cm^{-1} in the IR spectrum due to a complex which is decomposed as consequence of irradiation from a Hg lamp (no suggestions on the structure of this complex have been given). Considering the expected error in the calculated vibrational frequencies due to anharmonicity and partial allowance for electron correlation in the calculations, it is expected that for α-DMS:Cl_2 a band should be experimentally detected around 400 cm^{-1}. This could make α-DMS:Cl_2 a suitable candidate for the reaction intermediate observed in the DMS + Cl_2 → MDMS + HCl reaction, while the computed IR spectrum of structure β does not give good agreement with the experimental IR spectrum for the intermediate.

Concerning vertical ionization energies (VIEs), the results obtained by applying Koopmans' theorem to the molecular orbitals obtained at the Hartree-Fock level for the two structures of DMS:Cl_2 are listed in Table 4.12.

Table 4.12- VIEs of the two DMS:Cl_2 structures calculated with Koopmans' theorem at the HF/aug-cc-pVDZ level

KT calculated VIE (eV) α-DMS:Cl_2	KT calculated VIE (eV) β-DMS:Cl_2
9.626	9.093
11.401	11.772
11.427	12.198
12.601	12.243
13.826	13.257

Bearing in mind that the PE bands experimentally detected have VIEs at 9.69 and 10.62 eV, these results exclude β-DMS:Cl_2 as a possible candidate as the reaction intermediate, as its first calculated VIE is too low. The VIEs in Table 4.12 are in fact expected to be too high because of the approximations involved in Koopmans' theorem: if the values are scaled by the widely used 0.92 factor, the energies for the two first bands become 8.86 and 10.49 eV for the α structure and 8.37 and 10.83 for the β structure.

For a more reliable energy determination for the VIE of the first band of α-DMS:Cl_2, calculations at higher degrees of approximations have been conducted [24]. Coupled-cluster calculations with inclusion of the triples contribution (CCSD(T)) led to a VIE of 8.83 eV with the aug-cc-pVDZ basis set, while the estimate with the aug-cc-pVTZ basis set was calculated as 8.93 eV.

These values are too low compared to the experimental VIE of 9.66 eV. Therefore, computed VIEs for α-DMS:Cl_2 do not reproduce the experimental VIEs for the reaction intermediate. Despite the possible reasonable agreement for the IR spectrum, such a complex does not satisfy completely the requirements of the observed reaction intermediate in the PE spectrum.

4.5.2 MDMS:HCl

Three different structures have been obtained for the CH_3SCH_2Cl:HCl complex, according to the relative orientation of the HCl molecule with respect to the chlorine atom of MDMS. The three structures are presented in Figure 4.39. In this case, their differences are merely in orientation, so they can be considered as conformers of the same complex, in contrast with DMS:Cl_2 where the two complexes showed more marked differences in bond lengths and electronic and vibrational characteristics. The structures have been labelled *ortho*-, *meta*- and *para*-MDMS:HCl, to distinguish the relative positions of their HCl and CH_2Cl groups.

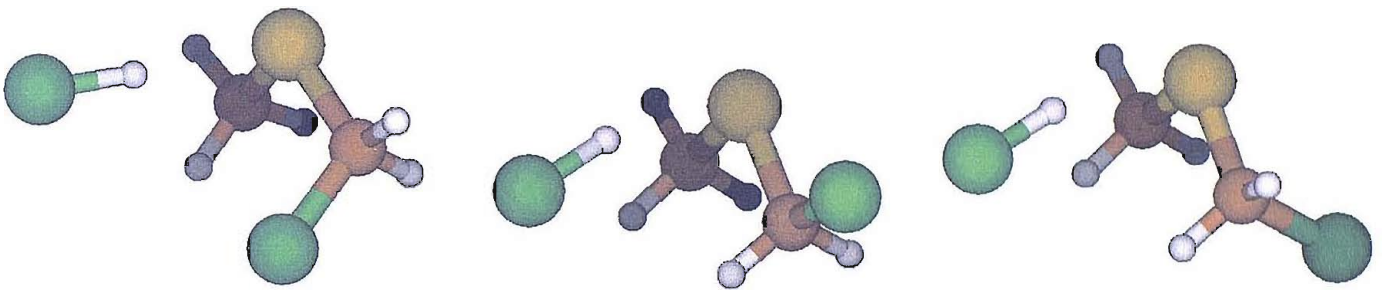

Figure 4.39- Optimized structures of MDMS:HCl at the MP2/aug-cc-pVDZ level. Left: *ortho*, centre: *meta*, right: *para*

The total and relative energies calculated for the three structures are reported in Table 4.13; structure *para* was found to be the most stable one, while structure *meta* is the least stable one.

Table 4.13- Total and relative energies of the three minimum energy conformers of MDMS:HCl calculated at the MP2/aug-cc-pVDZ level

Structure	Total energy (hartrees)	Relative energy (kcal/mol)
Ortho-MDMS:HCl	-1396.5423365	+0.756
Meta-MDMS:HCl	-1396.5395915	+2.479
Para-MDMS:HCl	-1396.5435419	0

Figure 4.40 presents in more detail the geometry of *para*-MDMS:HCl, and Table 4.14 lists its most significant geometrical parameters. There are no major differences in parameters between the conformers, apart from the angles of the chlorine atom to the MDMS unit: the only difference is in structure *ortho* where, due to steric hindrance between the chlorine atoms, the HCl unit is moved higher above the sulphur atom. The two S-C bonds are here slightly different, due to the presence of chlorine near one of them, while the H-Cl bond is just slightly longer than in free HCl (1.274 Å).

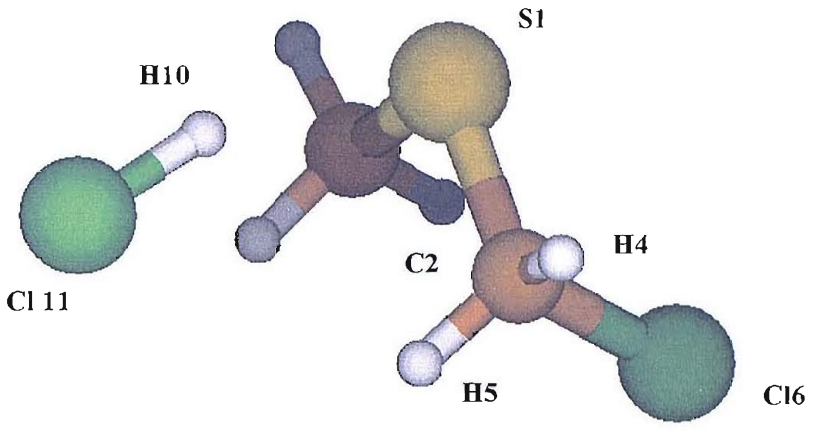

Figure 4.40- Optimized geometry of *para*-MDMS:HCl with the labelling of the atoms

Table 4.14- The most significant geometrical parameters for *para*-MDMS:HCl optimized at the MP2/aug-cc-pVDZ level

Bond	Distance (Å)	Angle	Value (°)
S1-C2	**1.810**	C2-S1-C3	**98.23**
S1-C3	**1.824**	Cl6-C2-S1	**113.57**
C2-H4	**1.098**	C2-S1-H10	**87.54**
C2-H5	**1.099**	S1-H10-Cl11	**161.70**
C2-Cl6	**1.805**	C2-H5-Cl11	**114.40**
H10-S1	**2.228**	H5-C2-S1-C3	**-53.17**
Cl11-H10	**1.315**	H5-C2-S1-H10	**37.18**
Cl11-H5	**3.124**	C2-S1-H10-Cl11	**-47.92**
C2-H10	**2.782**	Cl6-C2-S1-H10	**158.74**

Harmonic vibrational frequencies have been calculated at the MP2/aug-cc-pVDZ level for the three conformers. The complete spectra (presented with a Gaussian shape for the bands) are reported in Figure 4.41, while the vibrational frequencies with the largest calculated intensities are listed in Table 4.15.

The spectra are dominated by the H-Cl stretching band: this can vary considerably in frequency (100 cm^{-1} separate the peak of *ortho* structure to that of *meta* structure) according to whether the vibrational mode is close to the H-Cl value stretching for free HCl (calculated at 3084 cm^{-1} using the same basis set). It is evident that even if the computed spectra show a relatively strong band in the 350-450 cm^{-1} region, the full spectra cannot fit the experimental spectrum in the literature for the intermediate [9], where as a consequence of co-deposition of DMS and Cl_2 in a matrix, a strong band was observed at

360 cm^{-1} with much weaker bands at 1035 and 1331 cm^{-1}. Moreover, in FT-IR spectra acquired in this work (Section 4.5.1), the HCl bands are observed at the frequencies of free HCl, while according to calculations MDMS:HCl should absorb around 150 cm^{-1} lower.

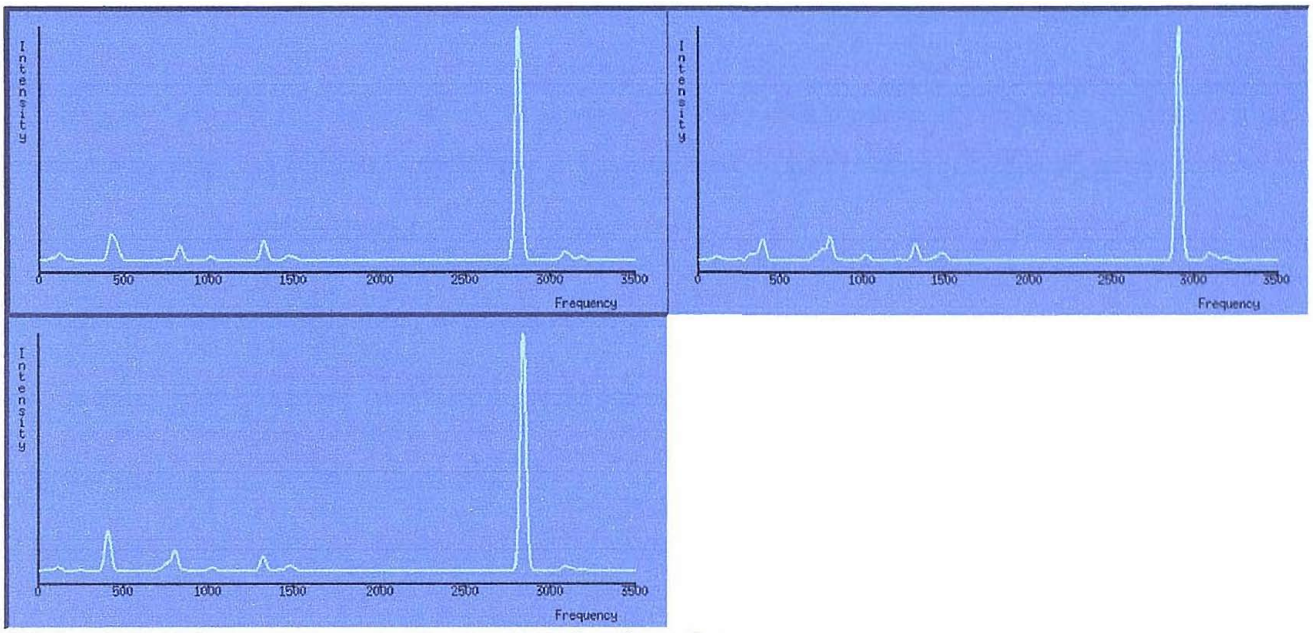

Figure 4.41- Calculated IR spectra for the MDMS:HCl conformers: above, *ortho* (left) and *meta* (right); below, *para* at the MP2/aug-cc-pVDZ level

Table 4.15- Calculated vibrational frequencies for the structures of MDMS:HCl (intensities of the bands reported in brackets)

***ortho*-MDMS:HCl frequencies (cm^{-1})**	***meta*-MDMS:HCl frequencies (cm^{-1})**	***para*-MDMS:HCl frequencies (cm^{-1})**	**Normal mode**
395.1 (44.19)		407.3 (90.67)	
	424.3 (62.88)	422.7 (18.22)	
709.3 (8.44)	457.6 (35.47)	710.7 (5.33)	
753.2 (23.89)	748.6 (3.22)	755.0 (21.68)	
802.4 (50.27)	828.6 (37.84)	802.5 (55.19)	S-C-Cl stretching
863.1 (1.87)	918.6 (1.50)	863.5 (2.29)	
1005.8 (3.27)	1008.2 (4.47)	1008.8 (3.39)	
1025.8 (9.14)	1015.1 (4.85)	1026.0 (7.78)	
1217.3 (2.30)		1220.4 (1.05)	
1317.7 (35.03)	1322.2 (51.76)	1319.8 (38.01)	
1405.2 (1.84)		1404.5 (1.88)	C-H scissoring
1440.4 (3.56)		1441.4 (2.29)	
1467.1 (9.88)	1463.3 (9.70)	1468.3 (10.51)	
1493.6 (9.17)	1499.2 (7.27)	1495.0 (8.94)	
2905.0 (504.64)	2809.6 (621.5)	2837.6 (621.12)	Cl-H···S stretch
3086.6 (14.38)	3079.4 (18.90)	3085.1 (13.22)	C-H stretching
3127.4 (9.08)	3111.7 (11.85)	3124.4 (6.68)	
3187.1 (4.98)	3176.2 (5.90)	3185.4 (3.35)	
3196.1 (1.32)	3189.0 (2.66)	3198.6 (1.10)	

From the computed vibrational intensities and frequencies, it is therefore not likely that MDMS:HCl could be the intermediate in the DMS + Cl_2 → MDMS + HCl reaction observed experimentally.

The vertical ionization energies (VIEs) calculated with Koopmans' theorem for the three conformers of MDMS:HCl are reported in Table 4.16

Table 4.16- VIEs of the three MDMS:HCl structures calculated with Koopmans' theorem at the HF/aug-cc-pVDZ level

KT calculated VIE (eV) *ortho*-MDMS:HCl	KT calculated VIE (eV) *meta*-MDMS:HCl	KT calculated VIE (eV) *para*-MDMS:HCl
10.266	10.271	10.307
11.975	12.103	12.027
12.291	12.333	12.301
12.358	12.516	12.638
12.370	12.572	12.664
13.245	13.036	13.264

Considering the usual overestimate made by Koopmans' theorem of the VIE value, the prediction for the first band is quite realistic: if a 0.92 scaling factor is used, the computed value for conformer *ortho* becomes 9.44 eV, compared to an experimental value of 9.66 eV. The four following VIEs are very close to each other: experimentally it would be possible that they all contribute to the same PE band; considering the 0.92 scaling factor, the value for the second VIE would be 11.02 eV. Even if this value is not be far from the observed VIE at 10.62 eV, the energy separation between the first and second band is too large (1.6 eV, compared to 0.9 eV experimentally). This problem was encountered also for calculations run on *ortho*-MDMS:HCl at higher levels of approximation [24]: despite the VIE of the first band being computed by coupled-cluster calculations to be at 9.42 eV (double-zeta basis set) or 9.53 eV (estimate at the triple-zeta basis set level), the value for the second VIE (not calculable with CCSD(T) because of the C_1 symmetry of the complex) was found to be above 11.2 eV with CIS, CASSCF and EOM-CCSD methods.

Therefore, even if the first computed VIE is in satisfactory agreement with the one observed in the PES experiments at 9.66 eV, no clear bases for the assignment to the second band of MDMS:HCl, with VIE at 10.62 eV, can be found. It is therefore unlikely that MDMS:HCl can be associated with the observed reaction intermediate.

4.5.3 $(CH_3)_2SCl_2$

$(CH_3)_2SCl_2$ was also considered as a possible candidate as the reaction intermediate observed in the PES experiments. When the structure was optimized at the MP2 level, it was found that the sulphur centre does not exhibit a tetrahedral or square-planar co-ordination, but instead it exhibits a pseudo octahedral co-ordination, in which two axial positions are unoccupied.

The computed structure for this sulphurane-like structure is reported in Figure 4.42, along with the atom labelling.

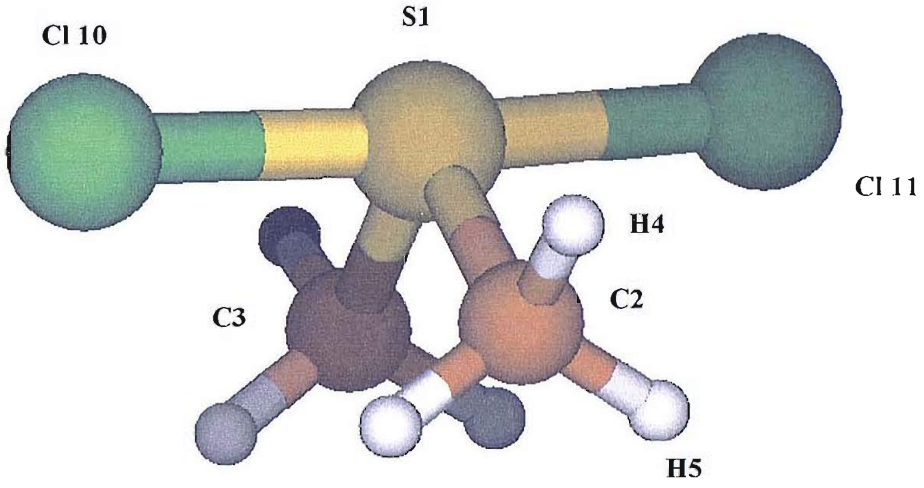

Figure 4.42- Structure of $(CH_3)_2SCl_2$ optimized at the MP2/aug-cc-pVDZ level

Even if slightly distorted (the angle Cl 10-S1-Cl 11 is not exactly 180°, and the angle C2-S1-C3 is not exactly 90°), the structure posses 2 planes of symmetry and a C_2 axis passing through the sulphur atom: its point group is therefore C_{2V}. The most relevant geometrical parameters are listed in Table 4.17.

Table 4.17- The most significant geometrical parameters of $(CH_3)_2SCl_2$ optimized at the MP2/aug-cc-pVDZ level

Bond	Distance (Å)	Angle	Value (°)
S1-C2	**1.828**	C2-S1-C3	**100.32**
C2-H4	**1.099**	H4-C2-S1	**106.08**
C2-H5	**1.096**	C2-S1-Cl 10	**90.79**
S1-Cl 10	**2.322**	Cl 10-S1-Cl 11	**178.11**
Cl 11-H5	**3.508**	H4-C2-S1-C3	**180.0**
		H4-C2-S1-H10	**-90.0**

It is noteworthy that the DMS unit is practically unchanged on bonding with the two Cl atoms, as its bond lengths and angles are almost identical for those of isolated DMS calculated at the same level (MP2/aug-cc-pVDZ).

The geometry of $(CH_3)_2SCl_2$ is very similar to the geometry calculated for $(CH_3)_2SCl$ at the UMP2/DZP level [5]: $(CH_3)_2SCl$ is the intermediate observed in the DMS + Cl reaction [1, 3]. In that case, the molecule is almost identical as $(CH_3)_2SCl_2$, only with one of the chlorine atoms removed from the sulphur. For example, the angle C-S-Cl is identical between the two structures, while the C-S and S-Cl distance are slightly different (S-Cl is longer in $CH_3)_2SCl$, while C-S is longer in $(CH_3)_2SCl_2$). Moreover, the structure of SCl_4 has been studied by means of *ab initio* calculations [25], and its geometry is very similar to the geometry of $(CH_3)_2SCl_2$, as both show a pseudo octahedral co-ordination around the sulphur atom.

The total energy calculated for this molecule (which is not a complex, as are the two $(CH_3)_2S{:}Cl_2$ structures previously described) is –1396.5182567 hartrees. The energy is therefore intermediate between those of $DMS{:}Cl_2$ and MDMS:HCl: at 0 K the most stable conformer of MDMS:HCl is 15.87 kcal/mol lower, while the most stable structure of $DMS{:}Cl_2$ is 16.81 kcal/mol lower.

Harmonic vibrational frequencies have been calculated at the MP2/aug-cc-pVDZ level for $(CH_3)_2SCl_2$. The frequencies are listed in Table 4.18, and the full computed IR spectrum is reported in Figure 4.43, which was obtained assuming a Gaussian contour for the bands.

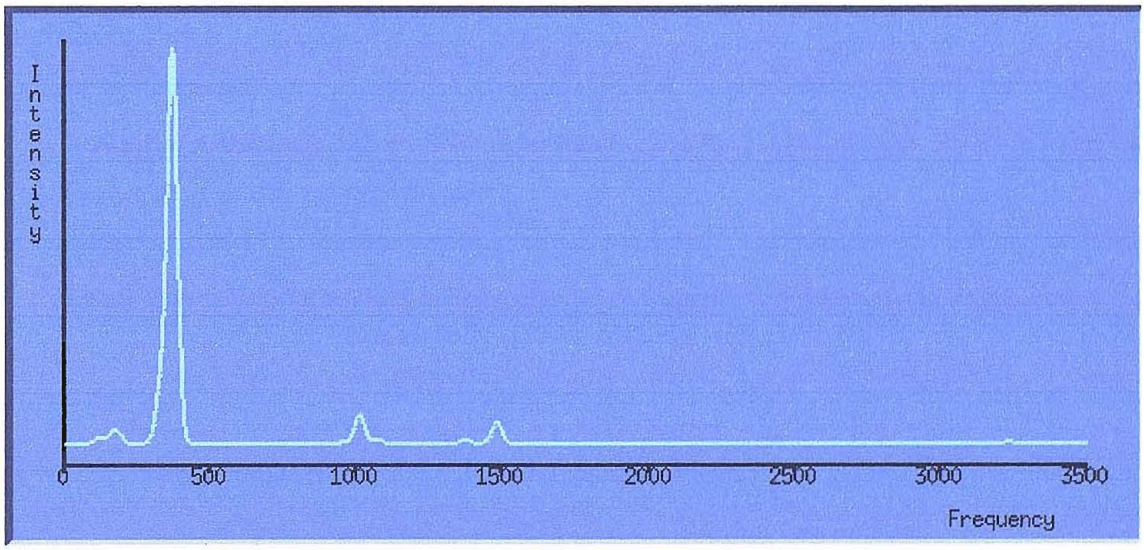

Figure 4.43- The IR spectrum of $(CH_3)_2SCl_2$ calculated at the MP2/aug-cc-pVDZ level

Table 4.18- Harmonic vibrational frequencies calculated for $(CH_3)_2SCl_2$

$(CH_3)_2SCl_2$ frequencies (cm^{-1})	Intensities (km/mol)	Normal mode
353.4	398.97	Asymmetric Cl-S-Cl stretch
972.4	1.95	
1035.8	25.23	
1090.6	7.14	
1411.8	2.94	C-H scissoring
1440.1	12.49	
1474.7	10.58	
1479.2	10.44	
3245.8	1.96	C-H stretching

The spectrum is clearly dominated by the S-Cl stretching band at 353 cm^{-1}, plus weak bands at around 1036 and 1475 cm^{-1}. The overall pattern is in very good agreement with the literature matrix isolation infrared evidence [9] that indicates that an intermediate produced by co-deposition of DMS and Cl_2 is characterized by a strong band at around 360 cm^{-1} and two weak bands at 1035 and 1331 cm^{-1}. The calculated value for the S-Cl band is slightly lower than the experimental one; nevertheless, this frequency is very dependent on the basis set chosen in the calculations. For example, when a 6-311++G(2p, 2d) basis set is used, the S-Cl stretching frequency increases to 373.6 cm^{-1}, a value that considering neglect of anharmonicity and partial allowance for electron correlation is in particularly good agreement with the experimental value of 360 cm^{-1}.

Therefore, $(CH_3)_2SCl_2$ has a calculated IR spectrum in very good agreement with the experimental matrix isolation spectrum recorded on co-deposition of DMS and Cl_2, both in band positions and intensity distribution.

Vertical ionization energies calculated with Koopmans' theorem are listed in Table 4.19, along with the values corrected by a 0.92 scaling factor.

Table 4.19- VIEs of $(CH_3)_2SCl_2$ calculated with Koopmans' theorem at the HF/aVDZ level

KT calculated VIE (eV)	0.92·KT calculated VIE (eV)
10.218	9.400
11.715	10.778
11.721	10.783
11.774	10.832
11.789	10.845

The second to the fifth calculated VIEs are very close: experimentally they would merge into the same photoelectron band. In fact, the molecular orbitals involved in these ionizations (MO 30-33) are very similar, being due to lone pairs on the chlorine atoms, plus a small σ-bonding contribution from the S-CH_3 bonds. The HOMO (MO 34) is mostly a σ-antibonding orbital along the Cl-S-Cl unit. The two HOMOs are reported in Figure 4.44: the three next highest HOMOs are almost identical with MO 33.

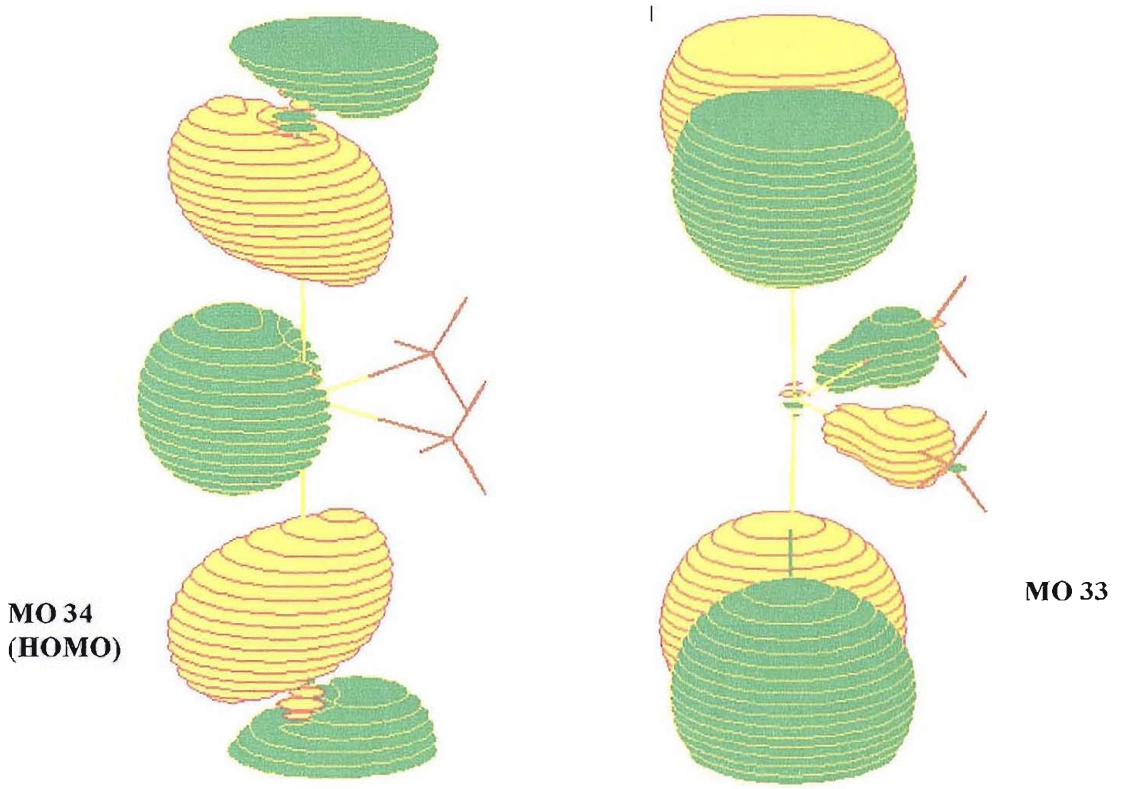

Figure 4.44- The two highest occupied molecular orbitals calculated for $(CH_3)_2SCl_2$

The results from Koopmans' theorem are somewhat similar to those obtained for MDMS:HCl. The value computed for the first band is encouraging (the experimental value is 9.66 eV), and the energy difference with the second one (experimental VIE at 10.62 eV) is still too high, but better than the values obtained for MDMS:HCl: there, the difference between the two first VIEs was about 1.6 eV; here it is ca. 1.4 eV. Calculations conducted with a coupled-cluster method considering triple contributions- CCSD(T)- have been performed using different basis sets in order to obtained more reliable values at least for the two first VIEs; the results are listed in Table 4.20.

Table 4.20- VIEs of the $(CH_3)_2SCl_2$ structure calculated with the CCSD(T) method with different basis sets, and compared wit the experimental VIEs

Ionization	CCSD(T) VIE (eV) Basis set: aVDZ	CCSD(T) VIE (eV) Basis set: aVTZ	CCSD(T) VIE (eV) Basis set: aV(T+d)Z	Experimental VIE (eV)
$(34\ a_1)^{-1} \rightarrow {}^2A_1$	9.535	9.633	9.643	9.66
$(33\ b_2)^{-1} \rightarrow {}^2B_2$	10.465	10.593	10.602	10.62
$(32\ a_1)^{-1} \rightarrow {}^2A_1$	-	-	-	
$(31\ b_1)^{-1} \rightarrow {}^2B_1$	-	10.623	-	
$(30\ a_2)^{-1} \rightarrow {}^2A_2$	-	10.655	-	

It was not possible to calculate the third VIE of $(CH_3)_2SCl_2$ by the CCSD(T) method because the symmetry of MO32 is the same as the HOMO. From the Koopmans' theorem values, however, the VIE value should be very close to that of the second VIE, that is around 10.60 eV.

The overall agreement between experiment and calculations is strikingly good, to the point that the error in the calibration of the experimental bands must be taken into account as a limit for the degree of accuracy of the calculations.

Therefore, on the basis of this evidence and the computed vibrational spectrum of $(CH_3)_2SCl_2$, the intermediate between the reagents DMS+Cl_2 and the products CH_3SCH_2Cl+HCl observed in the PES experiments is assigned to $(CH_3)_2SCl_2$; also from the energetic point of view, its relative energy is consistent with its relatively long lifetime.

Now that the reaction intermediate has been assigned to $(CH_3)_2SCl_2$, a study of the energy surface relating DMS + Cl_2 to the intermediate and products was carried out in order to explain the reaction mechanism. This will be presented in Section 4.7.

4.6 PROPOSED REACTION MECHANISM

From the experimental results, it was shown that the DMS + Cl_2 reaction first proceeds via the formation of $(CH_3)_2SCl_2$ without any other product being formed. Unfortunately, the possible formation of this intermediate was proposed after the acquisition of the IR spectra, so no investigation was carried out in the region below 400 cm^{-1} where this molecule is expected to display its strongest vibrational absorption; a confirmation of this hypothesis was given by the PES results and from the literature results on IR matrix isolation [9]. Moreover, the same kind of compound has been proposed for the reactions of DMS with F_2 [26] and of DMSe with Cl_2 [27, 28].

At later stages of the reaction, $(CH_3)_2SCl_2$ decomposes and MDMS and HCl are observed.

For increasing concentrations of chlorine relative to DMS, or at longer contact times, DDMS is observed, even if its presence was detected in a narrow range of experimental conditions: for example, in a closed cell its presence was almost completely hidden by the great abundance of TDMS.

An initial decomposition scheme can be visualized as

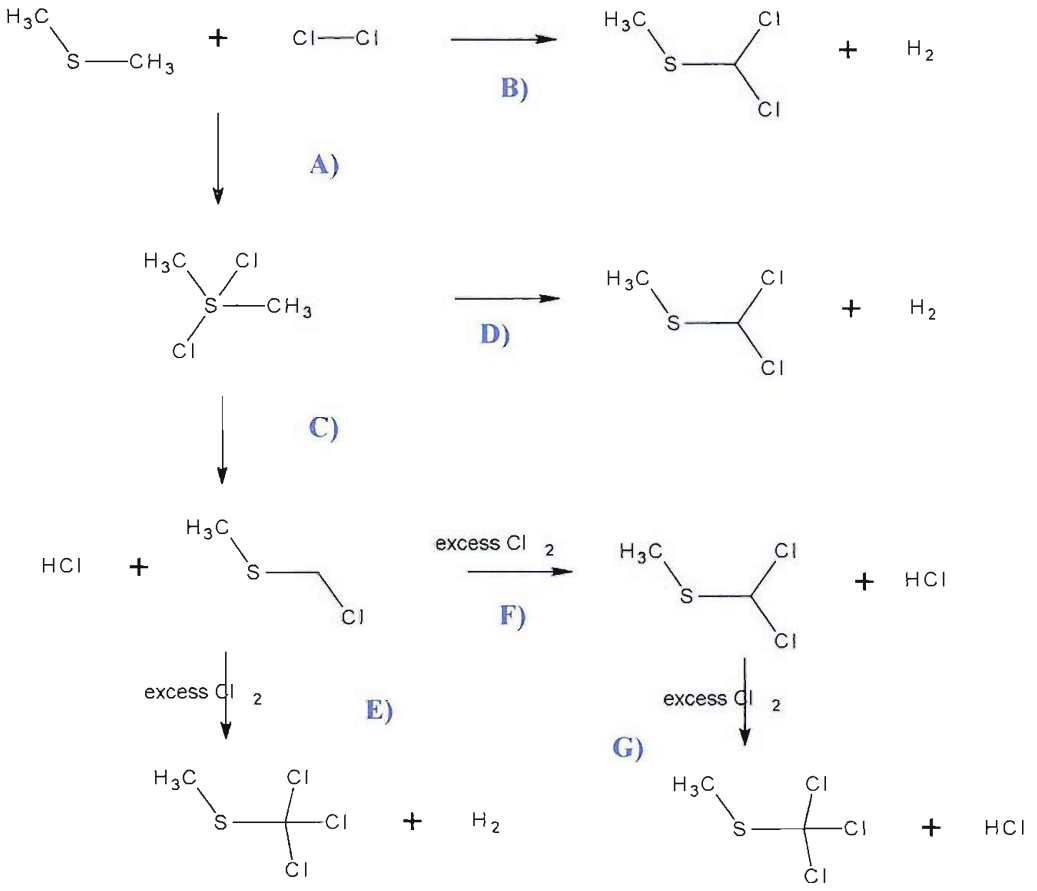

Route B is clearly disfavoured, because no DDMS has been observed in the initial stages of the reaction: route A is then the first step.

It is more problematic to state if route D is open or not: experimental evidence (Section 4.5.4) indicates that some DDMS is observed before $(CH_3)_2SCl_2$ has been totally consumed. Nevertheless, it is possible that DDMS can initially be produced (via routes C+F) when $(CH_3)_2SCl_2$ is not already fully decomposed to MDMS via route C. No *ab initio* calculations searching for a transition state for route D have been performed, but the nature of the process- with four bonds being broken and then four new ones formed- seems to suggest that route C should be favoured over route D.

The choice between route E and routes F+G is very difficult. On one hand, DDMS is experimentally detected, weakly in PES and more intensely in IR matrix isolation spectra. On the other, the intensities of DDMS bands are usually lower- both in IR and PES spectra- than those of MDMS or TTDMS (depending on the DMS:Cl_2 ratio or the mixing distance), and even in IR matrix results it appears that DDMS is better observed when MDMS is mixed with chlorine, rather than when the reaction is between DMS and chlorine. This probably suggests that when MDMS is formed as a reaction product from DMS, it has some kind of excess energy that allows the compound to react promptly with Cl_2 to form directly TDMS; when MDMS is the initial reactant, the reaction is much slower (in the same mixing ratio, and after the same deposition time, the amount of unreacted MDMS was higher than the equivalent amount of DMS, and TDMS was not observed) and DDMS is detected in higher abundance. It is also possible that DDMS is formed with a very short lifetime, that is route F could be open and route G can be a very rapid process.

An important discrimination can be done on the basis of the reaction partner: while route E proceeds without any formation of HCl with respect to MDMS, routes F+G implies the formation of additional HCl after all $(CH_3)_2SCl_2$ has decomposed to MDMS. Results must be handled with care, due to the difficulty of discerning when HCl begins to be formed as a consequence of route C or route F (that is, when MDMS is formed, or when it is already reacting: probably there is an overlapping between the two processes); still, from PES it seems that the increase of HCl when MDMS bands are almost stable is not very enhanced (Section 4.5.4), and from FT-IR results (Section 4.5.2) it can be seen that the bands associated with HCl do not increase between the conditions in which MDMS is obtained and those when TDMS is obtained. Comparing Figures 4.23 and 4.24, once the different total pressure is taken into account for the correction of the intensities, it can be seen that the HCl intensity, as judged from the sharp-like HCl spectrum, is almost the same, even if in one case MDMS is formed and in the other case TDMS is formed: the different Cl_2:DMS ratios do not seem to have much effect on the amount of HCl produced.

It is concluded that probably routes E and F+G are open at the same time, even if it is difficult to state clearly which one of them is more dominant in the decomposition pathway.

Considering all these aspects, a general scheme for the DMS + Cl_2 reaction can be proposed as in Figure 4.45.

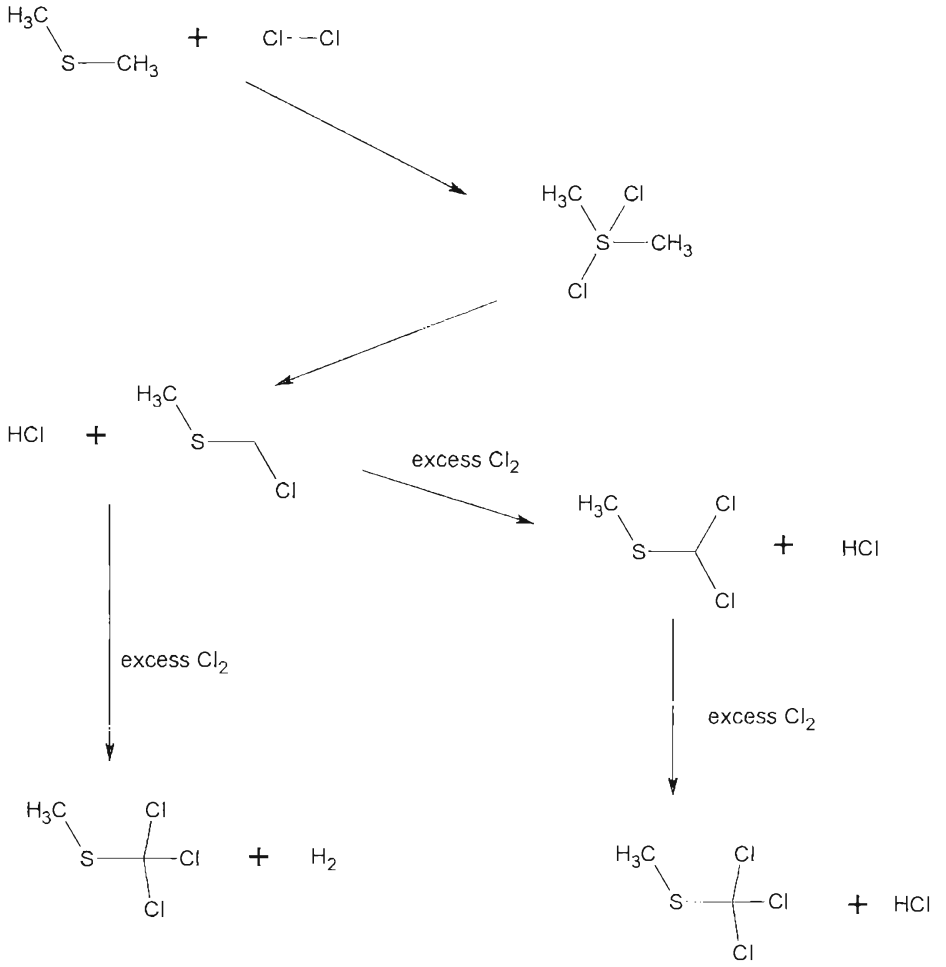

Figure 4.45- Proposed scheme for the DMS + Cl_2 reaction

The possibility that the intermediate $(CH_3)_2SCl_2$ directly reacts with Cl_2 to produce HCl, H_2 and TDMS was not considered (such a complex reaction is very unlikely to happen in a single step), and also it was assumed that DMS does not react directly with Cl_2 to produce directly MDMS and HCl: apart from the need to justify the presence of $(CH_3)_2SCl_2$, the reason why this direct route is not included is due to its higher transition state with respect to that producing the intermediate. This aspect will be described in more detail in the next section.

Finally, it must be borne in mind that the production of DDMS can start when the $(CH_3)_2SCl_2$ intermediate is not fully consumed: this explains why in some PE spectra it is possible to see weak intermediate bands when DDMS bands are already present (1 mm exit tube, at short mixing distances).

4.6.1 ENERGY LEVEL DIAGRAM AND TRANSITION STATES

In order to support the hypothesis of the formation of $(CH_3)_2SCl_2$ as an intermediate in the DMS + Cl_2 reaction, a study of the potential energy surface connecting DMS+Cl_2 to MDMS+HCl was conducted. No investigation was carried out on the steps of the reaction, which involve the formation of DDMS and TDMS.

The detailed study of the relevant parts of the energy surface (including the transition states) proved to be quite time consuming due to the size of the structures involved; this placed a limitation on the type of molecular orbital method and basis set that could be used. For example, at the MP2/6-31++G(2p, 2d) level the time required for the convergence of the calculations was too long and therefore no study an all the intermediates and transition states was carried out at this level. Relevant parts of the surface were therefore investigated with aug-cc-pVDZ, aug-cc-pVTZ and 6-31++G** basis sets.

When DMS and molecular chlorine are brought together, the DMS:Cl_2 complexes (α and β) described in Section 4.6.1 were formed; the interconversion between them should occur without an appreciable activation energy, as interconversion involves essentially a rotation of the Cl_2 group. From complex β-DMS:Cl_2 another intermediate was found, where one of the chlorine atoms is co-ordinated by the sulphur centre, while the second chlorine atom is moved further towards one of the methyl groups. This structure, which can be described as a $(CH_3)_2SCl$:Cl complex is characterized by all real frequencies: its geometry is shown in Figure 4.46 along with all the other intermediates and transition states on the DMS+Cl_2 surface. While the DMS:Cl_2 complexes were calculated to be more stable than DMS+Cl_2, $(CH_3)_2SCl$:Cl is characterized by a relatively high energy.

No transition state was found to connect such a complex to β-DMS:Cl_2. On the other hand, a transition state was found to connect $(CH_3)_2SCl$:Cl to the intermediate $(CH_3)_2SCl_2$ which is experimentally observed: the connection was confirmed by an IRC calculation. The two structures differ only by a displacement of the second chlorine atom towards the other side of the sulphur centre with respect to the first chlorine atom: therefore, the energy of the transition state (labelled TS1) was not much higher than the energy of $(CH_3)_2SCl$:Cl itself. The only imaginary vibrational frequency for such a transition state is correctly associated with the rotation of the Cl atom around the sulphur atom.

From TS1, the intermediate $(CH_3)_2SCl_2$, which is much lower in energy than DMS+Cl_2, is obtained.

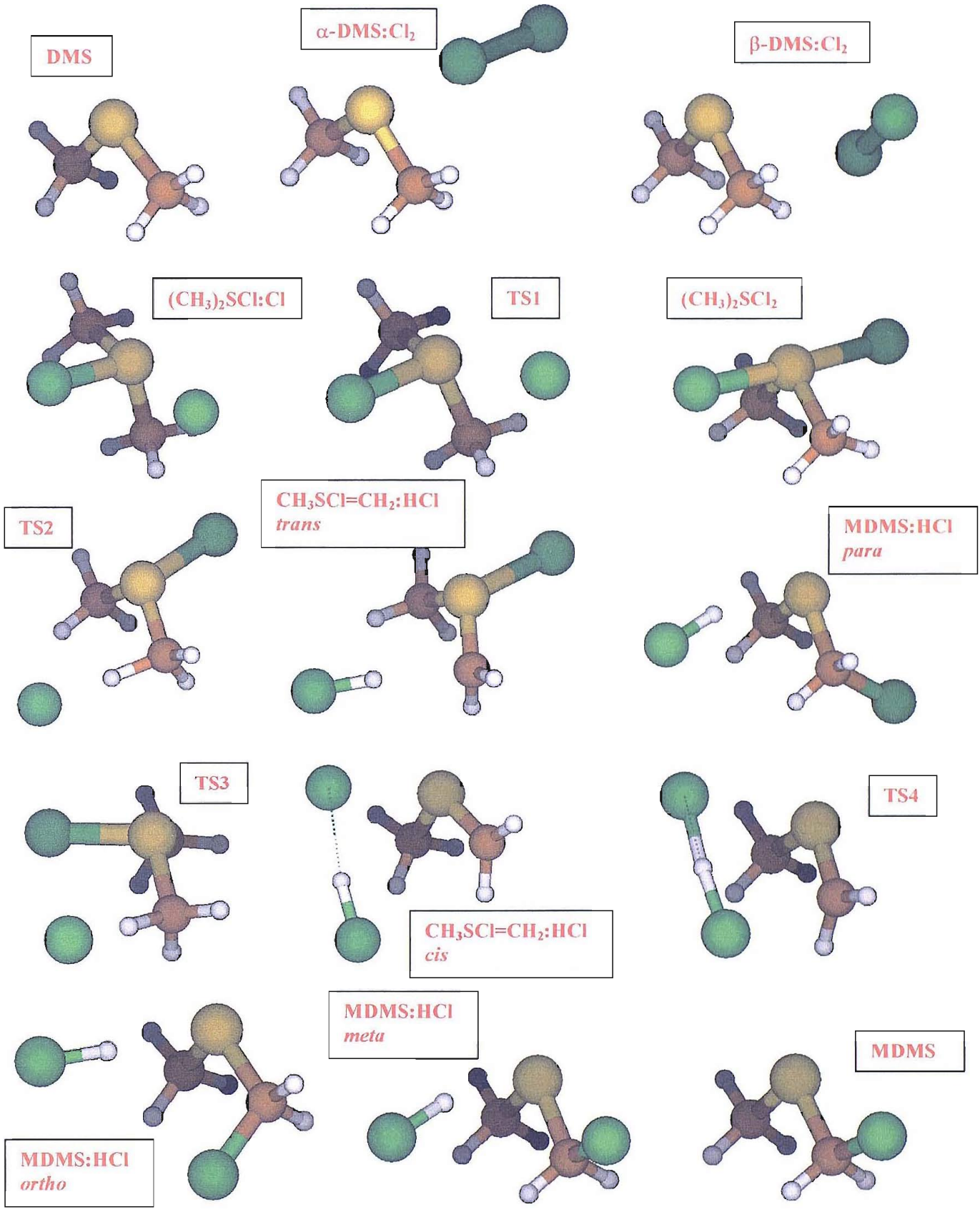

Figure 4.46- Geometries of intermediates and transition states on the DMS+Cl_2 surface located at the MP2/6-31G++ level. Refer to the energy diagrams (Figures 4.47 and 4.48) for the labelling of the transition states

From the $(CH_3)_2SCl_2$ intermediate, if one of the S-Cl bonds is broken or partially broken and the liberated chlorine atom is moved towards one of the methyl groups, the transition state TS2 is obtained: the imaginary frequency for this transition state corresponds to a movement bringing the Cl atom very close to one of the protons, which is detached from the methyl group to form HCl. HCl remains complexed with the rest of the molecule, forming an intermediate $CH_3SCl{=}CH_2{:}HCl$. This structure is characterized by a much shorter S-Cl bond (1.66 Å, against 1.82 Å for a normal S-Cl single bond), and a minimum energy structure that has all real vibrational frequencies.

From $CH_3SCl{=}CH_2{:}HCl$, if the chlorine left in the co-ordination sphere of the sulphur atom is moved towards the terminal methylene group in a concerted movement with the HCl molecule, *para*-MDMS:HCl is obtained. Even if this is much more stable than $CH_3SCl{=}CH_2{:}HCl$, the relative complexity of the change requires the location of a transition state to check the energy barrier for the process. This optimization was not carried out in this work, but it was assumed that the transition state required will not be higher in energy than TS2, which is the crucial transition state for the whole $(CH_3)_2SCl_2 \rightarrow$ MDMS+HCl reaction. *Para*-MDMS:HCl is the most stable structure on the surface: on moving HCl away from the MDMS molecule, the energy of the MDMS+HCl system is higher than that of the complexed species. The stepwise $DMS+Cl_2 \rightarrow (CH_3)_2SCl_2 \rightarrow$MDMS+HCl path has therefore been explored.

If a more direct route $DMS+Cl_2 \rightarrow$MDMS+HCl by-passing the sulphurane-like intermediate is searched for, *ab initio* calculations showed that no reaction is possible by moving the Cl_2 molecule towards one of the DMS methyl groups to produce HCl and MDMS in a concerted way, because the optimization always pushed the chlorine molecule away from DMS. It was therefore necessary to pass through a stepwise mechanism to produce MDMS+HCl.

Starting from $(CH_3)_2SCl{:}Cl$, if the outer chlorine atom is moved not towards the sulphur atom (as occurred when TS1 was obtained) but towards the other chlorine (which is bonded to the sulphur atom), then TS3 is obtained. Its geometry is somewhat similar to β-$DMS{:}Cl_2$, but the Cl_2 molecule is positioned so that one of the chlorine atoms is closer to the sulphur atom and the other closer to one of the methyl groups: the Cl-Cl bond is broken, and a new S-Cl bond is formed. This structure has a very high energy, and it is therefore the rate-determining energy barrier for the formation of MDMS which bypasses the $(CH_3)_2SCl_2$ intermediate. Its imaginary frequency is associated with a movement that in one direction leads to $(CH_3)_2SCl{:}Cl$ by pushing away the complexed chlorine from the methyl group, and in the other direction moves the Cl atom close to the methyl group so that it abstracts a proton from it.

The result is that from TS3 a structure of the type $CH_3SCl{=}CH_2{:}HCl$ is obtained. The difference with the analogous structure found in the $(CH_3)_2SCl_2$→ MDMS+HCl path is that here the second chlorine atom is more distant from the sulphur centre (in fact in Figure 4.46 no S-Cl bond is depicted) and that this time the HCl molecule lies on the same side of the sulphur as the second chlorine. This is why this structure, which has all real frequencies, has been labelled *cis*-$CH_3SCl{=}CH_2{:}HCl$, in contrast to the trans conformer previously encountered. Also in this case, the reduced bond length (1.64 Å) is consistent with the double bond nature of one of the S-Cl bonds.

In the geometry of *cis*-$CH_3SCl{=}CH_2{:}HCl$, the proton on HCl is roughly halfway between the two chlorine atoms: it was then quite simple to locate a transition state (TS4) in which this proton moves from one chlorine atom to the other, as shown by the mode associated with the imaginary frequency. From TS4, *ortho*-MDMS:HCl is then easily formed by making the isolated chlorine atom come closer to the methylene group. *Ortho*-MDMS:HCl can isomerize to *meta*-MDMS:HCl with a simple rotation of the CH_2Cl group, therefore without a proper energy barrier. If then HCl moves away from MDMS, the two separate products- experimentally detected- are obtained.

The study of the key regions for the DMS+Cl_2 surface has therefore been completed- apart for two transition states which are left to be searched in future work, but which should not alter the mechanism described.

A relative energy level diagram for the whole process can be presented. The relative energies of products, intermediates and transition states were found to be quite dependent on both the molecular orbital level (MP2 or CCSD(T)) and the basis set (aug-cc-pVDZ, aug-cc-pVTZ or 6-311++G**). The choice of the preferred method and basis set was determined by the relative energy value for the $(CH_3)_2SCl_2$ intermediate and the relative energy of the TS1 transition state: this choice was due to the fact that TS1 is the highest saddle point of the surface for the formation of the intermediate and for formation of the separate MDMS and HCl products (the path by-passing the intermediate via TS3 is in fact much higher in energy and should not be open). Given the fact that the reaction proceeds at room temperature, and so no thermal contributions help the reaction to overcome the energy barriers, it is necessary that the energy of TS1 relative to DMS+Cl_2 should not be higher than 7-8 kcal/mol, given the fact that at room temperature k_BT is around 0.6 kcal/mol.

A double-zeta basis set was found to achieve a relative energy of TS1 lower than 5 kcal/mol: it was therefore chosen as the "best" basis set to describe the potential energy surface for this system. The energy diagrams reported in the next figures will then be those obtained with such a basis set. Nevertheless, Table 4.21 lists the energies for $(CH_3)_2SCl_2$, MDMS+HCl and TS1 relative to DMS+Cl_2 to highlight the effects of the chosen method and basis set on the results of the calculations.

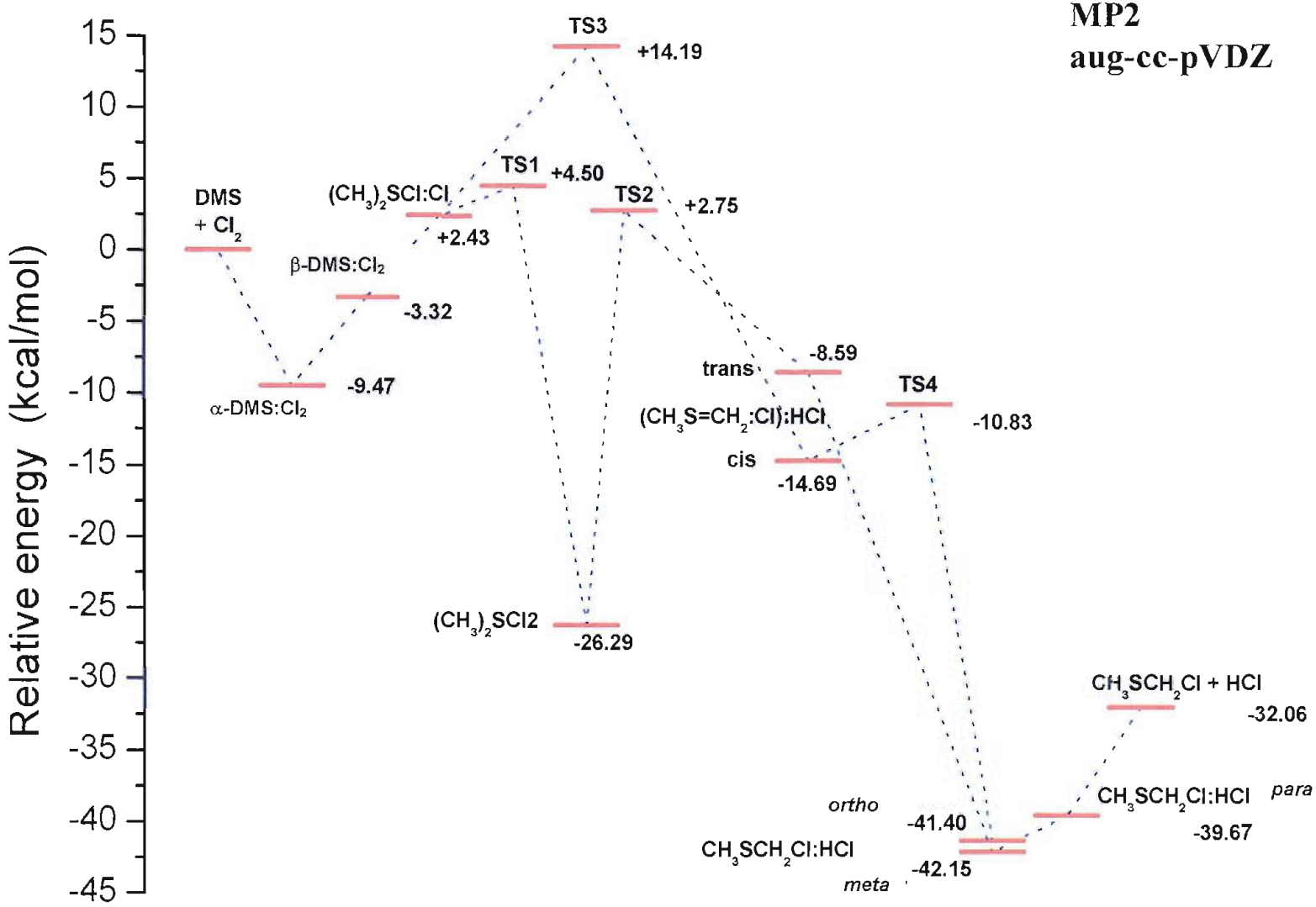

Figure 4.47- Relative energy diagram for the DMS+Cl_2 system calculated at 0 K at the MP2/aug-cc-pVDZ level

Table 4.21- Comparison of the computed energy values relative to DMS+Cl_2 for the most important species on the DMS+Cl_2 surface calculated at 0 K with different quantum chemical methods and basis sets. The MP2 values are calculated on the MP2 geometries optimized with each basis set, while CCSD(T) values are obtained from single-point calculations on the molecular geometry obtained by MP2 calculations with the same basis set

	MP2 6-31++G**	CCSD(T) 6-31++G**	MP2 aVDZ	CCSD(T) aVDZ	MP2 aVTZ	CCSD(T) aVTZ	MP2 aV(T+d)Z	CCSD(T) aV(T+d)Z
$(CH_3)_2SCl_2$	-15.05	-11.84	-26.29	-21.83	-24.46	-18.95	-25.21	-19.47
TS1	+13.75	+15.54	+4.50	+7.59	+6.37	+10.17	+5.43	+9.40
MDMS+HCl	-	-	-32.06	-29.72	-27.76	-25.10	-	-

From Table 4.21 it is evident that the MP2 method always gives lower energies for both TS1 and the intermediate $(CH_3)_2SCl_2$ than the CCSD(T) method.

It is quite surprising to notice that a double-Z basis set gives lower relative energies than a triple-Z basis set; the reason of this behaviour will not be discussed here. It will be remarked, however, that if a polarization function *d* is included within the basis set, then the relative energies are lower for a triple-Z basis set. In the following paragraphs the relative energy values obtained at the MP2/aug-cc-pVDZ level will be presented, as this seems the most favourable choice for the calculation of the energy of TS1 and also leads to calculations which can be completed in a reasonable time.

Figure 4.47 presents the 0 K relative energy level diagram for the DMS+Cl_2 surface: both routes to MDMS+HCl- via the intermediate $(CH_3)_2SCl_2$ or bypassing it- are reported. It is clear that the route passing through the intermediate is favoured, with the highest energy barrier (TS1) almost 10 kcal/mol lower than the highest one for the direct route (TS3). This explains why under certain conditions (see Section 4.5.4) only $(CH_3)_2SCl_2$ is observed without any trace of MDMS.

The contribution of zero point energy, of thermal energy and of entropy should also be considered: for this, a diagram of the relative free energies at 298 K is reported in Figure 4.48. The diagram was calculated at the MP2/6-31++G** level, due to the very time consuming procedure to calculate the entropy and thermal contribution with a double-Z basis set. In order to give an idea of the changes introduced passing from ΔE^0 to ΔG^{298}, a diagram of ΔE^0 at the MP2/6-31++G** level is reported in Figure 4.48, for the sake of comparing energy levels calculated with the same basis set. In this case, the energies are all much higher than at the MP2/aVDZ level, but a qualitative comparison can be made.

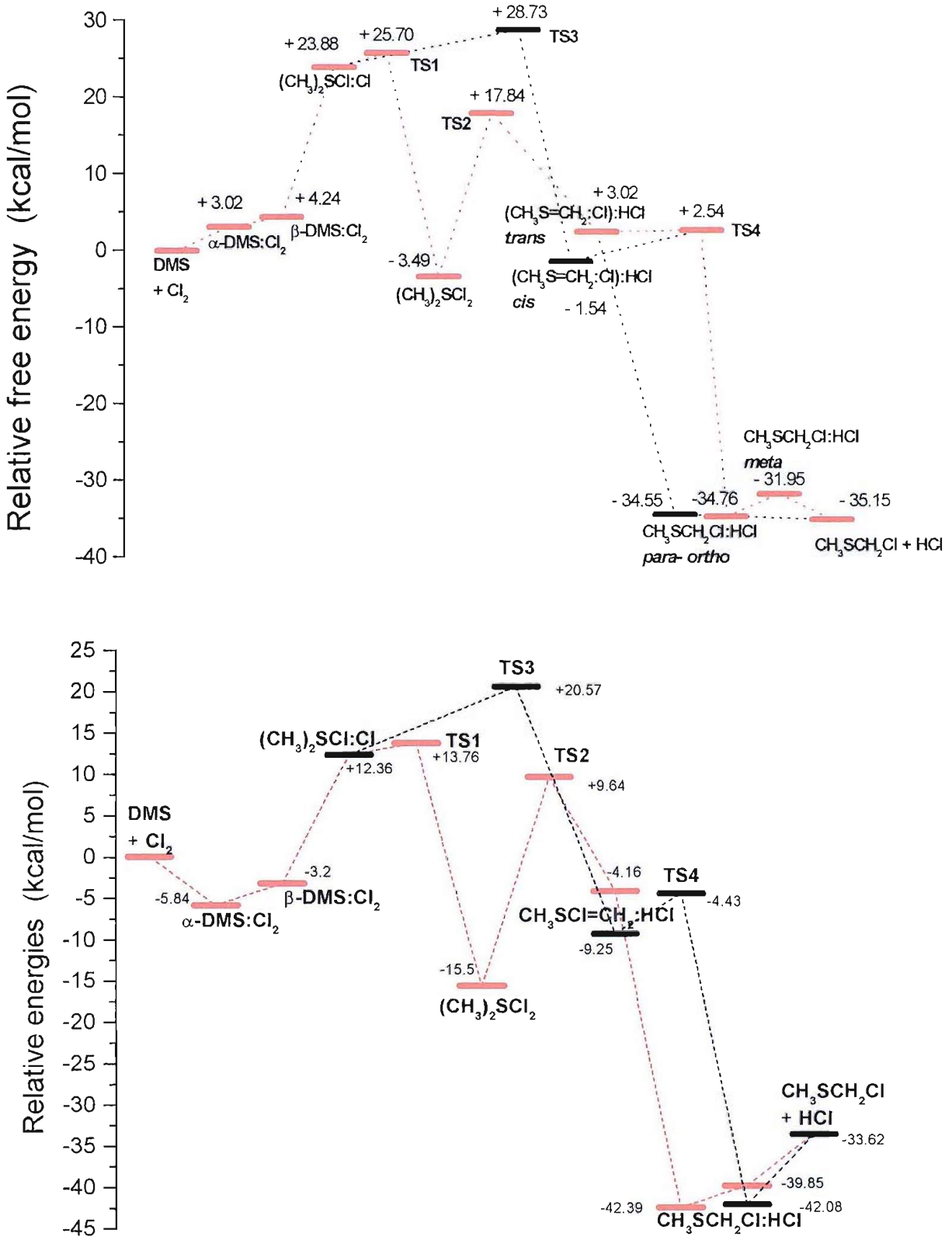

Figure 4.48- Diagrams of the relative ΔG^{298} (above) and ΔE^{0} (below) energies calculated at the MP2/6-31++G level**

Inclusion of entropy means that all the complexes and transition states are higher in energy with respect to DMS+Cl_2 or MDMS+HCl, because of their more ordered structure compared to two separated molecules. This explains why in the ΔG^{298} diagram the DMS:Cl_2 complexes are calculated to be less stable than DMS+Cl_2 compared to the ΔE^0 figures or the MDMS:HCl complexes are as stable as separated MDMS and HCl.

Also $(CH_3)_2SCl_2$ is raised in energy to reach a value comparable to DMS+Cl_2, and the transition states TS1 and TS3 are considerably higher in energy. As already stated, these ΔG^{298} values must not be taken as reliable values, because of the inadequacies of the 6-31++G** basis set in describing this system. In order to give a more precise idea of the changes introduced by comparing ΔE^0 and ΔG^{298} for some important points on the surface calculated at the MP2/aug-cc-pVDZ level, the results obtained at this level are reported in Table 4.22.

Table 4.22- ΔE^0 and ΔG^{298} for some significant points on the DMS+Cl_2 surface calculated at the MP2/aVDZ level

	ΔE^0 (kcal/mol)	ΔG^{298} (kcal/mol)
$(CH_3)_2SCl$:Cl	+2.43	+13.79
TS1	+4.50	+16.40
$(CH_3)_2SCl_2$	-26.29	-14.73
TS3	+2.75	+22.17
MDMS+HCl	-32.06	-33.37

Despite the fact that all the relative energies increase on passing from ΔE^0 to ΔG^{298}, it can be seen that the highest increase is for the transition state for the process which by-passes the $(CH_3)_2SCl_2$ intermediate (TS3), giving additional support for considering that the reaction proceeds mainly through the formation of the $(CH_3)_2SCl_2$ intermediate.

The fact that the values of the free energies are too high is proved by the inconsistency with the values for the rate constant of the DMS + Cl_2 reaction [10], measured as $3.4 \cdot 10^{-14}$ cm^3/molecule·s. Using the values for $\Delta H^{\#}$ and $\Delta S^{\#}$ from geometries obtained at the MP2/aug-cc-pVDZ level followed by fixed point CCSD(T) calculations ($\Delta H^{\#}$ = +4.89 kcal/mol, $\Delta S^{\#}$ = -37.8 cal/K·mol) to calculate the rate constant by means of the standard transition state expression, a value of $1.0 \cdot 10^{-20}$ cm^3/molecule·s is obtained. To be consistent with the experimental rate constant, the energy of TS1 relative to the reactants should be around 1-2 kcal/mol lower and the computed $\Delta S^{\#}$ should be less negative.

This discrepancy arises because single reference methods have been used to calculate the energy surface. A multireference treatment with a larger basis set is thought to give more accurate values for the relative energies of both intermediates and transition state.

4.7 CONCLUSIONS

The reaction between dimethyl sulphide and molecular chlorine has been studied in the gas-phase by photoelectron spectroscopy, FT-infrared and ultraviolet spectroscopy, and in a nitrogen matrix by infrared spectroscopy. Different molar ratios have been investigated, with particular attention being given to conditions of slight DMS excess in order to study the mechanism of the first chlorination step.
In PES, broad bands with VIEs at 9.69 and 10.62 eV have been observed under every condition in which the reaction had not totally consumed the initial DMS and Cl_2 partial pressures yet and not proceeded to completion and produced a full amount of monochloro-DMS. These bands- disappearing when DMS was totally consumed and MDMS was present- had the behaviour of those associated with a reaction intermediate, as was found out by measuring their relative intensity on varying the experimental parameters (mixing distance and molar ratio between DMS and Cl_2).
Ab initio calculations assigned the intermediate bands to a $(CH_3)_2SCl_2$ structure in which the central sulphur atom is tetra co-ordinated to the methyl and chlorine groups. The geometry is very similar to the geometry of $(CH_3)_2SCl$ [5], which is the intermediate observed in the reaction between DMS and atomic chlorine, and to the geometry of SCl_4 [25]. Such a structure is expected to have VIEs in very good agreement with the experimental VIEs. Moreover, the calculated IR spectrum of the intermediate displays a very strong band at around 355 cm^{-1} with weaker bands at 1035 and 1440 cm^{-1}: this is in very good agreement with the literature spectra recorded for DMS and Cl_2 co-deposited in a matrix. Calculations using different methods and basis sets have also been used to construct an energy level diagram for the DMS → MDMS surface, both involving and by-passing the formation of the intermediate.
Unfortunately, in the IR matrix isolation in this work no windows for radiation below 400 cm^{-1} were available, preventing the observation of $(CH_3)_2SCl_2$ by IR spectroscopy.
In FT-IR and UV gas-phase measurements, attention was focused on the formation of high chlorinated DMS species. It was found that the reaction proceeds stepwise to produce first MDMS, then DMDS and TDMS; while MDMS and TDMS were clearly detected, the signal of the dichlorinated species is very weak, suggesting that the reaction, once having produced MDMS, prefers to form predominantly the trichloro-DMS. This can be due either to a very fast reaction DMDS → TDMS or to a direct reaction MDMS → TDMS. Whatever the case, the spectra indicate that the reaction introduces the chlorine atoms on the same methyl group of the DMS molecule, attacking the other one only after the formation of TDMS- when no more hydrogen atoms can be removed from the first methyl group.

If the formation and removal of the complex in the gas-phase is represented as

$$DMS + Cl_2 + M \rightarrow (CH_3)_2SCl_2 + M \qquad (a)$$

$$(CH_3)_2SCl_2 \rightarrow MDMS + HCl \qquad (b)$$

then the results of this work suggest that the first step is the slow step and the second step is much faster. Hence the measured rate constant for the DMS + Cl_2 reaction corresponds to the rate of reaction (a).

Emphasis of future work could be both on *ab initio* calculations (the location of the remaining transition states to fully describe the potential energy surface for the first chlorination mechanism) and on experiments. In particular, co-deposition of DMS and Cl_2 in a matrix should be studied in the far infrared region to detect the band of the $(CH_3)_2SCl_2$ intermediate; also, the possibility of designing a flow-tube set-up for the detection of this intermediate in the gas-phase by means of FT-IR and UV spectroscopies should be considered.
Considering the importance of halogens above the ocean surface [28], a parallel study of the reaction of DMS with I_2 could be an interesting complement to the DMS+Cl_2 investigation.

REFERENCES

[1] a) R.E. Stickel, J.M. Nocovich, S. Wang, Z. Zhao, P.H. Wine, *J. Phys. Chem*, **96**, *1992*, 9875
b) S.P. Urbanski, P.H. Wine, *J. Phys. Chem*, **96**, *1992*, 9875

[2] J.E. Chateauneuf, *Chem. Commun., 1998*, 2099

[3] Y. Diaz-de-Mera, A. Aranda, D. Rodriguez, R. Lopez, B. Cabanas, E. Martinez, *J. Phys. Chem. A*, **106**, *2002*, 8627

[4] M.L. McKee, *J. Phys. Chem.*, **97**, *1993*, 10971

[5] a) S.M. Resende, W.B. De Almeida, *J. Phys. Chem. A*, **101**, *1997*, 9738
b) C. Wilson, D.M. Hirst, *J. Chem. Soc. Faraday Trans.*, **93**(16), *1997*, 2831

[6] N. Hooper, *Ph.D. thesis*, University of Southampton, *2002*

[7] W.E. Truce, G.H. Birum, E.T. McBee, *J. Amer. Chem. Soc.*, **74**, *1952*, 3594

[8] U.P. Agarwal, A.J. Barnes, W.J. Orville-Thomas, *Canad. J. Chem.*, **63**, *1985*, 1705

[9] N.P. Machara, B.S. Ault, *J. Phys. Chem.*, **91**, *1987*, 2046

[10] J.M. Dyke, M.V. Ghosh, D.J. Kinnison, G. Levita, A. Morris, D.E. Shallcross, *PCCP*, **7**, 2005, 868

[11] J.M. Dyke, N. Jonathan, A. Morris, *Electron spectroscopy Vol. 3 Chap. 4*, Edit. C.R. Brundle & A.D. Baker, *1979*

[12] M.J. Winter, *Ph.D. thesis*, University of Southampton, *1981*

[13] D.W. Turner, C. Baker, A.D. Baker, C.R. Brundle, *Molecular Photoelectron Spectroscopy*, Wiley Interscience, London, *1970*

[14] a) T. Ingham, D. Bauer, R. Sander, P. Crutzen, J. Crowley, *J. Phys. Chem. A*, **103** *1999*, 7199

b) S.P. Urbanski and P.H. Wine, J. Phys. Chem, A, **103**, *1999*, 10935

c) P. H. Wine, N.M. Kreuter, C.A. Gump, A.R. Ravishankara, *J. Phys. Chem.*, **85**, *1981*, 18

d) P. Limao-Vieira, S. Eden, P.A. Kendall, N.J. Mason, S.V. Hoffman, *Chem. Phys. Lett.*, **366**, *2002*, 34

[15] http://webbook.nist.gov/chemistry

[16] K.Kimura, S. Katsumata, *He(I) Photoelectron spectra of organic compounds*, Hokkaido University, Sapporo, *1978*

[17] S. De Frutos, *M. Phil. Thesis*, University of Southampton, *2002*

[18] F. Boberg, G. Winter, J. Moss, *Annalen der Chemie, Mai 1958*, 8

[19] L.E. Fernandez, A.B. Altabef, E.L Varetti , *J. Mol. Struc.*, **444**, *1998*, 227

[20] J.S. Ogden, University of Southampton, *private communication*

[21] A.M. Ellis, *Ph.D. thesis*, University of Southampton, 1989

[22] C. Moeller, M.S. Plesset, *Phys. Rev.*, **49**, *1934*, 618

[23] J. Simons, *J. Phys. Chem.*, **95**, *1991*, 1017

[24] E.P. Lee, University of Southampton, private communication

[25] Y. Drozdova, R. Steudel, W. Koch, K. Miaskiewicz, I.A. Topol, *Chem. Eur. J.*, **6**, *1999*, 1936

[26] N.P. Machara, B.S. Ault, *J. Mol. Struc.*, **172**, *1988*, 129

[27] N.P. Machara, B.S. Ault, *Inorg. Chem.*, **27**, *1988*, 2383

[28] a) S.M. Godfrey, C.A. McAuliffe, R.G. Pritchard, S. Sarwar, *J. Chem. Soc. Dalton Trans.*, *1997*, 1031

b) N. Kaltsoyannis, *J. Chem. Soc. Dalton Trans., 1997*, 4759

[29] C.W. Spicer, E.G. Chapman, B.J. Finlayson-Pitts, R.A. Plastridge, J.M. Hubbe, J.D. Fast, C.M. Berkowitz, *Nature*, **394**,*1998*, 353

CHAPTER 5

A SPECTROSCOPIC STUDY OF THE THERMAL DECOMPOSITION OF ALIPHATIC AZIDES

5.1 INTRODUCTION

Since the early work by Bock and Dammel [1-4], gas-phase UV-photoelectron spectroscopy has been used to study the pyrolysis of organic azides. The first azides studied were simple alkyl azides RCH_2-N_3, such as methylazide, or ethylazide: the compounds detected upon thermal decomposition of these azides were the corresponding imines RCH=NH (methylimine, ethylimine) and molecular nitrogen.

These pioneering studies suggested that the imines could be formed either via a 1,2- H shift mechanism (or a 1,2-Me shift) of the unstable nitrene radical RCH_2N: originating from the liberation of nitrogen from the azide or from a concerted process involving nitrogen elimination and the 1,2-hydrogen shift, which would therefore produce the imine without any nitrene formation. The initial study by Bock and Dammel preferred the latter mechanism, but this was apparently inconsistent with later experimental and theoretical works [5, 6].

The imines formed from the azide decomposition showed a limited temperature range in which they were stable, as they were usually decomposed at less than a hundred degrees above the temperature for complete azide pyrolysis. The decomposition involved elimination of hydrocarbons, such as methane or ethane, or other small molecules like HCN or CH_3CN.

More complex azides, for example azidoacetonitrile, showed no imine formation but instead the direct elimination of nitrogen and production of other small stable molecules. In cases where the imine was not detected, the presence of the observed products could be explained by molecular rearrangements following the same general pattern as for the alkyl azides.

In order to extend the interpretation of the thermal behaviour to more complex organic azides, a joint project between the PES groups of the Universities of Southampton and Lisbon has been undertaken; in order to provide an alternative identification fingerprint for the reaction intermediates and products, gas-phase monitoring by means of PES has been supported by parallel experiments carried out with

infrared matrix isolation spectroscopy. The azide studies made previously on azidoacetic acid, azidoacetone, azidoethanol and ethyl azidoacetate [10, 11, 12] showed that the thermal decompositions do not just give the products expected by following the same pathway as the simple alkyl azides, but also other products were observed whose presence can be explained only by suggesting alternative reaction mechanisms. The aim of the present project was to extend the study to investigate more classes of organic azides.

In this work, azidoacetamides, azidoesters and azidonitriles have been studied. For each compound, the specific objects of investigation were the temperatures of partial and complete pyrolysis and the nature of the products released along with molecular nitrogen- as these are the crucial pieces of information needed to characterize the azide decomposition. For example, when used as energy storage in synthesis it is important to know the nature of the decomposition products, or the thermodynamic stability of the azide when used in seismic explosives.

Each azide was pyrolyzed and the vapour monitored both by gas-phase PES and matrix isolation IR spectroscopy. The aim was to identify reaction products, to locate bands associated with reaction intermediates and to monitor their intensities as a function of pyrolysis temperature. Fundamental support to assist spectral assignments, to help in formulating the decomposition paths, and to calculate the relative energy between reactants and products, was provided by *ab initio* molecular orbital calculations.

Experimental PES and IR studies were carried out on: azidoacetamide, dimethylazidoacetamide, methyl- and ethyl-azidoformate, 2- and 3-azidopropionitrile, azidoacetonitrile, methyl azidoacetate, 2- and 3-methylazidoacetate. The first six of these compounds have been fully studied with the support of *ab initio* calculations, and the results will be presented in this Chapter. For the last four compounds, only a summary of the spectra and the initial interpretation of the results will be given in the final section of this Chapter.

From these studies, two alternative decomposition pathways have been proposed in order to explain the experimental evidences.

The first one, "Type 1", is characterized by the formation of an imine after the initial liberation of nitrogen from the azide, by means of a proton transfer on the iminic nitrogen atom from the adjacent carbon atom; this is consistent with the mechanism proposed by Bock and Dammel in their works [1-4] and can be written as:

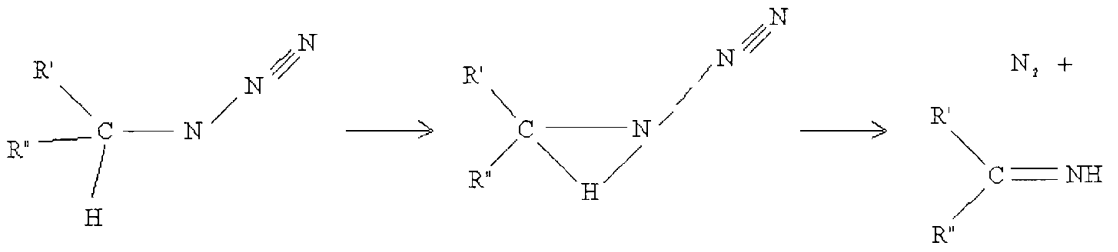

The second path, "Type 2", involves a nucleophilic attack of the electron-deficient nitrogen atom on a remote site of the molecule after the liberation of nitrogen has occurred: in this case fragmentation of the molecule or formation of cyclic products are possible. It was first recognised in the decomposition of azidoacetic acid [10], and in that case was represented as:

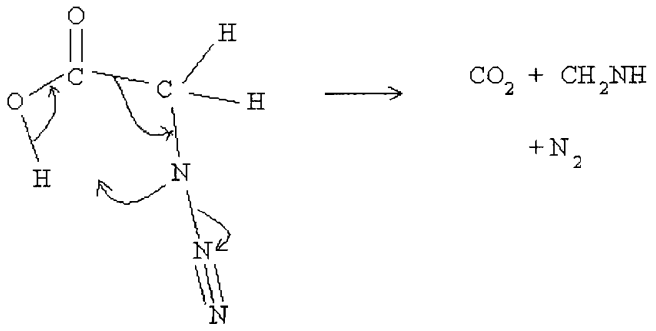

5.2 AZIDOACETAMIDE

5.2.1 EXPERIMENTAL SETUPS

Photoelectron spectroscopy

As azidoacetamide ($N_3CH_2CONH_2$) is a solid at room temperature, it does not have enough vapour pressure to be introduced into the ionization chamber of the spectrometer by simply evacuating a flask holding the sample connected to the inlet tube of the spectrometer via a needle valve. It was necessary to heat the substance in the spectrometer ionization chamber, in order to achieve a sample vapour pressure in the photoionization region high enough to produce spectra of acceptable signal-to-noise ratio -in this case when the pressure in the ionization chamber reached 10^{-4} torr. For this purpose, the spectrometer which has a radio-frequency induction heating system has been used. A description and a schematic diagram of this PE spectrometer has been given in Chapter 2, Section 2.1 [7].

The procedure for the acquisition and calibration of the photoelectron spectra followed the same pattern as described in Chapter 2. Calibration of spectra obtained on pyrolysis of the azide was normally achieved using the bands associated with the first vertical ionization energies (VIEs) of N_2 (15.58 eV), H_2O (12.62 eV), or HCN (13.60 eV) [8].

Matrix isolation IR spectroscopy

The apparatus and the procedure for the acquisition of infrared spectra in nitrogen matrices has been described in Chapter 2. Given the fact that azidoacetamide is a solid, it was found more convenient to pre-heat the sample and the inlet system to approximately 40 °C in order to obtain a sufficient vapour pressure. Deposition times were of the order of 30 to 60 minutes, and the matrix dilution ratios were estimated to be above 1000:1.

Spectra of ammonia and formamide have been acquired in a nitrogen matrix, to provide evidence for the possible presence and thermal behaviour of these compounds as pyrolysis products.

5.2.2 SAMPLE PREPARATION AND CHARACTERIZATION

PREPARATION

The sample was prepared by the Lisbon PES group using the following method: chloroacetamide was added slowly to a solution of sodium azide in water, until an approximate molar ratio chloroacetamide:sodium azide of 1:3 was reached. The mixture was stirred for 24 hours in an oil bath at 60 °C. After cooling the product was extracted with ethyl acetate and the water phase discarded. The organic phase was dried over anhydrous sodium sulfate and concentrated using a rotary evaporator. The azidoacetamide obtained was purified by re-crystallization from dichloromethane (m.p. 55–56 °C) by means of an Electrothermal apparatus.

CHARACTERIZATION

Azidoacetamide ($N_3CH_2CONH_2$) is a white crystalline solid at room temperature. It was characterized in the vapour phase by UV-photoelectron spectroscopy and electron impact mass spectrometry, and by ^{1}H- and ^{13}C-NMR in solution in deuterated chloroform. Characterization by infrared spectroscopy was conducted in a suspension in Nujol.

Mass spectrometry and NMR were performed to check for the presence of impurities in the samples: in practice, the spectra revealed that the azidoacetamide used in this work was pure.

Mass spectrometry: the 70 eV electron impact mass spectrum is reported in Figure 5.1. As expected, it displays the parent peak at 100 amu (intensity 2.1% relative to the base peak). Stronger peaks can be found at 28 amu (base peak, 100%) corresponding to N_2^+ and CH_2N^+ fragments, at 44 amu (17.1%) corresponding to $CONH_2^+$ and at 72 amu (2.6%) corresponding to $NCH_2CONH_2^+$. Signals are present also at 29 (4.9%, HCO^+) and 43 (2.6%, $HNCO^+$) amu.

In the 20 eV electron impact mass spectrum, the relative intensities of all the ions were enhanced with respect to the N_2^+ intensity. The relative intensities are 14.8% for the parent ion, 100% for $CONH_2^+$, 24.8% for $NCH_2CONH_2^+$, 20.9% for HCO^+ and 4.8% for $HNCO^+$.

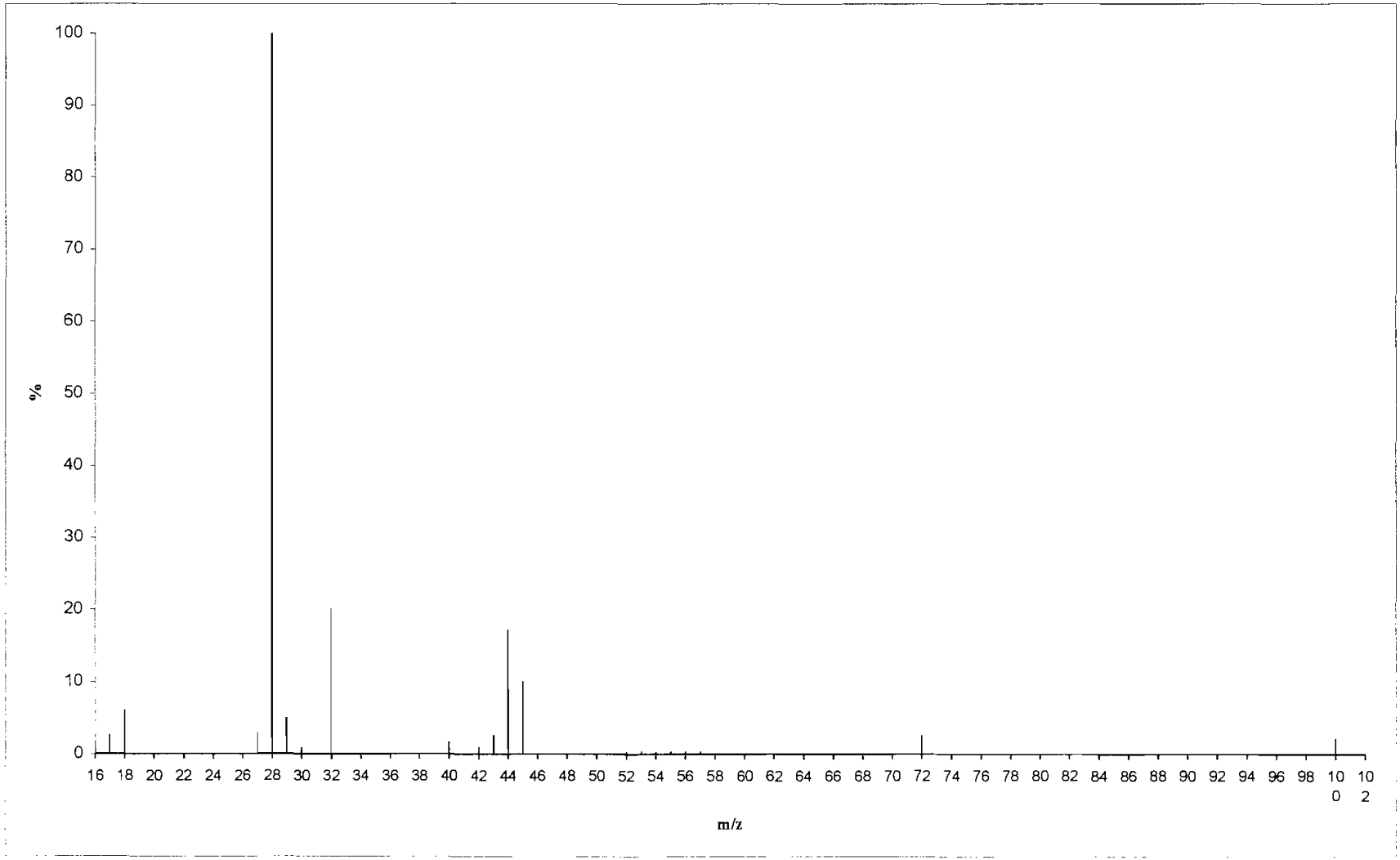

Figure 5.1- The 70 eV impact mass spectrum of azidoacetamide

^{1}H- and ^{13}C-NMR spectroscopy: the 300 MHz ^{1}H-NMR spectrum of azidoacetamide, recorded in $CDCl_3$ solution, is reported in Figure 5.2. It shows a single peak at 4.01 ppm relative to TMS corresponding to the two protons on the methylene group, while a lower, broad doublet at 6.46 ppm is due to the protons on the amidic nitrogen atom. The ratio between the integrals of the two peaks is 1.04:1. The doublet at 6.46 ppm is due to the inequivalent N-H proton signals in the azide

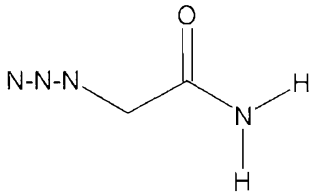

In the ^{13}C-NMR spectrum, also run in $CDCl_3$ solution, two peaks were observed, as can be seen in Figure 5.3; a peak at 52.7 ppm with respect to TMS is due to the methylene carbon atom, while the other one at 170.2 ppm is assignable to the carbonyl carbon atom.

Infrared spectroscopy: the IR spectrum of the compound dispersed in Nujol recorded between KBr plates is shown in Figure 5.4a. Apart from the Nujol bands at 1460 and 1377 cm^{-1} [9], it displays a broad band with peaks at 3373 and 3179 cm^{-1}, assigned to N-H stretching absorptions, strong bands at 2980-2920 cm^{-1} (C-H stretching overlapping with Nujol bands), and bands at 2117 cm^{-1} (N_3 stretching), 1630 cm^{-1} (C=O stretching), 1414 cm^{-1} and 1315 cm^{-1}.

The bands appear to have almost the same value in the matrix isolation IR spectrum recorded in a N_2 matrix (reported in Figure 5.10 in Section 5.1.3 dealing with the *ab initio* results), apart from the highest frequency of the N-H stretching mode above 3500 cm^{-1}: because of the elimination of any intermolecular hydrogen bonding in the matrix, the frequencies of the two modes rise respectively from 3373 and 3179 cm^{-1} to 3538 and 3420 cm^{-1}. A further analysis of the matrix IR spectrum will be found in the next section, when a comparison with the results of the *ab initio* calculations will be made.

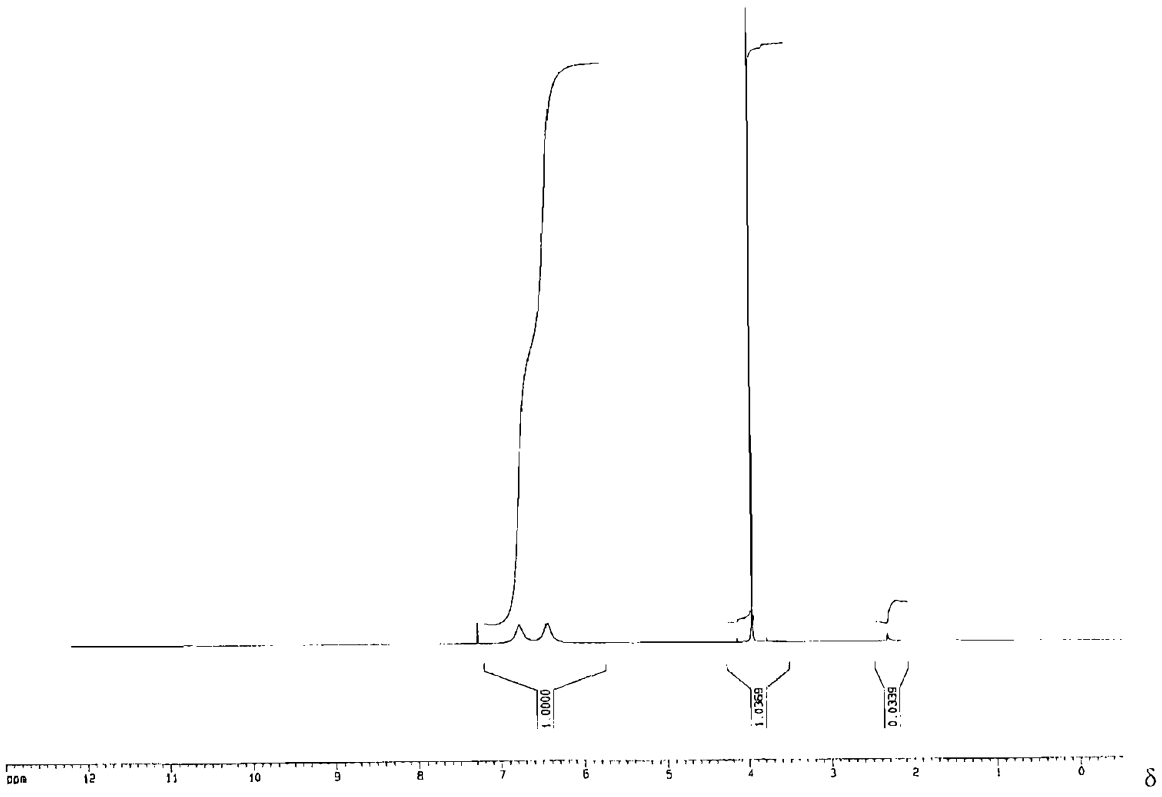

Figure 5.2- ^{1}H-NMR spectrum of azidoacetamide acquired in $CDCl_3$ with a 10s pulse delay

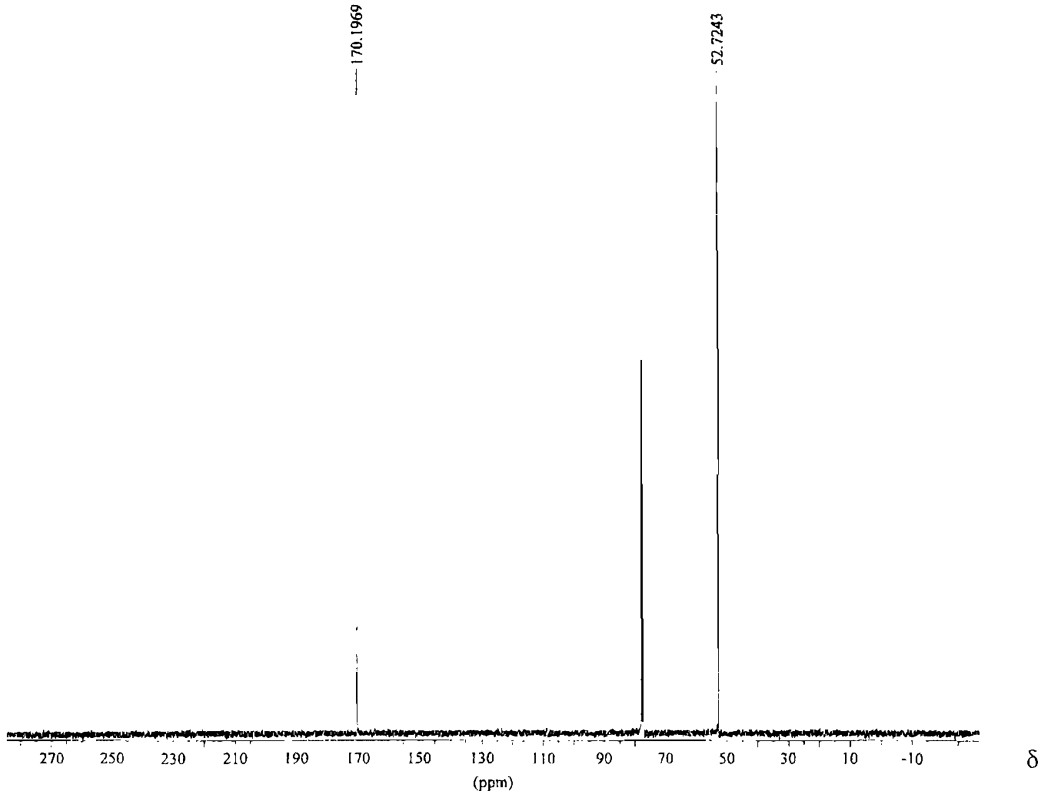

Figure 5.3- ^{13}C-NMR spectrum of azidoacetamide in $CDCl_3$ (triplet at 77 ppm)

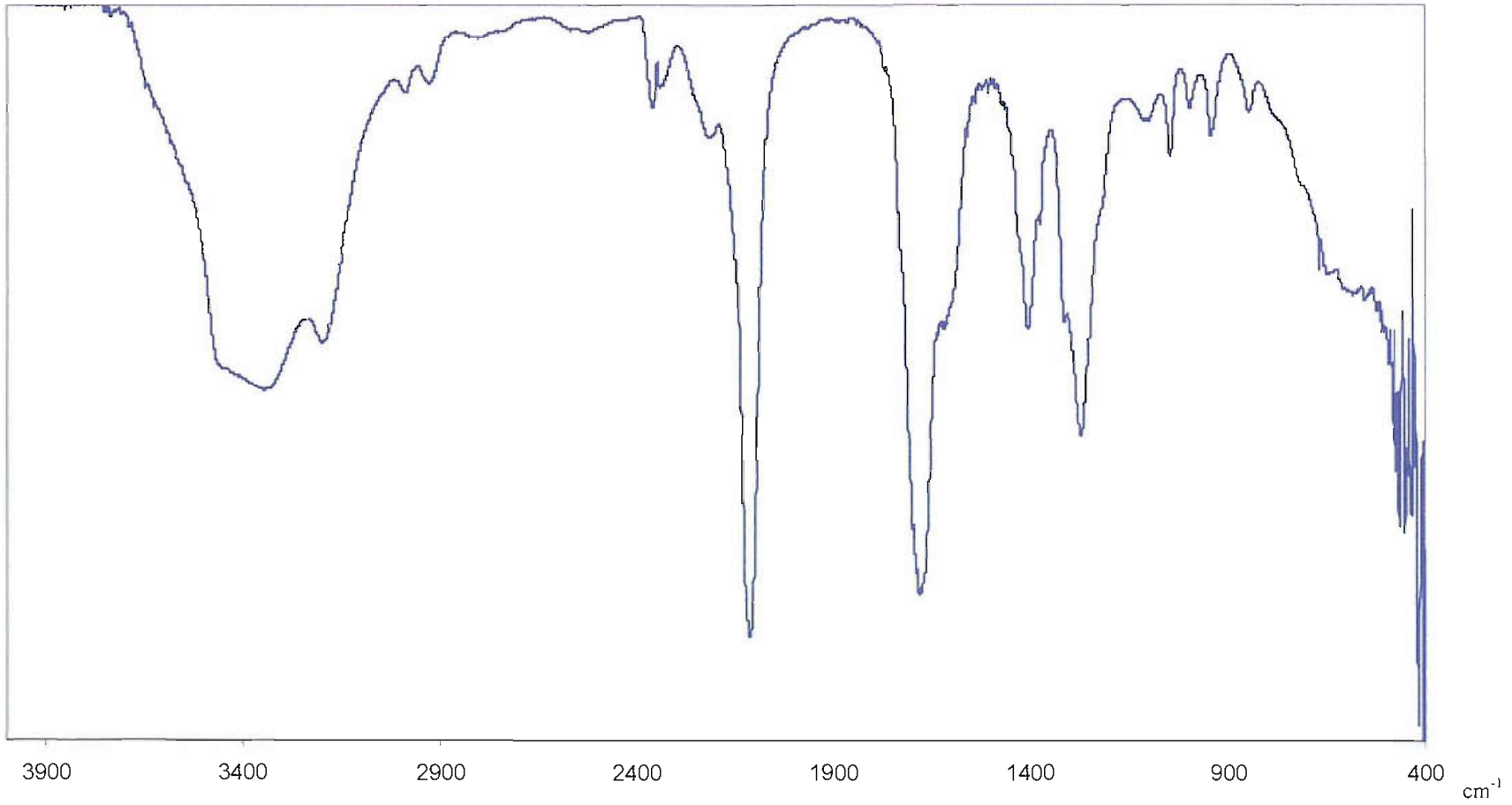

Figure 5.4- IR spectrum of azidoacetamide dispersed in Nujol, recorded between KBr plates

Photoelectron spectroscopy: the azidoacetamide UV-photoelectron spectrum (Figure 5.5) was obtained by warming the solid sample to 80 °C to obtain a suitable vapour pressure. The eight bands visible in the spectrum, and labelled A-H, were calibrated by averaging the vertical ionization energies of the bands calibrated from nine different spectra. The results are shown in Table 5.1 (see Figure 5.5 for the numbering of the bands in the spectrum). The asymmetric shape of band B arises, according to *ab initio* molecular orbital calculations (see later section), from the overlap of two different one-electron ionizations.

Table 5.1- Calibrated vertical ionization energies of azidoacetamide- see Figure 5.5 for band numbering

Band	**A**	**B**	**C**	**D**	**E**	**F**	**G**	**H**
VIE (eV) ±0.02	10.16	10.68	11.94	13.37	14.44	15.35	16.93	17.99

Spectra of the precursor of the azide (chloroacetamide) have also been recorded and calibrated in order to verify the absence of the precursor in the sample studied. It displayed the characteristic sharp band associated to the ionization from the lone pair on the chlorine atom in the 11.0-11.5 eV ionization energy region. Actually, all parent azide spectra were free of any detectable trace of the precursor used in the preparation: considering this, no comparison between the spectra of chloroacetamide and azidoacetamide will be presented here.

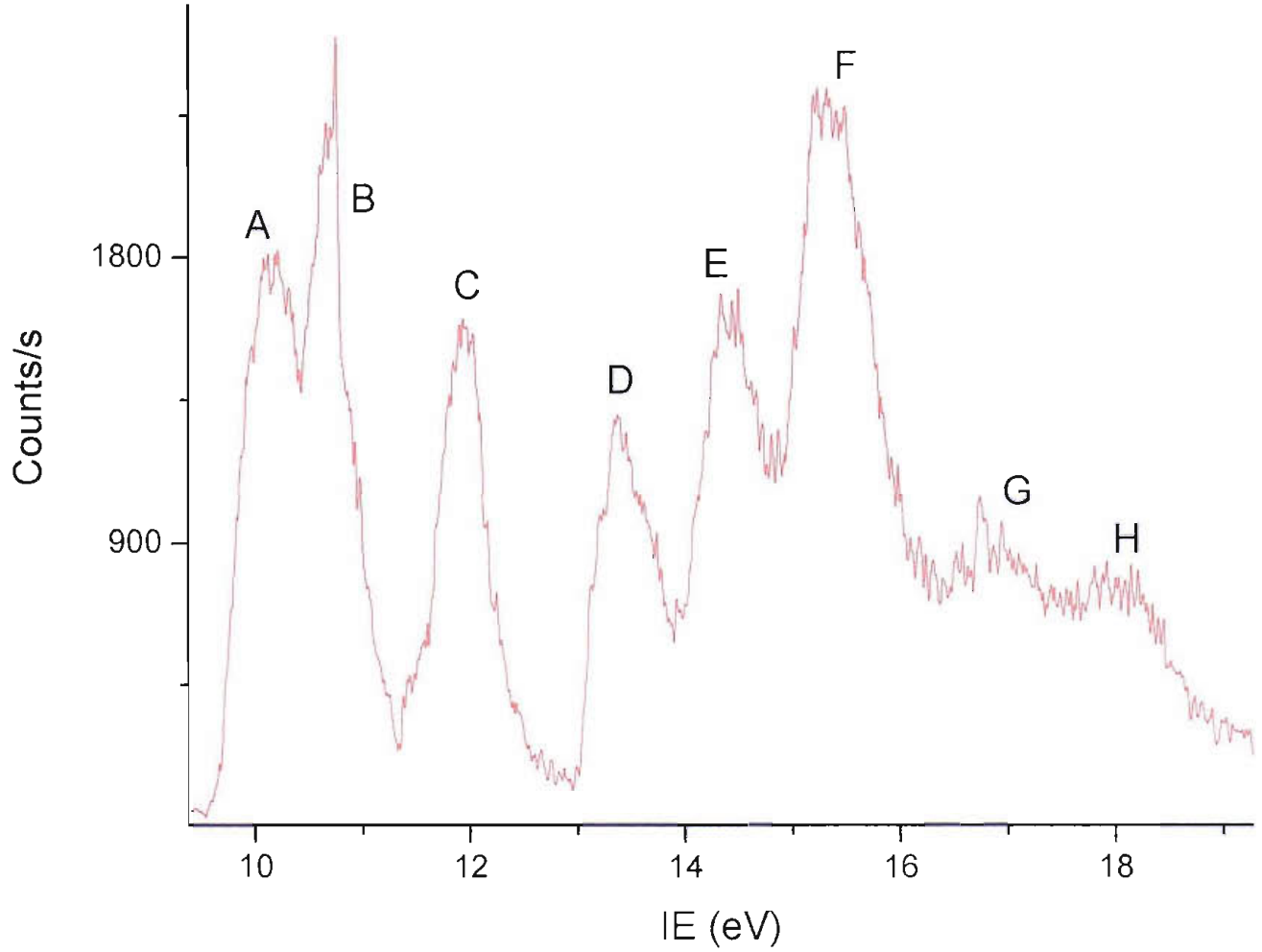

Figure 5.5- The HeI photoelectron spectrum of azidoacetamide recorded at a heater temperature of 80 °C

5.2.3 RESULTS OF MOLECULAR ORBITAL CALCULATIONS

At the MP2/6-31G** level of calculation, four minimum energy conformers have been found for $N_3CH_2CONH_2$ in its closed-shell singlet state, depending on the different relative positions (*cis* or *trans*) of the carbonyl, methylene and azide groups: their geometries are shown in Figure 5.6. They are not perfectly planar: in each case the CH_2 group and the N_3 chain are slightly out of the mirror plane (in structure *cis-trans* the chain is particularly out of the plane). Therefore they all have C_1 symmetry. Attempts to locate a minimum geometry structure in the C_s point group proved unsuccessful, both with this basis set and with a 6-311++G** basis set.

Table 5.2 reports the total and relative energies calculated for the four structures. The energies of three of the structures differ only by 2.0 kcal/mol, while structure *trans-cis* lies approximately 5.2 kcal/mol higher in energy than the most stable form, structure *cis-cis*. Due to the small differences in energy between *trans-trans*, *cis-cis* and *cis-trans* conformers, it is likely that all the three structures contribute to the experimental photoelectron and infrared spectra, considering that $k_B T$ at 300 K is around 0.60 kcal/mol.

Table 5.3 reports the most important geometrical parameters for the most stable conformer (see Figure 5.7 for the labelling of the atoms).

Table 5.4 reports the first nine VIEs for the most stable conformer (structure *cis-cis*), calculated with Koopmans' theorem, obtained by taking the negative of the orbital energies computed at the MP2/6-31G** level, and the first three VIEs calculated with ΔSCF method, and compares them with the experimental VIEs. Values in parentheses indicate doublet ionic states, calculated at the neutral minimum energy geometry, contaminated with higher multiplicity states: a state was considered contaminated when the spin quantum number S is such that $S^2 > 0.9$ for these states, where S^2 for a pure doublet state is 0.75.

Attempts to calculate adiabatic ionization energies (AIEs) by optimization of the geometry of the cation, starting from the geometry of the most stable neutral conformer (*cis-cis*), was prevented by the lack of convergence of the calculations both at the MP2 and Hartree-Fock level, either on removal of an electron from the HOMO or from the second HOMO.

Table 5.5 compares the calculated values of the VIEs for all four conformers obtained by Koopmans' theorem at the HF level.

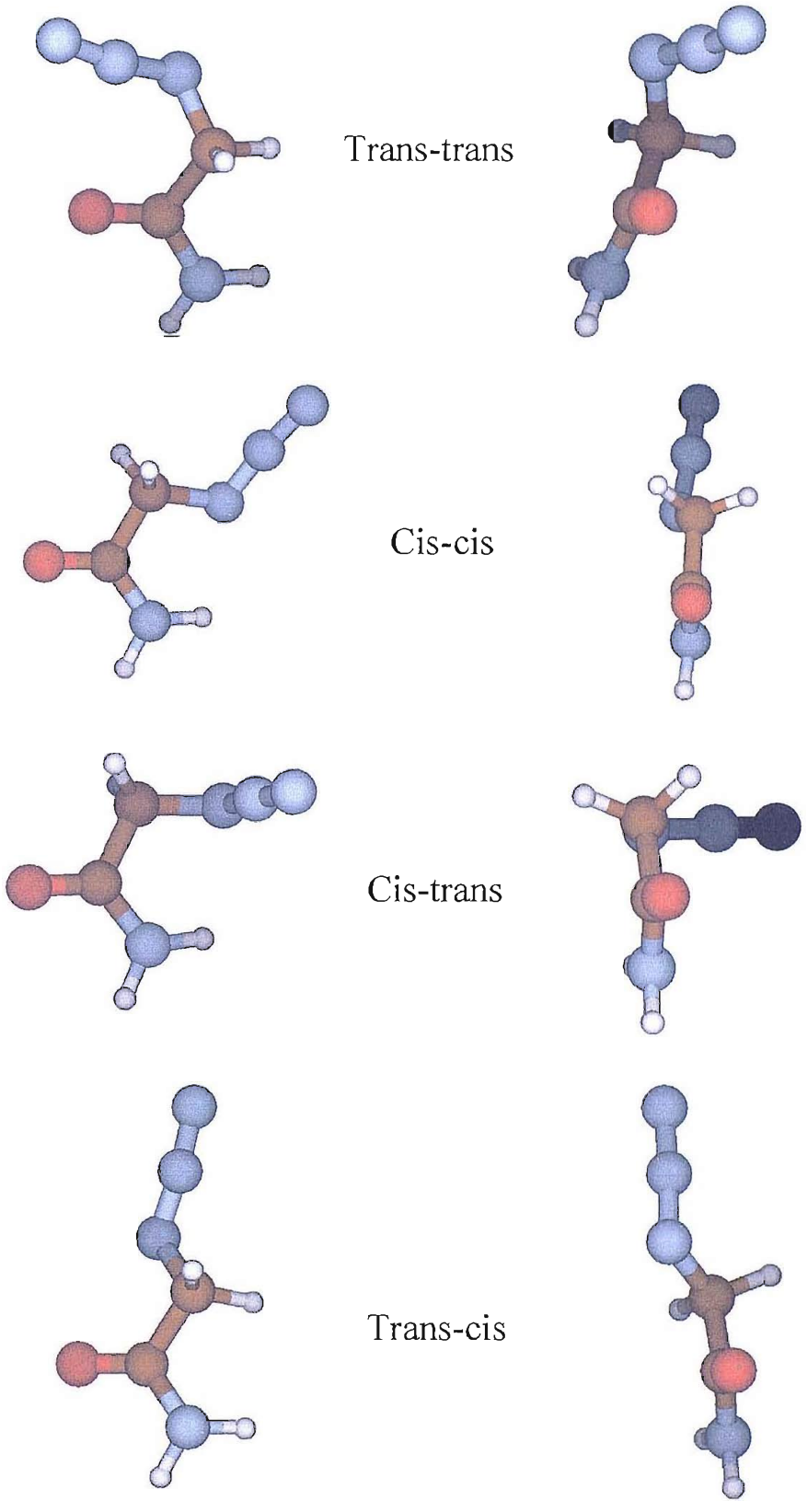

Figure 5.6- The four conformers of azidoacetamide obtained from *ab initio* calculations using the Gaussian98 program at the MP2/6-31G level; the labelling reflects the relative position of the methylene hydrogen atoms to the oxygen atom and of the azide chain to the methylene hydrogen atoms. As an example, structure *cis-trans* has oxygen and hydrogen atoms in the *cis* position with respect to the C-C bond, and the azide chain and the hydrogen atoms in the *trans* position with respect to the C-N bond.**

Table 5.2- Total energies of the conformers calculated for azidoacetamide at the MP2/6-31G** level

Structure	Energy (hartrees)	Relative energies (kcal/mol)
Trans-trans	-371.761257	1.96
Cis-cis	-371.7643758	0
Cis-trans	-371.7641118	0.17
Trans-cis	-371.7561247	5.18

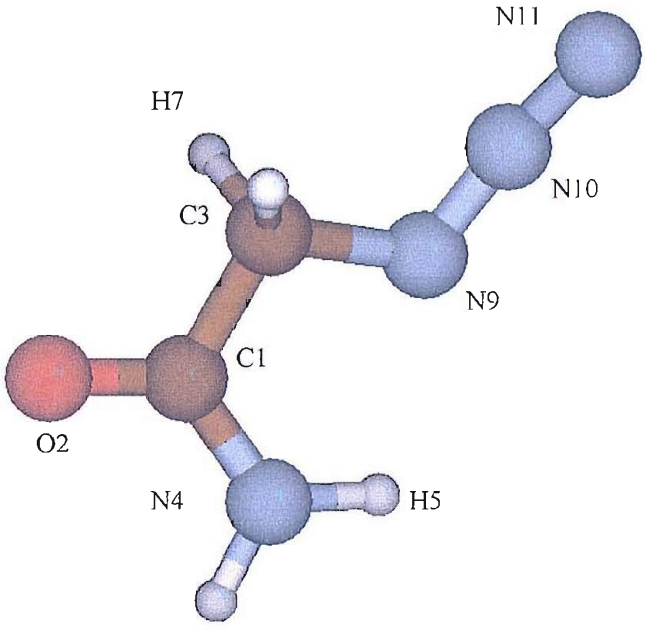

Figure 5.7- Atom labelling in structure *cis-cis* of azidoacetamide

Table 5.3- Geometrical parameters for the lowest energy structure of azidoacetamide

Bond	Length (Å)	Angle	Value (°)
N11-N10	1.163	N11-N10-N9	173.2
N10-N9	1.2455	N10-N9-C3	115.52
N9-C3	1.4776	N9-C3-H7	111.25
C3-H7	1.0913	N9-C3-C1	110.65
C3-C1	1.5243	O2-C1-N4	124.87
C1-O2	1.2291	C1-N4-H5	119.1
C1-N4	1.3573	N10-N9-C3-C1	189.3
N4-H5	1.0059	N9-C3-C1-O2	191.6

Table 5.4- Experimental and computed VIEs of *cis-cis* azidoacetamide

KT calculated VIE (eV)	KT calculated VIE · 0.92 (eV)	ΔSCF calculated VIE (eV)	S^2 for the ion	Experimental VIE (eV)	Band
10.69	9.83	10.24	0.86	10.16	A
11.34	10.43	(10.29)	0.954	10.68	B
11.70	10.76	10.40	0.795		
12.57	11.56			11.94	C
14.75	13.57			13.37	D
15.97	14.69			14.44	E
17.11	15.75			15.35	F
17.52	16.11			16.93	G

Table 5.5- Comparison between the VIEs of the four minimum energy conformers of azidoacetamide calculated with Koopmans' theorem (all expressed in eV)

Ionization	KT VIEs·0.92 *cis-cis*	KT VIEs·0.92 *cis-trans*	KT VIEs·0.92 *trans-trans*	KT VIEs·0.92 *trans-cis*	Exp. VIEs
(26 a)$^{-1}$→ ^{2}A	9.83	9.70	9.30	9.54	**10.16**
(25 a)$^{-1}$→ ^{2}A	10.43	10.48	10.68	10.55	**10.68**
(24 a)$^{-1}$→ ^{2}A	10.76	11.02	10.76	10.87	
(23 a)$^{-1}$→ ^{2}A	11.56	11.77	11.40	11.17	**11.94**
(22 a)$^{-1}$→ ^{2}A	13.57	13.52	13.79	13.74	**13.37**
(21 a)$^{-1}$→ ^{2}A	14.69	14.88	14.84	14.78	**14.44**
(20 a)$^{-1}$→ ^{2}A	15.75	15.54	15.18	15.50	**15.35**
(19 a)$^{-1}$→ ^{2}A	16.11	15.92	16.34	16.34	**16.93**

Calculations performed at the Hartree-Fock level led to location of only two minimum energy geometry conformers, corresponding to structures *cis-cis* and *trans-trans*. The description of the molecular orbitals for structures *cis-trans* and *trans-cis* have been obtained from a single point Hartree-Fock calculation assuming the geometries being those calculated at the MP2 level.

Figure 5.8 shows the shape of the first six MOs calculated for the most stable conformer of azidoacetamide (*cis-cis*) at the HF level.

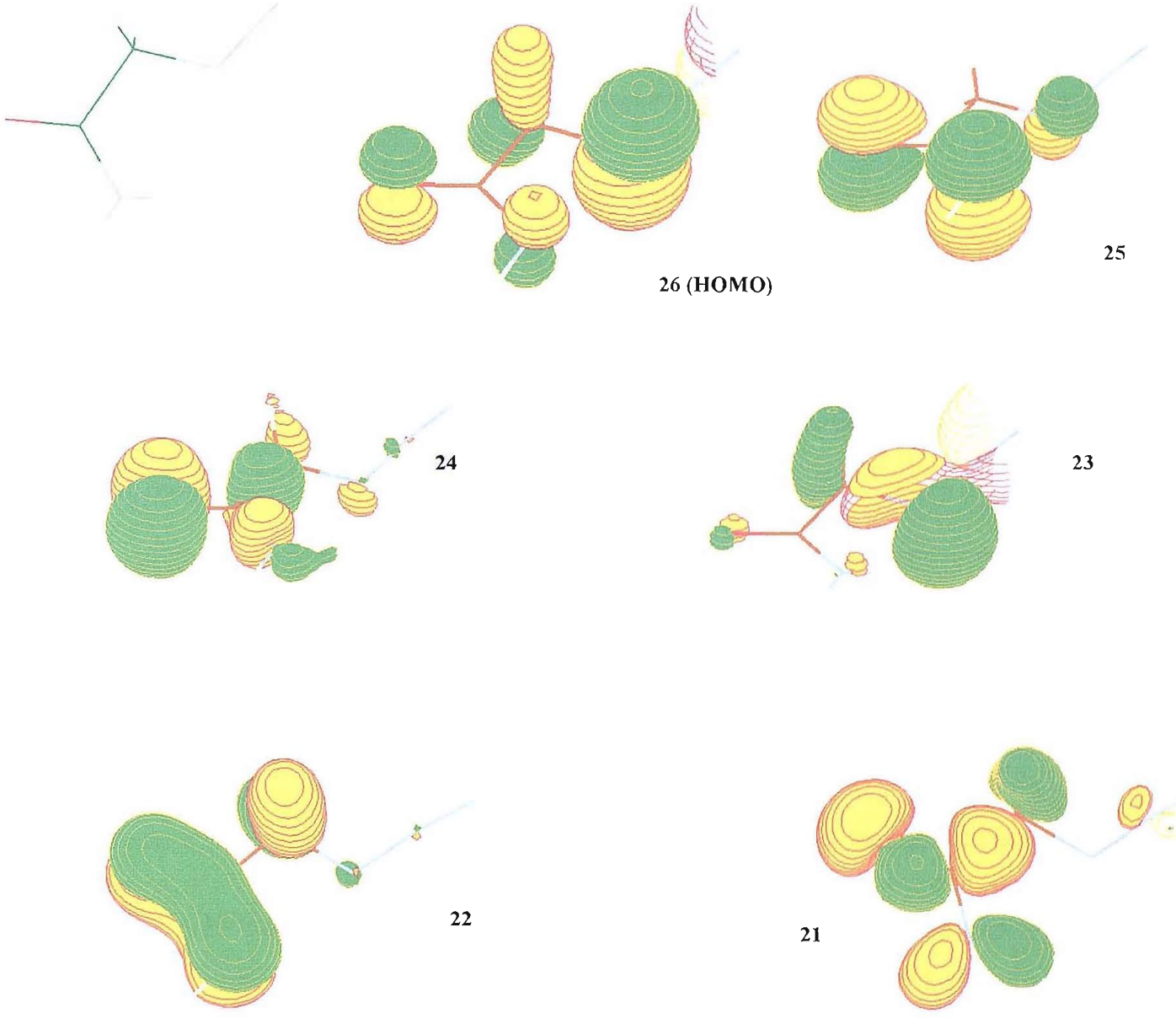

Figure 5.8- The six highest occupied molecular orbitals for structure *cis-cis* of azidoacetamide as obtained from calculations performed with the Gaussian98 program at the HF/6-31G level. Refer to Figure 5.7 for the identification of the atoms on the skeleton of the molecule (reported here in the top left corner).**

Assuming the main skeleton of the azide to be quasi-planar, molecular orbital 26 (the HOMO) is a delocalized orbital with mostly antibonding character: the major contribution is due to a p_π antibonding system between the last nitrogen atom of the azide chain and the adjacent carbon, and between the first and last nitrogen atoms of the azide chain. Lone pairs are also contributing from the oxygen and amidic nitrogen atoms.

MO 25 retains mostly π-type symmetry: it has mainly a p_π-bonding character on the NH_2 group, and a slight p_π-bonding character on the carbonyl group. A further contribution is due to the lone pair on the first nitrogen atom on the azide chain.

MO 24 is basically antibonding between the oxygen atom and the carbonyl carbon atom, still with p_π symmetry but this time with a nodal plane perpendicular to the plane of the molecule. The orbital has also σ-bonding character on the H_2N-C-CH_2 frame.

MO 23 is a delocalized orbital, mainly with p_π-antibonding character (and nodal plane perpendicular to the molecular plane) between the first and last nitrogen atoms of the azide chain and with bonding character on the methylene group.

MO 22 is strongly p_π-bonding on the O=C-NH_2 sector of the molecule, and p_π-antibonding between the carbonyl and the methylene carbon atoms.

MO 21 is p_π-antibonding between the amidic nitrogen and the adjacent carbon atom and σ-bonding on the carbonyl group and between the carbonyl and the methylene carbon atoms.

As expected, the highest occupied molecular orbitals have mainly antibonding or non-bonding character, but in contrast with previous calculations on other azides [10-12], the contribution of the azide chain to these HOMOs is relatively low. Molecular orbitals 20-26 are not widely delocalized: this is in agreement with the relatively sharp appearance of the photoelectron bands in the azide spectrum; the mostly localized molecular orbital, MO 25, is the one whose ionization produces band B, which is in fact the sharpest.

Comparing structure *trans-trans* of azidoacetamide with the *cis-cis* one, the main general difference between the molecular orbitals calculated for the two conformers is that in the *trans-trans* form the azide chain contributes more to the description of the outermost occupied MOs with respect to the *cis-cis* structure. This is particularly evident, for example, for MOs 23 and 24. In the case of the HOMO (MO 26), the major contribution is still due to the p_π- antibonding character on the H_2C-N bond, but in the case of the *trans-trans* structure there is a p_π- antibonding contribution on the carbonyl group and a p_π-bonding contribution between the amidic nitrogen and the carbonyl carbon atoms and between the

carbonyl and methylene carbon atoms: all of these characters were absent in the HOMO of structure *cis-cis*. Also, a more marked contribution of the lone pair of the last nitrogen atom of the azide chain can be identified.

The comparison between the HOMOs of the two conformers explains the big difference (0.53 eV) predicted by Koopmans' theorem for the vertical ionization energies of their first bands.

Harmonic vibrational frequencies have been calculated for the four conformers at the MP2/6-31G** level by means of calculations of second derivatives. Figure 5.9 displays the calculated IR spectra for each structure, while Table 5.6 reports the computed IR frequencies for the four conformers of azidoacetamide and compares them with the values for the most prominent experimental peaks.

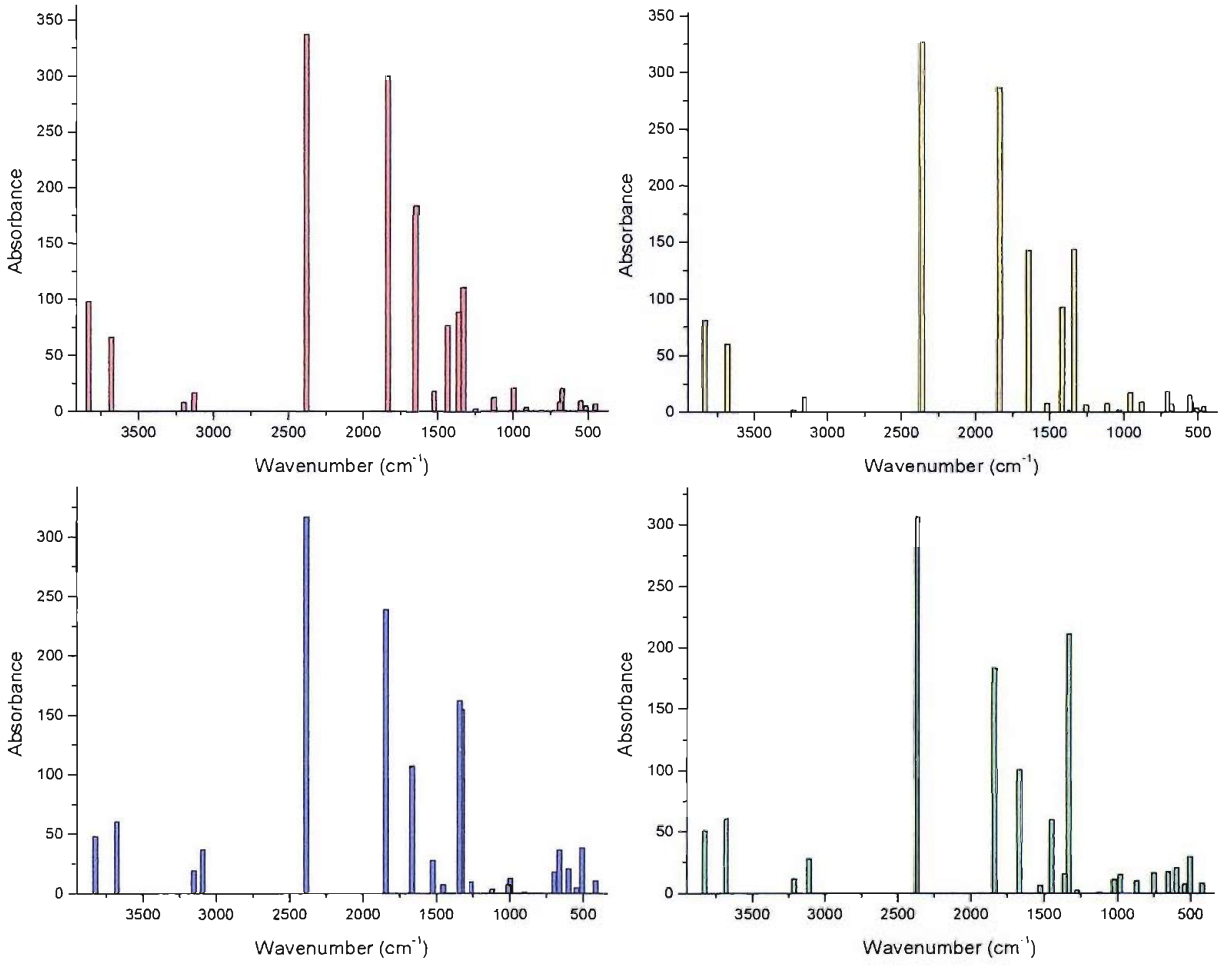

Fig. 5.9- The four IR spectra calculated for the conformers *cis-cis* (red lines), *cis-trans* (yellow lines), *trans-trans* (blue lines) and *trans-cis* (green lines) of azidoacetamide at the MP2/6-31G level**

Table 5.6- Calculated IR bands and intensities of the four minimum energy conformers of azidoacetamide at the MP2/6-31G level**

Cis-cis		*Cis-trans*		*Trans-trans*		*Trans-cis*			
Calculated frequency (cm^{-1})	Absorbance (Km/mol)	Calculated frequency (cm^{-1})	Absorbance (Km/mol)	Calculated frequency (cm^{-1})	Absorbance (Km/mol)	Calculated frequency (cm^{-1})	Absorbance (Km/mol)	Experim. frequency (cm^{-1})	Normal mode
449.5	6.04	460.3	5.13	414.8	10.02	420.8	7.96		
512.0	4.33	505.4	3.58	505.8	37.80	501.2	29.43		
541.9	3.78	542.0	8.30	542.6	4.35	540.2	7.32		
546.5	9.28	553.0	14.80	596.9	20.14	592.0	20.51		
670.6	20.43	677.0	6.80	660.9	35.98	650.2	17.40		
685.7	8.26	705.0	18.26	695.7	17.53	747.3	16.40		
910.7	2.83	877.8	8.55	898.3	1.03	866.5	9.65		
994.3	20.79	953.7	17.14	995.9	12.39	977.4	15.00		
1016.2	0.66	1031.0	2.14	1010.2	6.92	1018.5	11.13		
1125.7	11.84	1112.6	7.72	1119.3	3.31	1120.3	0.71		
1251.1	2.47	1254.3	6.42	1261.7	9.30	1274.2	2.28		
1332.0	110.10	1334.7	143.62	1327.9	154.11	1327.5	210.9		C-N=N stretch
1363.4	88.52	1365.4	1.33	1343.9	161.41	1357.5	15.6		$C-H_2$ wag
1434.2	76.75	1415.4	92.93	1454.5	7.10	1447.3	59.98		
1522.5	18.07	1517.4	7.50	1525.1	27.42	1523.5	6.27		$C-H_2$ scissor
1646.2	183.15	1641.4	142.62	1664.6	107.20	1664.2	100.54	**1574**	$N-H_2$ scissor
1835.1	299.50	1833.9	286.59	1842.4	237.92	1833.9	183.10	**1719**	C=O str.
2376.3	336.67	2356.9	326.84	2385.6	316.44	2364.7	306.02	**2126**	N-N-N str.
3127.8	16.10	3156.6	12.82	3096.9	36.36	3109.1	27.65		$C-H_2$ sym. str.
3196.1	7.70	3231.3	2.04	3155.5	18.71	3211.0	11.42		$C-H_2$ asym str
3680.1	65.84	3681.9	60.05	3678.4	59.46	3679.7	60.11	**3420**	$N-H_2$ sym. str.
3831.0	97.48	3833.0	80.99	3824.3	47.12	3827.2	50.50	**3538**	$N-H_2$ asym str

These computed results and the comparison with experimental IR spectra are particularly informative: the two most energetically stable structures- *cis-cis* and *cis-trans*- display an intensity ratio for the two highest vibrations (in the 3500-4000 cm^{-1} range) that reflect the experimental matrix IR spectra intensity ratio, while for structures *trans-trans* and *trans-cis* the relative intensities of the two bands are

reversed. This indicates that structures *cis-cis* and *cis-trans* are those which contribute most to the IR spectrum. The small satellite peaks around the N_3 stretching peak could reflect the co-presence of different conformers of azidoacetamide trapped in the matrix.

The two most stable structures (*cis-cis* and *cis-trans*) have similar spectra, but the one arising from the structure *cis-trans* is slightly closer to the experimental spectrum in the 1900-1300 cm^{-1} region, in particular the bands predicted at 1640 and 1330 cm^{-1} which in structure *cis-trans* have equal computed intensities and therefore reflect the experimental intensity ratio better. Figure 5.10 compares the experimental IR spectrum obtained in a nitrogen matrix with the one calculated for conformer *cis-trans* allowing the calculated frequencies to assume a Gaussian shape. The IR spectrum calculated for the *cis-trans* conformer has been chosen as it is in slightly better agreement with the experimental spectrum, and the energy difference with the most stable conformer- *cis-cis*- is negligible.

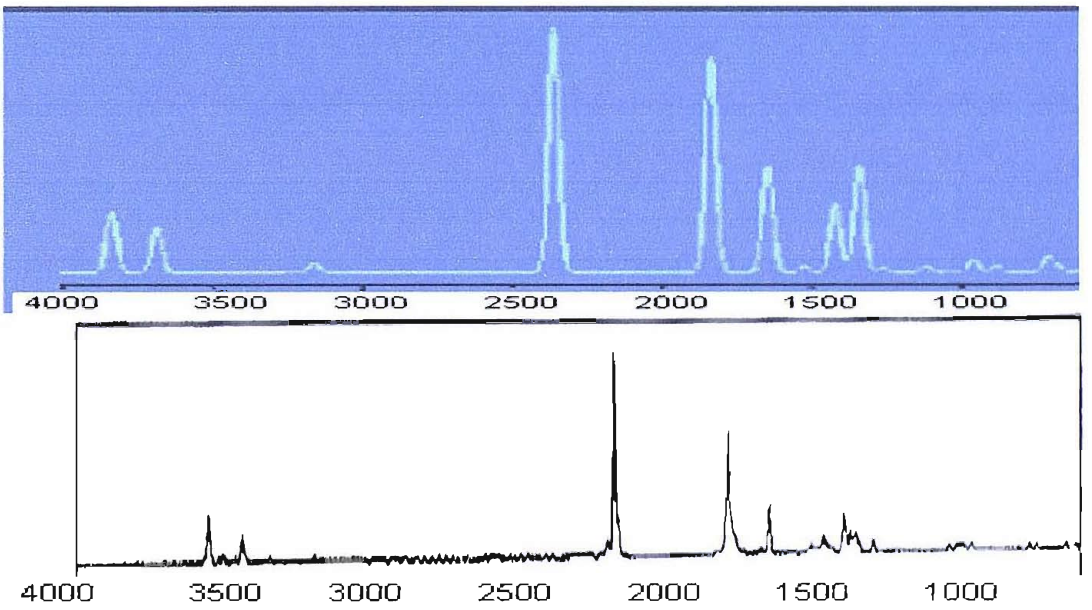

Fig. 5.10- The IR spectrum calculated for conformer *cis-trans* of azidoacetamide at the MP2/6-31G level, compared with the experimental spectrum recorded in the nitrogen matrix.**

The higher values of the calculated frequencies compared to the experimental values, especially for those above 3000 cm^{-1}, are expected considering that anharmonicity has been neglected, and that electron correlation was only partially taken into account in the calculations [13-15].

The differences between experiment and calculations are reduced if the possibility that two or more conformers of azidoacetamide are trapped in the matrix is considered: in this case, the agreement in the band pattern especially in the 500-2000 cm^{-1} region is very good, in particular for the number of bands detected in that region. The possibility of trapping more than just the *cis-cis* structure is confirmed by the relatively low energy difference between three of the four optimized structures.

5.2.4 THERMAL DECOMPOSITION EXPERIMENTS

Photoelectron spectroscopy

The first evidence of pyrolysis is the appearance of the first, sharp band of nitrogen with VIE at 15.58 eV [8] at around 210 °C. With increasing temperature the parent bands decrease, while four bands associated with three products appear simultaneously: a broad band at 10.66 eV (VIE) and a vibrationally resolved band at 12.50 eV (VIE) are both attributed [16] to methyl imine, CH_2NH. The vibrationally resolved band at 11.61 eV (VIE equal to AIE) is attributed [17] to isocyanic acid, HNCO. A very weak vibrationally structured band with VIE equal to the AIE at 13.60 eV indicates [8] the formation of HCN. All these bands increase in intensity when the temperature is raised, and- using as an indicator the first azide band with VIE at 10.16 eV- no bands associated to azidoacetamide are present anymore when the temperature reaches 600 °C.

At intermediate temperatures- when the degree of pyrolysis of the azide is relatively low- no clear features were observed which could be attributed to an imine intermediate, iminoacetamide $HN{=}CHCONH_2$ or a nitrene intermediate NCH_2CONH_2: however, according to ΔSCF calculations at the 6-31G** level, their photoelectron bands are expected to be very close in energy to those of the parent azide. The computed values for the two first VIEs of these compounds are 9.94 and 10.11 eV for $HN{=}CHCONH_2$ in its $X\ ^1A'$ state and 9.65 and 10.16 eV for NCH_2CONH_2 in its $X\ ^3A''$ state. The only possible indication of the formation of such a molecule can be the growth of the band at approximately 10.50 eV at temperatures around 300 °C: it is clear from the band at 10.16 eV that at those temperatures the azide is already consumed and that therefore there is an additional contribution to the band at 10.50 eV. CH_2NH contributes too, but considering the intensity of the band at 12.50 eV it seems that a further contribution must be invoked to explain the prominent feature around 10.50 eV. Considering the matrix isolation results- see following section- iminoacetamide is the most likely candidate.

Figure 5.11 reports four PE spectra of azidoacetamide vapour recorded at different degrees of pyrolysis, from 80 °C to 900 °C. Figure 5.12 shows in more detail two photoelectron spectra obtained at 280 °C (roughly 50% of azide decomposed) and 590 °C (roughly 100% of azide decomposed), where contributions from different products have been shaded.

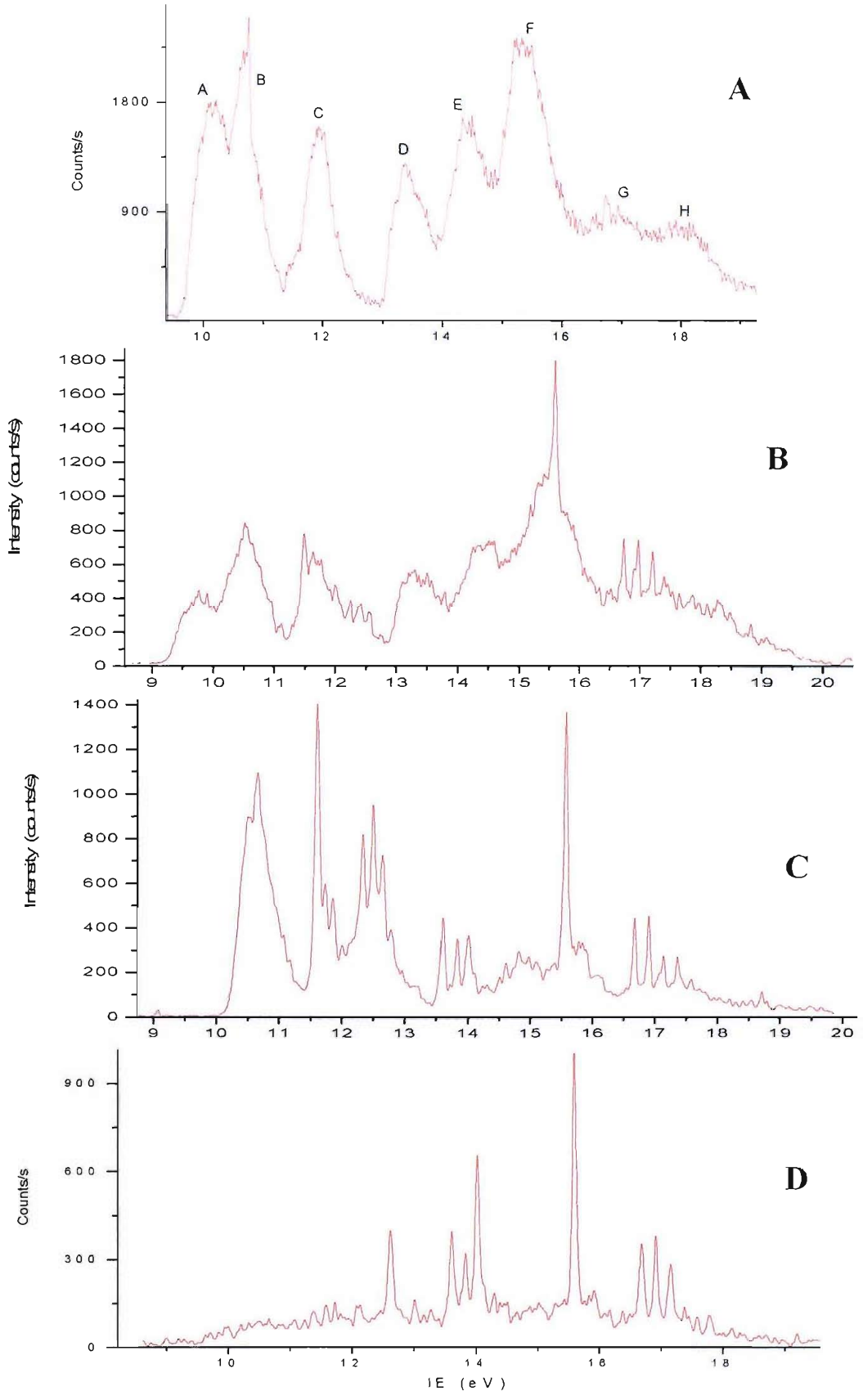

Figure 5.11- PE spectra of azidoacetamide recorded at heater temperatures of A) 90, B) 260, C) 580 and D) 900 C.

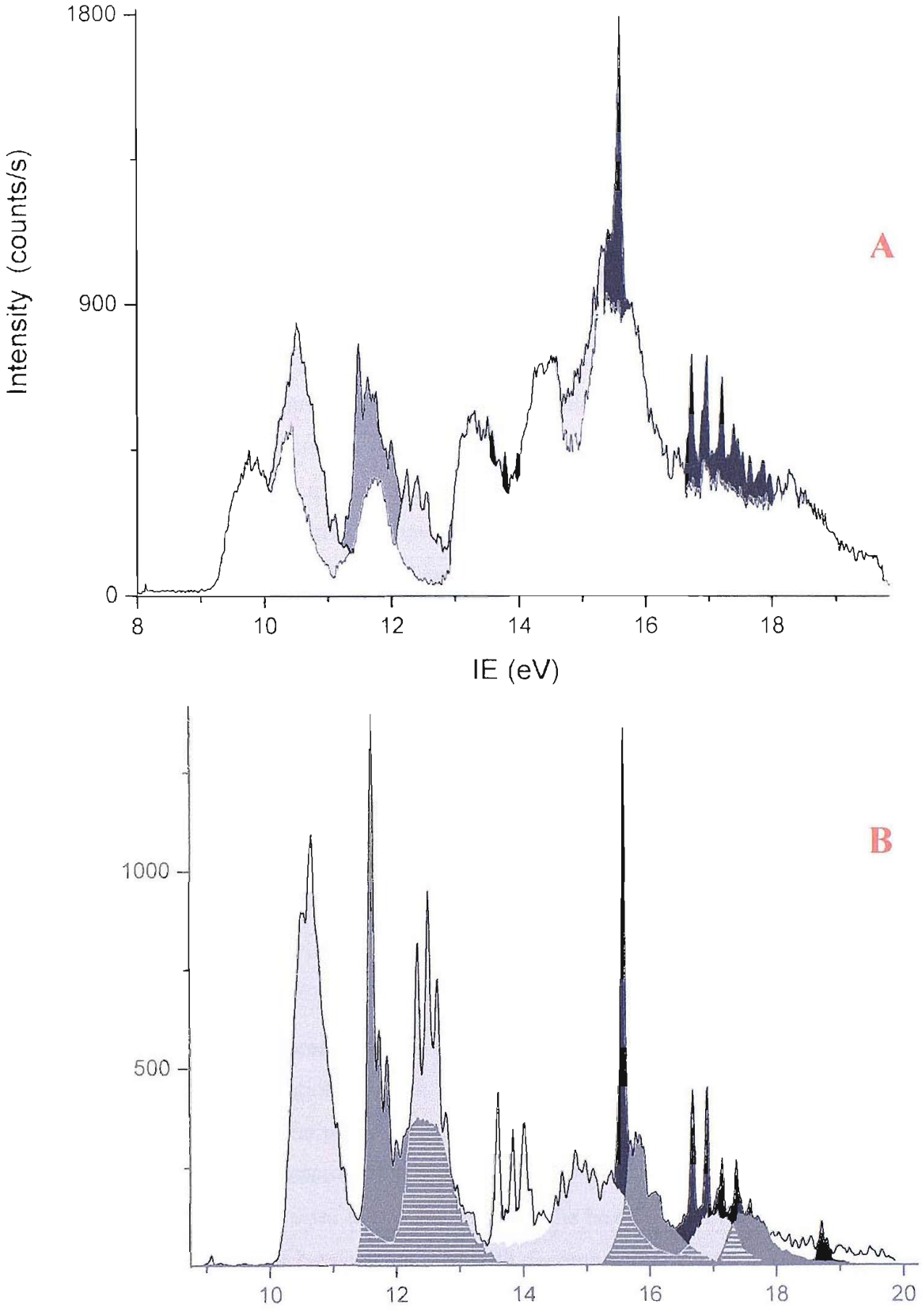

Figure 5.12- PE spectra of azidoacetamide vapours heated at A) 280 °C and B) 590 °C in which the contributions from different products have been shaded; light grey CH_2NH, dark grey HNCO, black N_2, white HCN.

At 600 °C, HCN is present, but in a relatively low amount (evaluated by the intensity of its first band, with VIE at 13.60 eV). A sharp feature at 14.01 eV, partially overlapping with the third vibrational component of the HCN first band, is attributed [8] to CO. The low intensity seems to indicate that these molecules- of high photoelectron cross section- are present in low partial pressures at early stages of the azide decomposition: as can be seen in the following chapters, other experiments which yield HCN or CO as major decomposition products of an azide show that the intensity of the photoelectron bands associated with these products is much greater. The fact that the band intensities increase when the temperature passes from 600 °C to 900 °C indicates that probably HCN and CO appear also as secondary decomposition products, from CH_2=NH and HNCO respectively.

At 900 °C N_2, HCN and CO are the only contributors to the spectrum (not considering the H_2O band at 12.62 eV due to residual water in the system): all the bands associated with other decomposition products are negligible. A spectrum at 900 °C was reported in Figure 5.11.

Other possible decomposition products have been considered in the spectral analysis, notably ammonia, hydrazine and formamide. In all the PES experiments, no clear evidence for bands assignable to these products is present. Formamide should display [8] a vibrationally resolved band at 10.13 eV quite different from the first band of the parent azide and of CH_2=NH. Hydrazine is characterized [18] by two broad bands partially vibrationally resolved: the first one has components at 9.91 and 10.64 eV. Ammonia should show [18] a very structured, broad band with VIE at 10.85 eV. From the spectra, no features that could be associated with $HCONH_2$, NH_2NH_2 or NH_3 are observed; however, the overlap of the bands of the azide and of CH_2=NH means that small contributions from these species cannot be ruled out.

Matrix isolation IR spectroscopy

A succession of matrix isolation infrared spectra recorded at increasing temperature is reported in Figure 5.13. Table 5.7 lists the molecules associated with the labels on the bands in this figure, along with the value of the most intense features in the spectra.

In infrared spectroscopy, nitrogen cannot be detected: the beginning of the azide pyrolysis is therefore marked by the appearance of bands associated with decomposition products. The first evidence can be identified at around 200 °C, when a band at 869 cm^{-1} begins to be observed.

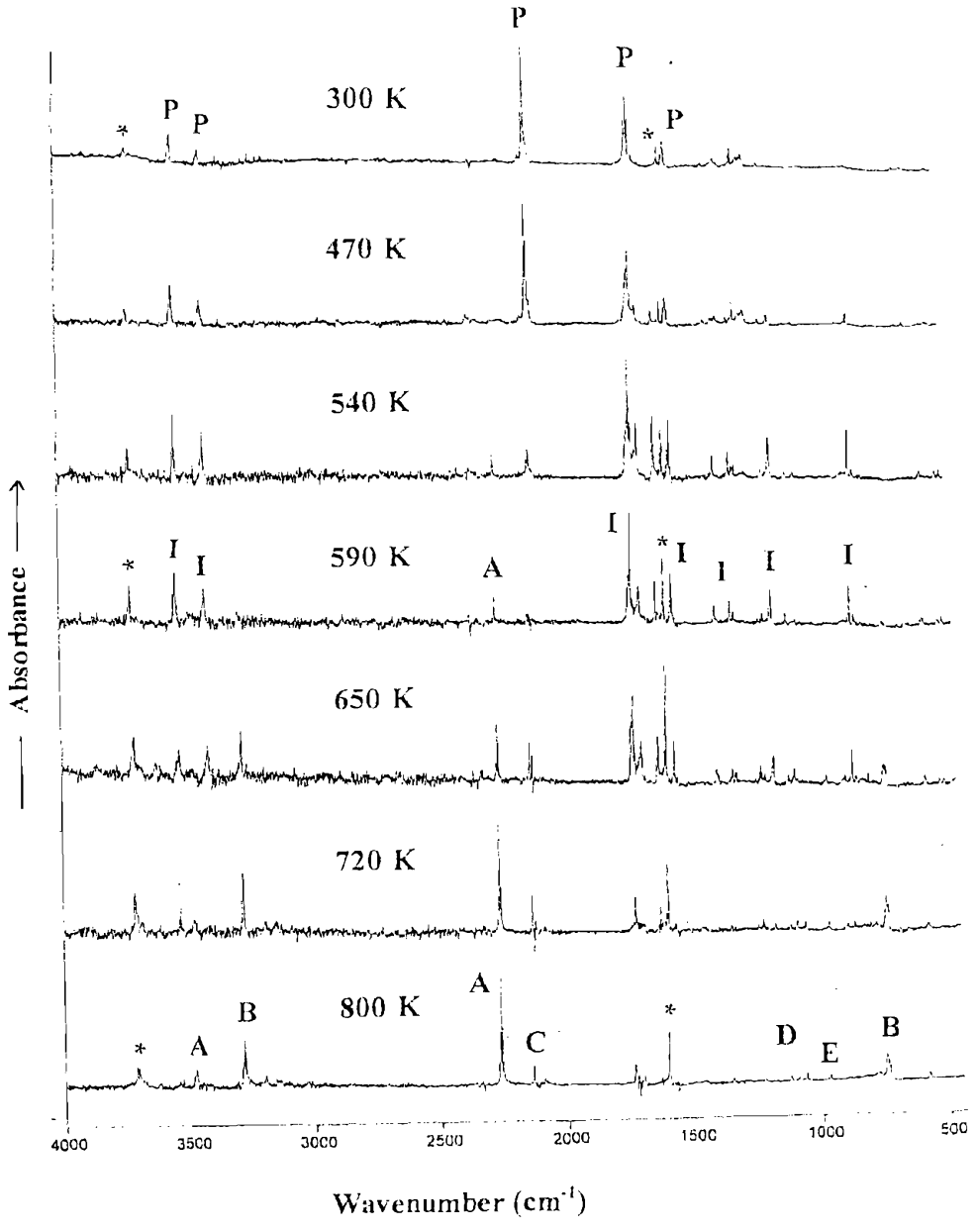

Figure 5.13- The IR spectra recorded for azidoacetamide vapours heated between 30 °C and 530 °C trapped in a nitrogen matrix

Table 5.7- Labels and assignment of the most significant IR bands observed in the matrix isolation study of azidoacetamide thermal decomposition (refer to Figure 5.13 for the labelling of the bands)

Label	*N_2 matrix frequency (cm^{-1})*	*Assignment*	*Reference*
P	3538,3420, 2126, 1719, 1574	**$H_2NCOCH_2N_3$**	
I	3538, 3418, 1728, 1566, 1399, 1339, 1178, 869	**$H_2NCOCHNH$**	
A	3483	**HNCO**	[19]
B	3287, 747, 737	**HCN**	[20]
C	2139	**CO**	[21]
D	3032, 2919, 1637, 1450, 1352, 1127, 1065	**CH_2NH**	[22]
E	970	**NH_3**	[23]

With increasing temperatures, the azide bands lower in intensity, as exemplified by the decrease of the strong N_3 absorption at 2126 cm^{-1}, while new bands appear. Among these, two types can be distinguished. A set of bands which increases steadily in intensity with the raising of the temperature: this is the case for example for the bands at 2265 (labelled A in Figure 5.13), 3287 (labelled B), 2139 (labelled C), 1127 cm^{-1} (labelled D) and 970 cm^{-1} (labelled E) which have been assigned- by referring to previous matrix IR studies- to HNCO, HCN, CO, CH_2NH and NH_3 respectively [19-23]. A second set of bands, identified with the label I in Figure 5.13, shows a different thermal behaviour, with an increase of intensity between 200 and 300 °C followed by a decrease for temperatures above 350 °C and a total disappearance beyond 450 °C: this suggests the presence of a reactive intermediate being formed as a consequence of the azide decomposition, and which is subsequently degraded to secondary products. The important evidence resulting from the analysis of the spectra is that all these bands, which cannot be assigned to HNCO, HCN, CO, CH_2NH and NH_3, display the same kind of intermediate thermal behaviour. Moreover, the fact that their relative intensity ratio is not altered by changing pyrolysis temperature, deposition time or other experimental parameters suggests that all the intermediate bands belong to the same species. The bands between 3600 and 3400 cm^{-1} and the strong band at 1728 cm^{-1} displayed by the intermediate give an initial indication of its structure, which must retain the N-H and the C=O groups from the parent azide. Comparisons with spectra of possible products such as formamide proved that this intermediate could not be associated with any stable reaction product. A full assignment of all the bands and of the compound associated with them can only be achieved with the support of *ab inito* calculations.

5.2.5 CHARACTERIZATION OF THE POSSIBLE REACTION INTERMEDIATES

Following the pattern already indicated in other azide decompositions [10-12], the formation of nitreneacetamide, $:NCH_2CONH_2$, was supposed as the initial step accompanying the release of nitrogen when azidoacetamide is pyrolysed, following the scheme

$$^1N_3CH_2CONH_2 \rightarrow {}^1N_2 + {}^1:NCH_2CONH_2$$

The established instability of nitrenes with respect to imines [6, 24], for example, by means of a 1,2-hydrogen shift like in

$$^1:NCH_2CONH_2 \rightarrow {}^1HN{=}CHCONH_2$$

required also the *ab initio* investigation of the possible imines related to nitreneacetamide.

Nitreneacetamide

The search for minimum energy structures of $:NCH_2CONH_2$ on the closed shell singlet surface at the MP2/6-31G** restricted level converged to the imines (see the following section for geometric and energetic details): singlet nitrene appears therefore to be unstable with respect to interconversion to an imine, at least at this level of calculation.

An unrestricted calculation at the MP2/6-31G** level on the open-shell triplet surface with configuration $...(a')^2(a'')^2(a')^1(a'')^1$ led to the identification of a minimum, with the planar structure shown in Figure 5.14.

No minimum energy structure with the nitrogen atom of the $-CH_2N$ group *cis* to the oxygen atom was obtained: the optimization gave rise to convergence to the *trans* conformer shown in Figure 5.14, probably because of the stabilizing interaction between the methylene protons and the oxygen, and between the terminal nitrogen and the iminic proton. The computed total energy of the triplet nitrene at the MP2/6-31G** level is -262.4949107 hartrees, and its electronic state is $^3A''$.

Considering that the ground state of azidoacetamide and the ground states of all possible stable decomposition products are singlets, spin conservation selection rules imply that the triplet nitrene is not produced among the possible pyrolysis products: the calculated vertical ionization energies and vibrational frequencies of triplet nitrene are therefore not reported.

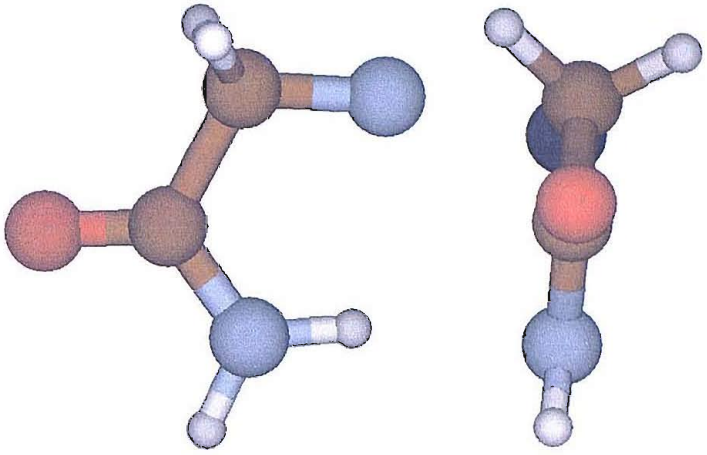

Figure 5.14- Structure of the triplet state conformer of nitreneacetamide obtained at the MP2/6-31G level**

Iminoacetamide

For $HN{=}CHCONH_2$ four conformers with all real vibrational frequencies have been located at the MP2/6-31G** level on the closed-shell singlet surface: their geometries are shown in Figure 5.15. Structures *cis-cis* and *trans-trans* are planar, structure *trans-cis* is very close to planarity, while structure *cis-trans* is characterized by a distinctly out of plane terminal NH group. The labelling nomenclature describes, as for azidoacetamide, the relative positions of the C-H hydrogen atom with respect to the oxygen atom and of the iminic hydrogen atom relative to the C-H hydrogen atom.

The two most stable structures, *cis-cis* and *trans-trans*, differ only by less than 1.7 kcal/mol, while structures *cis-trans* and *trans-cis* lie 5.3 and 7.7 kcal/mol respectively above structure *cis-cis*, which is the most stable one. It is likely that structures *trans-trans* and *cis-cis* contribute to the experimental photoelectron spectrum.

Table 5.8 reports the total energies of the four structures. The ground electronic state is $^1A'$. Figure 5.16 shows in greater detail the most stable of them, structure *cis-cis*; its geometrical parameters are listed in Table 5.9.

Table 5.10 reports the VIEs calculated by applying Koopmans' theorem to the orbital energies of *cis-cis* iminoacetamide, and the two first VIEs and the first AIE calculated via ΔSCF method.

Table 5.11 shows the computed IR frequencies and intensities for iminoacetamide and compares them with the bands detected in the IR matrix isolation experiments of thermal decomposition of azidoacetamide. Even if the most stable structure (the *cis-cis* conformer) is expected to be the one that mainly contributes to the experimental IR spectrum, vibrational frequencies for all the structures are shown. The experimental and computed spectra are shown in Figure 5.17.

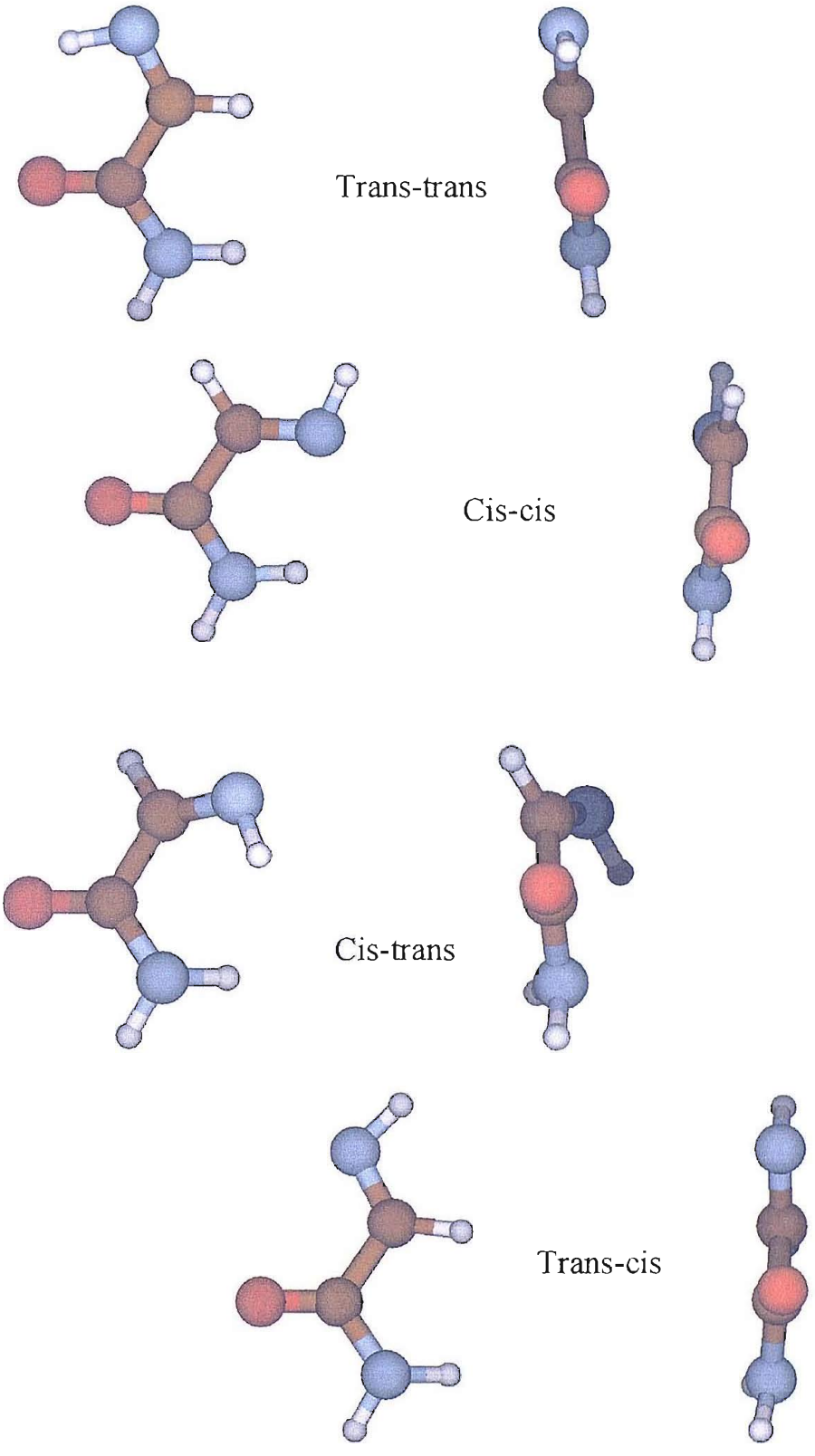

Figure 5.15- The four conformers of iminoacetamide obtained from *ab initio* calculations at the MP2/6-31G level; the labelling reflects the relative position of the methylene hydrogen to the oxygen atom and of the imine hydrogen to the methylene hydrogen. As an example, structure *cis-trans* has oxygen and hydrogen in a *cis* position with respect to the C-C bond, and the imine hydrogen and the methylene hydrogen in a *trans* position with respect to the C-N bond**

Table 5.8- Total and relative energies of iminoacetamide conformers at the MP2/6-31G** level

Structure	Symmetry	Energy (hartrees)	Relative energy (kcal/mol)
Trans-trans	C_S	-262.5898174	1.7
Cis-cis	C_S	-262.5924662	0
Cis-trans	C_1	-262.5840081	5.3
Trans-cis	C_1	-262.5801703	7.7

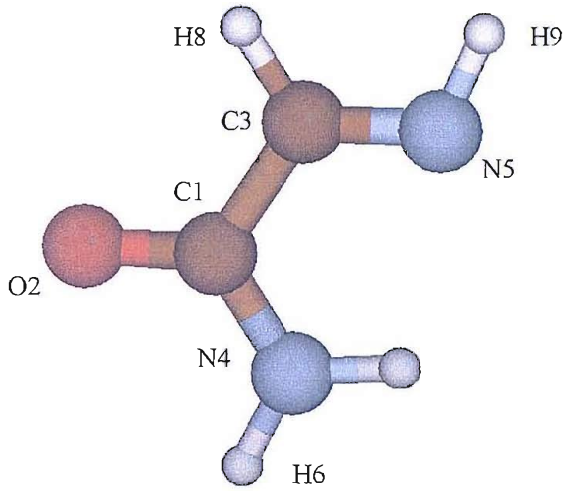

Figure 5.16- Atom labelling in structure *cis-cis* of iminoacetamide

Table 5.9- Geometrical parameters for the lowest energy structure of iminoacetamide (structure *cis-cis*)

Bond	Length (Å)	Angle	Value (°)
N5-H9	1.021	H9-N5-C3	110.54
N5-C3	1.284	N5-C3-C1	120.17
C3-H8	1.091	O2-C1-N4	125.64
C3-C1	1.506	C1-N4-H6	119.19
C1-O2	1.233	H9-N5-C3-C1	180.0
C1-N4	1.355	H8-C3-C1-O2	0.0
N4-H6	1.005	H6-N4-C1-C3	180.0

Table 5.10- Calculeted VIEs for structure cis-cis of iminoacetamide at the MP2/6-31G level**

KT calculated VIE (eV)	KT calculated VIE · 0.92 (eV)	ΔSCF calculated VIE (eV)	S^2 with the ion minimum energy geometry	ΔSCF calculated AIE (eV)	*Ionization*
11.21	10.31	9.94	0.75	9.65	$(19\ a'')^{-1} \rightarrow {}^2A''$
11.42	10.51	9.94	0.75		$(18\ a')^{-1} \rightarrow {}^2A'$
12.67	11.66	(10.11)	0.925		$(17\ a'')^{-1} \rightarrow {}^2A''$
12.95	11.91	10.93	0.789		$(16\ a')^{-1} \rightarrow {}^2A'$
16.03	14.75				
16.34	15.03				
17.76	16.34				

Table 5.11- Comparison between experimental IR bands of iminoacetamide and calculated IR bands for the minimum energy conformers of iminoacetamide (absorbances in Km/mol reported in brackets)

Calc. IR bands (cm^{-1})				Exp. bands (cm^{-1})	Calc. IR bands (cm^{-1})				Normal mode	Exp. bands (cm^{-1})
cis-cis	*cis-trans*	*trans-cis*	*trans-trans*		*cis-cis*	*cis-trans*	*trans-cis*	*trans-trans*		
522 (14.3)	463 (9.5)	465 (28.3)	475 (115.4)	**426 (s)**	1455 (40.4)	1478 (0.9)	1459 (71.0)	1424 (26.9)		**1566 (s)**
593 (7.0)	661 (40.6)	491 (48.2)	513 (19.0)		1637 (130.3)	1662 (101.1)	1663 (98.8)	1657 (81.6)	$N\text{-}H_2$ scissoring	**1630 (s)**
652 (3.0)	668 (12.6)	673 (39.9)	665 (54.0)		1688 (44.5)	1697 (10.3)	1709 (2.6)	1674 (35.0)	C=N stretching	**1695 (s)**
873 (49.4)	866 (17.6)	852 (12.0)	870 (15.1)	**869 (s)**	1826 (226.9)	1822 (233.9)	1832 (206.7)	1812 (195.6)	$H_2N\text{-}C{=}O$ stretching	**1728 (vs)**
893 (10.0)	867 (0.9)	871 (42.7)	891 (6.9)		3189 (21.4)	3194 (29.6)	3117 (50.2)	3236 (11.6)	C-H stretching	
1102 (18.1)	1105 (2.0)	1100 (16.6)	1110 (1.8)		3547 (0.1)	3453 (3.9)	3527 (0.2)	3502 (1.1)	N-H stretching	
1125 (12.8)	1177 (65.5)	1124 (13.6)	1171 (54.8)		3682 (69.7)	3691 (76.3)	3681 (60.1)	3664 (52.1)	$N\text{-}H_2$ symm. stretching	**3418 (s)**
1213 (63.4)	1255 (62.7)	1238 (77.1)	1241 (84.8)	**1178 (s)**	3840 (87.3)	3839 (60.4)	3826 (47.4)	3803 (48.1)	$N\text{-}H_2$ asym. stretching	**3538 (s)**
1390 (29.2)	1371 (190.2)	1352 (80.1)	1403 (73.5)	**1339/ 1399 (m)**						

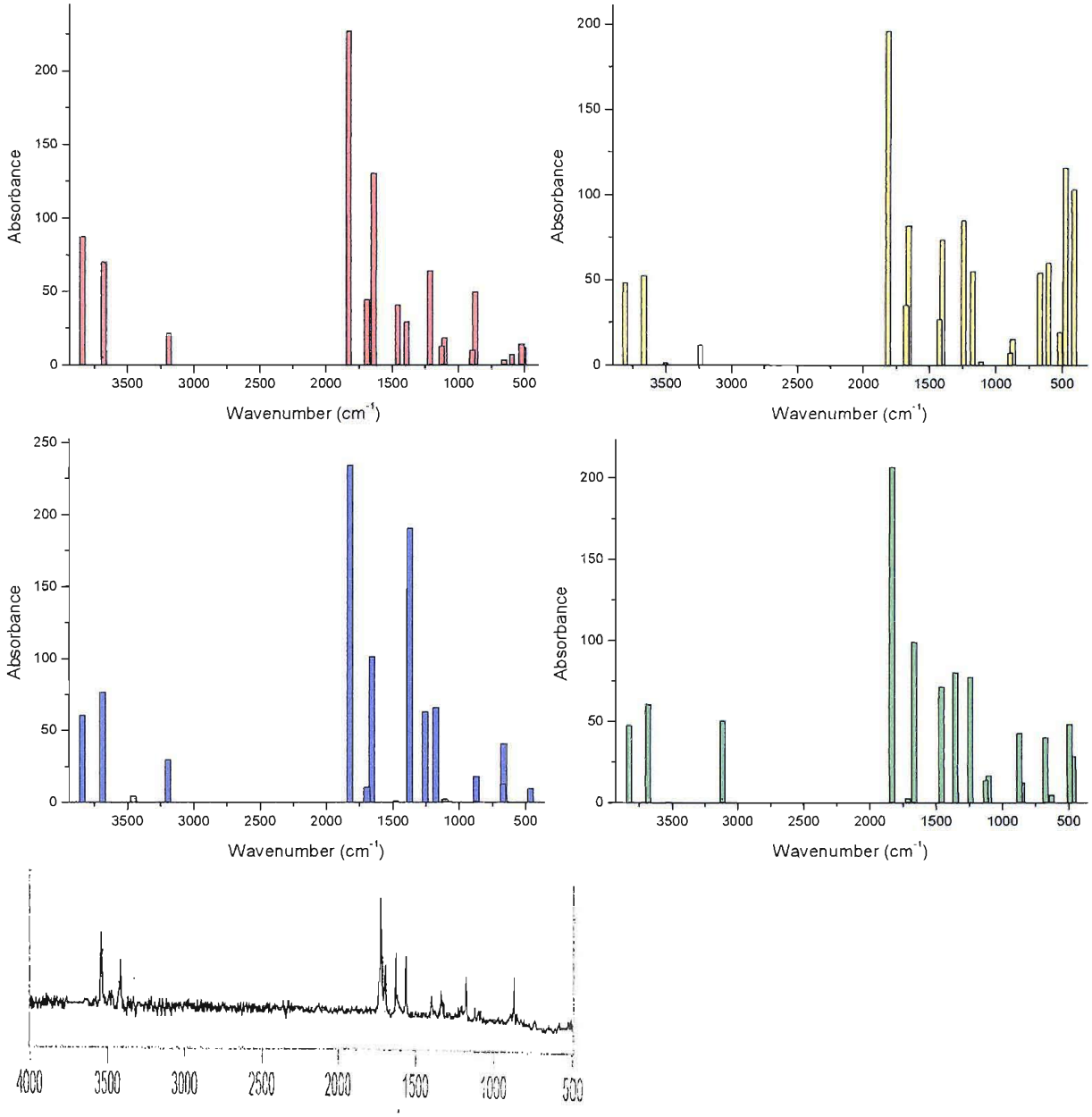

Fig. 5.17- The four IR spectra calculated for the conformers *cis-cis* (red lines), *cis-trans* (yellow lines), *trans-trans* (blue lines) and *trans-cis* (green lines) of iminoacetamide at the MP2/6-31G level.**

The agreement between the experimental and the calculated IR spectra, especially for the *cis-cis* structure, is remarkable: there are discrepancies between the calculated and experimental frequencies, in particular for the N-H stretching region above 3000 cm^{-1}, but this is an expected error considering that anharmonicity has not been considered in the calculations and that only partial allowance has been made for electron correlation. Moreover, the experimental spectrum has been obtained by considering only the bands with the correct thermal behaviour for an intermediate, and all the bands belonging to the azide or the other recognized decomposition products have been removed. It is therefore possible

that the subtracted spectrum is not the complete spectrum for iminoacetamide because some features could have been lost in the subtraction process. It is possible, however, to state that it represents the most significant bands for the intermediate.

The degree of agreement can be better clarified by considering the agreement between the computed and the experimental infrared spectra in the case of the parent azide. Figure 5.18 reports the comparison between the experimental azidoacetamide spectrum with the *ab initio* calculated spectra for the different conformers, and the comparison between the imine intermediate experimental spectrum with the spectra calculated for the iminoacetamide conformers. The quality of the agreement is comparable between the two compounds.

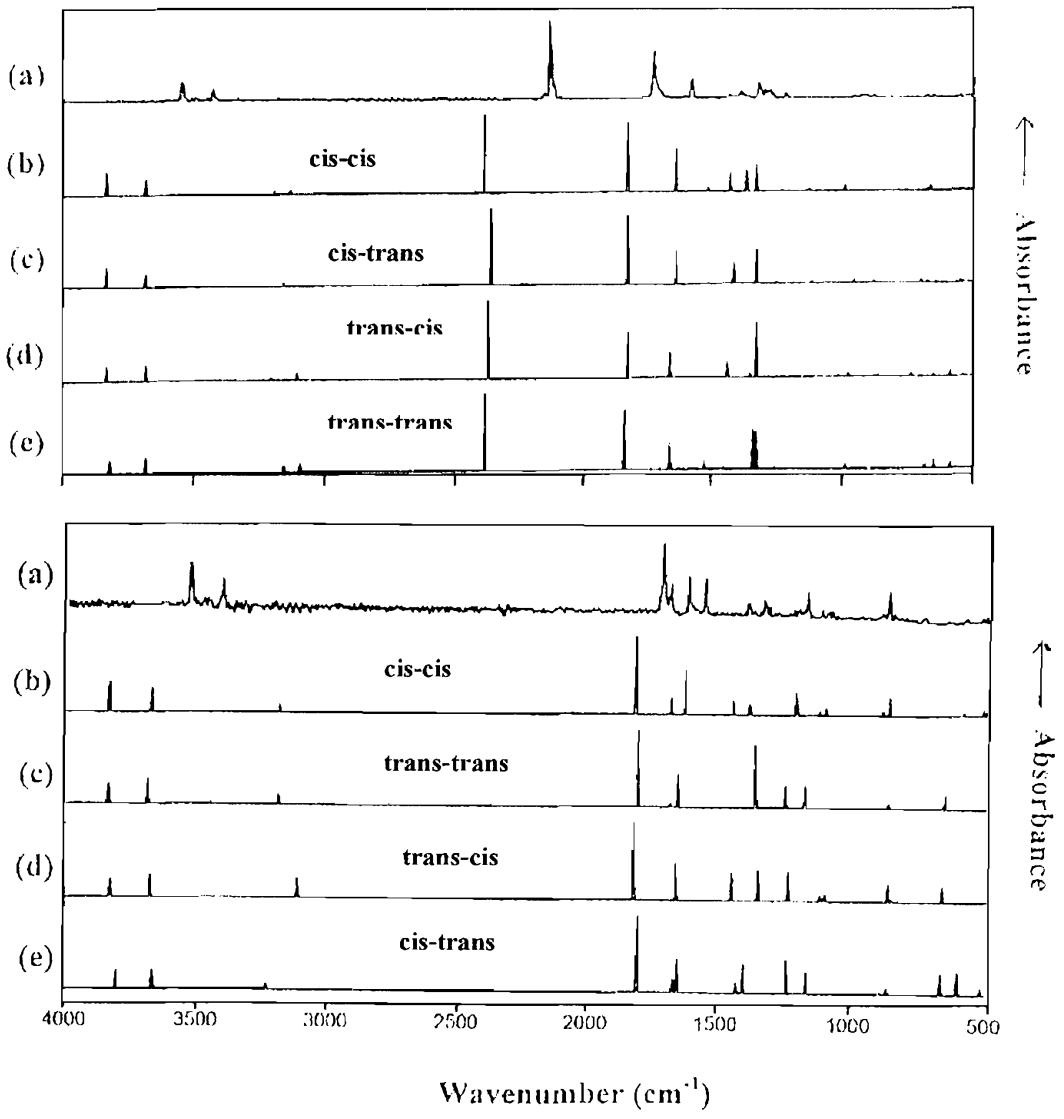

Figure 5.18- Comparison of the experimental and calculated IR spectra for azidoacetamide (above) and iminoacetamide (below). a) indicates the experimental spectra, b) to e) the calculated ones for the four conformers of both compounds- assignment reported on each spectrum

The computed imine spectra offer a significant contribution for the understanding of the reaction, because only the spectrum calculated for structure *cis-cis* provides the experimentally correct intensity ratio for the two highest energy bands (3680 and 3840 cm^{-1}). The differences between its calculated IR spectrum and the experimental one- which displays an additional band in the 1500-2000 cm^{-1} region and some more weak bands in the 500-1500 cm^{-1} region- are small and therefore do not contradict the assignment, and underline the fact that other possible intermediates are formed.

The first assumption is that structure *cis-cis*- despite being the structure better reproducing the experimental pattern- is not the only iminoacetamide conformer trapped in the matrix but that other conformers can be present. The differences between experiment and calculations are in fact lowered by adding the contribution of structure *trans-trans* to the spectrum. This reflects what was also found in the case of the parent azide.

Even with this assumption, the investigation of possible reaction intermediates must be widened to consider other types of imine (e.g. N-iminoacetamide).

N-iminoacetamide

So far, it was assumed that nitreneacetamide, $:NCH_2CONH_2$, undergoes a 1,2-H shift to form iminoacetamide. An alternative mechanism can nevertheless be invoked: *ab initio* calculations show that by removing the two terminal nitrogen atoms from one of the optimised structures of azidoacetamide- leaving intact the rest of the atomic coordinates- and letting the optimization procedure operate on the remaining nitrene, the terminal nitrogen atom does not acquire a proton from the adjacent carbon but instead prefers to attack the carbonyl atom. The net result is the production of N-iminoacetamide

$$:NCH_2CONH_2 \rightarrow CH_2{=}NCONH_2$$

Only one structure has been optimised for this molecule at the MP2/ 6-31G** level and its geometry is shown in Figure 5.19; the most important geometrical parameters are listed in Table 5.12. The calculated total energy was found to be -262.5905386 hartees, which is 1.11 kcal/mol higher in energy than *cis-cis* iminoacetamide..

It corresponds to a planar structure with the terminal methylene group in a *cis* position with respect to the oxygen atom; attempts to locate a stable geometry with *trans* orientation have not been successful, because in this structure the stabilizing interaction between the $-CH_2$ hydrogen atom and the oxygen is removed, and a repulsive interaction with the hydrogen atom on the $-NH_2$ group leads the optimization to converge back to the *cis* structure.

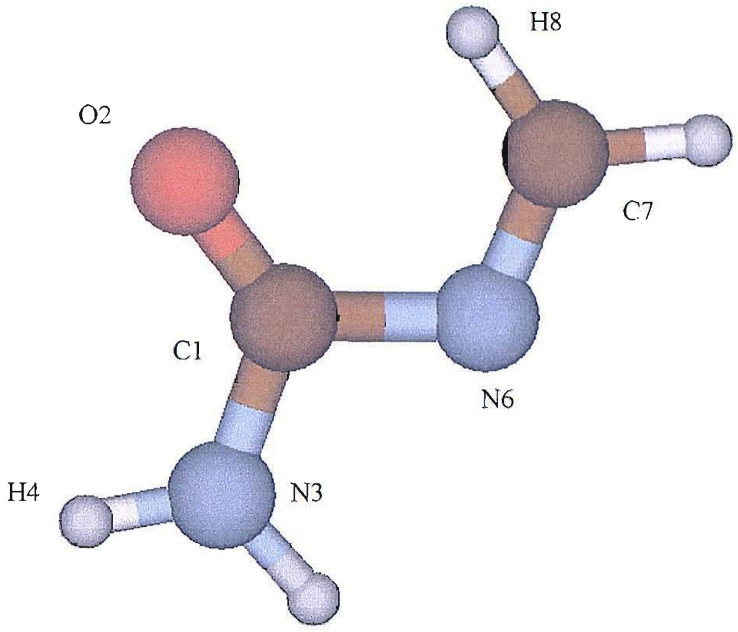

Figure 5.19- Optimized geometry of N-iminoacetamide calculated at the MP2/6-31G level**

Table 5.12- The most significant geometrical parameters of N-iminoacetamide calculated at the MP2/6-31G level**

Bond	Length (Å)	Angle	Value (°)
C7-H8	1.089	H8-C7-N6	122.31
N6-C7	1.282	C7-N6-C1	113.14
C1-N6	1.458	O2-C1-N3	125.17
N3-C1	1.355	C1-N3-H4	119.39
C1-O2	1.225	H8-C7-N6-C1	-0.07
H4-N3	1.004	C7-N6-C1-O2	-0.27
		H4-N3-C1-O2	-0.20

Table 5.13 reports the calculated vertical ionization energies for N-iminoacetamide. As can be seen from a comparison with Table 5.10, the differences with the VIEs of iminoacetamide are minimal.

Table 5.14 reports the most significant calculated vibrational frequencies for N-iminoacetamide: the associated IR spectrum is shown in Figure 5.20.

Table 5.13- Calculeted VIEs of N-iminoacetamide at the MP2/6-31G level**

KT calculated VIE (eV)	KT calculated VIE · 0.92 (eV)
11.27	10.37
11.33	10.42
12.16	11.18
13.02	11.98
16.04	14.76
16.42	15.11
16.96	15.60

Table 5.14- Calculated IR bands of N-iminoacetamide at the MP2/6-31G level**

Frequency (cm^{-1})	Intensity (km/mol)	Frequency (cm^{-1})	Intensity (km/mol)	Normal mode
487.2	4.69	1504.3	42.62	C-H_2 scissoring
557.1	6.68	1644.3	148.01	N-H_2 scissoring
653.5	5.00	1712.0	31.86	C=N stretching
656.4	5.54	1858.1	330.04	H_2N-C=O stretching
837.7	30.03	3171.3	16.54	C-H_2 symm. stretching
873.0	9.22	3294.8	11.06	C-H_2 asym. stretching
1117.4	14.57	3705.3	91.81	N-H_2 symm. stretching
1250.1	3.62	3861.2	75.61	N-H_2 asym. stretching
1385.3	192.13			

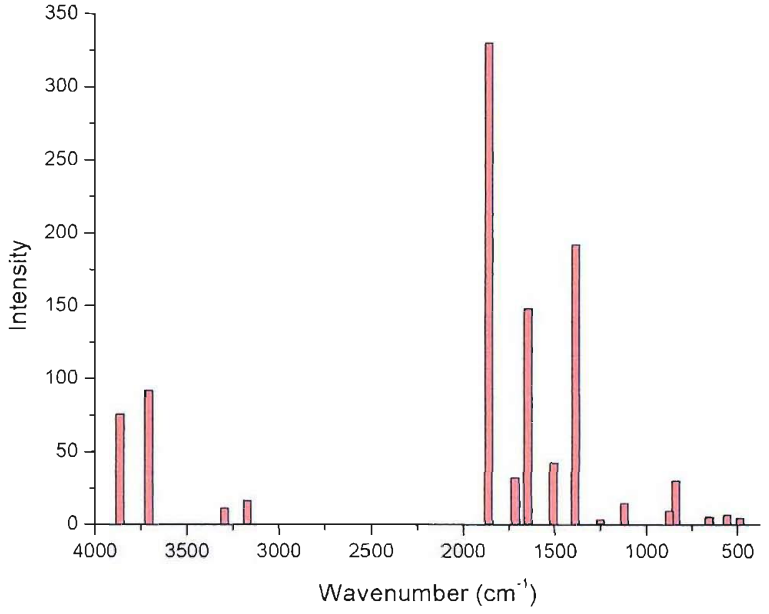

Figure 5.20- The infrared spectrum of N-iminoacetamide calculated at the MP2/6-31G level**

Iso-N-iminoacetamide

From N-iminoacetamide, it is possible to form a new type of compound by promoting a 1,2-H shift between the terminal methylene carbon and the adjacent nitrogen atom

$$CH_2{=}NCONH_2 \rightarrow CH{=}NHCONH_2$$

This new imine is expected to be clearly less stable than N-iminoacetamide, considering the fact that the carbon and nitrogen atoms between which the 1,2-H shift took place are negatively and positively charged respectively.

Nevertheless, optimization was carried out on the possible conformers of this new imine, labelled iso-N-iminoacetamide, because they could be important as reactive intermediates or precursors for the experimentally observed decomposition products of azidoacetamide.

Two structures have been optimized at the MP2/6-31G** level; their geometries are shown in Figure 5.21. The interatomic distances and angles are almost the same as in N-iminoacetamide, with the exception of slightly longer C=N and C-H bonds (1.32 and 1.1 Å). Structure *cis* (referring to the relative orientation of the terminal carbon atom with respect to the oxygen atom) is not planar due to

the repulsive interaction between the hydrogen atoms on the two different nitrogen atoms. Structure *trans*, which is planar and does not display intramolecular repulsions, is therefore the most stable conformer. Their total energies are calculated to be -262.5095464 and -262.5300254 hartrees respectively.

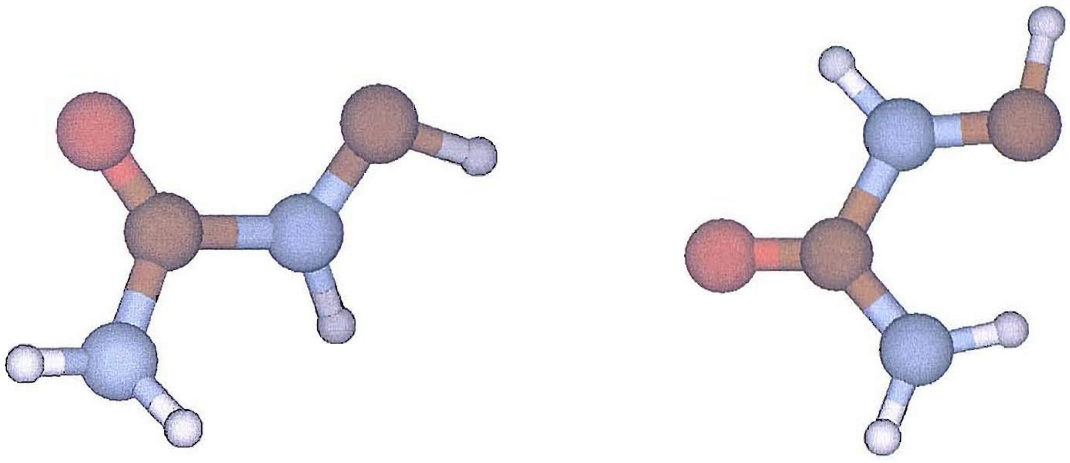

Figure 5.21- The two structures (*cis*, left; *trans*, right) of iso-N-iminoacetamide optimized at the MP2/6-31G level**

Given their high energies compared to the energy of iminoacetamide or N-iminoacetamide, it was assumed that neither of the iso-N-iminoacetamide structures could be formed in the azidoacetamide decomposition process. For this reason, the results obtained from *ab initio* calculations on vertical ionization energies and vibrational frequencies will not be reported here.

Interpretation of the *ab initio* calculations on the possible reaction intermediates

From the computed lowest VIEs, few differences are seen between the VIEs of iminoacetamide and N-iminoacetamide: the changes of VIE for each band are of the order of 0.1 eV, and the values are very similar to those calibrated for the second and third bands of azidoacetamide and the first band of CH_2=NH. It is therefore impossible to distinguish if these imines are both present as reaction intermediates, or which one is the predominant species.

Iso-N-iminoacetamide is computed to have a more distinct first band around 10.0 eV. Even if this is roughly 1.0 eV lower than the corresponding first band of iminoacetamide and N-iminoacetamide, it would overlap with the azide first band. During the thermal decomposition experiments, the shape of the first azide PE band does not seem to markedly change, and its decrease in intensity when increasing temperatures suggests that iso-N-iminoacetamide is not formed, or- more correctly- is not detected.

This is supported by its calculated total energy, which is much higher with respect to iminoacetamide or N-iminoacetamide.

The calculated IR spectra for iminoacetamide and N-iminoacetamide show some important differences, especially for the intensity ratio in the N-H stretching region: the spectrum of *cis-cis* iminoacetamide is the only one among all the iminoacetamide and N-iminoacetamide conformers which correctly reproduces the experiment in this region. The *cis-cis* iminoacetamide is therefore expected to be the dominant species produced. More complicated is to distinguish the additional contributions which will completely fit the experimental results in the 1000-2000 cm^{-1} region: from both the total energy and the IR pattern, is not possible to unambiguously distinguish if *trans-trans* iminoacetamide or N-iminoacetamide are formed.

5.2.6 SUGGESTED MECHANISM OF GAS-PHASE DECOMPOSITION

The combination of the results from UV-PES and matrix isolation IR experiments on the pyrolysis of azidoacetamide show that

- When the thermal decomposition begins, N_2 is released as the first product
- A reaction intermediate is formed when the azide is not yet completely decomposed (at around 200 °C) and before the appearance of other products: its IR spectrum matches the one calculated for iminoacetamide
- HNCO and CH_2NH are formed at the same temperature as when iminoacetamide approximately reaches its maximum partial pressure (280 °C)
- HCN, NH_3 and CO are formed at slightly higher temperatures and initially in lower partial pressure than HNCO and CH_2NH
- When iminoacetamide is almost completely consumed (450 °C), HNCO, CH_2NH, HCN, CO and NH_3 are all still present
- At very high temperatures –around 800 °C- only HCN and CO are observed.

It is clear that the first step of the decomposition is the formation of nitrogen and iminoacetamide, following the same behaviour of simpler alkyl azides [1-4, 25]. Production of N-iminoacetamide at the same time as iminoacetamide is thought to be a minor channel.

From this work, it is not clear whether a nitrene is first formed which then rearranges via a 1,2 H-shift or if an imine is produced at the same time as the nitrogen release. This point could of course be resolved if a nitrene could be detected experimentally.

Even if from these experiments it was not possible to detect the formation of the nitrene diradical as the consequence of the release of nitrogen,

$$N_3CH_2CONH_2 \rightarrow N_2 + :NCH_2CONH_2$$

recent theoretical [6] and experimental [5, 26] results on methylazide and ethylazide decomposition seem to confirm the formation of the nitrene as a preferred route in opposition to a concerted mechanism involving breaking of the N-N bond and 1,2-H shift to produce directly iminoacetamide.

A*b initio* calculations clearly indicate that the singlet nitrene is unstable and converges to different imines by undergoing **two** different isomerization processes, which will be called Type 1 and Type 2. Furthermore, it was not possible to locate a transition state between the azide and one of these imines by means of a concerted nitrogen release/1,2-H shift mechanism; the conclusion from this evidence is that the azide decomposes via a stepwise mechanism to a nitrene which has a very short lifetime and rapidly decomposes to the imine: this justifies the fact that experimentally they have not been observed. The two decomposition mechanisms for the nitrene are reported below.

Type 1:

This is the well established 1,2-H shift mechanism in which the electron deficient nitrogen atom acquires a proton from the adjacent carbon atom and a double bond is formed. As a general scheme it can be depicted as

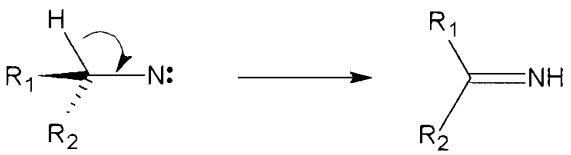

In this case, this would lead to the formation of iminoacetamide

$$:NCH_2CONH_2 \rightarrow HN{=}CHCONH_2$$

Type 2:

As an alternative to proton transfer, the nitrogen atom can compensate its electron deficiency by attacking a remote site of the molecule, forming a new bond. This can be seen as a type of nucleophilic substitution. In this case, the site is the carbonyl carbon atom, following the scheme

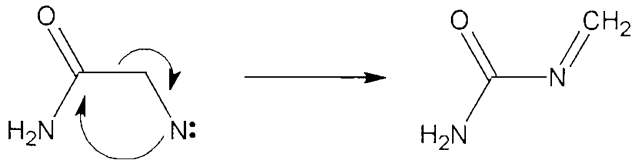

Ab initio calculations show that in the azidoacetamide case, type 2 would be the preferred path when all the nitrene geometrical parameters are left as they were in the azide; this is equivalent to saying that if the geometry of nitreneacetamide is exactly like the geometry of azidoacetamide-only with a very long length of the N-N bond which is broken in the azide decomposition- the optimization of the structure leads to the formation of N-iminoacetamide rather than of iminoacetamide.

In reality, the breaking of the N-N bond will most probably be accompanied by slight rearrangements of the remaining interatomic geometries, and with just a small geometry change in the initial nitrene, the optimization process leads to iminoacetamide. Moreover, the experimental IR spectrum shows that iminoacetamide is the main product. N-iminoacetamide can be formed as a minor product: this could improve the degree of agreement between the calculated and experimental infrared spectra.

From the experiments, it is therefore clear that azidoacetamide prefers a Type 1 mechanism for the decomposition path; Type 2 in this system- producing N-iminoacetamide- appears to be only a minor route, even it is not possible to completely rule it out.

The main decomposition products are HNCO, CH_2NH, HCN, NH_3 and CO. The presence of all of them can be explained with the decomposition of iminoaceamide (or N-iminoacetamide).

The most prominent products, isocyanic acid and methylimine, are formed from iminoacetamide by breaking the carbon-carbon bond and with a hydrogen shift from the amide nitrogen to imine carbon, i.e.

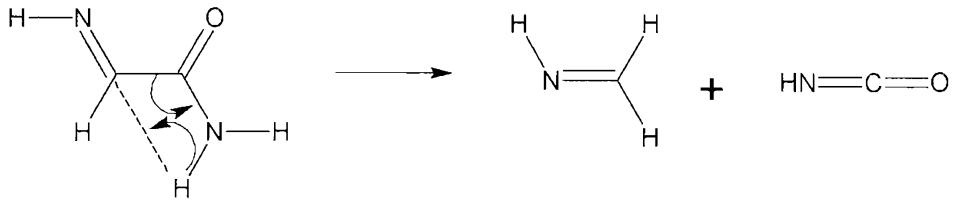

From N-iminoacetamide, a C-N bond has to be broken instead of a C-C bond, and the proton is transferred from a nitrogen atom to another nitrogen atom, instead of to a carbon atom.

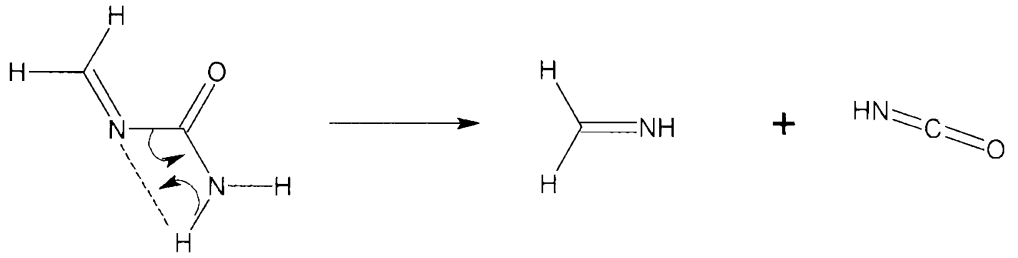

The formation of CH_2NH and HNCO via N-iminoacetamide is calculated to have a transition state roughly 5 kcal/mol lower in energy with respect to the one for iminoacetamide: this is probably due to the fact that in the first case the proton transfer is favoured by the absence of other protons on the receiving nitrogen atom. In the iminoacetamide case, the presence of a proton on the receiving carbon atom gives rise to a steric hindrance which could be the cause of the higher energy required in the process.

An alternative decomposition channel could lead to formamide, $HCONH_2$ and HCN, by breaking the carbon-carbon bond in the imine and forming a new carbon-hydrogen bond with one of the hydrogen atoms of the iminic group.

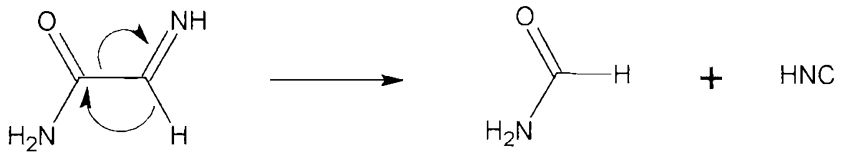

Ab initio studies [6, 24] have found that HNC is more favoured than HCN as the first released molecule: the isomerization takes place immediately, though, and HNC has never been experimentally detected from azide decompositions.

However, in the IR matrix isolation experiments, no bands were observed associated with pure formamide; in the PES experiments, no clear evidence for bands assignable to formamide was obtained. Therefore, formamide either is not formed at all, or it is formed in very small amount in the decomposition path. The partner decomposition product of formamide, HCN, is on the other hand clearly present even at low temperature, even if in small amount. Its formation should not be due to decomposition of CH_2=NH, which in a previous decomposition study of methylazide is reported to be stable up to 500 °C. It is therefore possible that the imine intermediate partially decomposes also to formamide and HCN, but that formamide is formed with such a high internal energy that is immediately decomposed to HN=C=O and hydrogen. A separate experiment was carried out on

formamide which showed that the decomposition to isocyanic acid is only partial at 300°C. The complete decomposition of formamide observed on pyrolysing azidoacetamide must be due to the fact that in this decomposition formamide is produced with very high internal energy.

Remarkably, no transition state was found for the N-iminoacetamide → formamide process; this difficulty in locating the transition state can indicate that N-iminoacetamide prefers to decompose to isocyanic acid and methylimine rather than to formamide. Such a result is in agreement with the PES evidence that at relatively low temperatures HCN is formed in lower amount than HNCO and CH_2NH.

Finally, a route leading to production of ammonia can be found by considering a concerted breaking of the C-C and C-N bonds adjacent to the carbonyl group and a proton transfer to the amidic nitrogen either from the iminic nitrogen or from the iminic carbon atom. From the *ab initio* results, the transfer from the carbon atom is favoured, due to the formation of HNC instead of HCN as one of the products.

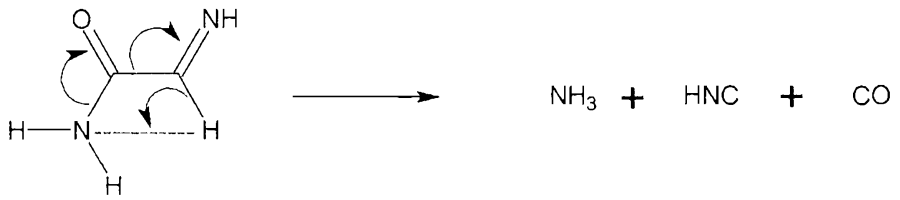

The production of ammonia, carbon monoxide and cyanic acid from N-iminoacetamide was thought to proceed via a two-step mechanism, the first producing ammonia and the HCNCO radical

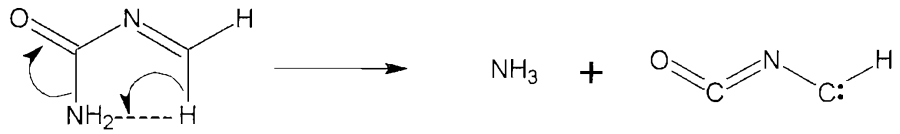

which is subsequently decomposed to HCN and CO: the second step is the most endothermic one.

The overall decomposition path can therefore be represented schematically as shown in Figure 5.22.

The calculated total energy level diagram at 0 K is reported in Figure 5.23. All the calculations were performed at the MP2/6-31G** level. To show the contribution of entropy to the decomposition path, a diagram of the relative free energies at 298 K for all products and transition states is reported in Figure 5.24 in which only the most stable conformer of azidoacetamide and iminoacetamide are shown; the geometries of the transition states are reported in Figure 5.25, and their energies listed in Table 5.15. For the sake of simplicity, in the N-iminoacetamide → ammonia route only the transition state producing the HCNCO radical is reported in the diagrams.

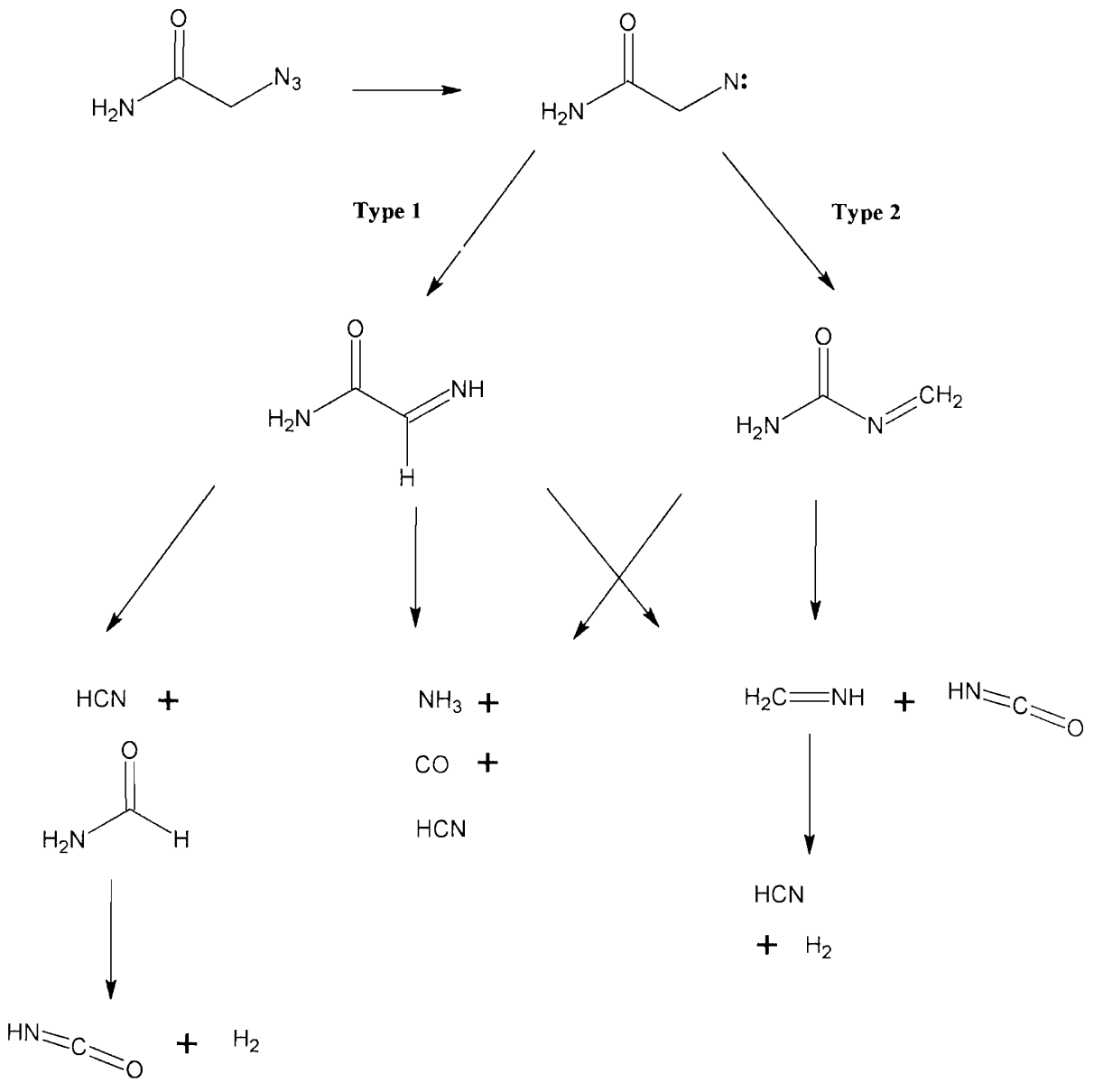

Figure 5.22- Schematic representation of the proposed thermal decomposition pattern of azidoacetamide

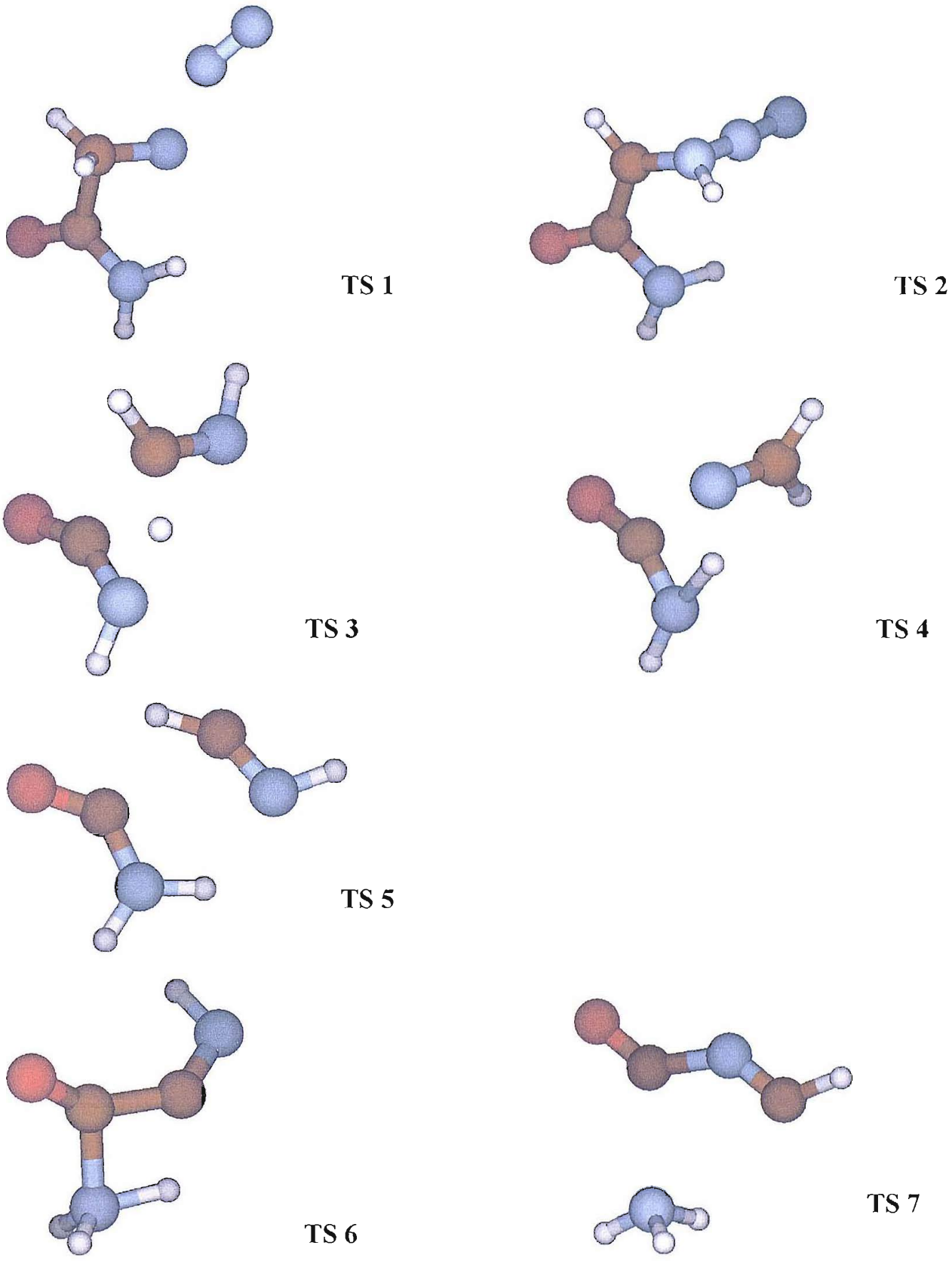

Figure 5.25- Optimized geometries of the transition states of the azidoacetamide decomposition system at the MP2/6-31G level. See figures 22-23 for the labelling of the transitin states**

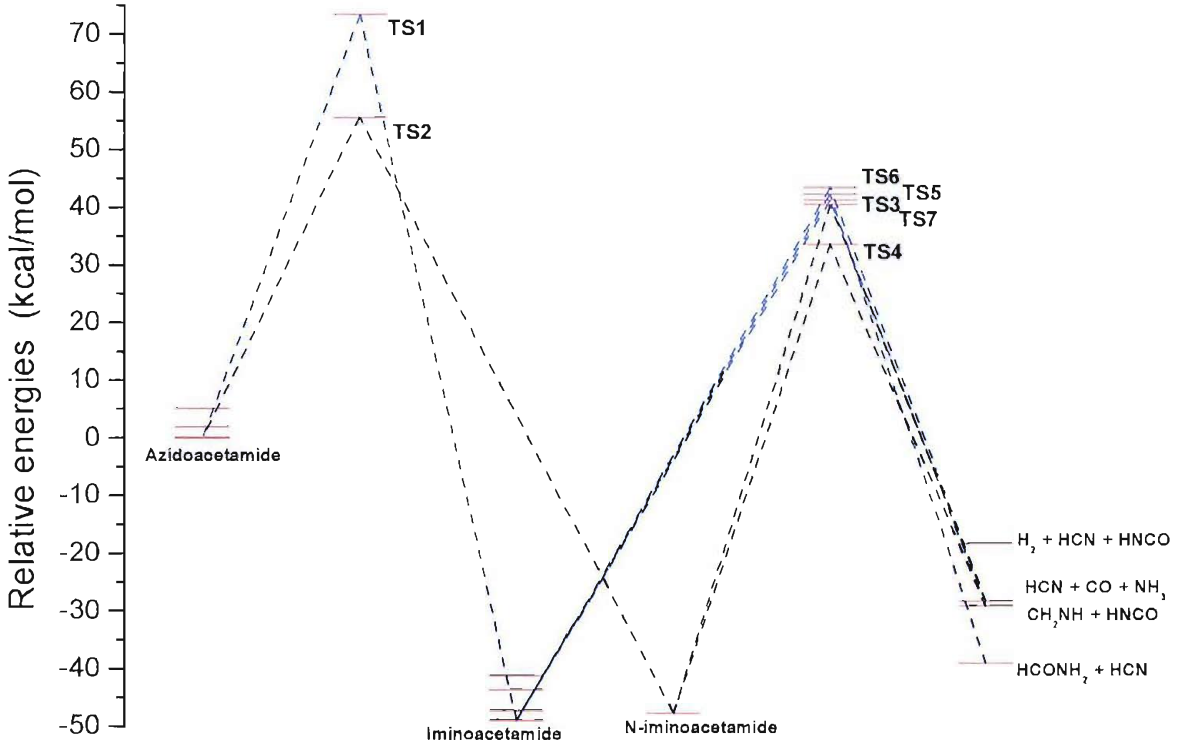

Figure 5.23- Diagram of the relative total energies of the species and transition states involved in azidoacetamide thermal decomposition calculated at the MP2-6/31G level. No thermal or zero point contributions are included.**

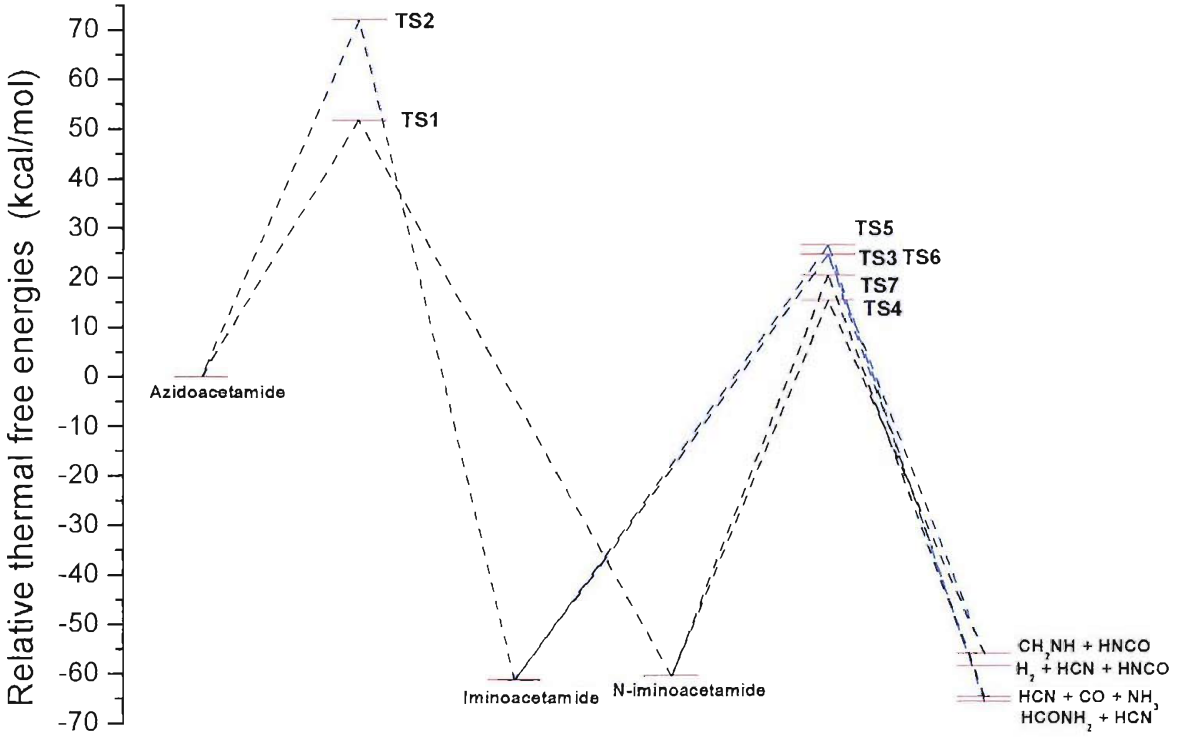

Figure 5.24- Diagram of the relative free energies of the species and transition states involved in azidoacetamide thermal decomposition calculated at the MP2-6/31G level. Thermal and zero point contributions are included.**

Table 5.15- ΔE_0 and ΔG_{298} values calculated at the MP2/6-31G level for intermediates, products and transition states of the azidoacetamide thermal decomposition system: azidoacetamide is chosen as the reference zero energy**

Compound	Relative energy at 0 K (kcal/mol)	Relative free energy at 298 K (kcal/mol)
Azidoacetamide	0	0
TS1	70.938	71.933
Iminoacetamide	-51.389	-61.313
TS2	52.532	51.887
N-iminoacetamide	-50.275	-60.423
TS3	35.335	24.728
TS4	25.715	15.548
$CH_2NH + HNCO$	-34.741	-55.954
TS5	34.648	24.861
$HCONH_2 + HCN$	-45.303	-64.588
$HNCO + H_2 + HCN$	-31.827	-58.343
TS6	36.497	26.701
TS7	34.173	20.612
$NH_3 + CO + HCN$	-36.908	-65.572

When ΔG^{298} is considered, the main effect in comparison to ΔE^0 is the lowering of the energies of the transition states between imines and main products, and of the energies of the main products. The free energies of the products span a smaller scale of values than for the total energies. Also, the transition states for the reactions iminoacetamide → products are very close in energy. On the basis of just the relative energy values, the predominance of CH_2NH and HNCO as decomposition products cannot be explained. The decisive factor for the large presence of methylimine and isocyanic acid is the route through N-iminoacetamide: from the graph in Figure 5.23 it can be seen that the initial transition state leading to its production is 20 kcal/mol lower in energy than the one leading to iminoacetamide, and the one leading to the CH_2NH and HNCO is almost 10 kcal/mol lower than the equivalent transition state from iminoacetamide. In this way, both the predominance of iminoacetamide over N-iminoacetamide and of CH_2NH and HNCO over the other main products is explained. It is also important to underline that according to the calculations, N-iminoacetamide does not seem to decompose to formamide: this- along with the possibility of its formation with high internal energy- explains the fact that formamide has not been detected in both PES and IR studies.

5.3 DIMETHYL AZIDOACETAMIDE

5.3.1 EXPERIMENTAL SETUPS

Photoelectron spectroscopy

Dimethylazidoacetamide ($N_3CH_2CON(CH_3)_2$) is a liquid which does not have a sufficiently high vapour pressure at room temperature to allow PE spectra with sufficient signal-to-noise ratio to be recorded. The vapour could not be introduced into the spectrometer ionization chamber by simply evacuating a flask holding the sample connected to the inlet tube of the spectrometer via a needle valve. As was the case for azidoacetamide, it was necessary to heat the substance in the ionization chamber, in order to achieve a sample vapour pressure in the photoionization region high enough to produce spectra of acceptable signal-to-noise ratio -when the sample pressure in the chamber reaches approximately 10^{-4} torr. Therefore two small glass vials were placed in the region immediately above the heated area on a small pad of glass wool (see Figure 2.5), where the temperature is lower than in the pyrolysis region but high enough to heat the sample to give suitable vapour pressures. In this way, run times of ~30 minutes could be achieved even at temperatures of 500 °C. The 10-cm mean hemisphere radius photoelectron spectrometer was used for this set of experiments: a description and a schematic diagram of this PE spectrometer is given in Section 2.1.

The procedure for the acquisition and calibration of the photoelectron spectra followed the same pattern as described in Chapter 2. Calibration of spectra obtained on pyrolysis of the azide was normally achieved using the bands associated with the first vertical ionization energies (VIE) of N_2 (15.58 eV), H_2O (12.62 eV), or HCN (13.60 eV) [8].

Matrix isolation IR spectroscopy

The apparatus and the procedure used for the acquisition of infrared spectra in nitrogen matrices have been described in Chapter 2. Given the fact that dimethylazidoacetamide is a viscous liquid, it was found more convenient to preheat the sample and the inlet system at approximately 35 °C in order to obtain a more suitable vapour pressure. Deposition times were in the order of 30 to 60 minutes, and the matrix dilution ratios were estimated to be above 1000:1.

Spectra of dimethylformamide (DMF) have been acquired in a nitrogen matrix, to provide evidence for its possible presence and thermal behaviour as a possible pyrolysis product, and to support the hypotheses made on the azide decomposition pathways.

5.3.2 SAMPLE PREPARATION AND CHARACTERIZATION

PREPARATION

The preparation follows the same method as the azidoacetamide preparation. Chloro-dimethylacetamide was added slowly to a solution of sodium azide in water, until an approximate molar ratio chloro-N-dimethylacetamide:sodium azide of 1:3 was reached. The mixture was stirred for 2 hours in an oil bath at 60 °C. After cooling the product was extracted with ethyl acetate and the water phase discarded. The organic phase was dried over anhydrous sodium sulphate and concentrated using a rotary evaporator. The dimethylazidoacetamide obtained was purified by distillation at reduced pressure.

CHARACTERIZATION

Dimethylazidoacetamide ($N_3CH_2CON(CH_3)_2$) is a viscous, low vapour pressure liquid at room temperature. It was characterized in the vapour phase by UV-photoelectron spectroscopy and electron impact mass spectrometry, and by ^1H- and ^{13}C-NMR in solution in deuterated chloroform. Infrared spectroscopy characterization was conducted on the pure liquid between KBr plates.
According to spectroscopic results, the dimethylazidoacetamide used in this work was pure.

Mass spectrometry: the 70 eV electron impact mass spectrum is reported in Figure 5.25. The parent peak is the expected one at 128 amu (intensity 3.4% relative to base peak). Stronger peaks can be found at 28 amu (corresponding to N_2^+ and CH_2N^+, 100%), at 42-43-44 amu (corresponding to $CH_2NCH_2^+$ 18.9%, $CH_3NCH_2^+$ 22.2%, and $CH_3NCH_3^+$ 5.9%), at 72 amu (corresponding to $CON(CH_3)_2^+$, 100%) and at 98-99-100 amu (corresponding to $NCOCH_2N_3^+$ 10.0%, $NCH_2CON(CH_3)CH_2^+$ 28.9%, and $NCH_2CON(CH_3)_2^+$ 8.1%). Signals were present also at 15 (CH_3^+) and 85 ($CHCON(CH_3)_2^+$, 0.8%) amu.

As was the case for azidoacetamide, in the 20 eV electron impact mass spectrum most of the relative intensities of the ions were enhanced with respect to the N_2^+ signal, compared to the 70 eV spectrum.

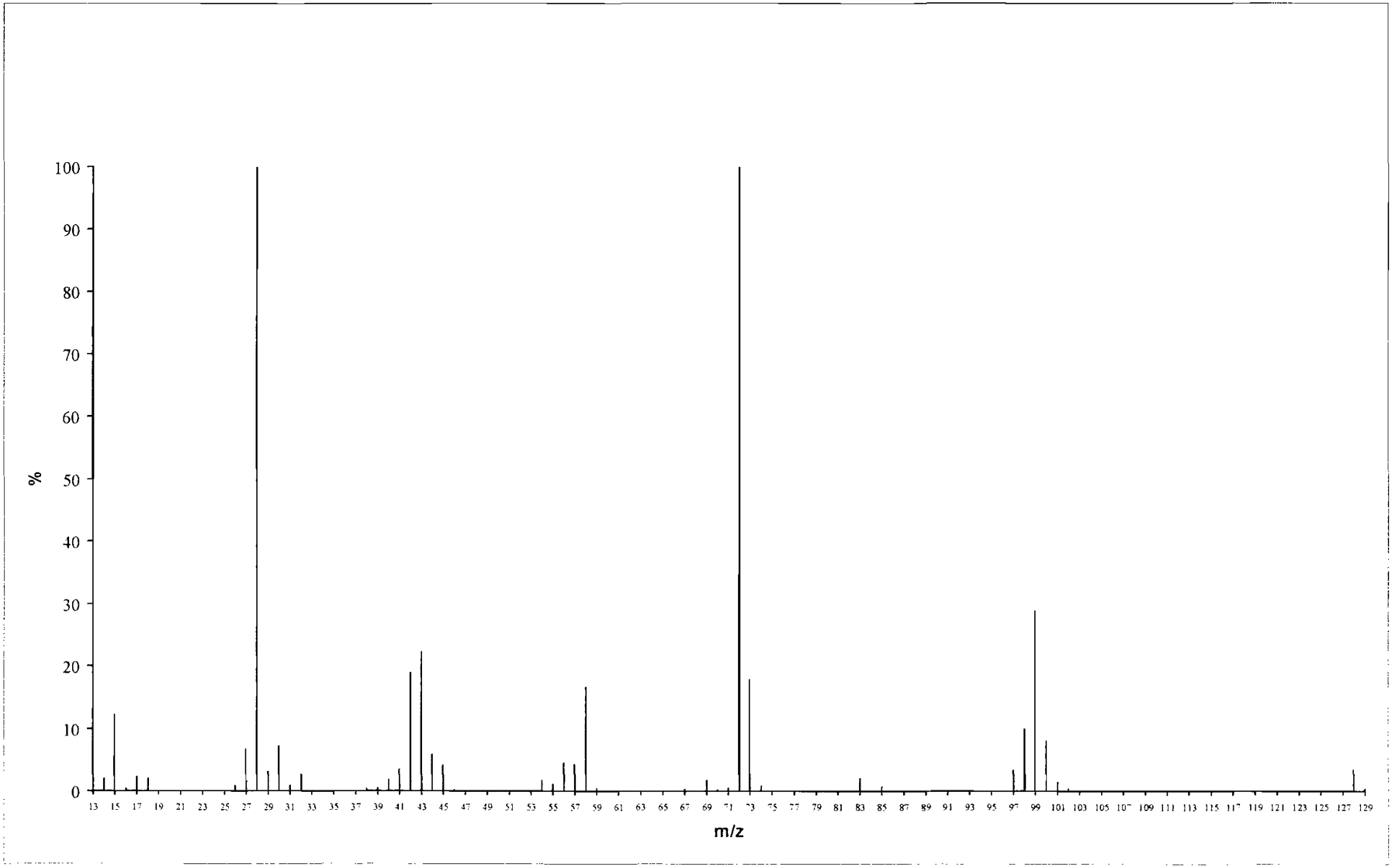

Figure 5.25- 70 eV impact mass spectrum of dimethylazidoacetamide

^{1}H- and ^{13}C-NMR spectroscopy: the 300 MHz ^{1}H-NMR spectrum of dimethylazidoacetamide, recorded in $CDCl_3$ solution, is reported in Figure 5.26. It shows a single peak at 3.68 ppm relative to TMS corresponding to the methylene protons on the carbon atom in the α position to the N_3 and the carbonyl groups, while a partially resolved doublet peak at 2.69 ppm relative to TMS is due to the protons on the methyl groups- which are chemically inequivalent

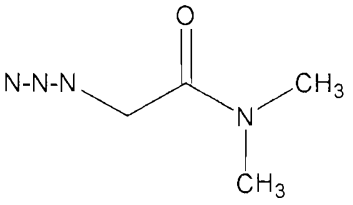

A closer investigation of the doublet at 2.69 ppm reveals that each component of the doublet is furthermore split, due to the non-equivalence between the two methyl groups due to their different orientation within the molecular arrangement (*cis* or *trans* with respect to the carbonyl group).
The intensity ratio between the signals at 2.69 and 3.68 has the value of 6:2 i.e. 3:1, consistent with the relative intensity expected for the $(CH_3)_2$ and CH_2 protons.

The ^{13}C-NMR spectrum, run in $CDCl_3$ solution, is reported in Figure 5.27. Four peaks can be identified: the double peak at 35.8 and 36.5 ppm with respect to TMS is due to the two different methyl groups. Another peak at 50.4 ppm corresponds to the methylene carbon atom, while one present at 167.3 ppm is assignable to the carbonyl carbon atom.

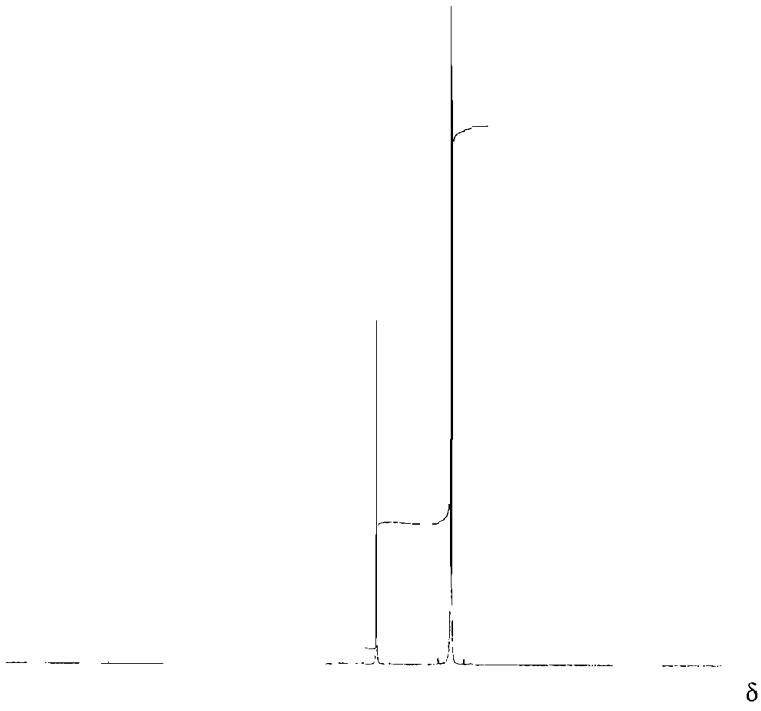

Figure 5.26- ^{1}H-NMR spectrum of dimethyl-azidoacetamide acquired in $CDCl_3$ solution with a 10s pulse delay

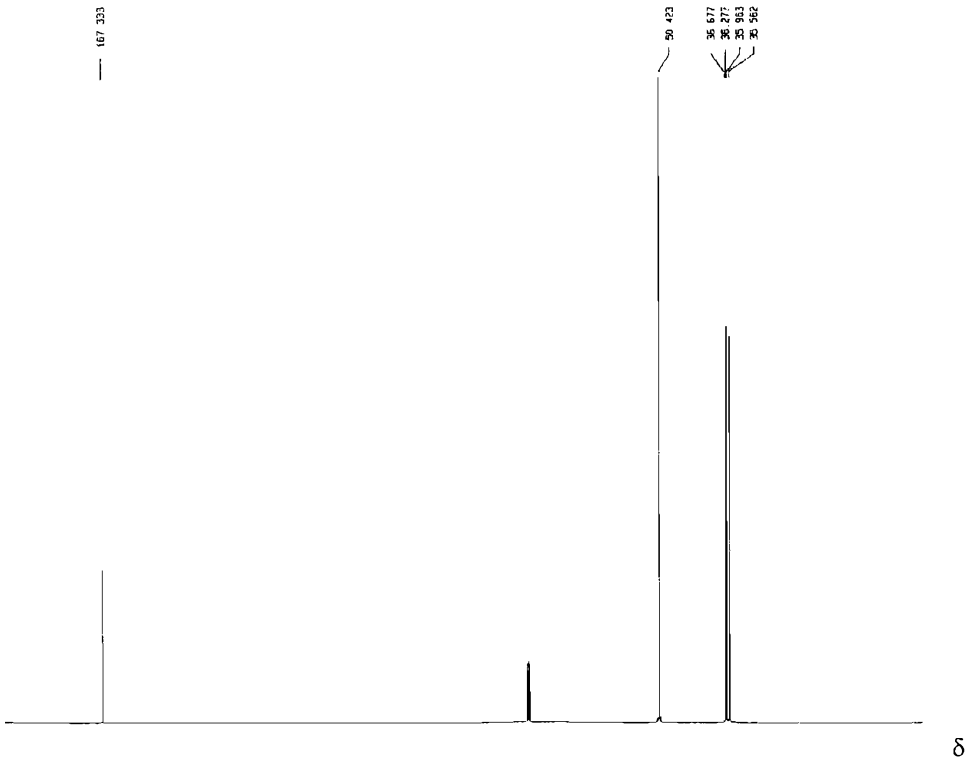

Figure 5.27- ^{13}C-NMR spectrum of dimethyl-azidoacetamide in $CDCl_3$ (triplet at 77 ppm)

Infrared spectroscopy: the IR spectrum of the liquid compound recorded between KBr plates (Figure 5.28) shows a relatively broad band with peaks at 2934 cm^{-1} and 2925 cm^{-1}, assigned to C-H stretching absorptions, and strong, sharp bands at 2107 cm^{-1} (N_3 stretching), 1660 cm^{-1} (C=O stretching). Other prominent features can be observed at 1403, 1284 and 1147 cm^{-1}.

As for azidoacetamide (see chapter 5.1), the infrared bands of the compound in the liquid phase have almost the same positions in the spectrum recorded in a N_2 matrix (spectrum reported in Figure 5.34 in Section 5.2.3 dealing with *ab initio* results), apart from the highest frequency of the N-H stretching modes above 3500 cm^{-1}: because of the elimination of any intermolecular hydrogen bonding in the matrix, the frequencies of the two modes rise respectively from 3373 and 3179 cm^{-1} to 3538 and 3420 cm^{-1}. A further analysis of the matrix IR spectrum will be found in the next section, when a comparison with the results of the *ab initio* calculations will be made.

Photoelectron spectroscopy: the dimethylazidoacetamide UV-photoelectron spectrum (Figure 5.29) was obtained by warming the liquid sample at 60 °C to obtain a suitable vapour pressure. The six most prominent bands in the spectrum (labelled A-F) were calibrated by averaging the vertical ionization energies (VIEs) of the bands obtained from measurement of seven different spectra. The results are shown in Table 5.16 (see Figure 5.29 for the numbering of the bands in the photoelectron spectrum).

Table 5.16- Calibrated vertical ionization energies of dimethylazidoacetamide

Band	**A**	**B**	**C**	**D**	**E**	**F**
VIE (eV) ±0.02 eV	9.19	9.85	11.36	13.31	14.22	16.03

Spectra of the precursor of the azide (dimethyl-chloroacetamide) have also been recorded and calibrated in order to verify the absence of the precursor in the sample studied. It displayed a characteristic sharp band associated to the ionization from the lone pair on the chlorine atom in the 11.0-11.5 eV region. Actually, all parent azide spectra were free of any detectable trace of the chlorinated precursor used in the preparation: considering this, no comparison between the spectra of the two compounds will be presented here.

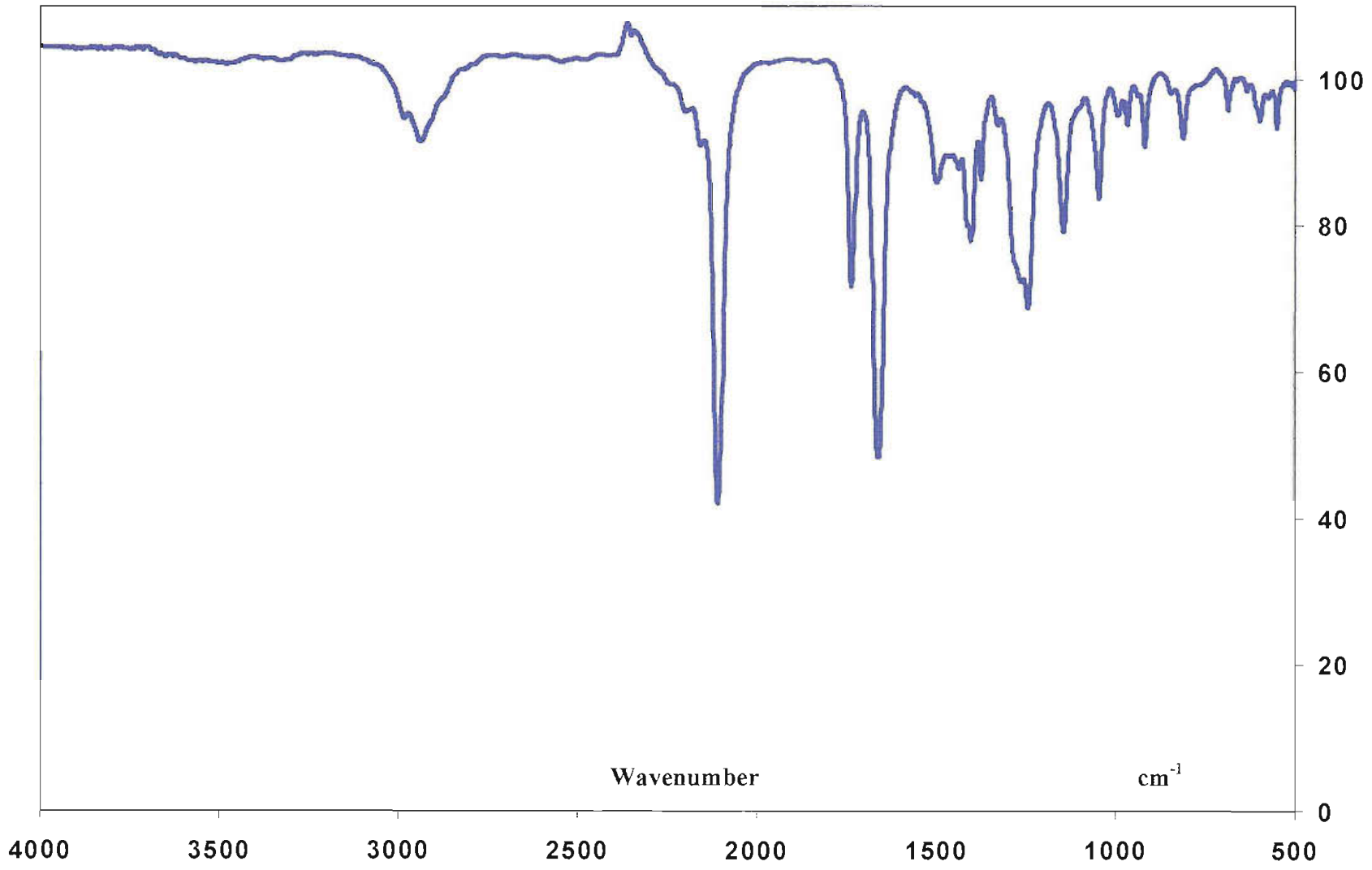

Figure 5.28- Infrared spectrum recorded for liquid dimethylazidoacetamide

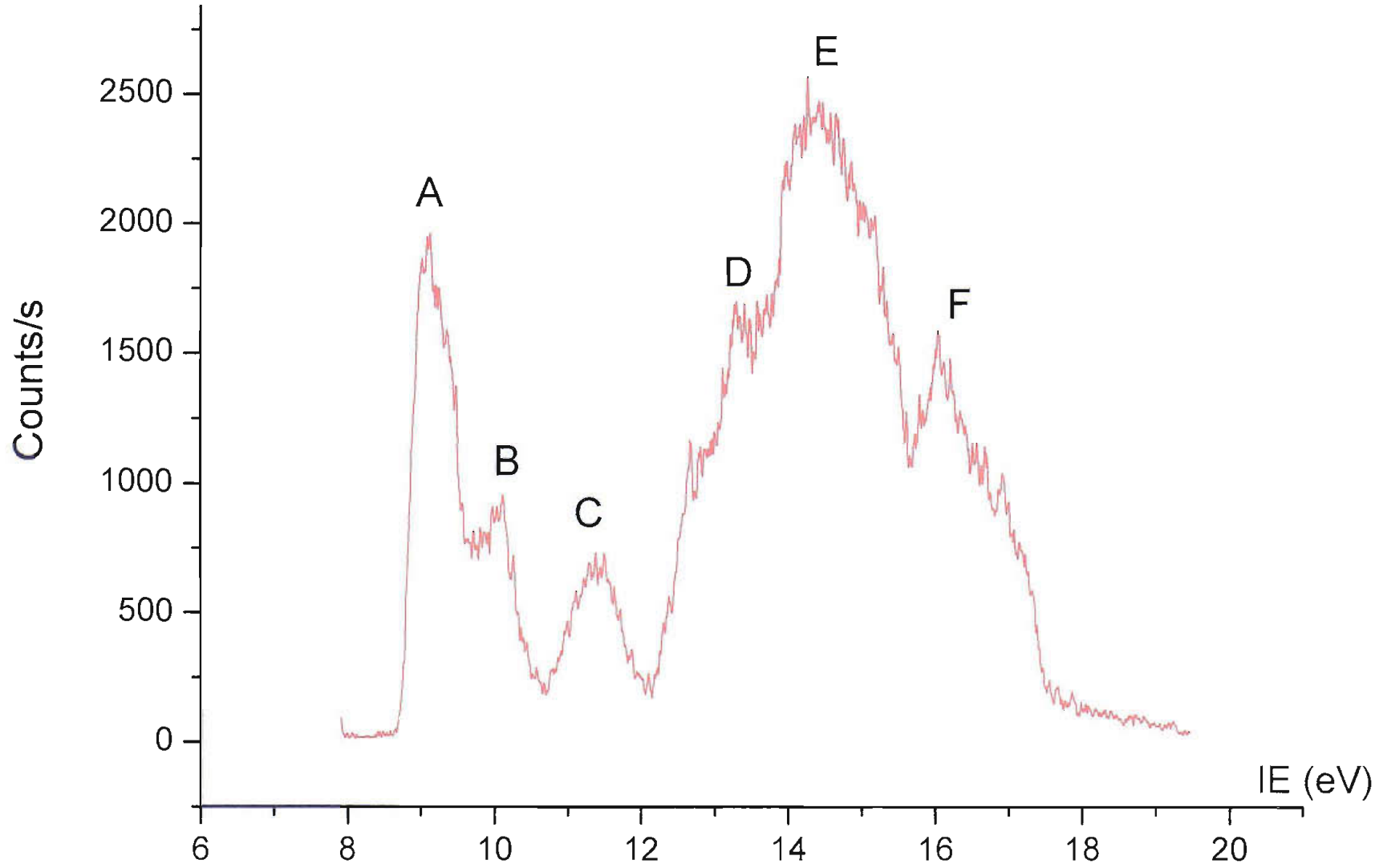

Figure 5.29- HeI photoelectron spectrum of dimethylazidoacetamide at a furnace temperature of 80 °C

5.3.3 RESULTS OF *AB INITIO* MOLECULAR ORBITAL CALCULATIONS

Four minimum energy conformers have been found for $N_3CH_2CON(CH_3)_2$ in its ground state (closed-shell singlet state) at the MP2/6-31G** level, according to the different relative orientations of the carbonyl, methylene and azide groups. They have C_1 symmetry, with their methyl and methylene groups and the N_3 chain out of the plane of the NC(=O)C backbone. Attempts to locate a minimum geometry structure in the C_s point group both with this basis set and with 6-311++G** as basis set proved unsuccessful.

The geometries of the stable structures are reported in Figure 5.30, the most stable one- labelled as *cis-trans*- is shown in greater detail in Figure 5.31, and Table 5.17 reports its most important calculated geometrical parameters.

Following the same nomenclature scheme for the different conformers as in azidoacetamide, the label describes the relative position of the carbonyl group to the methylene group, and of the methylene group to the azide group respectively. For example, structure *cis-trans* is the structure in which the carbonyl and the methylene groups are in the *cis* relative position, while the methylene and azide groups are in the *trans* orientation. Referring to Figure 5.31, this approximates to saying that an "ideal" *cis-trans* position is that when the dihedral angle O2-C1-C3-N9 is 180°, the dihedral angle C1-C3-N9-N10 is 0°: in this way the methylene hydrogen atoms are *cis* to the carbonyl group and *trans* to the azide chain. The actual optimized dihedral angles are not exactly 0° or 180°, due to the non-planarity of the molecule; an orientation is considered *trans* when the angle value is between -90° and 90° and *cis* when between 90° and 270°.

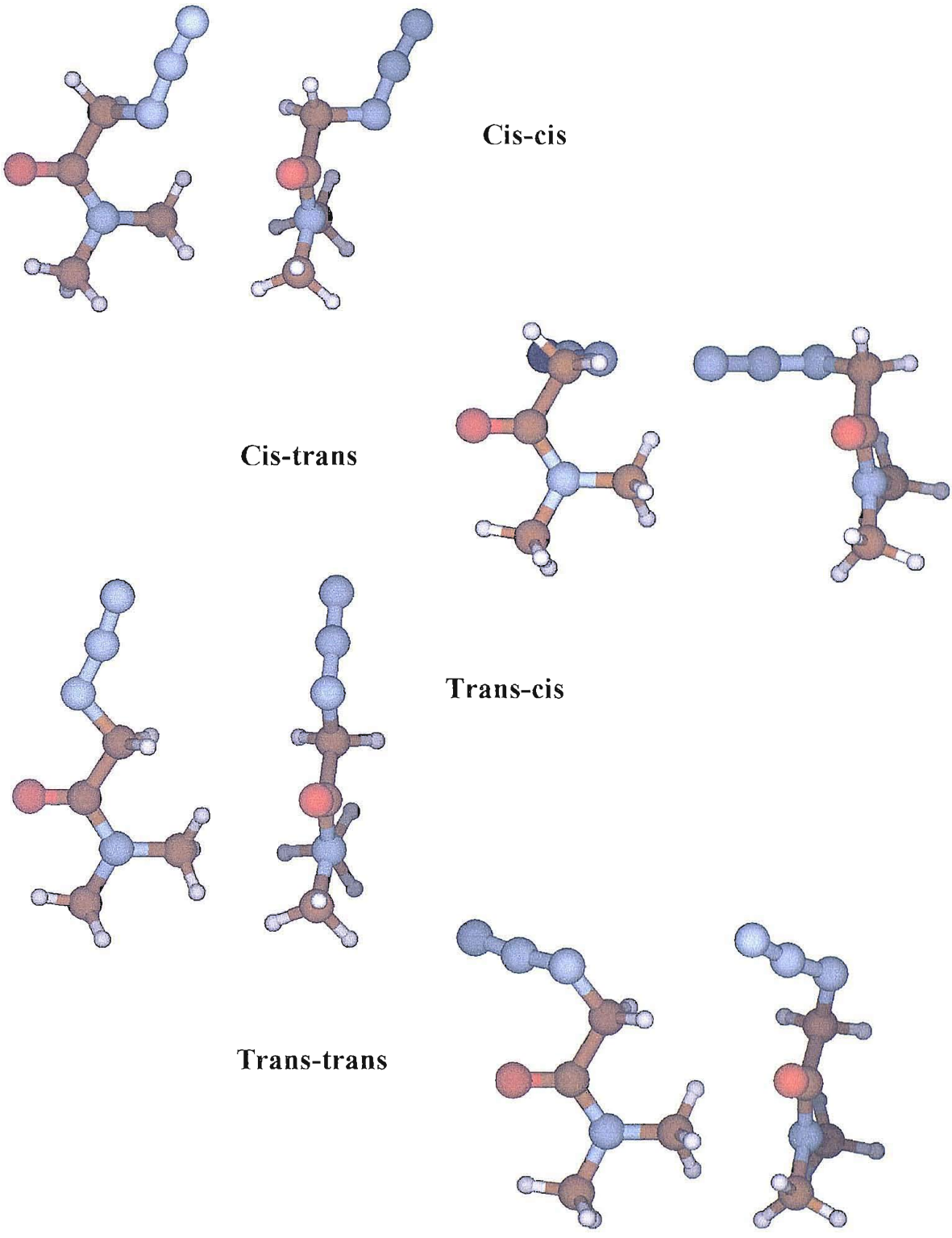

Figure 5.30- The four conformers of dimethylazidoacetamide obtained from *ab initio* calculations at the MP2/6-31G level. The labelling reflects the relative position of the methylene hydrogen atoms to the oxygen atom and of the azide chain to the methylene hydrogen atoms. For example, structure *trans-cis* is characterized by the oxygen atom in *trans* position to the methylene hydrogen atoms, and with methylene hydrogen atoms latter pointing in the same direction of the azide chain, therefore they are *cis***

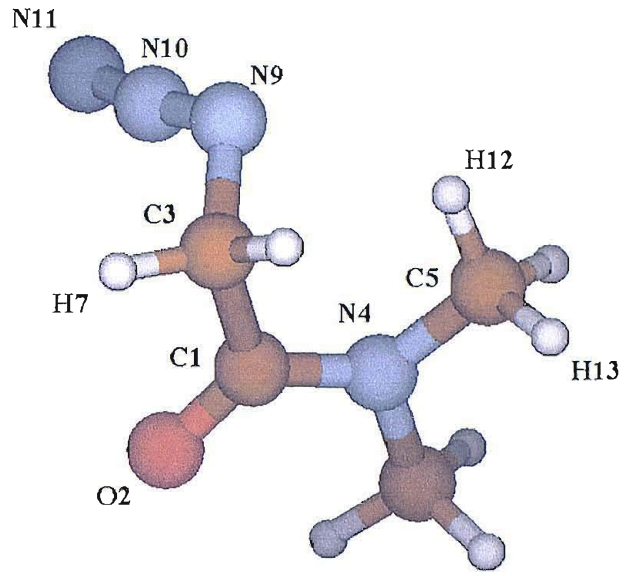

Figure 5.31- Atom labelling in structure *cis-trans* of dimethylazidoacetamide

Table 5.17- Geometrical parameters for the lowest energy structure of dimethylazidoacetamide

Bond	Length (Å)	Angle	Value (°)
N11-N10	1.1635	N11-N10-N9	172.08
N10-N9	1.2492	N10-N9-C3	114.66
N9-C3	1.4797	N9-C3-H7	108.28
C3-H7	1.09	N9-C3-C1	113.07
C3-C1	1.5304	O2-C1-N4	123.5
C1-O2	1.2369	C1-N4-C5	121.6
C1-N4	1.3668	N4-C5-H12	109.9
N4-C5	1.4536	N10-N9-C3-C1	62.3
C5-H12	1.0846	N9-C3-C1-O2	244.2
C5-H13	1.0931	C1-N4-C5-H12	11.3

Table 5.18 reports the total and relative energies calculated for the four structures: the differences are small, because the dihedral angles are very different from the 0° and 180° values and tend to lie in a relatively narrow range. For example, in structure *cis-trans* the values are 244.2° and 185.1°, while in structure *trans-trans* they are 13.7° and –58.7°.

These small differences in the orientations can be seen at a glance in Figure 5.30.

Table 5.18- Total energies of the four dimethylazidoacetamide conformers at the MP2/6-31G level**

Structure	Energy (hartrees)
Cis-cis	-450.1057254
Cis-trans	-450.1075181
Trans-cis	-450.1016063
Trans-trans	-450.1067725

The total energies of the three lowest energy structures differ by only 1.1 kcal/mol, while structure *trans-cis* (which is the structure closest to planarity) lies around 3.7 kcal/mol higher in energy than the most stable one. Due to the small differences in energy between conformers *cis-cis*, *cis-trans* and *trans-trans*, it is likely that the three structures will contribute to the experimental photoelectron and infrared spectra ($k_B T$ at 300 K is around 0.60 kcal/mol).

Table 5.19 reports the first VIEs for the most stable conformer (structure *cis-trans*), calculated with Koopmans' theorem, obtained by taking the negative of the orbital energies computed at the MP2/6-31G** level, and compares them with the experimental VIEs. The ΔSCF method was applied to the first two ionizations: values reported in parentheses indicate VIEs obtained for doublet ionic states, calculated at the neutral minimum energy geometry, contaminated with higher multiplicity states. In the case of dimethylazidoacetamide, the spin contamination on the first two ionic states is such that ΔSCF method is hardly reliable, as can be seen from the lower value obtained when an electron was removed from the third HOMO, which is free of spin contamination (a state was considered contaminated when the spin quantum number S is such that $S^2 > 0.9$ for these states, where S^2 for a pure doublet state is 0.75).

Also in this case, calculation of adiabatic ionization energies (AIEs) by optimization of the geometry of the cation, starting from the geometry of the most stable neutral conformer (*cis-trans*), was prevented by lack of convergence of the calculations at the MP2 level either on removing an electron from the HOMO (MO 33) or from the second HOMO (MO 32).

Koopmans' theorem has been applied to all four conformers. Table 5.20 compares the values obtained from the calculations at the Hartree-Fock level, after they have been scaled by 0.92 which is a factor widely used in the literature [27, 28].

Table 5.19- Experimental and computed (with Koopmans' theorem) VIEs for the *cis-trans* structure of dimethylazidoacetamide. Unrestricted calculations were performed on the cations.

KT calculated VIE (eV)	KT calculated VIE · 0.92 (eV)	ΔSCF calculated VIE (eV)	Ionization	Experimental VIE (eV)	Band
10.06	9.25	(10.01)	$(34\ a)^{-1} \rightarrow {}^2A$	9.19	A
10.30	9.47		$(33\ a)^{-1} \rightarrow {}^2A$		
11.67	10.74	9.83	$(32\ a)^{-1} \rightarrow {}^2A$	9.85	B
12.68	11.67			11.36	C
14.42	13.27			13.31	D
14.62	13.45				
15.32	14.09			14.22	E
15.39	14.16				
15.70	14.44				
16.08	14.79				
17.62	16.21			16.03	F
17.91	16.48				

Table 5.20- Comparison between the VIEs of the four minimum energy conformers of dimethylazidoacetamide calculated with Koopmans' theorem, all expressed in eV and scaled by the 0.92 factor

Ionization	KT VIEs·0.92 *cis-trans*	KT VIEs·0.92 *cis-cis*	KT VIEs·0.92 *trans-trans*	KT VIEs·0.92 *trans-cis*	Exp. VIEs
$(34\ a)^{-1} \rightarrow {}^2A$	9.25	9.32	9.16	9.29	**9.19**
$(33\ a)^{-1} \rightarrow {}^2A$	9.47	9.64	9.60	9.59	
$(32\ a)^{-1} \rightarrow {}^2A$	10.74	10.75	10.53	10.62	**9.85**
$(31\ a)^{-1} \rightarrow {}^2A$	11.67	11.28	11.17	10.99	**11.36**
$(30\ a)^{-1} \rightarrow {}^2A$	13.27	12.99	13.00	12.88	**13.31**
$(29\ a)^{-1} \rightarrow {}^2A$	13.45	13.38	13.58	13.55	
$(28a)^{-1} \rightarrow {}^2A$	14.09	13.95	14.23	14.09	**14.22**
$(27a)^{-1} \rightarrow {}^2A$	14.16	14.08	14.38	14.32	
$(26a)^{-1} \rightarrow {}^2A$	14.44	14.42	14.66	14.63	
$(25a)^{-1} \rightarrow {}^2A$	14.79	15.03	14.89	15.37	

Figure 5.32 shows the shape of the four highest occupied molecular orbitals calculated for the most stable conformer of dimethylazidoacetamide (*cis-trans*) at the HF level- the skeleton of the molecule is also reported to facilitate the identification of the atoms. The description of the molecular orbitals for the structures has been obtained from a single point Hartree-Fock calculation assuming the geometries being those calculated at the MP2 level. Calculations carried out at the Hartree-Fock level only produced three minimum energy geometry conformers (*cis-cis* and *cis-trans* structures optimised to the same structure), and therefore three different sets of molecular orbitals.

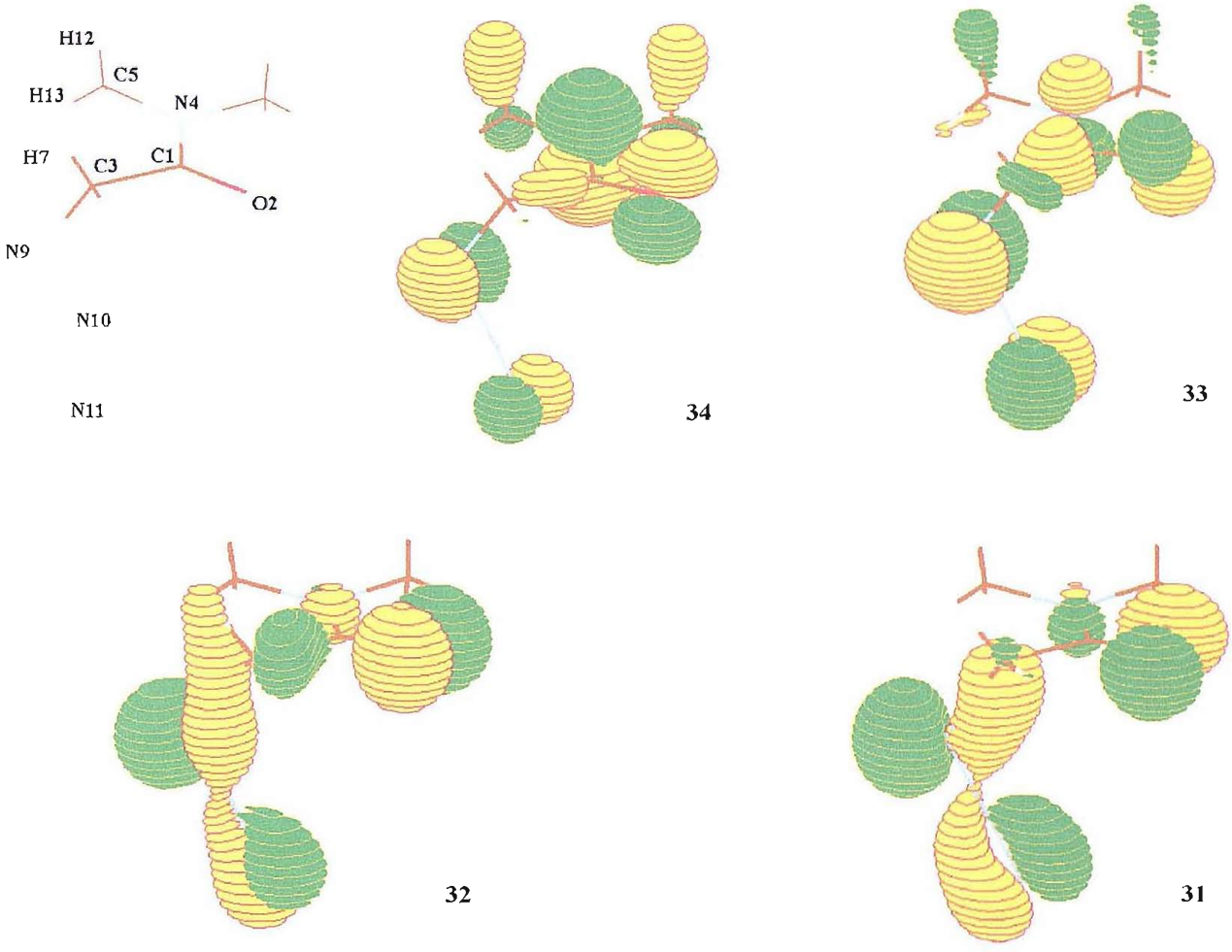

Figure 5.32- The four highest occupied molecular orbitals for structure *cis-trans* of dimethylazidoacetamide as obtained from calculations performed on the Gaussian98 program at the HF/6-31G level**

Assuming that C3, C1, O2, N4 and C5 lie in a plane, and C3, N9, N10 and N11 lie in another plane, molecular orbital 34 (the HOMO) can be described as a delocalized orbital with major p_{π}-bonding

character between C1 and N4, a p_π-antibonding contribution on the carbonyl group, and a p_π-antibonding character on the azide chain (the nodal plane is the C3-N9-N10-N11 one). There are also non-bonding contributions arising from the methyl carbon atoms.

MO 33 retains the p_π-antibonding character on the carbonyl group, but the nodal plane this time is orientated perpendicularly to the C3-C1-O2-N4-C5 plane; with respect to MO 34 there is a higher p_π-antibonding contribution from the azide chain.

MO 32 is strongly p_π-antibonding on the carbonyl group, with the nodal plane orientated perpendicularly to the C3-C1-O2-N4-C5 plane, and σ-bonding between C1 and N4 and between C1 and C3. There is also a strong p_π-bonding contribution between N11 and N10, as well as the strong p_π-antibonding character between N10 and N9: the nodal plane for both is perpendicular to the C3-N9-N10-N11 plane. An additional contribution can be seen in a σ-bond between C3 and H7.

MO 31 is similar to MO 32.

In comparison with the results on azidoacetamide, the contribution of the azide chain to these HOMOs is higher, especially for structure *cis-trans* (even if this time the differences in the shape of the HOMOs and in the corresponding VIEs between different conformers are smaller than between the azidoacetamide conformers), and therefore they show more similarities with the HOMOs obtained from previous calculations on other azides [10-12]. Also, all the molecular orbitals are more delocalized than in azidoacetamide (c.f. previous section): this explains the broader nature of the photoelectron bands (see Figure 5.29) in dimethylazidoacetamide, which especially in the 13.0-20.0 eV region are difficult to distinguish. Moreover, Table 5.19 shows that numerous bands have VIEs expected in the region between 13.0 and 17.0 eV: the overlapping of such one-electron ionizations leads to the broad appearance of the photoelectron spectrum in that region.

Harmonic vibrational frequencies have been calculated for the four conformers at the MP2/6-31G** level by means of second derivative calculations. Figure 5.33 displays the calculated IR spectra for each structure, while Table 5.21 reports the computed IR frequencies for the four conformers of dimethylazidoacetamide and compares them with the experimental values for the most prominent bands. For a more detailed evaluation of the agreement between the calculated and experimental spectrum, Figure 5.34 compares the calculated IR spectrum for structure *cis-cis* (even if it is not the most stable structure) with the experimental spectrum obtained in a nitrogen matrix. The conformer *cis-cis* has been chosen because it is the one for which the degree of agreement between the calculated and experimental IR spectrum can be better appreciated; moreover, its energy is comparable to the most stable conformer (*cis-trans*).

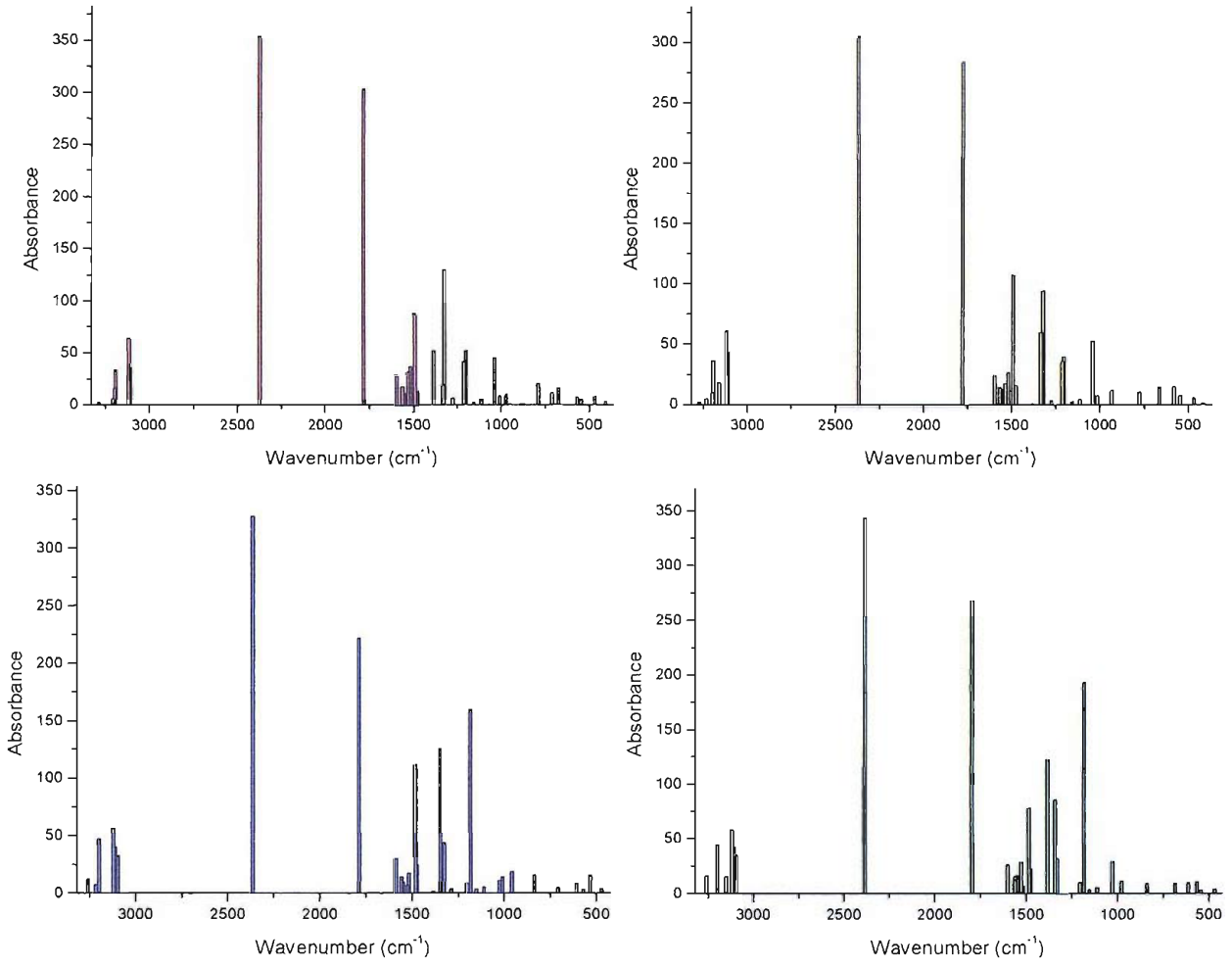

Figure 5.33- The IR spectra calculated for the structures *cis-cis* (red line), *cis-trans* (yellow line), *trans-trans* (blue line) and *trans-cis* (green line) of dimethylazidoacetamide at the MP2/6-31G level.**

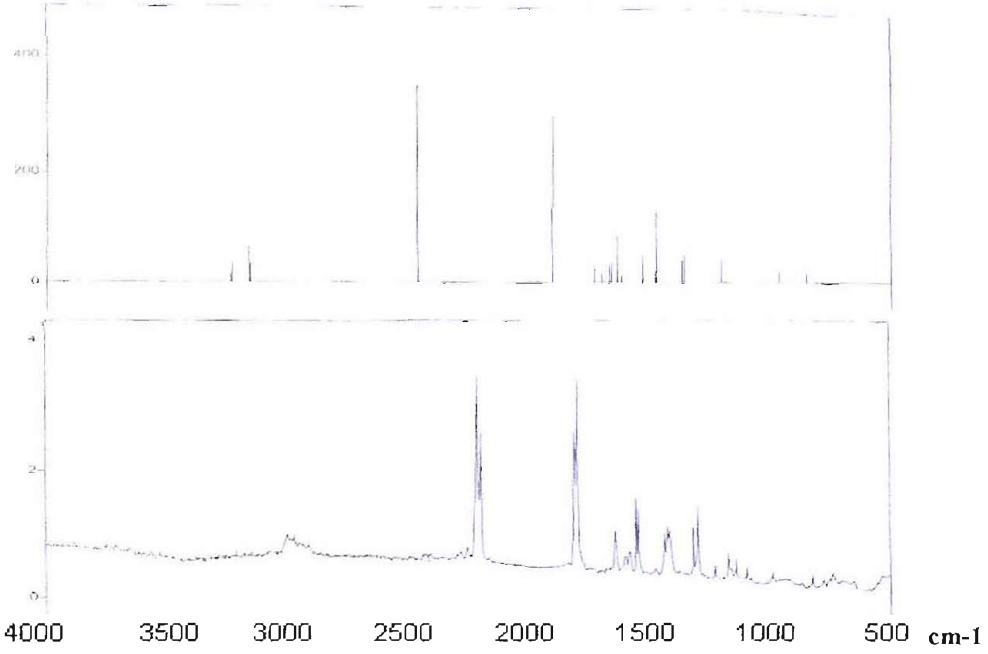

Figure 5.34- Comparison between the matrix IR spectra of dimethylazidoacetamide calculated at the MP2/6-31G level for structures *cis-cis* (above) and the experimental one.**

Table 5.21- The most intense calculated IR bands for the four conformers of dimethylazidoacetamide (absorbances in km/mol are reported in brackets for all the structures)

Cis-trans	*Cis-cis*	*Trans-trans*	*Trans-cis*		
IR frequency (cm^{-1})	**IR frequency (cm^{-1})**	**IR frequency (cm^{-1})**	**IR frequency (cm^{-1})**	**Experim. frequency (cm^{-1})**	**Normal mode**
	932 (11.6)	961 (18.4)	978 (10.9)		
		1011 (13.9)			
1038 (44.7)	1039 (52.5)	1027 (10.7)	1028 (29.1)		
1201 (51.8)	1201 (39.6)	1184 (159.2)	1183 (193.0)		
1211 (41.0)	1211 (35.6)				
1322 (129.4)	1319 (94.3)	1328 (43.0)	1326 (31.6)		
1329 (18.5)	1331 (59.9)	1348 (125.4)	1341 (85.7)		
1383 (51.4)			1383 (122.2)		
1475 (12.8)	1474 (15.6)	1475 (23.9)	1475 (22.3)		
1495 (87.0)	1489 (107.3)	1483 (111.3)	1484 (77.9)		
1520 (36.9)	1517 (26.6)	1520 (17.0)	1527 (28.6)		C-N=N stretching
1533 (31.7)	1533 (17.4)		1548 (16.2)		$C-H_2$ wagging
	1557 (12.3)	1560 (14.0)	1558 (15.7)		
1564 (17.4)	1565 (14.2)	1561 (11.7)	1562 (11.9)		$C-H_2$ scissoring
1595 (27.7)	1592 (23.9)	1589 (29.3)	1599 (25.8)		$N-H_2$ scissoring
1780 (303.0)	1775 (283.8)	1788 (220.9)	1795 (267.8)	**1685/1672**	C=O stretching
2374 (353.7)	2365 (305.1)	2366 (327.1)	2383 (343.0)	**2118/2104**	N-N-N stretching
3109 (35.6)	3110 (43.5)	3096 (32.4)	3091 (34.9)		$C-H_2$ sym. stretching
3112 (32.7)		3110 (39.4)	3106 (42.4)		$C-H_2$ asym stretching
3118 (64.1)	3119 (60.7)	3119 (56.1)	3117 (57.8)		$N-H_2$ sym. stretching
3192 (33.6)	3160 (18.1)		3149 (15.7)		
3199 (15.6)	3194 (36.2)	3199 (47.0)	3197 (44.6)		$N-H_2$ asym stretching
		3257 (12.6)	3258 (15.9)		

In the case of dimethylazidoacetamide minimum energy structures, the computed spectra do not display great differences in intensity ratios or peak position (for example the C=O stretch ranges from 1775 to 1795 cm^{-1}), so it is more difficult to state whether a given conformer contributes to the experimental IR spectrum more than the others; the calculated total energies for the four structures are so similar that is possible that all of them- with the possible exception of structure *trans-cis*- contribute to the IR spectrum. The actual experimental spectrum shows the carbonyl absorption to be more intense than the azide absorption, and it seems that structure *cis-trans* (which is also the most stable, as obtained in calculations) is the one that more closely resembles the correct intensity ratio between the peaks at ~2300 and ~1700 cm^{-1}.

The differences between experimental and calculated spectra are reduced by considering the possibility that two or more conformers of azidoacetamide are trapped in the matrix: in this case, the agreement in the band pattern especially in the 500-1500 cm^{-1} region is improved (the *cis-cis* and *cis-trans* structures alone cannot, even if they are the ones whose agreement seems more satisfactory with the experiment, reproduce the high intensity of the bands around 1200 cm^{-1}). Also the broad nature of the carbonyl band can be explained by the slightly different frequencies between the conformers that lead to a partial overlap of the bands associated to the C=O stretch.

The degree of agreement between experiment and calculations is good: the higher values of the calculated frequencies, especially above 3000 cm^{-1} e.g. the C-H and N-H stretches, are expected considering that anharmonicity has been neglected, and that electron correlation has only been partially allowed for in the calculations.

5.3.4 THERMAL DECOMPOSITION EXPERIMENTS

Photoelectron spectroscopy

Figure 5.35 shows the change in the photoelectron spectra when dimethylazidoacetamide vapour is heated at temperatures respectively of 100, 350 and 510 °C. In the spectrum at 350 °C, when roughly 50% of the azide has decomposed, the estimated contribution for DMF (red line) has been included.

The first evidence of pyrolysis is, as expected, the appearance of nitrogen (sharp band at 15.58 eV, structured band with AIE at 16.91 eV [8]): this occurs at temperatures around 250 °C. Around 300 °C the characteristic resolved band of hydrogen cyanide (VIE at 13.60 eV [8]) appears, along with the first sharp band of CO (VIE 14.01 eV [8]).

At the same time the first band of the azide begins to show the presence of an overlapping vibrationally resolved band at around 9.75 eV: this marks the appearance of dimethylformamide [8]. The characters of the HOMOs for both DMF and dimethylazidoacetamide are similar (the azide HOMO has a relatively small contribution from the azide chain), therefore the bands associated with these ionizations are quite similar: at temperatures between 200 and 300 °C it is difficult to distinguish which of the two compounds contributes more, and hence to establish the actual degree of pyrolysis. The visibility of the vibrational structure in the 9.75-10.10 eV is therefore the most reliable feature to detect the formation of DMF. At temperatures above 350 °C, the shape of the band in the 9.0-12.0 eV region is virtually the same as that of the DMF first band. It is therefore assumed that the parent azide is almost totally decomposed at that temperature.

The azide third band, centred at around 11.36 eV seems surprisingly persistent at increasing temperatures, and it only fully disappears beyond 480 °C: considering the thermal dependence of the other bands associated with the azide, this band was expected to disappear at lower temperatures. In fact, the band at 9.19 eV, which is associated with the parent azide, shows changes in its shape indicating that at those temperatures DMF is the main product and contributes to the 9.19 eV region. If the band at 11.36 eV is not associated with the azide (and is not associated with DMF, as can be seen from the pure PE spectrum of DMF shown in Figure 5.35b), this anomalous behaviour must be interpreted in terms of the presence of a reaction intermediate that shows a band in that region, given the fact that the band disappears with further increase of temperature.

Figure 5.36 shows the approximate residual contribution to the 9.0-12.0 eV IE region of the PE spectrum after DMF has been subtracted. This residual contribution can be attributed both to the imine being formed at that temperature and to some non-pyrolyzed azide. The similarity between the azide and DMF PE spectra makes deconvolution of spectra at intermediate degrees of pyrolysis difficult. It is

therefore difficult to estimate the amount of azide actually contributing to the spectrum in Figure 5.35b. Deconvolution attempts on this spectrum have nevertheless have shown that the PE band at 11.36 eV cannot be fully associated with the azide: even supposing that spectrum 5.35b is mainly originating from the azide rather than DMF, the azide contribution in the 11.36 eV region is not enough to fully represent the band experimentally observed.

By analogy with azidoacetamide, it is likely that dimethylazidoacetamide also decomposes first to dimethyliminoacetamide, which subsequently decomposes to DMF and HCN. *Ab initio* MO calculations on dimethyliminoacetamide using Koopmans' theorem predict the third VIE at 11.17 eV and the fourth VIE at 11.55 eV, therefore confirming the hypothesis of assigning such an intermediate to the thermally persistent band at 11.36 eV. The first two PE bands of the imine, predicted VIEs at 9.56 and 10.43 eV (see following section), are overlapping with strong bands of the parent azide and DMF and are therefore not clearly observed.

Beyond 500 °C the spectrum only shows bands associated with N_2, HCN, CO and DMF: no clear evidence was found either of isocyanic acid and its methylated equivalent, or of methyl- and ethylimine. In fact, $CH_3N{=}C{=}O$ is characterized [17] by an intense, vibrationally resolved band with VIE approximately 10.60 eV, while $CH_3CH{=}NH$ shows [4] a broad band at 10.17 eV and a vibrationally resolved band at 11.43 eV. While the energy of these bands is compatible with the observations in the decomposition spectra of dimethylazidoacetamide, their shapes, as is reported in literature [17, 4], do not seem to correctly represent the characteristics observed in the present series of PE spectra. Lacking a positive identification of the presence of these compounds, it is not possible to state that methyl isocyanate and ethyl imine are being formed in the thermal decomposition of dimethylazidoacetamide.

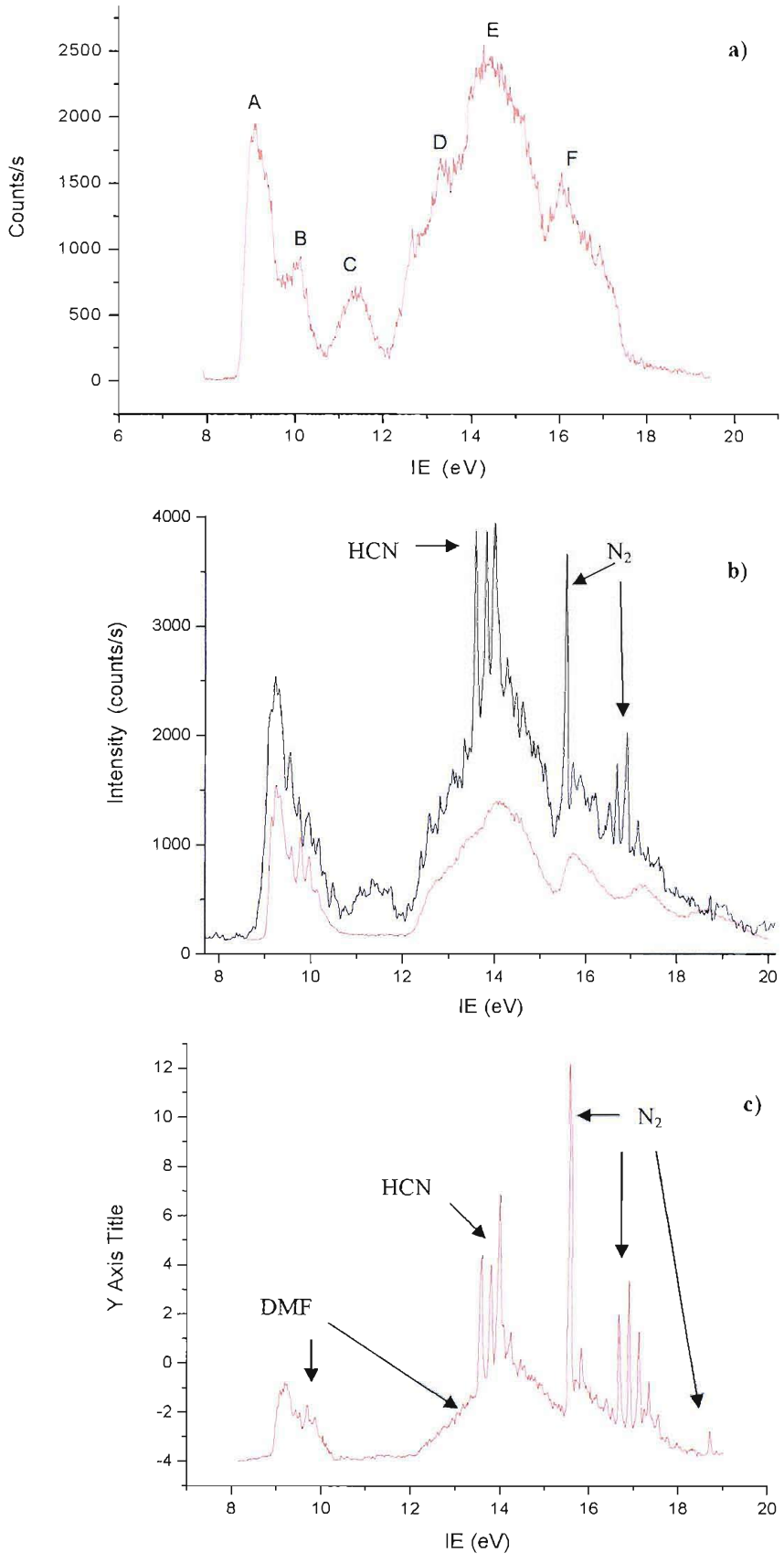

Figure 5.35- Pyrolysis HeI-photoelectron spectra (red line) of dimethylazidoacetamide vapours heated at 50 (a), 350 (b) and 510 °C (c). Red line in (b): pure dimethylformamide.

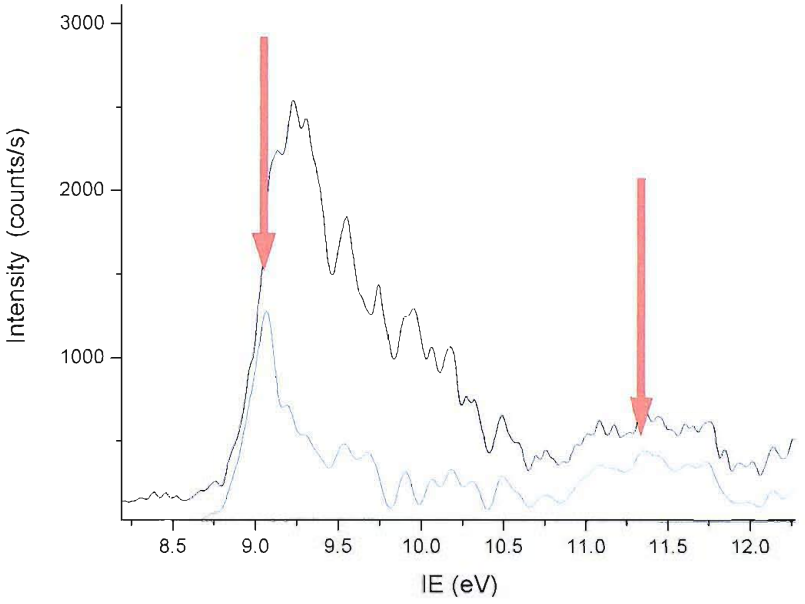

Figure 5.36- Residual contribution (blue line) obtained from the PE spectrum of the pyrolysis of dimethylazidoacetamide at 350 C (black line), after subtraction of the estimated DMF contribution. The red arrows indicate the positions of the VIEs of the bands of the possible reaction intermediate

Matrix isolation IR spectroscopy

A succession of matrix isolation infrared spectra recorded at increasing temperature of the furnace is reported in Figure 5.37. Table 5.22 lists the molecules associated with the labels of the bands, along with the vibrational wavenumber values of the most intense features in the spectra.

Table 5.22- Labels and assignment of the most important IR bands obtained experimentally in a nitrogen matrix in the thermal decomposition of dimethylazidoacetamide (see Figure 5.37 for the labelling of the bands)

Label	Vibrational wavenumbers (cm^{-1})	Assignment	Reference
	2118/2104, 1685/1672	$(CH_3)_2NCOCH_2N_3$	
D	1673, 1630, 1371, 1217	$(CH_3)_2NCOCH{=}NH$	
F	2139	CO	[21]
J	1694, 1384, 1082	DMF	[29]
K	2828, 2786, 1148, 1021	$(CH_3)_2NH$	[29]
M	3285, 747/737	HCN	[20]

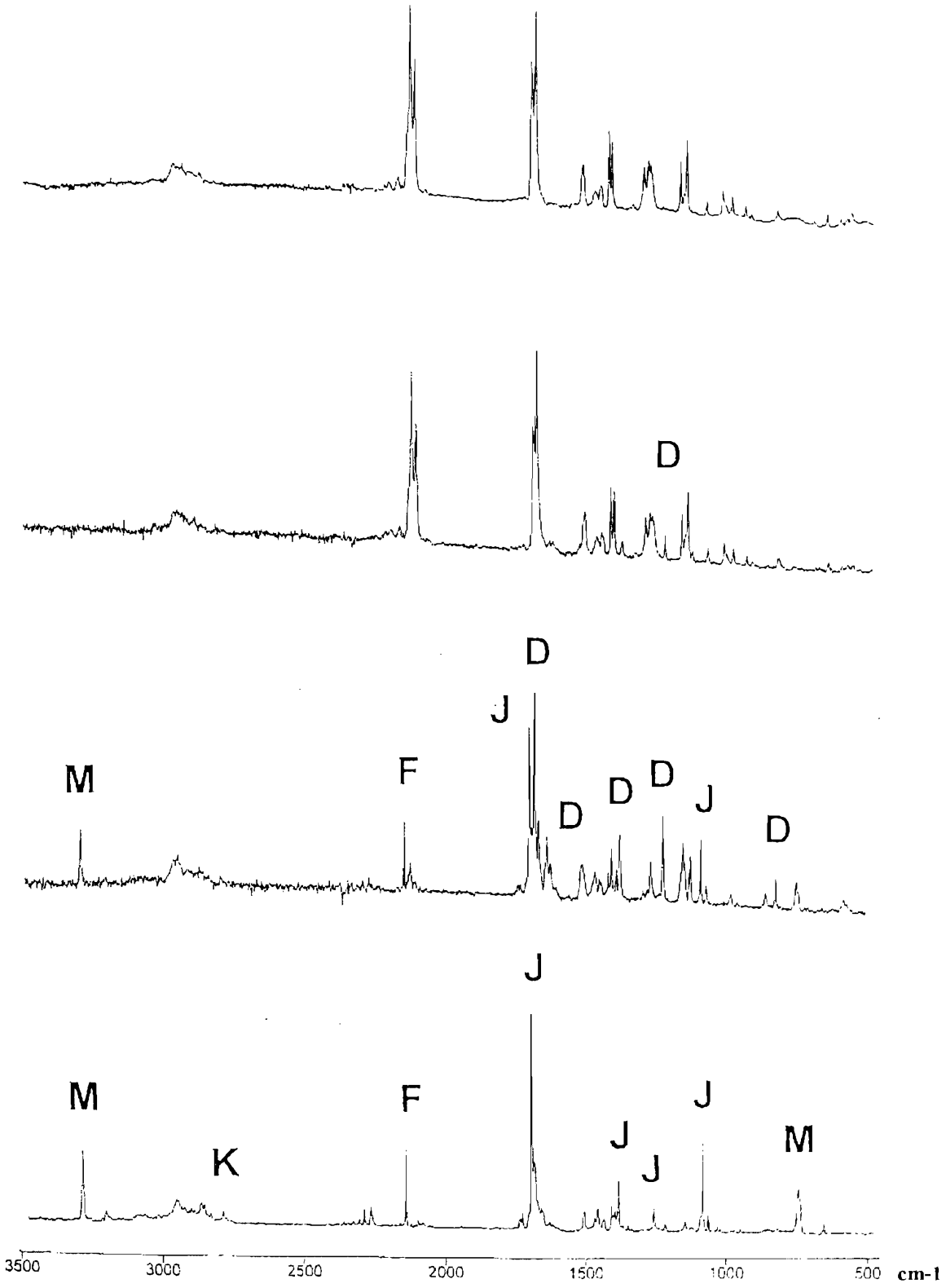

Figure 5.37- IR spectra recorded for dimethylazidoacetamide vapours heated between 30 and 530 °C and then trapped in a nitrogen matrix

As it is impossible to detect nitrogen in infrared spectroscopy, the start of the azide pyrolysis can be identified by the appearance of other bands associated with decomposition products. The first evidence occurs at around 160 °C, when a band at 1217 cm^{-1} begins to be observed. With increasing temperatures, the azide bands reduce in intensity, as exemplified by the decrease of the strong N_3 absorptions at 2118/2104 and at 1685/1672 cm^{-1}, while new bands appear. As happened in the azidoacetamide decomposition, two types of new bands can be distinguished according to their thermal dependence. A set of bands increases steadily in intensity with increasing temperature, indicating the formation of stable products which do not decompose even at relatively high temperatures: this is the case for example for the bands at 3285, 747/737 (labelled M in Figure 5.37), 2139 (labelled I) and 1694, 1384, 1082 cm^{-1} (labelled J), which have been assigned- by referring to previous matrix IR studies [20, 21, 29]- to HCN, CO and $HCON(CH_3)_2$ respectively. Also additional weak bands can be identified at temperatures above 210 °C which follow the same thermal behaviour: the bands at 3483, 2265, 780, 581 cm^{-1} (labelled G in Figure 13) are assigned to HNCO [19], while the bands at 2828, 2786, 1148, 1021 cm^{-1} (labelled K) are assigned to $(CH_3)_2NH$ [29].

A second set of bands (the most prominent are at 1673, 1630, 1371 and 1217 cm^{-1}, and are labelled D in Figure 5.37) shows a different thermal behaviour, with an increase of intensity between 160 and 250 °C followed by a decrease in intensity for temperatures above 300 °C and a total disappearance beyond 360 °C: this suggests the presence of a reactive intermediate as a product of the azide decomposition, which is subsequently decomposed to secondary products. Also in the case of the decomposition of dimethylazidoacetamide, all the bands not assigned to the thermally more stable products (HCN, CO, DMF, HNCO, dimethylamine) show the same kind of intermediate thermal behaviour, that is there is no evidence for more than one reaction intermediate being formed. The fact that their relative intensity ratio is not altered by changing pyrolysis temperatures, deposition times or other experimental parameters suggests that all the intermediate bands belong to the same species. An initial estimate of the structure of the intermediate is given by the bands above 3000 cm^{-1} and by the strong band at 1673 cm^{-1}: it is likely that the N-H and the C=O groups are retained from the parent azide. By analogy with the intermediate observed in the azidoacetamide thermal decomposition, a full assignment of the bands associated with the intermediate can only be achieved with the support of *ab inito* calculations: it was found that no match between these bands and those of some expected products like CH_3NCO or CH_3CHNH could be obtained.

5.3.5 CHARACTERIZATION OF THE POSSIBLE REACTION INTERMEDIATES

The chemical formula of dimethylazidoacetamide and the IR and PES evidence suggests a thermal decomposition path similar to azidoacetamide, the initial step being the release of nitrogen accompanied by the production of a nitrene diradical in its singlet spin multiplicity state following the scheme

$$^1N_3CH_2CON(CH_3)_2 \rightarrow {}^1N_2 + {}^1{:}NCH_2CON(CH_3)_2$$

$^1{:}NCH_2CON(CH_3)_2$ –nitreneacetamide- is expected to be highly unstable, as nitrenes have never been experimentally detected in the gas-phase in photoelectron spectra and in matrices in infrared matrix isolation spectra.

Moreover, *ab initio* MO calculations on dimethyl nitrenacetamide do not lead to the location of a minimum energy structure in the singlet multiplicity state, because all the attempted calculations led to the conversion into the imine during the optimization. Only the triplet state is found to be stable: an inter-system crossing to the triplet is therefore required for experimental detection, which is an unlikely process due to the breaking of the spin conservation rule.
Nitrene formation cannot be proved, so- by analogy with azidoacetamide- no details of the computational results on this diradical will be reported here. Only the products arising from one of the possible isomerization mechanisms of the nitrene will therefore be considered in the next paragraphs.

The first isomerization possibility from the nitrene is the Type 1 mechanism (see Section 5.1.5), in which dimethylnitreneacetamide undergoes a 1,2-hydrogen shift

$$^1{:}NCH_2CONH_2 \rightarrow {}^1HN{=}CHCONH_2$$

producing dimethyliminoacetamide which is a stable molecule with all real vibrational frequencies at the MP2/6-31G** level of calculations.

A Type 2 mechanism involves the attack of the nitrogen terminal atom at another site within the nitrene molecule so that a new bond is formed to compensate the electron deficiency of the nitrogen atom. By letting the *ab initio* calculation optimize the nitrene structure obtained by removing the two terminal nitrogen atoms (and leaving unchanged all the other geometrical parameters) from all the four different conformers of dimethylazidoacetamide, different Type 2 mechanisms are found.

One is the attack on the carbonyl carbon atom, already encountered in the azidoacetamide case, which in the present case can be represented as

$$:NCH_2CON(CH_3)_2 \rightarrow CH_2{=}NCON(CH_3)_2$$

where a new N-C bond is formed along with the formation of the iminic C=N double bond. This molecule is labelled dimethyl-N-iminoacetamide.

In contrast with azidoacetamide, an additional mechanism is possible, involving the attack of the nitrogen atom on the oxygen atom, leading to the formation of a four-membered ring. The geometrical strain of this structure and the presence of adjacent opposite charges is reflected by a very high energy of this molecule (the computed total energy is found to be around 100 kcal/mol higher than that of the two other imines). Therefore, despite the calculation predicting it having all real vibrational frequencies, this molecule is very unlikely to be formed in the decomposition process. Its calculated geometrical, energetic and spectroscopic characteristics will not be reported here.

Finally, a third possibility must be considered, that is the attack on one of the methyl groups: this leads to the formation of a cyclic structure.

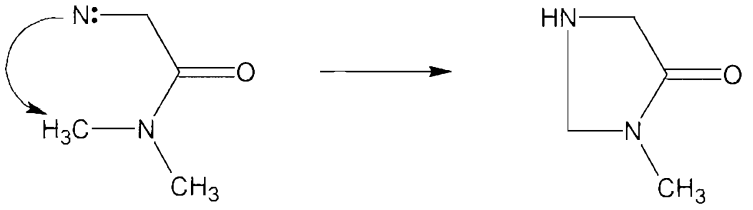

The most probable candidates as reaction intermediates for the dimethylazidoacetamide pyrolysis are then dimethyliminoacetamide, dimethyl-N-iminoacetamide and the five-membered cycle.

The most probable candidates as reaction intermediates for the dimethylazidoacetamide pyrolysis are then dimethyliminoacetamide, dimethyl-N-iminoacetamide and the above five-membered cyclic compound.

Dimethyliminoacetamide

For $HN{=}CHCON(CH_3)_2$ three conformers – and not four as was the case for iminoacetamide- with all real vibrational frequencies have been located at the MP2/6-31G** level on the closed-shell singlet surface: their geometries are shown in Figure 5.38. The labelling nomenclature describes, as for the

azide, the relative positions of the C-H hydrogen atom with respect to the oxygen atom and the iminic hydrogen atom relative to the C-H hydrogen atom. The structure, which at the beginning of the calculation had an initial geometry which was set in a *trans-cis* orientation, converged, during the optimisation process, to structure *cis-cis*, in which the C-H proton is in a *cis* position both to the N-H proton and the oxygen atom. This result is probably due to the presence of the methyl groups in the positions in which in iminoacetamide there are hydrogen atoms. This involves a new repulsive interaction of the C-H hydrogen with the methyl hydrogen atoms, in addition to the one with the proton on the terminal nitrogen atom: the effect is a rotation around the C-C bond of the molecule. Figure 5.39 shows in greater detail the most stable structure, structure *trans-trans*, and its most relevant geometrical parameters are listed in Table 5.23.

Even if the distortion from a C_s structure is not very large, the symmetry of the three structures is C_1, mainly due to the asymmetry of the methyl hydrogen atoms and, in the case of structure *cis-trans*, of the imine NH group placed markedly out of the -NC(=O)C- plane. The most stable structure has been calculated to be structure *trans-trans*, which is the closest to planarity. This is in contrast to the results on dimethylazidoacetamide, where the structure closer to planarity (*cis-trans*) was the least stable. Setting the energy of structure *trans-trans* as zero, structures *cis-cis* and *cis-trans* lie at energies 1.4 and 2.8 kcal/mol higher respectively. This small energy difference indicates that all structures could be formed in the pyrolysis experimental conditions, and therefore they all contribute to the photoelectron spectrum.

Table 5.24 reports the total energies of the three structures. The ground electronic state is $^1A'$.

Table 5.24- Total and relative energies of the three conformers of dimethyliminoacetamide at the MP2/6-31G level**

Structure	Energy (hartrees)	Relative energy (kcal/mol)
Trans-trans	-340.9337716	0
Cis-cis	-340.9315373	1.4
Cis-trans	-340.9292423	2.8

Table 5.25 reports the VIEs calculated by applying Koopmans' theorem to structure *trans-trans* of dimethyliminoacetamide and the two first VIEs calculated via the ΔSCF method. As no optimization of the geometry of the cation was achieved, the calculation of the first adiabatic ionization energy was not possible; values in parenthesis indicate high spin contamination ($S^2 > 0.9$).

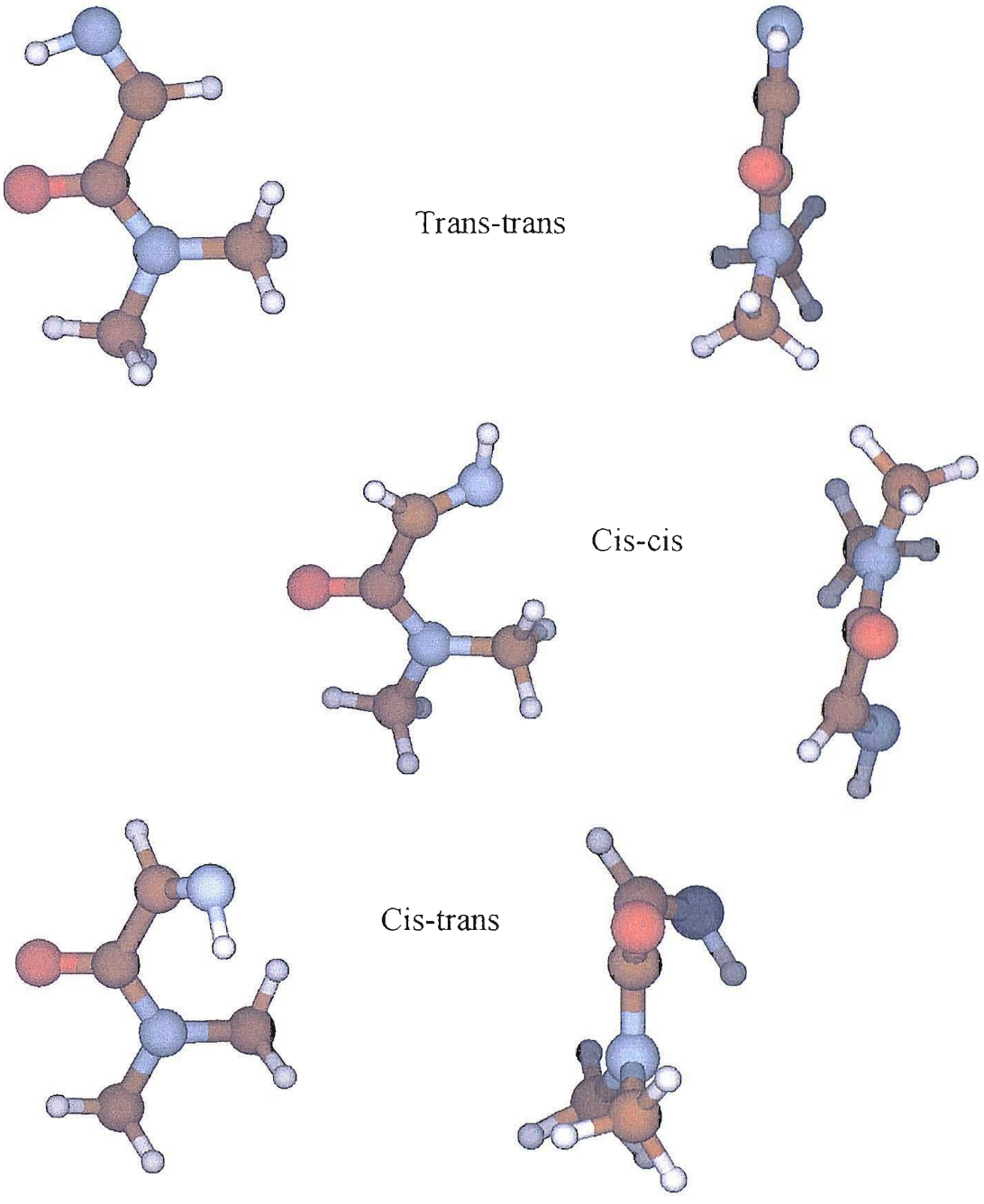

Figure 5.38- The three conformers of dimethyliminoacetamide computed with *ab initio* calculations at the MP2/6-31G level; the labelling reflects the relative position of the C-H proton in NH=CH to the oxygen atom and of the N-H proton to the C-H proton. For example, structure *cis-cis* means that the proton on the methyne group is in *cis* orientation with respect to the carbonyl oxygen and in *cis* also to the proton on the iminic nitrogen atom.**

Table 5.25- Calculated VIEs for structure *trans-trans* of dimethyliminoacetamide, using Koopmans' theorem and the ΔSCF method

KT calculated VIE (eV)	KT calculated VIE · 0.92 (eV)	ΔSCF calculated VIE (eV)	S^2 for the ion	Ionization
10.39	9.56	(9.34)	0.944	$(27\ a')^{-1} \rightarrow {}^2A$
11.34	10.43	10.06	0.762	$(26\ a')^{-1} \rightarrow {}^2A$
12.14	11.17	(9.34)	0.944	$(25\ a')^{-1} \rightarrow {}^2A$
12.55	11.55			
14.83	13.65			
15.14	13.93			
15.82	14.55			
15.84	14.57			
16.31	15.01			
16.70	15.36			
18.17	16.71			
18.29	16.83			

Table 5.26 shows the computed IR frequencies and intensities for dimethyliminoacetamide and compares them to the bands experimentally detected in IR matrix isolation experiments of thermal decomposition of dimethylazidoacetamide. Even if the most stable structure (the *trans-trans* conformer) is expected to be the one that mainly contributes to the experimental IR spectrum, vibrational frequencies for all the minimum energy structures are shown. The resulting spectra compared with the experimental one obtained in a nitrogen matrix are shown in Figure 5.40.

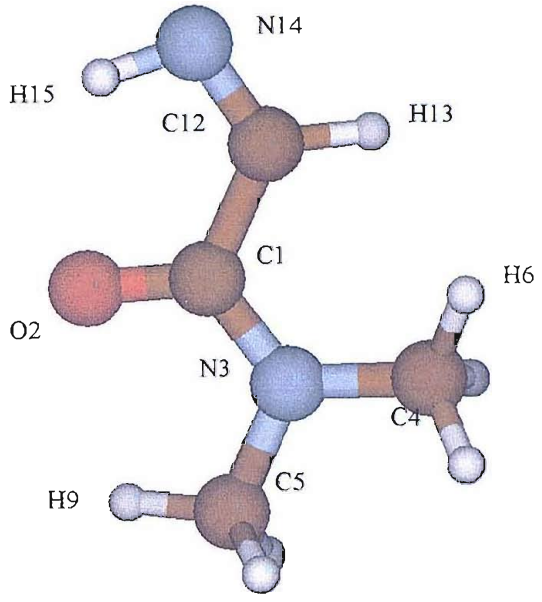

Figure 5.39- Structure and atom labelling in structure *trans-trans* of dimethyliminoacetamide

Table 5.23- Geometrical parameters for the lowest energy structure of dimethyliminoacetamide

Bond	Length (Å)	Angle	Value (°)
N5-H9	1.021	H9-N5-C3	110.54
N5-C3	1.284	N5-C3-C1	120.17
C3-H8	1.091	O2-C1-N4	125.64
C3-C1	1.506	C1-N4-H6	119.19
C1-O2	1.233	H9-N5-C3-C1	180.0
C1-N4	1.355	H8-C3-C1-O2	0.0
N4-H6	1.005	H6-N4-C1-C3	180.0

Table 5.26- Comparison between the computed and experimental IR bands of dimethyliminoacetamide (absorbances in km/mol are reported in brackets for all the three calculated structures)

Calc. IR bands (cm^{-1})			**Exp. bands (cm^{-1})**	*Calc. IR bands (cm^{-1})*			**Exp. bands (cm^{-1})**	*Normal mode*
trans-trans	***cis-trans***	***cis-cis***		***trans-trans***	***cis-trans***	***cis-cis***		
409.2 (5.35)	418.0 (2.39)			1507.4 (24.39)	1494.6 (65.90)	1480.4 (27.92)	**1460 (w)**	
500.6 (10.74)	463.8 (10.43)	444.3 (17.36)	**488 (s)**	1518.7 (15.11)	1523.0 (23.51)	1518.1 (12.67)		
580.9 (34.47)	570.3 (16.36)	579.4 (13.65)	**580 (w, br)**	1553.1 (11.28)	1535.7 (23.82)	1543.0 (3.02)		
628.8 (4.24)	705.3 (22.53)	727.0 (30.68)		1557.8 (17.00)	1556.1 (13.35)	1551.6 (12.58)		
843.9 (26.06)	730.0 (4.95)	727.7 (3.81)	**817 (s)**	1562.0 (14.06)	1560.4 (10.12)	1564.4 (11.28)		
	870.8 (49.49)	876.5 (8.09)		1588.1 (24.66)	1591.3 (22.23)	1589.7 (17.71)	**1506 (m)**	C-H_3 scissoring
1000.0 (3.11)	1020.4 (27.83)	1019.8 (29.56)	**973 (w)**	1678.0 (23.79)	1687.8 (50.22)	1670.3 (40.64)	**1630 (s)**	C=N stretching
1108.8 (5.95)	1111.2 (4.38)	1108.4 (5.08)	**1062 (w)**	1768.3 (259.73)	1759.2 (273.52)	1759.1 (256.78)	**1673 (vs)**	N-C=O stretching
1154.6 (3.66)	1129.7 (7.62)	1156.6 (2.58)		3118.1 (27.44)	3118.5 (30.61)	3114.2 (32.24)		asymm C-H_3 stretching
1182.4 (60.22)	1155.6 (1.13)	1173.1 (61.75)	**1082 (m)**	3122.1 (61.16)	3125.4 (64.85)	3118.6 (57.48)	**2930 (m, br)**	symm C-H_3 stretching
1192.0 (68.60)	1188.8 (91.59)	1201.2 (57.16)	**1120 (m)**		3171.5 (26.02)			
1202.9 (37.36)	1203.8 (8.35)	1203.8 (50.72)	**1148 (s)**	3199.6 (36.22)	3196.1 (47.25)	3190.1 (28.87)		C-H_3 asymm stretching
1263.9 (115.13)	1287.1 (16.24)	1267.5 (41.21)	**1217 (s)**	3207.3 (9.12)	3200.9 (7.39)	3204.1 (17.48)		C-H_3 asymm stretching
1323.2 (45.48)	1323.2 (44.34)	1318.5 (37.12)	**1261 (m)**	3243.9 (18.74)		3226.7 (15.78)		C-H stretching
1440.2 (121.31)	1424.3 (20.85)	1428.1 (24.93)	**1371 (s)**	3275.7 (14.53)	3302.0 (4.01)	3276.2 (4.46)		C-H_3 symm
1474.7 (18.30)	1473.1 (13.04)	1478.0 (87.70)	**1399 (m)**	3449.7 (4.64)		3495.7 (2.36)		N-H rocking
			1450 (w)					

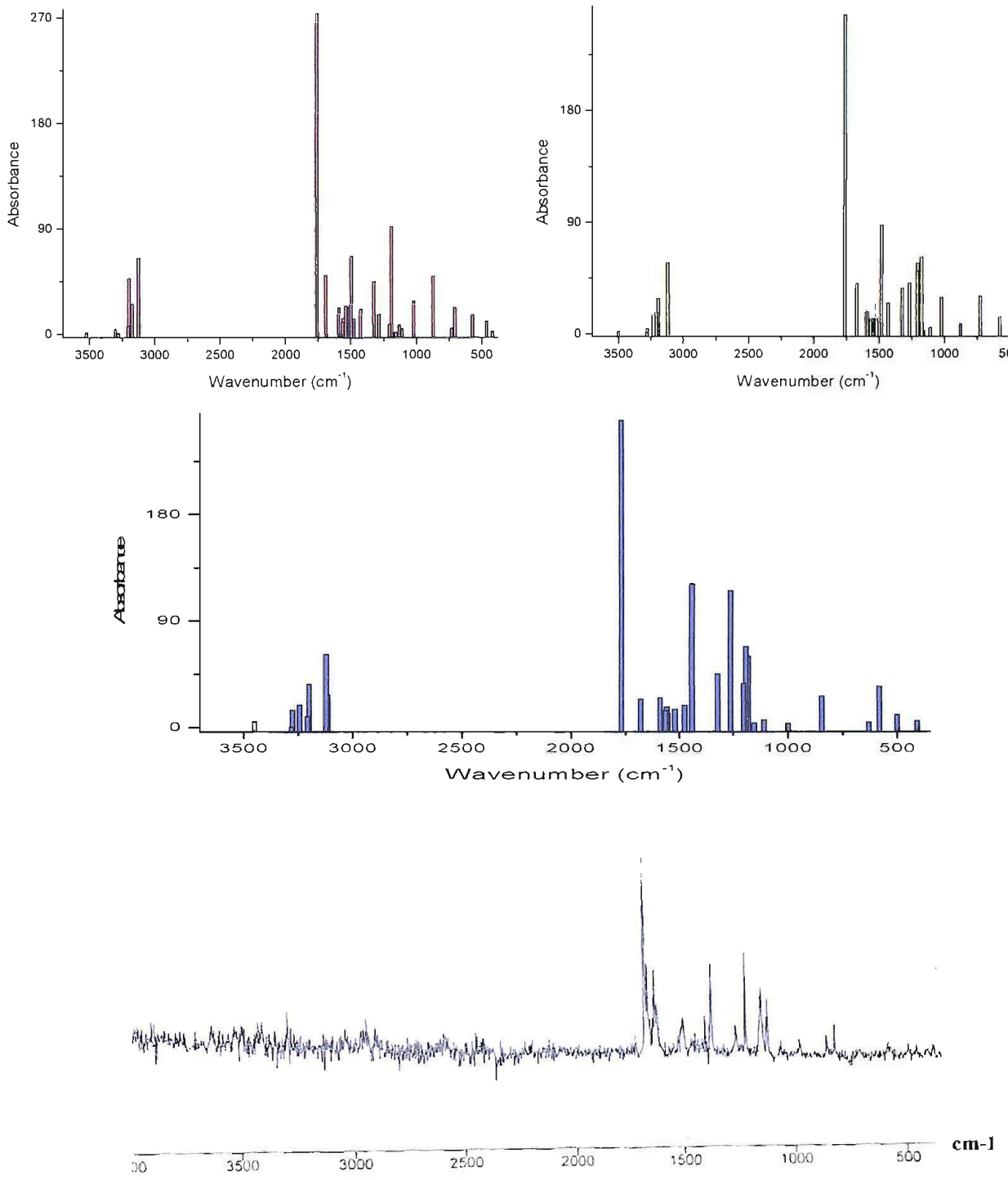

Fig. 5.40- The three IR spectra calculated for the conformers *cis-cis* (red lines), *cis-trans* (yellow lines) and *trans-trans* (blue lines) of dimethyliminoacetamide at the MP2/6-31G level and the experimental matrix isolation IR spectrum**

For dimethyliminoacetamide, the computed spectra for the different structures are very similar, so at first it seems difficult to make clear statements about which conformer contributes more to the experimental matrix IR spectrum. Nevertheless, the agreement between the experimental and the calculated IR spectrum of the *trans-trans* structure is particularly good, both in the frequency distribution and the intensity pattern, once the effect of neglecting anharmonicity and of only partial allowance for electron correlation in the calculations has been considered: this leads to a higher value of the calculated frequencies, in particular for the N-H stretching region above 3000 cm^{-1}. It is therefore possible to state with confidence that dimethyliminoacetamide is present as a reaction intermediate from the thermal decomposition of dimethylazidoacetamide: this reflects the results obtained for azidoacetamide. For the individual conformers, the intensity ratio of the bands between 1500 and 1100 cm^{-1} in the experimental spectrum seems to prove, anyway, that structure *trans-trans* is characterised by an infrared spectrum in overall better agreement with the experimental one, so it is the conformer most likely to be present in higher concentrations under the conditions in which the experimental spectra have been recorded: this reflects the fact that structure *trans-trans* is the lowest in energy among those calculated for dimethyliminoacetamide.

Concerning the causes of discrepancies between experimental and calculated spectra- which anyway do not contradict the assignment-, it must be emphasised that the experimental spectrum cannot represent the true spectrum of the intermediate because it has been obtained by removing all the bands belonging to species –either the starting azide or the decomposition products- which do not show the proper thermal dependence for a reaction intermediate. The experimental spectrum shown in Figure 5.40 therefore represents the most important features of the intermediate, but it does not represent the "true" one, especially for low intensity peaks, because of the subtraction procedure used.

As was the case for azidoacetamide, the degree of agreement can be better clarified by considering the agreement in the case of the parent azide (dimethylazidoacetamide). As can be seen by comparing Figures 5.40 and 5.34, the quality of the agreement between the experimental spectrum and the one calculated for the most stable conformer is comparable between the two compounds.

Finally, to obtain better agreement with the experimental IR spectrum, especially in the 1700-1000 cm^{-1} region, the possibility must be considered of other intermediates being trapped in the matrix: this can involve both different conformers of dimethyliminoacetamide, which are very close in energy to the *trans-trans* one, and a different imine arising from a degradation of the starting nitrene via an alternative pathway to the 1,2-H shift, as it was the case for azidoacetamide.

For this, investigations on the other possible reaction intermediates arising from a "Type 2" mechanism have been considered.

Dimethyl-N-iminoacetamide

In the same way as occurred for azidoacetamide, *ab initio* calculations show that by removing the two terminal nitrogen atoms from one of the optimised structures of dimethylazidoacetamide- leaving intact the remaining structure- and letting the optimisation procedure operate on the remaining nitrene, the terminal nitrogen atom does not acquire a proton from the adjacent carbon but instead prefers to attack the carbonyl atom. The net result is the production of dimethyl-N-iminoacetamide

$$:NCH_2CON(CH_3)_2 \rightarrow CH_2{=}NCON(CH_3)_2$$

Only one structure has been optimised for this molecule at the MP2/ 6-31G** level and its geometry is shown in Figure 5.41; the most important geometrical parameters are listed in Table 5.27. The calculated total energy was found to be -340.9367223 hartees.

It corresponds to a structure which is close to planarity; as was the case for N-iminoacetamide, only the structure with the terminal methylene group in the *cis* position with respect to the oxygen atom was optimised; attempts to locate a stable geometry with *trans* orientation have not been successful, because in this disposition the stabilising interaction between a $-CH_2$ hydrogen atom and the oxygen is removed, and a repulsive interaction of the $-CH_2$ protons with the protons on the methyl group leads the optimisation to converge back to the *cis* structure.

Table 5.28 reports the calculated VIEs for dimethyl-N-iminoacetamide. The differences with the dimethyliminoacetamide VIEs are minimal, as can be seen from a comparison with Table 5.25.

Table 5.29 reports the most significant calculated vibrational frequencies for N-iminoacetamide: the associated IR spectrum is shown in Figure 5.42, where a Gaussian envelope for the bands has been assumed.

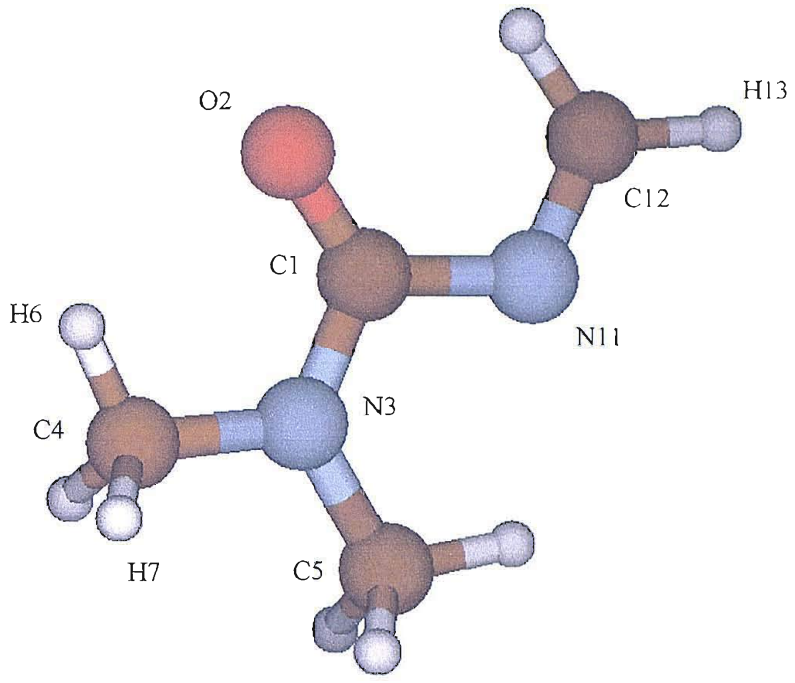

Figure 5.41- Optimized geometry of dimethyl-N-iminoacetamide calculated at the MP2/6-31G level**

Table 5.27- The most significant geometrical parameters for dimethyl-N-iminoacetamide

Bond	Length (Å)	Angle	Value (°)
C12-H13	1.0848	H13-C12-N11	118.34
N11-C12	1.2824	C12-N11-C1	113.17
C1-N11	1.4541	O2-C1-N3	124.08
N3-C1	1.3619	C1-N3-C4	118.73
C1-O2	1.2326	H6-C4-N3	108.65
C4-N3	1.4522	H13-C12-N11-C1	179.6
C5-N3	1.4534	C12-N11-C1-O2	-6.8
H6-C4	1.0844	C4-N3-C1-O2	0.8
H7-C4	1.0918	H6-C4-N3-C1	-1.5

Table 5.28- Calculated VIEs of dimethyl-N-iminoacetamide at the MP2/6-31G level**

KT calculated VIE (eV)	KT calculated VIE · 0.92 (eV)
10.00	9.21
11.09	10.21
11.96	11.00
12.78	11.76
14.45	13.29
14.96	13.77
15.09	13.88
15.14	13.93
15.84	14.58

Table 5.29- Calculated IR bands of dimethyl-N-iminoacetamide at the MP2/6-31G level**

Frequency (cm^{-1})	Intensity (km/mol)	Frequency (cm^{-1})	Intensity (km/mol)	Frequency (cm^{-1})	Intensity (km/mol)	Normal mode
400.3	5.12	1198.8	175.71	1592.7	30.83	C-H_3 symm. scissoring
413.0	19.40	1211.0	3.58	1708.7	24.67	C=N stretching
532.4	7.16	1246.1	1.84	1805.5	379.07	C=O stretching
570.0	11.02	1326.9	52.87	3113.5	33.52	C-H_3 symm. stretching
619.5	7.14	1470.5	21.81	3119.1	82.52	C-H_3 symm. stretching
797.1	7.56	1483.1	92.18	3171.2	21.47	C-H_2 symm. stretching
860.2	10.50	1490.4	8.70	3185.0	44.24	C-H_3 asymm. stretching
1015.5	6.91	1515.6	104.49	3194.2	16.18	C-H_3 asymm. stretching
1106.2	5.35	1558.9	17.64	3291.7	11.94	C-H_2 asym. stretching
1113.9	14.06	1561.6	16.65			C-H_2 scissoring

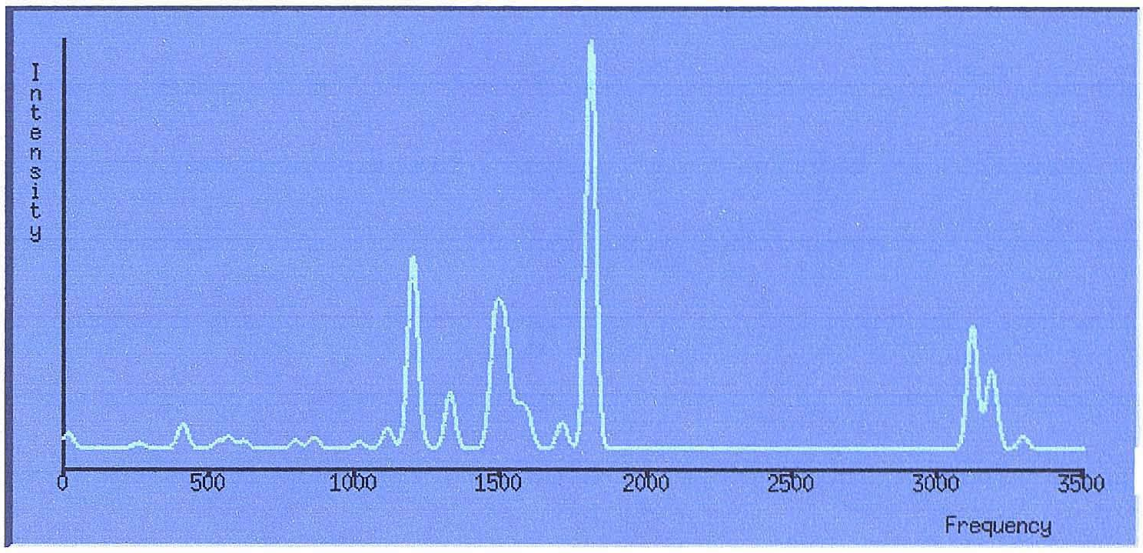

Figure 5.42- The infrared spectrum of dimethyl-N-iminoacetamide calculated at the MP2/6-31G level**

Five-membered cyclic intermediate

When the attack of the electron deficient nitrogen atom in the nitrene is towards the closest of the methyl groups- which is 3.1 Å away from the nitrogen atom- a five membered ring is formed. Its optimized structure is reported in Figure 5.43, and its most important geometrical parameters are listed in Table 5.30. The pentagon formed is not planar, mostly because of the N-H group, even if the lengths of the bonds forming the pentagonal structure are almost equal; the overall symmetry of the molecule is therefore C_1 even if the distortion from planarity is not large.

Its calculated total energy was found to be -340.9502777 hartrees: this is the lowest energy value for all the imine intermediates considered for this system.

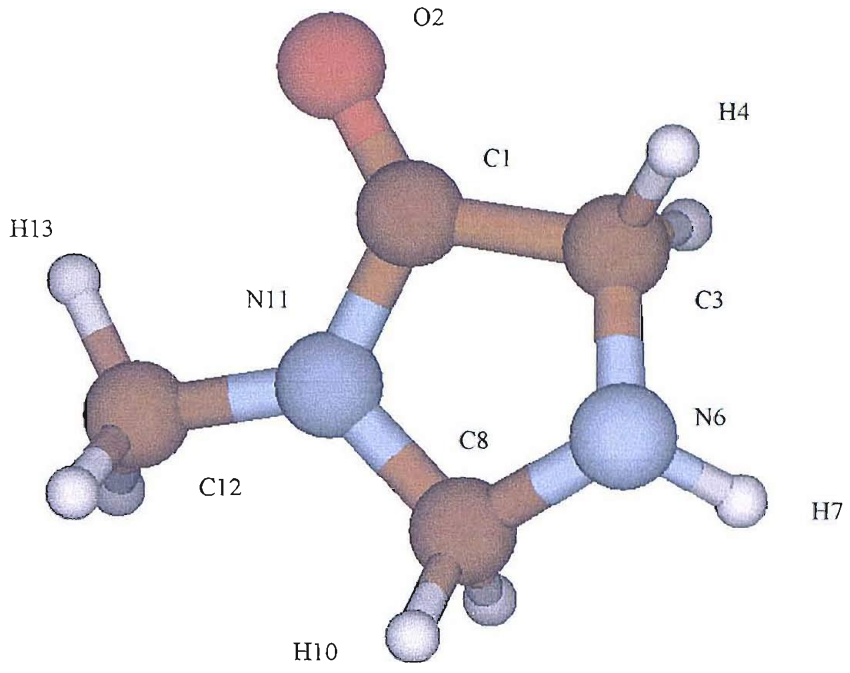

Figure 5.43- Optimized structure at the MP2/6-31G level for the cyclic intermediate obtainable in the decomposition of dimethylazidoacetamide**

Table 5.30- The most significant geometrical parameters calculated for the five-membered ring intermediate

Bond	Length (Å)	Angle	Value (°)
C1-O2	1.229	02-C1-C3	127.55
C1-C3	1.521	C1-C3-N6	103.40
C3-N6	1.464	C3-N6-C8	106.60
N6-C8	1.465	N6-C8-N11	102.49
C8-N11	1.445	C8-N11-C1	112.96
C1-N11	1.368	C8-N11-C12	123.45
N11-C12	1.443	02-C1-C3-N6	165.18
C3-H4	1.089	C3-N6-C8-N11	-28.92
N6-H7	1.013	C12-N11-C1-02	3.18
C8-H10	1.094	H7-N6-C3-H4	-91.65
C12-H13	1.087	H13-C12-N11-C1	-6.18

The first six vertical ionization energies (VIEs) obtained by applying Koopmans' theorem to the molecular orbital energies obtained at the MP2/6-31G** level are reported in Table 5.31.

Table 5.31- Vertical ionization energies obtained by Koopmans' theorem applied to the molecular orbitals obtained at the MP2/6-31G level for the five membered ring intermediate obtained from dimethylazidoacetamide pyrolysis**

Ionization	KT calculated VIE (eV)	0.92* KT calculated VIE (eV)
$(27\ a')^{-1} \rightarrow {}^2A$	10.02	9.22
$(26\ a')^{-1} \rightarrow {}^2A$	10.80	9.93
$(25\ a')^{-1} \rightarrow {}^2A$	11.23	10.33
$(24\ a')^{-1} \rightarrow {}^2A$	13.97	12.85
$(23\ a')^{-1} \rightarrow {}^2A$	14.58	13.42
$(22\ a')^{-1} \rightarrow {}^2A$	15.05	13.84

Harmonic vibrational frequencies have been calculated, and it should be noted that only a partial allowance for electron correlation was included in the calculations. The most significant bands are reported in Table 5.32, along with some of the normal vibrational modes with which they are associated; the full calculated infrared spectrum is reported (with Gaussian shaped bands) in Figure 5.44.

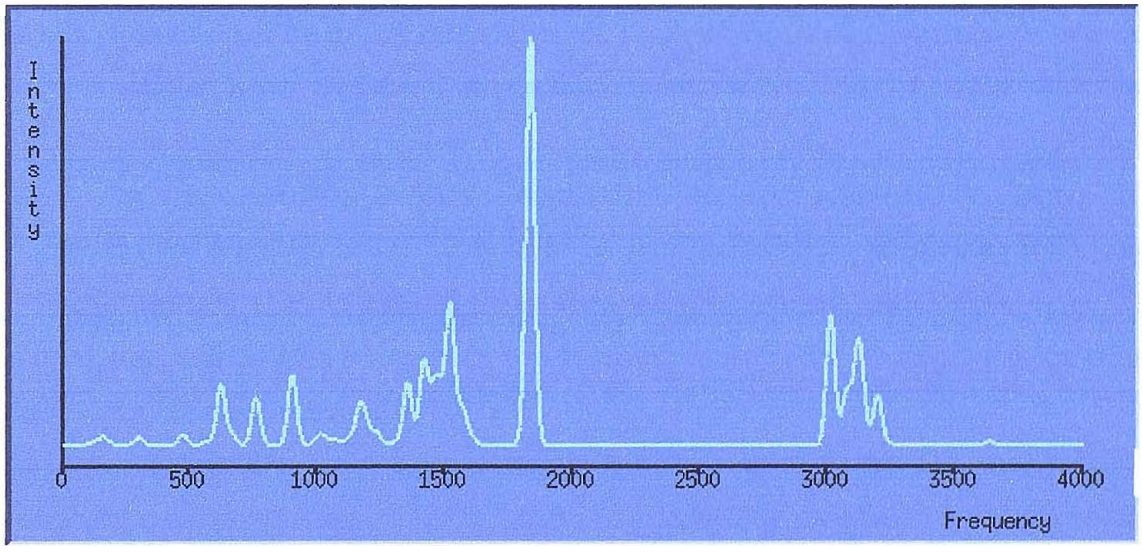

Figure 5.44- Calculated IR spectrum of the five-membered ring at the MP2/6-31G level**

Table 5.32- Calculated IR bands of the five-membered ring obtainable from the thermal decomposition of dimethylazidooacetamide at the MP2/6-31G level**

Frequency (cm^{-1})	Intensity (km/mol)	Frequency (cm^{-1})	Intensity (km/mol)	Frequency (cm^{-1})	Intensity (km/mol)	Normal mode
623.5	50.44	1231.1	6.80	1576.5	21.06	C-H_3 symm. scissoring
760.8	39.23	1235.9	4.40	1612.0	4.41	CH_2 scissoring
903.4	58.36	1301.1	3.05	1834.1	336.34	C=O stretching
1005.6	6.16	1354.8	52.22	3014.3	107.18	C-H_2 symm. stretching
1028.9	5.49	1417.9	68.91	3076.3	43.67	C-H_2 symm. stretching
1067.9	4.93	1457.0	36.70	3115.0	47.55	C-H_3 symm. stretching
1122.6	4.71	1480.6	35.81	3133.1	53.08	C-H_2 asymm. stretching
1161.9	20.89	1520.5	113.18	3196.2	27.23	C-H_3 asymm. stretching
1178.9	16.11	1549.6	8.48	3200.8	14.48	C-H_2 asym. stretching
1194.4	9.76	1557.5	7.67	3636.6	3.13	N-H stretching

Interpretation of the *ab initio* calculations on possible reaction intermediates

In the IR matrix isolation experiments, the sequence of spectra recorded at increasing temperatures shows the increase in intensity of some bands (while those of dimethylazidoacetamide decrease) not associated with HCN or DMF, then their decay at higher temperatures. This indicates an intermediate is formed and then decomposed.

By analogy with azidoacetamide, an imino intermediate has been proposed, originating from the nitrogen release from the azide and a 1,2-H shift: *ab initio* calculations on dimethyliminoacetamide have been performed and VIEs, vibrational frequencies and vibrational intensities computed.

As mentioned, the prediction for the imine of two PE bands in the 11.1-11.6 eV region can explain the thermal persistency of a band centred at 11.4 eV.

A comparison of the calculated IR spectra of dimethyliminoacetamide for the different conformers and the experimental spectrum (between 2000 and 400 cm^{-1}) derived by removal of all bands not showing the thermal behaviour of an intermediate is shown in Figure 5.40. Three minimum energy structures have been located in the calculations, and their relative energies are quite similar: the most stable

structure has been calculated to be structure *trans-trans*, with structures *cis-cis* and *cis-trans* lying at energies 1.4 and 2.8 kcal/mol higher respectively. Strangely, the *cis-trans* structure is the most stable for the azide and the least stable for the imine.

The presence of two methyl groups attached to the amidic nitrogen atom makes both the experimental and calculated vibrational spectra richer in bands than the ones of azidoacetamide: the assignment of bands is therefore more complex. The matrix isolation IR experiments seem to suggest that structures *cis-cis* and *trans-trans* contribute most to the experimental IR spectrum: the latter displays a better agreement in the intensity distribution. As an example, the calculated frequencies of the two strong bands observed at around 1370 and 1220 cm^{-1} are 1440 and 1264 cm^{-1} for the *trans-trans* conformer and 1478 and 1267 cm^{-1} for the *cis-cis* conformer, with the intensity ratio better described by the *trans-trans* conformer spectrum (see Figure 5.40).

Dimethyliminoacetamide and dimethyl-N-iminoacetamide have, according to calculations, almost the same energy: dimethyl-N-iminoacetamide lies about 1.85 kcal/mol below the most stable dimethyliminoacetamide conformer.

The cyclic intermediate is calculated to be much lower in energy (by about 10.34 kcal/mol).

The three lowest VIEs of dimethyliminoacetamide, dimethyl-N-iminoacetamide and the cyclic imine structure differ by a mean of 0.2-0.3 eV, with a maximum difference of around 0.4 eV for the first VIE: even if these differences are higher than those observed between iminoacetamide and N-iminoacetamide (where the variations within each band vertical ionization energy were of the order of 0.1 eV), it is not possible to discern which compound is contributing to the observed intermediate PE bands, especially the band at 11.36 eV. Moreover, the values are very similar to those of dimethylazidoacetamide and DMF. From PES it is therefore impossible to distinguish if the imines are both present as reaction intermediates, or which one is the predominant species.

Concerning the calculated IR spectra, they show the most important differences in the 1000-1500 cm^{-1} region: the spectrum of *trans-trans* dimethyliminoacetamide is the one that best reproduces the experiment, therefore justifying the assumption that *trans-trans* dimethyliminoacetamide is the dominant species produced. Despite its predicted higher stability, the cyclic imine is the one whose IR spectrum does not fit the experimental results, because of the lack of more than one strong band in the 1000-1500 cm^{-1} region. It is possible to conclude that the cyclization mechanism is not active in the thermal decomposition of dimethylazidoacetamide, or is active to a very minor extent.

It could be, however, that a contribution of more than one isomer of dimethyliminoacetamide or dimethyl-N-iminoacetamide could produce an IR spectrum in good agreement with the experimental

one. It is difficult to distinguish the additional contribution which will completely fit the experimental results, especially in the 1000-1500 cm^{-1} region: still, it is possible to state that the computed spectrum of dimethyl-N-iminoacetamide does not fit the experimental one to the same degree as the dimethyliminoacetamide conformers do.

Even if from both the total energies and the IR spectra, it is not possible to unambiguously distinguish if dimethyl-N-iminoacetamide is formed at all, it is nevertheless clear from the IR pattern that dimethyl-N-iminoacetamide should be present only as a minor decomposition route, the major route being the production of dimethyliminoacetamide especially in its *trans-trans* structure. A Type I mechanism is then the one playing a major role in the decomposition.

5.3.6 SUGGESTED MECHANISM OF GAS-PHASE DECOMPOSITION

The combination of the results from UV-PES and matrix isolation IR experiments on the pyrolysis of dimethylazidoacetamide show that

- When the thermal decomposition begins, N_2 is released as the first product
- A reaction intermediate is formed when the azide is not yet completely decomposed (around 160 °C) and before the appearance of other products: its IR spectrum matches the one calculated for dimethyliminoacetamide
- HCN, CO and $HCON(CH_3)_2$ (dimethylformamide) are formed at the same temperature as when iminoacetamide approximately reaches its maximum concentration (210 °C)
- $(CH_3)_2NH$ (dimethylamine) and HNCO are formed in lower concentration than HCN, CO and DMF when dimethyliminoacetamide is almost completely consumed (360 °C)

From this evidence, the first step of the decomposition follows the same behaviour of azidoacetamide, that is the formation of nitrogen and dimethyliminoacetamide.

From the experiments it was not possible to detect the formation of the nitrene diradical

$$^1N_3CH_2CON(CH_3)_2 \rightarrow {}^1N_2 + {}^1{:}NCH_2CON(CH_3)_2$$

as the consequence of the release of nitrogen. However, recent theoretical and experimental results [5, 6, 26] on methylazide and ethylazide decompositions seem to confirm the formation of the nitrene as a

preferred route as opposed to a concerted mechanism involving breaking of the N-N bond and a 1,2-H shift to produce directly dimethyliminoacetamide. *Ab initio* calculations performed in this work seem to confirm this hypothesis, as it was not possible to locate a transition state for the azide → imine concerted mechanism. The nitrenes were optimized as true minima only in the triplet spin state; in the singlet state they converged to imines, suggesting that the lifetime of this diradical in its singlet state is very short and isomerization takes place almost immediately after nitrogen has been released from the azide.

Ab initio calculations clearly indicate that also for dimethylazidoacetamide the unstable nitrene can undergo Type 1 and Type 2 isomerisation processes for its decomposition.

Type 1:

This is the 1,2-H shift mechanism in which the electron deficient nitrogen atom acquires a proton from the adjacent carbon atom and forms a double bond. In this case it would lead to the formation of dimethyliminoacetamide

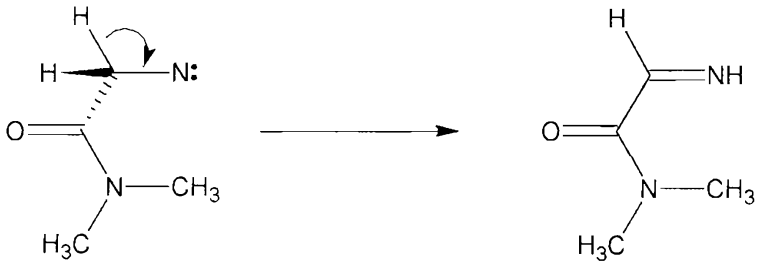

Type 2:

As an alternative to proton transfer, the nitrogen atom can compensate its electron deficiency by attacking a remote site of the molecule, forming a new bond as a type of nucleophilic substitution. In this case, the site is the carbonyl carbon atom, following the scheme

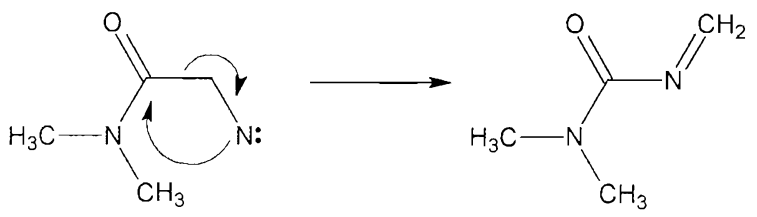

In partial contrast with azidoacetamide, *ab initio* calculations show that in the decomposition of the nitrene produced from dimethylazidoacetamide, Type 1 is the preferred mechanism when all the nitrene geometrical parameters- left as they were in the azide but with a very long value for the N-N bond which is going to be broken- are allowed to fully optimise: the process leads to the formation of dimethyliminoacetamide rather than of dimethyl-N-iminoacetamide.

This result confirms the IR evidence: the experimental spectrum shows that dimethyliminoacetamide is the main contributor to the bands of the reaction intermediate. Dimethyl-N-iminoacetamide should be formed only as a minor product.

The main decomposition products, HCN, CO, DMF, $(CH_3)_2NH$ are formed from the decomposition of dimethyliminoacetamide (or of dimethyl-N-iminoacetamide).

The most prominent products are HCN and DMF: this behaviour is in contrast with what was observed for iminoacetamide, where HCN was a secondary product and formamide could not be observed at all. In that case, isocyanic acid and methylimine were the predominant species, while in the dimethylazidoacetamide decomposition isocyanic acid is only a very minor product, methylimine is not observed, and no methylated equivalent of these two compounds could be observed.

HCN and dimethylformamide are formed from dimethyliminoacetamide by breaking the carbon-carbon bond adjacent to the HN=CH- group and prompting a hydrogen shift between the two carbon atoms

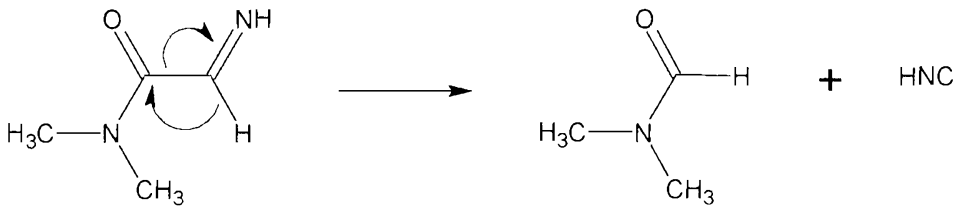

Following the indications obtained from iminoacetamide, a mechanism involving the initial production of HNC (and therefore a 1,2-hydrogen shift) is more favoured over a mechanism producing HCN accompanied by a 1,3-hydrogen shift. Unfortunately, the bigger size of the dimethyliminoacetamide molecule with respect to iminoacetamide has prevented a successful determination of the transition states involved in the decomposition pathway. It was therefore assumed that the results obtained from iminoacetamide- like the preference of HNC formation as the exit molecule rather than HCN- have a parallel equivalent in dimethyliminoacetamide.

For this, dimethyl-N-iminoacetamide is a poorer precursor for the DMF + HCN route, because it is not possible to produce HNC by a single proton transfer from the terminal carbon atom, but instead a different mechanism producing HCN is required

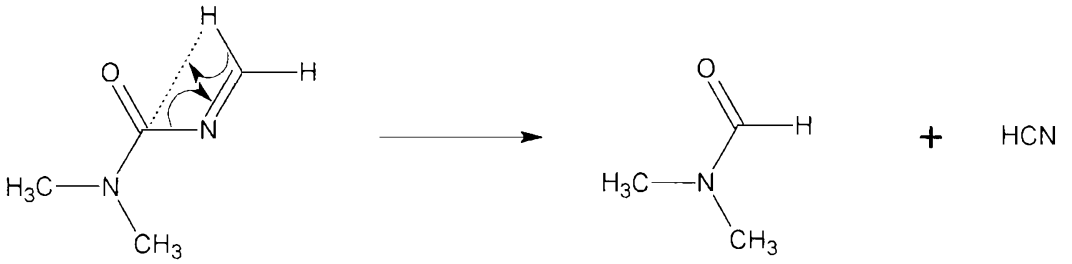

Given the fact that no CH_3NCO, $CH_3N{=}CH_2$ or $CH_3CH{=}NH$ have been observed, no alternative decomposition channel is open. This is in contrast to azidoacetamide, where the main channel was the one leading to the formation of isocyanic acid and methylimine. It is probable that the migration of a methyl group from the amidic nitrogen is much less feasible than the hydrogen migration involved in the formation of HNCO and CH_2NH from azidoacetamide. The difficulty of obtaining satisfactory information on the transition states involved in the decomposition from *ab initio* investigations prevents a quantitative explanation of this marked difference in the major pyrolysis channel between the two different azides.

The other main decomposition product, carbon monoxide, is formed along with DMF and HCN, at lower temperatures than was the case in azidoacetamide. Two mechanisms can be invoked to explain its presence.

It is possible that DMF partially decomposes to CO and $(CH_3)_2NH$ even at relatively low temperatures, when it is produced as a thermal decomposition product, presumably with internal energy, which can be better dissipated if the molecule breaks up. This reflects the assumption that was made in the previous chapter on formamide being completely decomposed to HNCO and H_2, if formed with high internal energy. The reason why dimethylformamide decomposes to CO and $(CH_3)_2NH$ while formamide decomposes to HNCO and H_2 (and not to CO and NH_3) can be traced to the difficulty of breaking the carbon-nitrogen bonds in the amidic part of the molecule: this follows the fact that dimethyliminoacetamide also decomposes with retention of the $(CH_3)_2N$- part.

The second route leading to production of carbon monoxide (and dimethylamine) can be due to a concerted breaking of the C-C and C-N bonds adjacent to the carbonyl group and a proton transfer to the amidic nitrogen either from the iminic nitrogen or from the iminic carbon atom.

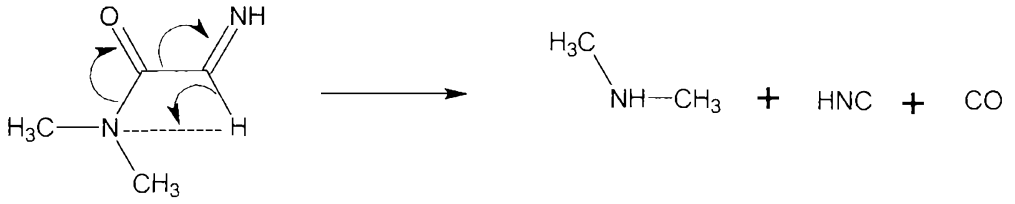

This is an exact parallel of the concerted route producing NH_3 and CO from iminoacetamide From the *ab initio* results on that system, the transfer from the carbon atom is supposed to be favoured, due to the formation of HNC instead of HCN as one of the leaving groups. For this reason, dimethyliminoacetamide should also be a better precursor than dimethyl-N-iminoacetamide for the mechanism leading to CO and $(CH_3)_2NH$.

The fact that in PES dimethylamine is not observed and that in IR it is observed only at higher temperatures than carbon monoxide, can be explained by the big difference in cross section between the two molecules for the two spectroscopic techniques. As the route to CO and $(CH_3)_2NH$ is a minor one, the combination of low concentration and low cross section explains the weakness of the bands associated with $(CH_3)_2NH$ (moreover, in PES its first band would be overlapping with the first band of DMF, due to the similarity of their HOMO energies).

The overall decomposition path can therefore be represented schematically as shown in Figure 5.45.

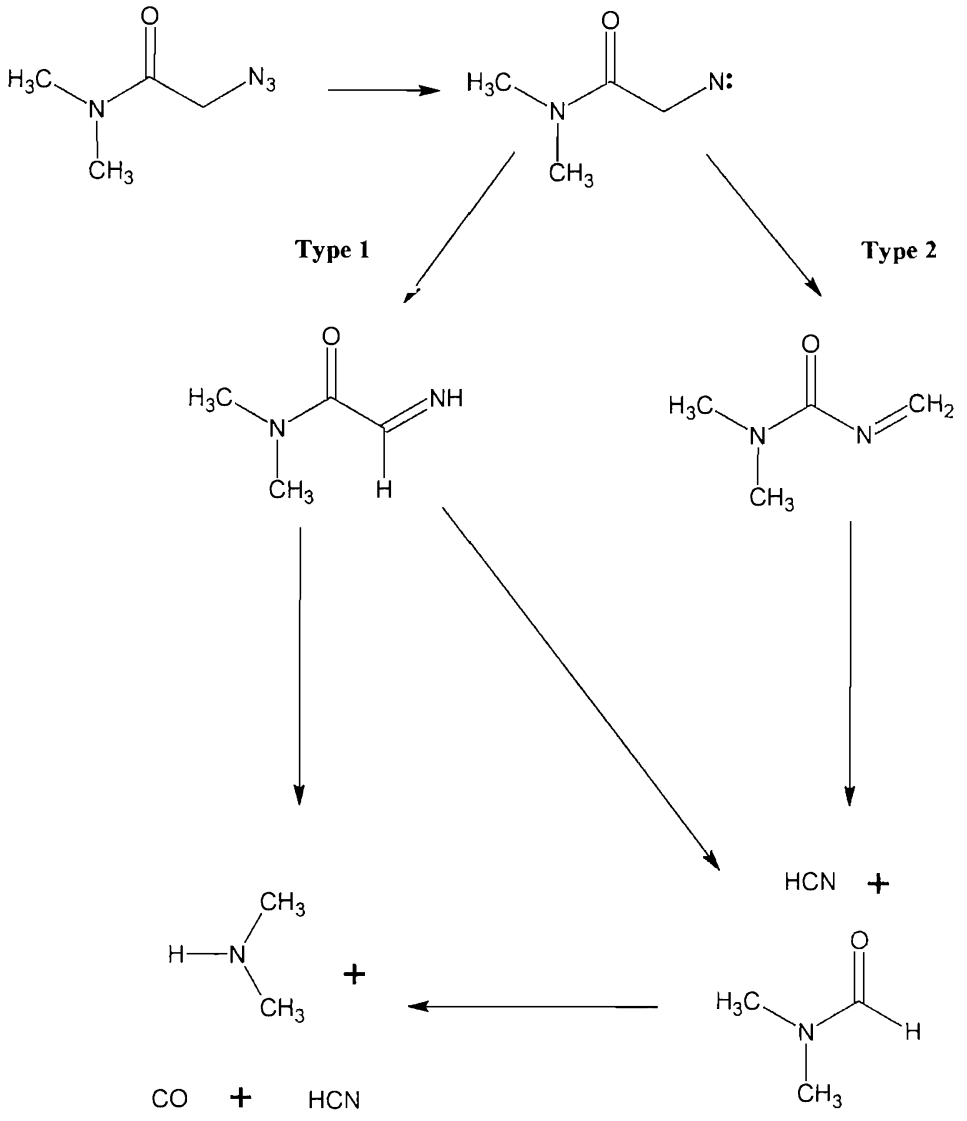

Figure 5.45- Schematic representation of the proposed thermal decomposition pattern of dimethylazidoacetamide

The calculated total energy level diagram at 0 K is reported in Figure 5.46. All the calculations were performed at the MP2/6-31G** level. To show the contribution of entropy to the decomposition path, a diagram of the relative free energies at 298 K for all products is reported in Figure 5.47 in which only the most stable conformer of dimethylazidoacetamide and dimethyliminoacetamide are shown. The calculated relative energies and free energies of all the reactants and products are listed in Table 5.33.

Table 5.33- ΔE^0 and ΔG^{298} values calculated at the MP2/6-31G level for possible intermediates and products of the thermal decomposition of the dimethylazidoacetamide system: the azide is chosen as the reference zero energy**

Compound	Relative energy at 0 K (kcal/mol)	Relative free energy at 298 K (kcal/mol)
Dimethylazidoacetamide	0	0
Dimethyliminoacetamide	-47.78	-60.70
Dimethyl-N-iminoacetamide	-49.63	-63.27
$CH_3CH{=}NH + CH_3NCO$	-40.25	-68.18
$CH_2{=}NCH_3 + CH_3NCO$		
DMF + HCN	-42.93	-68.07
$(CH_3)_2NH + CO + HCN$	-24.80	-62.61

When ΔG^{298} is considered, the main effect in comparison to ΔE^0 is the lowering of the energies of the products in comparison to the intermediate imines, and their narrower difference in energy. The much lower amount of dimethyl amine produced in comparison to the amount of DMF produced is clearly justified from their energy difference. Nevertheless, just from the relative energy values, it is not possible to explain the absence of CH_3CHNH and CH_3NCO as decomposition products. A possible solution could have been the *ab initio* investigation of the transition states leading to the different sets of products, as this provided an explanation of the absence of formamide from the azidoacetamide pyrolysis, but this was not possible to achieve, probably because of the size of the azide molecule.

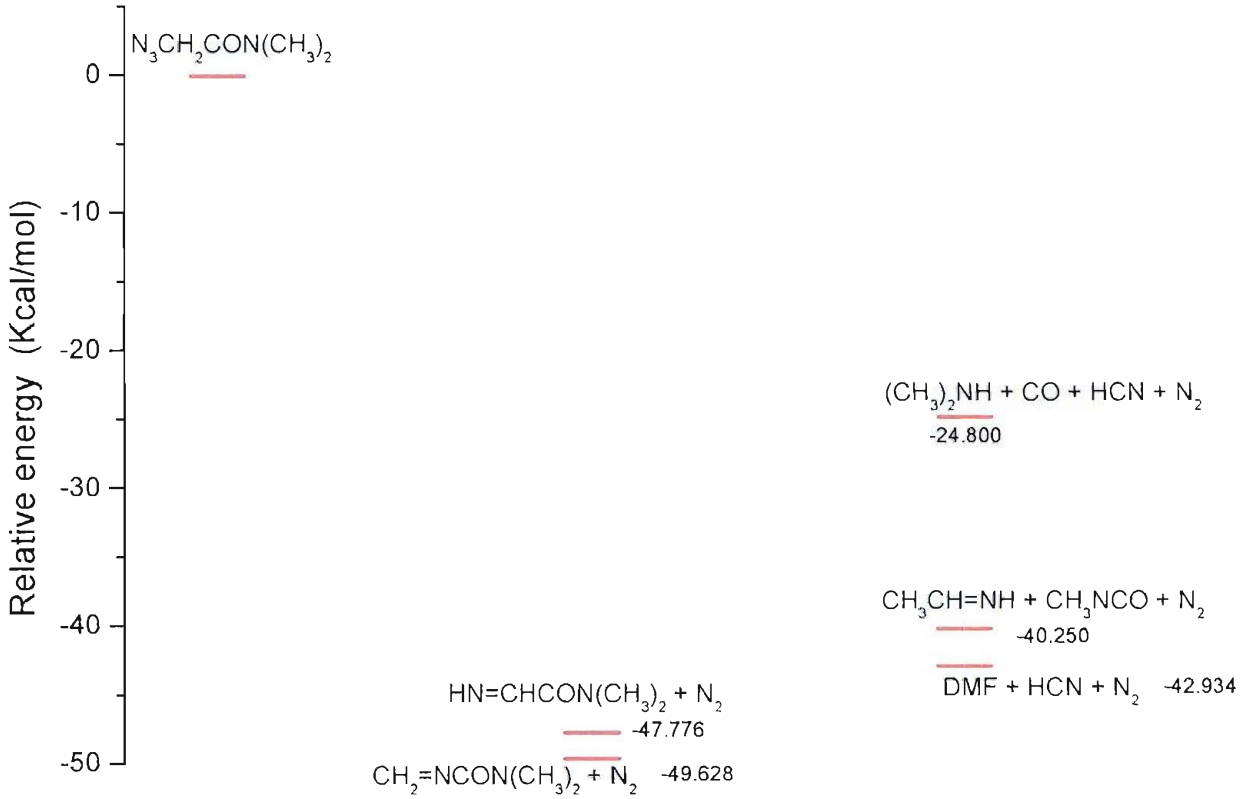

Figure 5.46- Diagram of the relative energies of the species involved in the dimethylazidoacetamide thermal decomposition calculated at the MP2-6/31G level. Thermal and zero point contributions are not included.**

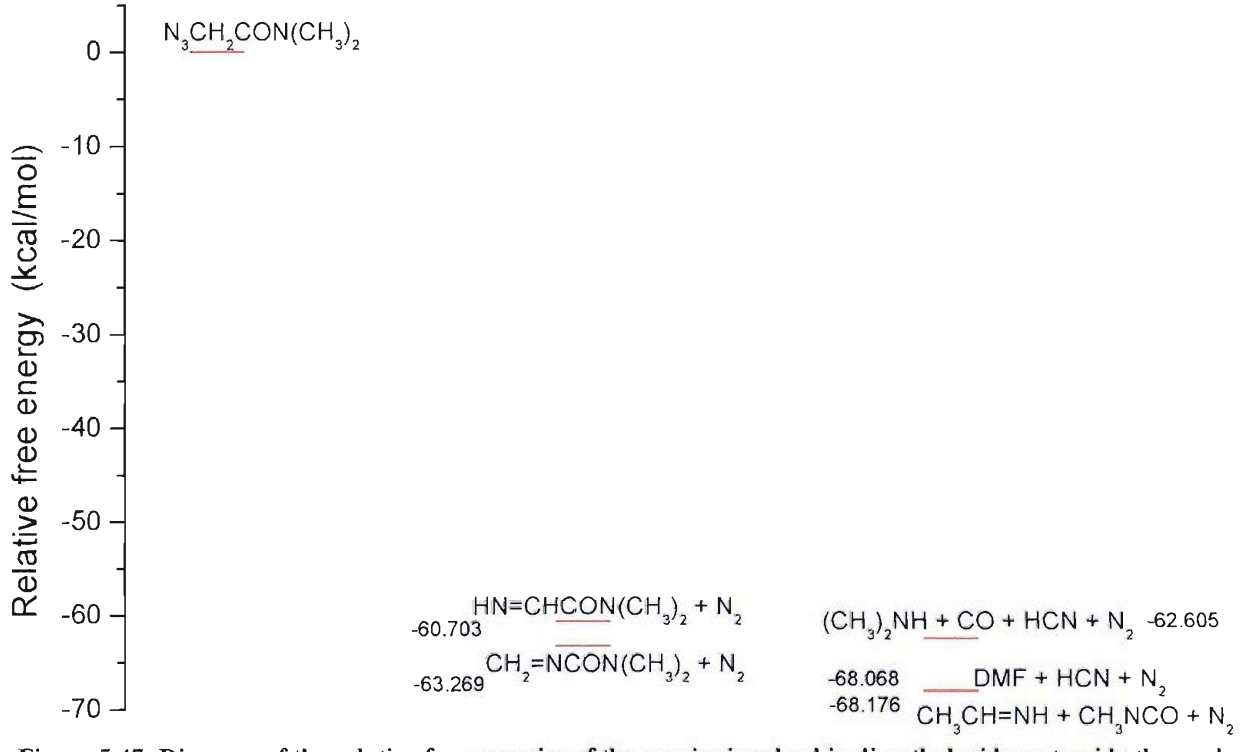

Figure 5.47- Diagram of the relative free energies of the species involved in dimethylazidoacetamide thermal decomposition calculated at the MP2-6/31G level. Thermal and zero point contributions are included.**

5.4 ETHYL AZIDOFORMATE

5.4.1 EXPERIMENTAL SECTION

Photoelectron spectroscopy

Ethyl-azidoformate ($N_3COOCH_2CH_3$) is a liquid that at room temperature has sufficient vapour pressure to produce spectra of acceptable signal-to-noise ratio by simply evacuating a flask holding the sample connected to the inlet tube of the spectrometer via a needle valve

For the pyrolysis study, a resistive heating system was found sufficient to reach temperatures at which total decomposition of the azide is achieved.

The 20-cm mean hemisphere radius photoelectron spectrometer of the Lisbon PE group was used for this set of experiments: a description and a schematic diagram of this PE spectrometer has been given in Section 2.1.

The procedure for the acquisition and calibration of the photoelectron spectra followed the same pattern as described in Chapter 2. Calibration of spectra obtained on pyrolysis of the azide was normally achieved using the bands associated with the first vertical ionization energies (VIEs) of N_2 (15.58 eV, [8]), H_2O (12.62 eV, [8]), CO_2 (13.78 eV, [8]), or of residual CH_2Cl_2 (12.21 eV, [18]), which is the solvent used for the preparation of the azide in the samples.

Matrix isolation IR spectroscopy

The apparatus and the procedure for the acquisition of infrared spectra in nitrogen matrices have been described in Chapter 2. Deposition times were in the order of 30 to 60 minutes, and the matrix dilution ratios were estimated to be above 1000:1.

Spectra of 2-oxazolidone have also been acquired in a nitrogen matrix, to provide evidence for its possible presence and thermal behaviour as a possible pyrolysis product, and to support the hypotheses made on the azide decomposition pathways.

5.4.2 SAMPLE PREPARATION AND CHARACTERIZATION

PREPARATION

Ethyl chloroformate was added slowly to a solution of sodium azide (3 equiv) in distilled water. The mixture was stirred for 24 hours in an oil bath at 50°C. After cooling, the product was extracted with dichloromethane, dried over anhydrous sodium sulphate and the organic phase concentrated in a rotary evaporator. The azidoformate was purified by distillation in a Kugelrohr at reduced pressure (10 mbar; b.p. 20 °C).

CHARACTERIZATION

Ethyl azidoformate ($N_3COOCH_2CH_3$) is a colourless liquid at room temperature. It was characterized in the vapour phase by UV-photoelectron spectroscopy and electron impact mass spectrometry, and by ^1H- and ^{13}C-NMR in solution in deuterated chloroform. Infrared spectroscopy characterization was conducted on the pure liquid between KBr plates.

According to spectroscopic results, the ethyl-azidoformate used in this work was pure, apart from some samples in which a non negligible amount of solvent (dichloromethane) was present: in this case, as the two liquids had very different boiling points, it was necessary to leave the sample connected to the low pressure inlet of the ionization chamber of the spectrometer (roughly 10^{-5} mbar), so that the residual solvent was eliminated by pumping it off.

Mass spectrometry: the 70 eV electron impact mass spectrum is reported in Figure 5.48. It displays a parent peak at 114 amu- corresponding to the de-protonated molecule- and the most intense peak (base peak) at 29 amu (corresponding to N_2H^+ and $CH_2CH_3^+$). Strong peaks were also present at 70 amu (corresponding to N_3CO^+, 34.50%), 27 amu (corresponding to CH_3C^+, 17.46%), 43 amu (corresponding to N_3H^+, 6.77%), 73 amu (corresponding to $CH_3CH_2OCO^+$, 5.30%), 42 amu (corresponding to N_3^+ and NCO^+, 5.11%) and 100 amu (corresponding to $N_3COOCH_2^+$, 3.45%).

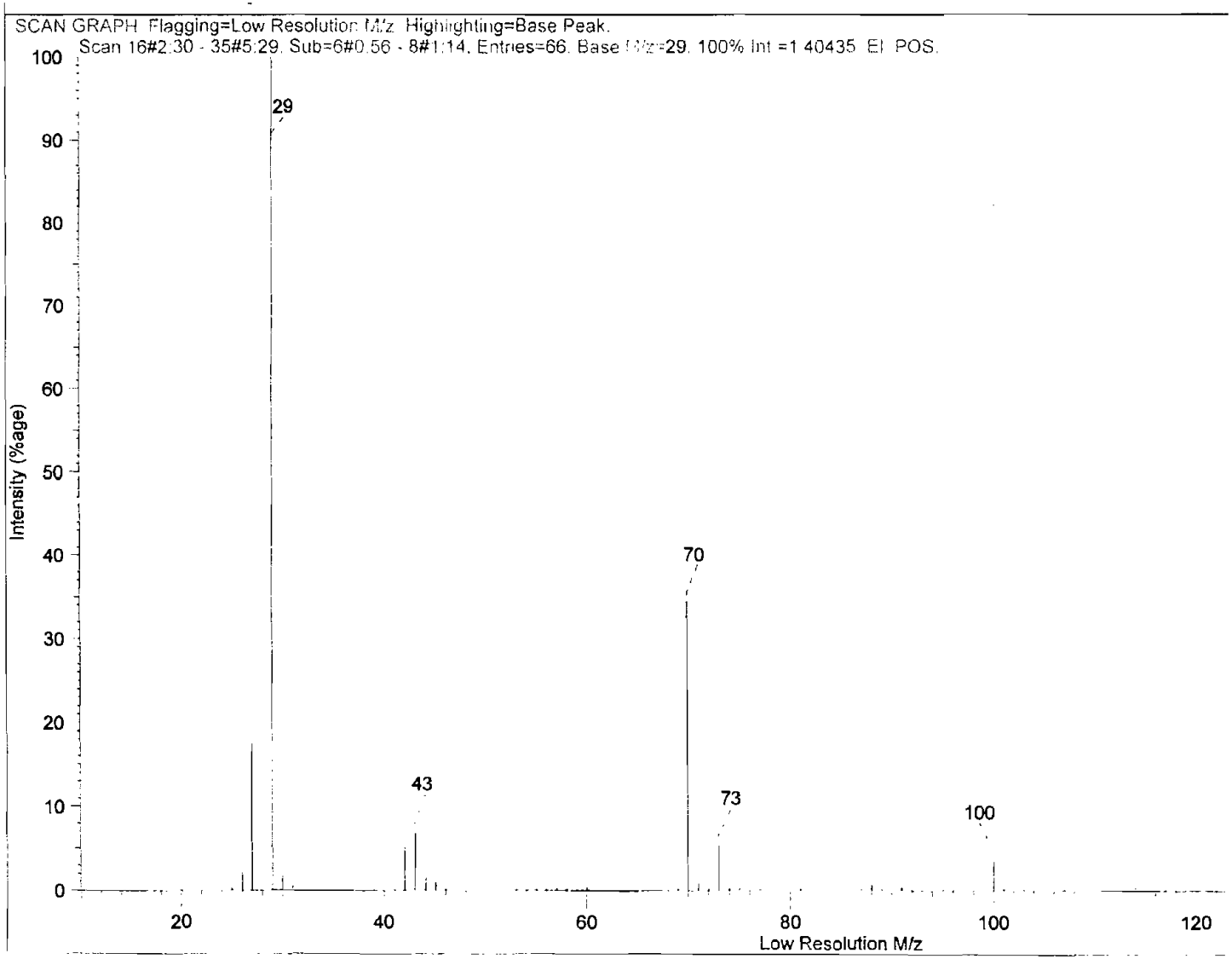

Figure 5.48- The 70 eV electron impact mass spectrum of ethyl-azidoformate

^{1}H- and ^{13}C-NMR spectroscopy: in the ^{1}H-NMR spectrum, recorded in $CDCl_3$ solution and presented in Figure 5.49, a triplet peak centred at 1.32 ppm relative to TMS corresponds to the methyl group, while the quartet centred at 4.27 ppm is associated to the methylene group. Their relative intensity ratio is very close to the expected value of 1.5.

In the ^{13}C-NMR spectrum, run in $CDCl_3$ solution, three peaks were observed: a peak at 13.9 ppm with respect to TMS is due to the methyl carbon atom, a peak at 64.6 ppm is associated with the methylene carbon, while the last one at 157.3 ppm is assignable to the carbonyl carbon atom.

Infrared spectroscopy: as can be seen from Figure 5.50a, the IR spectrum of the pure compound recorded between KBr plates showed peaks at 2986 cm^{-1}, assigned to C-H stretching absorptions, and strong bands at 1724 cm^{-1} (C=O stretching), 1220 cm^{-1} (N-N-C-O stretching), 1021 cm^{-1} and 751 cm^{-1}. A double band with maxima at 2179 and 2132 cm^{-1} is assigned to N_3 stretching vibrations.

The infrared spectrum of the compound in the liquid phase shows remarkable differences with the spectrum recorded in a N_2 matrix (reported in Figure 5.50b): apart from the higher frequencies of the C-H stretching- which is expected because of the elimination of any intermolecular hydrogen bonding in the matrix- the intensity pattern appears affected in the sense that in the matrix the bands associated with the azide group and carbonyl stretching modes (respectively at around 2130 cm^{-1} and around 1720 cm^{-1}) are much more intense with respect to the band at 1220 cm^{-1} than in the matrix. No clear explanation has been found for this discrepancy. A further analysis of the matrix IR spectrum will be found in the next section, when a comparison with the results of the *ab initio* calculations will be made.

Photoelectron spectroscopy: the bands in the ethyl-azidoformate HeI-photoelectron spectrum (reported in Figure 5.51) were calibrated by averaging the vertical ionization energies of the bands calibrated from seven different spectra. The results are shown in Table 5.34 (see Figure 5.51 for the numbering of the bands in the spectrum).

Table 5.34- Calibrated vertical ionization energies of ethyl azidoformate- see Figure 5.51 for band numbering

Band	A	B	C	D	E	F	G	H
VIE (eV) ± 0.02 eV	10.72	11.36	12.98	13.50	14.68	15.64	16.32	17.47

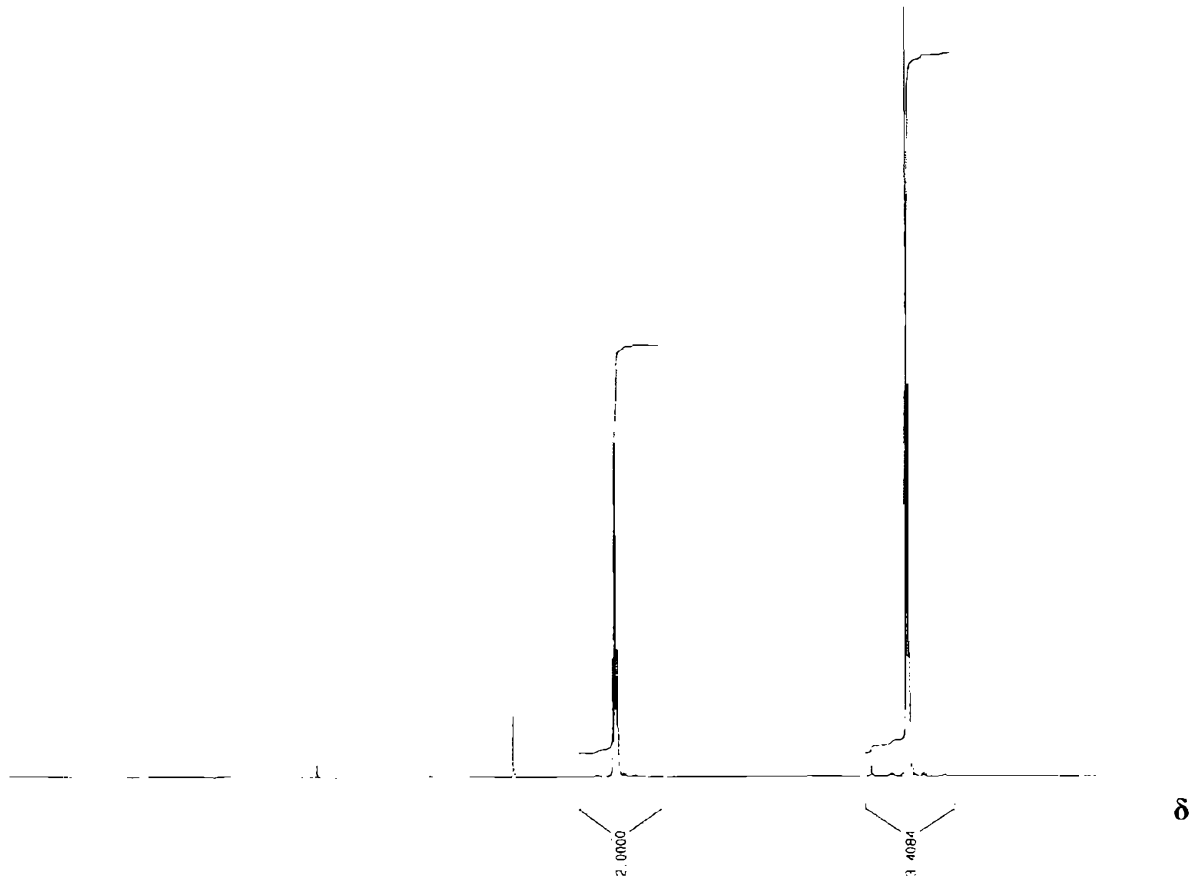

Figure 5.49- The ^{1}H-NMR spectrum of ethyl-azidoformate in $CDCl_3$ solution

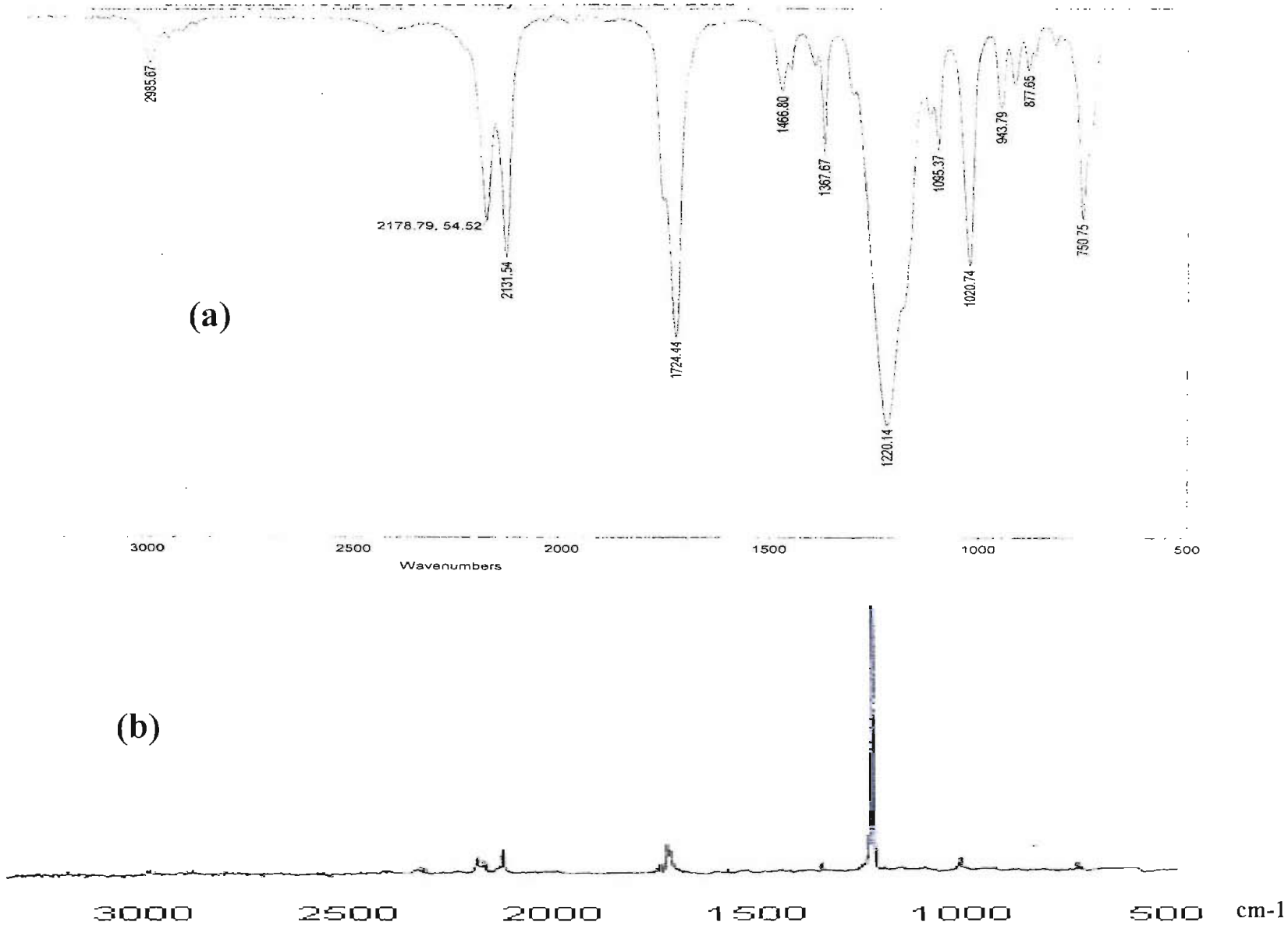

Figure 5.50- The infrared spectrum of ethyl-azidoformate recorded (a) in liquid phase between KBr plates, (b) in a nitrogen matrix

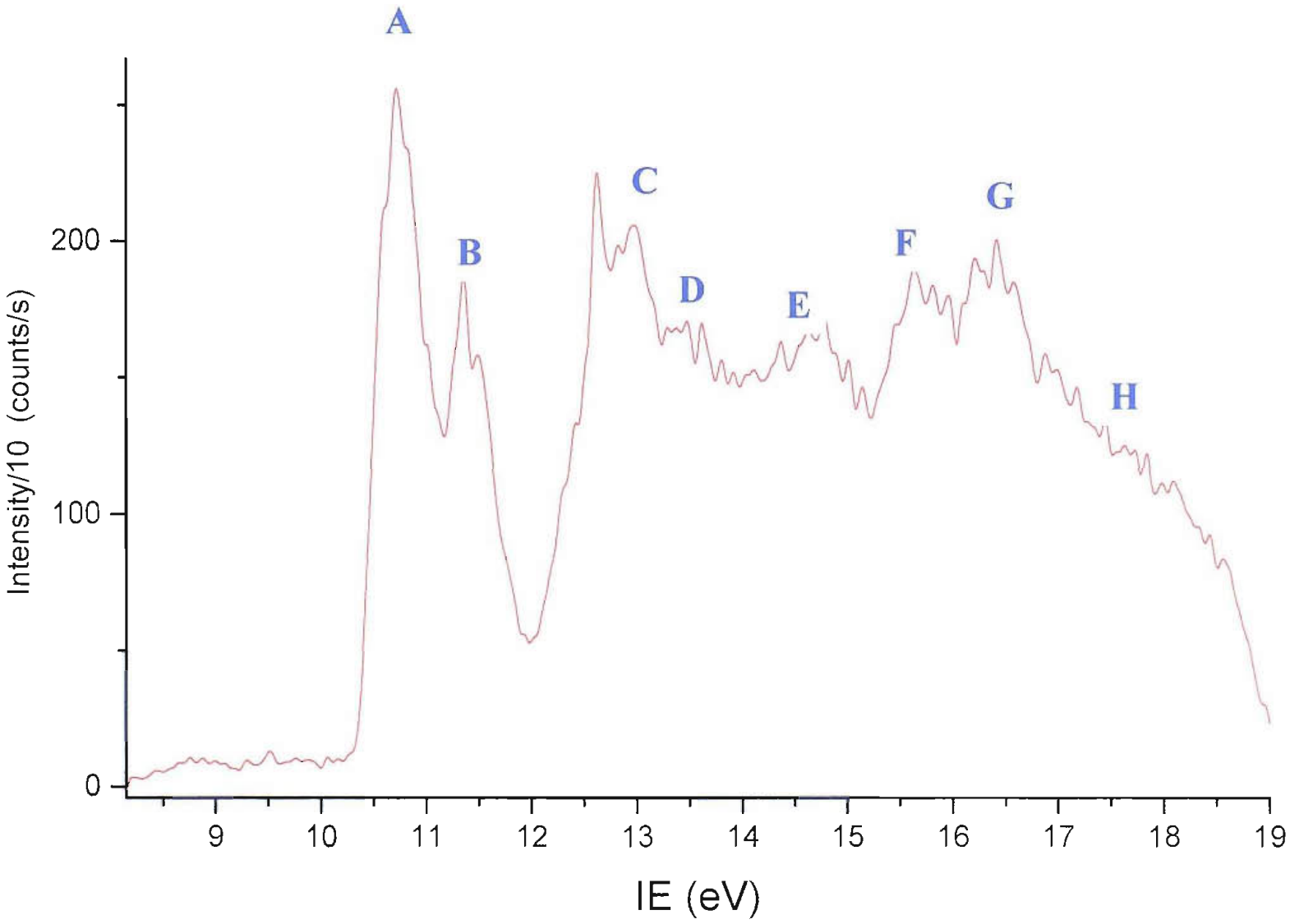

Figure 5.51- HeI-PE spectrum of ethyl-azidoformate recorded at room temperature

5.4.3 RESULTS OF MOLECULAR ORBITAL CALCULATIONS

Ab initio calculations have been performed at the MP2/6-31G** level to help the interpretation of photoelectron and infrared spectra, and to establish geometrical, electronic and vibrational characteristics of ethyl-azidoformate.

Seven minimum energy conformers have been found for $N_3COOCH_2CH_3$ in its closed-shell singlet state, depending on the different relative positions of the carbonyl, methyl, methylene and azide groups. The conformers have been named with a double *cis trans* nomenclature, and a subsequent number. The alphabetical part refers for the first label to the relative position of the azide chain with respect to the carbonyl group, and for the second label to the relative orientation of the carbonyl and the methylene groups. The number added to the name is to distinguish the different orientations of the methyl group with respect to the orientation of the oxygen atom (label 1 means that the methyl group is pointing in the same direction as the carbonyl, label 2 means that it points in the opposite direction). So, for example, structure *cis-trans2* refers to a structure in which the N_3 chain is *cis* with respect to the C–O group, the C=O group is in a *trans* position with respect to the CH_2 group and the terminal CH_3 group points in the same direction as the oxygen atom. A representation of all the geometries with the visualization of the nomenclature can be seen in Figure 5.52.

The five most stable structures lie within 4.25 kcal/mol in energy, while the two structures *trans-trans* lie 12.37 and 12.76 kcal/mol higher in energy with the respect to the most stable one (*cis-cis1*, see Table 5.35). Table 5.36 reports the most important geometrical parameters calculated for the most stable conformer (structure *cis-cis1*, which is reported in detail in Figure 5.53 along with the labelling of the atoms). Table 5.37 reports the first seven VIEs for this most stable conformer, calculated with Koopmans' theorem, and the first three VIEs calculated with ΔSCF method by calculating the energy of the cation and neutral using the neutral molecule geometry, and compares them with the experimental VIEs. The agreement with the experimental VIEs is good, especially if the values obtained from Koopmans' theorem are scaled by a 0.92 factor [27, 28]. Because of the small differences in energy between the conformers *cis-cis*, *trans-cis*, and *cis-trans*, it is possible that these three structures all contribute to the experimental gas phase spectrum. Vertical ionization energies have been computed for these structures using Koopmans' theorem and they were found to be very similar. The ΔSCF values are not particularly reliable, because the states obtained by ionization from the HOMOs were, apart from the third one, highly contaminated by higher multiplicity states.

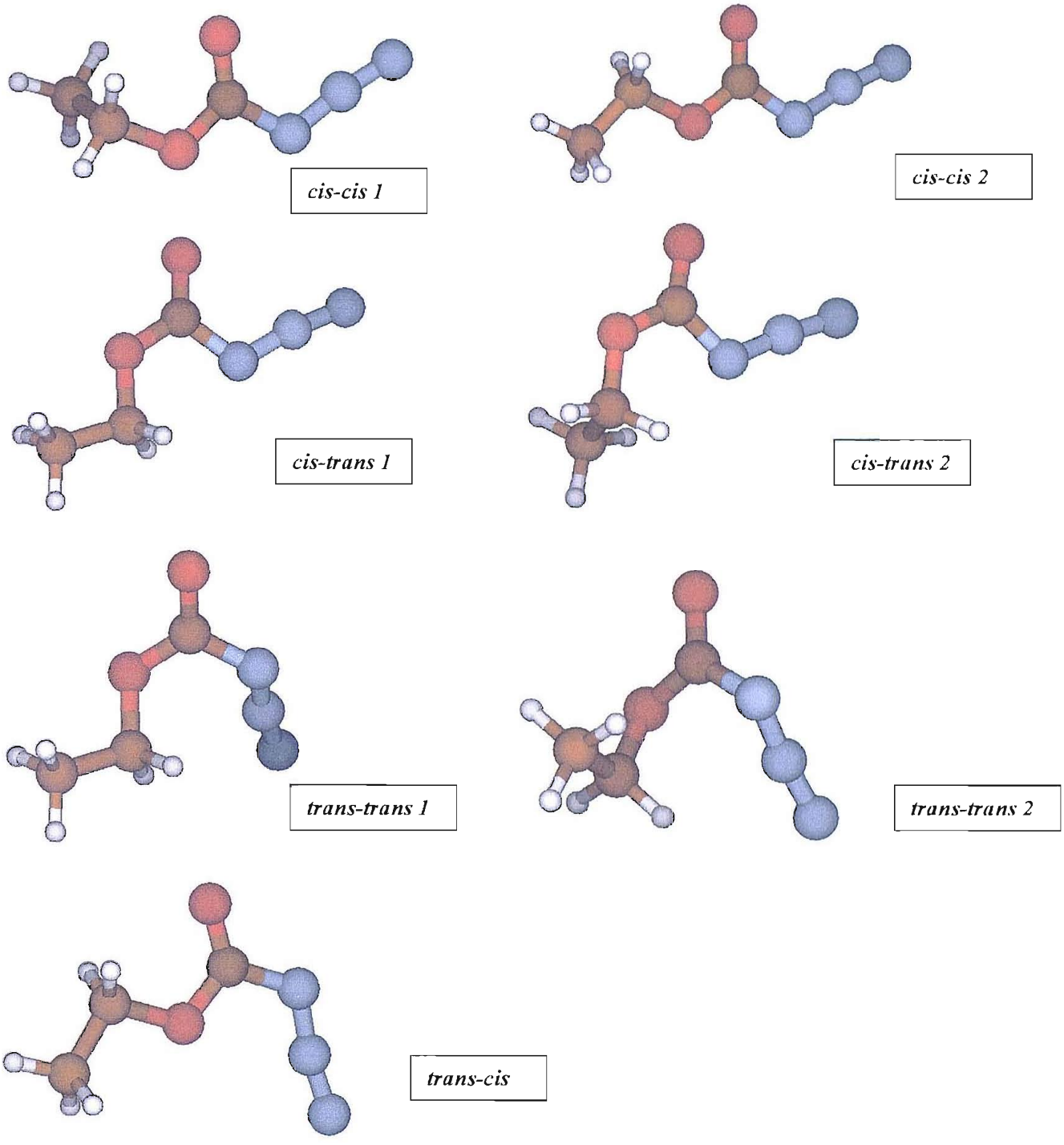

Figure 5.52- The seven conformers of ethyl-azidoformate obtained from *ab initio* calculations at the MP2/6-31G level. The labelling used reflects the relative position of the methyl group to the carbonyl group, of the methylene group to the carbonyl group and of the carbonyl group to the azide chain: for example, in structure *cis-trans2* the N_3 chain is *cis* with respect to the C=O group, the C=O group is in a *trans* position with respect to the CH_2 group and the terminal CH_3 group points in the same direction as the oxygen atom**

Table 5.35- Total and relative energies of the seven conformers of ethyl-azidoformate at the MP2/6-31G level**

Structure	Total energy (hartrees)	Relative energy (kcal/mol)	Point group
Cis-cis1	-430.7842669	0	C_1
Cis-cis2	-430.7839814	0.179	C_s
Cis-trans1	-430.777496	4.249	C_s
Cis-trans2	-430.7775001	4.246	C_1
Trans-cis	-430.7820778	1.374	C_1
Trans-trans1	-430.7645604	12.366	C_1
Trans-trans2	-430.7639391	12.756	C_s

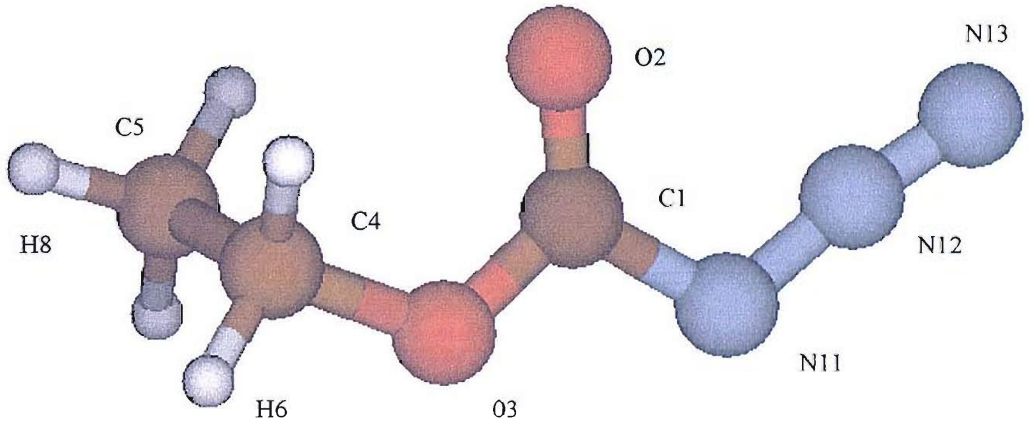

Figure 5.53- Structure *cis-cis1* of ethyl-azidoformate optimized at the MP2/6-31G level**

Table 5.36- The most relevant geometrical parameters for the lowest energy structure of ethyl azidoformate (*cis-cis1*)

Bond	Length (Å)	Angle	Value (°)
N13-N12	1.159	N13-N12-N11	172.4
N12-N11	1.253	N12-N11-C1	113.06
N11-C1	1.421	N11-C1-O3	106.69
C1-O2	1.219	O1-C1-O3	127.21
C1-O3	1.34	C1-O3-C4	114.29
O3-C4	1.454	O3-C4-C5	110.85
C4-C5	1.513	N13-N12-N11-C1	179.77
C4-H6	1.087	N12-N11-C1-O3	-179.82
C5-H8	1.09	C1-O3-C4-C5	81.51

Table 5.37- Experimental and computed VIEs of *cis-cis1* ethyl azidoformate

Koopmans' theorem (KT) calculated VIE (eV)	KT calculated VIE · 0.92 (eV)	ΔSCF calculated VIE (eV)	S^2 for the ion	Experimental VIE (eV)	Band
11.40	10.49	12.09	1.022	10.72	A
12.33	11.34	12.66	1.018	11.36	B
12.81	11.79	11.70	0.790		C
13.77	12.67			12.98	D
14.30	13.15			13.50	E
14.75	13.57				F
15.06	13.86			14.68	G
16.03	14.75			15.64	H

Figure 5.54 shows the shape of the highest six occupied molecular orbitals calculated for the *cis-trans1* conformer of ethyl-azidoformate at the Hartree-Fock level. The description of the molecular orbitals has been obtained from a single point Hartree-Fock calculation assuming the geometries being those calculated at the MP2 level. The choice of showing the MOs of structure *cis-trans1* instead of the most stable one is due to the simplicity of representing a planar structure, and because structure *cis-trans1* is the one used as the azide starting point in the search of the transition states which form the nitrene. In every case, the MOs for the most stable structure, structure *cis-cis1*, are very similar.

Molecular orbital 30 (the HOMO) is a slightly delocalized orbital with a major p_π-antibonding contribution from the lone pairs on the first and third nitrogen atoms of the azide group, and from this latter atom and the carbonyl oxygen.

In contrast, MO 29 is a largely delocalized orbital; it has mainly p_π-bonding character between the first two nitrogen atoms of the azide chain (in this case the nodal plane is perpendicular to the molecular plane), σ-bonding character between the nitrogen of the chain and the adjacent carbon, between the carbonyl carbon and the ester oxygen, and between the methylene and methyl carbon. A p_π-antibonding character (still with the π plane perpendicular to the molecular one) is evidenced between the first and third nitrogen atom of the azide chain and along the carbonyl group.

MO 28 is a delocalized orbital with mostly p_π-antibonding character on the plane of the molecule all along the $-CH_2OC(=O)N-$ backbone; the only p_π-bonding contribution is found on the carbonyl group.

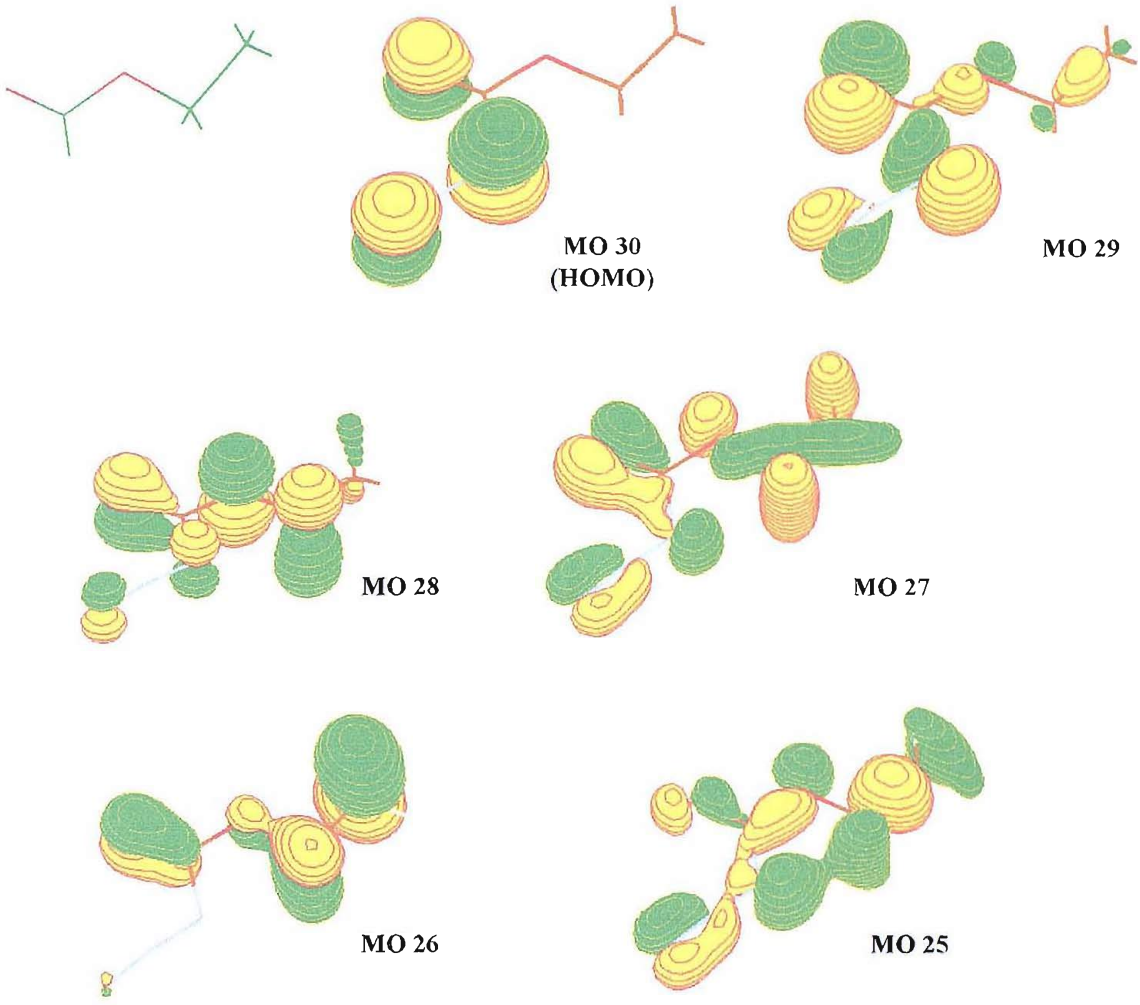

Figure 5.54- The six highest occupied molecular orbitals for structure *cis-cis* of azidoacetamide as obtained from calculations performed on the Gaussian98 program at the HF/6-31G level. The skeleton of the molecule is reported in the top left corner of the figure, to help the identification of the character of the orbitals**

MO 27 is mostly dominated by the p_π-bonding contribution between the terminal nitrogen atoms of the azide chain, the p_π-bonding character on the carbonyl group and the σ-bonding system stretching along the O-CH_2-CH_3 end of the molecule.

MO 26 is a lot more localized orbital with a mainly p_π-bonding character in the molecular plane between the carbonyl group and p_π-antibonding character between the methylene and methyl carbons. No contribution arises from the azide chain.

Harmonic vibrational frequencies have been calculated for all the conformers at the MP2/6-31G** level by means of second derivative calculations. Figure 5.55 displays the calculated IR spectra for each structure.

The spectra are similar for the frequencies of the bands, but display a marked difference in intensity distribution. The result is quite surprising considering that the structures are computed to be relatively close in energy and geometry.

For evaluation of the agreement between the computed IR spectra and the experimental spectra, the difference between liquid phase and matrix spectra must be considered (see Figure 5.50). Apart from the expected higher values of the calculated frequencies due to neglecting anharmonicity and only partially allowing electron correlation, the degree of agreement with the liquid phase spectra is remarkable, especially considering structure *cis-trans2* due to the stronger intensity of the weak bands in the 1000-1500 cm^{-1} region and to the azide and carbonyl bands in comparison to the N-N-C band at 1220 cm^{-1}. The broad appearance of the experimental band centred around 1220 cm^{-1} is explained, according to the calculations, by the overlap of three bands computed between 1360 and 1260 cm^{-1}. The only differences between the experimental and the calculated spectrum for this structure are the relative intensities of the carbonyl and azide stretching bands, the prediction of weaker intensity for the bands below 1000 cm^{-1} and the fact the experimental spectrum shows a subdivision of the N_3 chain stretching peak at around 2130 cm^{-1}. The structure whose calculated spectrum follows the best the experimental one is not the lowest in energy: this fact is nevertheless only a partial contradiction because the energy differences are relatively small between five of the seven conformers, so it is very likely that they contribute almost at the same level in the spectrum acquired at room temperature. Given the enhanced differences in intensity distribution among different spectra, it is possible that the spectrum of structure *cis-trans2* is the most similar to the one obtainable by averaging the five spectra.

As can be seen from Figure 5.50, the effect on the IR spectrum of trapping the azide in the nitrogen matrix with respect to the liquid phase is the dramatic decrease of intensity of the bands at 1720 and 2130 cm^{-1}; the effect was expected considering that the most stable structures, conformers *cis-cis*, are those displaying the lower intensity for those bands. Nevertheless, the extent of this decrease largely exceeds even the possibility of having trapped in the matrix only the two most stable conformers. For reasons which are not clear, the calculations overestimate the intensity of the bands associated to the C=O and N-N-N stretching modes.

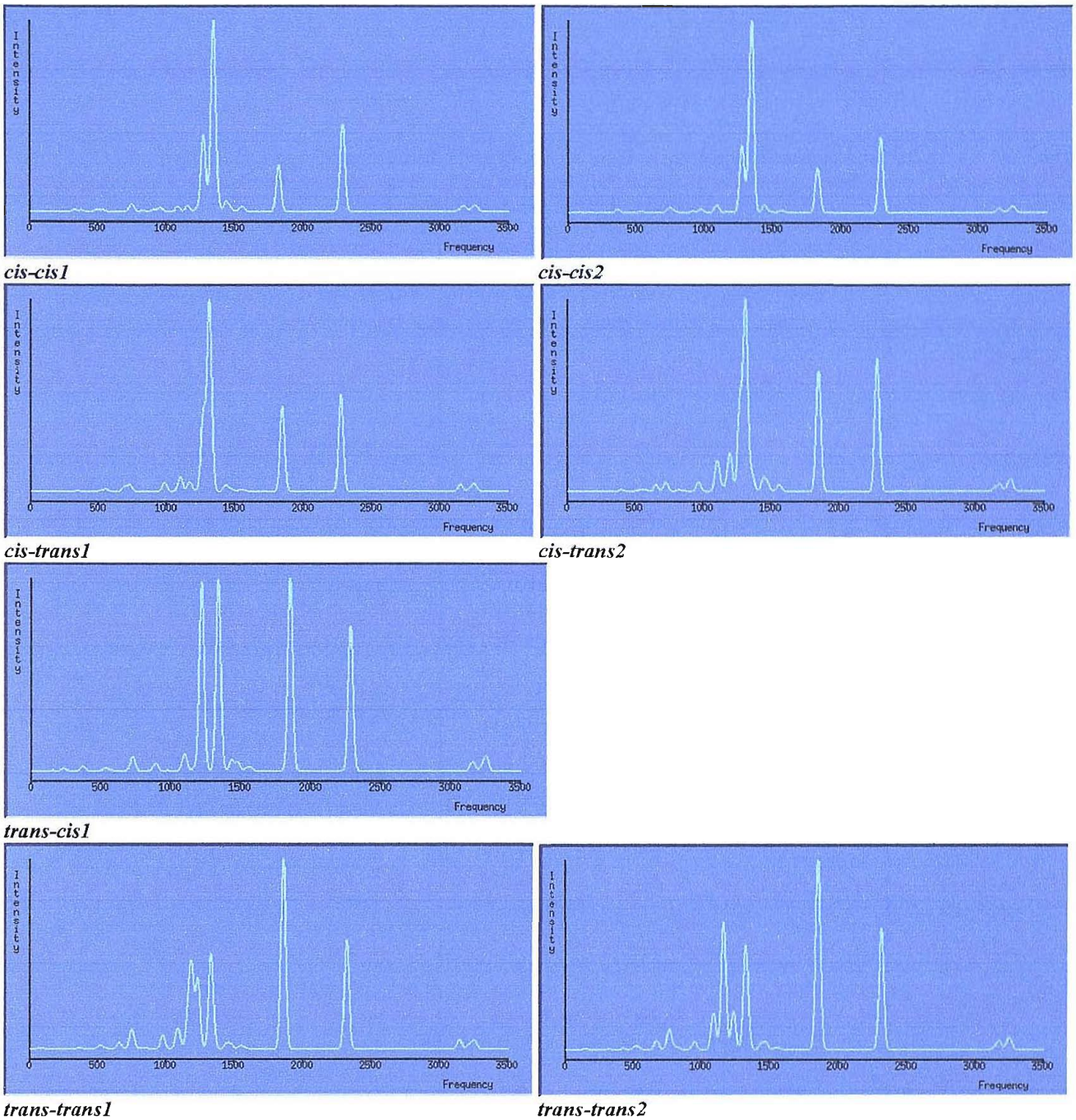

cis-cis1 *cis-cis2*

cis-trans1 *cis-trans2*

trans-cis1

trans-trans1 *trans-trans2*

Fig. 5.55- The IR spectra calculated for the seven conformers *cis-cis* (*1* and *2*, first line), *cis-trans* (*1* and *2*, second line), *trans-cis1* (third line) and *trans-trans* (*1* and *2*, fourth line) of ethyl-azidoformate at the MP2/6-31G level. All the frequencies are expressed in cm^{-1}**

Table 5.38 reports the computed IR frequencies for the *cis-cis1* and *cis-trans2* conformers of ethyl-azidoformate and compares them with the calibrated values for the most prominent experimental bands.

Table 5.38- Comparison between experimental liquid phase IR bands of ethyl-azidoformate and calculated IR bands for the conformers *cis-cis1* and *cis-trans2* of ethyl-azidoformate (all frequencies are expressed in cm^{-1}; absorbances in Km/mol are reported in brackets)

Cis-cis1 frequencies	*Cis-trans2 frequencies*	*Experimental frequencies*	*Cis-cis1 frequencies*	*Cis-trans2 frequencies*	*Experimental frequencies*	**Normal mode**
494.5 (10.00)	512.9 (1.89)		1362.6 (112.14)	1360.1 (51.00)		C-H twisting
538.7 (4.77)	541.4 (4.63)		1438.9 (47.06)	1442.2 (37.94)	1367.7	C-H in phase wagging
546.3 (2.10)	579.1 (4.64)		1471.2 (11.14)	1470.1 (23.70)		C-H out of phase wagging
745.7 (19.85)	655.2 (19.90)		1544.5 (8.34)	1544.5 (1.77)		$C-H_3$ scissoring
751.0 (14.53)	728.4 (27.78)	750.8	1550.2 (7.24)	1555.5 (11.51)	1466.8	C-H out of phase scissoring
831.3 (5.53)	826.6 (5.44)		1565.5 (8.24)	1565.4 (7.77)		C-H in phase scissoring
910.6 (8.65)	871.5 (1.55)	877.6	1821.8 (214.10)	1846.3 (377.32)	1724.4	C=O stretching
959.1 (16.45)	968.2 (29.97)	943.8	2288.3 (399.56)	2279.5 (416.92)	2132 / 2179	N-N-N stretching
1083.4 (22.96)	1104.3 (95.06)	1020.7	3143.7 (10.16)	3142.4 (9.27)		$C-H_3$ symmetric stretching
1155.2 (26.35)	1152.2 (13.65)		3176.5 (23.64)	3174.8 (21.00)		$C-H_2$ symmetric stretching
1230.2 (14.36)	1196.9 (120.2)	1095.4	3239.0 (15.67)	3237.6 (8.65)		C-H asymmetric stretching
1271.9 (353.82)	1272.0 (263.96)		3244.3 (2.47)	3239.6 (11.30)		$C-H_3$ symmetric/ $C-H_2$ asymmetric
1342.5 (822.28)	1312.6 (585.96)	1220.1	3264.1 (18.16)	3260.1 (25.45)	2985.7	C-H asymmetric stretching

5.4.4 THERMAL DECOMPOSITION EXPERIMENTS

Photoelectron spectroscopy

Photoelectron spectra of ethyl azidoformate at different degrees of pyrolysis are shown in Figures 5.56-5.58 –corresponding to roughly 30% pyrolysis at 250 °C and to 100% pyrolysis at 410 °C. A spectrum at 500 °C is reported, to show further decomposition of the primary products and results in CO production.

The first evidence of pyrolysis can be detected around 170 °C; along with the appearance of nitrogen (the sharp band with VIE at 15.58 eV, [8]), there is evidence of acetaldehyde and carbon dioxide being produced at the same time (the sharp bands associated with these products are clearly visible respectively at 10.26 eV and 13.78 eV, [8]). At increasing temperatures, as usual the parent bands decrease while bands of new products appear and gain intensity: a broad band at around 10.20 eV (VIE) and a partially resolved band at around 11.40 eV (VIE) are attributed to $CH_3CH{=}NH$ [4]. The vibrationally resolved band at 11.61 eV (VIE equal to AIE) is assigned to HNCO [17]. There is also evidence of a broad band at roughly 11.05 eV, which cannot be associated either to the azide or to the products so far considered. At around 400 °C, the pyrolysis is virtually complete, and the second band of acetaldehyde (broad band with VIE= 13.24 eV) is visible. The 14.0-16.0 eV region is where bands associated with acetaldehyde and ethylimine overlap, leading to the broad plateau in the spectrum. There is also clear evidence of the second and third bands of N_2 and CO_2 at higher ionization energies. The band at 11.05 eV is still present, indicating the presence of a product with remarkable thermal stability, and therefore not a reaction intermediate. This band has been attributed to the third PE band of a cyclic compound, 2-oxazolidone [30]: in the 10.0-13.0 eV region its PE spectrum consists of four bands, at 10.21, 10.71, 11.07 (the most intense one) and 12.82 eV. The former two are hidden by the envelope of the ethylimine first band, but evidence of the fourth can be found in the spectra. Also for ethyl azidoformate, a further increase in temperature leads to production of CO, whose first band is at 14.01 eV VIE [8]. Its presence is attributed to partial decomposition of HNCO or- more likely- of acetaldehyde, due to the fact that the bands associated with CH_3CHO are those that decrease in intensity on passing from 410 to 500 °C.

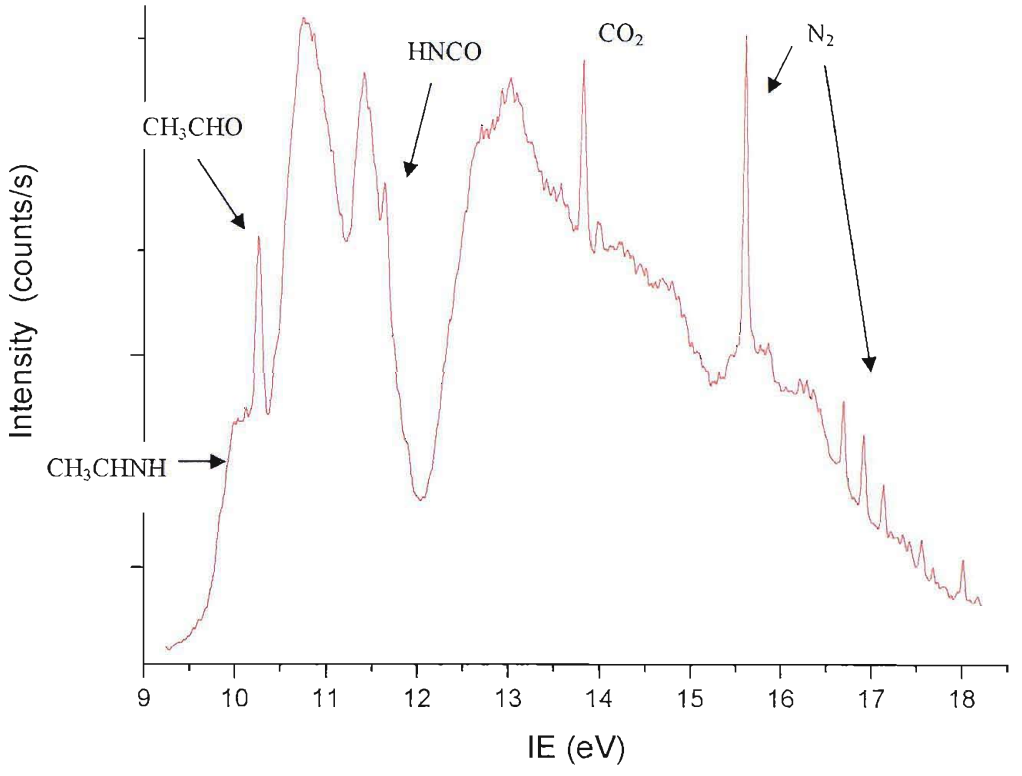

Figure 5.56- HeI PE spectrum of ethyl azidoformate pyrolysis at 250 °C

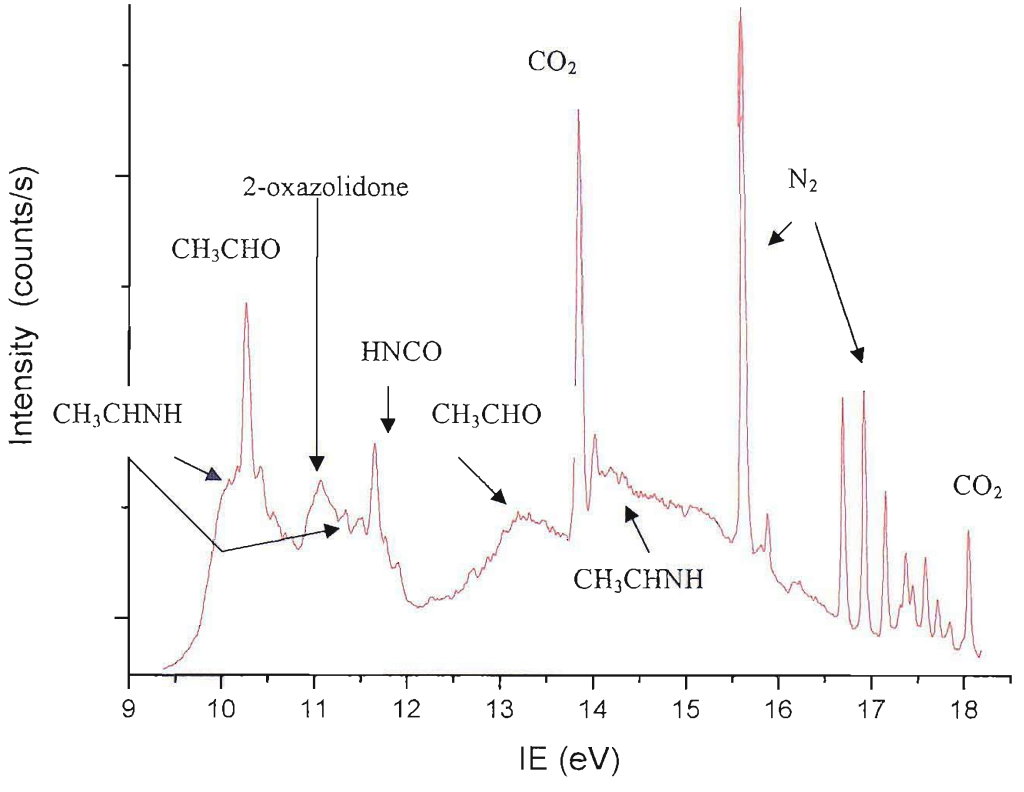

Figure 5.57- HeI PE spectrum of ethyl azidoformate pyrolysis at 410 °C

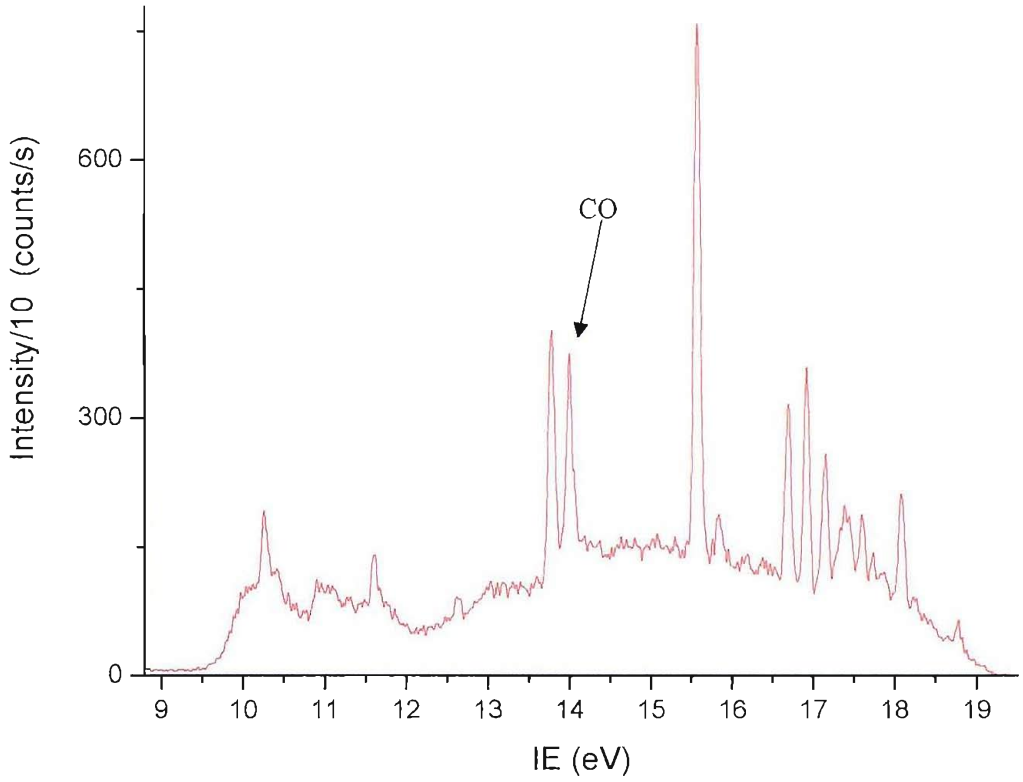

Figure 5.58- HeI PE spectrum of ethyl azidoformate pyrolysis at 500 °C

Matrix isolation IR spectroscopy

A comparison of the matrix infrared spectrum of the parent azide with the one obtained when the temperature is raised to around 280°C is reported in Figure 5.59. It can be seen that the azide is practically completely decomposed under these conditions. Table 5.39 lists the products associated with the labels of the bands in the spectrs, along with the value of the most intense features in the spectra.

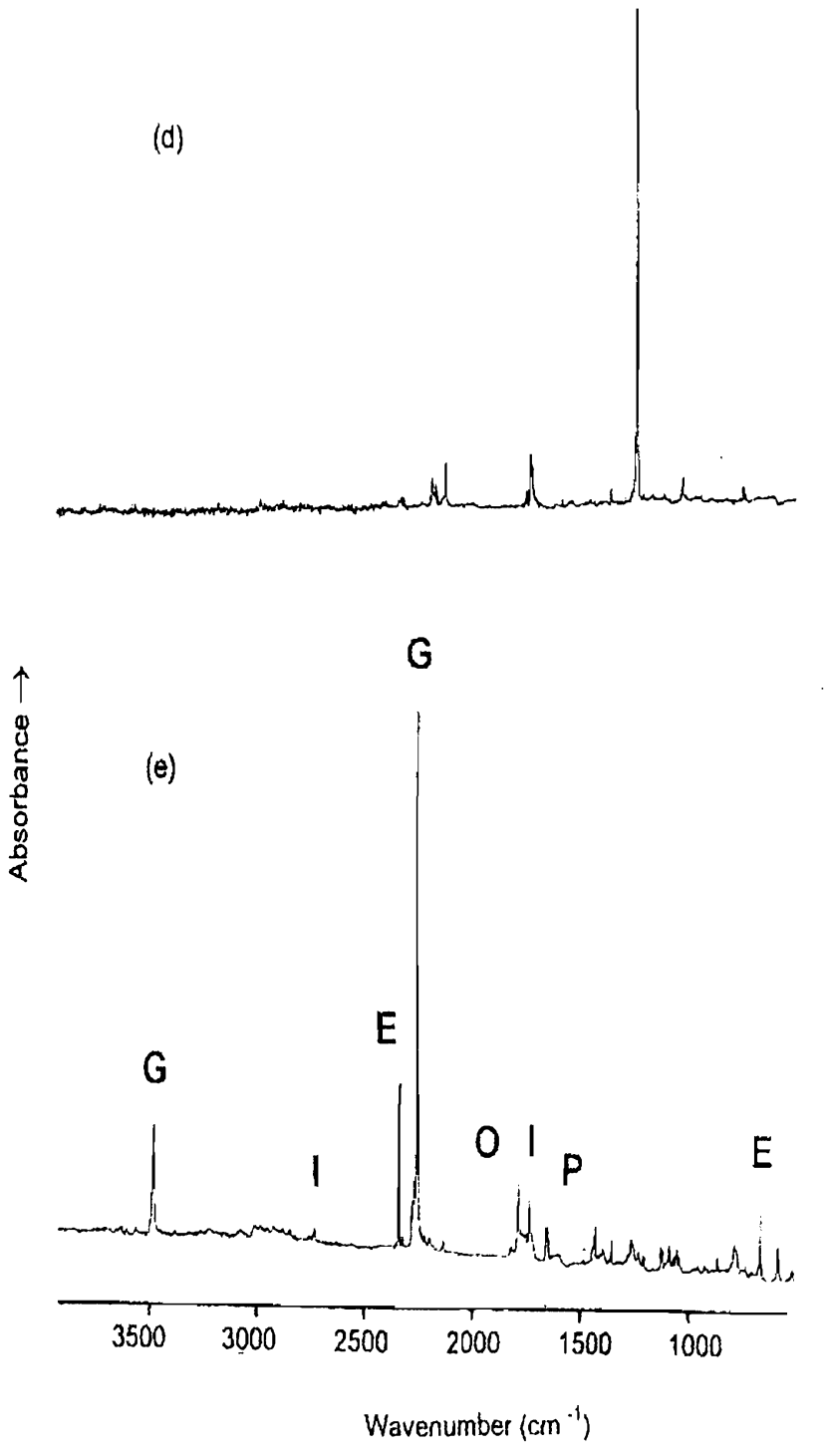

Figure 5.59- Matrix IR spectrum of ethyl-azidoformate at room temperature (d) and when heated at 280 °C (e)

Table 5.39- Labels and assignment of the most significant IR bands observed in the matrix isolation study of ethyl-azidoformate thermal decomposition (refer to Figure 5.59 for the labelling of the bands)

Label	*N_2 matrix frequency (cm^{-1})*	*Assignment*	*Reference*
A	2204, 2143, 1740, 1250	**$N_3COOCH_2CH_3$**	
E	2345, 662	**CO_2**	[31]
G	3483, 2265, 780, 581	**HNCO**	[19]
I	2734, 1737, 1431, 1121	**CH_3CHO**	[29]
P	1654	**CH_3CHNH**	[32]
O	1791, 1226, 1201, 1081	**2-Oxazolidone**	[29]

In matrix infrared spectroscopy experiments, the beginning of the azide pyrolysis is marked by the appearance of bands associated with decomposition products, of which the first one to be observed is that at 2265 cm^{-1} assigned to HNCO [19].

Only spectra at 0% and 100% degree of pyrolysis are reported, because ethyl-azidoformate decomposes without any formation of intermediates. In fact, apart from the bands associated with the azide which obviously decrease at increasing temperature, all bands increase steadily in intensity with the raising of the temperature: this can be seen for the bands at 2265 and 3483 cm^{-1} (labelled G in Figure 13), 2345 cm^{-1} (labelled E), 1654 cm^{-1} (labelled P), 2734 and 1737 cm^{-1} (labelled I) and 1791 cm^{-1} (labelled O) which have been assigned- by referring to previous matrix IR studies- to HNCO, CO_2, CH_3CHNH, CH_3CHO and 2-oxazolidone respectively [19, 29, 31, 32]. Their relative intensity ratio is not altered by changing pyrolysis temperatures, deposition times or other experimental parameters. The only band showing a slightly different behaviour is the weak one at around 2140 cm^{-1} (not labelled in spectrum b in Figure 13): it is assigned to CO [21], and it starts to be observed at higher temperature than the bands associated with the other decomposition products. Furthermore, its intensity keeps increasing at high temperatures, when the intensities of the other bands are roughly constant. Carbon monoxide is therefore a secondary product arising either from a minor decomposition route or from partial decomposition of one of the primary products- most likely acetaldehyde.

5.4.5 SUGGESTED MECHANISM OF GAS-PHASE DECOMPOSITION

The combination of the results from UV-PES and matrix isolation IR experimental data on the pyrolysis of ethyl-azidoformate show that

- When the thermal decomposition begins, HNCO and N_2 are observed as the first products to be released (roughly 170 °C)
- HNCO, CO_2 and CH_3CHO are observed at the same temperature, slightly higher than when nitrogen begins to appear (190 °C)
- CH_3CHNH and 2-oxazolidone are observed at slightly higher temperatures than the other set of products; however, this can be due to their lower photoionization cross sections and dipole moment than for the other molecules, so that their PE and IR bands are weaker and observable only at higher concentrations in the reaction region, or when the bands of the azide have almost disappeared
- At higher temperatures –around 500 °C- bands associated with CO are present in the PE spectra, indicating that a new route is open, or that one of the primary products begins to decompose.
- No bands which suggest the presence of a reaction intermediates were observed

As a general rule for azides, the first step in the decomposition is the formation of nitrogen: no evidence could be found that a nitrene is formed, even with an extremely short lifetime, or if a concerted rearrangement occurs in the molecule at the same time as the nitrogen release. Following the evidence obtained theoretically for other azides [6, 24] and experimentally for methyl- and ethyl-azide [5, 26], it will be assumed that the route which proceeds via a nitrene intermediate

$$N_3CH_2CONH_2 \rightarrow N_2 + :NCH_2CONH_2$$

is favoured over a concerted mechanism involving breaking of the N-N bond and a rearrangement to produce the decomposition products.

Azidoformates present a peculiarity over other azides, in the sense that they have no hydrogen atoms attached to the carbon atom adjacent to the N_3 chain. This means that no 1,2 hydrogen shift between the carbon and nitrogen atoms is possible when molecular nitrogen is released when the azide decomposes.

This fact rules out one of the two possible isomerization processes that a*b initio* calculations have indicated as the decomposition routes for the unstable nitrene, the one labelled Type 1 and that in general can be depicted as

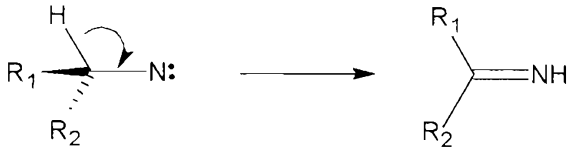

In this case the absence of hydrogen atoms adjacent to the N_3 chain prevents the formation of an imine.

The only possibility for isomerization is therefore the Type 2 mechanism in which the electron deficient nitrogen atom attacks a remote site of the molecule, forming a new bond. In the case of ethyl-azidoformate, there are two different sites to which the attack can be directed, that is either the methylene or the methyl carbon atoms.

In the first case, the nitrogen atom attacks the γ position to form a four membered ring

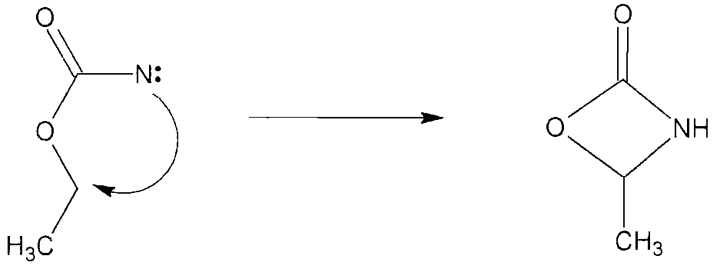

If on the other hand the attack is on the methyl carbon in the δ position, 2-oxazolidone is formed

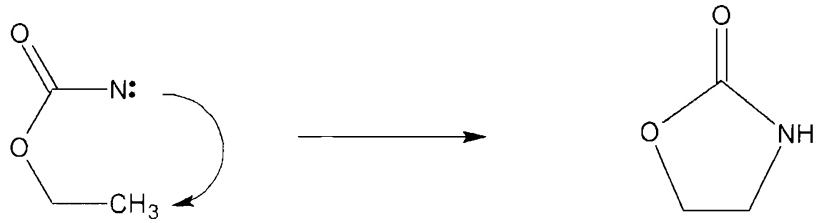

A five membered ring lacks the strain of a four membered one, and this is confirmed by the fact that 2-oxazolidone is a solid commercially available, while no proof of the existence of the four memebered ring- originating from the first type of attack- has been reported.

To take into account the optimised structures, the energy differences and the spectroscopic properties, *ab initio* calculations have been performed on all reactant, nitrenes and products involved in the

thermal decomposition of ethyl-azidoformate. Calculations were necessary not only *a posteriori* to explain the possible decomposition pathways, but also *a priori* to determine the decomposition pathways themselves: in fact, PE and IR bands of 2-oxazolidone were initially unassigned as no valid candidates could be found.

Before considering the decomposition process to produce the other main observed products (HNCO, CH_3CHNH, CO_2, CH_3CHO and CO), a summary of the *ab initio* calculations on the nitrenes and the cyclic products results will be presented.

Significantly, no attempt of optimization conducted in this work was possible for the amine that can be obtained by hydrogen abstraction from the methyl group onto the nitrogen atom followed by a molecular rearrangement, following a Type 2 mechanism like

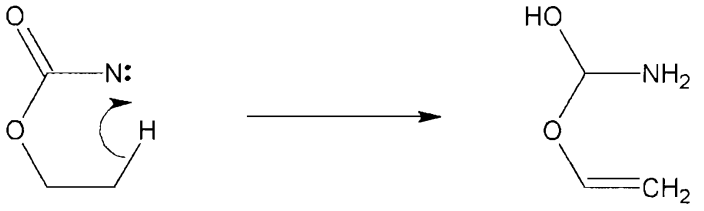

5.4.5.1 *Ab initio* calculations results on ethyl nitreneformate and cyclic molecules

Ethyl-nitreneformate

Calculations have been carried out for the nitrene that could be formed from ethyl azidoformate after release of molecular nitrogen. Four structures have been optimised for ethyl nitreneformate in its singlet spin multiplicity state- according to the possible different mutual dispositions of the alkyl groups and the oxygen and nitrogen atoms- and four structures were optimised for the triplet state, which is the ground state, all of them with all real vibrational frequencies. The location of minimum nitrene structures in the singlet spin state is remarkable, as this was not possible for nitrenes derived from other classes of azides such as azidoacetamides or azidopropionitriles, at least at the MP2/6-31G** level, as during the optimization the structures converged to those of the imines formed by isomerization via Type 1 or Type 2 mechanisms. It is possible that the absence of hydrogen atoms in the α position to the diradical nitrogen- and therefore the prevention of one of the possible isomerization routes (Type 1)- gives the singlet nitrene structures a higher stability.

The singlet state nitrene geometries have very similar energy (ΔE = 1.61 kcal/mol), while in the triplet state the difference among the conformers is more marked (7.27 kcal/mol). Tables 5.40 and 5.41 report the computed total energies for the four singlet structures, indicated by *cis* or *trans* according to the relative orientation of the methylene group with respect to the carbonyl group and the number referring to the different orientation of the methyl group with respect to the methylene group.

Table 5.40- Total energies of the conformers of ethyl-nitreneformate calculated at the MP2/6-31G level in the singlet spin multiplicity state**

Structure	*Energy (hartrees)*
Singlet *cis1*	-321.4835435
Singlet *cis2*	-321.483202
Singlet *trans1*	-321.4809725
Singlet *trans2*	-321.4818635

Table 5.41- Total energies of the conformers of ethyl-nitreneformate calculated at the MP2/6-31G level in the triplet spin multiplicity state**

Structure	*Energy (hartrees)*
Triplet *cis1*	-321.4847452
Triplet *cis2*	-321.484728
Triplet *trans1*	-321.4959516
Triplet *trans2*	-321.4963135

Given the fact that the decomposition path, for spin conservation, will be on the singlet surface, no further discussion will be given in this section on the nitrenes in their triplet spin multiplicity state.
The four optimised structures for singlet ethyl-nitreneformate are reported in Figure 5.60. Two of them are planar, while the other two show a marked out of plane orientation of the methyl group.

Strictly speaking, the conformers characterized by a cyclic C-O-N structure are not nitrenes: the N-O bond length is calculated as 1.75 Å which probably indicates a weak electrostatic interaction arising from a structure of the type

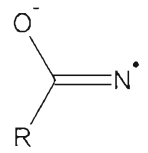

rather than from a structure of the type

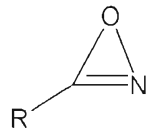

Moreover, the very small energy difference between the cyclic and the non-cyclic structures allows consideration of the four structures as the same set of unstable molecules, all arising from by nitrogen elimination from the different conformers of ethyl-azidoformate.

Setting as zero the energy of the most stable conformer of the azide, the relative energies of the nitrenes (plus molecular nitrogen) are about 32 kcal/mol higher: because of this high energy and because of their well known instability, the calculated VIEs and infrared bands of these nitrenes will not be reported here.

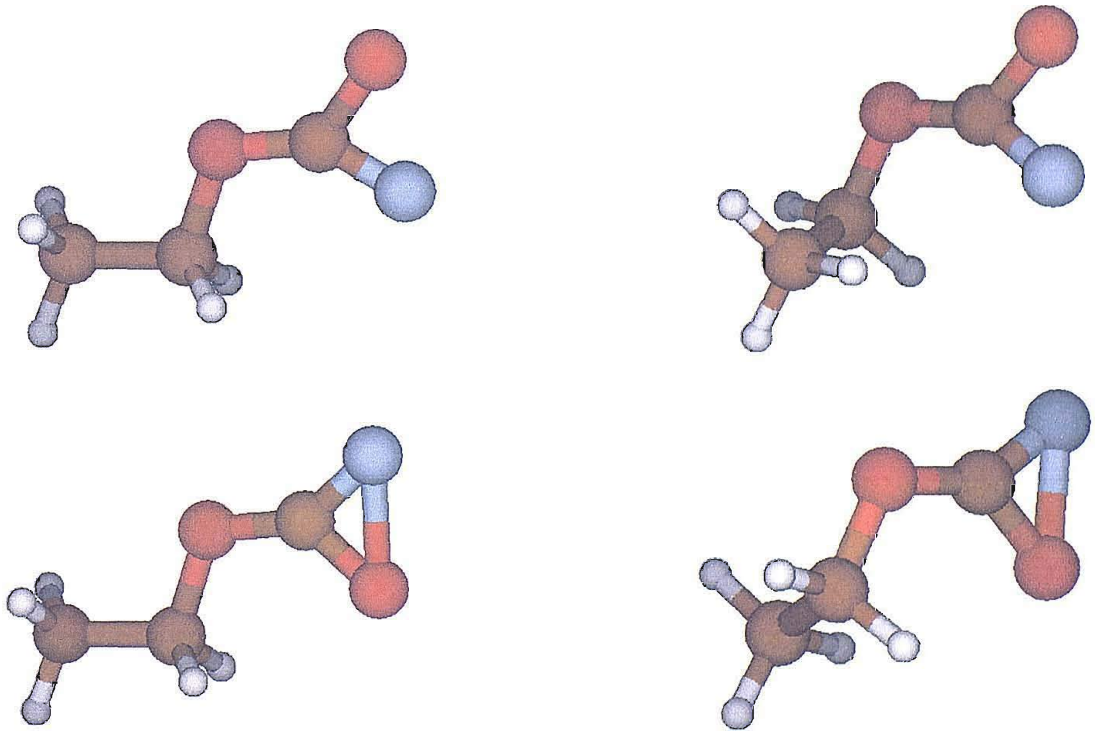

Figure 5.60- Optimized structures of singlet spin state ethyl-nitreneformate at MP2/6-31G level**

Cyclic products

As mentioned, the understanding of the pathway of the thermal decomposition of ethyl-azidoformate relies on the rationalization of the geometries and the energies of the reactants, transition states and products involved in the process. The hypothesis of the formation of cyclic molecules was based on the evidence that MO *ab initio* searches of a transition state between the nitrenes and the different sets of products always converged to one of these ring structures. Although some literature data were available on 2-oxazolidone [30], the existence of other possible ring structures is not proved: calculations were therefore carried out to obtain the relative energies and spectroscopic characteristics of such structures to confirm either their presence as decomposition products or to validate the hypothesis that they are an intermediate stage between the azide and the final pyrolysis products

The first option is the four-membered ring arising from the nitrogen attack on the methylene group, and can be labelled A) and represented as

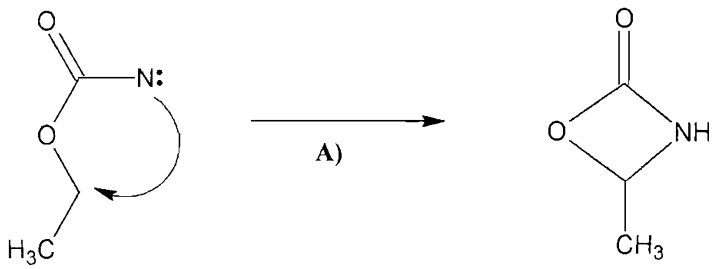

The optimized geometry for this cyclic compound is reported in Figure 5.61, and Table 5.42 reports its most important geometrical parameters. It is an almost square ring structure, but with significant out of plane contributions, notably for the hydrogen atoms bonded to the nitrogen and carbon atoms. The methyl group external to the ring is markedly out of the pseudo-plane of the ring itself.

The calculated total energy at the MP2/6-31G** level is -321.6102883 hartrees.

The first vertical ionization energies (VIEs)- calculated either by applying Koopmans' theorem to the energies of the molecular orbitals or by the ΔSCF method calculating the energy of the cation and neutral using the geometry optimized for the neutral molecule at the MP2/6-31G** level- are reported in Table 5.43.

The ΔSCF method alters the ionization energy order, because the ionization from MO 22 appears at higher VIE than the one from MO 21. If this swap is considered, the net effect of the ΔSCF method is a narrowing of the interval spammed by the bands: this effect is probably over-estimated by the method, as can be pointed out in the discussion on the calculations on 2-oxazolidone (see later in the section).

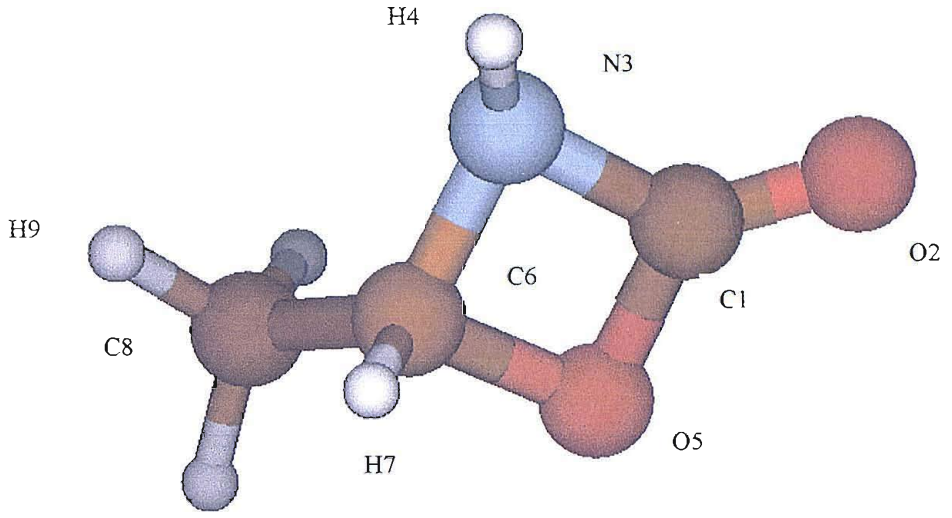

Figure 5.61- Optimized structure for the four membered ring intermediate in the decomposition of ethyl-azidoformate

Table 5.42- The most significant geometrical parameters calculated for the four-membered ring intermediate at the MP2/6-31G level**

Bond	*Length (Å)*	*Angle*	*Value (°)*	*Dihedral angle*	*Value (°)*
C1-O2	1.202	N3-C1-O2	135.89	C6-N3-C1-O2	186.7
C1-N3	1.401	C1-O5-C6	88.21	C1-N3-C6-O5	-7.0
N3-H4	1.011	O5-C6-N3	88.88	H4-N3-C1-O5	137.2
N3-C6	1.464	N3-C1-O5	94.13	H7-C6-N3-C1	104.2
C1-O5	1.396	C6-N3-C1	87.87	C8-C6-O5-C1	124.8
O5-C6	1.461	H4-N3-C1	121.21	H9-C8-C6-O5	186.3
C6-H7	1.093	H7-C6-N3	113.96		
C6-C8	1.502	C8-C6-O5	112.63		
C8-H9	1.090	H9-C8-C6	110.04		

Table 5.43- Vertical ionization energies obtained by Koopmans' theorem on the molecular orbitals obtained at the MP2/6-31G level for the four membered ring intermediate**

Ionization	*KT calculated VIE (eV)*	*0.92* KT calculated VIE (eV)*	*ΔSCF calculated VIE (eV)*
$(23a')^{-1}$	11.71	10.78	10.98
$(22a')^{-1}$	12.61	11.60	11.73
$(21a')^{-1}$	13.51	12.43	11.08
$(20a')^{-1}$	14.87	13.68	
$(19a')^{-1}$	14.89	13.70	
$(18a')^{-1}$	15.14	13.93	
$(17a')^{-1}$	16.24	14.94	
$(16a')^{-1}$	16.71	15.37	

The calculated harmonic vibrational frequencies obtained by second derivative calculations are listed in Table 5.44, while the full computed IR spectrum is presented in Figure 5.62, assuming a Gaussian shape for the bands.

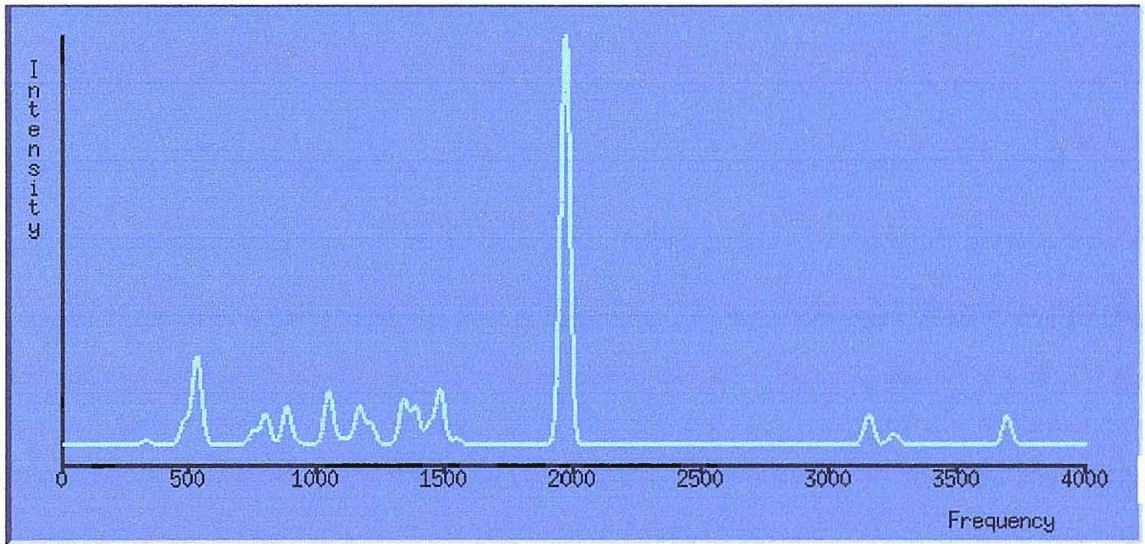

Figure 5.62- Calculated infrared spectrum of the four membered ring intermediate at the MP2/6-31G level**

Table 5.44- Calculated vibrational frequencies for the four-membered intermediate at the MP2/6-31G level**

Frequency (cm^{-1})	*Absorbance* (km/mol)	*Frequency* (cm^{-1})	*Absorbance* (km mol)	*Frequency* (cm^{-1})	*Absorbance* (km mol)	**Normal mode**
479.8	31.88	1092.0	5.77	1540.9	3.12	C-H_3 asymmetrical scissoring
526.4	112.29	1123.9	5.73	1543.4	5.01	C-H_3 symmetrical scissoring
544.0	15.58	1163.8	52.06	1963.3	572.63	C=O stretching
748.7	18.54	1208.3	28.58	3140.5	5.81	C-H_3 symmetrical stretching
796.2	41.65	1336.5	62.34	3153.7	38.23	C-H stretching
879.8	52.28	1382.3	51.48	3238.8	9.01	C-H_3 asymmetrical stretching
921.2	2.72	1437.7	28.53	3259.9	9.04	C-H_3 asymmetrical stretching
1043.2	75.32	1478.8	74.50	3689.7	39.48	N-H stretching

The second cyclization possibility is the one leading to the formation of a five-membered cyclic structure, 2-oxazolidone, as consequence of the attack of the nitrogen group onto the methyl group. This route can be labelled as B) and represented as

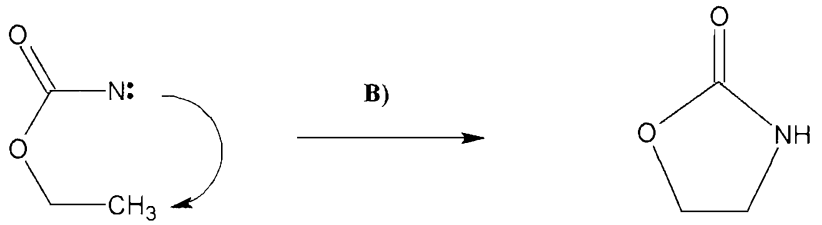

Even if 2-oxazolidone is a commercially available product, calculations were performed to determine its relative energy compared to the other pyrolysis products- and therefore to make a proposal on the decomposition route- and to have another validation test for the quality of the agreement between calculations and experiments: this latter aspect is particularly important, because 2-oxazolidone could be used as a reference for all the possible cyclic intermediates encountered in the azide decomposition pathways. Therefore it can provide a scaling factor to be used for the IR frequencies for the four membered ring discussed earlier.

The optimised geometry of 2-oxazolidone is reported in Figure 5.63, and the most important geometrical values are listed in Table 5.45. The distortion from a planar geometry is quite marked.
Its total energy has been calculated as -321.6259169 hartrees, which means it is about 10 kcal/mol lower than the total energy of the four membered-ring.

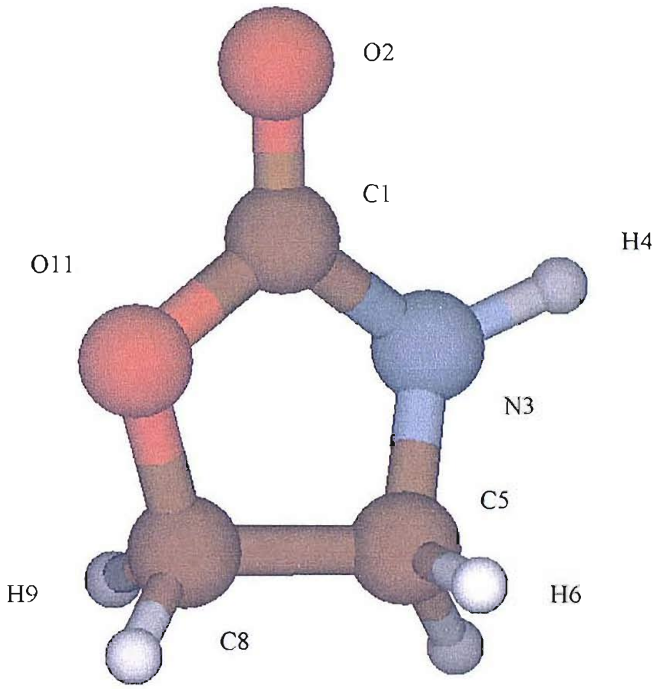

Figure 5.63- Optimized structure of 2-oxazolidone at the MP2/6-31G level**

Table 5.45- Optimized values of the most significant geometrical parameters of 2-oxazolidone

Bond	*Length (Å)*	*Angle*	*Value (°)*
C1-O2	1.212	O2-C1-N3	128.21
C1-N3	1.387	C1-N3-C5	110.02
N3-C5	1.451	N3-C5-C8	98.75
C8-C5	1.528	C5-C8-O11	104.18
O11-C8	1.439	C8-O11-C1	108.42
C1-O11	1.378	H4-N3-C5	121.45
H4-N3	1.008	O2-C1-N3-C5	163.44
H6-C5	1.094	C8-O11-C1-N3	-4.75
H9-C8	1.091	H4-N3-C5-C8	169.32
		H6-C5-C8-H9	-155.39

The VIEs- calculated either with Koopmans' theorem or by the ΔSCF method at the MP2/6-31G** level- are reported in Table 5.46, and compared to the experimental VIEs reported in literature [30].

Table 5.46- Vertical ionization energies obtained by Koopmans' theorem to the molecular orbital energies obtained at the MP2/6-31G level for 2-oxazolidone**

Ionization	KT calculated VIE (eV)	0.92* KT calculated VIE (eV)	Experimental VIE (eV)	ΔSCF calculated VIE (eV)
$(23a')^{-1}$	11.27	10.37	10.21	10.53
$(22a')^{-1}$	12.23	11.25	10.71	10.45
$(21a')^{-1}$	12.45	11.45	11.07	10.51
$(20a')^{-1}$	14.47	13.31	12.82	
$(19a')^{-1}$	15.71	14.45		
$(18a')^{-1}$	16.07	14.79		
$(17a')^{-1}$	16.40	15.09		
$(16a')^{-1}$	16.74	15.40		

The agreement between theory and experiment is not particularly good: the calculated values are higher by about 1.0 eV for the first VIE and about 1.5 eV for the second to fourth VIEs: even if a scaling factor improves the agreement, the separation between the first and second band is predicted by Koopmans' theorem to be around 1.0 eV, while experiments show that it is 0.5 eV in reality.
The VIEs obtained by the ΔSCF method show first of all an alteration of the VIE ordering: the ionization from the HOMO is higher than those from MO 22 and 21. Even taking into account this alteration, the VIEs span a too narrow interval (0.08 eV instead of the experimental 0.86 eV).

Therefore, 2-oxazolidone reveals that, at least at the MP2/6-31G** level, the calculated VIEs can only offer an indicative prediction about the experimental VIEs of a cyclic intermediate like the four-membered structure discussed earlier. Experimentally no clear evidences were found of the bands associated with the four-membered intermediate, although they could be overlapping with the first bands of 2-oxazolidone and HNCO. The presence of such a four-membered molecule is therefore not confirmed by the PES evidence.

Harmonic vibrational frequencies of 2-oxazolidone have been calculated at the MP2/6-31G** level and are reported in Table 5.47; the full IR spectrum is shown in Figure 5.64.

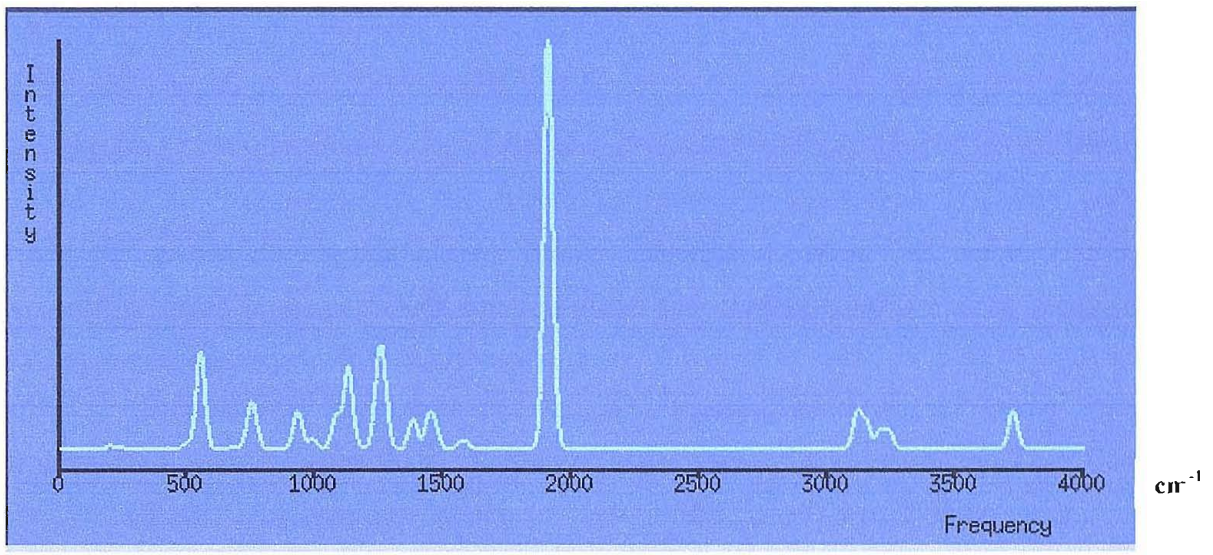

Figure 5.64- Calculated IR spectrum of 2-oxazolidone at the MP2/6-31G level**

Table 5.47- Calculated vibrational frequencies for 2-oxazolidone at the MP2/6-31G level**

Frequency (cm^{-1})	*Absorbance (km/mol)*	*Frequency (cm^{-1})*	*Absorbance (km/mol)*	*Frequency (cm^{-1})*	*Absorbance (km/mol)*	**Normal mode**
501.4	6.93	1082.8	41.69	1466.7	23.88	
554.2	122.78	1130.0	102.61	1570.7	4.28	C-H_3 asymmetrical scissoring
681.1	2.39	1168.8	2.82	1584.5	7.80	C-H_3 symmetrical scissoring
746.8	36.80	1246.1	79.01	1910.8	518.10	C=O stretching
763.3	29.14	1266.9	77.47	3116.6	44.19	C-H_3 symmetrical stretching
925.5	14.14	1271.3	2.91	3152.1	31.43	C-H stretching
934.9	34.13	1382.0	37.41	3207.2	21.91	C-H_3 asymmetrical stretching
991.0	12.82	1444.2	34.17	3241.8	20.78	C-H_3 asymmetrical stretching
				3724.5	47.88	N-H stretching

In the case of the vibrational frequencies, the agreement is much better than for the VIEs: the experimental pattern follows quite closely the pattern obtained from calculations. The most intense band, the C=O stretch, is observed at 1791 cm^{-1} (calculated value 1911 cm^{-1}), while the strong bands calculated at 1267, 1246 and 1130 cm^{-1} are observed experimentally at 1226, 1201 and 1081 cm^{-1}.

By comparing the vibrational frequencies of the two cyclic compounds, it is expected that the most intense band for the four-membered ring would be experimentally detected around 1840 cm^{-1}; nevertheless, the spectra do not display any clearly detectable band in this region. Therefore, no evidence could be found to support the formation of the four-membered structure: it is possible that, despite the predicted stability, its lifetime is very short.

The four-membered cyclic structure is the most suited precursor for the formation of CO_2 + CH_3CHNH and of HNCO + CH_3CHO, by breaking the opposite sides of the pseudo-square of the structure.
In one case the mechanism (labelled A1) can be represented as

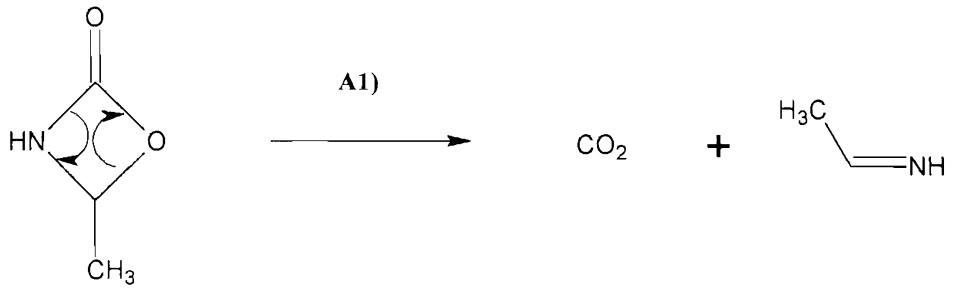

In the alternative case, the scheme (labelled A2) is

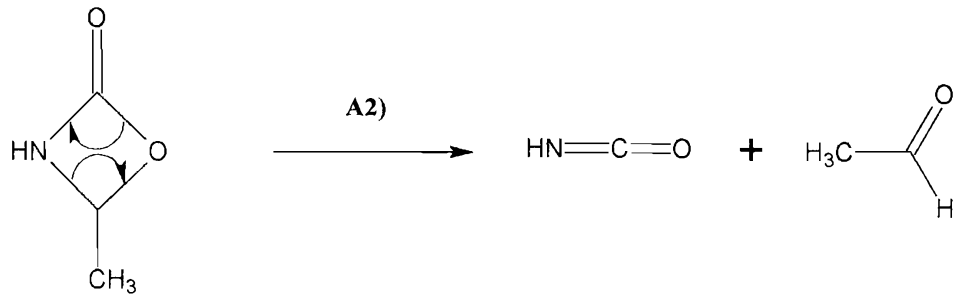

Therefore, the formation of the four-membered ring as an intermediate explains the formation of all the products, apart from 2-oxazolidone: this last molecule is formed in the other independent cyclization mechanism.

On the basis of the experimental results, 2-oxazolidone appears at roughly the same temperatures as the other products, and it is stable even at high temperatures, showing no trace of decomposition into the other sets of products: this indicates that the two channels for the production of the cyclic structures (A and B) are open at the same time and that increasing temperature does not alter the preference for one of the decomposition routes.

The overall mechanism, assuming that the nitrene is actually formed, can be therefore represented as in Figure 5.65.

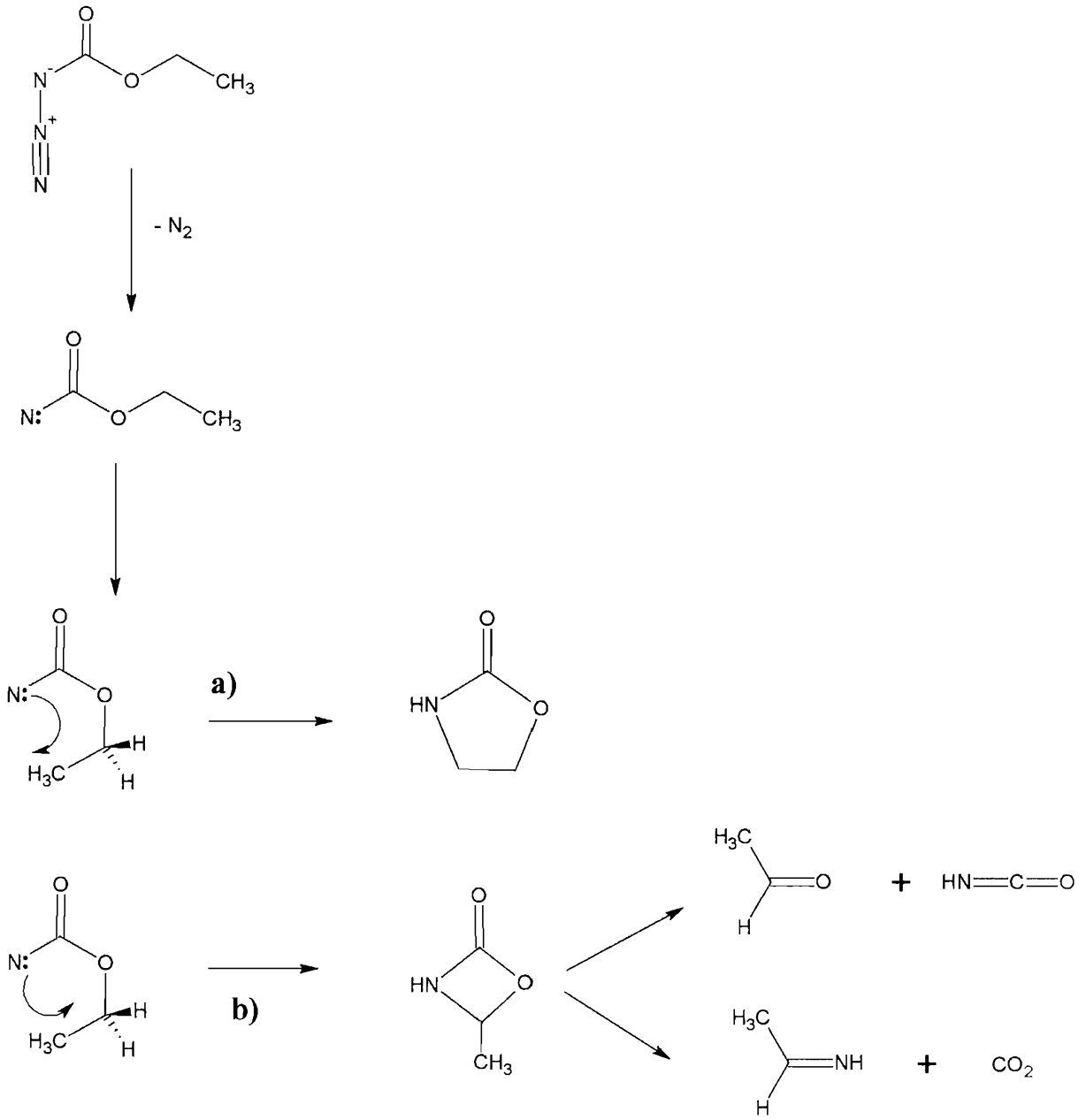

Figure 5.65- Proposed decomposition scheme for ethyl-azidoformate

The preference for the assumption that the nitrene is actually formed- even if with a very short lifetime- arises from the fact that *ab initio* calculations are able to locate transition states for forming the cyclic structures only from the nitrene. All the calculations carried out on the decomposition mechanism did not converge to an appropriate structure for the transition state between the azide and the two cyclic intermediates with a concerted mechanism between the release of nitrogen and the closure of the ring. From these results, the cyclic intermediates are likely to be preferably formed via the nitrenes.

In the same way, it was not possible to locate a valid transition state for the direct nitrene → products route: this confirms that even if not detected experimentally the four-membered ring is crucial for the production of the smaller molecules observed on decomposition, as they are not formed from the nitrene.

The 0 K energy level diagram for the stepwise mechanism is reported in Figure 5.66. To take into account the contribution of zero point energy, of thermal energy and of entropy (important especially for the formation of the final products), a free energy diagram at 298 K is reported in Figure 5.67. In both cases the zero is set to correspond with the energy of the most stable conformer of ethyl-azidoformate. The geometries of the transition states found in the calculations- and reported in the energy level diagram- are shown in Figure 5.68.

For the location of the transition states between the nitrene and the ring structures, it has been found that the two cyclic structures are more easily formed from two different nitrenes. In the study of the azide → nitrene process only one transition state (TS1) was considered, because all the other nitrene geometries can be obtained from the one resulting from TS1 by a simple rotation of the methyl or carbonyl groups.

When the contributions of entropy are considered, the effect is- as expected- a lowering of the relative energies of the final products in comparison with the energy of the cyclic products, which themselves are lowered with respect to the azide. According to ΔG^{298} values, the energies of the two sets of products arising from the four-membered ring are lower than those of the cyclic structures. Also, despite the marked difference in energy, the two sets of products CO_2+CH_3CHNH and HNCO+CH_3CHO are formed via transition states differing only by less than 4 kcal/mol, which confirms the fact that the two sets are experimentally observed and with an approximate constant molar ratio with increasing temperatures.

Remarkably, the transition states between 2-oxazolidone and the other sets of products are much higher in energy than those from the four-membered ring: 2-oxazolidone therefore seems a stable structure requiring high amounts of energy to decompose, as it has already been found from the experimental results. The other products are attributed to the decomposition of the four-membered ring.

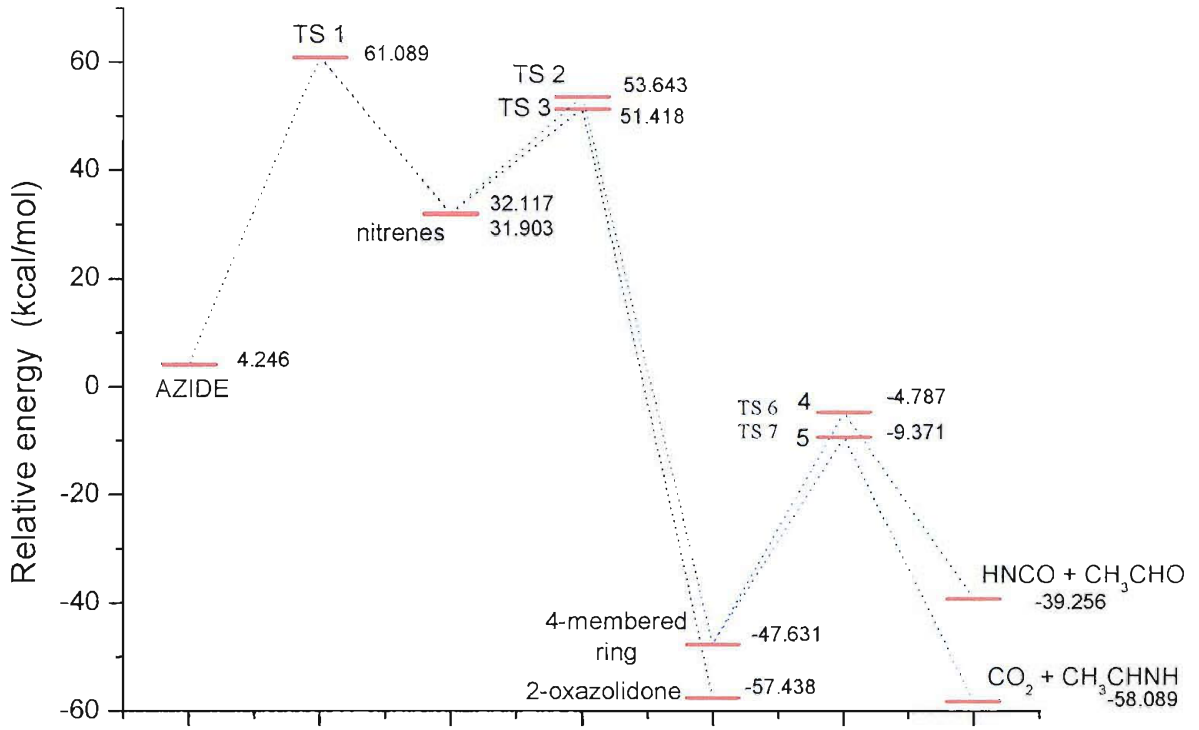

Figure 5.66- Energy diagram at 0 K for the decomposition of ethyl-azidoformate calculated at the MP2/6-31G level. The zero value is set for the most stable azide conformer**

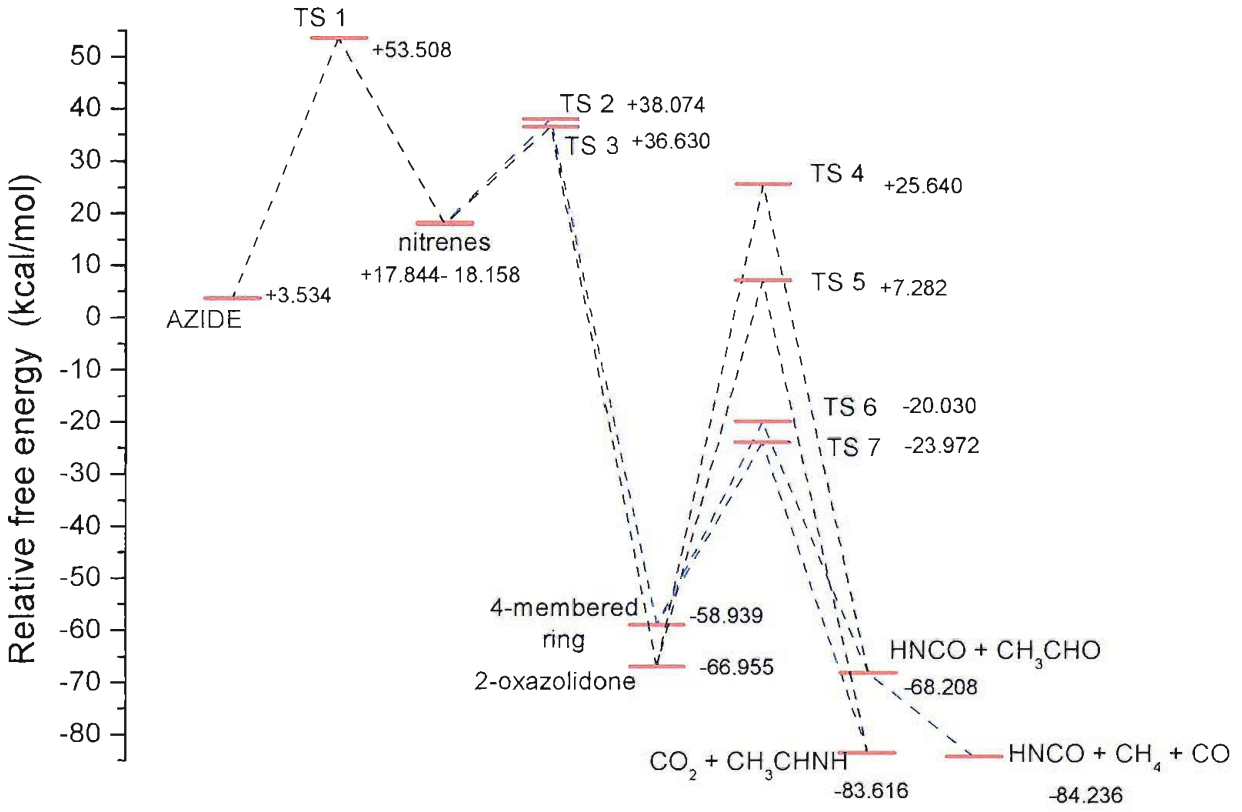

Figure 5.67- Free energy diagram at 298 K for the decomposition of ethyl-azidoformate calculated at the MP2/6-31G level. The zero value is set for the most stable azide conformer**

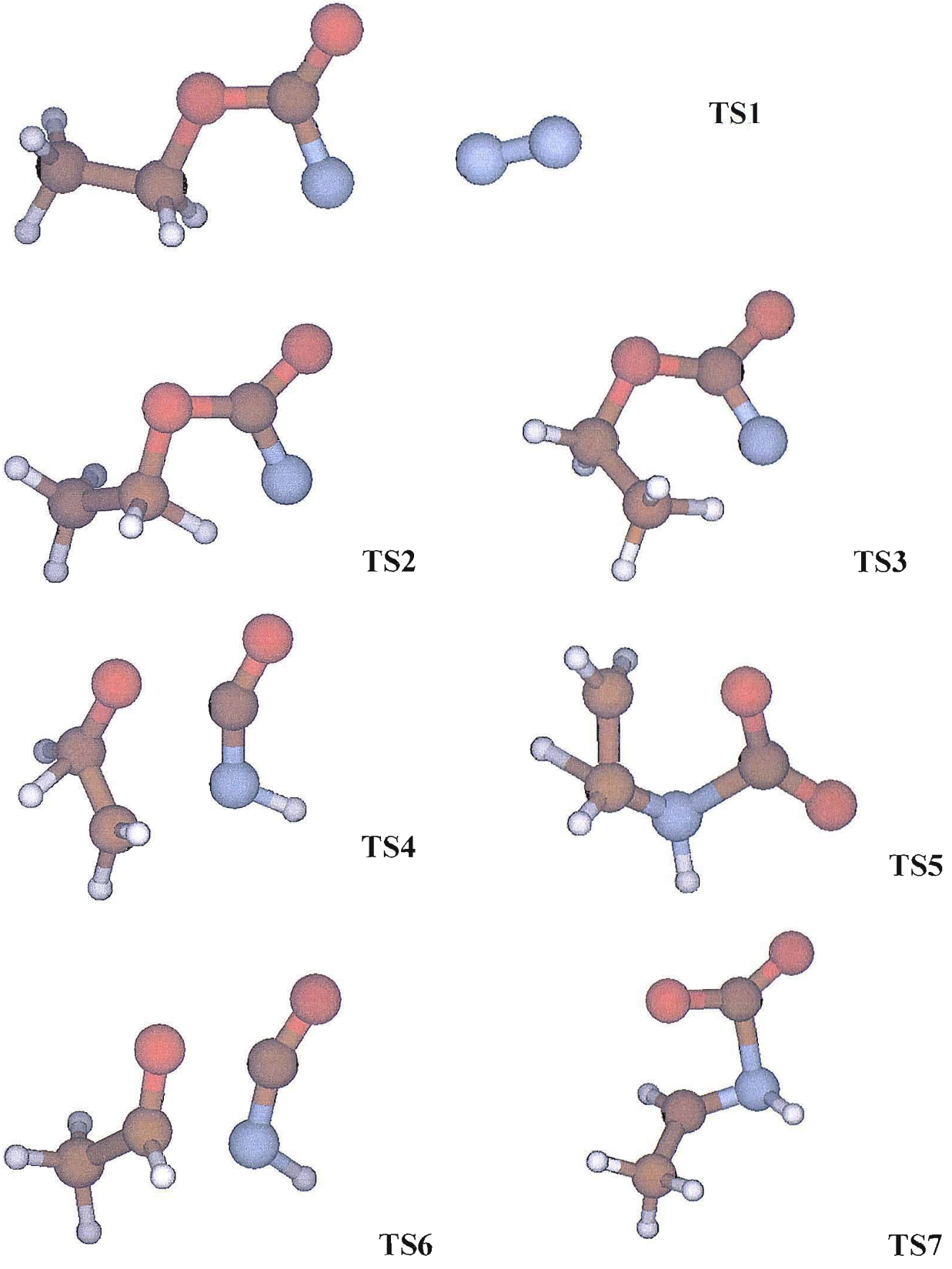

Figure 5.68- Geometries of the transition states optimized in the ab initio study of the thermal decomposition of ethyl-azidoformate. Labels refer to the TS labels in the energy diagrams in Figures 5.66-5.67

5.5 METHYL AZIDOFORMATE

5.5.1 EXPERIMENTAL SECTION

Photoelectron spectroscopy

Methyl-azidoformate (N_3COOCH_3), with a chemical structure similar to ethyl-azidoformate and with a methylene group less, is a liquid that at room temperature has enough vapour pressure to produce spectra of acceptable signal-to-noise ratio simply by evacuating a flask holding the sample connected to the inlet tube of the spectrometer via a needle valve

For the pyrolysis study, a resistive heating system was found sufficient to reach temperatures at which total decomposition of the azide is achieved.

The 20-cm mean hemisphere radius photoelectron spectrometer of the Lisbon PE group was used for this set of experiments: a description and a schematic diagram of this PE spectrometer were given in Section 2.1.

The procedure for the acquisition and calibration of the photoelectron spectra followed the same pattern as described in Chapter 2. Calibration of spectra obtained on pyrolysis of the azide was normally achieved using the bands associated with the first vertical ionization energies (VIEs) of N_2 (15.58 eV), H_2O (12.62 eV), CO_2 (13.78 eV), or of residual CH_2Cl_2 (12.21 eV) [8]., which is the solvent used for the preparation of the azide, in the samples

Matrix isolation IR spectroscopy

The apparatus and the procedure for the acquisition of infrared spectra in nitrogen matrices have been described in Chapter 2. Deposition times were in the order of 30 to 60 minutes, and the matrix dilution ratios were estimated to be above 1000:1.

5.5.2 SAMPLE PREPARATION AND CHARACTERIZATION

PREPARATION

Methyl chloroformate was added slowly to a solution of sodium azide (3 equiv) in distilled water. The mixture was stirred for 24 hours in an oil bath at 50°C. After cooling, the product was extracted with dichloromethane, dried over anhydrous sodium sulphate and the organic phase concentrated using a rotary evaporator. Methyl azidoformate was purified by distillation in a Kugelrohr at reduced pressure (10 mbar; b.p. 20 °C).

CHARACTERIZATION

Methyl azidoformate (N_3COOCH_3) is a colourless liquid at room temperature. It was characterized in the vapour phase by UV-photoelectron spectroscopy and electron impact mass spectrometry, and by ^1H- and ^{13}C-NMR in solution in deuterated chloroform. Infrared spectroscopy characterization was conducted on the pure liquid between KBr plates.

According to the spectroscopic results, the methyl-azidoformate used in this work was pure, apart from some samples in which a non-negligible amount of solvent (dichloromethane) was present: in this case, having the two components with very different boiling points, it was necessary to leave the sample connected to the low pressure inlet of the ionization chamber of the spectrometer, so that the residual solvent was pumped away.

Mass spectrometry: the 70 eV electron impact mass spectrum is reported in Figure 5.69. It displays a parent peak at 101 amu (corresponding to the unfragmented azide, 0.86%) and the most intense peak (base peak) at 59 amu (corresponding to CH_3OCO^+). Strong peaks were also present at 70 amu (corresponding to N_3CO^+, 36.47%), 28 amu (corresponding to N_2^+, 17.92%), 29 amu (corresponding to N_2H^+ and COH^+, 14.28%) and 42 amu (corresponding to N_3^+ and NCO^+, 12.27%).

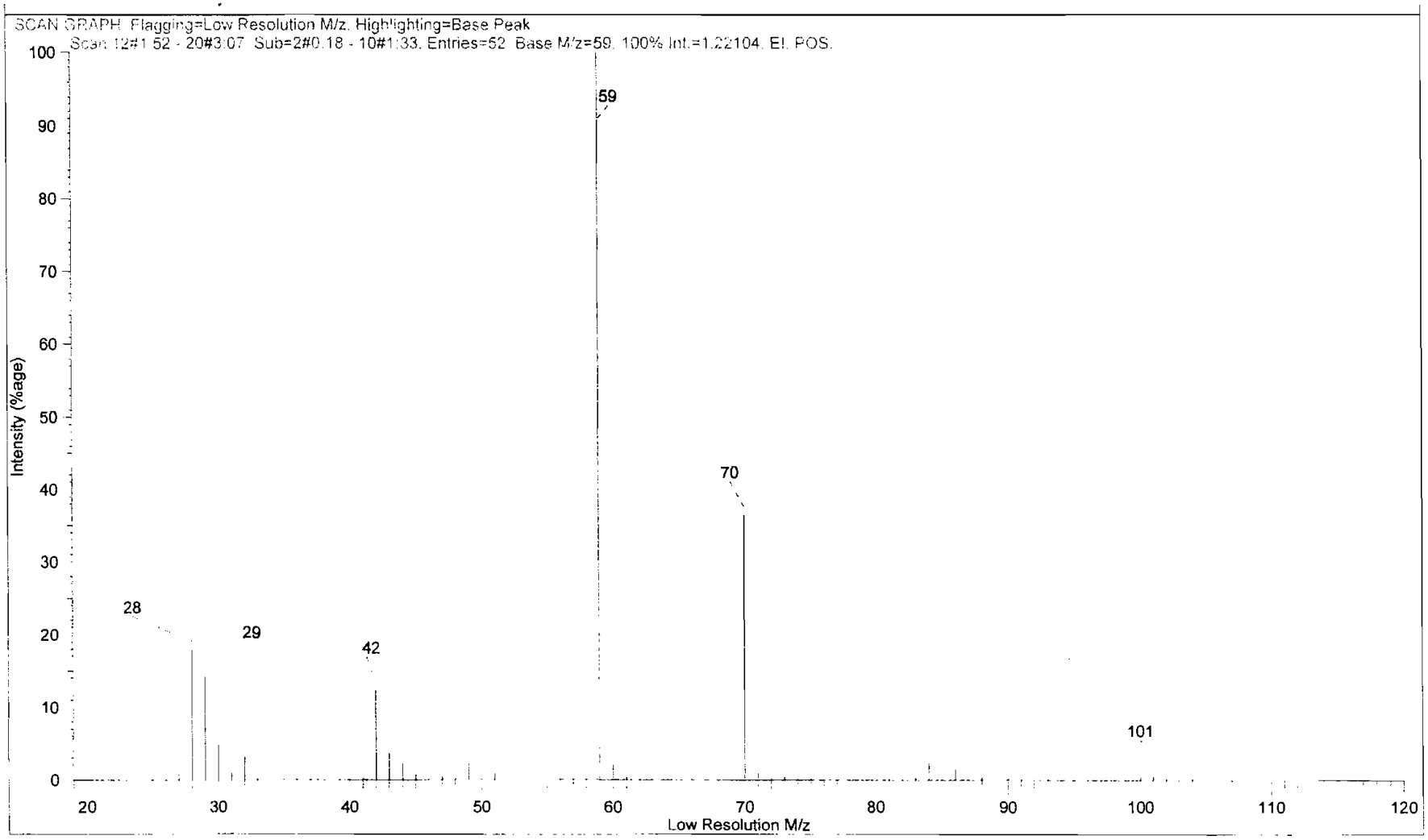

Figure 5.69- The 70 eV electron impact mass spectrum of methyl-azidoformate

^{1}H- and ^{13}C-NMR spectroscopy: in the 300 MHz ^{1}H-NMR spectrum, recorded in $CDCl_3$ solution and presented in Figure 5.70, only a singlet peak is observed, at 3.83 ppm relative to TMS. It corresponds to the protons on the methyl group. A much weaker peak at 3.76 ppm (roughly intensity ratio 1:130 relative to the one at 3.83 ppm) is due to an impurity- already present in the starting methyl-chloroformate used in the azide preparation- of unknown nature but whose low intensity indicated a very low relative concentration.

In the ^{13}C-NMR spectrum, run in $CDCl_3$ solution, two peaks were observed: a peak at 55.0 ppm is associated with the methyl carbon atom, while the one at 157.9 ppm is assignable to the carbonyl carbon atom. The full spectrum is reported in Figure 5.71.

Infrared spectroscopy: Figure 5.72a presents the IR spectrum of the liquid compound recorded between KBr plates. It shows peaks at 2958 cm^{-1}, assigned to C-H stretching absorptions, strong bands at 1727 cm^{-1} (C=O stretching), 1437 cm^{-1} (C-H scissoring), 1240 cm^{-1} (N-N-C-O stretching), 905 cm^{-1} and 727 cm^{-1}. The band associated with the N_3 group stretching is a very broad, consisting of roughly 5 main components ranging from 2133 to 2256 cm^{-1}.

Similar to the case of ethyl-azidoformate, for methyl-azidoformate the infrared spectrum of the compound in the liquid phase (Figure 5.72b) displays some differences in the intensity distribution of the bands with the one recorded in the N_2 matrix (apart from the expected highest frequencies of the C-H stretching). As was the case for ethyl-azidoformate, the main difference between the spectrum in the liquid phase and in the matrix is the much higher intensity of the band at 1240 cm^{-1} in the matrix with respect to those associated to the azide and carbonyl stretching modes (at around 2150 cm^{-1} and 1730 cm^{-1}). A further analysis of the matrix IR spectrum will be found in the next section, when a comparison with the results of the *ab initio* calculations will be made.

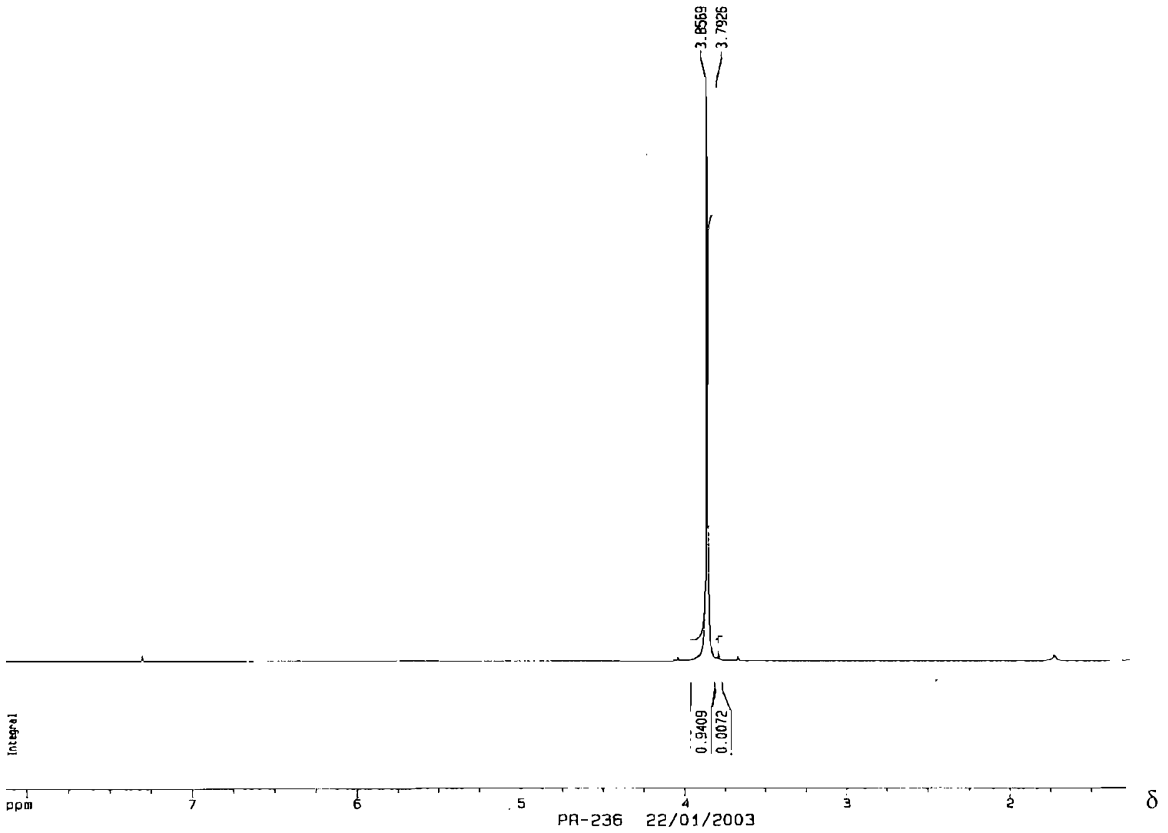

Figure 5.70- The ^{1}H-NMR spectrum of methyl-azidoformate in a $CDCl_3$ solution

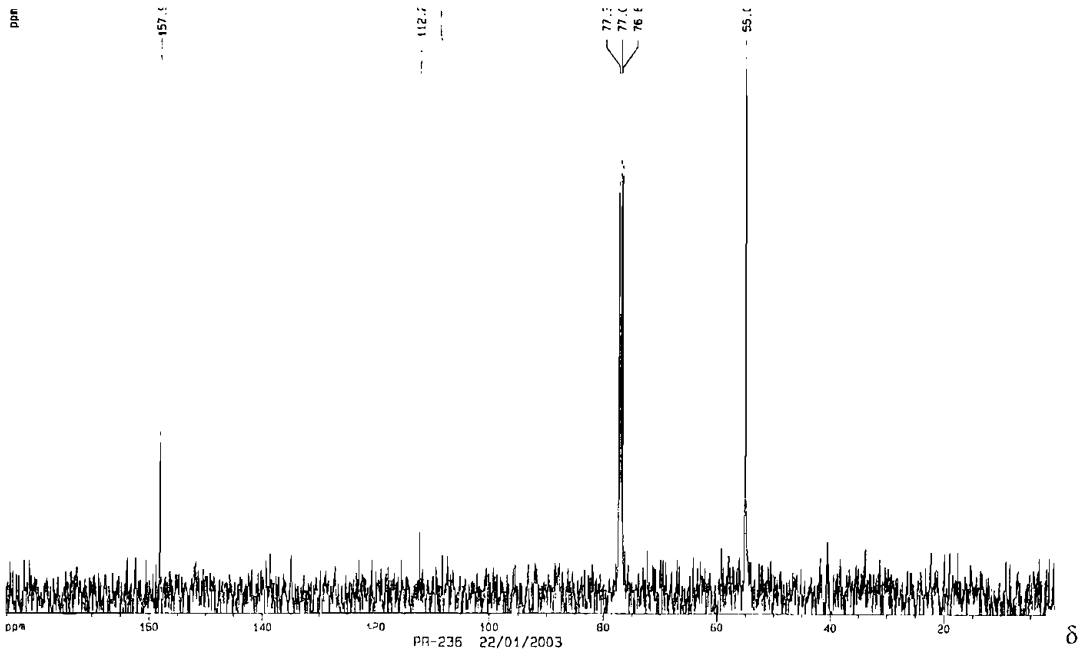

Figure 5.71- The ^{13}C-MR spectrum of methyl-azidoformate in a $CDCl_3$ solution

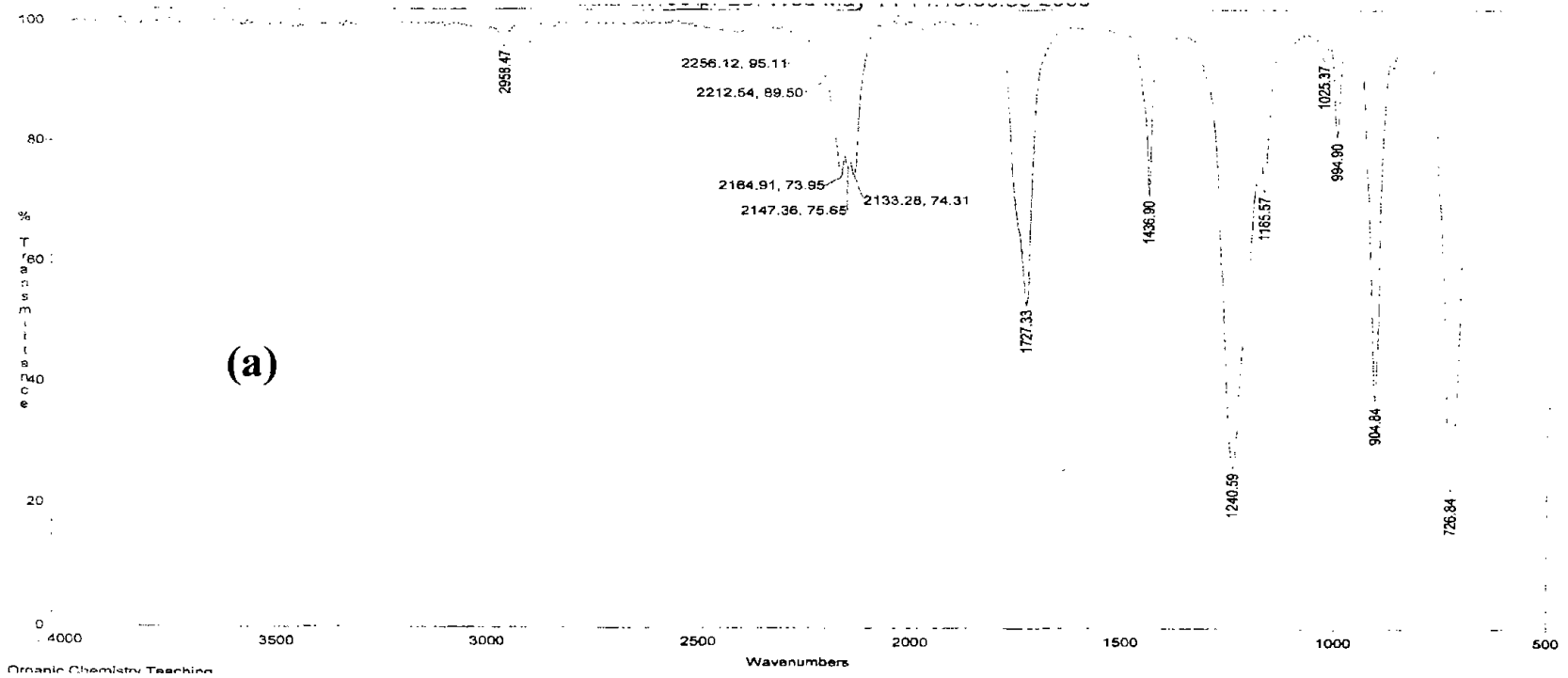

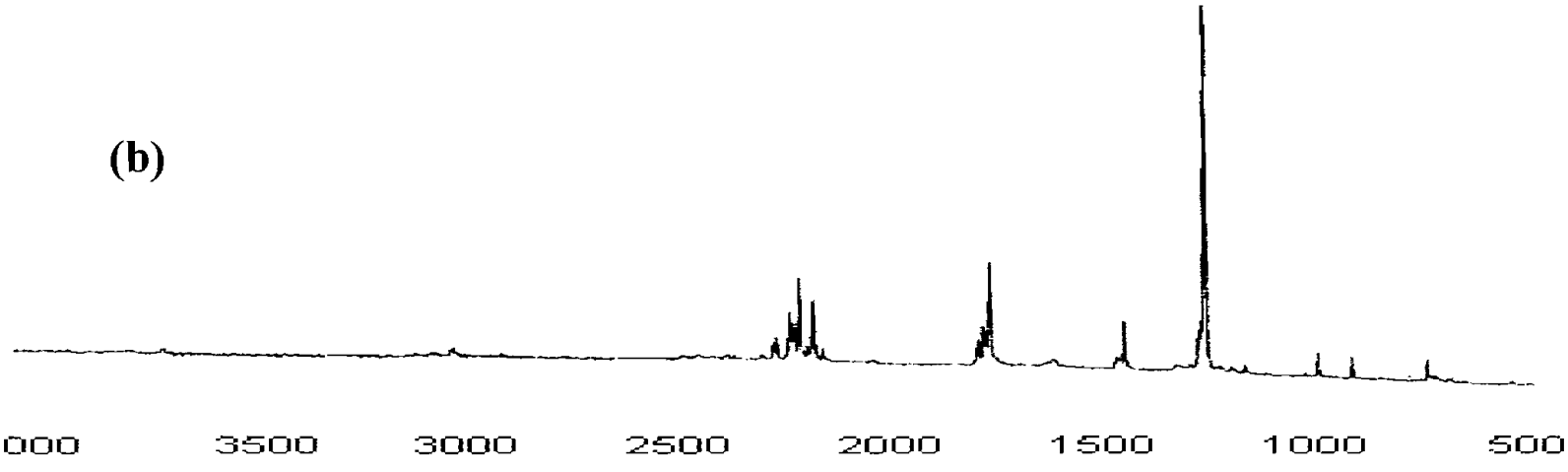

Figure 5.72a- The IR spectrum of methyl-azidoformate recorded (a) in liquid phase between KBr plates and (b) in a nitrogen matrix

Photoelectron spectroscopy

The bands in the methyl-azidoformate photoelectron spectrum (reported in Figure 5.73) were calibrated by averaging the VIEs of the bands calibrated from six different spectra. The results are shown in Table 5.48 (see Figure 5.73 for the labelling of the bands in the spectrum).

Table 5.48- Calibrated vertical ionization energies of methyl-azidoformate- see Figure 5.73 for band labelling

Band	A	B	C	D	E	F	G	H
VIE (eV) ±0.02 eV	*10.85*	*11.59*	*12.83*	*13.51*	*14.37*	*15.43*	*15.93*	*16.40*

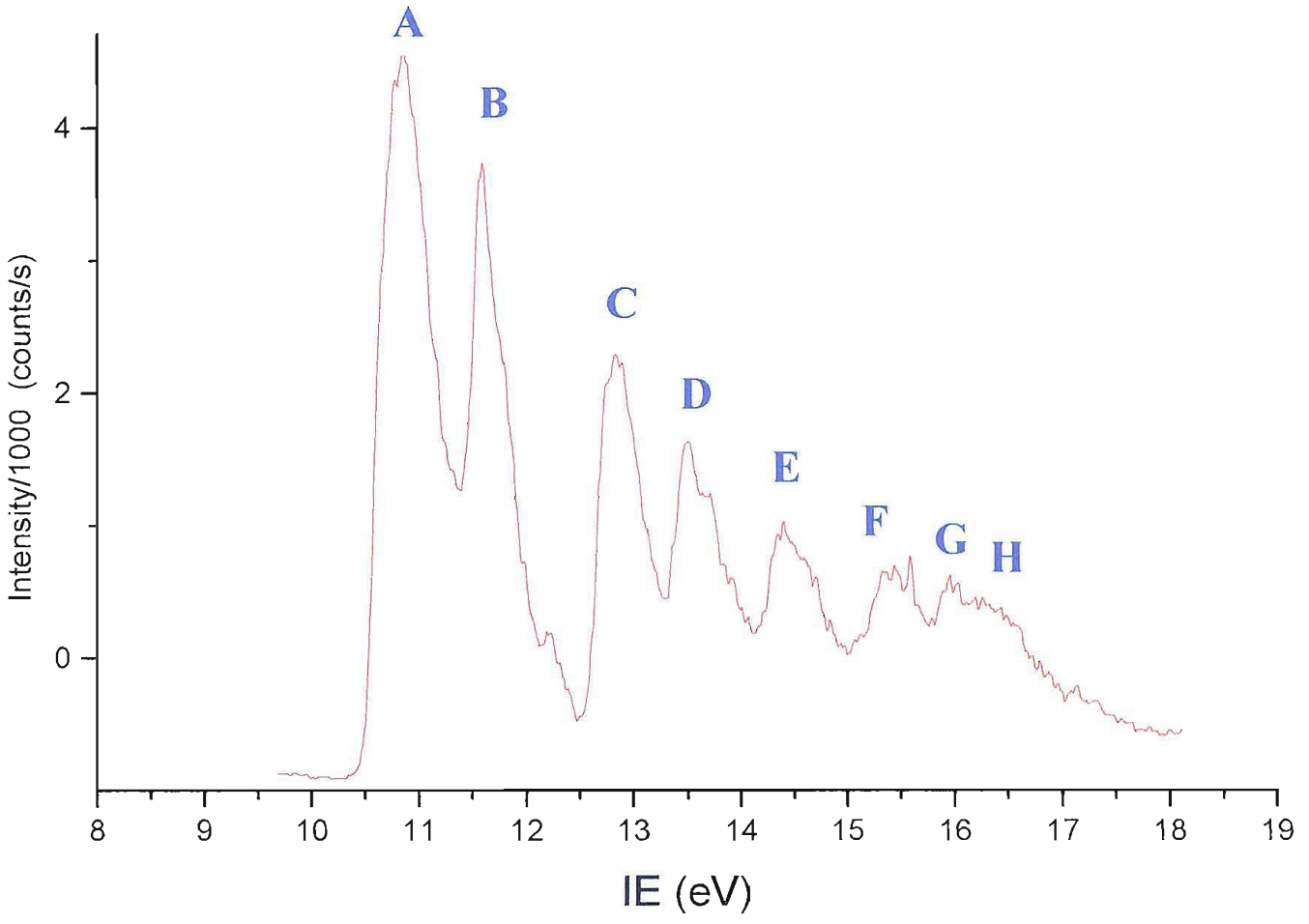

Figure 5.73- HeI- PE spectrum of methyl-azidoformate at room temperature

5.5.3 RESULTS OF MOLECULAR ORBITAL CALCULATIONS

Ab initio calculations have been performed at the MP2/6-31G** level to help the interpretation of photoelectron and infrared spectra, and to establish geometrical, electronic and vibrational characteristics of methyl-azidoformate.

Four minimum energy conformers have been found for N_3COOCH_3 in its closed-shell singlet state, depending on the different relative positions of the carbonyl, methyl and azide groups: they are reported in Figure 5.74. The conformers have been named with a double *cis trans* nomenclature, with the first label referring to the relative position of the azide chain relative to the carbonyl group and with the second label referring to the relative position of the carbonyl and the methyl groups. For example, structure *trans-cis* refers to a structure in which the N_3 chain is *trans* with respect to the C=O group, and the C=O group is in a *cis* position with respect to the terminal CH_3.

The three most stable structures are very close in energy, lying within 4.3 kcal/mol, while structure *trans-trans* lies 12.7 kcal/mol higher in energy with the respect to the most stable one, structure *cis-cis* (see Table 5.49). Structure trans-trans is also the only non-planar one, all the others belonging to the C_s symmetry group. Table 5.50 reports the most important geometrical parameters calculated for the most stable conformer, *cis-cis*, which is shown in detail in Figure 5.75 along with the labelling of the atoms. Table 5.51 reports its first seven VIEs, calculated with Koopmans' theorem, and the first three VIEs calculated with ΔSCF method by calculating the energy of the cation and the neutral at the neutral geometry, and compares them with the experimental VIEs. The agreement is good, especially if the values obtained from Koopmans' theorem are scaled by a 0.92 factor [27, 28]. The ΔSCF values are not particularly reliable because apart from ionization from the third HOMO, the ion states are not purely doublet states but are heavily contaminated by higher multiplicity states (S^2 for a pure doublet state is 0.75).

Because of the small differences in energy between the conformers *cis-cis*, *trans-cis*, and *cis-trans*, it is possible that these three structures all contribute to the experimental gas phase PE spectrum. VIEs have been computed for these structures using Koopmans' theorem and they were found to be very similar.

Figure 5.76 shows the shape of the first five molecular orbitals calculated for the *cis-cis* conformer of methyl-azidoformate at the HF level. The description of the molecular orbitals has been obtained from a single point Hartree-Fock calculation using as geometries those calculated at the MP2 level.

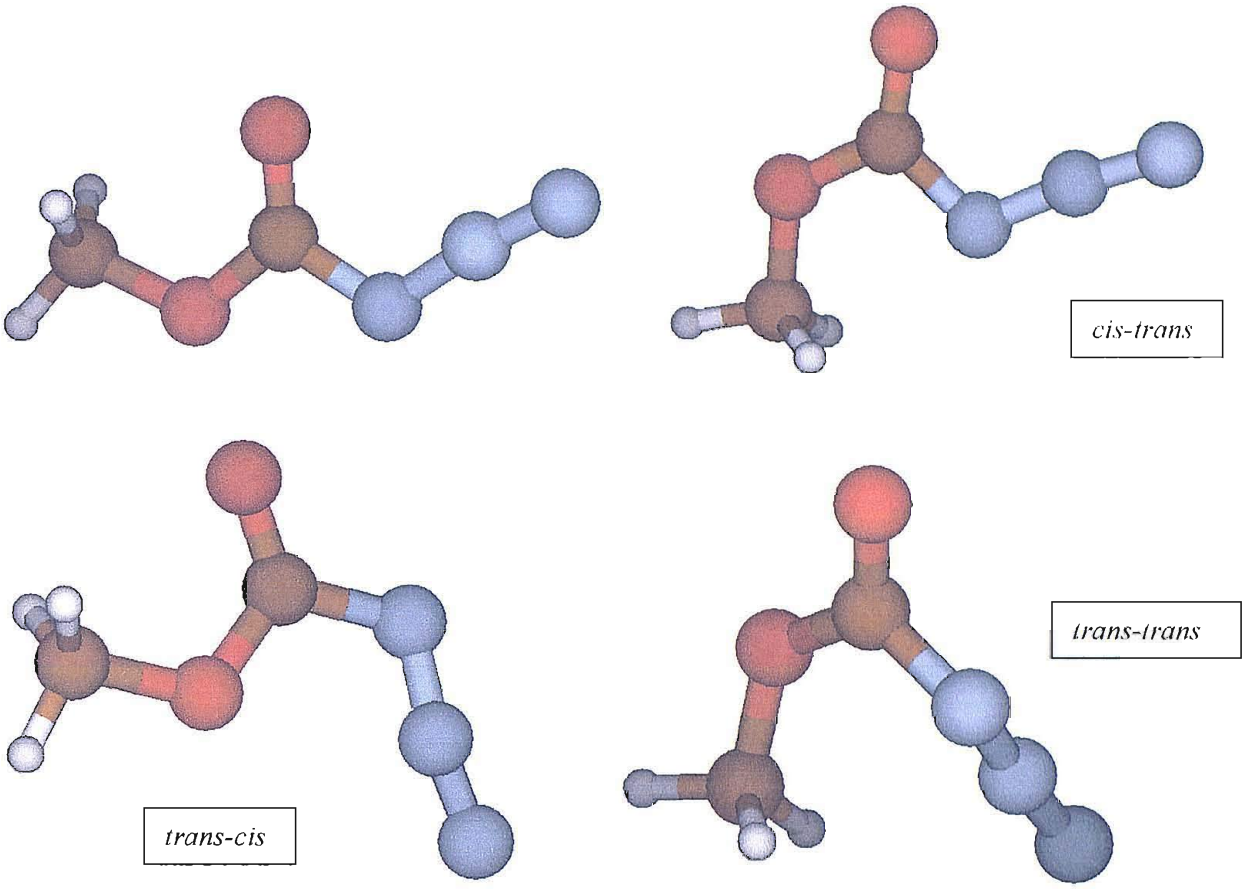

Figure 5.74- The four minimum energy conformers of methyl-azidoformate obtained from *ab initio* calculations at the MP2/6-31G level. The labelling reflects the relative position of the carbonyl group to the azide chain and of the methyl group to the carbonyl group**

Table 5.49- Total and relative energies of the four conformers of methyl-azidoformate at the MP2/6-31G level**

Structure	Total energy (hartrees)	Relative energy (kcal/mol)	Point group
Cis-cis	-391.5979684	0	C_s
Cis-trans	-391.5912249	+4.232	C_s
Trans-trans	-391.5776744	+12.735	C_s
Trans-cis	-391.5960435	+1.208	C_1

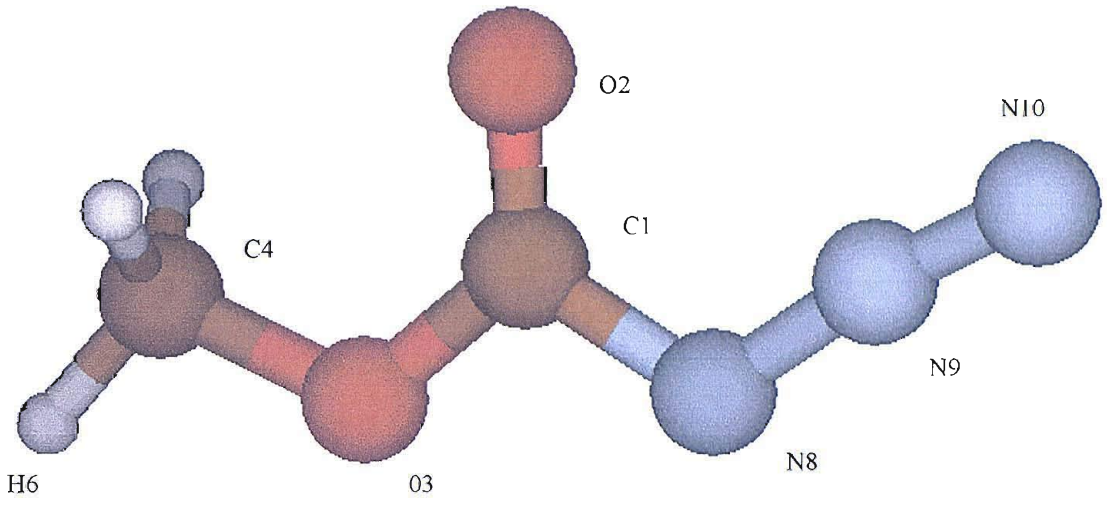

Figure 5.75- Structure *cis-cis* of methyl-azidoformate optimized at the MP2/6-31G level**

Table 5.50- The most relevant geometrical parameters of the lowest energy structure (*cis-cis*) of methyl-azidoformate

Bond	Length (Å)	Angle	Value (°)
N10-N9	1.159	N10-N9-N8	172.32
N9-N8	1.253	N9-N8-C1	113.07
N8-C1	1.419	N8-C1-O2	126.54
C1-O2	1.218	C1-O3-C4	113.22
C1-O3	1.341	O3-C4-H6	104.80
O3-C4	1.443	N10-N9-N8-C1	180.0
C4-H6	1.084	N9-N8-C1-O3	180.0
		O2-C1-O3-C4	0.0

Table 5.51- Experimental and computed VIEs of *cis-cis* methyl-azidoformate

KT calculated VIE (eV)	KT calculated VIE · 0.92 (eV)	ΔSCF calculated VIE (eV)	S^2 for the ion	Experimental VIE (eV)	Band
11.45	10.53	10.96	1.027	10.85	A
12.40	11.41	12.91	1.022	11.59	B
13.06	12.01	11.81	0.790	12.83	C
14.23	13.10			13.51	D
15.08	13.87			14.37	E
15.54	14.30				
16.86	15.51			15.43	F

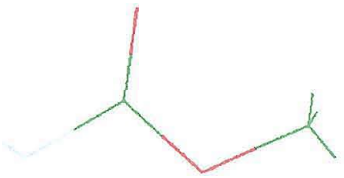

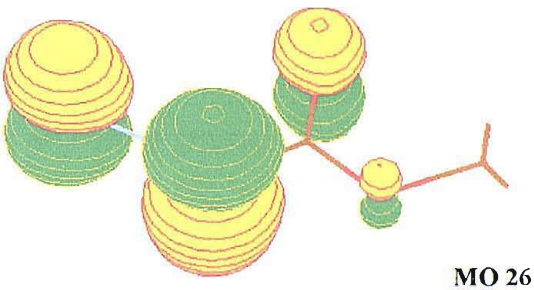

MO 26

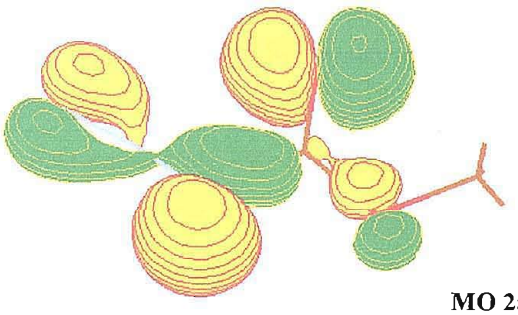

MO 25

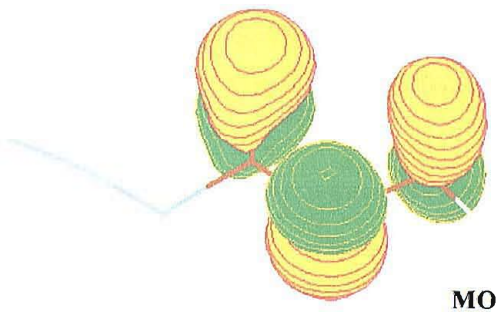

MO 24

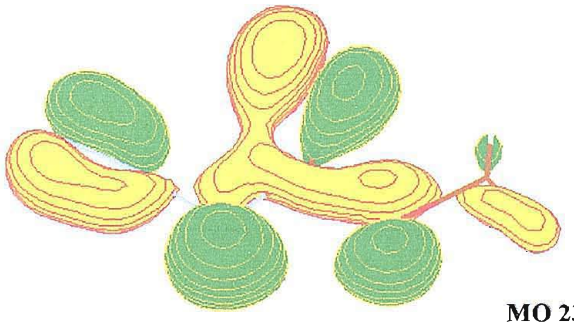

MO 23

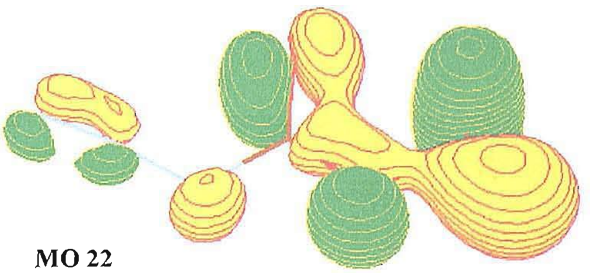

MO 22

Figure 5.76- The five highest occupied molecular orbitals for structure *cis-cis* of methyl-azidoformate as obtained from calculations performed with the Gaussian98 program at the HF/6-31G level. Refer to Figure 5.75 for the identification of the atoms on the skeleton of the molecule, here reported in the top left corner**

Molecular orbital 26 (the HOMO) is a relatively localized orbital with a major p_π-antibonding contribution between the first and third nitrogen atoms of the azide group arising from their lone pairs, and between this latter atom and the carbonyl oxygen. A smaller contribution- still p_π-antibonding in character- comes from the ester oxygen atom.

MO 25 is a more delocalized orbital with mainly p_π-antibonding character (with the nodal planes of the π orbitals perpendicular to the molecular plane) between the first and third nitrogen atoms of the azide chain and along the carbonyl group. Also, p_π-bonding character is shown between the first two nitrogen atoms of the azide chain, and σ-bonding character between the nitrogen of the chain and the adjacent carbon, and between the carbonyl carbon and the ester oxygen.

MO 24 is a very localized orbital with mostly p_π-antibonding character between the methyl carbon, the ester oxygen and the carbonyl group, with a p_π-bonding contribution within the carbonyl group. No contribution arises from the azide chain.

MO 23 is characterized by the p_π-bonding contribution between the terminal nitrogen atoms of the azide chain and along the carbonyl group, and by the σ-bonding system stretching along the N-C-O backbone.

MO 22 is a delocalized orbital with still mainly p_π-bonding character (perpendicular to the molecular plane) along the carbonyl group and σ-bonding along the O-C-O-CH_3 end of the molecule.

MO 21 is dominated by the p_π-bonding contribution of the carbonyl group and the terminal azide nitrogen atoms, and the non-bonding contribution of the methyl carbon atom, all with a nodal plane corresponding to the molecular plane.

In general, the characters of each molecular orbital are very similar between methyl- and ethyl-azidoformate: this is consistent with the very similar VIEs of the PE bands and their distribution. Only the shape of the molecular orbitals are slightly different, in the sense that those of ethyl-azidoformate are more delocalized, and therefore the experimental bands are broader than those of the methyl-equivalent.

Harmonic vibrational frequencies have been calculated for all the conformers at the MP2/6-31G** level by means of second derivatives calculations. Figure 5.77 displays the calculated IR spectra for each structure (with a Gaussian shape assumed for the peaks).

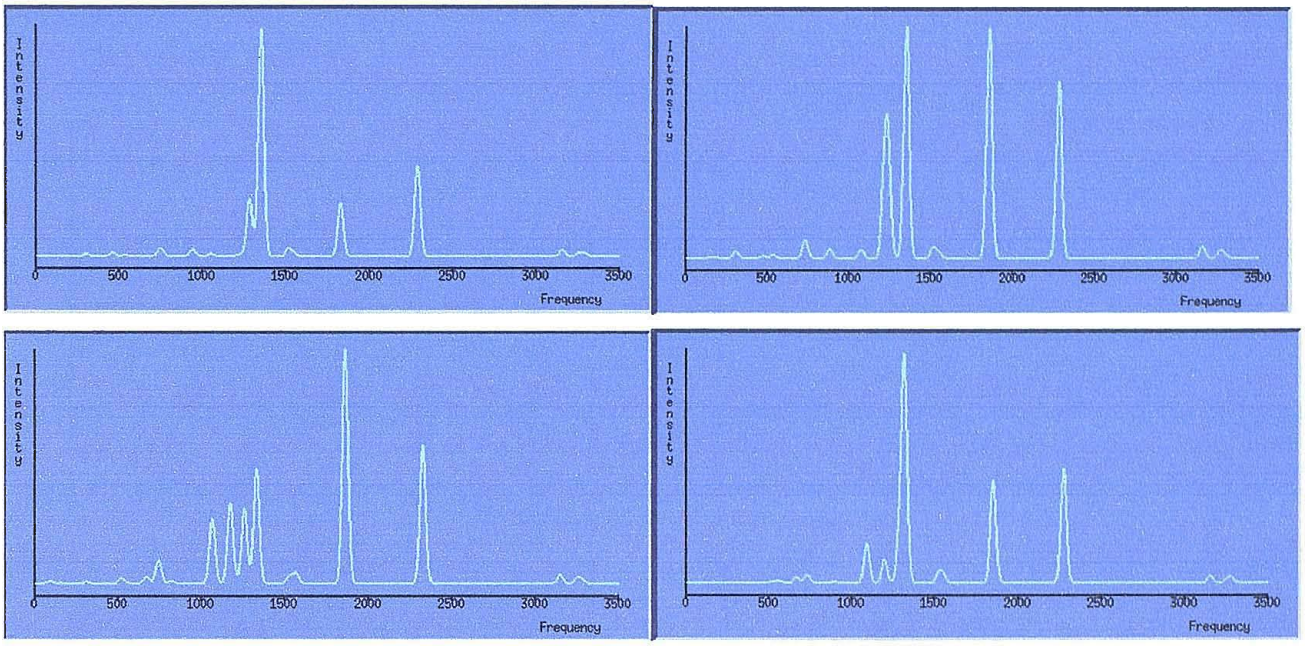

Fig. 5.77- The IR spectra calculated for the four conformers of methyl-azidoformate at the MP2/6-31G level. All the frequencies are reported in cm^{-1}**

The calculated frequencies (listed in Table 5.52) are very similar between the four different conformers but, as was found for ethyl-azidoformate, their intensity distribution shows important differences.

As previously mentioned, the experimental IR spectra in the liquid phase and in the matrix show remarkable differences (see Figure 5.72), especially in the low-frequency region, where all the bands in the liquid phase show higher intensities. Due to the small energy difference between three of the four structures, it is likely that those three structures contribute almost equally to the liquid phase spectrum, which is therefore a sum of the spectra of these structures: the breadth and subdivision of the azide stretching peak around 2150 cm^{-1} seems to support this assumption.

In the matrix, the intensities of all the bands with respect to the band at 1240 cm^{-1} decrease, and the intensity pattern shows a better agreement with the calculated spectrum of structure *cis-cis*. This result is in agreement with the fact that this is the lowest energy conformer. Still, the azide stretching region presents distinct absorptions, which probably indicates the co-presence of more than one conformer trapped in the matrix; in this case, the high intensity of the band at 1240 cm^{-1} is unclear- given that only in structure *cis-cis* is such a feature predicted. As for ethyl-azidoformate, the calculations overestimate the C=O and N-N-N stretching intensities, and underestimate the C-H scissoring and C-N stretching intensities.

Table 5.52- Comparison between experimental liquid phase and the calculated IR bands for the minimum energy conformers of ethyl-azidoformate (absorbances in km/mol reported in brackets; all frequencies are quoted in cm^{-1})

Cis-cis frequencies	*Cis-trans frequencies*	*Trans-cis frequencies*	*Trans-trans frequencies*	*Experimental frequencies*	**Normal mode**
463.4 (13.94)	511.8 (1.84)	475.9 (3.86)	515.9 (7.36)		
538.4 (4.96)	540.2 (5.06)	532.6 (6.82)	543.2 (3.50)		
747.2 (27.24)	570.3 (5.30)	732.8 (26.77)	673.8 (15.84)		
757.0 (9.66)	666.5 (21.26)	734.2 (10.42)	745.0 (52.50)		
941.8 (29.19)	730.6 (29.33	884.0 (18.06)	821.1 (5.99)		
1052.7 (9.06)	891.9 (4.30)	1076.9 (16.31)	1067.3 (142.18)	**905**	
1205.9 (1.41)	1091.2 (135.88)	1205.6 (1.60)	1174.2 (175.84)	**995**	
1233.1 (8.45)	1198.0 (78.94)	1218.7 (180.20)	1203.3 (7.97)		C-H twisting
1283.4 (245.44)	1288.2 (158.06)	1241.4 (185.99)	1259.2 (166.12)	**1166**	C-H in phase wagging
1352.1 (971.68)	1317.4 (754.95)	1350.9 (470.08)	1331.7 (252.57)	**1241**	C-H out of phase wagging
1517.2 (31.49)	1525.3 (34.56)	1515.0 (21.58)	1525.9 (14.22)		$C-H_3$ scissoring
1545.0 (5.94)	1548.7 (5.88)	1543.9 (5.94)	1553.2 (9.34)		C-H out of phase scissoring
1554.8 (6.80)	1553.4 (20.320	1555.7 (7.03)	1570.9 (17.17)	**1437**	C-H in phase scissoring
1828.7 (228.91)	1851.7 (355.96)	1857.2 (464.88)	1862.5 (516.76)	**1727**	C=O stretching
2289.0 (383.22)	2275.5 (395.97)	2282.8 (357.89)	2326.1 (304.58)	**2147**	N-N-N stretching
3156.5 (25.40)	3152.4 (24.05)	3158.8 (22.68)	3148.3 (19.82)	**2958**	C-H asymmetric stretching
3259.8 (15.01)	3258.4 (16.10)	3264.8 (13.61)	3252.4 (12.94)		$C-H_3$ symmetric/ $C-H_2$ asymm. stretching
3293.3 (10.45)	3280.8 (15.41)	3292.7 (8.18)	3279.5 (8.07)		C-H asymmetric stretching

5.5.4 THERMAL DECOMPOSITION EXPERIMENTS

Photoelectron spectroscopy

Figures 5.78-5.80 show PE spectra recorded at increasing temperatures, corresponding roughly to respectively 10%, 50% and 100% of pyrolysis. Figure 5.81 reports a spectrum at higher temperature to show the increasing formation of CO when the temperature is raised well beyond the temperature required for complete azide pyrolysis.

The liberation of nitrogen, which is the first consequence of all azide decompositions, is effective at temperatures as low as 140-150 °C: methyl-azidoformate is the azide with the lowest decomposition temperature among all those considered in this project.

Despite this, the intensity of the nitrogen first band (sharp peak at 15.58 eV, [8]) remains low until the temperatures reach 300 °C, and the intensity of the azide bands remain relatively unchanged: this seems to indicate that despite partial decomposition beginning at low temperatures, it is not until temperatures higher than 300 °C that the azide begins to be appreciably pyrolyzed. The only change in the spectra is the appearance of a weak band at 13.78 eV indicating the formation of CO_2 [8].

The spectra abruptly change when the temperatures reach 300 °C: the change is surprisingly fast in comparison with the very similar spectra obtained for the temperatures between 200 and 300 °C. The azide passes from about 10% to about 50% of pyrolysis in a few tens of degrees, as seen by the change in the band intensities. At temperatures beyond 300 °C, the appearance at almost the same time of two sharp bands- one at 10.88 eV and one at 11.60 eV- and of a structured band centred around 12.50 eV indicate the formation of H_2CO, HNCO and CH_2NH [8, 16, 17]; at this stage, the bands associated with the parent azide are remarkably lower in intensity.

Heating up further, the intensity of the azide bands decrease to zero while those of the products increase, showing that the pyrolysis reaches completeness as the temperature approaches 400 °C.

On going to 500 °C, the only change is an increased production of CO; this is probably due to the decomposition of one of the primary products, HNCO or- most likely- H_2CO.

No clear evidence of other stable products or of reaction intermediates were observed; nevertheless, a shoulder on the low energy side of the first methylimine band (VIE at 10.46 eV) remains present in the temperature range between 400 and 500 °C. The position of this shoulder was calibrated as 9.85 ± 0.05 eV. No explanations can be given for the presence of this shoulder.

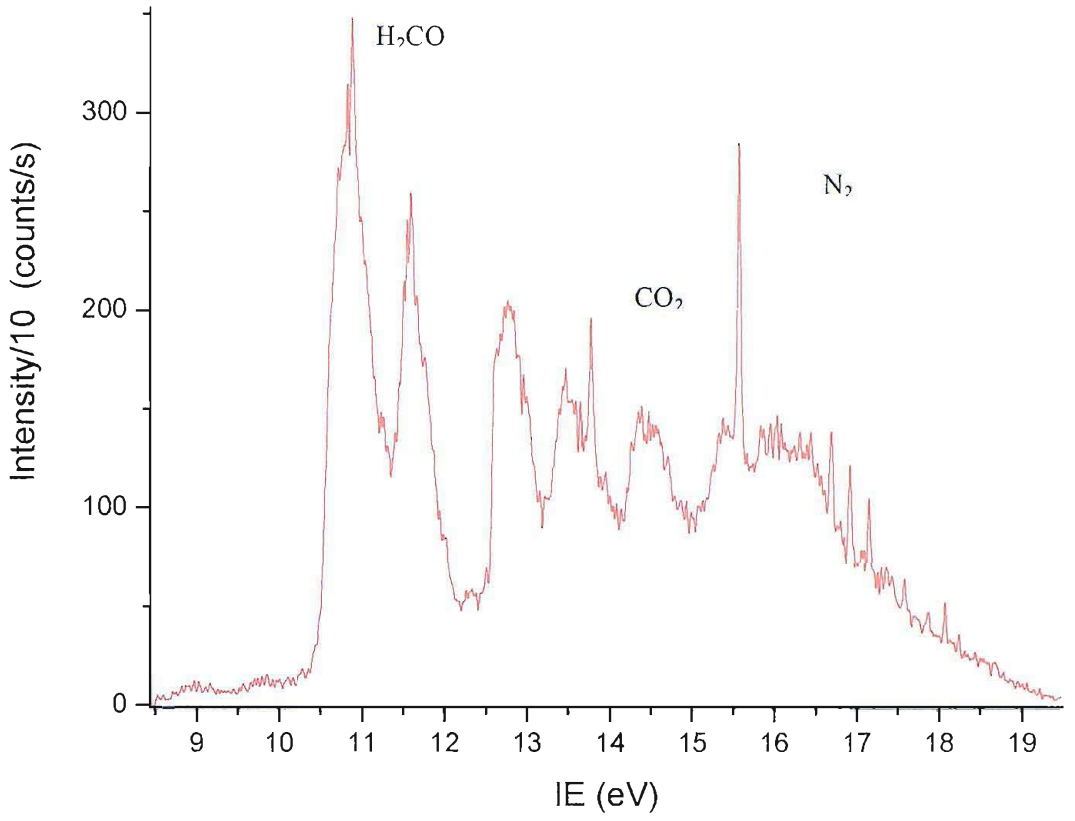

Figure 5.78- HeI PE spectrum of methyl-azidoformate pyrolysis at 170 °C

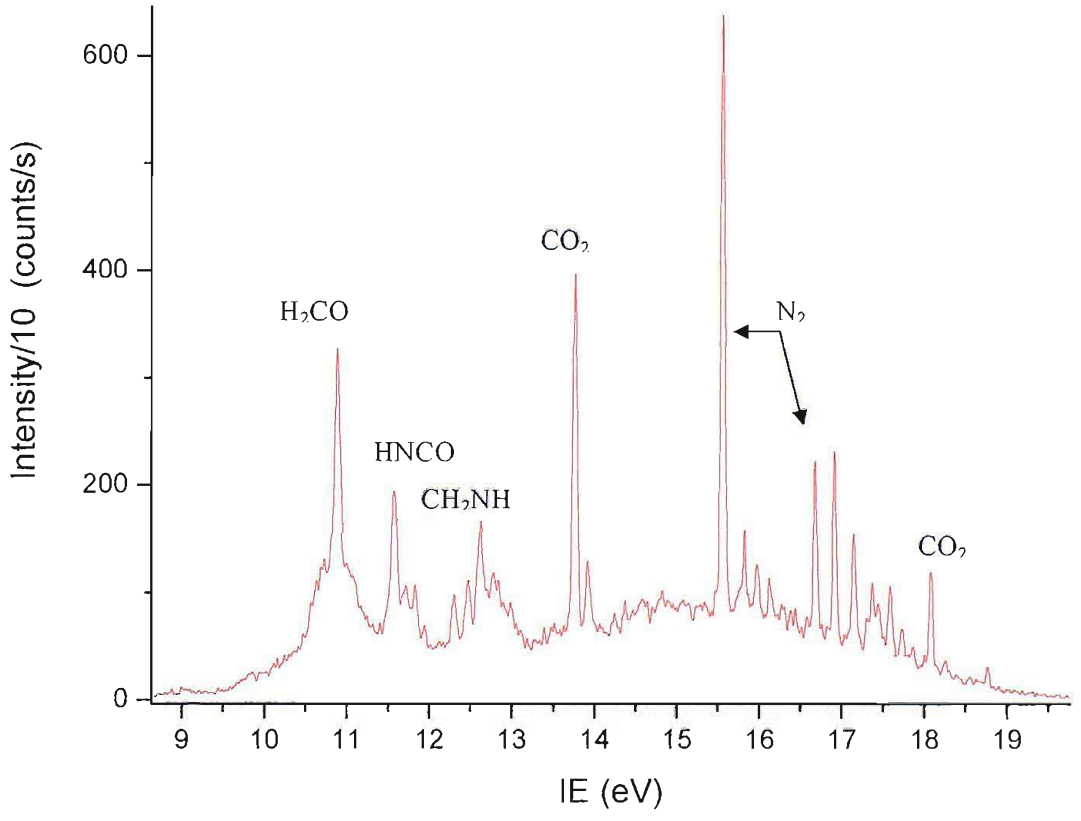

Figure 5.79- Decomposition HeI PE spectrum of methyl-azidoformate at 335 °C

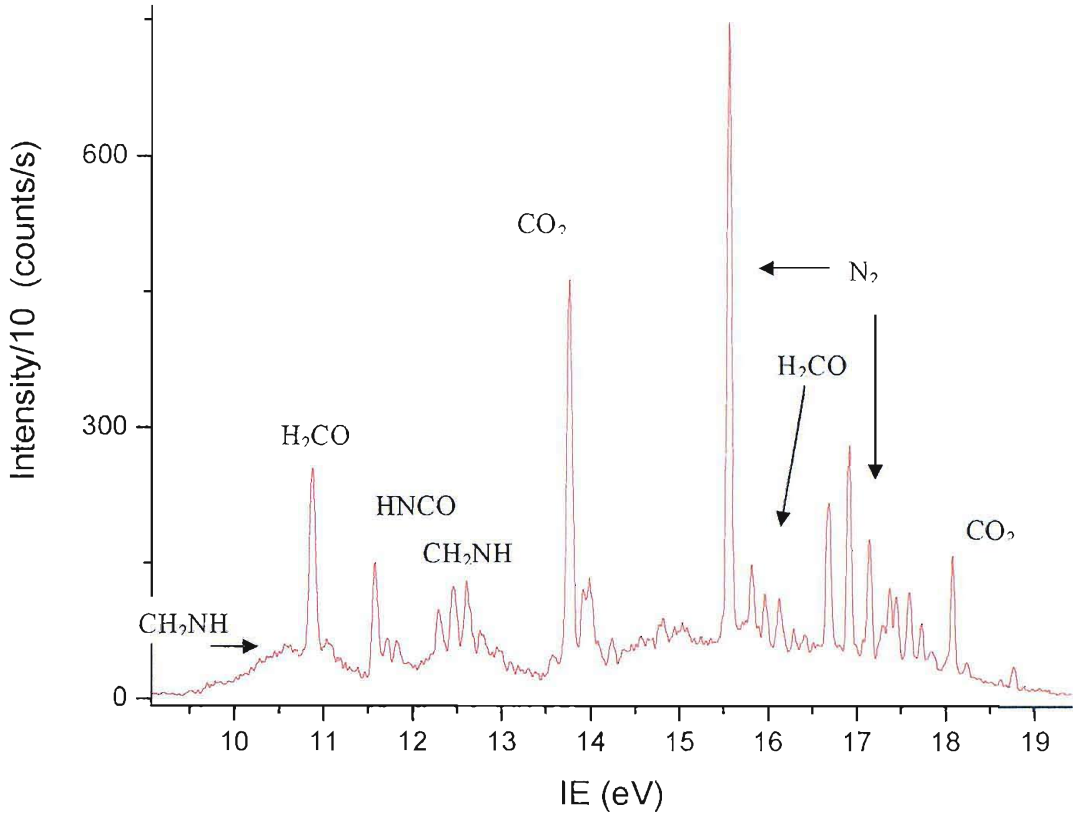

Figure 5.80- Decomposition spectrum of methyl-azidoformate at 420 °C

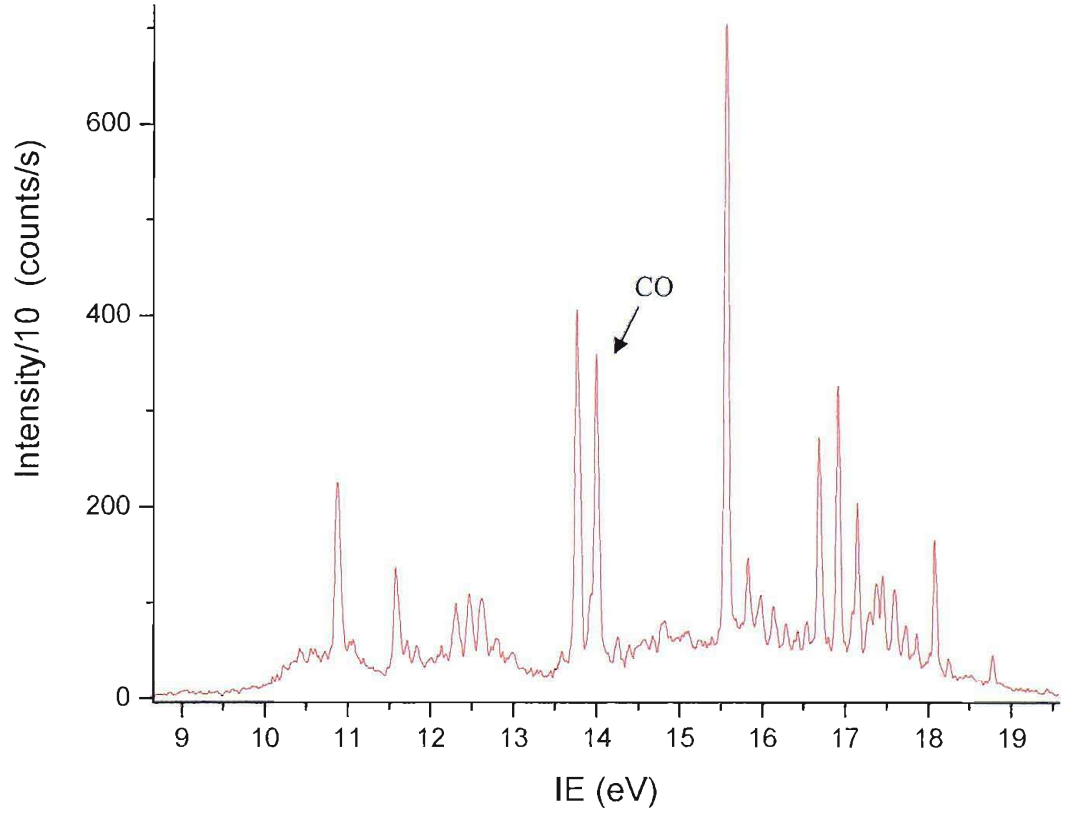

Figure 5.81- Decomposition spectra of methyl-azidoformate at 490 °C

Matrix isolation IR spectroscopy

A comparison of the matrix infrared spectrum of the parent azide with the one obtained when the azide vapours are heated at a temperature around 280°C- and therefore completely decomposed- is reported in Figure 5.82 (it should be noted that the temperature for full decomposition in the matrix experiments is different from that in the PES experiments). Table 5.53 lists the products associated with the labels given to the bands associated with the most intense bands found in the spectrum.

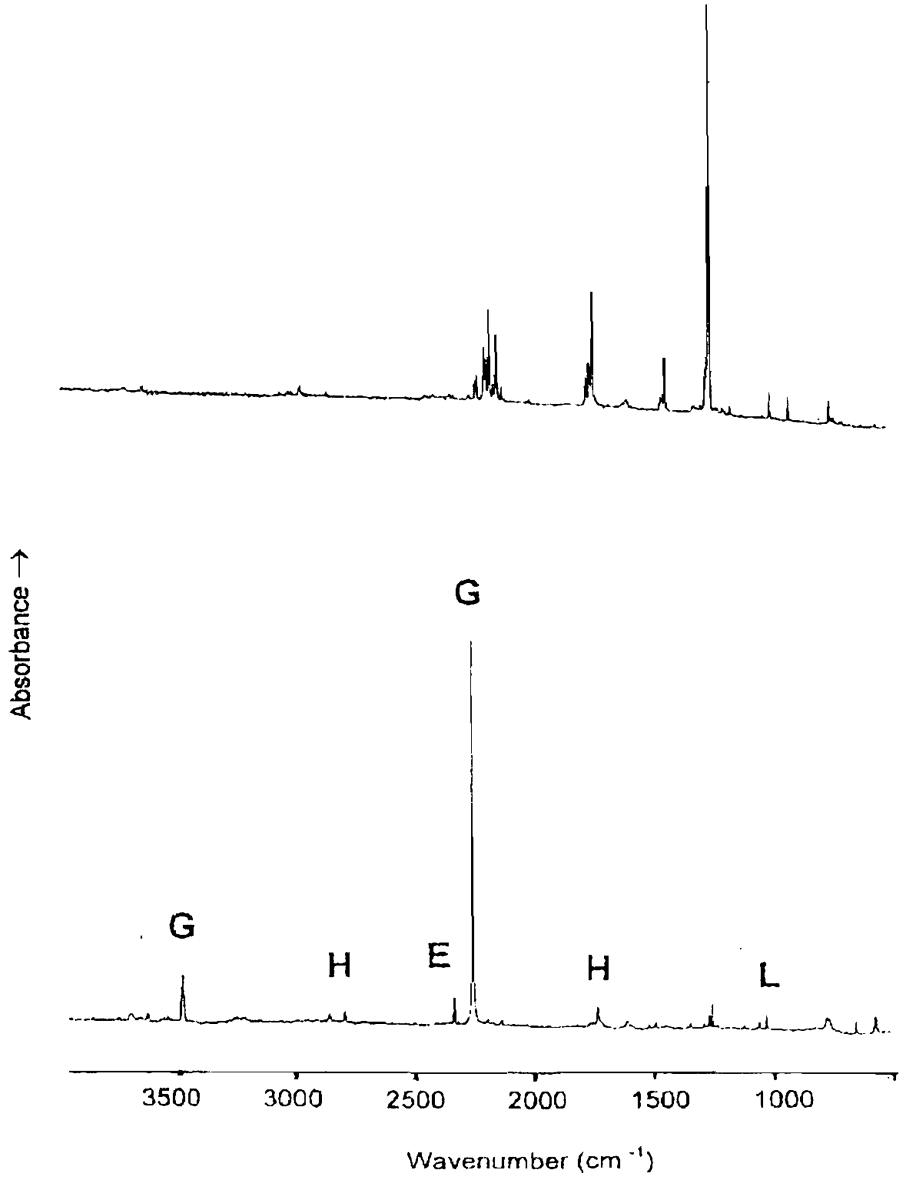

Figure 5.82- IR spectra recorded in a nitrogen matrix for methyl-azidoformate (upper spectrum) and for the vapour obtained on heating at roughly 280 °C when the pyrolysis is complete and only bands of the decomposition products are present

Table 5.53- Labels and assignment of the most significant IR bands observed in the matrix isolation study of methyl-azidoformate thermal decomposition (refer to Figure 5.82 for the labelling of the bands)

Label	*N_2 matrix frequency (cm^{-1})*	*Assignment*	*Reference*
A	2174, 2143, 1743, 1260	**$N_3COOCH_2CH_3$**	
E	2345, 662	**CO_2**	[31]
G	3483, 2265, 780, 581	**HNCO**	[19]
H	2864, 2799, 1739, 1497	**HCHO**	[33]
L	1352, 1127, 1065	**CH_2NH**	[22]

The beginning of the pyrolysis is marked by the appearance of the band at 2265 cm^{-1}- assigned to HNCO [19]- at around 160 °C.

As was observed for ethyl-azidoformate, methyl-azidoformate decomposes without formation of any observable intermediate, so that only the spectra at 0% and 100% degree of pyrolysis are reported. All the bands associated with decomposition products increase steadily in intensity with the increase in temperature, as can be seen for the bands at 2265 and 3483 cm^{-1} (labelled G in Figure 13), 2345 cm^{-1} (labelled E), 2799 and 1739 cm^{-1} (labelled H), and 1065 cm^{-1} (labelled L); they have been respectively assigned- by referring to previous matrix IR studies- to HNCO, CO_2, CH_2NH, and HCHO [19, 22, 31, 33]. Their relative intensity ratio is not altered by changing pyrolysis temperatures, deposition times or other experimental parameters.

The only band showing a slightly different behaviour is the weak one at around 2140 cm^{-1} (not labelled in spectrum b in Figure 5.82): it is assigned to CO [21], and it starts to be observed at higher temperatures than the bands associated with the other decomposition products, and its intensity keeps increasing at high temperatures, when the intensities of the other bands are roughly constant. Carbon monoxide is therefore a secondary product arising either from a minor decomposition route or from partial decomposition of one of the primary products- most likely formaldehyde.

5.5.5 SUGGESTED MECHANISM OF GAS-PHASE DECOMPOSITION

The combination of the results from UV-PES and matrix isolation IR experimental data on the pyrolysis of methyl-azidoformate show that

- When the thermal decomposition begins, HNCO (in matrix IR) and N_2 (in PES) are observed as the first products to be released (roughly 150- 160 °C)
- CO_2 and HCHO are observed at approximately the same temperature, slightly higher than when nitrogen and isocyanic acid begin to appear (170 °C)
- CH_2NH is observed at slightly higher temperatures than the other set of products, probably because of its lower photoionization cross section and dipole moment than the other molecules: their PE and IR bands are weaker and observable only at higher concentrations in the reaction region, or when the overlapping bands of the azide have almost disappeared
- At higher temperatures –almost 500 °C- bands associated with CO are present in the PE spectra, indicating that a new route is open, or that one of the primary products begins to decompose.
- No clear bands which could be associated with the presence of reaction intermediates were observed

As a general rule for azides, the first step in the decomposition is the formation of nitrogen: no evidence could be found for nitrene formation, even with an extremely short lifetime, or if a concerted rearrangement operates in the molecule with nitrogen release. Following evidence found theoretically for other azides [6, 24] and experimentally for methyl- and ethyl-azide [5, 26], it will be assumed that the route proceeding via a nitrene intermediate

$$N_3COOCH_3 \rightarrow N_2 + :NCOOCH_3$$

is favoured over a concerted mechanism involving breaking of the N-N bond and a rearrangement to produce the decomposition products.

As was the case for ethyl-azidiformate, methyl-azidoformate does not have hydrogen atoms attached to the carbon atom adjacent to the N_3 chain, meaning that no 1,2 hydrogen shift between the carbon and nitrogen atoms is possible when molecular nitrogen is released when the azide decomposes.

The only possibility for isomerization is therefore the Type 2 mechanism in which the electron deficient nitrogen atom attacks a remote site of the molecule, forming a new bond. In contrast to the case of ethyl-azidoformate, there is only one site to which the attack can be directed, the methyl carbon atom.

In this case, the nitrogen atom attacks the γ position to form a four membered ring similar to the one formed in the decomposition of ethyl-azidoformate, but without the additional methyl group on it

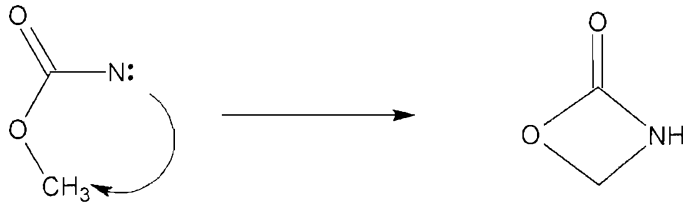

This ring structure was not observed experimentally and no proof of the existence of this four membered ring has been so far reported in the literature; therefore *ab initio* calculations were performed on this molecule to estimate its total energy and understand the role it plays in methyl-azidoformate decomposition. *Ab initio* calculations have been performed on all reactants, nitrenes and products involved in the thermal decomposition of methyl-azidoformate.

5.5.5.1 Results of *ab initio* calculations on methyl-nitreneformate and the cyclic compound

Methyl-nitreneformate

Calculations have been carried out for the nitrene that could be formed from methyl azidoformate after release of molecular nitrogen. Two structures have been optimised for methyl nitreneformate in its singlet spin multiplicity state- according to the possible different mutual dispositions of the methyl group to the carbonyl group- and two structures were optimized for the triplet state, which is the ground state, all of them having real vibrational frequencies. As was the case for ethyl-azidoformate, it was possible to locate minimum energy structures in the singlet spin state at the MP2/6-31G** level, which was not possible for other classes of azides. The explanation for this could be that hydrogen atoms are absent in the α position to the diradical nitrogen -and therefore this prevents one of the possible isomerization routes (Type 1)- and gives the singlet nitrene structures a higher stability.

As happened for ethyl-nitreneformate, the singlet state nitrene geometries differ in energy by just 1.38 kcal/mol, while in the triplet state the difference among the stable conformers is more marked (7.43

kcal/mol). Table 5.54 reports the computed energies for the two singlet and the two triplet structures, indicated with *cis* or *trans* according to the relative orientation of the methylene group with respect to the carbonyl group.

Table 5.54- Energies of the minimum energy conformers of methyl-nitreneformate calculated at the MP2/6-31G level in their singlet and triplet spin multiplicity states**

Structure	*Energy (hartrees)*
Singlet *trans*	-282.2964605
Singlet *cis*	-282.2942641
Triplet *trans*	-282.3099753
Triplet *cis*	-282.2981329

Given the fact that the decomposition path, for spin conservation, will be on a singlet surface, nitrenes in their triplet spin multiplicity state will not be discussed further in this section.

The optimised structures for singlet methyl-nitreneformate are reported in Figure 5.82. Both of them are planar. Also in this case, a minimum energy structure is found with a cyclic C-O-N structure, which in theory should not be attributed to a nitrene structure. Nevertheless, the long N-O bond distance probably indicates an electrostatic interaction between the two atoms more than a truly cyclic structure.

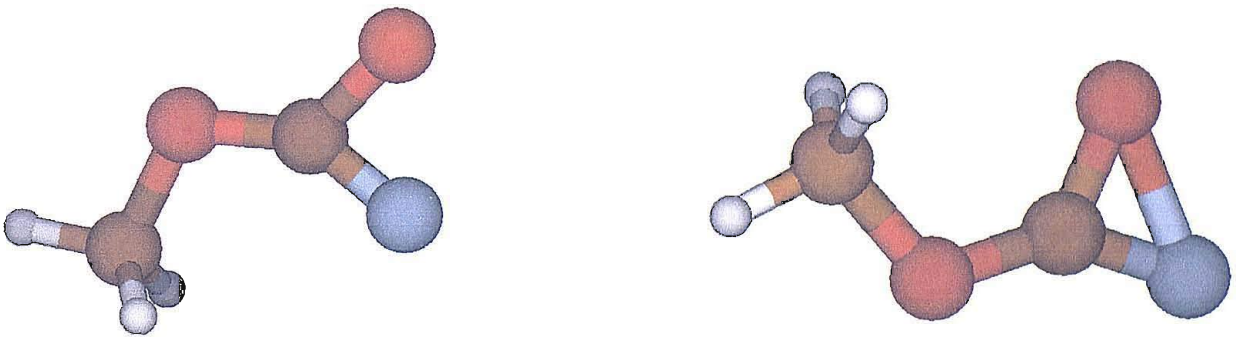

Figure 5.82- Optimized structures of the *trans* (left) and *cis* (right) conformers of the singlet spin state methyl-nitreneformate at MP2/6-31G level**

The energy of the two singlet nitrenes (plus N_2) is around 33 kcal/mol higher than the energy of the azide. This high value, and their well known instability, makes their formation and experimental observation highly unlikely: as a result, their calculated VIEs and infrared bands will not be reported here.

Cyclic product

The hypothesis of the formation of a cyclic molecule was based on the similar structure of methyl- and ethyl-azidoformate, which could therefore display the same decomposition path. This was confirmed by the results of *ab initio* searches for a transition state between the nitrenes and the different sets of products always converged to the ring structure, whose existence is not proved. Calculations were therefore carried out to study the energetic and spectroscopic characteristics of the ring structure to investigate its possible presence as a decomposition product.

The optimized geometry for the cyclic compound is reported in Figure 5.83, and Table 5.55 reports its most important geometrical parameters. It is an almost square ring structure, but with significant out of plane contributions, notably for the hydrogen atoms bonded to the nitrogen atom.

The total energy at the MP2/6-31G** level was computed to be -282.4177495 hartrees.

The first four vertical ionization energies (VIEs)- calculated either by applying Koopmans' theorem to the energies of the molecular orbitals or by the ΔSCF method calculating the energy of the cation and the neutral using the geometry optimized for the neutral molecule at the MP2/6-31G** level- are reported in Table 5.56.

The ΔSCF method alters the ionization energy order, and it dramatically narrows the interval spanned by the bands: this effect is probably intrinsic in this method when applied to this type of cyclic structures, as was pointed out in the discussion on the calculations on the cyclic compounds in ethyl-azidoformate decomposition (see section 5.3.5.1). The exceeding narrow differences in the computed VIEs lead to the conclusion that the results of ΔSCF calculations are unreliable for calculating the experimental VIEs, even if for all the ionization the S^2 value is 0.75 and therefore no contamination by spin states higher than the doublet are present in the doublet ionic states considered.

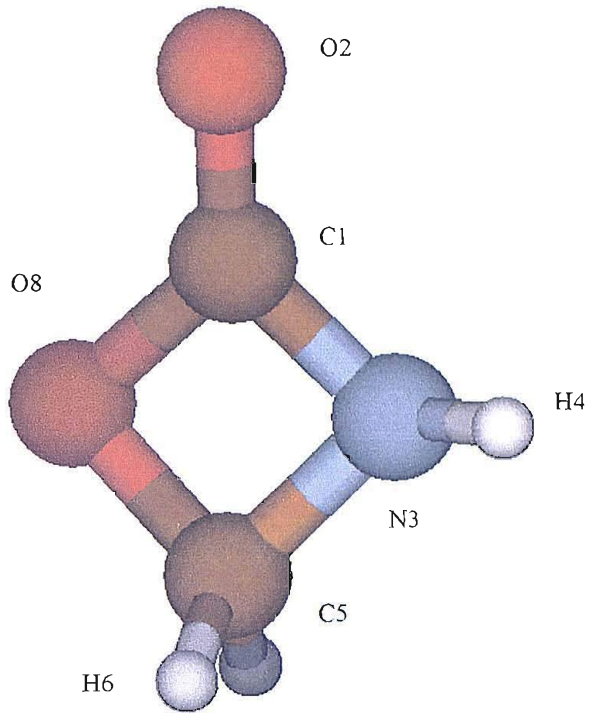

Figure 5.83- Optimized structure of the four-membered ring intermediate in the methyl-azidoformate decomposition

Table 5.55- The most significant geometrical parameters calculated for the four-membered ring intermediate at the MP2/6-31G level**

Bond	*Length (Å)*	*Angle*	*Value (°)*	*Dihedral angle*	*Value (°)*
C1-O2	1.200	N3-C1-O2	136.06	C5-N3-C1-O2	173.5
C1-N3	1.402	C1-O8-C5	88.07	C1-N3-C5-O8	6.9
N3-H4	1.011	O8-C5-N3	89.43	H4-N3-C5-O8	134.3
N3-C5	1.458	N3-C1-O8	93.92	H6-C5-O8-C1	110.6
C5-H6	1.090	H6-C5-O8	111.47		
C5-O8	1.452	H4-N3-C1	121.47		
C1-O8	1.399				

Table 5.56- Vertical ionization energies obtained by Koopmans' theorem applied to the molecular orbitals obtained at the MP2/6-31G level for the four membered ring intermediate**

Ionization	*KT calculated VIE (eV)*	*0.92* KT calculated VIE (eV)*	*ΔSCF calculated VIE (eV)*
$(19a')^{-1}$	11.85	10.90	11.21
$(18a')^{-1}$	12.80	11.77	11.94
$(17a')^{-1}$	13.66	12.57	11.31
$(16a')^{-1}$	15.51	14.27	11.16
$(15a')^{-1}$	15.81	14.55	
$(14a')^{-1}$	16.38	15.07	

The experimental PE spectra show no trace of an intermediate band formed, or bands associated with molecules other than N_2, CO_2, HNCO, CH_2NH and HCHO. The only unclear evidence is the broad shoulder on the low energy side of the CH_2NH first band: this broad shoulder is roughly centred at 9.85 eV. Whatever the calculation method, this experimental value is too low in comparison to the computed first VIE of the four-membered cyclic compound, whose first band should be expected to be close to 11.0 eV. No confirmation of such a molecule can therefore be found from PES. No explanation for the shoulder at 9.85 eV has been found, if it is not actually part of the structure of the methylimine first band (e.g. vibrationally excited CH_2=NH). In these experiments no measurements on pure methylimine have been performed, so that the knowledge of its PE spectum is just based on literature spectra [4] in which the quality of the graphic representation of the bands is quite poor, therefore allowing a certain degree of uncertainty in the exact shape of the experimental bands.

The calculated harmonic vibrational frequencies obtained by second derivative calculations are listed in Table 5.57, while the full IR spectrum is presented in Figure 5.84 (with Gaussian envelopes for the bands).

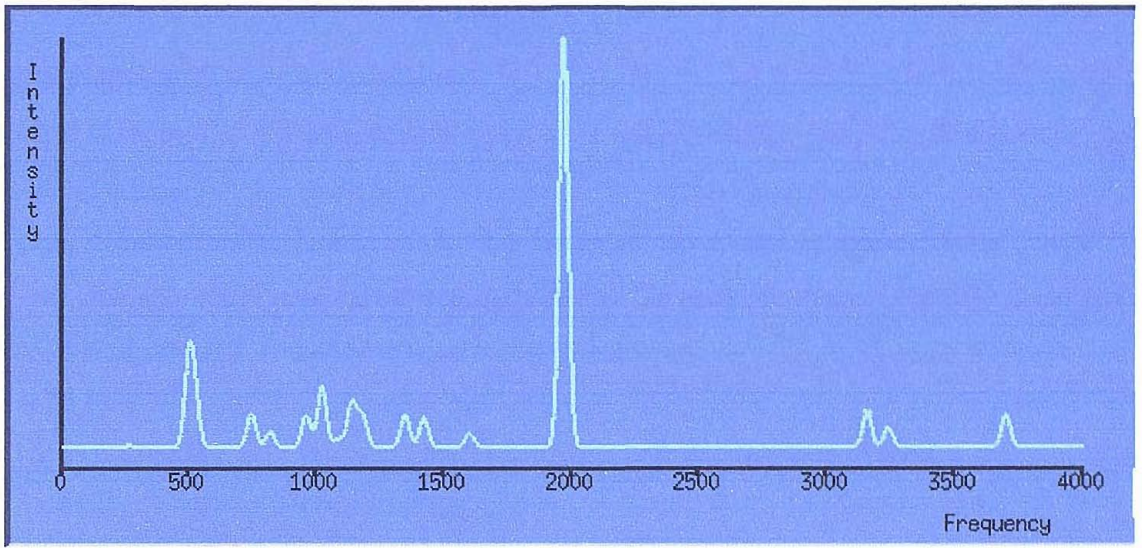

Figure 5.84- Calculated infrared spectrum of the four membered ring intermediate at the MP2/6-31G level**

Table 5.57- Calculated vibrational frequencies for the four-membered intermediate at the MP2/6-31G level**

Frequency (cm^{-1})	*Absorbance* (km/mol)	*Frequency* (cm^{-1})	*Absorbance* (km/mol)	**Normal mode**
501.5	113.44	1348.1	44.07	N-H bending
525.6	64.46	1422.2	39.99	C-H wagging
746.0	46.14	1601.3	18.10	C-H scissoring
819.2	20.86	1968.8	552.97	C=O stretching
960.9	43.64	3158.3	45.72	C-H symmetrical stretching
1022.4	80.93	3240.7	25.94	C-H asymmetrical stretching
1086.1	11.83	3699.2	42.30	N-H stretching
1136.4	47.20			
1152.3	19.50			
1182.4	41.44			

By comparing the vibrational frequencies of the cyclic compound with those obtained for 2-oxazolidone, it is expected that the most intense band for the four-membered ring would be experimentally detected around 1850 cm^{-1}; however, the experimental IR spectra do not display any clearly detectable band in that region. Therefore, no evidence could be found from the matrix IR

spectra to support the formation of the four-membered structure: it is possible that, despite the predicted stability, its lifetime is very short.

As was the case in the thermal decomposition of ethyl-azidoformate, the four-membered cyclic structure is a suitable precursor for the formation of the observed products, and this explains the fact that it is not observed as an intermediate. The two sets of products experimentally detected, CO_2 + CH_2NH and HNCO + HCHO, are produced by breaking the opposite sides of the pseudo-square.

In one case the mechanism (labelled A) can be represented as

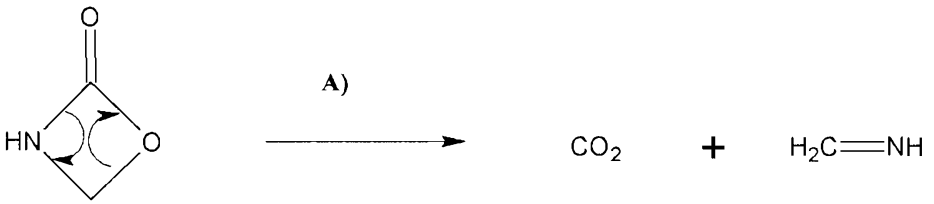

In the alternative case, the scheme (labelled B) is

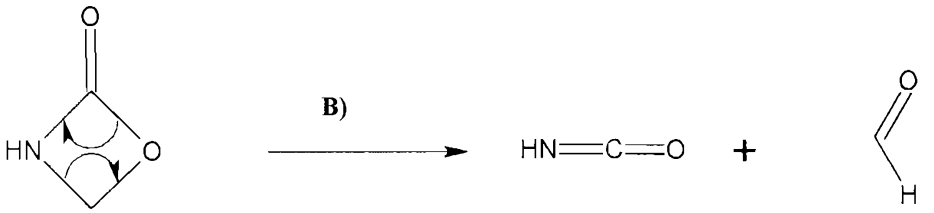

Therefore, the formation of the four-membered ring as an intermediate explains the formation of all the products. The two mechanisms appear to be open at the same time, and given the temperature dependence of all bands, no change in the relative amounts of products from paths A) and B) is observed. A determination of which of the two channels contributes more to the decomposition mechanism is difficult because no precise data on the relative PES and IR cross sections for the products are available: this prevents obtaining the relative concentration of a molecule from its band intensities in the spectra. The two mechanisms, however, seem to operating roughly to the same degree, even if the channel producing carbon monoxide should be more energetically favoured (see following paragraphs).

The overall mechanism, assuming that the nitrene is actually formed, can be therefore represented as in Figure 5.85.

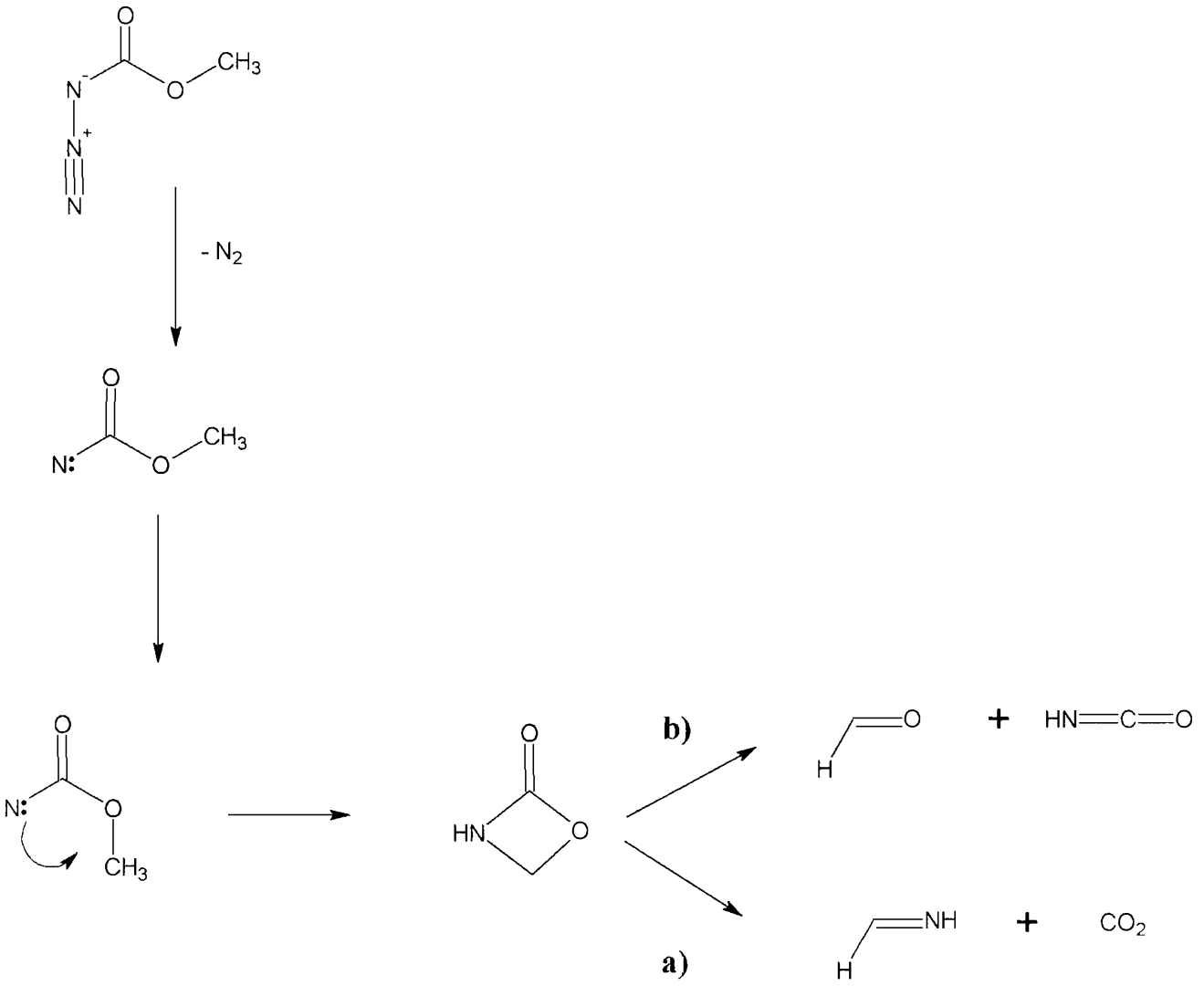

Figure 5.85- Proposed decomposition scheme for methyl azidoformate

The preference for the assumption that the nitrene is actually formed- even if with a very short lifetime- arises from the fact that *ab initio* calculations locate a transition state for forming the cyclic structures only from the nitrene; this is exactly what was found for ethyl-azidoformate. All the calculations carried out to find a transition state between the azide and the two cyclic intermediates (with a concerted mechanism involving the release of nitrogen and the closure of the ring) did not converge to an appropriate structure. From these results, the cyclic intermediates are likely to be preferably formed via the formation of the nitrenes.

In the same way, it was not possible to locate a valid transition state for the direct nitrene → products route: this confirms that even if not detected experimentally the four-membered ring is crucial for the production of the smaller decomposition products, as they are not formed directly from the nitrene.

The 0 K energy level diagram for the stepwise mechanism is reported in Figure 5.86. To take into account the contribution of zero point energy, of thermal energy and of entropy (important especially for the formation of the final products) a free energy diagram at 298 K is reported in Figure 5.87. In both cases the zero is set to correspond with the energy of the most stable conformer of methyl-azidoformate.

The geometries of the transition states found in the calculations- and reported in the energy level diagram- are shown in Figure 5.88.

When the contribution of entropy is considered, the effect is- as expected- a lowering of the relative energy of the final products in comparison to the energy of the cyclic structure, which in turn is lowered with respect to the azide. According to ΔG^{298}, the energies of both the two sets of products arising from the four-membered ring are lower than those of the cyclic structure itself: this explains why they are observed and the four-membered ring is not. Despite the marked difference in energy, the two sets of products CO_2+CH_3CHNH and HNCO+CH_3CHO are formed via transition states differing only by less than 4 kcal/mol, which confirms the fact that the two sets are experimentally observed and with an approximate constant molar ratio with increasing temperatures.

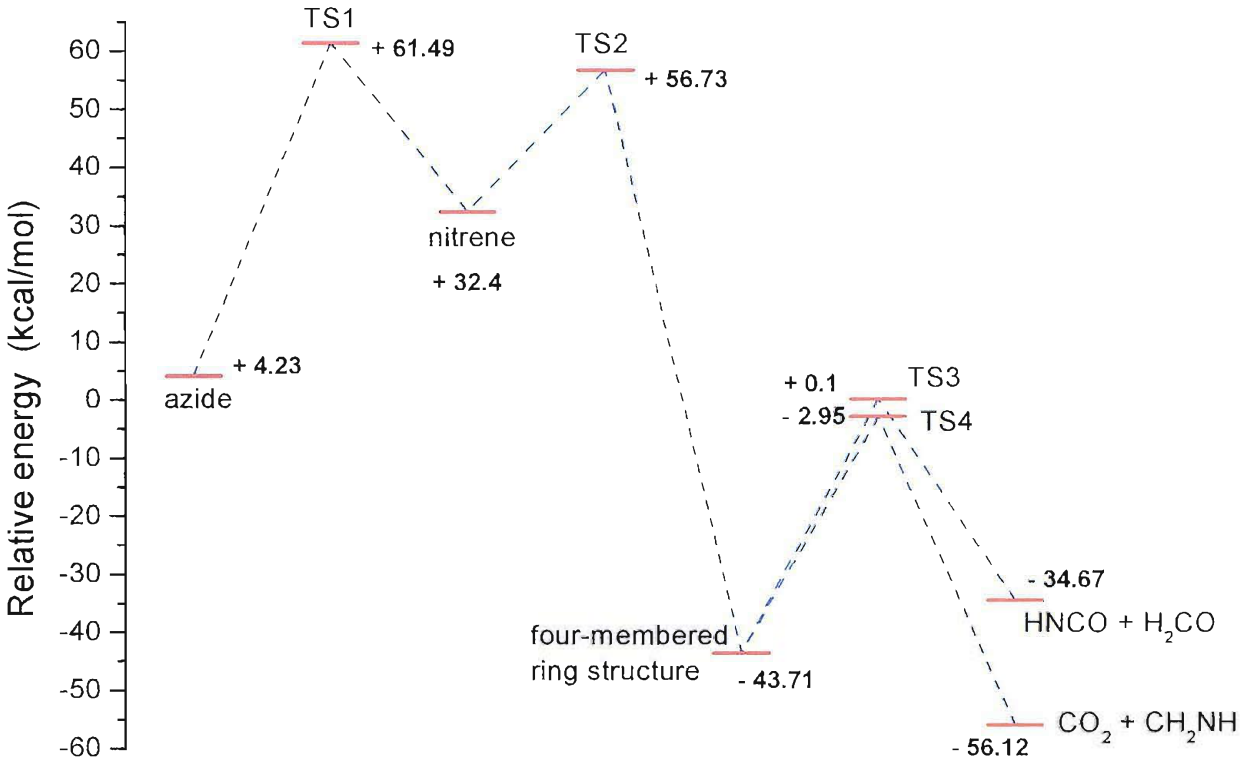

Figure 5.86- Energy diagram at 0 K for the decomposition of methyl-azidoformate calculated at the MP2/6-31G level. The zero value is set for the most stable azide conformer**

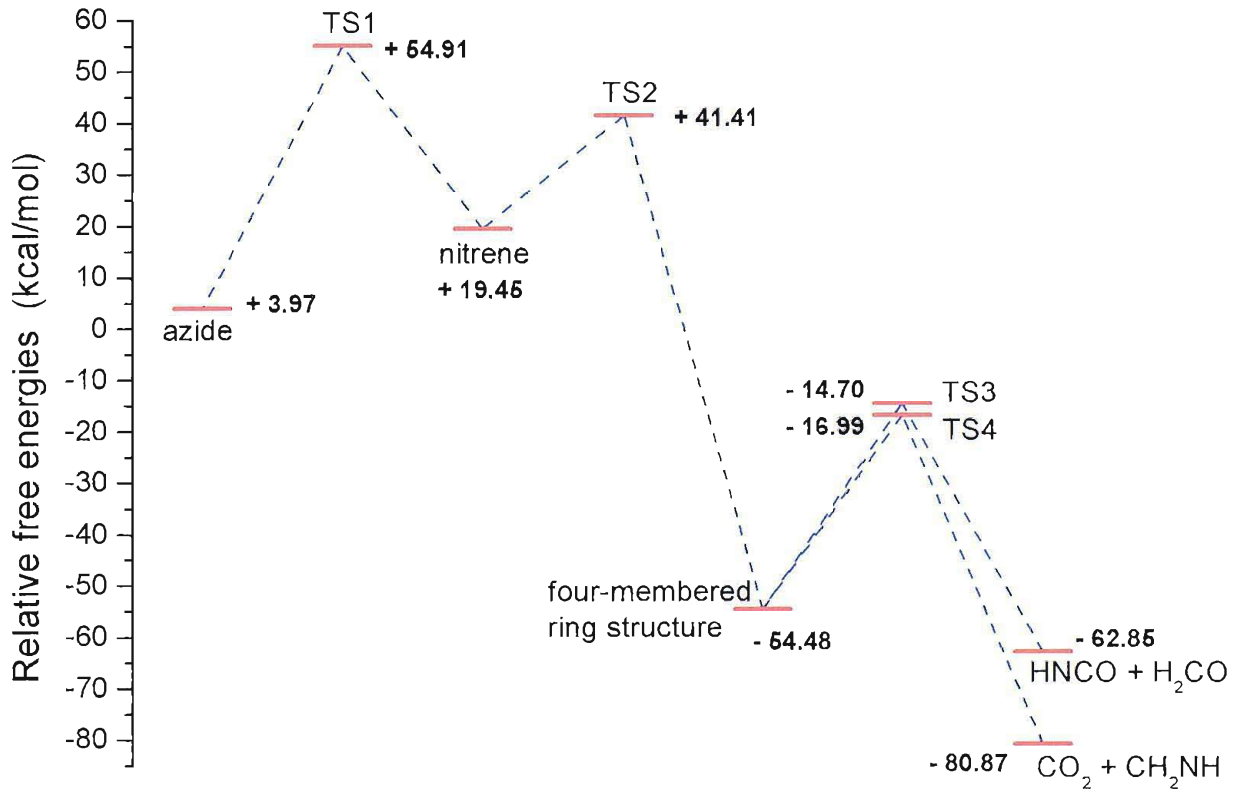

Figure 5.87- Free energy diagram at 298 K for the decomposition of methyl-azidoformate calculated at the MP2/6-31G level. The zero value is set for the most stable azide conformer**

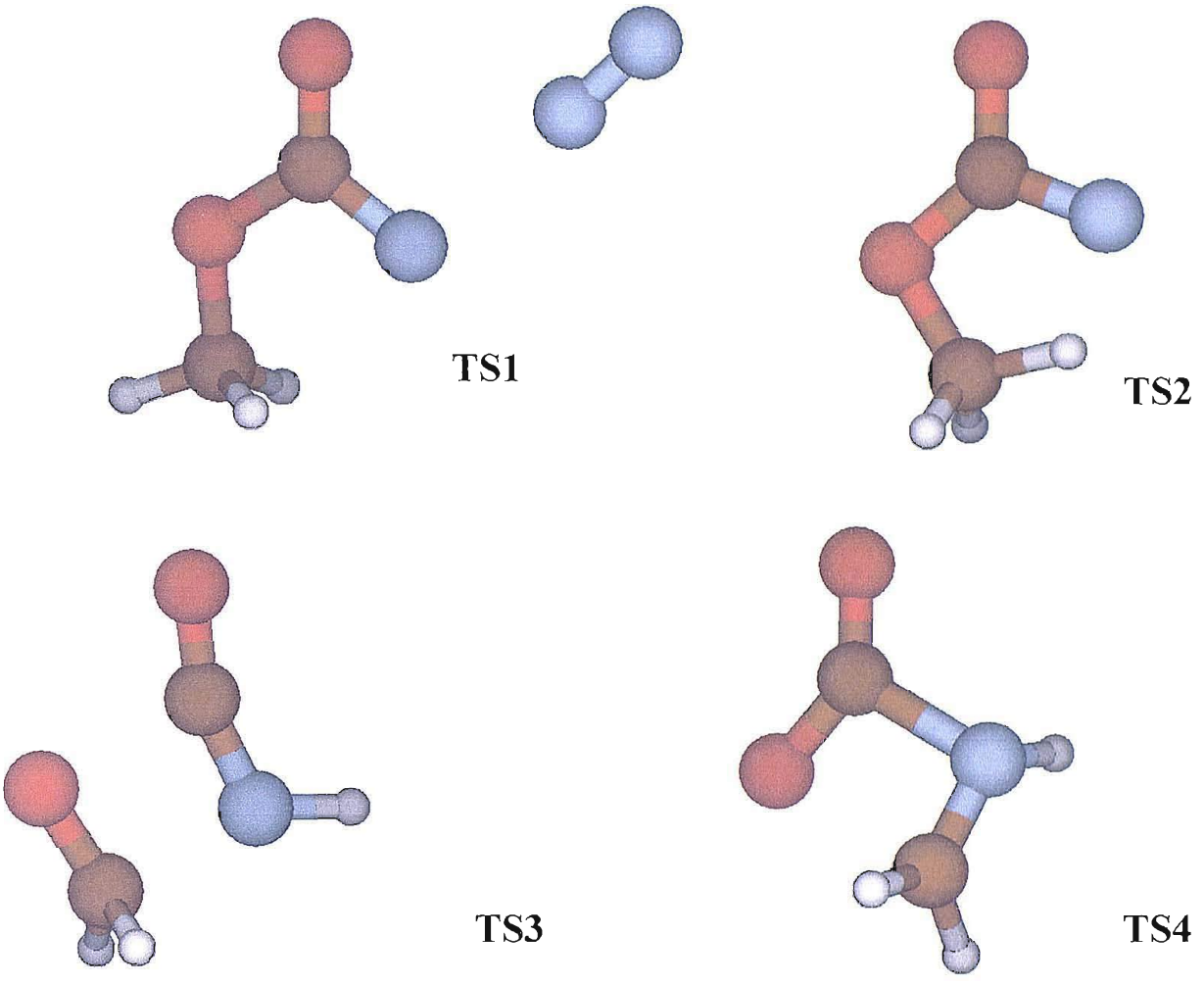

Figure 5.88- Geometries of the transition states optimized in the *ab initio* study of the thermal decomposition of methyl-azidoformate. Labels refer to the TS labels in the energy diagrams in Figures 5.86-5.87

5.6 2-AZIDOPROPIONITRILE

5.6.1 EXPERIMENTAL SECTION

Photoelectron spectroscopy

2-azidopropionitrile ($N_3CH(CH_3)CN$) is a liquid volatile enough to be introduced into the ionization chamber of the photoelectron spectrometer by simply evacuating the flask holding the sample via a needle valve: in this way, the low pressure created by the diffusion pumps evacuating the ionization chamber is enough to ensure a constant vapour pressure allowing the recording of PE spectra with acceptable signal-to-noise ratio.

The temperature of full decomposition proved to be low enough to allow a resistive heating system to be used on the photoelectron spectrometer with 10 cm-mean radius of the hemispheres [7].

The procedure for the acquisition and calibration of the photoelectron spectra followed the same pattern as described in Section 2.1. Calibration of spectra obtained on pyrolysis of the azide was normally achieved using the bands associated with the first vertical ionization energies (VIEs) of N_2 (15.58 eV), H_2O (12.62 eV) or of HCN (13.60 eV) [8].

Matrix isolation IR spectroscopy

The apparatus and the procedure for the acquisition of infrared spectra in nitrogen matrices have been described in Chapter 2. Deposition times were of the order of 30 to 60 minutes, and the matrix dilution ratios were estimated to be above 1000:1.

5.6.2 SAMPLE PREPARATION AND CHARACTERIZATION

PREPARATION

Samples of 2-azidopropionitrile ($N_3CH(CH_3)CN$) were obtained from the reaction of 2-chloropropionitrile with sodium azide using DMSO as solvent. In this preparation, 2-chloroacetamide was added slowly to 3 equivalents of sodium azide. The mixture was stirred for 24 hours in an oil bath at 60 °C. After cooling, the product was extracted with diethyl ether, and the organic phase, in which the azide was dissolved, was dried over anhydrous sodium sulfate, filtered and concentrated using a rotary evaporator. The impure azide was purified by distillation in a Kugelrohr apparatus under vacuum.

CHARACTERIZATION

2-Azidopropionitrile ($N_3CH(CH_3)CN$) is a colourless liquid. It was characterized in the vapour phase by ultraviolet photoelectron spectroscopy and electron impact mass spectrometry, and in the liquid phase by ^{1}H- and ^{13}C-nuclear magnetic resonance (Bruker AMX-400), and by infrared spectroscopy (Mattson Satellite FT-IR).

Mass spectrometry: the 70 eV electron impact mass spectrum is reported in Figure 5.89, and it shows the parent peak at 96 amu, with a weaker peak at 97 amu corresponding to the protonated azide. The base peak (i.e. the most intense one) was found at 53 amu, corresponding to CH_3CCN^+. Strong peaks were found at 54 (CH_3CHCN^+), 28 (N_2^+, CH_2N^+), 42 (N_3^+), 67 (CH_3CNCN^+) and 27 (CH_3C^+, HCN^+) amu. For each of these signals, other peaks were present at 1 and 2 amu lower, indicating a high probability of deprotonation of the fragment during the electron impact.

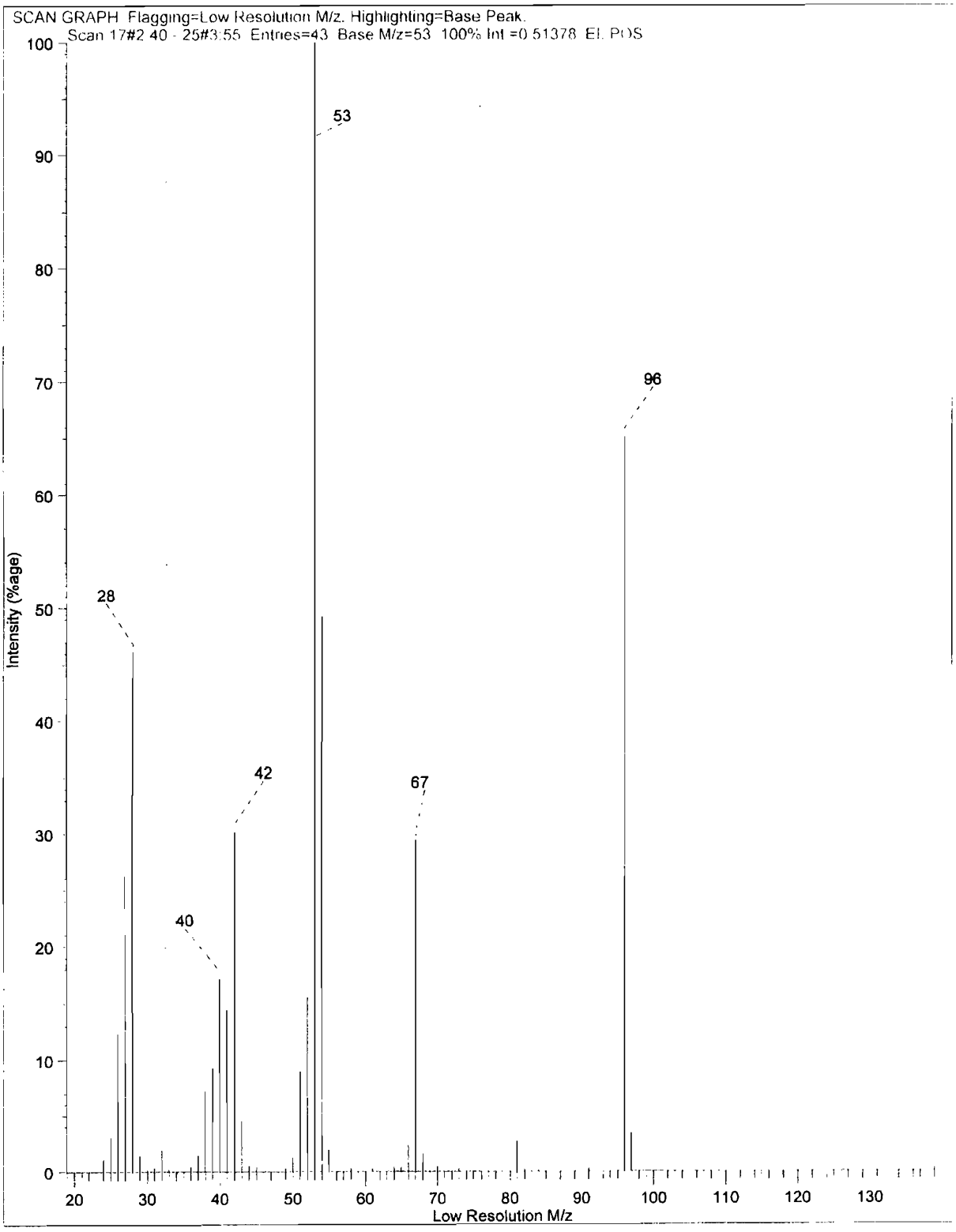

Figure 5.89- The 70 eV electron impact mass spectrum of 2-azidopropionitrile

^{1}H- and ^{13}C-NMR spectroscopy: the ^{1}H-NMR spectrum in $CDCl_3$ solution, presented in Figure 5.90, displays a doublet centred at 1.595 ppm relative to TMS corresponding to the methyl protons, and a quartet centred at 4.245 ppm assigned to the methyne group. The multiplet structure of the signals is due to the number of hydrogen atoms adjacent to the resonating protons. The ratio between the two signal intensities was 3.45:1, slightly higher than the expected 3.0 value. The higher value is probably due to small impurities contained in the sample whose protons resonate in the same chemical shift region as the methyl protons of the azide. The nature of these impurities has not been found, but it has been noted- from spectra on the chlorinated precursor- that they were already present in the starting material (2-chloropropionitrile) from which the azide was obtained.

The ^{13}C-NMR spectrum in $CDCl_3$ solution (Figure 5.91) shows peaks at 18.16 ppm (relative to TMS) assigned to the methyl carbon, at 46.39 ppm, assigned to the methyne carbon and at 117.34 ppm, assigned to the cyanide carbon.

Infrared spectroscopy: the IR spectrum of the pure compound in the liquid phase was recorded between KBr plates, and is reported in Figure 5.92a. The most intense band is a relatively broad doublet, with peaks at 2089 and 2122 cm^{-1}: the assignment of this band is not straightforward, because in that region of the spectrum both the azide N-N-N and the C≡N stretching modes are expected. It is therefore not clear if the doublet is due to the two different vibrational modes, or if the C≡N stretch (which is expected to be lower in intensity- see Section 5.5.3 on the *ab initio* calculations on the 2-azidopropionitrile conformers) is assignable to one of the weak satellites of the main band, or it is overlapped by it. The bands associated to the C-H stretching modes at 2997 and 2942 cm^{-1} are very weak, while a very strong band is found at 1236 cm^{-1} corresponding to the C-N-N stretch. Other prominent bands were found at 1448, 1382, 1321, 1087, 1019, 880 and 713 cm^{-1}.
Figure 5.92b shows the IR spectrum of 2-azidopropionitrile obtained in a nitrogen matrix. As can be seen, in contrast with the spectrum acquired in the liquid phase, in the matrix the bands associated with the N-N-N and C≡N stretches are resolved and some bands in the 1500-1000 cm^{-1} region display a different intensity pattern.
In the next section the IR spectra of 2-azidopropionitrile in the liquid phase and in a N_2 matrix will be presented in comparison with the results obtained from *ab initio* calculations on the vibrational frequencies.

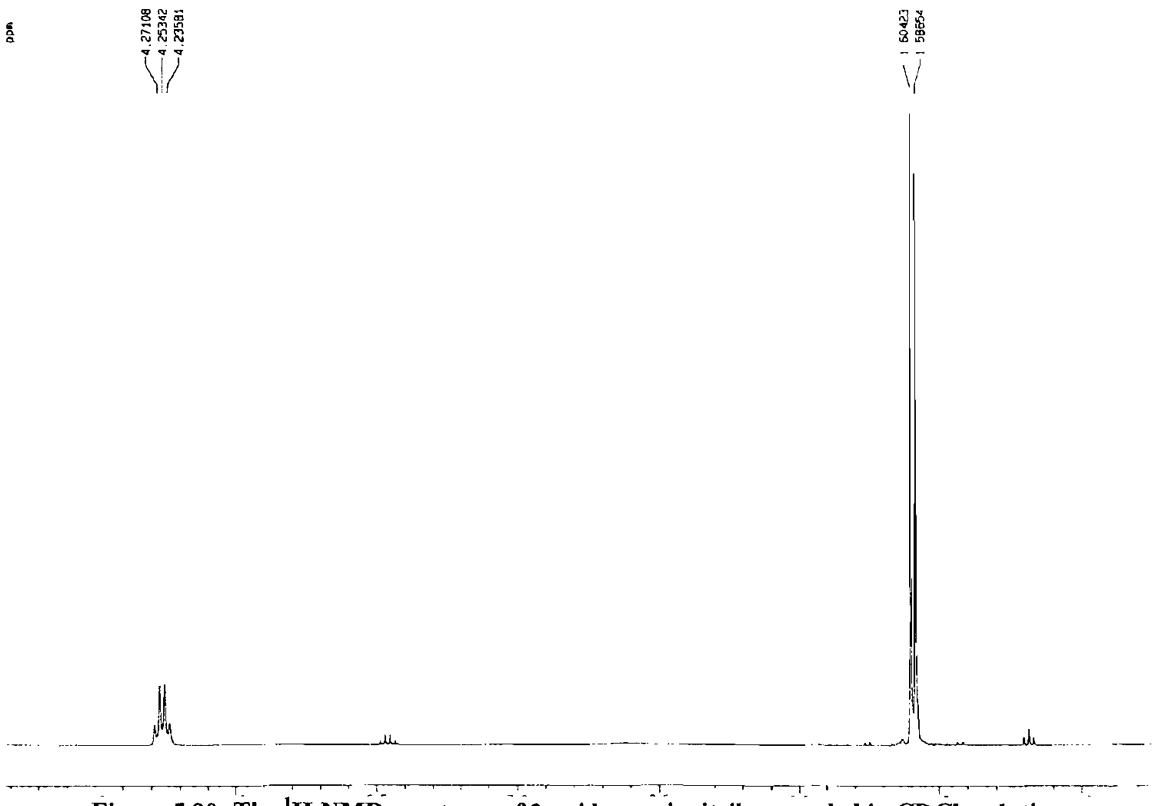

Figure 5.90- The ^{1}H-NMR spectrum of 2-azidopropionitrile recorded in $CDCl_3$ solution

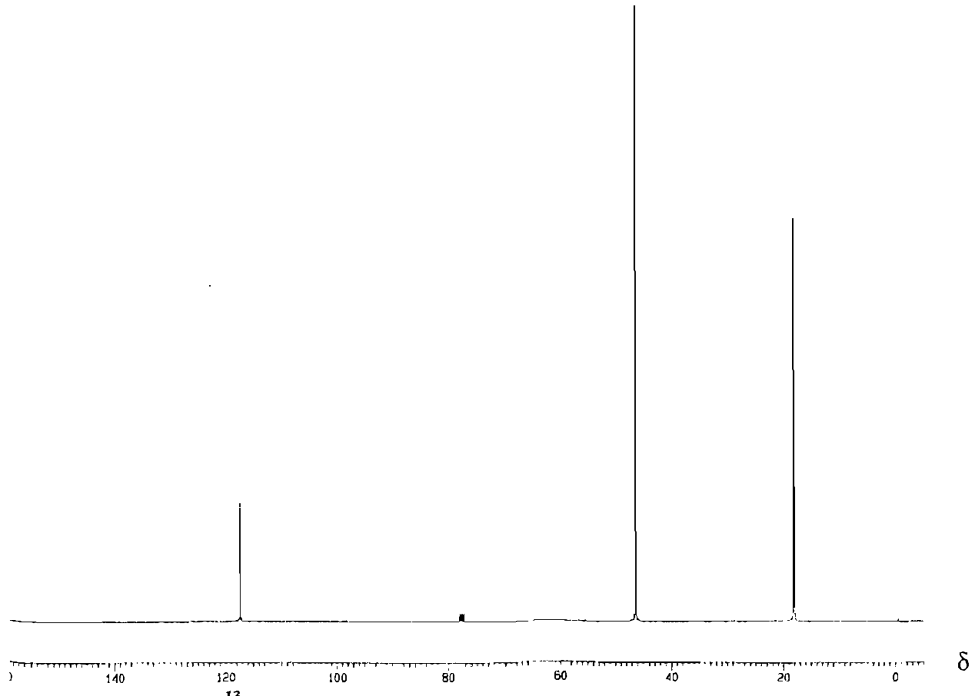

Figure 5.91- The ^{13}C-NMR spectrum of 2-azidopropionitrile in $CDCl_3$ solution

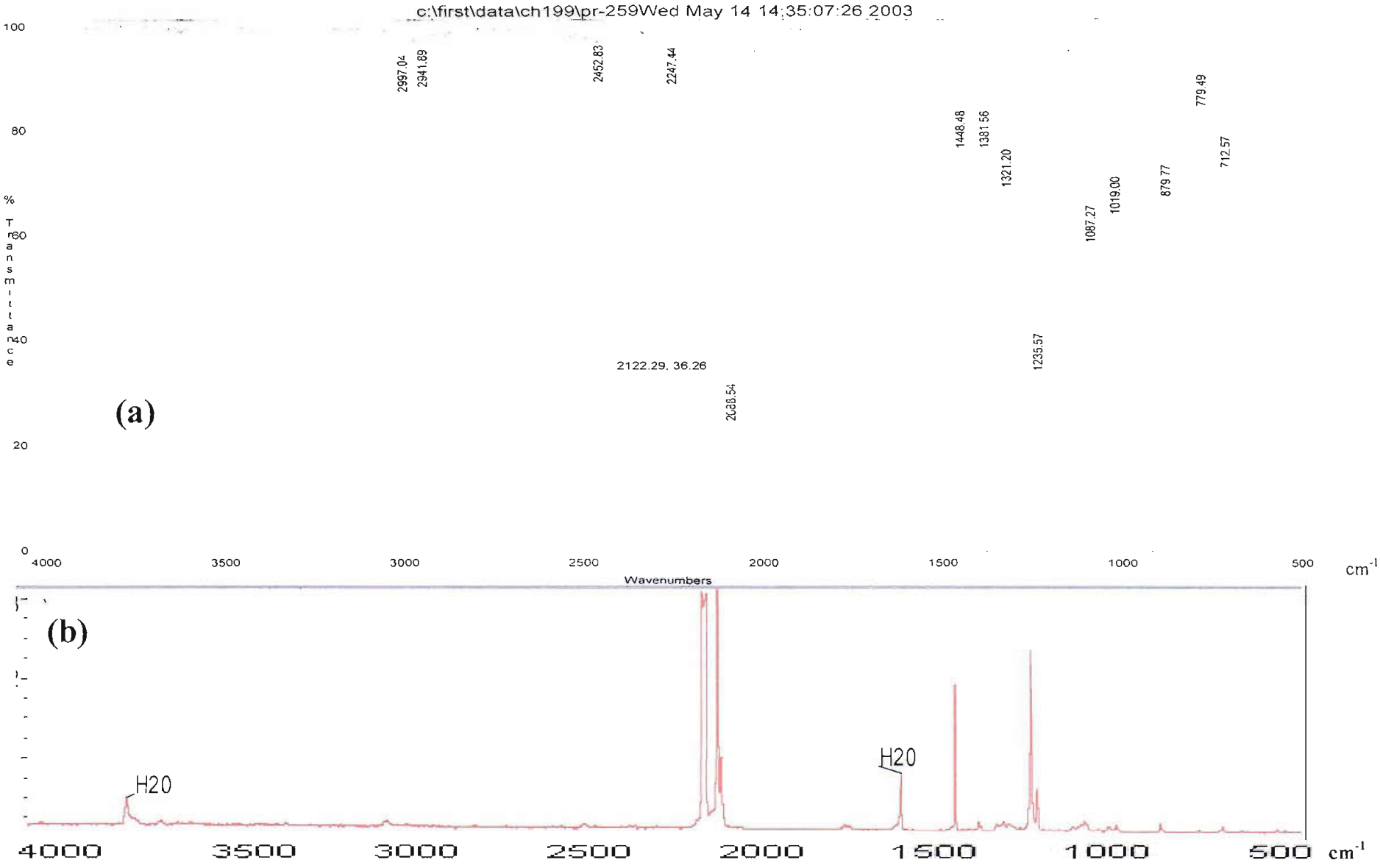

Figure 5.92b- The IR spectrum of 2-azidopropionitrile recorded (a) in liquid phase between KBr plates and (b) in a nitrogen matrix

Photoelectron spectroscopy

All the spectra were recorded using HeIα radiation (21.22 eV). Photoelectron spectra of the parent azide were calibrated using argon and methyl iodide [18] added to the ionization chamber along with the azide vapour samples. The photoelectron spectra of the azide precursor, 2-chloropropionitrile, were also recorded and calibrated to check for its possible presence as an impurity in the azide spectra, but all the 2-azidopropionitrile samples seemed free from any detectable trace of the precursor used in the preparation. The pressure of the azide in the ionization region was set at approximately 10^{-4} torr.

Figure 5.93 shows the PE spectrum of 2-azidopropionitrile recorded at room temperature, along with the labelling of the bands. These have been calibrated by averaging the VIEs obtained from six different spectra, and the values are presented in Table 5.58. A more detailed description of the molecular orbitals involved in the ionizations associated with the photoelectron bands will be reported in the following session.

Table 5.58- Calibrated vertical ionization energies of 2-azidopropionitrile- see Figure 5.93 for band labelling

Band	A	B	C	D	E	F	G
VIE (eV) ±0.02 eV	10.34	11.69	12.31	12.71	13.31	13.83	15.32

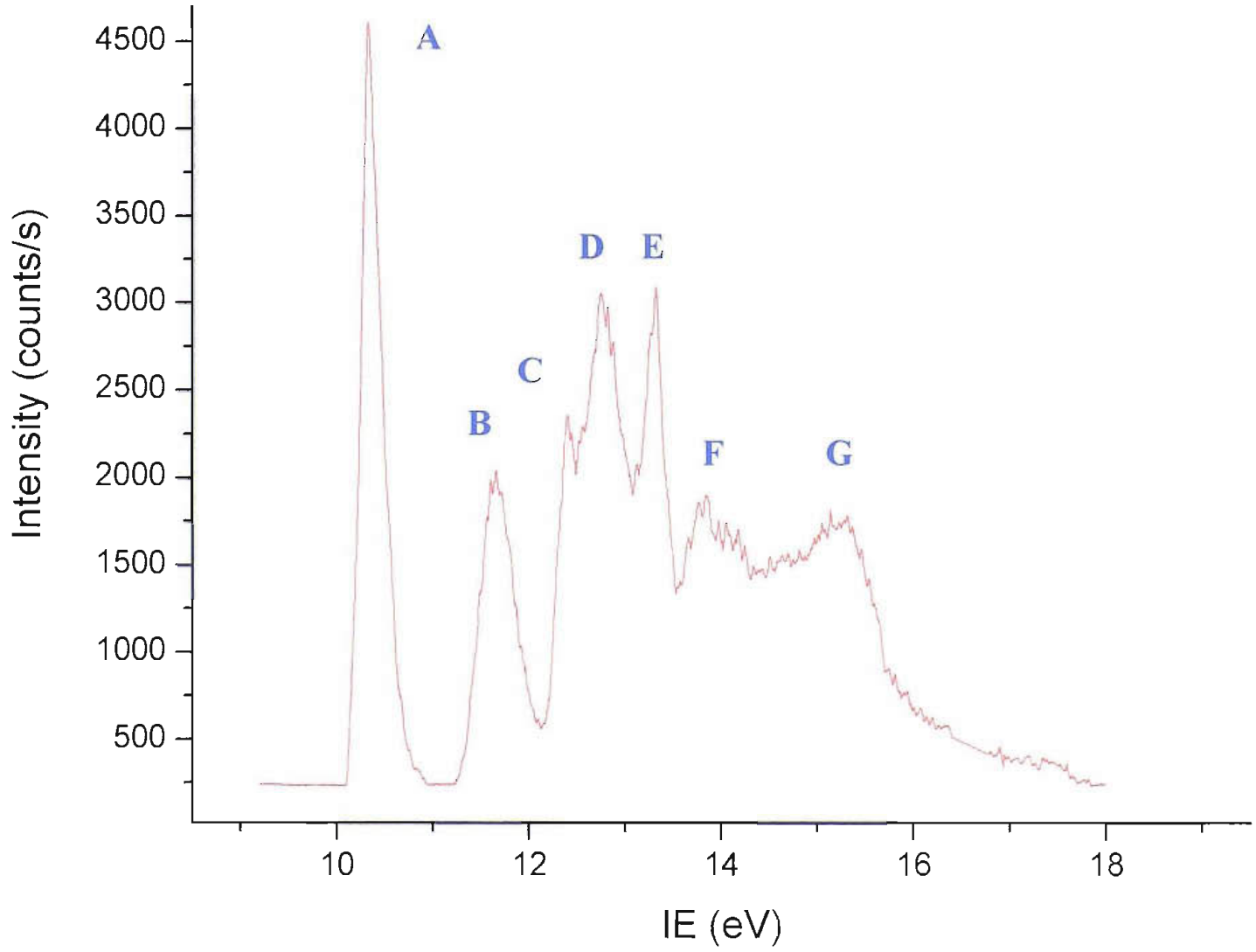

Figure 5.93- PE spectrum of 2-azidopropionitrile at room temperature, with bands labelled A to G

5.6.3 RESULTS OF *AB INITIO* MOLECULAR ORBITALS CALCULATIONS

Molecular orbital calculations were carried out at the MP2/6-31G** level on the parent azide and on its decomposition products to facilitate the spectral interpretation and the assignments of the bands by calculating vertical ionisation energies (VIEs) and infrared frequencies and intensities. Also, the geometry of the azide and the imines were computed, and relative energy diagrams were constructed in order to trace the energy surface for the decomposition reaction.

Two conformers of 2-azidopropionitrile were optimized, according to the relative orientation of the azide chain with respect to cyano group. This is the only possible geometrical change in the molecule, since all other groups cannot be differently orientated.

The geometries of the two structures are shown in Figure 5.94, and as can clearly be seen by the absence of any symmetry element, their point group is C_1. They have been labelled *cis* and *trans* according to the relative position of the azide chain with respect to the C≡N group.

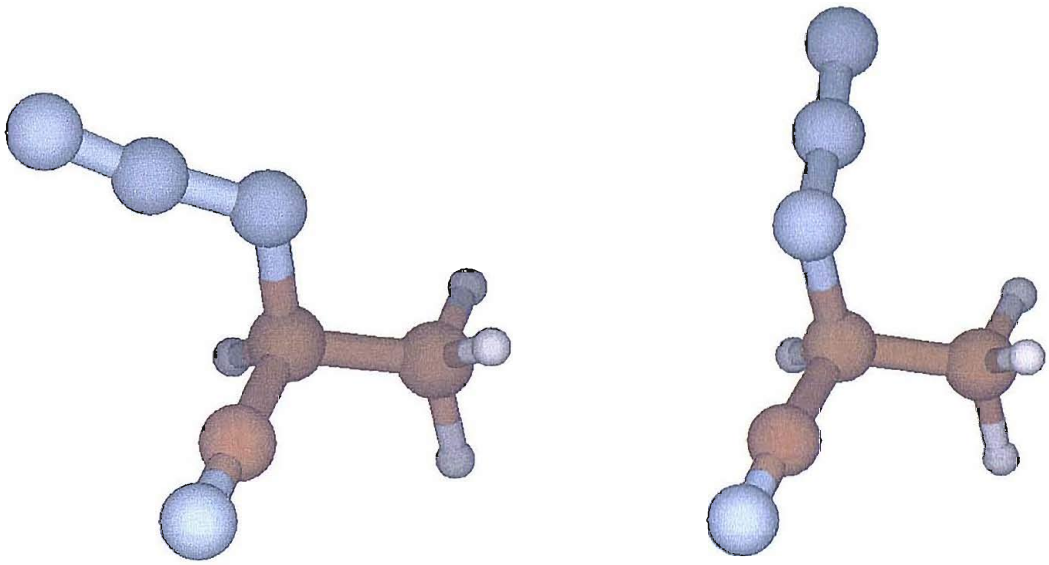

Figure 5.94- The structures of 2-azidopropionitrile optimized at the MP2/6-31G level, *cis* (left) and *trans* (right)**

The two structures are very close in energy (1.05 kcal/mol). Figure 5.95 shows in detail the most stable of the two, labelled "*trans*", along with the labelling of the atoms, while Table 5.59 summarizes its most significant geometrical parameters.

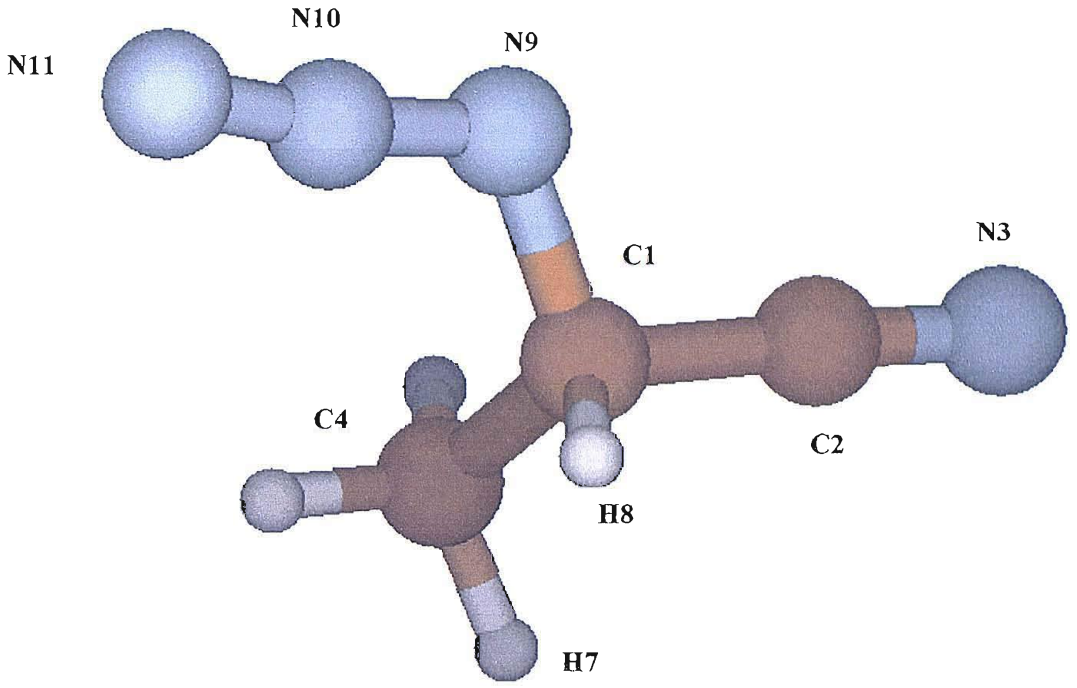

Figure 5.95- Structure *trans* of 2-azidopropionitrile calculated at the MP2/6-31G level**

Table 5.59- Most significant geometrical parameters for the lowest energy structure of 2-azidopropionitrile

Bond	Length (Å)	Angle	Value (°)
N11-N10	1.162	N11-N10-N9	172.66
N10-N9	1.251	N10-N9-C1	113.71
N9-C1	1.483	N9-C1-C2	106.33
C1-H8	1.095	N9-C2-C4	111.84
C1-C2	1.469	C1-C2-N3	177.34
C1-C4	1.528	C1-C4-H7	109.61
C2-N3	1.182	N10-N9-C1-C2	193.5
C4-H7	1.090	N9-C1-C4-H7	-62.4

Table 5.60 reports vertical ionization energies for the two conformers as calculated by applying Koopmans' theorem to the energies of the molecular orbitals obtained at the MP2/6-31G** level. The agreement is good for the first four bands, while the higher ones show clear differences between computed values and experiment; it is possible that 6-31G** is not a good enough basis set to describe this azide, or that Koopmans' theorem is a too crude approximation of the true vertical ionization energies because of neglect of reorganization and correlation effects. To allow for reorganization effects, VIEs using the ΔSCF method- calculating the energy of the azide cation at the same geometry of the neutral- were calculated. Unfortunately, only ionization from the higher molecular orbitals were possible, due to the fact that on removing an electron from a lower lying orbital the same values of energies as from the ones of higher energy were obtained because the calculation converged to the lower state; this means that for a molecule of C_1 symmetry, calculations at the ΔSCF level are not possible for higher VIEs.

Table 5.60- Experimental and calculated vertical ionization energies (VIEs) of the first seven bands of 2-azidopropionitrile in both its conformers

Band	"cis" KT calculated VIE (eV)	"cis" KT calculated VIE *0.92 (eV)	Experimental VIE (eV)	"trans" KT calculated VIE (eV)	"trans" KT calculated VIE *0.92 (eV)	ΔSCF calculated VIE (eV)
A	10.89	10.02	10.34	10.97	10.09	11.58
B	12.44	11.45	11.69	12.22	11.24	13.06
C	12.63	11.62	12.31	12.67	11.66	12.29
D	13.00	11.96	12.71	13.37	12.230	
E	15.09	13.88	13.31	15.09	13.88	
F	15.62	14.37	13.83	15.57	14.32	
G	16.13	14.84	15.32	15.72	14.46	

Figure 5.96 represents the highest occupied molecular orbitals for structure *trans* of 2-azidopropionitrile obtained at the Hartree-Fock level on the geometry optimized at the MP2/6-31G** level.

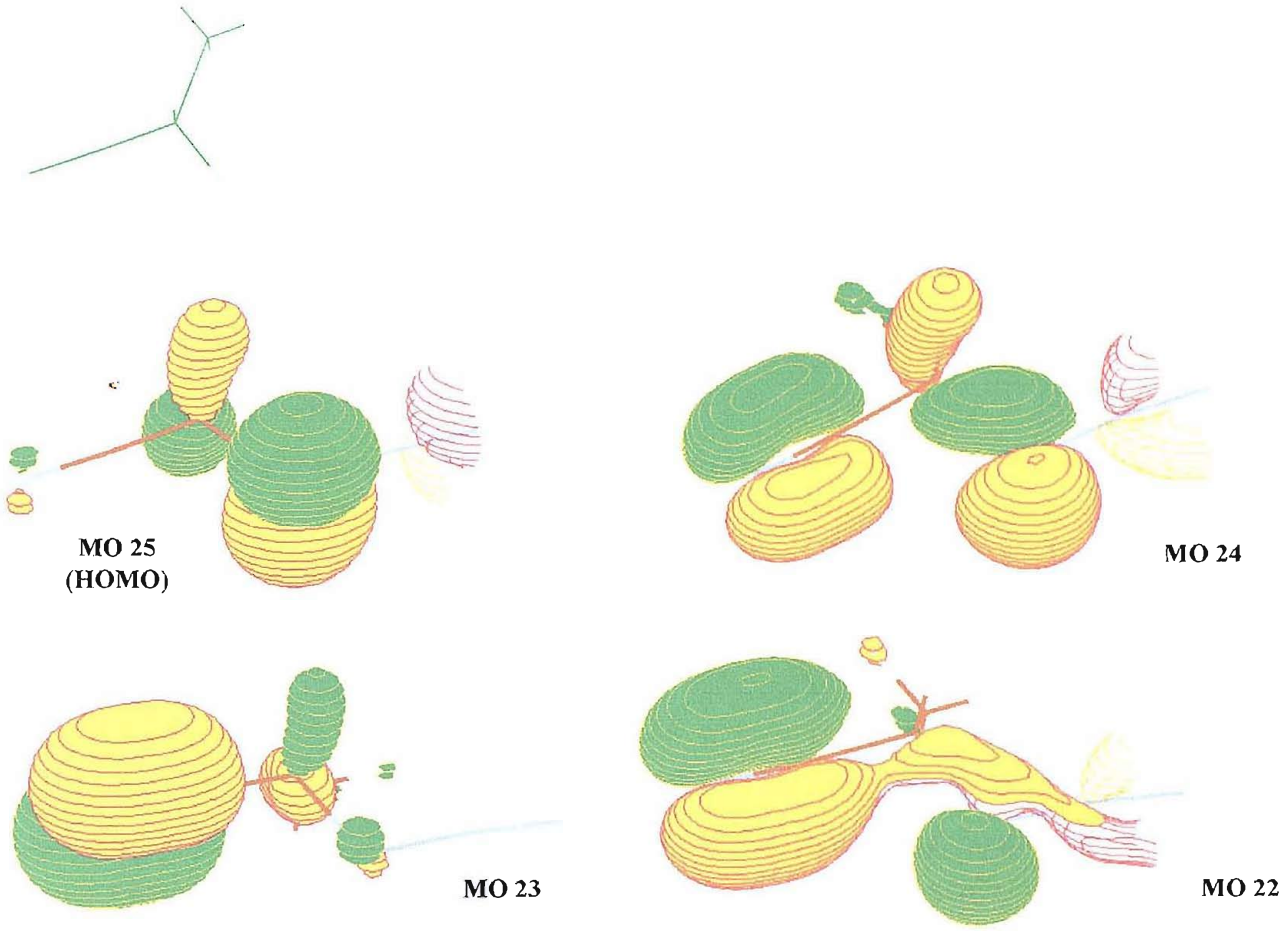

Figure 5.96- The four highest occupied molecular orbitals (HOMOs) calculated for 2-azidopropionitrile

For the most stable conformer (conformer *trans*), molecular orbital 25 (the HOMO) is quite a localized orbital, mostly π-antibonding in character: assuming the N-N-N-CH-CN frame to be almost planar, the HOMO consists of p_π orbitals centred on the first and last nitrogen atoms of the azide chain, plus a p_π antibonding character between the first nitrogen of the azide and the adjacent methyne carbon. All of them have the nodal plane corresponding to the pseudo-plane of the molecule. The p_π character on the methyne group is not due to a lone pair on the carbon atom, but to the σ-bonds between the methyne carbon atom and the methyl and the hydrogen groups.

MO 24 is a delocalized orbital, with major p_π-bonding contribution from the C≡N group, a p_π antibonding character between the cyano carbon atom and the methyne carbon atom, and a σ-bonding contribution between the methyne carbon atom and the first azide nitrogen atom of the azide group, plus a p_π bonding character on the two terminal nitrogen atoms of the azide chain and a p_π antibonding character between the first and second nitrogen atoms of the azide chain. In this case, all the p_π orbitals have the nodal plane perpendicular to the pseudo molecular plane.

MO 23 is almost totally characterized by a strong π-bonding contribution on the C≡N group and to a lesser extent by a σ-bonding contribution between the methyne and methyl carbon atoms: these two contributions create also a p_π antibonding system between the cyano and the methyne carbon atoms.
MO 22 is very similar to MO 24, without the contribution arising from the σ-bonds between the methyne carbon and the methyl and hydrogen groups.

Harmonic vibrational frequencies have been calculated for the two conformers of 2-azidopropionitrile via second derivative calculations at the MP2/6-31G** level, with only partial allowance for electron correlation, the calculated frequencies are then expected to be higher than the experimental ones. The computed IR spectra are reported in Figure 5.97, and the computed frequencies and intensities of the bands are listed in Table 5.61.
Considering the approximations used in the calculations, the predicted distribution of the frequencies is good. As was found in previous calculations on azides, the calculations overestimate the intensity of the strongest bands relative to the others. Therefore, the experimental spectrum displays a much higher intensity for the series of bands between 500 and 1200 cm^{-1}. The bigger discrepancy is however the contribution of the C≡N stretch, which according to calculations should be a weak band roughly 100 cm^{-1} wavenumbers lower than the azide stretch: in the experimental spectra; in practice there is actually a band as intense as the azide one at around 2080 cm^{-1}. It is not possible to definitely assign this band to the C≡N stretch or to the azide stretch of the second conformer trapped in the matrix: assuming the assignment to the C≡N stretch, the discrepancy between the predicted and the observed band is remarkable.
The two conformers show very similar band patterns: the only main difference is the shape of the two bands almost overlapping around 1300 cm^{-1}. The spectrum recorded in the liquid phase shows a better agreement with the *cis* structure of 2-azidopropionitrile, even if this is the high in energy structure. The difference is however so small (just 1.0 kcal/mol) that it is possible that at room temperature the two structures are both present: the experimental spectrum reproduces probably an average of the two spectra of the pure conformers *cis* and *trans*. In the matrix it is evident that the band centred at around 1450 cm^{-1} displays a much enhanced intensity relative to the band observed in the liquid phase: this behaviour is not reflected by the bands expected from the calculations, and the effect was attributed to an impurity in the sample.

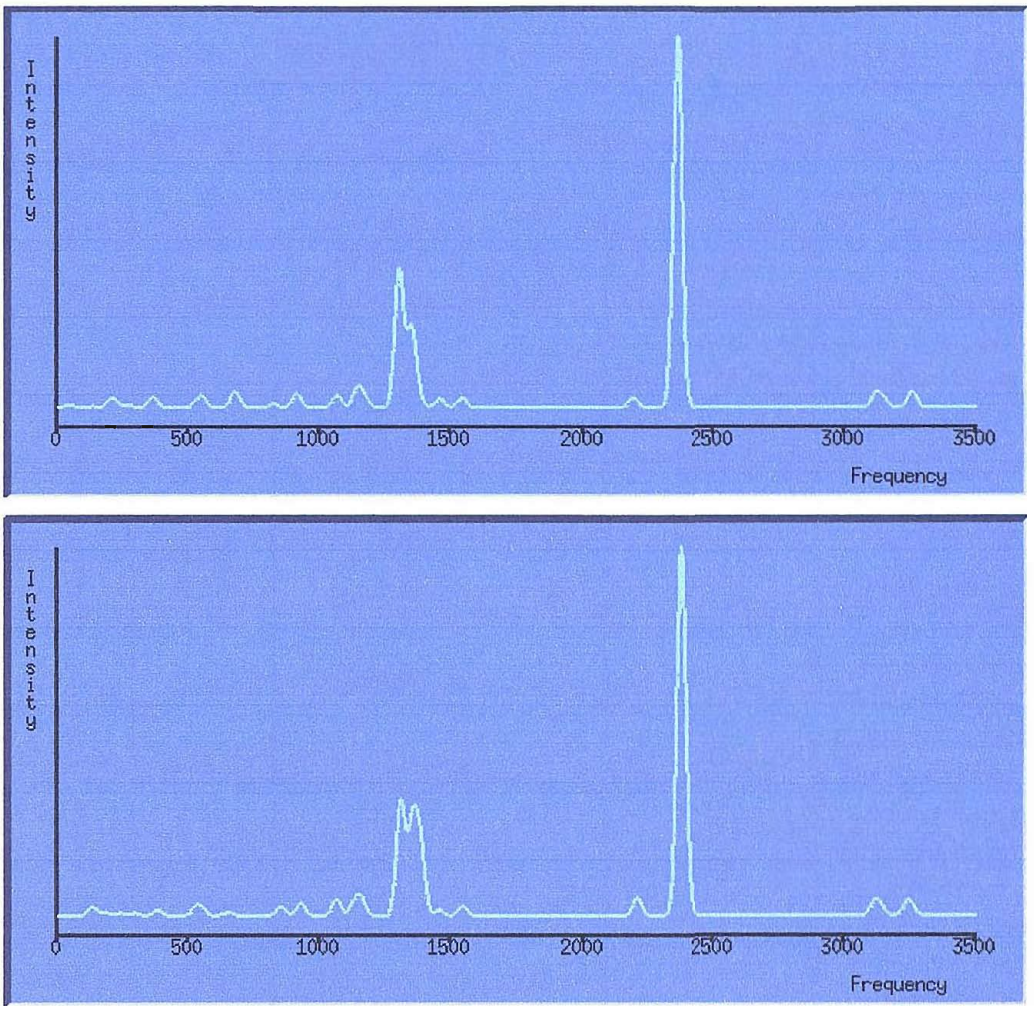

Figure 5.97- Infrared spectra for the two conformers of 2-azidopropionitrile calculated at the MP2/6-31G level**

Table 5.61- Comparison between the experimental liquid phase IR bands and the calculated band positions and intensities for the minimum energy conformers of 2-azidopropionitrile (absorbances in Km/mol, frequencies in cm^{-1})

Cis frequencies	*Intensity*	*Trans frequencies*	*Intensity*	*Experimental frequencies in liquid phase*	**Normal mode**
544.0	5.27	536.0	4.45		
560.1	5.02	554.9	4.63		
681.0	12.96	654.0	3.19		
828.2	3.14	854.7	7.30		
915.2	11.50	931.0	9.50		
1068.8	10.37	1065.8	12.70		
1145.7	15.00	1132.0	9.20	1019.0	
1173.4	7.93	1158.7	13.95	1087.3	
1306.7	111.81	1311.1	90.56	1235.6	
1353.1	62.56	1355.9	71.33		
1379.4	8.20	1385.7	55.03	1321.2	C-H bending
1460.2	7.21	1457.5	5.11	1381.6	$C-H_3$ wagging
1542.0	5.22	1546.5	7.01	1448.5	$C-H_3$ in phase scissoring
1551.5	3.17				$C-H_3$ out of phase scissoring
2193.3	8.18	2209.8	14.18	2088.5	C≡N stretching
2363.5	300.64	2378.6	294.71	2122.3	N-N-N stretching
3122.8	11.14	3117.1	10.36		C-H stretching
3149.4	5.51	3139.6	5.47		$C-H_3$ symmetric stretching
3255.1	7.05	3239.7	8.78	2941.9	$C-H_3$ asymmetric stretching
3262.2	5.88	3258.1	5.02	2997.0	$C-H_3$ asymmetric stretching

5.6.4 THERMAL DECOMPOSITION RESULTS

Photoelectron spectroscopy

Figure 5.98 represents the UV-photoelectron spectra recorded when the vapour of 2-azidopropionitrile is heated at respectively 350, 390 and 470 °C.

The first evidence of pyrolysis, as in every organic azide, is the release of nitrogen (sharp band at 15.58 eV): in the case of 2-azidopropionitrile the loss of nitrogen was observed to begin at approximately 170 °C. At approximately 190 °C HCN is also produced (observation of a vibrationally structured band with VIE at 13.60 eV). Apart from N_2 and HCN, the first bands associated with decomposition products appear at approximately 210 °C; notably, two sharp bands at 11.27 and 13.14 eV. Their shape and position correspond to the bands expected for methyl isocyanide and methyl cyanide [8]. At relatively low pyrolysis temperature the band of the isocyanide is more intense than that of the cyanide, while at higher temperatures (beyond 420 °C) the intensity ratio moves in favour of CH_3CN. This behaviour was expected both from previous experiments [34] and from the predicted thermodynamic stability order for the methyl isocyanide/cyanide system [4]: the minimum energy structure of the isocyanide is calculated to have a total energy value 28.35 kcal/mol higher than that of the cyanide at the MP2/6-31G** level.

The spectrum at 350 °C shows that the intensity ratio between the first two azide bands is reflecting a higher relative intensity for the second one (centred at 11.7 eV), which also shows a slight change of its shape: this can be due to the presence of an additional contribution arising from a newly formed molecule. It is possible that an intermediate is being formed, due to the fact that when the temperature is further raised no remaining contribution is observed in that region. However, it is not possible to clearly state that an intermediate band is actually present, due to the overlapping of this possible intermediate band with the second azide band.

At temperatures above 400 °C, the azide is totally decomposed into CH_3NC, CH_3CN and HCN.

Figure 5.99 reports the thermal behaviour of the intensities of the main band of each compound: the normalization was carried out by simply considering the height of the band, not its integral, and setting as 1.0 the height of the band at the temperature at which its intensity was the maximum among all the spectra.

According to their observed thermal behaviour in the 400-500 °C region, HCN and CH_3CN will eventually be the only products at temperatures higher than 600 °C, which in these experiments could not be achieved.

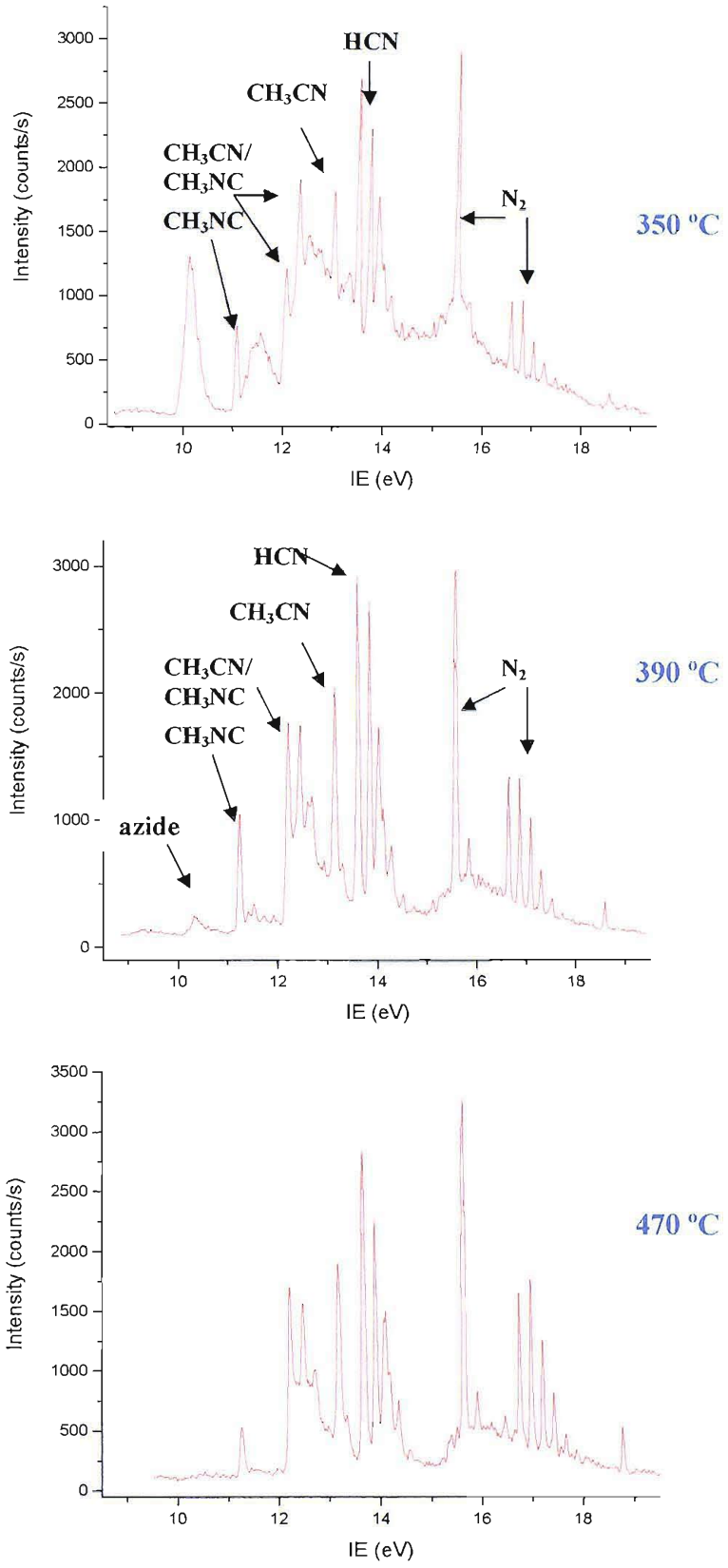

Figure 5.98- Decomposition photoelectron spectra of 2-azidopropionitrile at 350, 390 and 470 °C

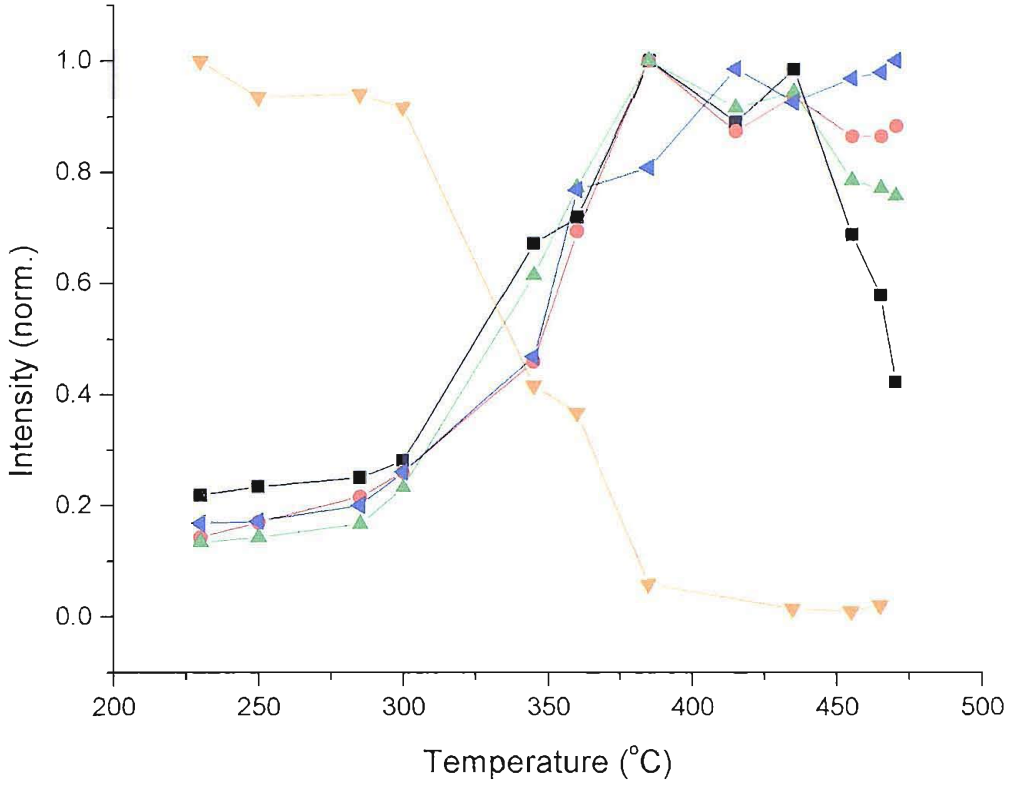

Figure 5.99- Thermal behaviour of the normalized intensities of the main species present in the 2-azidopropionitrile pyrolysis. Orange diamonds: 2-azidopropionitrile; black squares: methyl isocyanide; red circles: methyl cyanide; blue inclined triangles: nitrogen; green triangles: HCN

Of great importance is a very weak, broad band centred around 9.22 eV: its thermal behaviour, increasing in intensity with increasing temperature then suddenly disappearing at temperatures above 400 °C, is typical of a reaction intermediate. An initial assignment of this band to 2-iminopropionitrile, $HN{=}CHCH_2CN$, proved not to be satisfactory due to the first VIE calculated with Koopmans' theorem being at 11.80 eV, a value exceeding the experimental value, 9.22 eV, beyond any reasonable estimate for the Koopmans' theorem value. The band was subsequently assigned to ketenimine, $CH_2{=}C{=}NH$, which has been studied by PES in the past [35]: this is a C_2H_3N isomer with comparable energy to CH_3NC, but with much lower stability (reported lifetime of roughly 1 second at 1 torr) [35]: its first band is in very good agreement with that found in these experiments, both in its VIE and in its shape.

Infrared matrix isolation spectroscopy

Figure 5.100 presents the infrared spectra obtained when vapours of 2-azidopropionitrle were heated at increasing temperatures and trapped into a nitrogen matrix.

The onset of the pyrolysis was observed at 210° C by the appearance of the HCN bands at 3282 and 797 cm^{-1} [20]. With increasing temperature, the azide bands decrease and all the bands associated with the products start to increase; the summary of the most significant absorptions for the molecules released in the decomposition of 2-azidopropionitrile are listed in Table 5.62.

Some of the bands show an increase in intensity with increase of the temperature, marking the presence of thermally stable compounds: apart from HCN, this is the case of methyl cyanide (CH_3CN) whose most prominent peak is observed at 1447 cm^{-1} [36]. With the obvious exception of the azide bands which constantly decrease in intensity with increasing temperature (and completely disappear above 360° C), two other sets of bands show a behaviour typical of a reaction intermediate, with intensity decrease when the vapours are heated above 300° C. The first set was assigned to methyl isocyanide (CH_3NC) and its most intense band can be found at 2161 cm^{-1} [37]; the second set is weaker (most intense band at 2038 cm^{-1}), and was attributed to ketenimine, CH_2CNH [38]. The assignments, evidenced in Table 5.63, reflected the results obtained from PES data.

Two additional pieces of evidence were found: HCN is not observed as a monomer, but instead the vibrational frequencies suggest its existence in a dimeric form $(HCN)_2$ [29], or even a polymeric form.

Finally, it was not possible to assign the band at 1742 cm^{-1}, which shows the thermal behaviour of a stable product: a possible explanation of this is the presence of a decomposition product of the impurity detected in the azide sample absorbing at 1447 cm^{-1}. If on the other hand the band is associated to a "true" decomposition product of 2-azidopropionitrile, an assignment may only be achieved following an *ab initio* calculations of the vibrational frequencies of all the possible products. This will be presented in the next section.

Table 5.62- Labels and assignment of the most significant IR bands observed in the matrix isolation study of ethyl-azidoformate thermal decomposition (refer to Figure 13 for the labelling of the bands)

Label	*N_2 matrix frequency (cm^{-1})*	*Assignment*	*Reference*
M	2141/2135, 2102/2091, 1242, 1224	$N_3CH(CN)CH_3$	
HCN	3282, 3270, 799/795	Polymeric cyanic acid	[29]
CH3CN	2256, 1447, 1407, 1378, 1040, 916	Methyl cyanide	[36]
CH3NC	2161, 947	Methyl isocyanide	[37]
CH2CNH	2038, 1125 997, 885, 697	Ketenimine	[38]

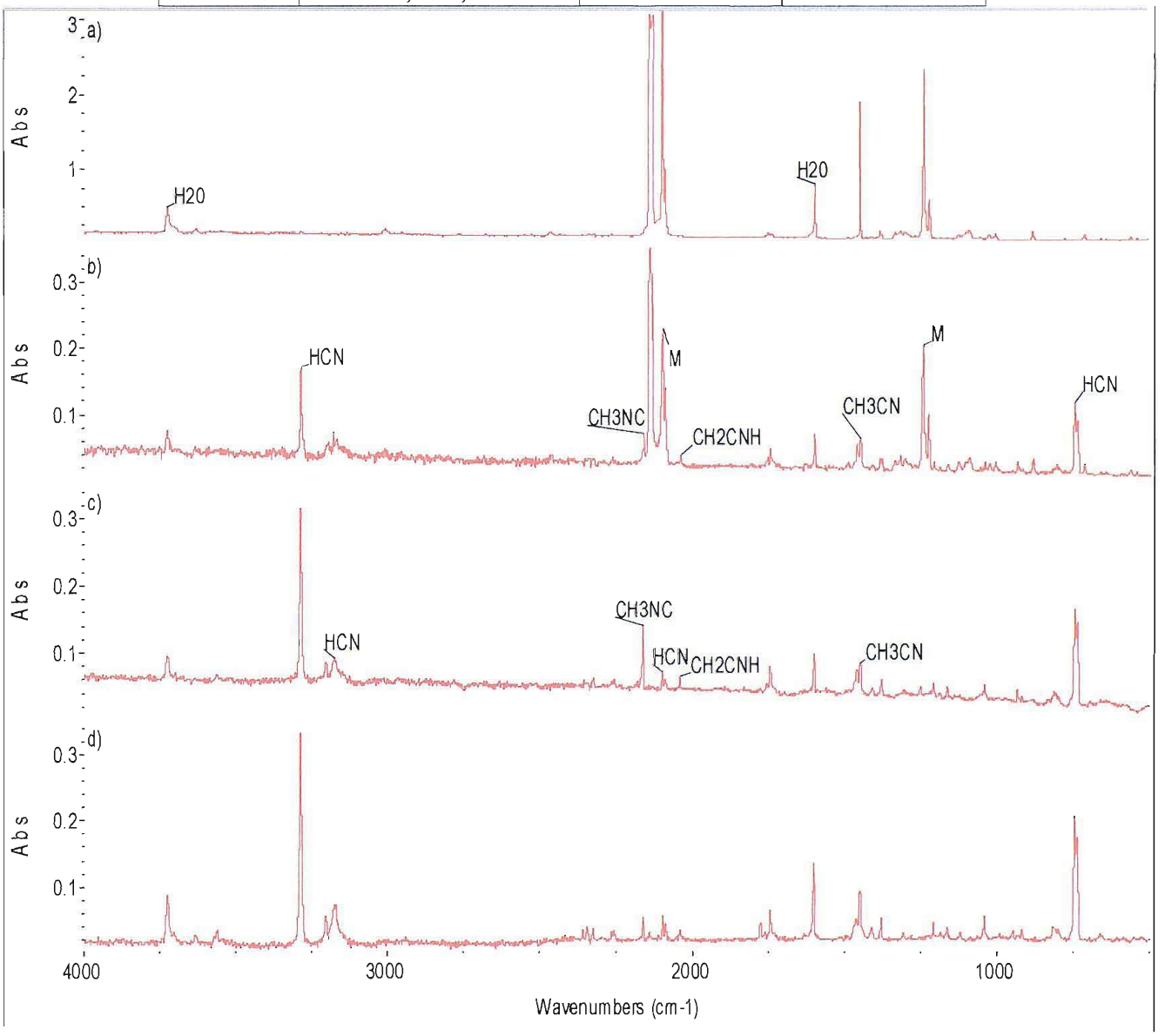

Figure 5.100- Matrix IR spectra of vapours of 2-azidopropionitrile heated at respectively 30, 250, 360 and 470 C

Summary of the experimental results

The experimental results from both PES and matrix IR data show that this azide decomposes releasing nitrogen, cyanic acid and methyl cyanide as stable molecules; in addition to that, methyl isocyanide and- in a lesser amount- ketenimine are formed as reaction intermediate. Methyl isocyanide has a longer thermal stability, and it is still present at temperatures above 500 °C, while ketenimine has a much lower stability which precludes its observation above 400 ° C.

The apparent simplicity of the system disguises a much more complex situation when the geometries of the molecules are considered, and when *ab initio* studies of the transition states leading to the products are carried out.

The formation of methyl cyanide, CH_3CN, when 2-azidopropionitrile is thermally decomposed is easily explained by considering the structure of the azide (see Figure 5.95). However, the formation of methyl isocyanide (CH_3NC) and ketenimine (CH_2=C=NH) cannot be immediately rationalized on the basis of the geometry of the starting azide. A study of the potential energy surface connecting 2-azidopropionitrile with the observed decomposition products has therefore been carried out by *ab initio* molecular orbital calculations at the MP2/6-31G** level.

5.6.5 *AB INITIO* RESULTS ON THE DECOMPOSITION INTERMEDIATES

As usual with aliphatic azides, it was supposed that 2-azidopropionitrile initially decomposes releasing molecular nitrogen and forming a nitrene, according to the reaction

$$N_3CH(CH_3)CN \rightarrow N_2 + :NCH(CH_3)CN$$

It was found out from *ab initio* molecular orbital calculations that the nitrene is not stable in its singlet state, because during the optimization the nitrene structure converges to an imine structure; this was expected according to the previous results on other azides (see earlier sections). Nevertheless, the calculations showed that on optimization of the nitrene initial geometry, initially set as the one of the azide but removing the last two nitrogen atoms of the N_3 chain, instead of simply undergoing a 1,2-H shift to produce 2-iminopropionitrile, $CH_3C(CN)=NH$, following Type 1 mechanism, the nitrene nitrogen prefers to attack other electron deficient sites within the molecule, therefore following a Type 2 mechanism.

There are two different sites to which the nitrogen atom can attack: one is the methyl carbon atom, the other is the cyanic carbon atom.

In addition to these, the possibility of the formation of 2-iminopropionitrile via a Type 1 mechanism is still present, because it is possible that during the release of molecular nitrogen the azide partially modifies its geometrical parameters so that the route to 2-iminopropionitrile becomes favoured.

Ab initio calculations were therefore necessary on all these molecules, both to interpret the spectroscopic results and to build a reasonable decomposition mechanism for 2-azidopropionitrile with an associated energy level diagram.

As mentioned, in principle three different possible routes for the decomposition of the nitrene arising from 2-azidopropionitrile are possible, one following a Type 1 mechanism and two following a Type 2 mechanism. These three initial hypotheses have been considered for the *ab initio* study of the pyrolysis reaction.

Type 1 mechanism: 2-iminopropionitrile

Following this route, 2-nitrenepropionitrile decomposes via a 1,2-hydrogen shift following the scheme

$$:NCH(CH_3)CN \rightarrow HN=C(CH_3)CN$$

The two structures of the imine obtained, 2-iminopropionitrile, were optimized at the MP2/6-31G** level of calculation, and they are reported in Figure 5.101; Table 5.63 reports the most significant geometrical parameters for the most stable structure, labelled *cis* by referring to the relative orientation of the iminic proton with respect to the cyano group. Both are planar structures, therefore their point group is C_s. Their total energies were calculated as -225.5241063 and -225.5219504 hartrees: this corresponds to an energy difference of 1.35 kcal/mol.

Due to the small difference in energy, the two structures are likely to contribute equally to the experimental spectra- if they are formed at all. Nevertheless, the calculated VIEs and vibrational frequencies of both structures will be reported in the following paragraphs.

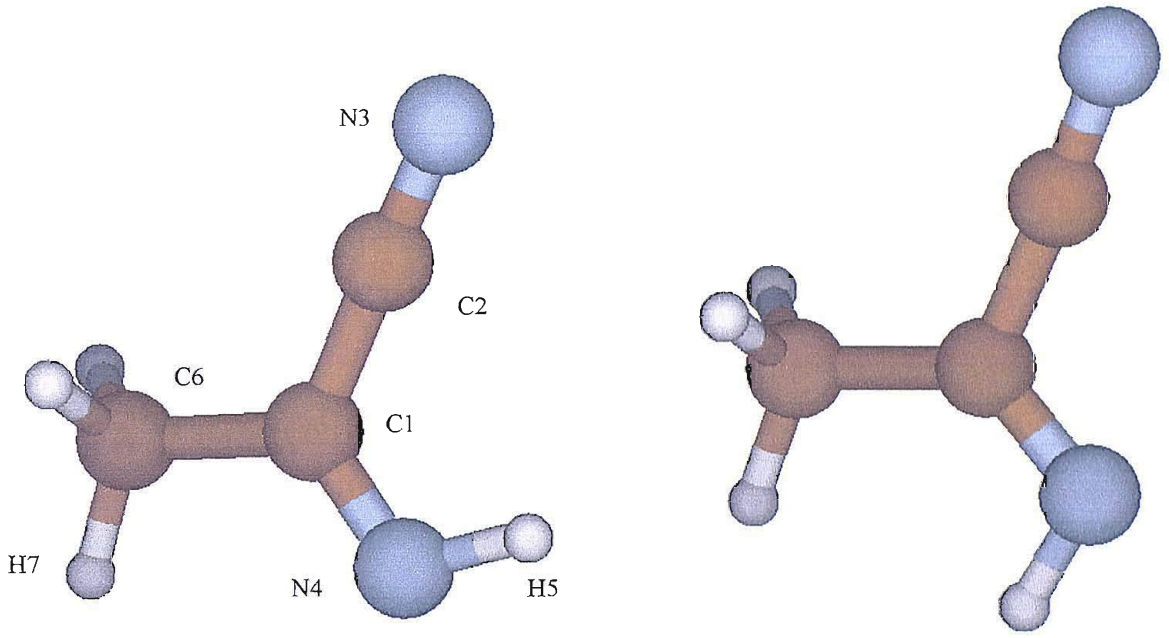

Figure 5.101- The optimized structures of 2-iminopropionitrile at the MP2/6-31G level, *cis* (left) and *trans* (right)**

Table 5.63- Most significant geometrical parameters for structure *cis* of 2-iminopropionitrile- see Figure 5.101 for the labelling of the atoms

Bond	Length (Å)	Angle	Value (°)
C2-N3	1.185	**N3-C2-C1**	178.88
C1-C2	1.458	**C2-C1-N4**	122.54
C1-N4	1.289	**C1-N4-H5**	110.37
N4-H5	1.023	**C6-C1-N4**	120.98
C1-C6	1.499	**H7-C6-C1**	108.69
C6-H7	1.087	**N3-C2-C1-N4**	10.11

To obtain VIEs, Koopmans' theorem has been applied to the orbital energies obtained for the MP2/6-31G** optimized structure. The results are listed in Table 5.64.

The two conformers show an important difference in their computed third band: in structure *trans* it is practically overlapping with the second one with VIE at 12.78 eV, while in structure *cis* it is an isolated band with VIE at 13.28 eV. Considering the usual overestimation of the experimental VIEs by Koopmans' theorem, it is likely that only structure *cis* would display a band in the 12.5- 13.5 eV region of the photoelectron spectrum.

Table 5.64- The calculated vertical ionization energies for the conformers of 2-iminopropionitrile

"cis" KT calculated VIE (eV)	"cis" KT calculated VIE *0.92 (eV)	"trans" KT calculated VIE (eV)	"trans" KT calculated VIE *0.92 (eV)
11.80	10.85	11.70	10.76
12.67	11.66	12.78	11.76
13.28	12.22	12.79	11.77
14.03	12.90	13.92	12.80
15.61	14.36	15.33	14.10

Harmonic vibrational frequencies at the MP2/6-31G** level have been calculated for the two conformers, and the computed infrared spectra are reported in Figure 5.102. The frequencies and intensities of the bands are listed in Table 5.65.

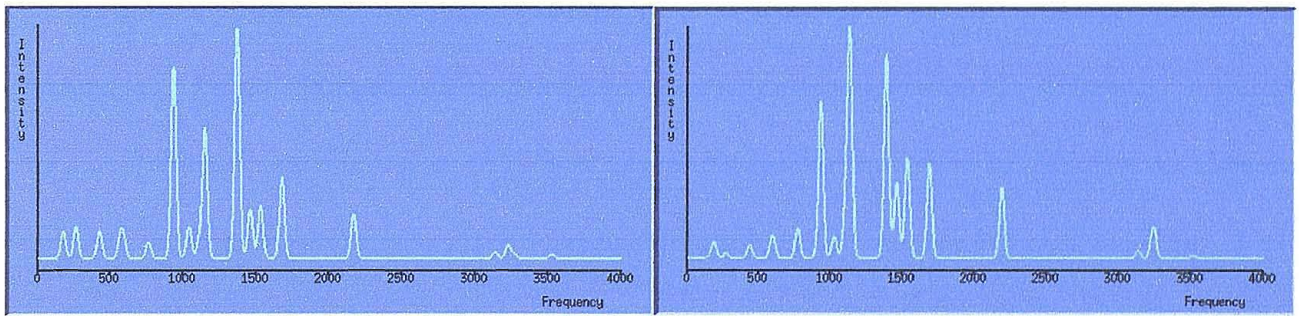

Figure 5.102- The infrared spectra for the two conformers cis (left) and trans (right) of 2-iminopropionitrile calculated at the MP2/6-31G level. The frequencies are reported in cm^{-1}**

It is evident that there is a very different distribution of the intensities of the bands- which are very similar in frequencies- between the two conformers. In particular, the *trans* conformer shows an

increased intensity of the band at 1132 cm^{-1} and of all those bands above 1530 cm^{-1} relative to the band at 1387 cm^{-1} which is not the most intense band as it was in the case of the *cis* conformer. The *cis* conformer structure also shows the highest intensity for the band predicted at 933 cm^{-1}.

Table 5.65- Calculated infrared bands for the two conformers of 2-iminopropionitrile (absorbances in Km/mol, frequencies expressed in cm^{-1})

Cis frequencies	*Intensity*	*Trans frequencies*	*Intensity*	**Normal mode**
426.1	9.80	437.5	3.82	
568.8	7.47			
591.3	5.74	598.2	6.18	
762.9	5.64	770.1	8.76	
933.5	68.28	930.7	45.36	
1038.9	11.29	1024.8	6.06	
1110.8	6.52	1102.2	14.24	
1148.6	45.91	1132.5	64.35	
1368.9	81.62	1386.6	59.40	N-H bending
1458.8	17.17	1457.1	21.77	C-H_3 wagging
1529.0	9.42	1523.5	8.11	C-H_3 in phase scissoring
1530.3	9.46	1535.1	22.45	C-H_3 out of phase scissoring
1676.0	28.93	1686.1	27.53	C=N stretching
2166.7	15.75	2187.8	20.72	C≡N stretching
3136.6	2.36	3131.4	2.25	C-H_3 symmetric stretching
3225.4	4.81	3227.2	2.85	C-H_3 asymmetric stretching
3265.5	1.68	3243.0	6.98	C-H_3 asymmetric stretching
3526.5	1.46			N-H stretching

Type 2 mechanism:

In principle, 2-nitreneacetamide, originating from 2-azidopropionitrile by nitrogen release, should have just one possible geometry: when the initial geometry of the nitrene is set as the one of the azide with a very long distance for the N-N bond which is going to be broken and the calculation is let to fully optimize the structure, the nitrene diradical proved to be unstable and isomerized by attacking a remote site of the molecule. However, two conformers of the azide were optimized: by using the two different

geometries of 2-azidopropionitrile as the starting geometry for the initial nitrene geometry, two different attack sites for the nitrogen atom were found.

When the geometrical parameters of the singlet nitrene are set as in structure *cis* of 2-azidopropionitrile, the attack site is the methyl group, leading to the production of $CH_3N{=}CHCN$ with the mechanism:

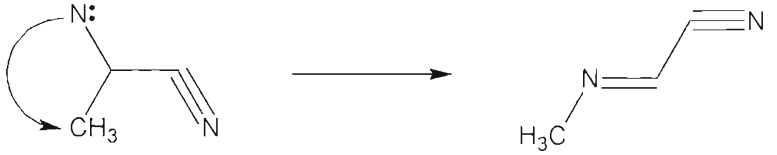

When structure *trans* is used as the starting point for the singlet nitrene geometry, the attack is directed to the cyanic carbon atom, leading to the production of $CH_3CH{=}NCN$ following the scheme:

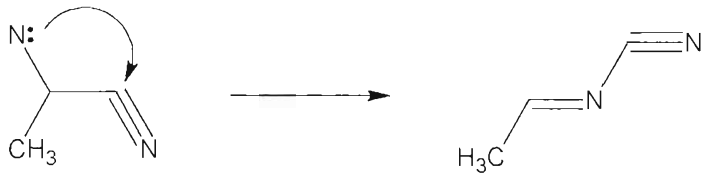

It is important to state that by using these initial geometries for the singlet nitrene for the *ab initio* optimization, no isomerization following a Type 1 mechanism (the 1,2-hydrogen shift) was observed.

It is important also to note that attempts to locate a transition state directly leading to the formation of 2-iminopropionitrile from 2-azidopropionitrile by a concerted nitrogen elimination-1,2 hydrogen shift mechanism were not successful.

In the singlet nitrene these two sites are favoured to be attacked by the nitrogen atom because of geometrical alignment: in the *cis* conformers of the azide (Figure 5.94), the N_3, CH and CH_3 groups are basically in the same plane, while in the *trans* conformer the azide chain is rotated so that this time the N_3, CH and CN group are in the same plane. This means that when nitrogen is released and the azide chain is broken, the N-N bond breaking is accompanied by a relative movement of the nitrogen atoms so that the one remaining on the nitrene is moved closer to these two electron deficient sites. In one case the direction of the movement (found by the imaginary frequency for the transition state between the azide and the nitrene in consequence of the nitrogen elimination) makes the nitrogen move towards the methyl group (structure *cis*), in the other case it moves towards the cyano group (structure *trans*).

The result is that the nitrene isomerizes to two imines, different from 2-iminopropionitrile.

CH_3N=CHCN

Two geometries for this imine were optimized, they were labelled *cis* and *trans* according to the relative positions of the methyl and cyano groups, and are reported in Figure 5.103. They are planar structures, and therefore belong to the C_s point group. Table 5.66 lists the most significant geometrical parameters for structure *trans*, which is the most stable of the two, as labelled in Figure 5.103.

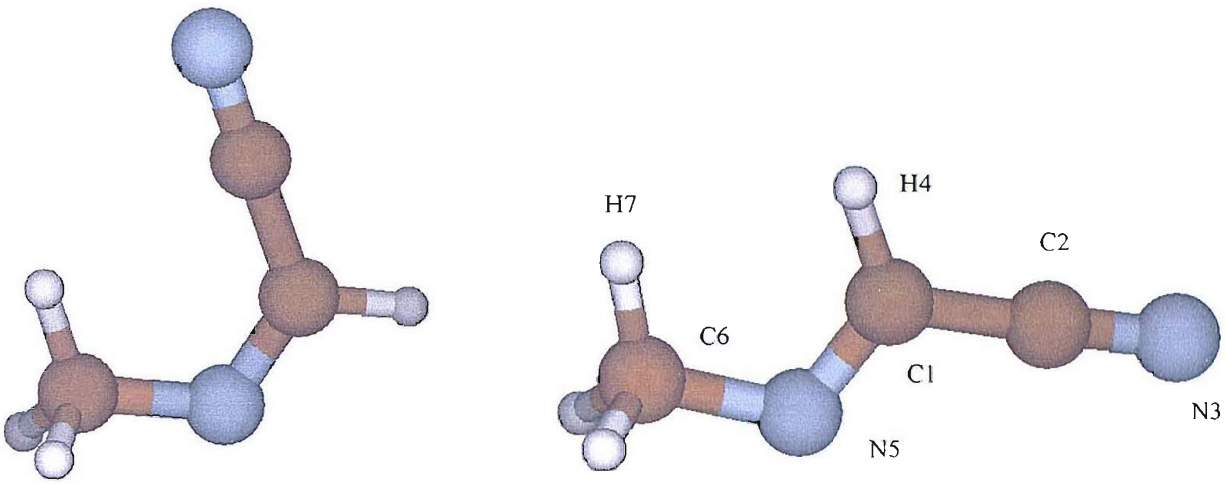

Figure 5.103- The two minimum energy structures *cis* (left) and *trans* (right) of CH_3N=CHCN optimized at the MP2/6-31G level**

Table 5.66- The most significant geometrical parameters for structure *trans* of CH_3N=CHCN - see Figure 5.103 for the labelling of the atoms

Bond	Length (Å)	Angle	Value (°)
C2-N3	1.184	N3-C2-C1	177.51
C1-C2	1.444	C2-C1-N5	119.56
C1-H4	1.094	H4-C1-N5	124.24
C1-N5	1.283	C6-N5-C1	115.93
N5-C6	1.455	H7-C6-N5	113.77
C6-H7	1.095	N3-C2-C1-N5	179.53

The total energy of the *cis* and *trans* structures was calculated as -225.5091045 and -225.5091953 hartrees, which means a difference of just 0.057 kcal/mol. Such a small energy difference means that both structures will be produced- if they are formed at all- as reaction intermediates: the calculated VIEs and vibrational frequencies of both conformers will therefore be reported in the following paragraphs.

VIEs have been calculated by means of Koopmans' theorem applied to the molecular orbital energies obtained for the MP2/6-31G** structures: they are listed in Table 5.67 for both conformers.

Table 5.67- The calculated vertical ionization energies for the two conformers of CH_3N=CHCN

"cis" KT calculated VIE (eV)	"cis" KT calculated VIE *0.92 (eV)	"trans" KT calculated VIE (eV)	"trans" KT calculated VIE *0.92 (eV)
11.50	10.58	11.39	10.48
12.35	11.36	12.48	11.49
13.01	11.97	12.77	11.75
14.13	13.00	14.09	12.96
15.42	14.19	15.19	13.98

Also in the case of CH_3N=CHCN the differences between the VIEs of the two conformers are very small: the only difference could be the fact that-as happened for 2-iminopropionitrile, structure *trans* should have the third band overlapping with the second, while in structure *cis* these should be separated. Only structure *cis* would therefore display a band in the 12.0-13.0 eV region of the photoelectron spectrum.

Harmonic vibrational frequencies have been calculated for both conformers at the MP2/6-31G** level. They are reported in Table 5.68 along with a description of the normal mode they are associated with; the full calculated IR spectra are presented in Figure 5.104, assuming a Gaussian shape for the peaks. The main difference is in the distribution of the intensities of the bands- which are very similar in frequencies- between the two conformers, notably the band at 3110 cm^{-1}, which is stronger in the *cis* spectrum, and the band at 1016 cm^{-1}, which is stronger in the *trans* structure. For both conformers, the most intense band is the one due to the C=N stretch, which as an average is calculated at 1685 cm^{-1}.

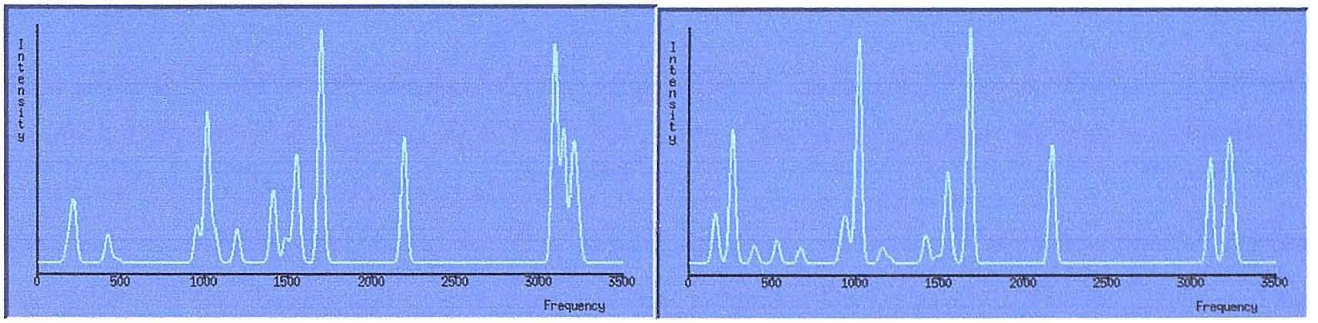

Figure 5.104- The infrared spectra for the conformers *cis* (left) and *trans* (right) of CH_3N=CHCN calculated at the MP2/6-31G level. The frequencies are expressed in cm^{-1}**

Table 5.68- Calculated infrared bands for the two conformers of CH_3N=CHCN (absorbances in Km/mol)

Cis frequencies	*Intensity*	*Trans frequencies*	*Intensity*	**Normal mode**
528.5	3.68	422.2	4.71	
669.1	2.40			
920.2	4.96	955.3	6.23	
946.5	5.37	1015.8	25.24	
1014.8	36.07	1061.8	5.20	
1156.9	2.52	1194.8	5.60	
1417.9	4.57	1410.8	12.14	C-H bending
1482.7	1.04	1485.6	4.14	$C-H_3$ wagging
1539.2	4.88	1532.2	3.89	$C-H_3$ out of phase scissoring
1551.6	10.67	1553.6	16.33	$C-H_3$in phase scissoring
1676.8	38.06	1695.4	39.05	C=N stretching
2168.5	19.02	2191.8	21.05	C≡N stretching
3110.6	16.91	3090.9	36.59	$C-H_3$ symmetric stretching
3213.2	13.05	3144.1	22.10	$C-H_3$ asymmetric stretching
3231.5	7.89	3202.2	17.74	$C-H_3$ asymmetric stretching
3246.9	5.98	3229.7	8.43	C-H stretching

- On inspecting the *cis* structure, it is evident that another isomerization is possible from CH_3N=CHCN, that is a 1,2-hydrogen shift from the iminic carbon atom to the adjacent nitrogen atom: in this way, a CH_3NH=CCN diradical can be formed as follows:

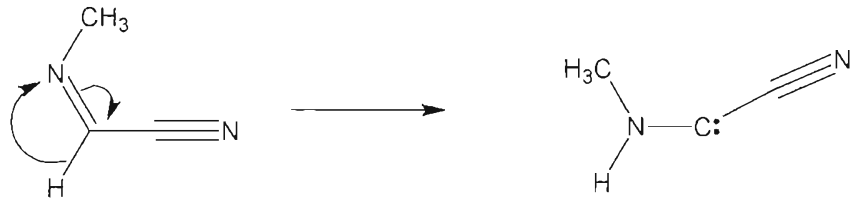

This radical is expected to be less stable than the originating imine. Nevertheless, calculations have been performed also on this radical because, as it will be seen in the following sections, it has been found that it can act as a precursor for the formation of the decomposition products experimentally detected in the 2-azidopropionitrile pyrolysis.

Two structures have been found for this radical, labelled *cis* or *trans* according to the relative orientation of the methyl and cyano groups. Their geometries are shown in Figure 5.105, and the important geometrical parameters for the most stable *trans* structure are listed in Table 5.69. Both are planar structures (point group C_s).

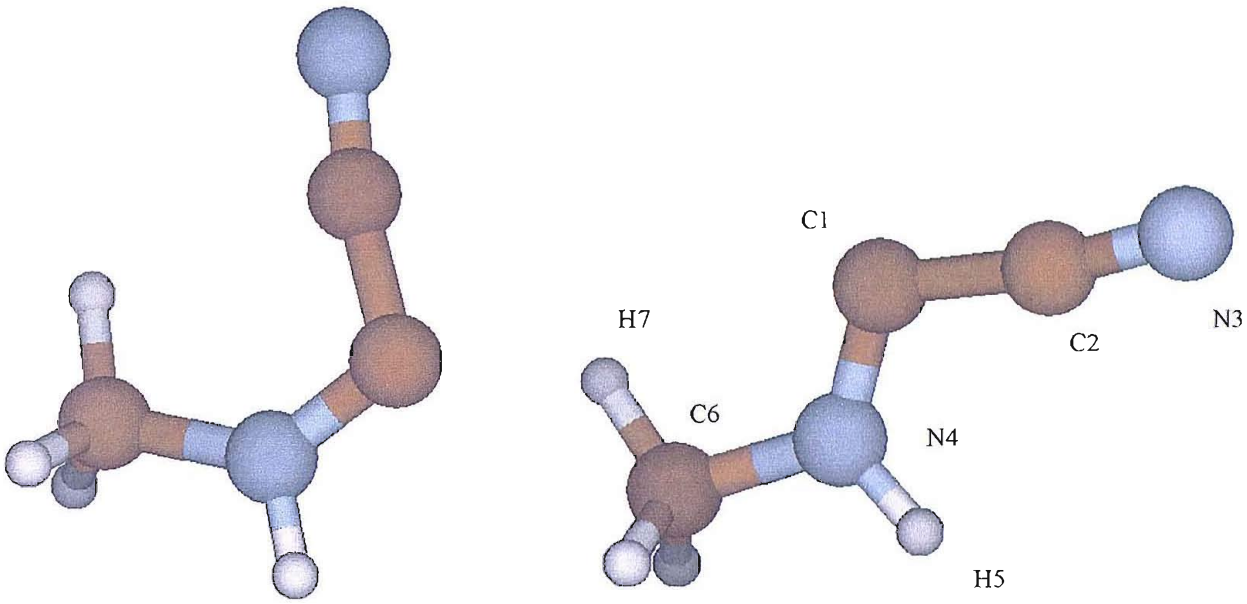

Figure 5.105- Structures *cis* (left) and *trans* (right) of CH_3NH=CCN optimized at the MP2/6-31G level**

Table 5.69- The most significant geometrical parameters for structure *trans* of CH_3NH=CCN - see Figure 5.105 for the labelling of the atoms

Bond	Length (Å)	Angle	Value (°)
C2-N3	1.187	**N3-C2-C1**	172.14
C1-C2	1.445	**C2-C1-N4**	110.89
C1-N4	1.312	**H5-N4-C1**	123.05
N4-H5	1.021	**C6-N4-C1**	121.81
N4-C6	1.459	**H7-C6-N5**	106.98
C6-H7	1.085	**N3-C2-C1-N4**	179.86

The most relevant difference between the geometries of this radical and the imine it originated from is the long bond distance between the carbon and nitrogen atoms on which the 1,2-H shift has undergone: from 1.28 Å it has increased to 1.31 Å. This is expected from the loss of double bonding character between these two atoms. However, the small increase shows that the bond has still some double bond character: this indicates that the radical prefers to redistribute its electron density forming a charged imine, with a negative charge on the carbon and a positive charge on the nitrogen, following the scheme

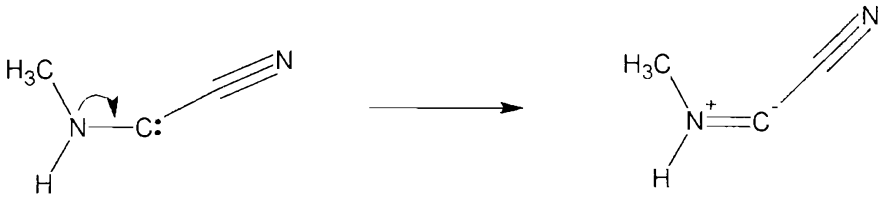

From the calculated bond lengths, it appears that this molecule prefers to exist in the iminic form: therefore, the molecule should be better treated as a charged imine rather than a radical.

The two optimized structures have total energies of respectively -225.4572496 (*cis*) and -225.4586603 (*trans*) hartrees. Their energy difference is then 0.885 kcal/mol, a value comparable with the difference between the conformers of the originating imine CH_3N=CHCN. The difference between the trans conformers of the two imines (which are the most stable conformers for both molecules) is 31.711 kcal/mol, indicating- as expected- a much reduced stability for the charged imine.

The large energy gap makes unlikely the experimental observation of this charged imine in the 2-azidopropionitrile thermal decomposition process. No details of the calculated VIEs and vibrational frequencies will be reported here. Only the computed IR spectra are displayed- in Figure 5.106- to show that no relevant bands are expected in the region above 1650 cm^{-1}, that is where the experimental IR matrix isolation results show the presence of a band associated with a stable pyrolysis product (1724 cm^{-1}). In fact, structure trans of this charged imine shows a relevant peak at 1656 cm^{-1}, associated with the C=N stretching mode. This value is very close to the one predicted for CH_3N=CHCN for the same vibration (around 1685 cm^{-1}).

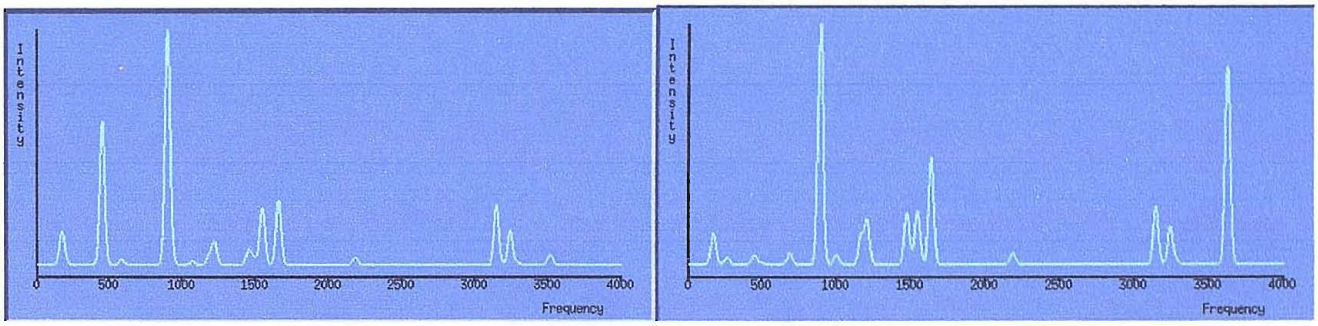

Figure 5.106- The infrared spectra for the conformers *cis* (left) and *trans* (right) of CH_3NH=CCN calculated at the MP2/6-31G level. The frequencies are reported in cm^{-1}**

Moreover, it was found that the singlet nitrene can undergo a different isomerization, leading to the formation of a cyclic amine, (cyc-CH_2NHCH)-CN: the first step of this process is the same as that leading to the formation of CH_3N=CHCN, that is the attack of the nitrogen onto the methyl group followed by a 1,2-H shift from the carbon to the nitrogen.

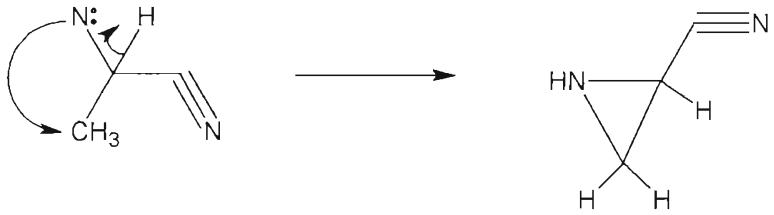

(cyc-CH_2NHCH)CN

Two structures have been optimized for the cyclic amine, according to the possible relative orientation of the cyano group to the aminic hydrogen (*cis* if both on the same side of the ring, *trans* if on opposite sides). Their geometries are reported in Figure 5.107, and the most relevant geometrical parameters for structure *cis*- the most stable one- are listed in Table 5.70.

Their calculated total energies are respectively -225.4937989 (*cis*) and -225.4925642 (*trans*) hartrees, corresponding to a difference of 0.775 kcal/mol. The two structures are therefore both likely to be produced in the pyrolysis of 2-azidopropionitrile.

The VIEs of these two structures obtained by applying Koopmans' theorem to the energy of the molecular orbitals for the MP2/6-31G** structures are reported in Table 5.71. The main difference between the two structures- apart from the mean 0.2 eV shift of the first two PE bands- is the fact that in structure *trans* the computed value for the third VIE is very close (0.27 eV) to that for the second VIE: in the experimental photoelectron spectrum the two would probably merge into the same band.

For structure *cis* the separation is bigger (0.43 eV), so that it should be possible to distinguish them experimentally.

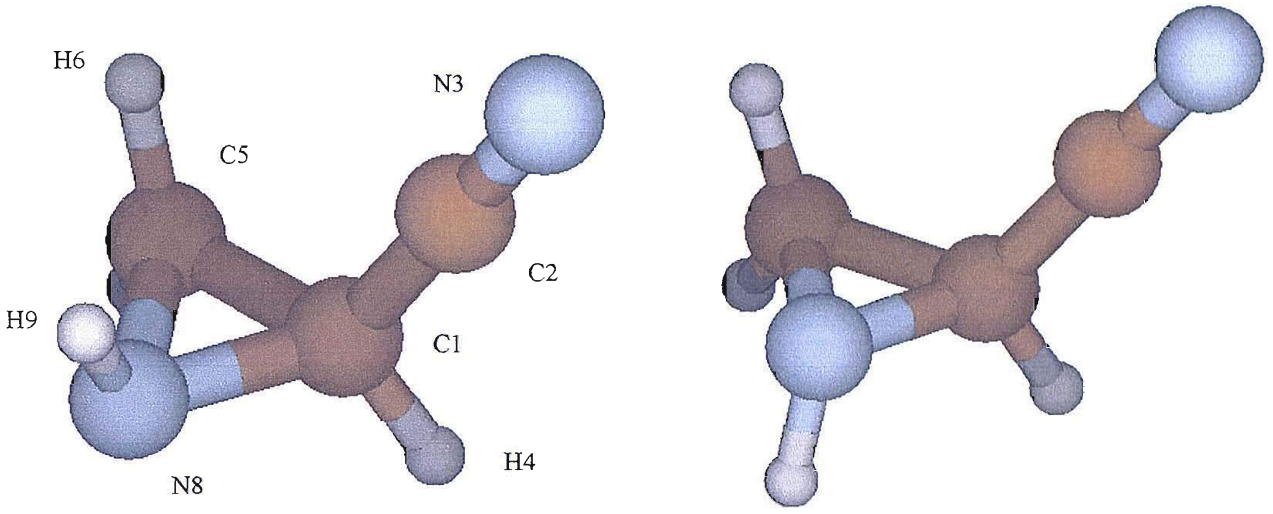

Figure 5.107- The structures *cis* (left) and *trans* (right) of (cyc-CH_2NHCH)CN optimized at the MP2/6-31G level**

Table 5.70- The most significant geometrical parameters for structure *cis* of (cyc-CH_2NHCH)CN - see Figure 5.107 for the labelling of the atoms

Bond	Length (Å)	Angle	Value (°)
C2-N3	1.183	**N3-C2-C1**	178.85
C1-C2	1.446	**C2-C1-N8**	119.30
C1-H4	1.082	**H4-C1-C5**	121.63
C1-C5	1.490	**H6-C5-C1**	119.60
C1-N8	1.478	**H9-N8-C5**	109.97
C5-N8	1.465	**C5-N8-C1**	60.85
H6-C5	1.083	**H9-N8-C1-C2**	4.49
H9-N8	1.018	**H6-C5-C1-H4**	-148.06
		C5-N8-C1-C2	107.13

Table 5.71- The first six calculated vertical ionization energies for the two conformers of (cyc-CH_2NHCH)CN

"cis" KT calculated VIE (eV)	"cis" KT calculated VIE *0.92 (eV)	"trans" KT calculated VIE (eV)	"trans" KT calculated VIE *0.92 (eV)
11.19	10.30	11.39	10.48
12.51	11.51	12.26	11.28
13.09	12.04	12.53	11.53
14.52	13.36	14.50	13.34
14.79	13.61	14.88	13.69
15.27	14.05	15.12	13.91

Harmonic vibrational frequencies have been calculated for both conformers at the MP2/6-31G** level, and are reported in Table 5.72. The full IR spectra are shown in Figure 5.108. As can be seen, the most relevant differences appear in the region below 1300 cm^{-1} in which structure *cis* displays all the bands with increased intensity- with the exception of the band at 550 cm^{-1}- with respect to the one at 890 cm^{-1} which is the strongest for both conformers. Noteworthy is also the fact that no relevant contributions are expected in the region between 1500 and 2000 cm^{-1} and that the C≡N stretching mode is expected to be very weak, in particular for the *cis* conformer.

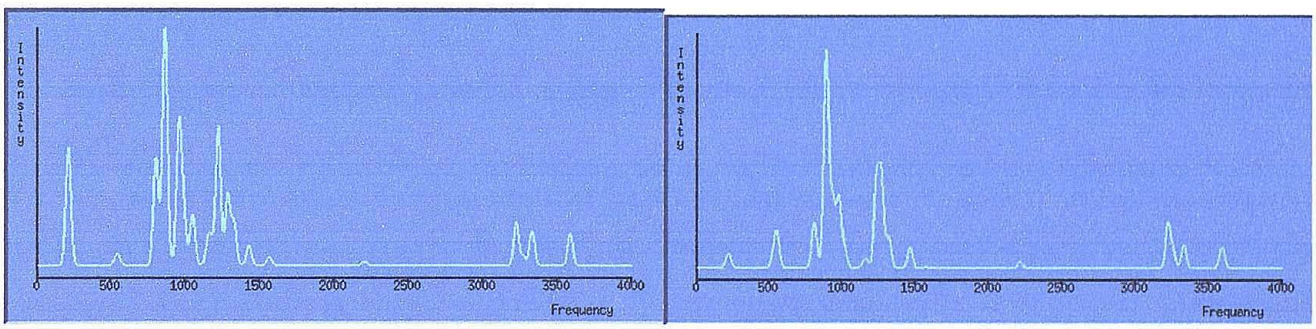

Figure 5.108- The infrared spectra for the conformers *cis* (left) and *trans* (right) of (cyc-CH_2NH=CH)CN calculated at the MP2/6-31G level and assuming a Gaussian shape for the peaks. Frequencies are expressed in cm^{-1}**

Table 5.72- Calculated infrared bands for the two conformers of (cyc-CH_2NH=CH)CN (absorbances in Km/mol, frequencies in cm^{-1})

Cis frequencies	*Intensity*	*Trans frequencies*	*Intensity*	**Normal mode**
547.3	1.55	526.7	2.85	
801.5	19.26	552.7	7.19	
862.1	42.41	807.2	9.82	
955.6	24.34	888.7	47.41	
985.8	9.60	933.9	14.48	
1047.4	9.04	975.8	15.07	
1151.5	3.95	1013.8	3.81	
1174.0	3.33	1159.6	1.80	
1220.4	24.80	1232.6	18.86	
1284.4	12.60	1266.9	19.30	
1325.9	7.68	1315.1	6.51	
1427.3	3.55	1461.6	4.50	C-H bending
1564.3	1.45			C-H_2 scissoring
		2211.5	1.31	C≡N stretching
3223.1	7.64	3221.6	9.39	C-H_2 symmetric stretching
3269.4	1.63	3253.1	3.49	C-H stretching
3329.2	6.12	3329.1	5.03	C-H_2 asymmetric stretching
3584.7	5.68	3590.0	4.47	N-H stretching

CH_3CH=NCN

As already mentioned, when the pseudo-nucleophilic attack of the nitrogen atom occurs on the cyano group, CH_3CH=NCN is formed.

Two structures have been optimized at the MP2/6-31G** level, according to the relative orientation of the cyano and the methyl groups, and consequently are labelled as *cis* or *trans* structures. Their geometries are reported in Figure 5.109 and the most important geometrical parameters for the most stable one, structure *trans*, are listed in Table 5.73. Being planar, their point group is C_s.

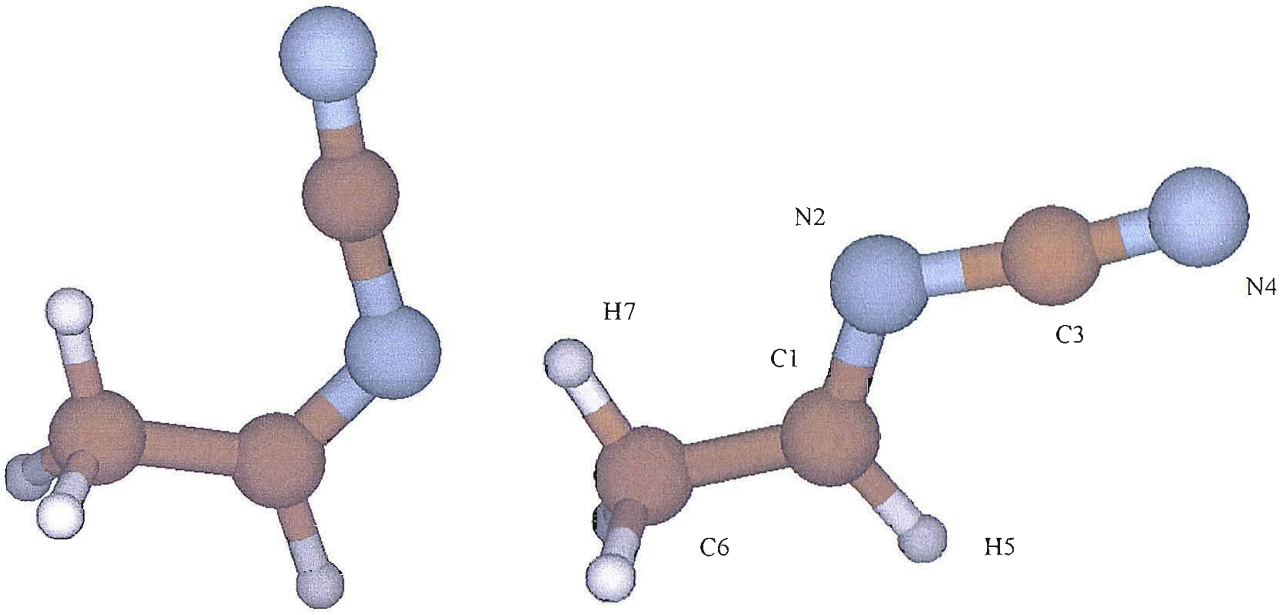

Figure 5.109- The structures *cis* (left) and *trans* (right) of CH_3CH=NCN optimized at the MP2/6-31G level**

Table 5.73- The most significant geometrical parameters for structure *trans* of CH_3CH=NCN - see Figure 5.109 for the labelling of the atoms

Bond	Length (Å)	Angle	Value (°)
C3-N4	1.187	**N4-C3-N2**	174.75
N2-C3	1.357	**C3-N2-C1**	117.38
C1-N2	1.292	**H5-C1-N2**	121.63
C1-H5	1.092	**C6-C1-N2**	120.35
C1-C6	1.487	**H7-C6-C1**	110.12
C6-H7	1.087	**N4-C3-N2-C1**	179.99

The calculated total energies are -225.5130145 (*cis*) and -225.5135792 (*trans*) hartrees, meaning a difference between the two conformers of only 0.354 kcal/mol.

Given this very small difference in stability, the two structures will both contribute to the experimental PE and IR spectra- assuming that CH_3CH=NCN is formed in the pyrolysis of 2-azidopropionitrile. Therefore both structures will be considered when VIEs and vibrational frequencies are presented.

VIEs obtained for the MP2/6-31G** structures by applying Koopmans' theorem to the molecular orbital energies are listed in Table 5.74.

Table 5.74- First five calculated vertical ionization energies for the two conformers of $CH_3CH=NCN$

"cis" KT calculated VIE (eV)	"cis" KT calculated VIE *0.92 (eV)	"trans" KT calculated VIE (eV)	"trans" KT calculated VIE *0.92 (eV)
11.14	10.25	11.10	10.22
11.340	10.49	11.47	10.552
14.02	12.90	13.95	12.83
14.79	13.60	14.81	13.63
15.15	13.94	15.12	13.91

The two structures display the same pattern of bands; it is possible that given the small difference between the energy of the first and second VIEs, a single band would be observed in the experimental photoelectron spectrum in the 10.5 eV region.

The harmonic vibrational frequencies, calculated at the MP2/6-31G** level, are listed for both conformers in Table 5.75. The computed IR spectrum is reported in Figure 5.110.

The spectrum of structure cis, apart from a higher intensity of the band at 1525 cm^{-1}, displays a more congested series of bands in the region below 1200 cm^{-1}. Both conformers are characterized by a strong peak at 1725 cm^{-1} due to the C=N stretching mode.

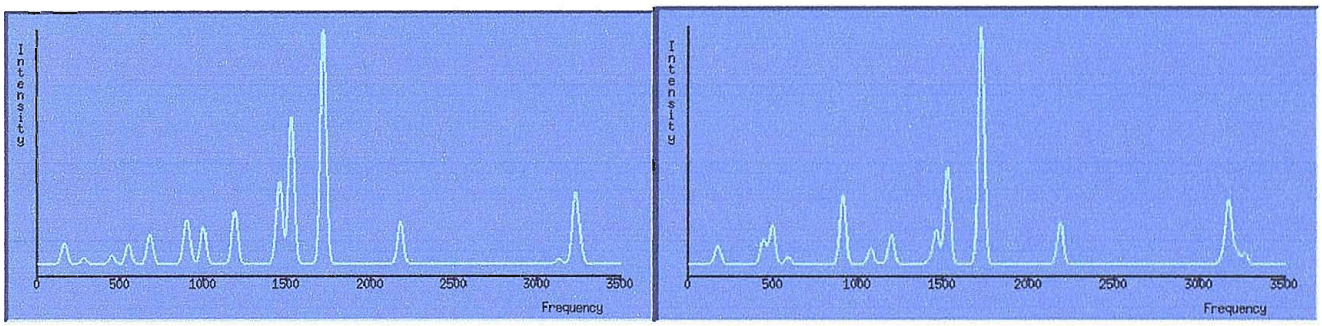

Figure 5.110- The infrared spectra for the conformers *cis* (left) and *trans* (right) of $CH_3CH=NCN$ as calculated at the MP2/6-31G level and assuming a Gaussian shape for the peaks. Frequencies are expressed in cm^{-1}**

Table 5.75- Calculated infrared bands for the two conformers of $CH_3CH=NCN$ (absorbances in Km/mol, frequencies in cm^{-1})

Cis frequencies	*Intensity*	*Trans frequencies*	*Intensity*	**Normal mode**
450.9	1.91	444.7	7.48	
549.7	4.45	497.7	11.70	
678.7	6.26	588.6	2.37	
889.4	5.11	909.1	14.11	
908.0	6.02	913.0	7.23	
998.1	8.09	1074.8	4.83	
1187.7	11.57	1195.8	9.01	
1435.4	2.93	1420.0	1.33	C-H bending-$C-H_3$ wagging
1457.6	16.58	1459.7	10.21	$C-H_3$ wagging-C-H bending
1526.0	21.97	1523.3	19.69	$C-H_3$ in phase scissoring
1527.5	9.85	1528.2	9.99	$C-H_3$out of phase scissoring
1718.1	51.01	1723.3	71.55	C=N stretching
2179.2	9.14	2185.3	12.68	N-C≡N stretching
3129.2	1.03	3130.3	2.05	$C-H_3$ symmetric stretching
3214.3	2.90	3167.7	19.21	$C-H_3$ asymmetric stretching
3226.3	12.20	3212.2	4.58	C-H stretching
3253.9	3.86	3265.3	3.45	$C-H_3$ asymmetric stretching

- As it was the case for $CH_3N=CHCN$, in $CH_3CH=NCN$ it is evident that in structure *cis* it is easy to promote a 1,2-hydrogen shift between the carbon and the nitrogen atoms to form a charged imine with formula $CH_3C=NHCN$.

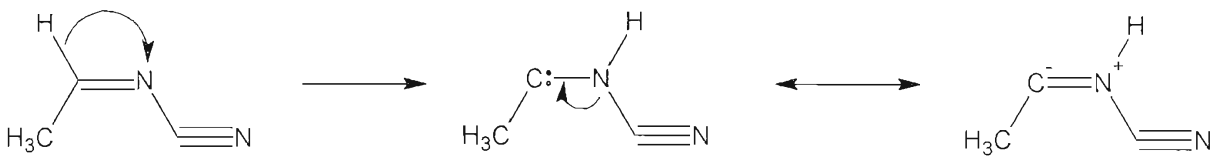

Also for this imine, two planar structures, *cis* and *trans*, have been optimized at the MP2/6-31G** level with different orientations of the cyano and methyl groups: they are reported in Figure 5.111, and Table 5.76 lists the most relevant geometrical parameters for structure *cis*, which in this case is the most stable one probably because of the lack of repulsion between the hydrogen atoms on the nitrogen and those on the methyl group which characterize structure *trans*. The value of the C=N bond distance (1.34 Å) is very close to the one in the originating CH_3CH=NCN imine, confirming that also in this case the newly formed structure shows the character of an imine with charges on the iminic carbon (-) and nitrogen (+) atoms rather than a diradical character.

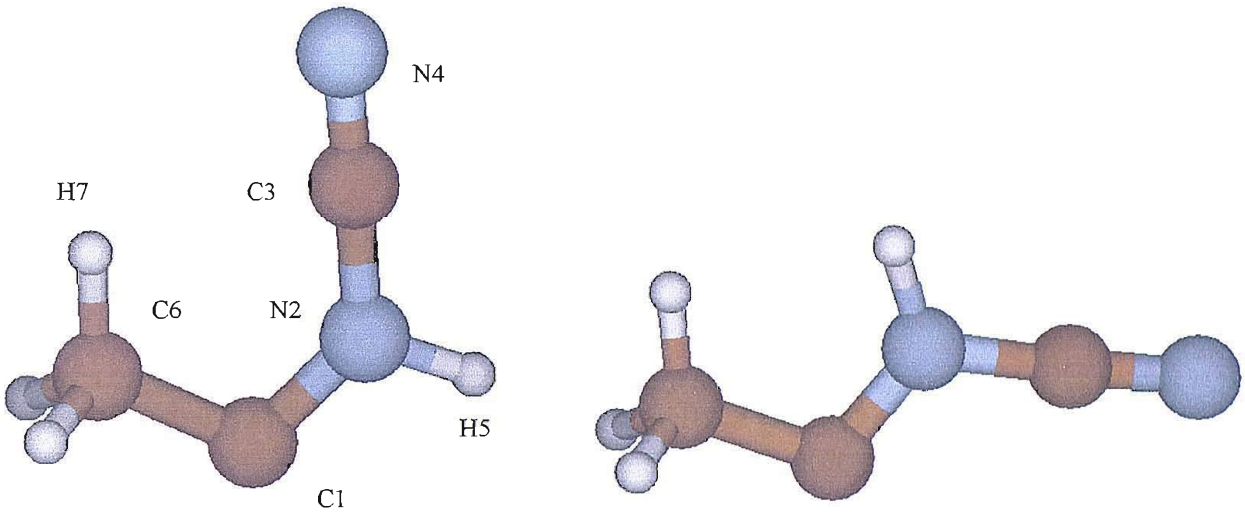

Figure 5.111- The structures *cis* (left) and *trans* (right) of CH_3C=NHCN optimized at the MP2/6-31G level**

Table 5.76- The most significant geometrical parameters for structure *cis* of CH_3C=NHCN - see Figure 21 for the labelling of the atoms

Bond	Length (Å)	Angle	Value (°)
C3-N4	1.183	**N4-C3-N2**	179.17
N2-C3	1.382	**C3-N2-C1**	128.27
C1-N2	1.341	**H5-N2-C1**	117.67
N2-H5	1.013	**C6-C1-N2**	112.65
C1-C6	1.494	**H7-C6-C1**	118.19
C6-H7	1.094	**N4-C3-N2-C1**	-0.31

The total energies for the two structures have been calculated as -225.4324657 and -225.4324485 hartrees: this means a difference between the two conformers of just 0.011 kcal/mol. The difference between the most stable conformers of $CH_3C{=}NHCN$ and $CH_3CH{=}NCN$ (the initial imine undergoing the 1,2-hydrogen shift) is 50.90 kcal/mol: such a marked difference in stability makes highly unlikely the experimental observation of $CH_3C{=}NHCN$ in the pyrolysis experiments of 2-azidopropionitrile. Therefore, no details on the calculated VIEs and vibrational frequencies on this imine will be reported here. Only the calculated IR spectra are shown in Figure 5.112, to show that in this case no strong bands in the 1600-1800 cm^{-1} region are expected, therefore discounting $CH_3C{=}NHCN$ as the species associated with the band at 1742 cm^{1} observed in the decomposition experiments conducted in the nitrogen matrix. It is noteworthy that- despite the almost identical total energies between the *cis* and *trans* structures- the calculated IR spectra of the two conformers show marked difference in the intensity ratios of the bands, especially above 1400 cm^{-1}.

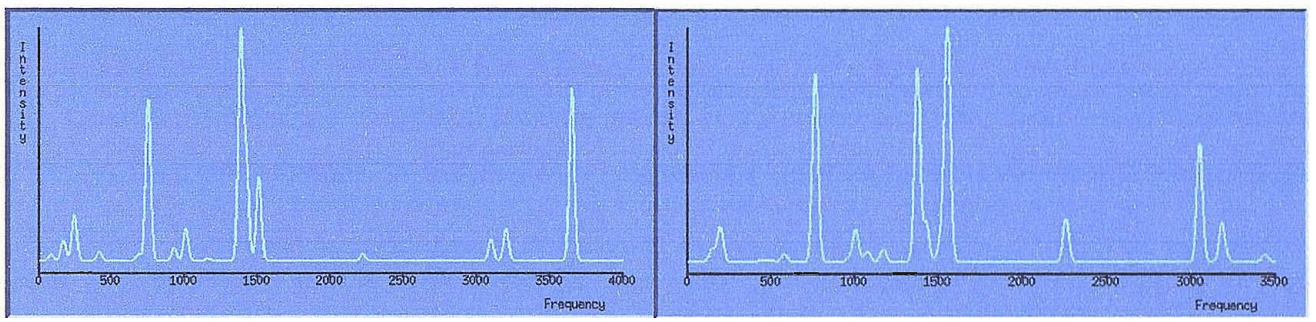

Figure 5.112- The infrared spectra for the conformers *cis* (left) and *trans* (right) of $CH_3C{=}NHCN$ as calculated at the MP2/6-31G level with a Gaussian shape for the bands. Frequencies expressed in cm^{-1}**

5.6.5.1 SUMMARY OF THE *AB INITIO* RESULTS ON THE INTERMEDIATES

Five possible imines and a cyclic amine have been considered as intermediates for the thermal decomposition of 2-azidopropiopnitrile, and the geometries of their different conformers have been optimized. These molecules are:

- $CH_3C(CN)=NH$
- $CH_3N=CHCN$
- $CH_3NH=CCN$
- $CH_3CH=NCN$
- $CH_3C=NHCN$
- (cyc-CH_2NHCH)CN

The relative energies indicate a marked stability of the imine + N_2 system in comparison to the azide: $CH_3C(CN)=NH$ + N_2 is located at an energy 51.2 kcal/mol lower than 2-azidopropionitrile, $CH_3N=CHCN$ + N_2 at 41.9 kcal/mol lower and $CH_3CH=NCN$ + N_2 at 44.6 kcal/mol lower.
The two other imines are formed as a consequence of 1,2-hydrogen shifts from $CH_3N=CHCN$ and $CH_3CH=NCN$, and are much higher in energy (respectively -10.1 and +6.3 kcal/mol with respect to the azide).
Also the cyclic amine proved to be stable, its energy having been located 32.2 kcal/mol below the one of the azide.
Considering the higher energies of the two charged imines, it was assumed that it is likely that they will not been observed even as short-lived molecules in the 2-azidopropionitrile thermal decomposition process and hence they will not be considered when the spectroscopic characteristics of the intermediates are discussed.

The first five VIEs calculated for the most stable conformers of these four molecules (and scaled by the 0.92 factor [27, 28]) are listed in Table 5.77.
From the experimental results, the only possible sign of a PE band associated with an intermediate is the one with VIE at roughly 11.7 eV; from the calculation, three of the suggested compounds are expected to present a band in that region. Only $CH_3CH=NCN$ is not expected to show bands in the 11-13 eV IE region. However, it must be considered that the results from Koopmans' theorem are not completely reliable because of neglect of reorganization and electron correlation change on ionization. Considering also the uncertainty of the experimental evidence, it is therefore not safe to rule out $CH_3CH=NCN$ from the possible observed compounds.

Table 5.77- Ionization energies calculated with Koopmans' theorem at the MP2/6-31G level for the most stable products originating from the isomerization of the nitrene produced by decomposition of 2-azidopropionitrile**

cis-$CH_3C(CN)NH$ KT calculated VIE*0.92 (eV)	*trans*-CH_3NCHCN KT calculated VIE *0.92 (eV)	*trans*-CH_3CHNCN KT calculated VIE *0.92 (eV)	*cis*-(cyc-$CH_2NHCH)CN$ KT calculated VIE *0.92 (eV)
10.85	10.48	10.22	10.30
11.66	11.49	10.55	11.51
12.22	11.75	12.83	12.04
12.90	12.96	13.63	13.36
14.36	13.98	13.91	13.61

For the IR bands, the only sign of a reaction product not assignable to any of those clearly detected (HCN, CH_3CN, CH_3NC, CH_2=C=CN) is the thermally stable band at 1742 cm^{-1}: the presence of an impurity in the starting azide makes uncertain the attribution of this band to a genuine decomposition product of the azide, because it could be a product originating from the decomposition of the impurity. The infrared bands above 1300 cm^{-1} calculated for the four most stable candidate compounds are listed in Table 5.78. As can be seen, only CH_3CH=NCN presents a band in the 1600-1700 cm^{-1} region, and knowing that calculated frequencies are always overestimates of the experimental ones, it is difficult to say if the experimental band at 1742 cm^{-1} could be attributed to the C=N stretching in CH_3CH=NCN.

Table 5.78- Harmonic vibrational frequencies calculated at the MP2/6-31G level for the most stable products originating from the isomerization of the nitrene produced by decomposition of 2-azidopropionitrile**

cis-$CH_3C(CN)NH$ frequencies (cm^{-1})	*trans*-CH_3NCHCN frequencies (cm^{-1})	*trans*-CH_3CHNCN frequencies (cm^{-1})	*cis*-(cyc-$CH_2NHCH)CN$ frequencies (cm^{-1})
1368.9			1325.9
	1410.8	1420.0	1427.3
1458.8	1485.6	1459.7	
1529.0		1523.3	
1530.3	1532.2	1528.2	
	1553.6		1564.3
1676.0	1695.4	1723.3	
2166.7	2191.8	2185.3	
	3090.9		
3136.6	3144.1	3130.3	
	3202.2	3167.7	
3225.4	3229.7	3212.2	3223.1
3265.5		3265.3	3269.4
			3329.2
3526.5			3584.7

5.6.6 PROPOSED DECOMPOSITION MECHANISM AND ENERGY LEVELS

The results of the *ab initio* calculations do not support the presence of either an intermediate- as suggested by PES- or a stable product- as suggested by matrix IR- other than the observed stable products (nitrogen, cyanic acid, methyl cyanide, methyl isocyanide, ketenimine). The six intermediates found in the calculations- five imines and a cyclic amine- formed by isomerization of 2-nitrenepropionitrile are therefore assumed not to be experimentally observed.

Nevertheless, these molecules are crucial in the definition of an energy surface connecting the azide to its decomposition products.

Summarizing, 2-azidopropionitrile is supposed to decompose by first forming 2-nitrenepropionitrile, whose structure has not been optimized and therefore it is supposed that it immediately decomposes in a very short time after its formation. Even if there is still the possibility that the imines or the products could be obtained directly from the azide with a concerted mechanism, the fact that it was possible to locate transition states originating from the nitrene leads to the assumption that the nitrene is actually formed, as consequence of the release of molecular nitrogen from the azide, even with a very short lifetime. A concerted mechanism forming N_2, HCN and CH_3CN at the same time from the azide directly might be possible, avoiding any kind of nitrene formation, but attempts at locating a suitable transition state for this process have not proved successful.

The nitrene isomerizes through four alternative pathways, three of them producing a different imine intermediate and the fourth producing the cyclic amine; this amine can further isomerize to $CH_3N{=}CHCN$. On the basis of the structure of $CH_3N{=}CHCN$, the formation of methyl isocyanide is therefore explained. $CH_3CH{=}NCN$ is on the other hand a good precursor for ketenimine. $CH_3C(CN){=}NH$ (2-iminopropionitrile) has been found to be a suitable intermediate for the production of all the observed decomposition products, CH_3CN, ketenimine and CH_3NC (this latter compound via a further isomerization).

Despite their predicted stability, the imine intermediates have not been experimentally detected: this could be due to the high internal energy with which they are formed. Figure 5.113a reports the energy level diagram at 0 K for the decomposition paths of 2-azidopropionitrile. The calculations showed that the energy surface is very complex, with different transition states linking the stable products.

In the diagram all the minimum energy structures located have been included, including the two different imines formed by a 1,2-H shift on the primary imines (e.g. $CH_3N{=}CHCN \rightarrow CH_3NH{=}CCN$). Although all of these intermediates have not been experimentally observed, they have been included in

the diagram because they can explain the formation of ketemine, which is observed- although weakly- in the experiments.

To illustrate the contribution of entropy to the reaction, a free energy level scheme at 298 K is reported in Figure 5.113b: in this diagram, for the sake of clarity, a simplification was made by considering only the most likely pathways (those with lower transition states). The general free energy level diagram is reported in more detail in Figure 5.114, and the labelling and geometries of the transition states are shown in Table 5.79 and Figure 5.115.

As expected, considering ΔS, the energies of the product relative to the azide are all significantly lower, by around 25 kcal/mol. Also the transition states and the intermediate imines are lowered in energy, but to a lesser extent (about 10-15 kcal.mol).

From the diagram it is seen how the free energies of the observed products are not- apart from CH_3CN channel- lower than those of the intermediate imines: simple energetic considerations do not explain why experimentally the imines are not clearly detected. The crucial factor must be the fact that the high temperatures at which these imines are formed lead to the formation of products with a high internal energy: for big molecules such as the imines or the cyclic amine, the possibility of dissipating this excess energy into translational, rotational and vibrational energy is not enough to keep the molecule intact. It is possible that some vibrational modes are so excited that the molecule falls apart into smaller fragments: in this way the internal energy is better dissipated, and only the smaller molecules (HCN, CH_3CN, CH_3NC and CH_2=C=NH) are experimentally detected, even if the energy of methyl isocyanide and ketenimine are not as favoured as those of the imines or the cyclic amine.

The imines, even if not experimentally observed, could nevertheless be present as very reactive species on the decomposition path: the calculations show that is much easier to find a series of transition states for the stepwise mechanism involving the formation of imines rather than locating a single transition state for a concerted path. Moreover, the stepwise path can explain the small amount of ketenimine observed in the IR and PE spectra: the energy barriers for the formation of ketenimine are lower than those leading to the formation of the cyanides. As can be seen in the diagram, ketenimine can be formed on either side of the energy surface, both parallel to CH_3CN formation or to CH_3NC formation. Experimentally, the amount of CH_3NC produced decreases with increasing temperature: this is despite the fact that the activation energy barrier for the production of the isocyanide is the highest and therefore likely to be produced more at higher temperatures. This partial contradiction is explained by the fact that at those temperatures the thermodynamic equilibrium between isocyanide and cyanide is much in favour of CH_3CN, so that at very high temperature only CH_3CN will be observed.

The overall thermal decomposition mechanism of 2-azidopropionitrile can be drawn schematically- without taking into account the intermediate steps via the imines obtained by 1,2-hydrogen shift- as:

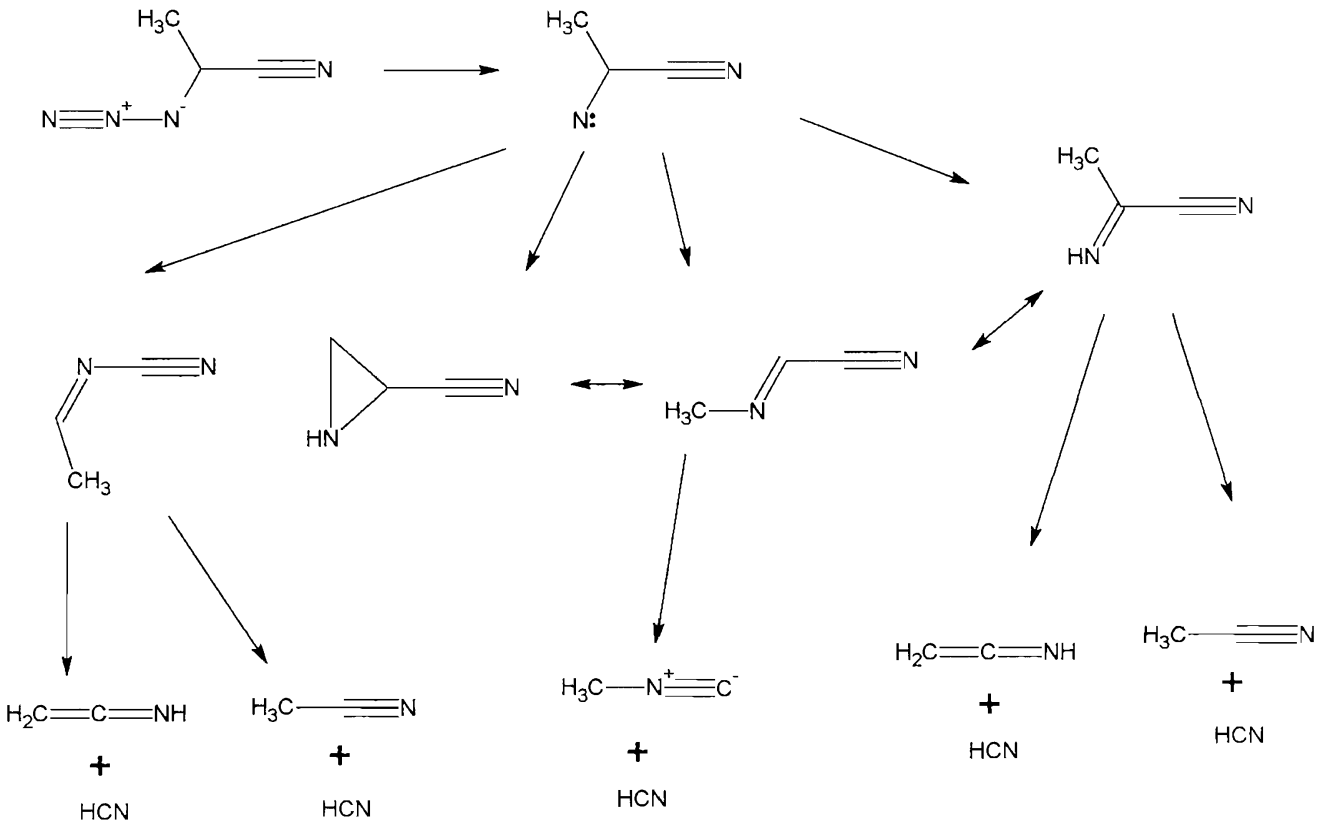

in which only the products in the last row are experimentally detected.

Table 5.79 reports the relative energies (at 0 K) and free energies (at 298 K) of the optimized structures and of the transition states found, setting as zero the total energy of the parent azide. Figure 5.115 shows the geometries of all the transition states of the system optimised at the MP2/6-31G** level, and it shows how the imines that have been located are necessary to explain the formation of molecules, such as CH_3NC and CH_2=C=NH, whose formation are not immediately explained from the geometries of the 2-azidopropionitrile conformers. The labelling of the transition states reflects that used in Figure 5.114 and explained in Table 5.79.

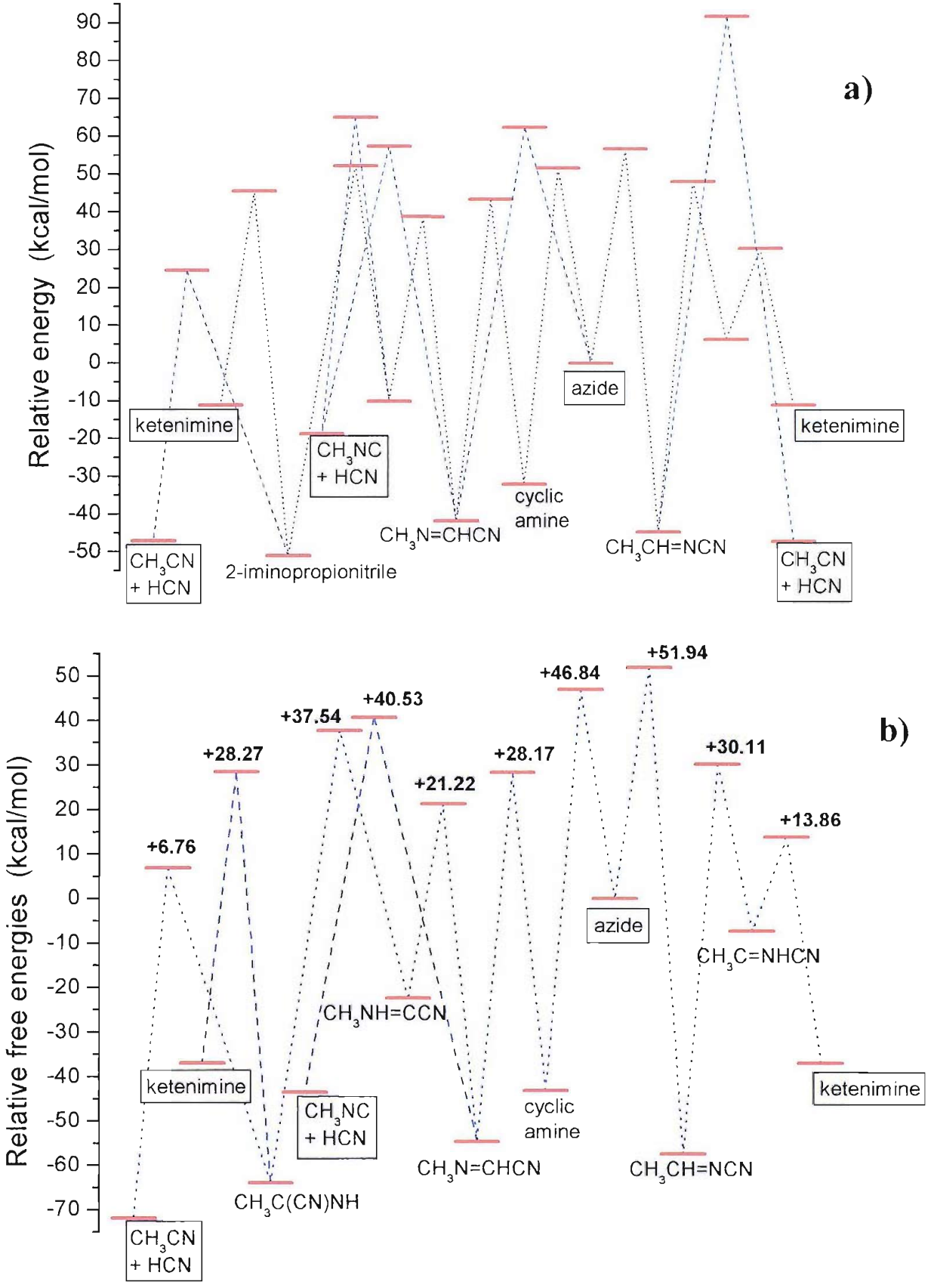

Figure 5.113- The energy level (a) and a simplified free energy level at 298 K (b) diagrams for 2-azidopropionitrile decomposition. The experimentally detected products are shown in boxes in this figure

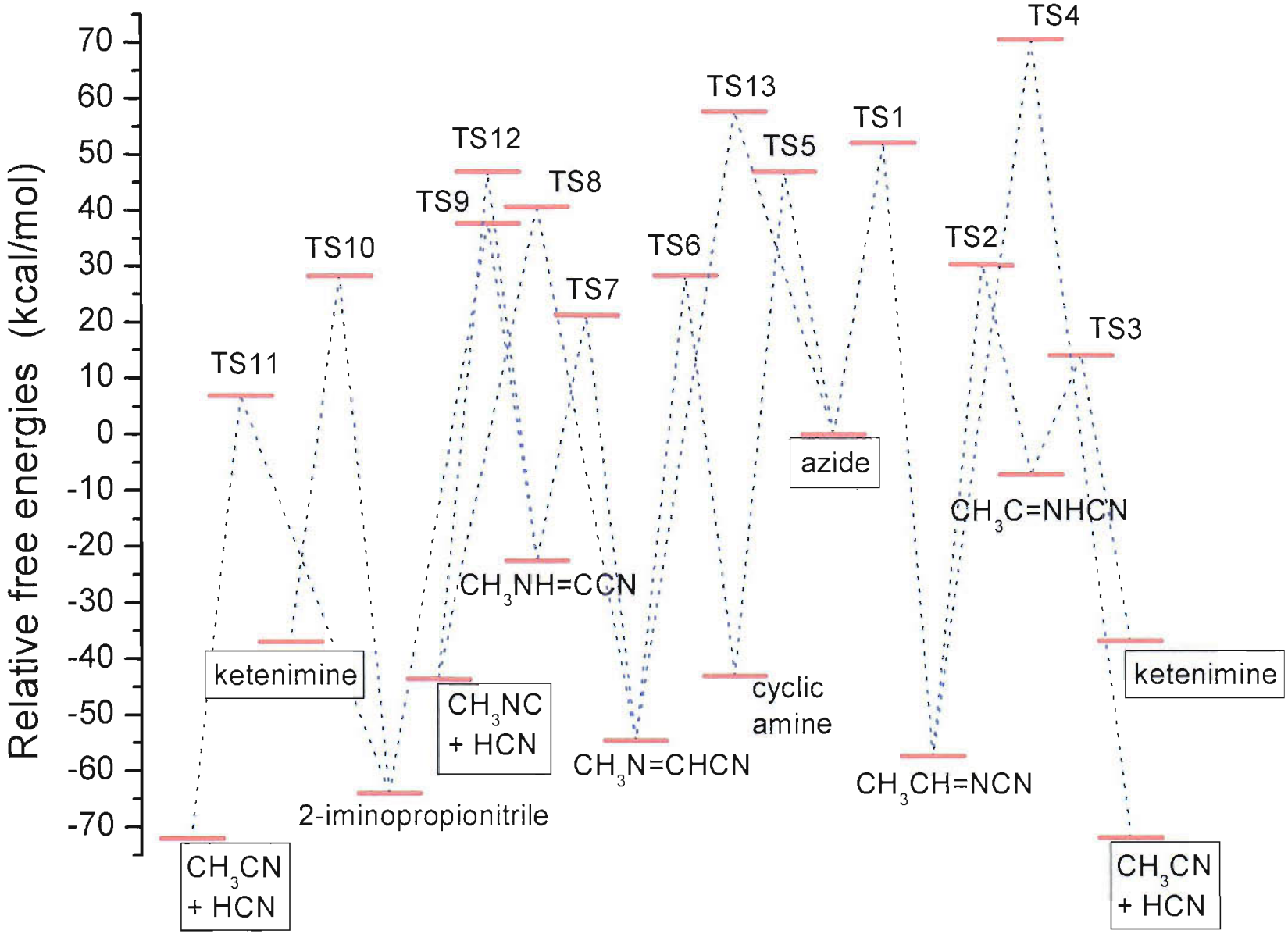

Figure 5.114- Diagram of the free energies at 298 K calculated at the MP2/6-31G level for the decomposition surface of 2-azidopropionitrile**

Table 5.79- Relative energy and free energy values calculated at MP2/6-31G level for products and transition states of the 2-azidopropionitrile decomposition system**

Structure	Energy (kcal/mol)	Free energy (kcal/mol)	Transition state	TS label	Energy (kcal/mol)	Free energy (kcal/mol)
$CH_3CH(CN)N_3$	0	0	TS azide-cyclic amine	TS5	51.55	46.84
(cyc-CH_2NHCH)-CN	-32.19	-43.23	TS azide-CH_3N=CHCN	TS13	62.27	57.54
CH_3N=CHCN	-41.85	-54.62	TS azide-CH_3CH=NCN	TS1	56.65	51.94
CH_3NH=CCN	-10.14	-22.45	TS cyclic amine-CH_3N=CHCN	TS6	43.35	28.17
CH_3CH=NCN	-44.60	-57.53	TS CH_3N=CHCN-CH_3NH=CCN	TS7	38.70	21.22
CH_3C=NHCN	+ 6.30	-7.29	TS CH_3N=CHCN-CH_3NC	TS8	57.29	40.53
CH_3C(CN)=NH	-51.21	-63.98	TS CH_3NH=CCN-CH_3NC	TS12	64.90	46.72
CH_2=C=NH + HCN	-11.25	-37.06	TS CH_3NH=CCN-CH_3C(CN)NH	TS9	52.14	37.54
CH_3NC + HCN	-18.78	-43.70	TS CH_3C(CN)NH -CH_3CN	TS11	24.50	6.76
CH_3CN + HCN	-47.13	-72.09	TS CH_3C(CN)NH -ketenimine	TS10	45.54	28.27
			TS CH_3CH=NCN-CH_3C=NHCN	TS2	47.94	30.11
			TS CH_3CH=NCN-CH_3CN	TS4	91.58	70.38
			TS CH_3C=NHCN-ketenimine	TS3	30.37	13.86

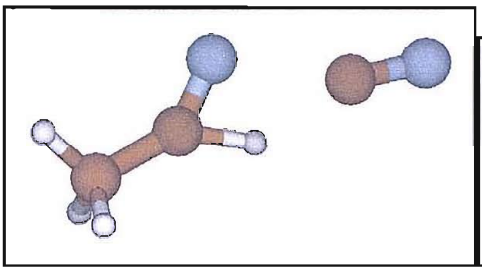

TS4

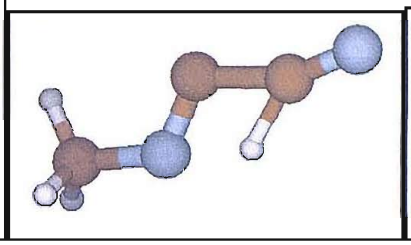

TS8

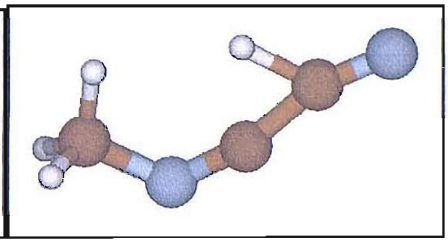

TS12

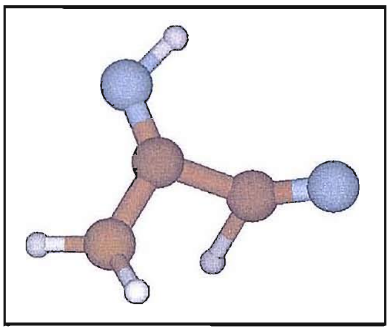

TS10

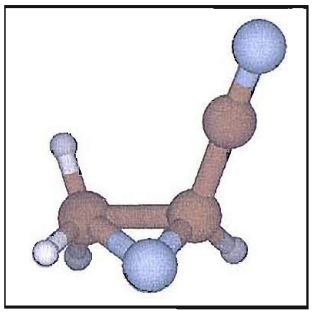

TS6

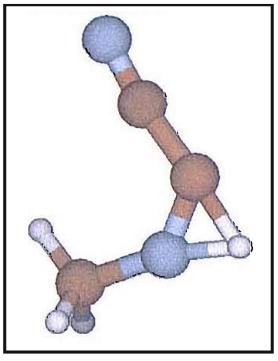

TS7

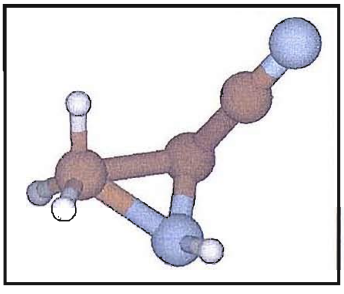

TS9

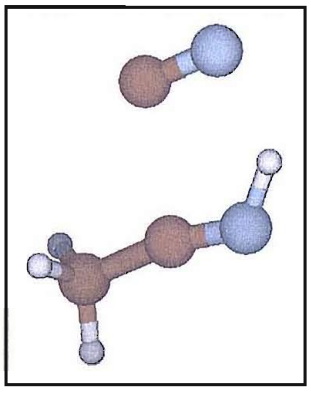

TS11

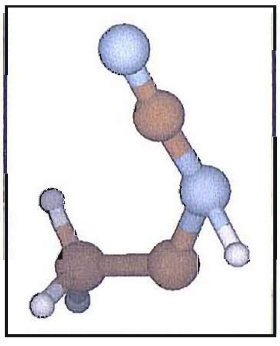

TS2

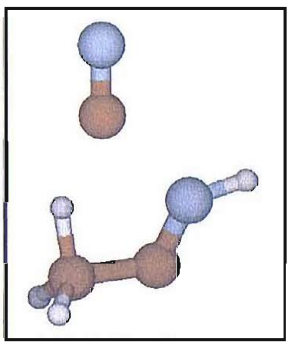

TS3

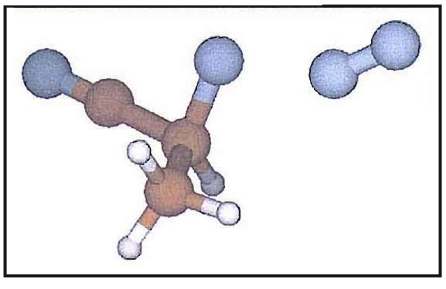

TS1

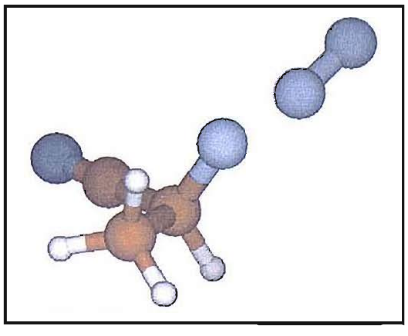

TS5

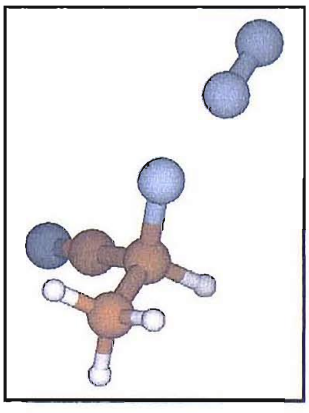

TS13

Figure 5.115- The geometries of the transition states optimised on the decomposition surface of 2-azidopropionitrile

5.7 3-AZIDOPROPIONITRILE

5.7.1 EXPERIMENTAL SECTION

Photoelectron spectroscopy

Despite the fact that they are isomers, 2- and 3-azidopropionitrile have remarkably different vapour pressures: 3-azidopropionitrile ($N_3CH_2CH_2CN$) is a much less volatile liquid than 2-azidopropionitrile. In order to obtain a PE spectrum of 3-azidopropionitrile it was necessary to place the sample in two small glass vials which were held by some glass wool at roughly 2 centimetres above the heating region: this meant that the sample was in an intermediate temperature zone, therefore helping the vaporization process, but the result of using a small amount of sample was reflected in a reduced time available for the acquisition of spectra. The time available for a pyrolysis run was therefore reduced with respect to that for 2-azidopropionitrile; nevertheless, in this way, the PE spectra obtained were of about the same signal-to-noise ratio as for 2-azidopropionitrile.

Also in the case of 3-azidopropionitrile the temperature of full decomposition was low enough to allow a resistive heating system to be used on the photoelectron spectrometer with a 10 cm-mean radius of the hemispheres of the analyzing chamber (see Figure 2.1).

The procedure for the acquisition and calibration of the photoelectron spectra followed the same pattern as described in Chapter 2. Calibration of spectra obtained on pyrolysis of the azide was normally achieved using the bands associated with the first vertical ionization energies (VIEs) of N_2 (15.579 eV), H_2O (12.616 eV) or of HCN (13.60 eV) [8].

Matrix isolation IR spectroscopy

The apparatus and the procedure for the acquisition of infrared spectra in nitrogen matrices have been described in Chapter 2. Deposition times were of the order of 30 to 60 minutes, and the matrix dilution ratios were estimated to be above 1000:1.

5.7.2 SAMPLE PREPARATION AND CHARACTERIZATION

PREPARATION

Samples of 3-azidopropionitrile ($N_3CH_2CH_2CN$) were obtained from the reaction of 3-chloropropionitrile with sodium azide using water as solvent. In this preparation, 3-chloroacetamide was added slowly to 3 equivalents of sodium azide (3 equiv). The mixture was stirred for 24 hours in an oil bath at 60 °C. After cooling, the product was extracted with dichloromethane, and the organic phase, in which the azide was dissolved, was dried over anhydrous sodium sulphate, filtered and concentrated using a rotary evaporator. The impure azide was purified by distillation in a Kugelrohr apparatus under vacuum.

CHARACTERIZATION

3-Azidopropionitrile ($N_3CH_2CH_2CN$) is a colourless liquid. It was characterized in the vapour phase by ultraviolet photoelectron spectroscopy and electron impact mass spectrometry and in the liquid phase by ^{1}H- and ^{13}C-nuclear magnetic resonance (Bruker AMX-400), and by infrared spectroscopy (Mattson Satellite FT-IR).

Mass spectrometry: the 70 eV electron impact mass spectrum shows the parent peak at 96 amu, with a weaker peak at 97 amu corresponding to the protonated azide. The base peak was found at 28 amu, corresponding to N_2^+ and CH_2N^+ ions. Strong peaks were found at 53 ($CHCH_2CN^+$), 54 ($CH_2CH_2CN^+$), 40 (CH_2CN^+, CCH_2N^+), 41 (CH_3CN^+, $CHCH_2N^+$), 42 (N_3^+), 67 (NCH_2CHCN^+) and 27 (CH_2CH^+, HCN^+) amu. For each of these signals, other peaks were present at 1 and 2 amu lower, indicating a high probability of deprotonation of the fragment during the electron impact.

^{1}H- and ^{13}C-NMR spectroscopy: the ^{1}H-NMR spectrum in $CDCl_3$ solution, presented in Figure 5.117, displays two triplets due to the methylene groups, one centred at 2.572 ppm relative to TMS, and one centred at 3.571 ppm. By comparison with the results obtained for previous azides, they have been assigned respectively to the methylene group adjacent to the cyano group and to that adjacent to the azide chain. The spectrum reported in Figure 5.117 was recorded before distilling the sample: as can be clearly seen, there are two additional triplets, centred at 2.51 and 2.95 ppm, reflecting a not negligible amount of impurities. When the spectrum was recorded on the distilled sample, these signals practically disappeared: in this case, the ratio between the integrals of the two triplets of 3-azidopropionitrile was exactly 1.0:1.0.

The ^{13}C-NMR spectrum (in $CDCl_3$ solution, Figure 5.118) shows peaks at 18.2 ppm (relative to TMS) assigned to the carbon adjacent to the cyano- group, at 46.6 ppm assigned to the carbon adjacent to the azide group, and at 117.7 ppm, assigned to the cyanide carbon.

Infrared spectroscopy: the IR spectrum of the pure compound in the liquid phase was recorded between KBr plates, and is reported in Figure 5.119a. The most intense band was once again that associated with the azide stretch: a broad band was observed at 2095 cm^{-1}; in contrast with 2-azidopropionitrile, here a sharp satellite band is visible at 2251 cm^{-1}: it is not clear if this corresponds to an additional stretching mode of the chain or it can be associated to the C≡N stretch, because according to *ab initio* calculations (see Section 5.6.3) this band should appear at a lower wavenumber than the N-N-N stretch. The second most intense band was a broad one at 1268 cm^{-1}, associated with the C-N-N stretch, while the bands associated with the C-H stretching modes were found at 2942 and 2886 cm^{-1}. The other most important bands were at 1456, 1418, 1351, 1332, 1054, 1011, 953, 911, 833 and 773 cm^{-1}.

Figure 5.119b shows the IR spectrum of 3-azidopropionitrile obtained in a nitrogen matrix. As happened for 2-azidopropionitrile, in contrast with the spectrum acquired in the liquid phase, in the matrix the bands associated with the N-N-N and C≡N stretches are better resolved, and also the bands in the 1500-1000 cm^{-1} region display a different intensity pattern: in general however, the differences between the spectra acquired with the two techniques are negligible, and smaller than in 2-azidopropionitrile.

In Section 5.6.3 the IR spectra of 3-azidopropionitrile in the liquid phase and in a N_2 matrix will be presented in comparison with the results obtained from *ab initio* calculations of the vibrational frequencies.

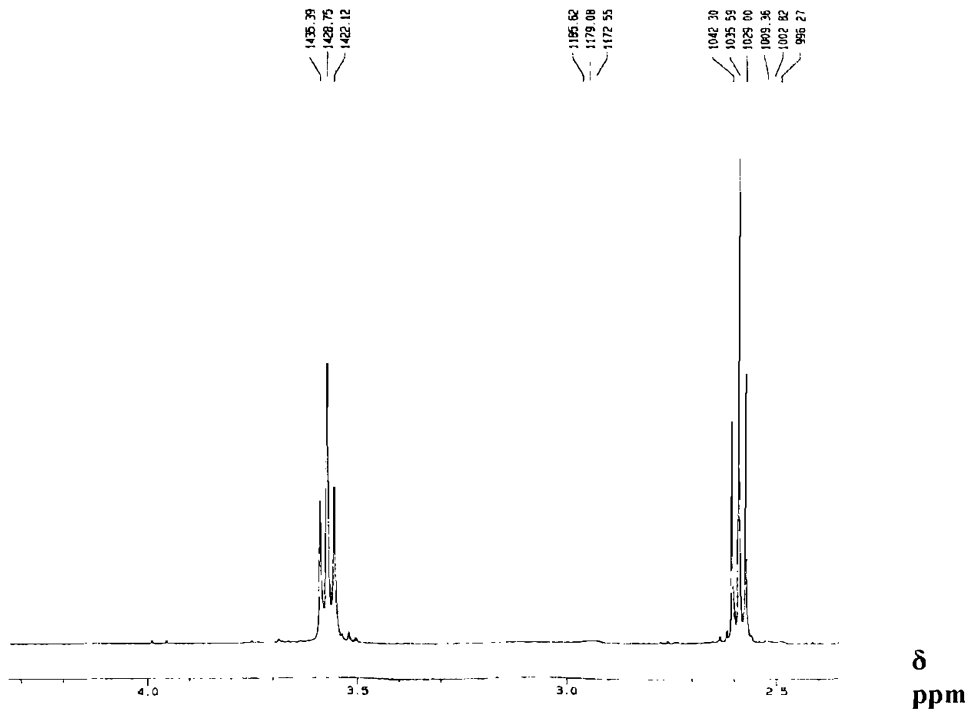

Figure 5.117- ^{1}H-NMR spectrum of 3-azidopropionitrile recorded in $CDCl_3$ solution

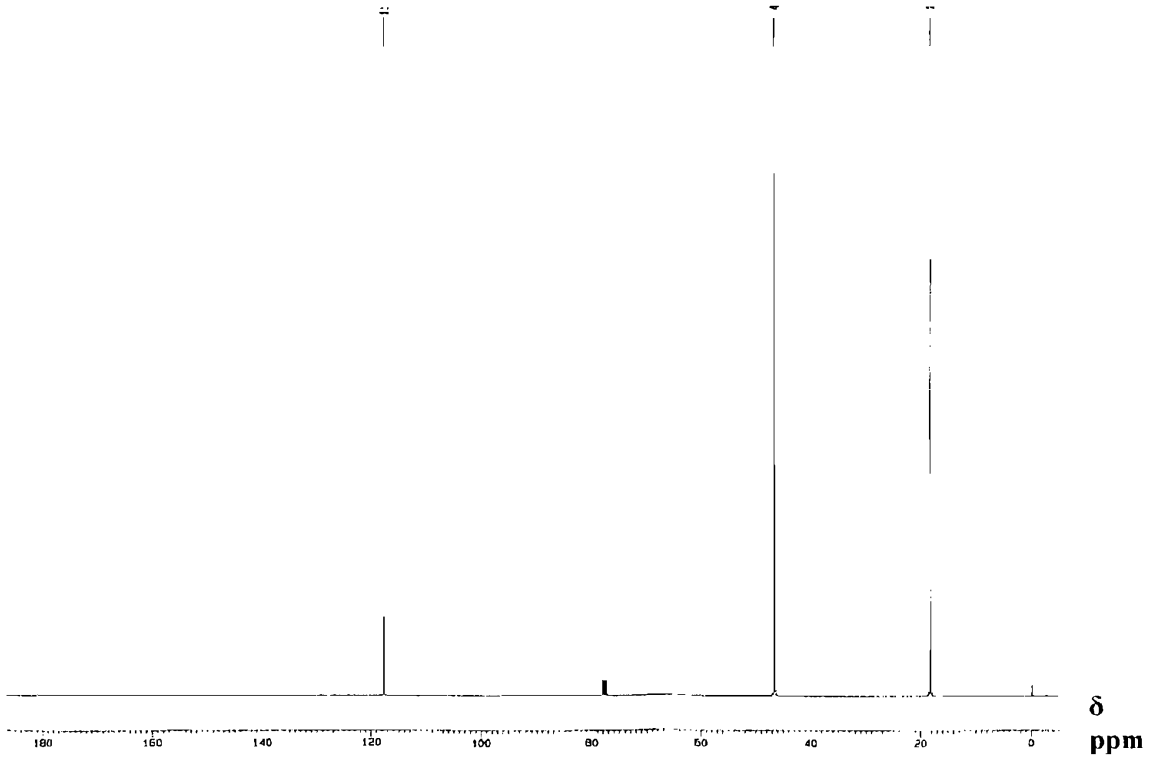

Figure 5.118- ^{13}C-NMR spectrum of 3-azidopropionitrile recorded in $CDCl_3$ solution

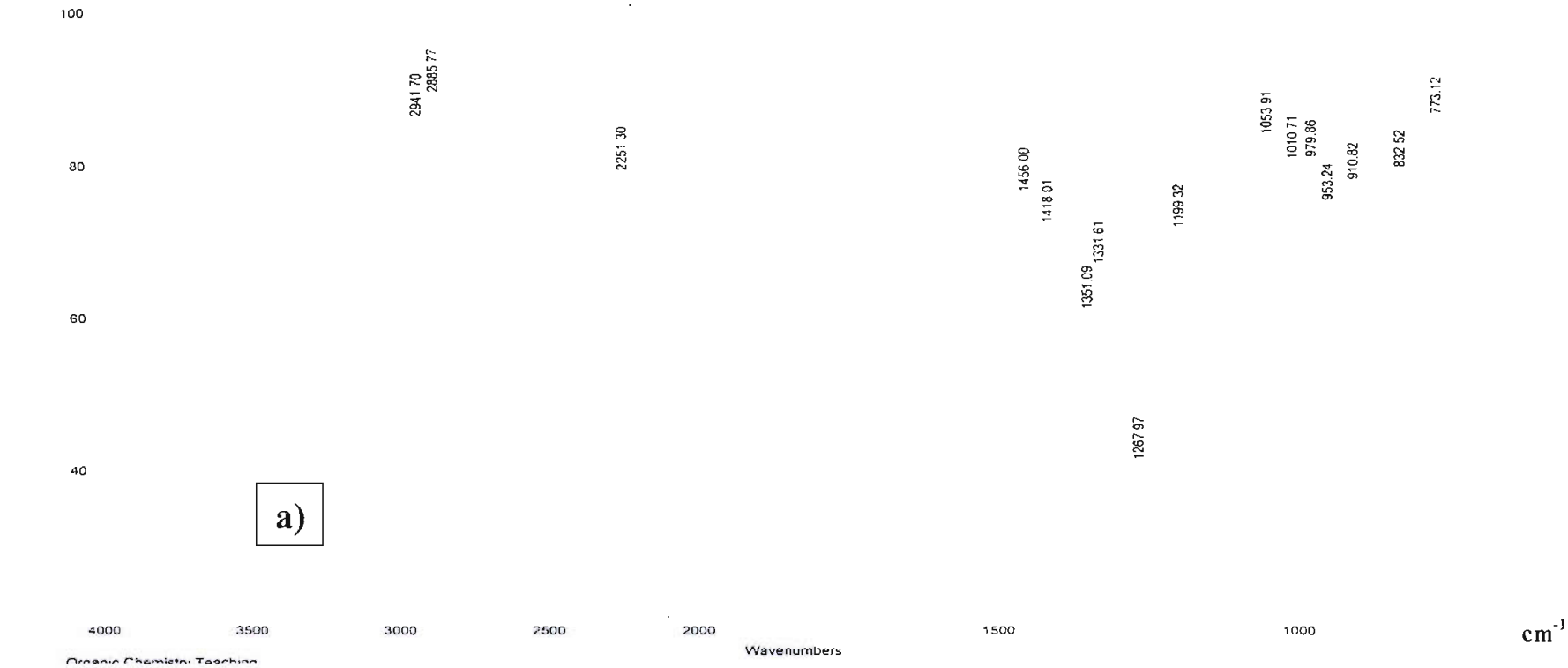

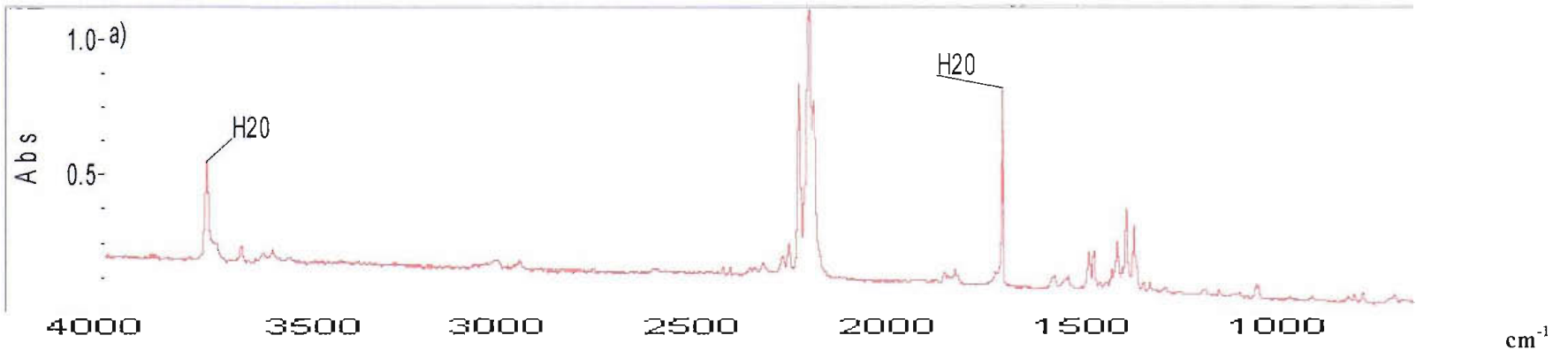

Figure 5.119- IR spectrum of 3-azidopropionitrile recorded in liquid phase between KBr plates (a) and trapped in a nitrogen matrix (b)

Photoelectron spectroscopy: all the spectra were recorded using He(I) radiation (21.22 eV). Photoelectron spectra of the parent azide were calibrated using argon and methyl iodide [18] added to the ionization chamber along with the azide vapour samples. The photoelectron spectra of the azide precursor, 3-chloropropionitrile, were also recorded and calibrated to check for its possible presence as in impurity in the azide spectra, but all the 3-azidopropionitrile samples seemed free from any detectable trace of the precursor used in the preparation. The pressure of the azide in the ionization region was set at approximately 10^{-4} torr.

Figure 5.120 shows the PE spectrum of 3-azidopropionitrile at room temperature, along with the labelling of the bands. These have been calibrated by averaging the values obtained in seven different spectra, and the values are presented in Table 5.80. A more detailed description of the molecular orbitals involved in the ionizations associated with the photoelectron bands will be reported in the following section.

Table 5.58- Calibrated vertical ionization energies of 3-azidopropionitrile- see Figure 5.93 for band labelling

Band	**A**	**B**	**C**	**D**	**E**	**F**	**G**	**H**
VIE (eV) ±0.02 eV	10.05	11.55	12.26	12.51	13.12	14.24	14.96	15.40

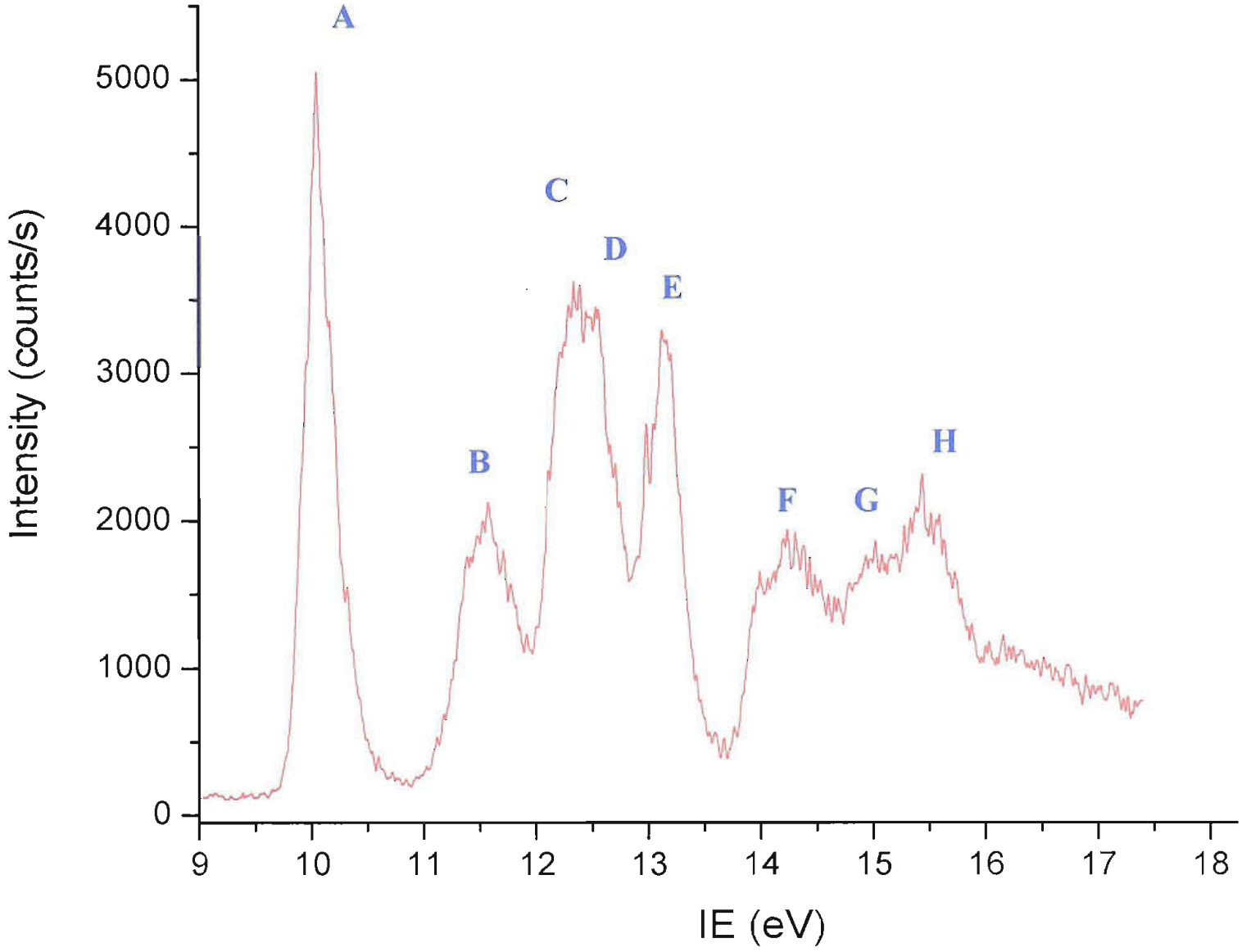

Figure 5.120- PE spectrum of 3-azidopropionitrile recorded at room temperature, with labelling of the bands

5.7.3 RESULTS OF *AB INITIO* MOLECULAR ORBITAL CALCULATIONS

Molecular orbital calculations were carried out at the MP2/6-31G** level on the parent azide and on its decomposition products to facilitate the spectral interpretation and the assignments of the bands by calculating vertical ionisation energies (VIEs) and infrared frequencies and intensities. Also, the geometry of the azide and the imines were computed, and relative energy diagrams were constructed in order to trace the energy surface for the decomposition reaction.

Four conformers of 2-azidopropionitrile were optimized, according to the relative orientation of the azide chain with respect to the cyano group and the methylene groups.
The geometries of the four structures are reported in Figure 5.121: one of them is planar (point group C_s), while the other three have no symmetry element, and their point group is C_1.

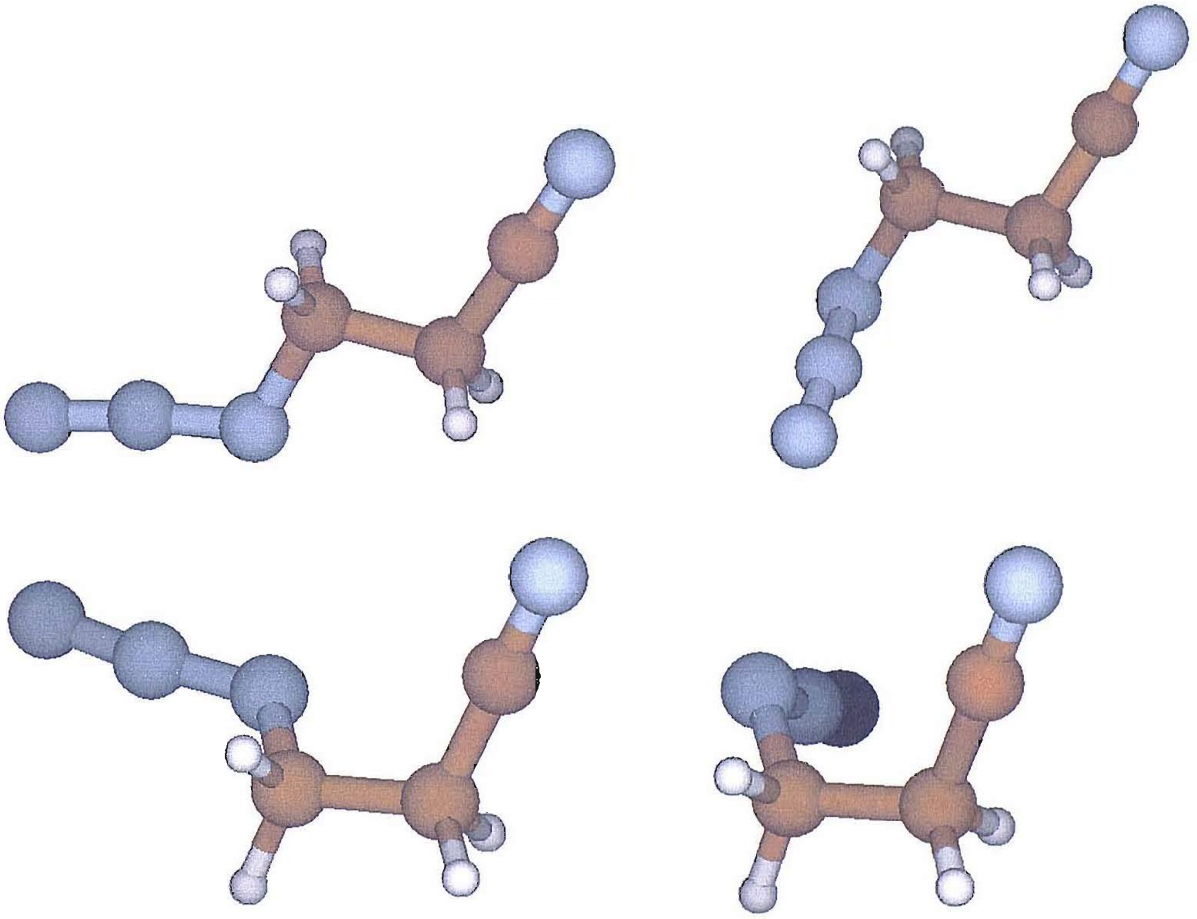

Figure 5.121- The four structures of 3-azidopropionitrile optimized at the MP2/6-31G level: clockwise from top left, they have been labelled *trans-trans*, *trans-cis*, *cis-cis* and *cis-trans*.**

The labelling nomenclature has been chosen in a slightly different way from the one followed by the other azides: in this case, as can be seen from Figure 5.121, there are conformers in which it is ambiguous to state if the relative orientation of the cyano group to the protons of the methylene group adjacent to the azide chain is *cis* or *trans*. A different labelling method has therefore been used, reflecting directly the relative orientation of the azide and cyano groups: when the first nitrogen atom of the azide chain forms a 180° dihedral angle with the cyano group (top row structures in Figure 5.121), a first *trans* label is given, while *cis* is given when this angle is 60° (bottom row). The second *trans* or *cis* label is added to differentiate if the chain is pointing in roughly the opposite direction of the cyano group (left column structures of Figure 5.121) or in roughly the same direction (right column). The most stable structure is structure *trans-cis*; however, the four structures are surprisingly very close in energy (0.36 kcal/mol), suggesting that there should be almost free interconversion between the conformers which would therefore all contribute to the experimental spectra. The total and relative energies calculated for the four conformers are reported in Table 5.81.

Table 5.81- Total and relative energies of the four conformers of 3-azidopropionitrile at the MP2/6-31G level**

Structure	Total energy (hartrees)	Relative energy (kcal/mol)
Cis-cis	-334.6934514	+0.355
Cis-trans	-334.6935443	+0.297
Trans-trans	-334 .6936499	+0.231
Trans-cis	-334.6940179	0

Figure 5.122 reports in detail the most stable of the four minimum energy structures, labelled *trans-cis*, along with the labelling of the atoms, while Table 5.82 summarizes its most significant geometrical parameters.

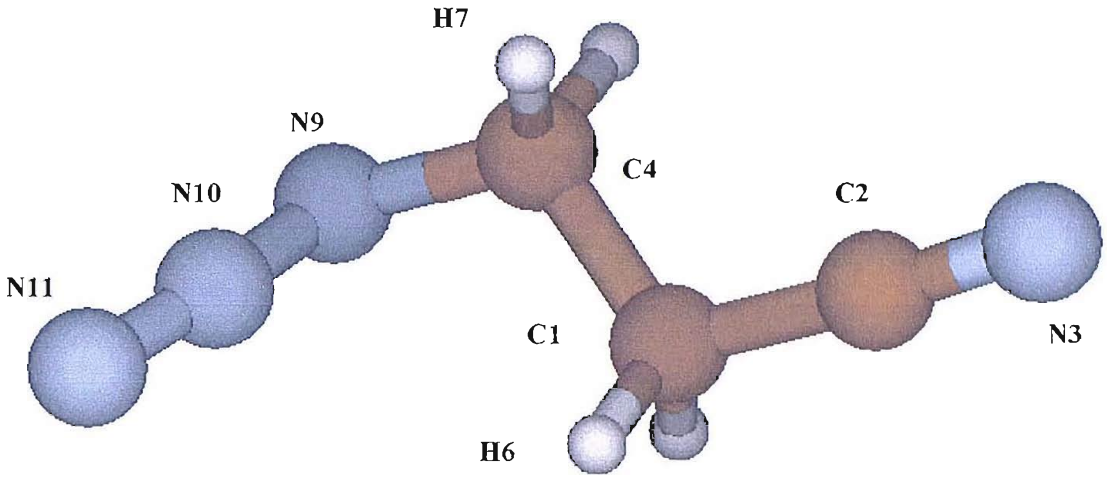

Figure 5.122- Structure *trans-cis* of 3-azidopropionitrile calculated at the MP2/6-31G level**

Table 5.82- The most significant geometrical parameters for the lowest energy structure of 3-azidopropionitrile (see Figure 5.122 for atom labelling)

Bond	Length (Å)	Angle	Value (°)
N11-N10	1.164	**N11-N10-N9**	172.38
N10-N9	1.249	**N10-N9-C4**	115.04
N9-C4	1.474	**N9-C4-C1**	111.01
C4-H7	1.087	**C4-C1-C2**	111.10
C1-C4	1.535	**C1-C2-N3**	177.96
C1-C2	1.464	**N10-N9-C4-C1**	72.2
C2-N3	1.182	**N9-C4-C1-C2**	176.5
C1-H6	1.092	**C4-C1-C2-N3**	

Table 5.83 reports the VIEs for the two conformers as calculated by applying Koopmans' theorem to the energies of the molecular orbitals obtained at the MP2/6-31G** level. The agreement is good for the first four bands, while the following bands show remarkable differences between theory and experiment; it is possible that 6-31G** is not an accurate enough basis set to describe this azide, or that Koopmans' theorem is a too crude approximation of the true VIEs. For this, VIEs using the ΔSCF method- calculating the energy of the azide cation at the same geometry of the neutral- were calculated. Unfortunately, only one VIE from ionization from the outer molecular orbitals could be calculated, due to the fact that on removing an electron from a lower lying orbital convergence occurred to a lower

ionic state; this means that for a molecule of C_1 symmetry, higher VIEs could not be calculated with the ΔSCF method.

Table 5.83- Experimental and calculated vertical ionization energies (VIEs) of the first seven bands of 2-azidopropionitrile in its *trans-cis* conformer

Band	Experimental VIE (eV)	KT calculated VIE (eV)	KT calculated VIE *0.92 (eV)	ΔSCF calculated VIE (eV)
A	10.05	10.711	9.791	11.584
B	11.55	12.457	11.461	13.061
		12.468	11.470	12.289
		12.523	11.521	
B	12.26	12.999	11.959	
C	12.51	15.181	13.967	
D	13.12	15.577	14.331	
E	14.24	16.088	14.801	

Figure 5.123 represents the five highest occupied molecular orbitals for structure *trans* of 3-azidopropionitrile obtained at the Hartree-Fock level on the geometry optimized at the MP2/6-31G** level.

The shape and energy of these orbitals are quite similar to those obtained for 2-azidopropionitrile: this explains the similarity of the experimental PE spectra of the two isomeric azides, both in the VIEs and the shape of the bands.

For the most stable conformer (conformer *trans-cis*), molecular orbital 25 (the HOMO) is mostly π-antibonding in character: assuming the N-CH_2-CH_2-CN frame to be almost planar, the HOMO consists of p_π orbitals centred on the first and last nitrogen atoms of the azide chain, plus p_π antibonding character also seen between the first nitrogen of the azide and the adjacent methylene carbon. The p_π electronic density on the first methylene group is orientated so as to form a σ-bond with the adjacent methylene carbon atom and the hydrogen atoms. A very small contribution arises also from the lone pair on the nitrogen atom of the cyano group.

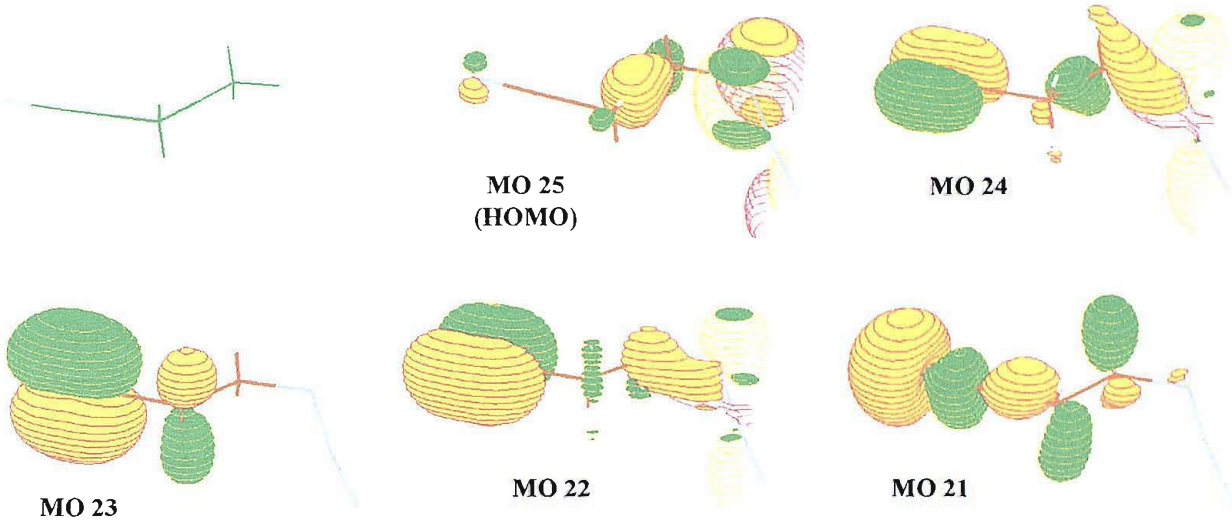

Figure 5.123- The six highest occupied molecular orbitals calculated for structure *trans-cis* of 3-azidopropionitrile

MO 24 is a delocalized orbital, with major p_π-bonding contribution from the C≡N group, and from a p_π antibonding character between the first and last nitrogen atoms of the azide chain; one of the lobes of this latter p_π antibonding density becomes a σ-bonding distribution between the last nitrogen of the azide chain and the adjacent methylene carbon atom and its hydrogen. There is also a σ-bond character between the two methylene groups.

MO 23 is much localized orbital, almost totally characterized by a strong π-bonding contribution on the C≡N group- this time with a nodal plane corresponding to the N-CH_2-CH_2-CN plane- and by a σ-bonding contribution between the methylene and its hydrogen atoms: these two contributions are also p_π antibonding between the cyano carbon and the adjacent methylene group.

MO 22 is very similar to MO 23, with in addition a σ-bond between the second methylene group and the first nitrogen atom of the azide chain and a p_π antibonding character arising from the lone pairs on the first and last nitrogen atoms of the azide group.

Harmonic vibrational frequencies have been calculated for the four conformers of 3-azidopropionitrile via second derivative calculations at the MP2/6-31G** level, with only partial allowance for electron correlation [15]. The calculated frequencies are higher than the experimental ones. The computed IR spectra are reported in Figure 5.124, and the frequencies and intensities of the bands are listed in Table 5.84.

Also for 3-azidopropionitrile, the computed distribution of the frequencies is in good agreement with the experimental results, if the approximations used in the calculations are considered. As usual for azides, the calculations overestimate the intensity of the strongest bands relatively to the others. Therefore, the experimental spectrum displays a much higher intensity for the series of bands between 500 and 1200 cm^{-1}. The bigger discrepancy, as in 2-azidopropionitrile, is the contribution of the C≡N stretch, which according to calculations should be a weak band roughly 100 cm^{-1} wavenumbers lower than the azide stretch: in the experimental spectra, the weak band satellite of the N-N-N one is actually 55 cm^{-1} higher. It is not possible to definitely assign this band to the C≡N stretch: in this case, the discrepancy between the predicted and the observed band would be remarkable. Moreover, in the experiment an inverted intensity ratio between the C-H stretching bands calculated at around 3100 cm^{-1} was observed, because the higher frequency band is experimentally also the strongest in intensity.

The main difference between the spectra of the four conformers is the shape of the two bands between 1300 and 1400 cm^{-1}: in some cases, they are well separated, in others they almost merge, and their intensity ratio varies from 1:1 to 7:1. The spectrum recorded in the liquid phase shows a better agreement with the *trans-cis* structure, which is in fact the lowest in energy. The difference in energy is however so small (just 0.36 kcal/mol) that at room temperature the four structures are probably all present and the experimental spectrum probably reproduces an average of the four pure spectra.

The spectra in the nitrogen matrix are in this case very similar to those obtained in the liquid phase.

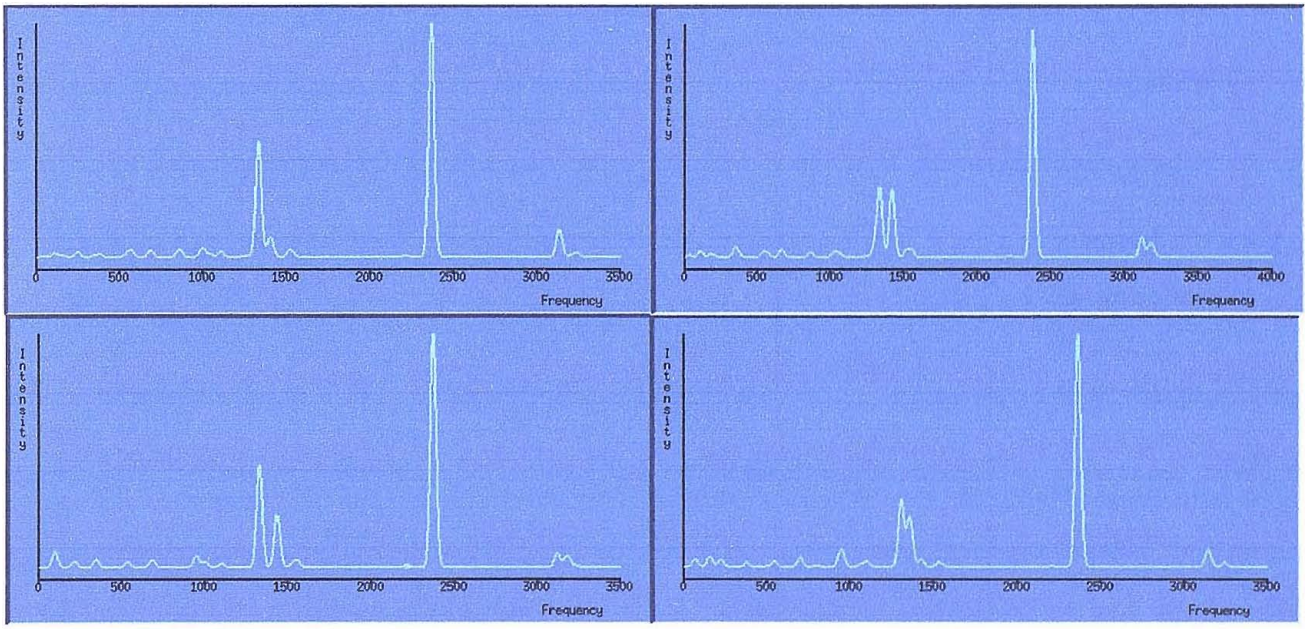

Figure 5.124- Infrared spectra for the four conformers of 3-azidopropionitrile calculated at the MP2/6-31G level (first line conformers *cis-cis* and *trans-cis*, second line conformers *cis-trans* and *trans-trans*; frequencies are in cm^{-1})**

Table 5.84- Comparison between the experimental liquid phase IR bands and the calculated ones for the minimum energy conformers of 3-azidopropionitrile (absorbances reported in parentheses in Km/mol; frequencies in cm^{-1})

Cis-cis frequencies	*Cis-trans frequencies*	*Trans-trans frequencies*	*Trans-cis frequencies*	*Experimental frequencies in liquid phase*	**Normal mode**
538.1 (6.96)	544.8 (4.15)	537.5 (6.44)	547.1 (7.02)		
570.8 (4.14)	572.6 (8.41)				
662. 1 (10.36)	687.5 (8.65)	685.2 (9.74)	700.2 (11.69)		
852.0 (1.93)	851.4 (2.54)		798.3 (1.98)		
865.9 (4.77)	861.2 (8.09)	949.6 (15.41)	946.8 (23.07)		
1024.6 (7.30)	998.6 (11.56)	1003.3 (6.57)	976.3 (1.26)		
1061.0 (4.38)	1043.1 (3.84)	1095.0 (1.11)	1069.0 (3.71)		
	1109.1 (7.01)	1105.2 (3.32)	1104.0 (6.30)		
1246.0 (1.58)	1248.2 (1.21)				
1298.0 (18.69)	1291.8 (1.87)	1326.6 (10.76)	1308.4 (86.07)	1199.3	
1334.3 (94.33)	1334.8 (141.39)	1329.5 (129.76)	1339.7 (4.35)	1268.0	
1403.0 (13.79)	1402.7 (20.79)		1360.5 (61.49)	1331.6	C-H bending
1420.0 (83.88)	1417.9 (5.49)	1436.4 (71.17)	1427.8 (9.84)	1351.1	$C-H_3$ wagging
1514.0 (8.94)	1521.4 (8.68)	1528.3 (4.64)	1525.1 (4.29)	1418.0	$C-H_3$ in phase scissoring
1551.6 (10.25)	1545.8 (2.24)	1557.2 (8.25)	1550.5 (2.83)	1456.0	$C-H_3$ out of phase scissoring
2216.0 (1.95)	2214.2 (1.75)	2215.2 (1.43)	2211.8 (1.03)	2251.3	C≡N stretching
2377.2 (311.55)	2369.0 (285.9)	2373.8 (320.62)	2366.4 (302.80)	2095.3	N-N-N stretching
3114.7 (27.11)	3131.1 (25.59)	3119.2 (18.72)	3140.0 (13.88)	2885.8	C-H stretching
3151.5 (2.35)	3139.9 (8.84)	3159.2 (2.45)	3148.6 (6.20)		$C-H_3$ symmetric stretching
3178.8 (18.66)	3196.4 (1.90)	3180.5 (14.44)		2941.7	$C-H_3$ asymmetric stretching
3214.7 (1.97)	3237.7 (5.70)	3221.8 (2.52)	3240.8 (5.35)		$C-H_3$ asymmetric stretching

5.7.4 THERMAL DECOMPOSITION RESULTS

Photoelectron spectroscopy

Figure 5.125 represents the change in UV-photoelectron spectra when the vapours of 3-azidopropionitrile are heated at respectively 70, 390, 420 and 450 °C.

The first evidence of pyrolysis, as in every organic azide, is the release of nitrogen (sharp band at 15.58 eV, [8]): in the case of 2-azidopropionitrile the loss of nitrogen was observed to begin at approximately 160 °C. HCN is produced at approximately 180 °C, as can be seen from the vibrationally structured band with VIE at 13.60 eV [8], that appears in a region where no azide bands are present. Apart from N_2 and HCN, the shape of the PE spectrum remains almost unaltered until 300 °C, except for the constant lowering of the intensity of the azide bands, especially the first one. The first bands associated with decomposition products, other than nitrogen and cyanic acid, only appear at approximately 310 °C, when two sharp bands at 12.21 and 12.45 eV are visible on top of the azide third band. Their shape and position correspond to the vibrational components of the first band expected for methyl cyanide [8]: its second band overlaps perfectly with the fourth azide bands at 13.13 eV VIE. No sign of methyl isocyanide (sharp band at 11.27 eV, [8]) is ever witnessed, but at temperatures above 350 °C the broad first band of ketenimine is clearly visible at around 9.2 eV [35]. Its relative intensity is much higher than that observed in 2-azidopropionitrile, therefore indicating a decomposition channel open more than in the isomeric azide. The character of ketenimine is nevertheless that of a reaction intermediate, because the band, after maximising in intensity around 400 °C (when the azide is roughly 80% pyrolysed), abruptly disappears when temperatures approach 450 °C. Given the relatively intense signal, attempts to study ketenimine first band with slow acquisition time were carried out in order to resolve vibrational structure: the band nevertheless appears practically unstructured even under these conditions (see Figure 5.126). It was possible, on the other hand, to observe its second band, which is a vibrationally structured band with VIE at 11.94 eV: in the spectra acquired at 390 and 420 °C this weak band can be seen on top of the azide second band.

At temperatures beyond 450 °C the azide is totally decomposed into CH_3CN and HCN only.

Figure 5.127 reports the thermal behaviour of the intensities of the main band of each compound: the normalization was carried out by simply considering the height of the band, not its integral, and setting as the 1.0 value the height of the band at the temperature at which its intensity was the maximum among all the spectra.

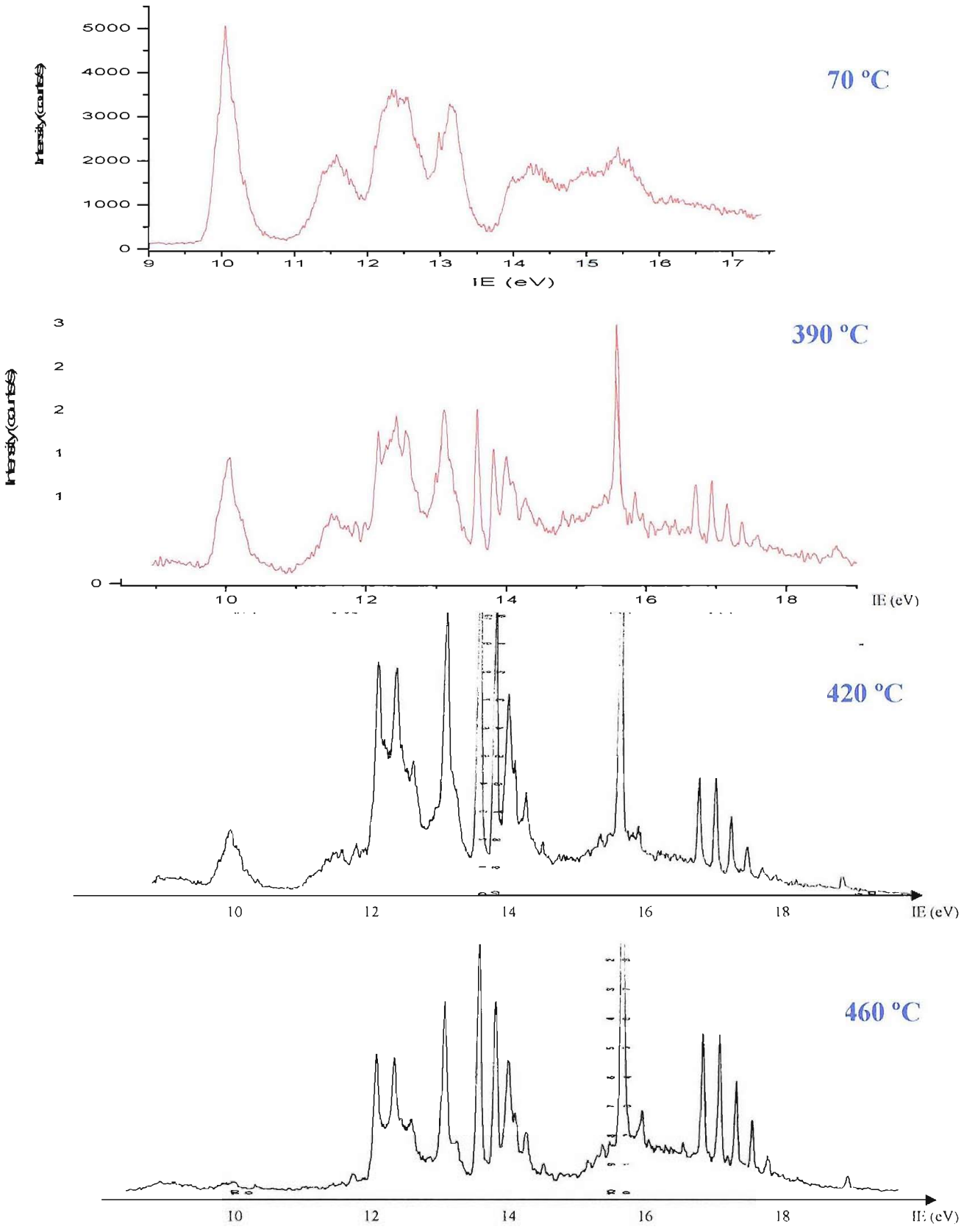

Figure 5.125- Decomposition photoelectron spectra of 3-azidopropionitrile vapours heated at 70, 390, 420 and 450 °C

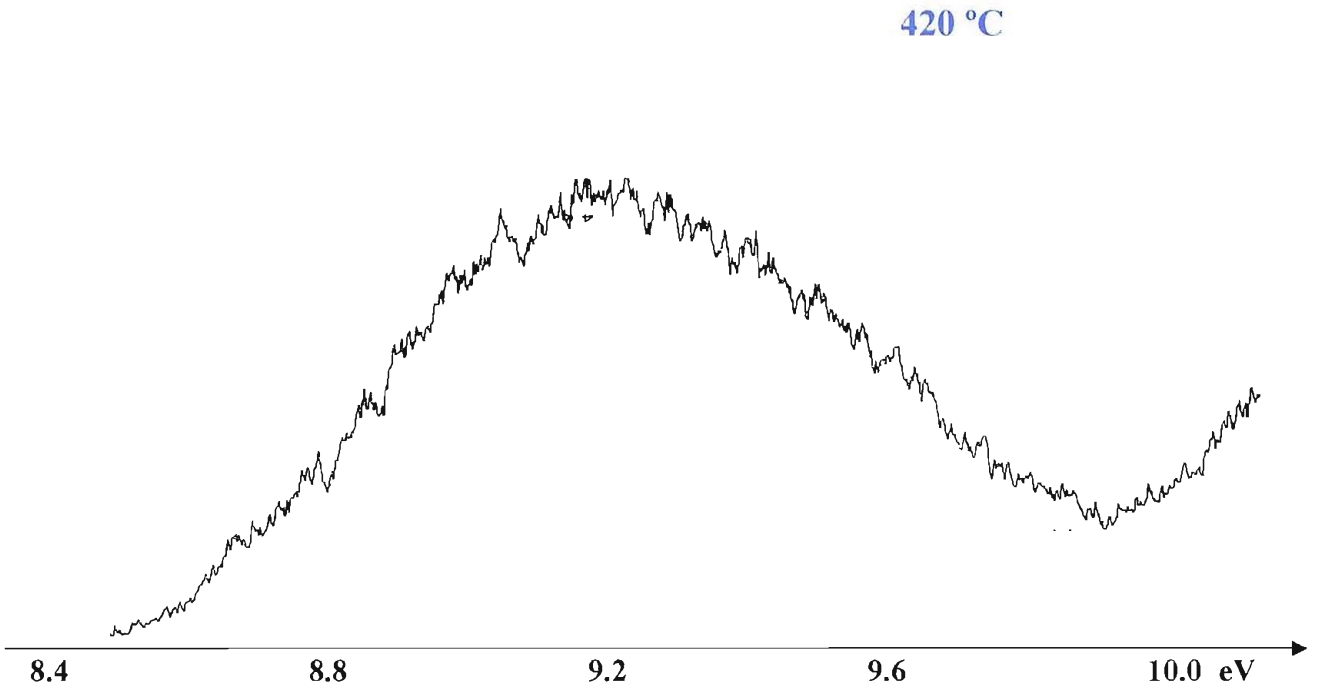

Figure 5.126- A scan of the first photoelectron band of ketenimine: no sign of vibrational structure is present

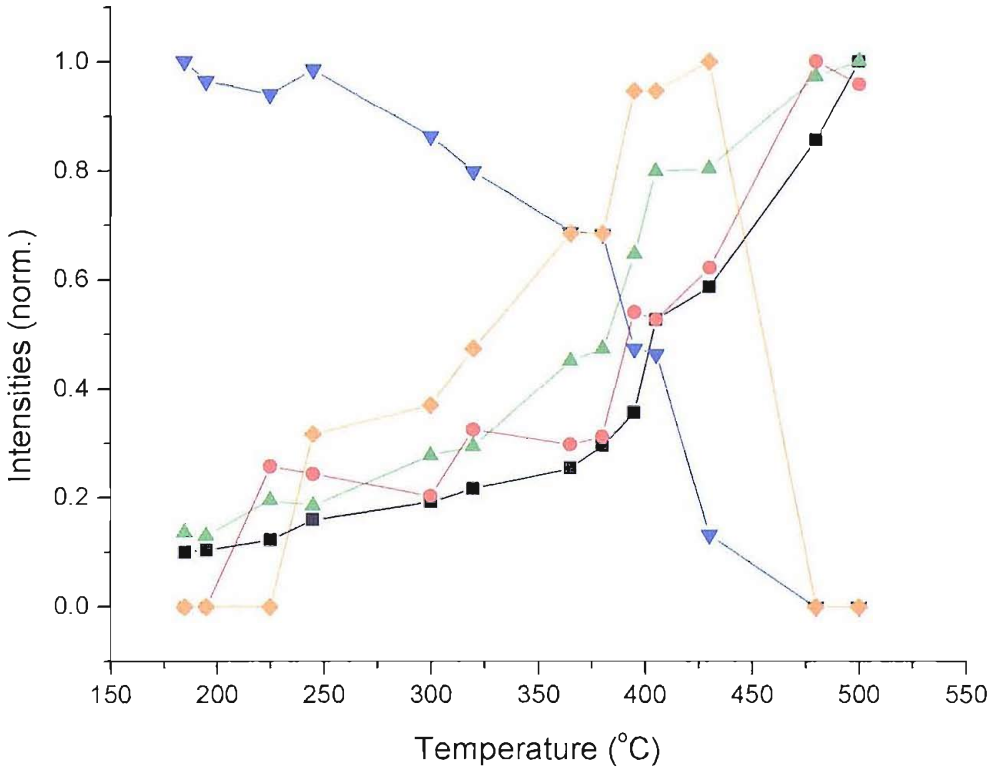

Figure 5.127- Thermal behaviour of the normalized intensities of the species present in the 3-azidopropionitrile pyrolysis. Downward blue triangles: 3-azidopropionitrile; red circles: methyl cyanide; upward green triangles: HCN; black squares: nitrogen; orange diamonds: ketenimine

Infrared matrix isolation spectroscopy

Figure 5.128 represents the infrared spectra obtained when vapours of 3-azidopropionitrle were heated at increasing temperatures and trapped into a nitrogen matrix.

The beginning of the pyrolysis was evidenced at 230° C by the appearance of the HCN bands at 3282 and 797 cm^{-1} [20]. With increasing temperature, the azide bands decrease and all the bands associated with the products start to increase; the summary of the most significant absorptions for the molecules released in the decomposition of 3-azidopropionitrile are listed in Table 5.85. The temperature after which all the azide bands had disappeared, and therefore the pyrolysis is complete, was observed to be 370° C.

Another set of bands shows an increase in intensity with the increasing of the temperature, marking the presence of thermally stable compounds: apart from cyanic acid, this is the case of methyl cyanide (CH_3CN) whose most prominent peak is observed at 1447 cm^{-1} [36]. All the bands attributed to both CH_3CN and HCN increase constantly in all the spectra up to 580 °C.

Finally, another set of bands shows a typical reaction intermediate behaviour, with intensity decrease when the temperature is increased above 450° C. This set of bands (whose most intense band is at 2038 cm^{-1}) was attributed to ketenimine, CH_2CNH [38]. It is important to note that ketenimine is still present in high concentration when the azide is already totally pyrolyzed (see spectrum at 370 °C).

The assignments, shown in Table 5.85, reflected the results obtained from the PE spectra.

Also in the case of 3-azidopropionitrile, HCN is not observed as a monomer, but instead the vibrational frequencies suggest [29] its existence in dimeric form $(HCN)_2$, or even polymeric form.

Table 5.85- Labels and assignment of the most significant IR bands observed in the matrix isolation study of 3-azidopropionitrile thermal decomposition (refer to Figure 5.128 for the labelling of the bands)

Label	*N_2 matrix frequency (cm^{-1})*	*Assignment*
M	2142, 2118/2114/2105, 1369/1355, 1293, 1268, 1247	**$N_3CH(CN)CH_3$**
HCN	3282, 3270, 799/795	**Polymeric cyanic acid**
CH3CN	2256, 1447, 1407, 1378, 1040, 916	**Methyl cyanide**
CH2CNH	2038, 1125 997, 885, 697	**Ketenimine**

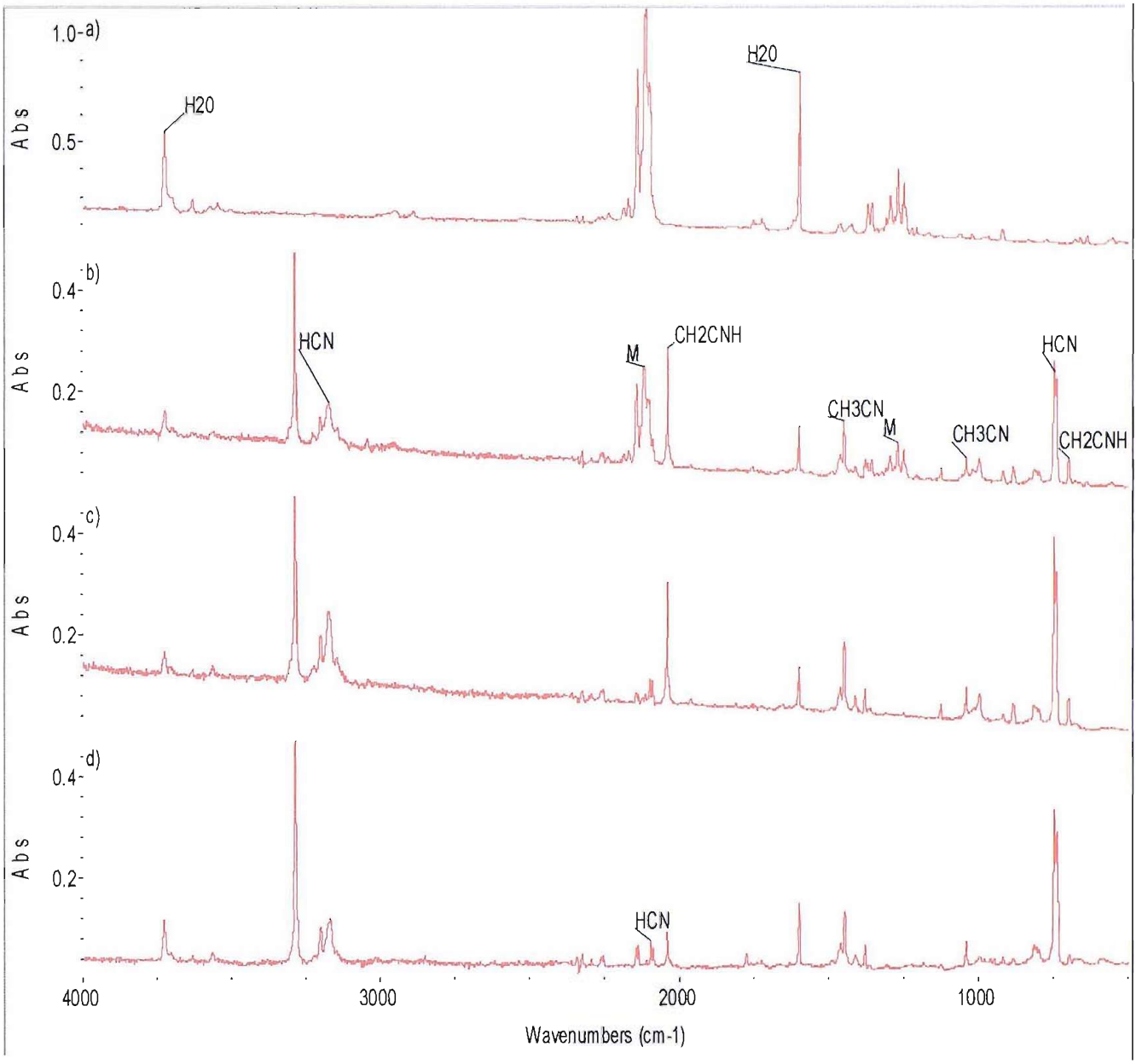

Figure 5.128- Matrix IR spectra of vapours of 3-azidopropionitrile heated at respectively 30, 260, 370 and 580 °C

5.7.5 *AB INITIO* RESULTS ON THE INTERMEDIATES

The experimental results from both PES and matrix IR show that the azide decomposes releasing nitrogen, cyanic acid and methyl cyanide as stable molecules; in addition to that, ketenimine is formed as a short-lived species, decomposing at temperatures above 450 °C. No other reaction intermediates were observed in either technique.

The system displays one less decomposition product with respect to 2-azidopropionitrile, therefore its pyrolysis path should be less complex; nevertheless, *ab initio* studies of the transition states leading to the products are needed to rationalize the mechanism.

A study of the potential energy surface connecting 3-azidopropionitrile with the observed decomposition products has been performed by means of *ab initio* molecular orbital calculations at the MP2/6-31G** level

As usual with aliphatic azides, it was supposed that 3-azidopropionitrile initially decomposes releasing molecular nitrogen and forming a nitrene, according to the reaction

$$N_3CH_2CH_2CN \rightarrow N_2 + :NCH_2CH_2CN$$

As was found for 2-azidopropionitrile, the nitrene is not stable in its singlet state, because during the optimization its structure converges to an imine structure; this was expected from the previous results on other azides. Nevertheless, the calculations showed that on leaving the calculation to optimize the nitrene initial geometry, initially set as the one of the azide but removing the last two nitrogen atoms of the N_3 chain, the optimization does not undergo a 1,2-H shift to produce 3-iminopropionitrile, $HN{=}CHCH_2C{\equiv}N$, following a Type 1 mechanism, but the nitrene nitrogen prefers to attack another electron deficient sites within the molecule, therefore following a Type 2 mechanism.

Despite the possibility of different sites on which the nitrogen atom can attack (for example the cyanic carbon atom), the calculations showed the methylene group is where this attack takes place.

In addition to this, the possibility of the formation of 2-iminopropionitrile via a Type 1 mechanism is still present, because it is possible that during the release of molecular nitrogen the azide partially modifies its geometrical parameters so that the route to 3-iminopropionitrile becomes favoured.

Ab initio calculations were therefore necessary on all these molecules, both to interpret the spectroscopic evidence and to build a reasonable decomposition mechanism for 3-azidopropionitrile and a related energy level diagram.

As mentioned, in principle three different possible routes for the decomposition of the nitrene arising from 3-azidopropionitrile are possible, one following a Type 1 mechanism and one following a Type 2 mechanism. These three initial hypotheses have been considered for the *ab initio* study of the pyrolysis reaction.

Type 1 mechanism: 3-iminopropionitrile

Following this route, 3-nitrenepropionitrile decomposes via a 1,2-hydrogen shift following the scheme

$$: NCH_2CH_2CN \rightarrow HN = CHCH_2CN$$

Four structures of the imine obtained, 3-iminopropionitrile, were optimized at the MP2/6-31G** level of calculation, and they are reported in Figure 5.129. Their total and relative energies are reported in Table 5.86; the total energy difference between them is 1.89 kcal/mol.

Due to the small difference in energy, the four structures are likely to contribute equally to the experimental spectra- if they are formed at all. Nevertheless, the calculated VIEs and vibrational frequencies of only the most stable structure (structure *cis-cis*) will be reported in the following paragraphs.

Table 5.87 reports the most significant geometrical parameters for the most stable structure, presented in Figure 5.130 and labelled *cis-cis*, referring to the relative orientation of the hydrogen atom on the iminic nitrogen with respect to the one on the adjacent carbon atom, and to the relative orientation of this latter hydrogen to the cyano group. The structures with *trans* orientation of the cyano group to the hydrogen on the methyne are planar structures, (therefore point group C_s), whereas those whose disposition is *cis* are not planar (and therefore have a point group C_1).

Table 5.86- Total and relative energies of the four conformers of 3-iminopropionitrile at the MP2/6-31G level**

Structure	Total energy (hartrees)	Relative energy (kcal/mol)
Cis-cis	-225.5190082	0
Cis-trans	-225.517263	+1.095
Trans-trans	-225.5185632	+0.279
Trans-cis	-225.5160027	+1.886

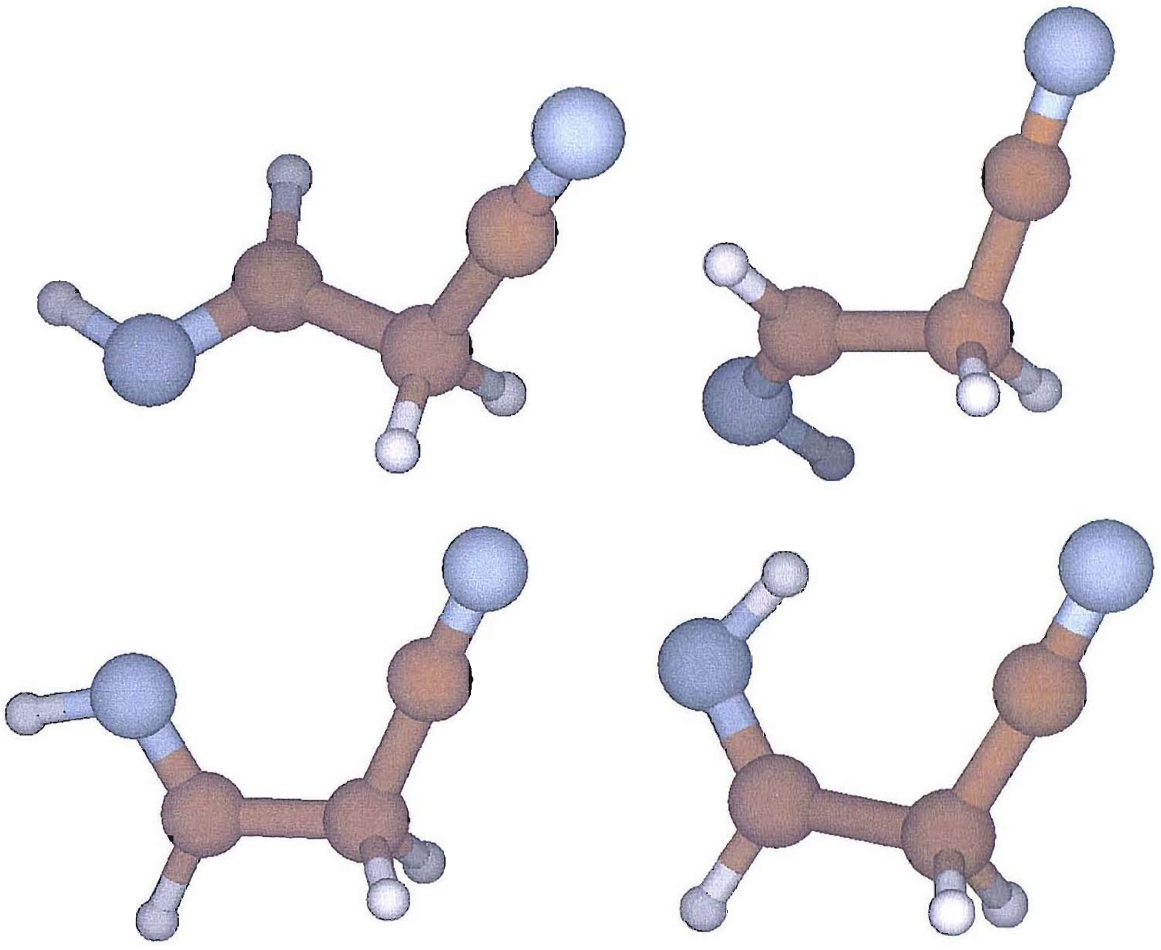

Figure 5.129- The four optimized structures of 3-iminopropionitrile at the MP2/6-31G level, *cis-cis*, *trans-cis* (top line), *cis-trans* and *trans-trans* (bottom line)**

To obtain VIEs, Koopmans' theorem has been applied to the orbital energies obtained at the MP2/6-31G** level for the *cis-cis* structure. The results are listed in Table 5.88.

Considering the results scaled by the 0.92 correcting factor [27, 28], 3-iminopropionitrile is expected to display two bands with VIEs at ≈11.2 and 11.7 eV, and a third band with VIE at ≈14.0 eV.

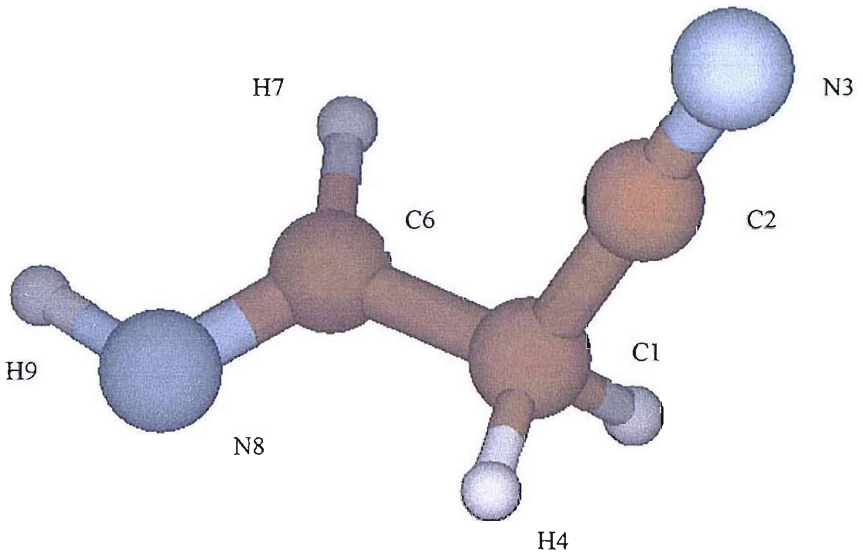

Figure 5.130- The optimized structure of *cis-cis* 3-iminopropionitrile at the MP2/6-31G level, with atom labelling**

Table 5.87- Most significant geometrical parameters for structure *cis-cis* of 3-iminopropionitrile- see Figure 5.130 for the labelling of the atoms

Bond	Length (Å)	Angle	Value (°)
C2-N3	1.181	**N3-C2-C1**	178.81
C1-C2	1.466	**C2-C1-C6**	111.48
C1-H4	1.090	**C1-C6-N8**	119.09
C1-C6	1.510	**H9-N8-C6**	109.68
C6-H7	1.093	**N3-C2-C1-C6**	
C6-N8	1.281	**C2-C1-C6-N8**	-129.13
N8-H9	1.022	**H7-C6-N8-H9**	0.34

Table 5.88- The calculated vertical ionization energies for the *cis-cis* conformer of 3-iminopropionitrile

KT calculated VIE (eV)	KT calculated VIE *0.92 (eV)
12.077	11.111
12.216	11.239
12.652	11.640
12.818	11.793
15.194	13.978

Harmonic vibrational frequencies at the MP2/6-31G** level have been calculated with partial allowance electron correlation for the four conformers: the calculated infrared spectra are reported in Figure 5.131. The frequencies and intensities of the bands are listed in Table 5.89.

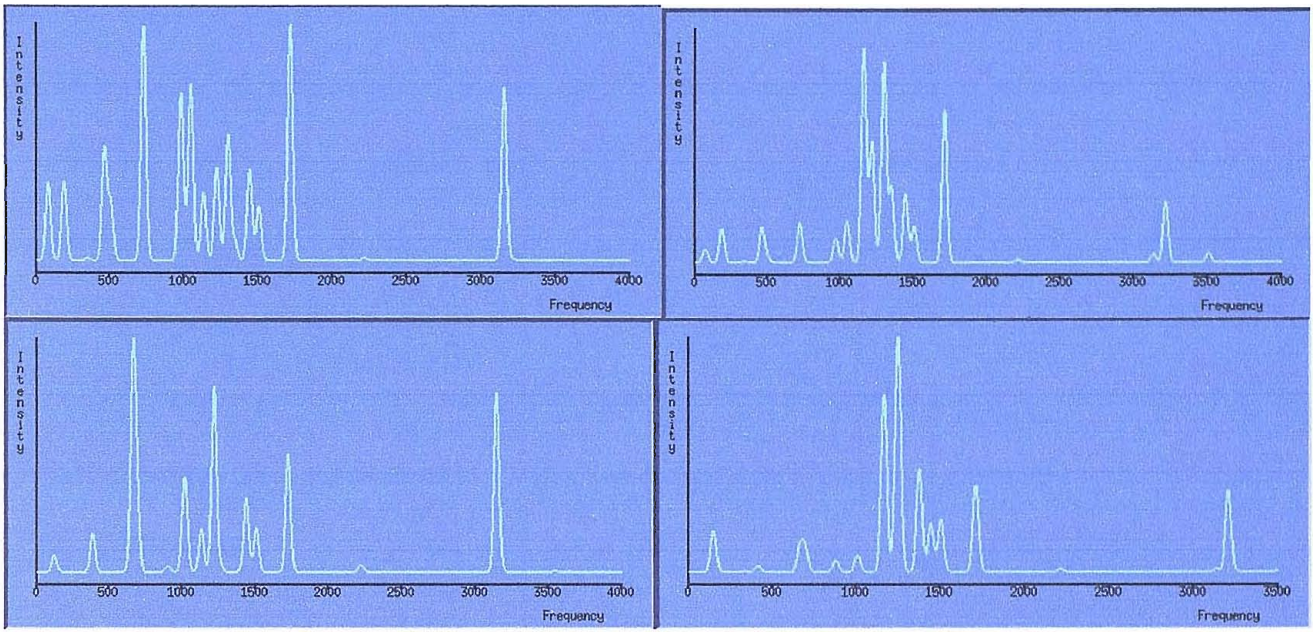

Figure 5.131- The infrared spectra for the four conformers of 3-iminopropionitrile calculated at the MP2/6-31G level (first line conformers *cis-cis* and *trans-cis*, second line conformers *cis-trans* and *trans-trans*; frequencies are expressed in cm^{-1})**

The different distribution patterns of the band intensities is immediately evident from Figure 5.131. The conformers in which the protons on the iminic nitrogen atom and on the adjacent carbon atom are in a *cis* relative orientation (spectra in the left column) show much higher intensity of the C-H stretching band at around 3150 cm^{-1} with respect to the two conformers in which the same orientation is *trans* (right column): the same happens for the band at around 730 cm^{-1}. In general, the differences in the intensities of the bands below 1700 cm^{-1} are very marked between all the four conformers of 3-iminopropionitrile.

Table 5.89- Calculated infrared bands for the four conformers of 3-iminopropionitrile (absorbances reported in parentheses in Km/mol, frequencies are expressed in cm^{-1})

cis-cis *frequencies*	*trans-cis* *frequencies*	*cis-trans* *frequencies*	*trans-trans* *frequencies*	**Normal mode**
465.0 (19.40)	463.2 (9.04)		415.4 (1.94)	
508.1 (10.04)	497.3 (1.17)	663.2 (56.41)	664.3 (7.74)	
728.2 (40.53)	721.3 (10.37)	689.6 (22.08)	695.1 (8.25)	
971.9 (6.48)		902.4 (1.66)	879.0 (3.62)	
982.6 (23.60)	966.5 (5.95)	1009.6 (12.39)	1006.9 (4.53)	
1046.2 (30.61)	1044.9 (10.91)	1022.7 (15.49)	1010.6 (1.02)	
1132.2 (11.72)	1159.7 (55.40)	1130.2 (11.76)	1165.6 (57.36)	
1221.1 (16.09)	1214.4 (31.05)	1217.1 (50.65)		N-H bending
1297.9 (21.70)	1296.6 (51.98)	1261.8 (1.99)	1249.1 (75.23)	C-H_3 wagging
1343.6 (3.23)	1349.0 (19.55)		1376.4 (33.46)	C-H_3 in phase scissoring
1442.4 (16.01)	1444.4 (17.86)	1437.3 (20.09)	1444.9 (15.56)	C-H_3 out of phase scissoring
1504.4 (9.45)	1503.3 (9.41)	1505.3 (12.11)	1504.9 (17.00)	C=N stretching
1715.9 (40.80)	1710.3 (39.74)	1722.6 (32.07)	1711.9 (27.90)	C≡N stretching
		2220.4 (1.90)	2212.9 (1.08)	C-H_3 symmetric stretching
3138.7 (1.19)	3130.9 (2.17)	3144.3 (48.47)	3135.6 (1.03)	C-H_3 asymmetric stretching
3154.2 (29.07)	3215.0 (15.62)		3206.4 (26.50)	C-H_3 asymmetric stretching
	3506.5 (2.23)			N-H stretching

Type 2 mechanism:

As was the case for nitrenes originating from the other aliphatic azides, the nitrene originating from 3-azidopropionitrile by nitrogen release, 3-nitreneacetamide, did not optimize at the MP2/6-31G** level in its singlet spin state, but it isomerizes to an imine instead.

The isomerization can be seen as a nucleophilic attack of the electron-deficient nitrogen atom on the methylene group adjacent to the cyano group: this leads to CH_2=NCH_2CN following the mechanism

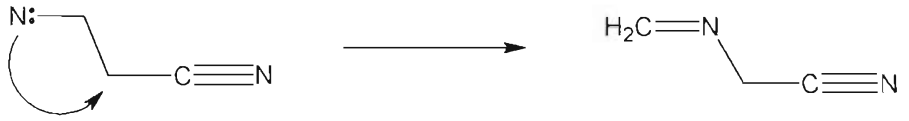

Two isomers have been found for CH_2=NCH_2CN, according to the relative orientation of the cyano group with respect to the terminal methylene group. They have been labelled *cis* and *trans*, and their geometries are shown in Figure 5.132.

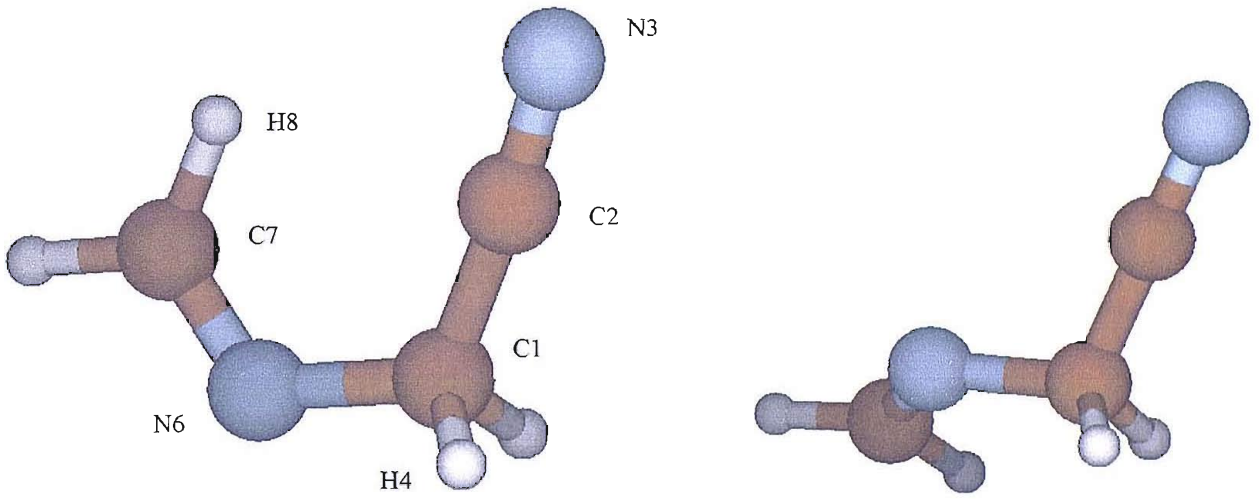

Figure 5.132- The geometries of structures *cis* (left) and *trans* (right) of CH_2=NCH_2CN optimized at the MP2/6-31G level**

Structure *cis* is a planar structure, while structure *trans* has no symmetry element (C_1 point group). Their energies are respectively -225.5061078 and -225.5040369 hartrees: this means a lower energy for the planar structure *cis* of about 1.30 kcal/mol, probably because of the stabilizing interaction between N8 and C3. It should be noted that only structures in which the dihedral angle C2-C1-N6-C7 (see Figure 5.132 for the labelling of the atoms) is either 0° or 120° have been optimized: no minimum energy structures with this dihedral angle 60° or 180° were found to be stable; they converged back to the two structures presented in Figure 5.132.

Table 5.90 reports the most significant geometrical parameters for structure *cis*, which is the most stable one for CH_2=NCH_2CN.

Table 5.90- Most significant geometrical parameters for structure *cis* of CH_2=NCH_2CN- see Figure 5.132 for the labelling of the atoms

Bond	Length (Å)	Angle	Value (°)
C2-N3	1.181	**N3-C2-C1**	178.81
C1-C2	1.466	**C2-C1-C6**	111.48
C1-H4	1.090	**C1-C6-N8**	119.09
C1-C6	1.510	**H9-N8-C6**	109.68
C6-H7	1.093	**N3-C2-C1-C6**	
C6-N8	1.281	**C2-C1-C6-N8**	-129.13
N8-H9	1.022	**H7-C6-N8-H9**	0.34

For both structures, VIEs calculated with Koopmans' theorem from the energies of the molecular orbitals are listed in Table 5.91.

Table 5.91- The first five VIEs for the two structures of CH_2=NCH_2CN calculated with Koopmans' theorem

Cis KT calculated VIE (eV)	*Cis* KT calculated VIE *0.92 (eV)	*Trans* KT calculated VIE (eV)	*Trans* KT calculated VIE *0.92 (eV)
11.947	10.991	11.875	10.925
11.978	11.019	12.249	11.269
12.787	11.764	12.386	11.395
12.807	11.782	12.791	11.767
15.299	14.075	15.054	13.849

The predicted pattern for the VIEs is very similar to that of 3-iminopropionitrile, with two close bands, one with VIE at around 11.0 eV and one at around 11.8 eV, and one at much higher energy (around 14.1 eV). These values are so close to those calculated for 3-iminopropionitrile (see previous section) that it would be practically impossible to distinguish the two compounds by means of UV-photoelectron spectroscopy.

Harmonic vibrational frequencies at the MP2/6-31G** level have been calculated for the four conformers by means of second derivative calculations: the whole calculated infrared spectra are reported in Figure 5.133. The frequencies and intensities of the bands are listed in Table 5.92.

The differences between the two conformers can be mainly found in the C-H stretching region above 3000 cm^{-1}, where the *trans* conformer shows a stronger component than the one observed in the *cis* conformer; the band at around 1400 cm^{-1} shows as well a stronger intensity in the *trans* conformer, and the series of bands around 1000 cm^{-1} is characterized by an overall different intensity pattern between the two conformers, as can be seen in Figure 5.133. Also some frequencies are calculated to be remarkably different among the two conformers; for example, some C-H stretching modes can differ by roughly 60 cm^{-1}, and the C≡N stretching mode appears with a difference of 20 cm^{-1}.

The calculated IR spectra of CH_2=NCH_2CN and 3-iminoporpionitrile are remarkably different (see Figure 5.133), because CH_2=NCH_2CN displays two strong bands in the region between 3100 and 3150 cm^{-1} (a single band in 3-iminopropionitrile), and quite an intense band associated with the C≡N stretch (around 2200 cm^{-1}) that in 3-iminopropionitrile is almost invisible.

The two molecules should therefore be distinguishable on the basis of their IR spectrum; nevertheless, the experimental results from the pyrolysis of 3-azidopropionitrile do not clearly support any evidence of the formation of these imines, because no intense bands associated with one or both of them can be traced in the matrix IR spectra, even as short-lived species. From the experiments it can only be assumed that the imines- if formed- have a very short lifetime that prevents their observation.

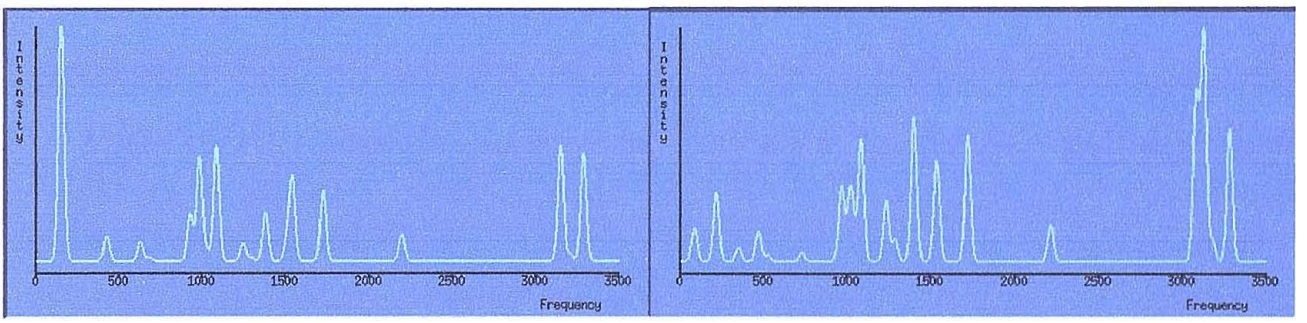

Figure 5.133- Calculated IR spectra of CH_2=NCH_2CN conformers, *cis* (left) and *trans* (right), at the MP2/6-31G level. Frequencies are expressed in cm^{-1}**

Table 5.92- Calculated infrared bands for the two conformers of CH_2=NCH_2CN

cis frequencies (cm^{-1})	*Absorbance (km/mol)*	*trans frequencies (cm^{-1})*	*Absorbance (km/mol)*	**Normal mode**
427.7	3.97	470.5	4.26	
630.1	3.08	730.5	1.22	
928.9	7.34	967.4	10.71	
983.7	16.51	1017.8	9.43	
1026.4	1.72	1041.2	3.04	
1085.7	18.33	1084.3	17.40	
		1233.4	8.68	
1245.5	2.91	1287.4	3.13	N-H bending
1380.2	7.71	1399.5	20.47	C-H_3 wagging
1509.6	3.39	1524.0	1.41	C-H_3 in phase scissoring
1541.3	12.95	1536.2	13.18	C-H_3 out of phase scissoring
1726.6	11.21	1721.2	18.06	C=N stretching
2197.9	4.26	2215.6	5.07	C≡N stretching
3149.5	16.72	3081.6	23.49	C-H_3 symmetric stretching
3153.3	1.51	3126.3	32.54	C-H_3 asymmetric stretching
3203.7	1.17	3181.1	2.95	C-H_3 asymmetric stretching
3285.6	17.11	3281.6	18.97	N-H stretching

CH=$NHCH_2CN$

From CH_2=NCH_2CN, it is possible to produce a different imine by means of a simple 1,2-hydrogen shift between the carbon and nitrogen atoms linked by the double bond. This results in producing a charged imine following the scheme:

$$CH_2=NCH_2CN \rightarrow CH=NHCH_2CN$$

This imine is expected to be more unstable than CH_2=NCH_2CN because of the presence of a negatively charged carbon atom adjacent to a positively charged nitrogen atom, but its structure makes it a good precursor for the formation of ketenimine, which is one of the products arising from the thermal decomposition of 3-azidopropionitrile: *ab initio* calculations have then been performed also on this charged imine.

Two conformers have been optimized for $CH{=}NHCH_2CN$, with different relative orientations of the iminic protons (*cis* or *trans*). It must be emphasized that only structures in which the proton on the nitrogen atom is in a *trans* position with respect to the cyano group have been found as minimum energy structures at the MP2/6-31G** level: when the two groups are in a *cis* position, one imaginary vibrational frequency was obtained, both in the C_s and in the C_1 point groups. Of the four possible different orientations of the protons and the cyano group, only two of them are minimum energy structures of the imine: they are presented in Figure 5.134.

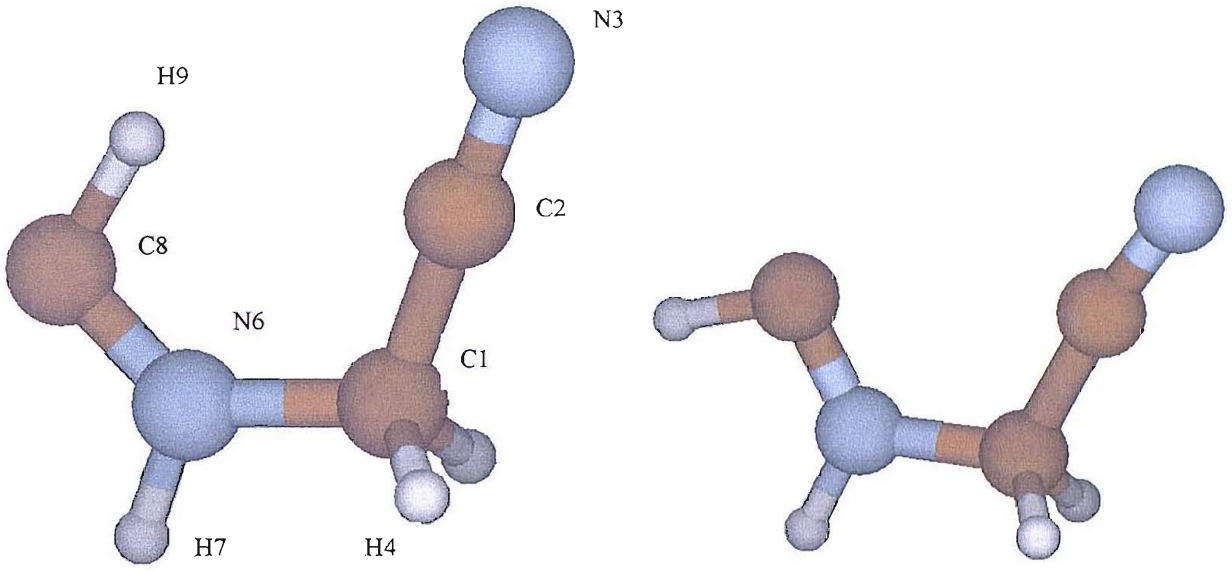

Figure 5.134- The geometries of structures *trans* (left) and *cis* (right) of $CH{=}NHCH_2CN$ optimized at the MP2/6-31G level**

Both are planar structures (point group C_s), and their difference in stability is just 0.137 kcal/mol (the total energies are -225.4321818 and -225.4319631 hartrees for the *trans* and *cis* structure respectively), with structure *trans* as the most stable of the two. As expected the difference in energy between the most stable conformers of $CH_2{=}NCH_2CN$ and of $CH{=}NHCH_2CN$ is large, being calculated in 46.39 kcal/mol.

The geometrical parameters of *trans*-$CHNH{=}CH_2CN$ are listed in Table 5.93 (see Figure 5.134 for the labelling of the atoms), while Table 5.94 reports the vertical ionization energies (VIEs) for the two conformers calculated with Koopmans' theorem at the Hartree-Fock level.

Table 5.93- Most significant geometrical parameters for structure *trans* of $CH{=}NHCH_2CN$- see Figure 5.134 for the labelling of the atoms

Bond	Length (Å)	Angle	Value (°)
C2-N3	1.181	N3-C2-C1	181.31
C1-C2	1.462	C2-C1-N6	111.78
C1-H4	1.092	C1-N6-C8	132.07
C1-N6	1.484	H9-C8-N6	106.10
N6-H7	1.015	N3-C2-C1-N6	180.0
N6-C8	1.314	C2-C1-N6-C8	0..0
C8-H9	1.104	H7-N6-C8-H9	180.0

Table 5.94- The first five VIEs for the two conformers of $CH{=}NHCH_2CN$ calculated with Koopmans' theorem

Cis KT calculated VIE (eV)	*Cis* KT calculated VIE *0.92 (eV)	*Trans* KT calculated VIE (eV)	*Trans* KT calculated VIE *0.92 (eV)
9.77	8.99	9.63	8.86
12.13	11.16	12.55	11.54
12.41	11.41	12.98	11.94
13.27	12.21	13.41	12.34
15.00	13.80	15.49	14.25

From the calculated values, the experimental photoelectron spectrum of $CH{=}NHCH_2CN$ should be characterized by a band with a VIE around 9.0 eV and by a broad series of bands between 11.5 and 12.0 eV. The two conformers have a similar pattern of the calculated VIEs (with the exception of the fifth band whose VIE values differ by 0.5 eV between the two conformers, and the fact that the third and fourth VIEs are more separated in conformer *cis* than in the *trans* one), but present important differences from the pattern expected for 3-iminopropionitrile or for $CH_2{=}NCH_2CN$, where the first two VIEs are expected to be very close to each other at ionization energies above 11.0 eV. In UV-photoelectron spectroscopy $CH{=}NHCH_2CN$ should then be clearly distinguishable from the two other imines.

Nevertheless, experimentally in the PE spectra no bands assignable to an intermediate or other stable products other than N_2, HCN, CH_3CN or $CH_2{=}C{=}NH$ are observed on pyrolysing 3-azidopropionitrile.

Harmonic vibrational frequencies have been calculated for the two conformers at the MP2/6-31G** level, and are reported in Table 5.95; the overall IR spectra are presented in Figure 5.135.

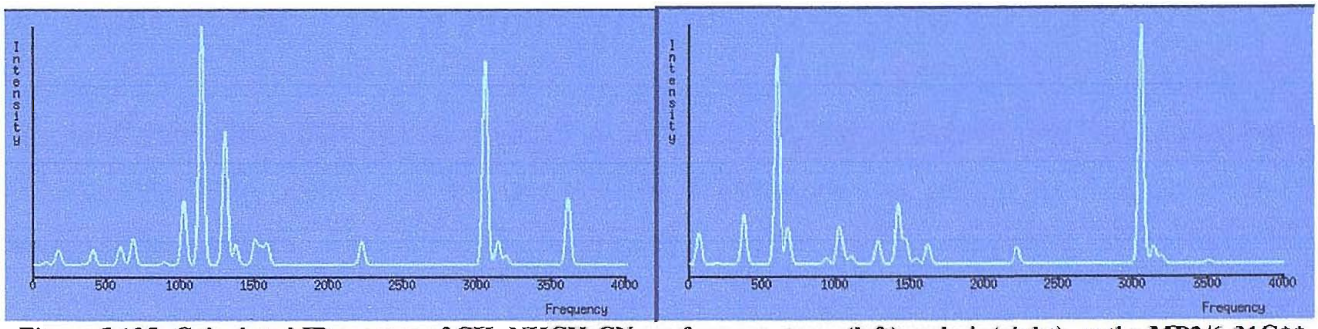

Figure 5.135- Calculated IR spectra of $CH{=}NHCH_2CN$ conformers, *trans* (left) and *cis* (right), at the MP2/6-31G level. Frequencies are reported in cm^{-1}**

The two spectra show very marked differences in intensity pattern. Conformer *trans* has a band for the N-H stretch which is almost invisible in the cis conformer, and a much more intense system of bands in the 1000-1400 cm^{-1} region. On the other hand, the cis conformer is characterized by a stronger set of bands below 600 cm^{-1}, in particular a band at around 590 cm^{-1}. The two conformers should then be distinguished in IR matrix isolation experiments.

Table 5.95- Calculated infrared bands for the two conformers of $CH{=}NHCH_2CN$

trans frequencies (cm^{-1})	*Absorbance (km/mol)*	*cis frequencies (cm^{-1})*	*Absorbance (km/mol)*	**Normal mode**
591.1	5.17	596.9	111.53	
677.8	7.37	673.8	19.71	
		933.4	2.99	
1018.2	16.74	1018.6	17.08	
1021.6	1.63	1041.5	6.07	
1138.0	67.68	1100.4	4.51	
		1277.4	10.15	
1298.2	37.87	1291.4	2.93	N-H bending
1370.3	5.71	1417.2	31.90	$C\text{-}H_3$ wagging
1498.7	7.14	1466.3	12.83	$C\text{-}H_3$ in phase scissoring
1538.6	4.87	1539.7	2.82	$C\text{-}H_3$ out of phase scissoring
1581.1	6.23	1616.4	10.39	C=N stretching
2219.5	6.74	2218.4	8.86	C≡N stretching
3051.8	57.72	3051.3	127.05	$C\text{-}H_3$ symmetric stretching
3137.3	6.89	3134.6	9.42	$C\text{-}H_3$ asymmetric stretching
3194.7	2.48	3189.3	4.34	$C\text{-}H_3$ asymmetric stretching
3610.3	19.20	3504.8	1.35	N-H stretching

SUMMARY OF THE RESULTS FROM *AB INITIO* CALCULATIONS

Three different imines have been considered as possible intermediates in the thermal decomposition of 3-azidopropionitrile, according to the two possible isomerization mechanisms that can occur for the nitrene (Type 1 or 2).

- $HN{=}CHCH_2CN$ (3-iminopropionitrile)
- $CH_2{=}NCH_2CN$
- $CH{=}NHCH_2CN$

$CHNH{=}CH_2CN$ was obtained from $CH_2{=}NCH_2CN$ by a 1,2-H shift, and it is a imine characterized by the presence of opposite electrostatic charges on the carbon and nitrogen atoms forming the iminic bond.

After optimization of all the possible conformers for each of these imines, it was found that the most stable of them is 3-iminopropionitrile. By setting its total energy as zero, the relative energies of the two remaining imines were calculated as +8.095 kcal/mol for $CH_2{=}NCH_2CN$ and as + 54.484 kcal/mol for $CH{=}NHCH_2CN$.

Table 5.96 compares the values of the first five VIEs calculated by Koopmans' theorem for the three imines (scaled by the 0.92 factor): it is evident that there is a similar pattern between 3-iminopropionitrile and $CH_2{=}NCH_2CN$, while $CH{=}NHCH_2CN$ is expected to display a different distribution of the PE bands.

Table 5.96- Comparison of the first five VIEs for the most stable conformers of 3-iminopropionitrile, $CH_2{=}NCH_2CN$ and $CH{=}NHCH_2CN$, calculated with Koopmans' theorem

3-iminopropionitrile KT calculated VIE (eV)*0.92	$CH_2{=}NCH_2CN$ KT calculated VIE *0.92 (eV)	$CH{=}NHCH_2CN$ KT calculated VIE *0.92 (eV)
11.11	10.99	8.86
11.24	11.02	11.54
11.64	11.76	11.94
11.79	11.78	12.34
13.98	14.07	14.25

The most important vibrational bands calculated for the most stable conformer of each of the three imines are reported in Table 5.97. As can be also seen from a visual comparison of the calculated IR spectra of Figures 5.131, 5.133 and 5.135, each of them should display a typical series of bands which allow them to be distinguished from one another in an experiment.

Table 5.97- Calculated infrared bands for the most stable conformers of 3-iminopropionitrile, CH_2=NCHCN and CH=NHCH$_2$CN at the MP2/6-31G level (frequencies are expressed in cm^{-1})**

3-iminopropionitrile frequencies	*CH_2=NCH$_2$CN frequencies*	*CH=NHCH$_2$CN frequencies*
982.6	983.7	
	1026.4	1018.2 / 1021.6
1046.2	1085.7	
1132.2		1138.0
1221.1		
1297.9	1245.5	1298.2
1343.6	1380.2	1370.3
1442.4		
1504.4	1509.6	1498.7
	1541.3	1538.6
		1581.1
1715.9	1726.6	
	2197.9	2219.5
3138.7	3149.5	3051.8
3154.2	3153.3	3137.3
	3203.7	3194.7
	3285.6	3610.3

By comparison with the experimental results both from PES and from IR matrix isolation, it is found that none of these intermediates is actually detected in the thermal decomposition of 3-azidopropionitrile: in fact, no reaction intermediates apart from ketenimine were seen during the pyrolysis. The imines considered so far are nevertheless important for the understanding of the decomposition mechanism, as will be shown in the next section.

5.7.6 PROPOSED THERMAL DECOMPOSITION PATH

On the basis of the experimental and *ab initio* results obtained in this work, it is possible to propose a decomposition path for 3-azidopropionitrile based on parallel routes, one leading to CH_3CN + HCN, the other to CH_2=C=NH + HCN.

It was found that the two pairs of products appear at roughly the same temperature, and their partial pressures in the reaction chambers increase until all the azide is totally consumed. It is only at high temperature that ketenimine is consumed, most likely because at high temperature ketenimine is a less favoured C_2H_3N isomer in comparison to methyl cyanide [4, 35]: the interconversion between the two forms is therefore assumed to be responsible for the elimination of ketenimine from the reaction chamber at high temperatures. In contrast to the pyrolysis of 2-azidopropionitrile, ketenimine is present in relatively high amount, while no traces of CH_3NC were observed. The route leading to ketenimine plays here a more relevant role than what was the case in 2-azidopropionitrile.

A transition state for the reaction between 3-iminopropionitrile and methyl cyanide was found, following the scheme

but none was found for the ketenimine production, because in 3-iminopropionitrile all the structures have a too large distance between the hydrogen atoms of the methyl group and the terminal nitrogen atom on which one of those protons must be transferred in order to form CH_2=C=NH. This fact highlights the importance of the other two imines produced by Type 2 mechanism, because from CH=NHCH$_2$CN a transition state leading to ketenimine was successfully optimized, following the scheme

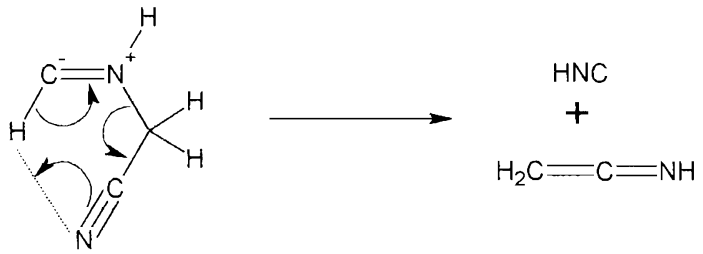

On the other hand, no transition state leading to CH_3CN was found: this could initially look quite surprising, in view of the geometry of $CH{=}NHCH_2CN$, but it is explained by the fact that HNC is a much better leaving molecule than HCN, therefore a suitable transition state is one forming HNC. This condition is not easy to be reached from $CH{=}NHCH_2CN$ due to the long distance between the terminal proton on the negatively charged carbon atom and the methylene group to which it should be transferred. The necessity of forming HNC as a leaving group is also the justification for the fact that no transition states were searched starting from $CH_2{=}NCH_2CN$, with the obvious exception of the one leading to $CH{=}NHCH_2CN$.

The importance of the imines obtained with a Type 2 mechanism is also seen from the fact that when the nitrene- obtained when molecular nitrogen is removed from 3-azidopropionitrile- is allowed to be optimized, then the isomerization takes place following this type of mechanism, that is with a nitrogen attack on the methylene group. A Type 1 mechanism is nevertheless to be fully considered, because even a slight change in the nitrene initial geometry makes the optimization follow this mechanism, involving a 1,2-hydrogen shift between the carbon and the nitrogen atoms. The two mechanisms were then assumed as having an equal probability of being followed when the nitrene is formed. The nitrene diradical is expected to be a highly unstable molecule with such a short lifetime that prevents its experimental detection, as proved in previous studies on other azides. Also in this case, 3-nitrenepropionitrile was not observed in either technique.

It is remarkable that no transition state for the azide → nitrene reaction was found: apart from problems in finding a suitable initial estimate for such a transition state, this fact could also indicate that the 3-azidopropionitrile can decompose to 3-iminopropionitrile also following a concerted path not involving the formation of a nitrene, following the scheme

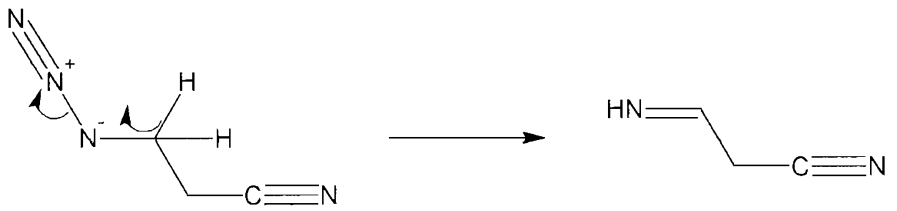

On the other hand, it is unlikely that the azide directly decomposes to N_2, HCN and CH_3CN in a single, concerted mechanism, because this would involve formation of HCN as a leaving group; for this reason, and because of the difficulty in defining a transition state where three bonds are broken at the same time, no transition states have been found for the azide → N_2 + HCN + CH_3CN mechanism.

Considering the possible formation of 3-iminopropionitrile ($HN{=}CHCH_2CN$) from the azide both via a concerted path and via a stepwise mechanism via the nitrene, the overall decomposition scheme of 3-azidopropionitrile can therefore be visualized as reported in Figure 5.136.

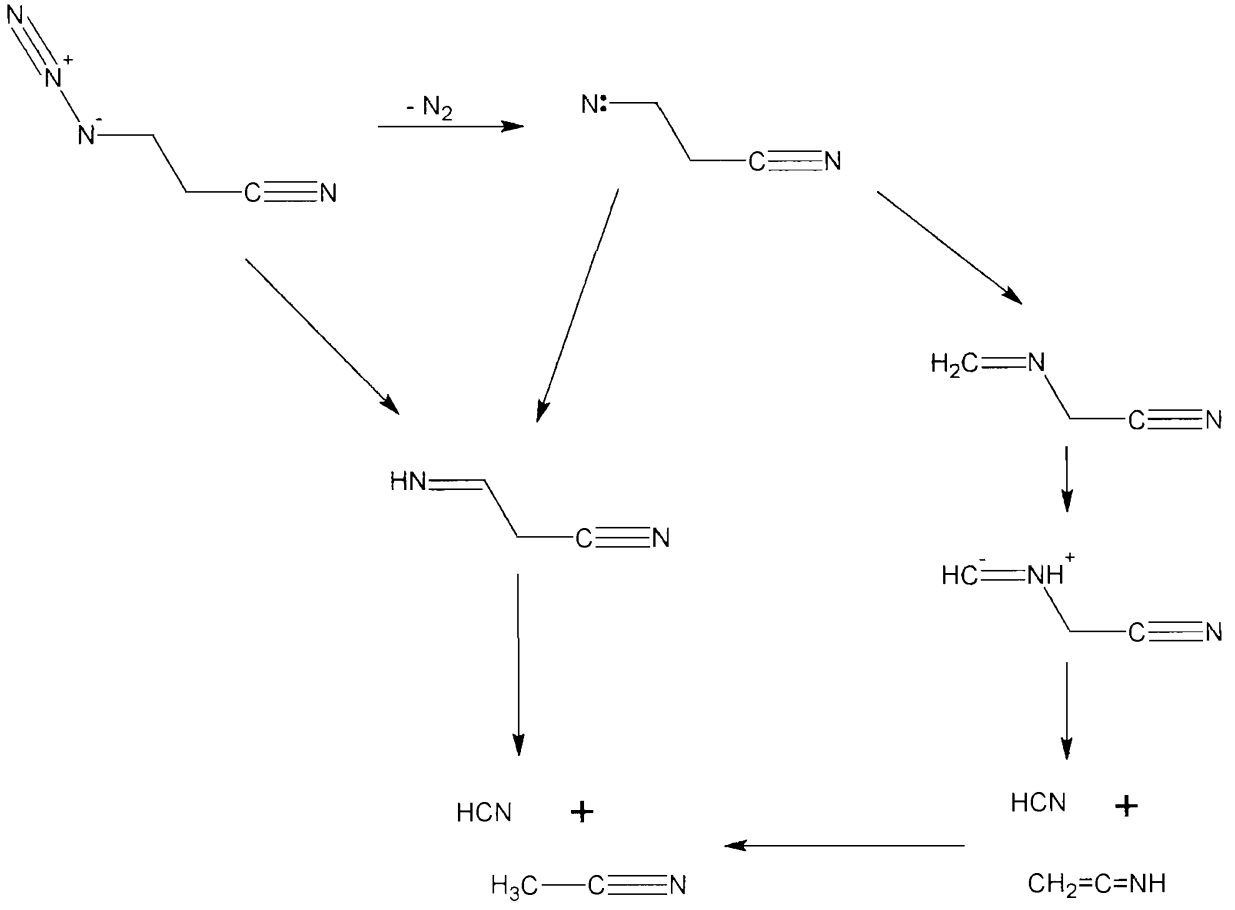

Figure 5.136- Representation of the thermal decomposition scheme for 3-azidopropionitrile

The impossibility of locating some transition states in the above scheme is reflected in the diagram of the relative energies of reactants and products at 0 K, which is presented in Figure 5.137.

The diagram in Figure 5.138 reports the relative free energy levels at 298 K, in order to take into account the contributions of zero point energy, of thermal energy and of entropy: as expected, in this scheme all the energies of the products relative to the energy of 3-azidopropionitrile are lowered in comparison to the scheme of Figure 5.137 where energies at 0 K were considered. This is particularly evident in the case of $CH_2{=}C{=}NH$ + HCN and of CH_3CN + HCN, mostly because of the entropic contribution: the result is that when ΔG^{298} is considered, methyl cyanide becomes the thermodynamically most stable product, and ketenimine is comparable in energy with 3-iminopropionitrile and $CH_2{=}NCH_2CN$.

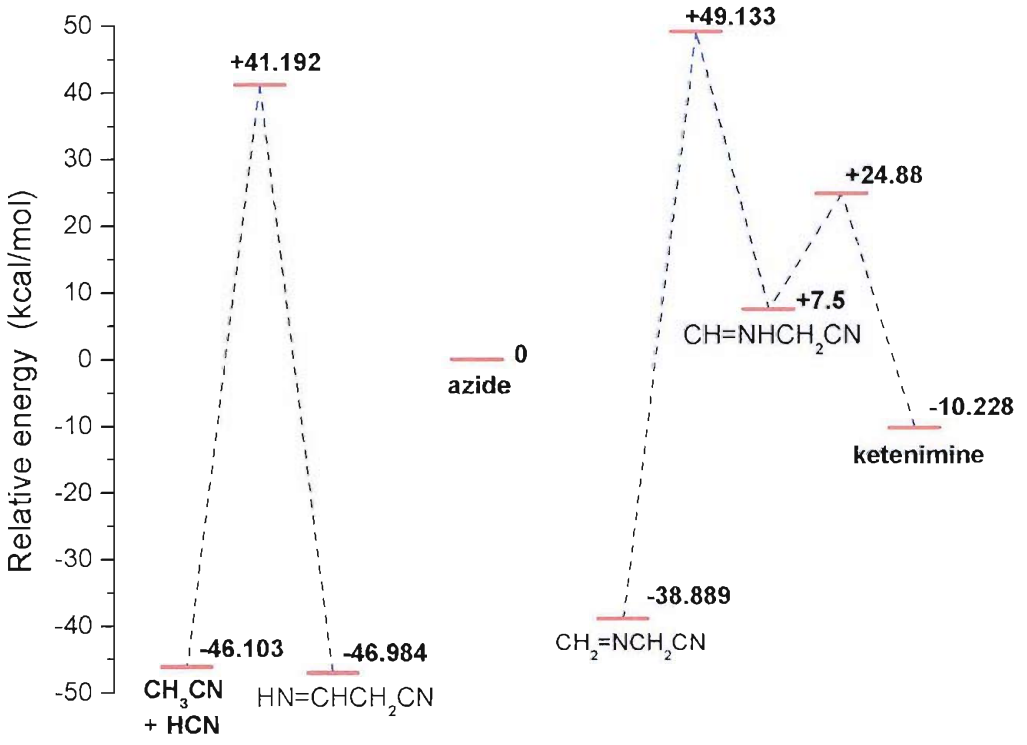

Figure 5.137- Diagram of the relative energies at 0 K for the products involved in the thermal decomposition of 3-azidopropionitrile calculated at the MP2/6-31G level (experimentally detected products reported in bold)**

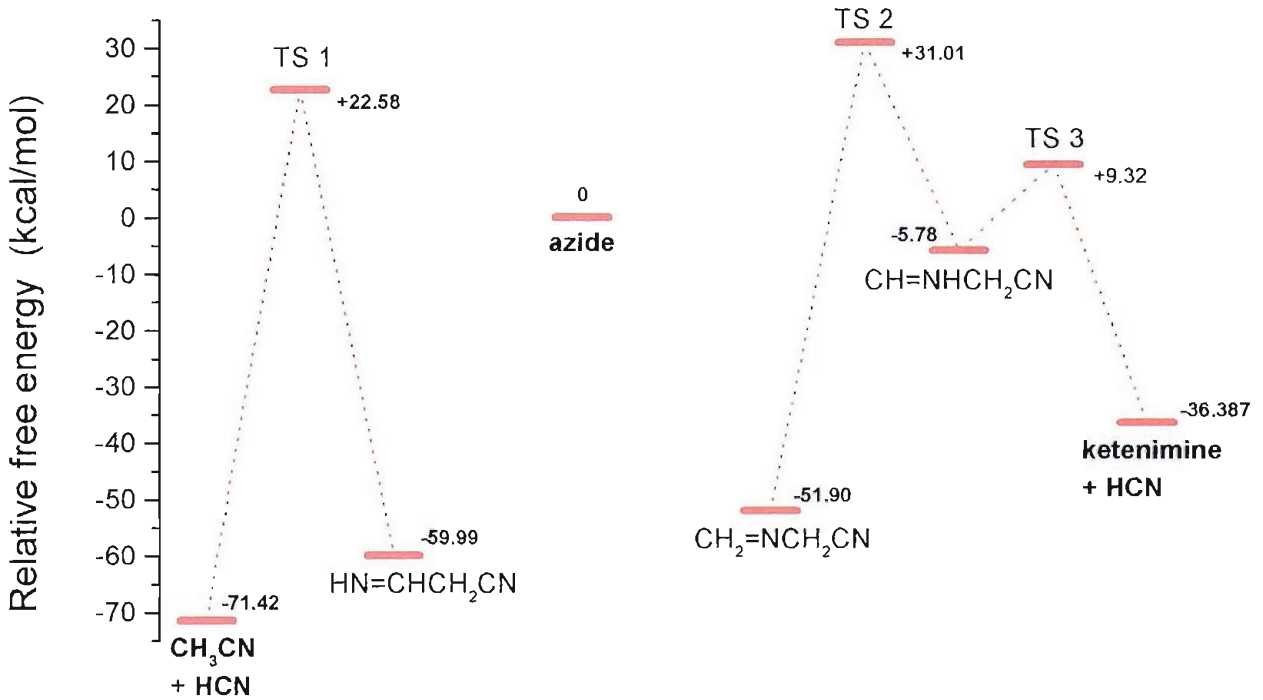

Figure 5.138- Diagram of the relative free energies at 298 K for the products involved in the thermal decomposition of 3-azidopropionitrile calculated at the MP2/6-31G level (experimentally detected products reported in bold)**

Even taking into account the entropy contributions, according to the expected relative energy values the imines should be observable. Once again, the explanation for the lack of detection of the intermediate imines lies in the high temperature at which the azide decomposes: beyond 400 °C 3-iminopropionitrile, for example, will be formed with a large amount of internal energy which is impossible to dissipate in the vibrational modes without breaking the molecule. For this reason, it is more favourable to produce HCN and ketenimine which, despite the lower thermodynamic stability of this system, can dissipate the excess energy by breaking the C-N bond in the imine and distributing it to two separate molecules. Further increases of temperatures then favour CH_3CN, and ketenimine is totally decomposed.

Figure 5.139 reports the geometries of the transition states found in the scheme, and which are reported and labelled in Figures 5.137 and 5.138.

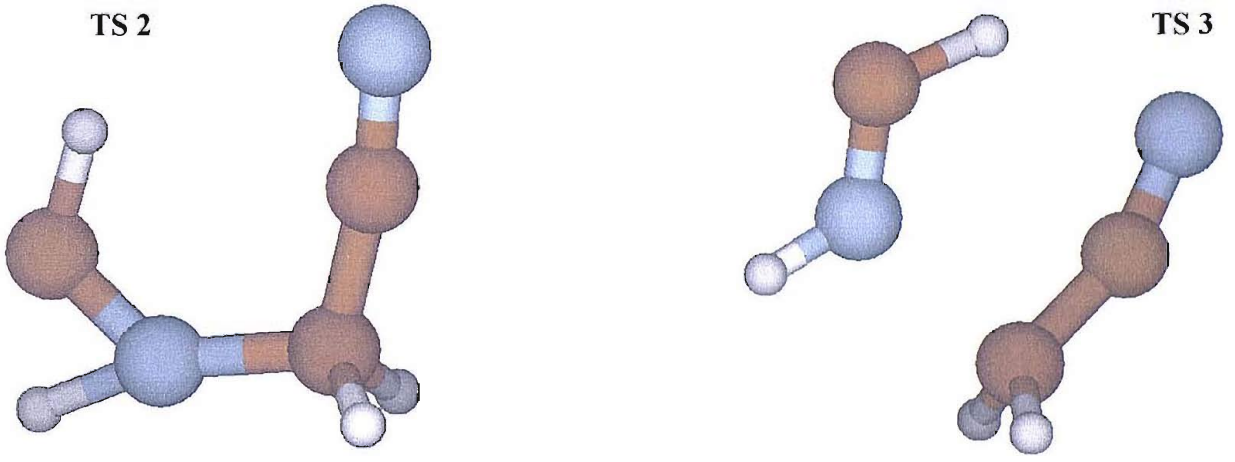

Figure 5.139- The geometries of the transition states optimized at the MP2/6-31G level for the decomposition scheme of 3-azidopropionitrile. The labels reflect the transition states indicated in Figure 5.138 and 5.139.**

5.8 INITIAL INTERPRETATION OF THE SPECTROSOPIC RESULTS ON OTHER ALIPHATIC AZIDES

In the course of the project on aliphatic azides, methyl-azidoacetate, 2-methylazidopropionate and 3-azidopropionate have also been studied. On these compounds, only initial work was started on the interpretation of the spectra, both UV-PES and IR matrix isolation spectra, and on *ab initio* molecular orbital calculations.

The importance of these azides is due to the fact that they are closely related to other azides previously studied, so that the understanding of their thermal behaviour allows an understanding of the decomposition scheme of the whole class of aliphatic azides to which they belong. For example, methyl-azidoacetate would be compared to the ethyl-azidoacetate previously studied in the Southampton PES group, and both these acetates can be compared with the equivalent formates discussed in this work.

At this stage, the experimental results from UV-PES will be briefly presented and –where available- the IR matrix isolation results will be presented. The preliminary stage of the *ab initio* calculations prevents an unambiguous assignment of some of the bands in the spectra and a full understanding of the decomposition paths. All the three azides in fact present, upon pyrolysis, bands due either to intermediate products or to stable products which are not yet fully identified: initial suggestions on the origins of such bands will be reported.

5.8.1 Methyl-azidoacetate ($N_3CH_2COOCH_3$)

Methyl-azidoacetate was prepared following the same method as the other aliphatic azides, that is by reacting methyl-chloroacetate with an excess of sodium azide at a temperature of 60 °C. The aliphatic azide was then extracted in an organic phase, dried and distilled. It was characterized as usual by 70 eV electron impact mass spectrometry, ^{1}H- and ^{13}C-NMR, and by IR spectroscopy in the liquid phase and in a nitrogen matrix. The samples used in the experiments proved to be of satisfactory purity.

Methyl azidoacetate is a colourless, moderately volatile liquid, so it was possible to introduce it into the ionization chamber of the photoelectron spectrometer by directly connecting the flask containing the sample to the quartz inlet system via a needle valve.

Figure 5.140 reports the UV-PE spectrum of methyl-azidoacetate recorded at 30 °C, with the labelling of the main bands. Calibration was carried out averaging VIEs of six spectra when methyl iodide and argon [18] were added to the ionization chamber of the spectrometer: the results of the calibration are listed in Table 5.98 and compared with VIE values calculated from *ab initio* calculations on one of the possible conformers of methyl-azidoacetate.

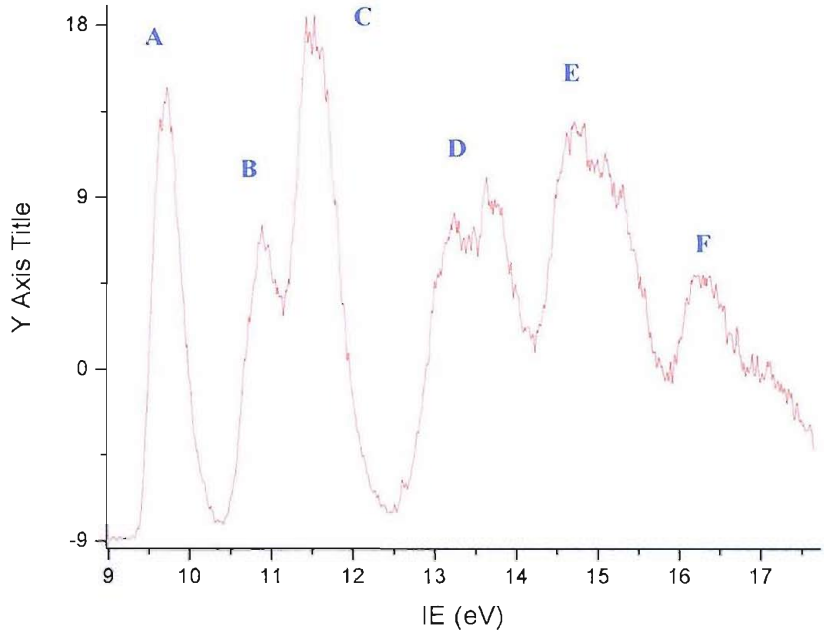

Figure 5.140- HeI-photoelectron of methyl-azidoacetate recorded at room temperature

Table 5.98- Experimental and calculated vertical ionization energies (VIEs) of the first six bands of methyl azidoacetate

Band	Experimental VIE (eV)	KT calculated VIE (eV)	KT calculated VIE *0.92 (eV)
A	9.78	10.827	9.961
B	10.96	12.306	11.322
		12.335	11.348
C	11.58	12.629	11.618
D	13.31	14.378	13.228
E	14.67	15.240	14.021
F	16.22		

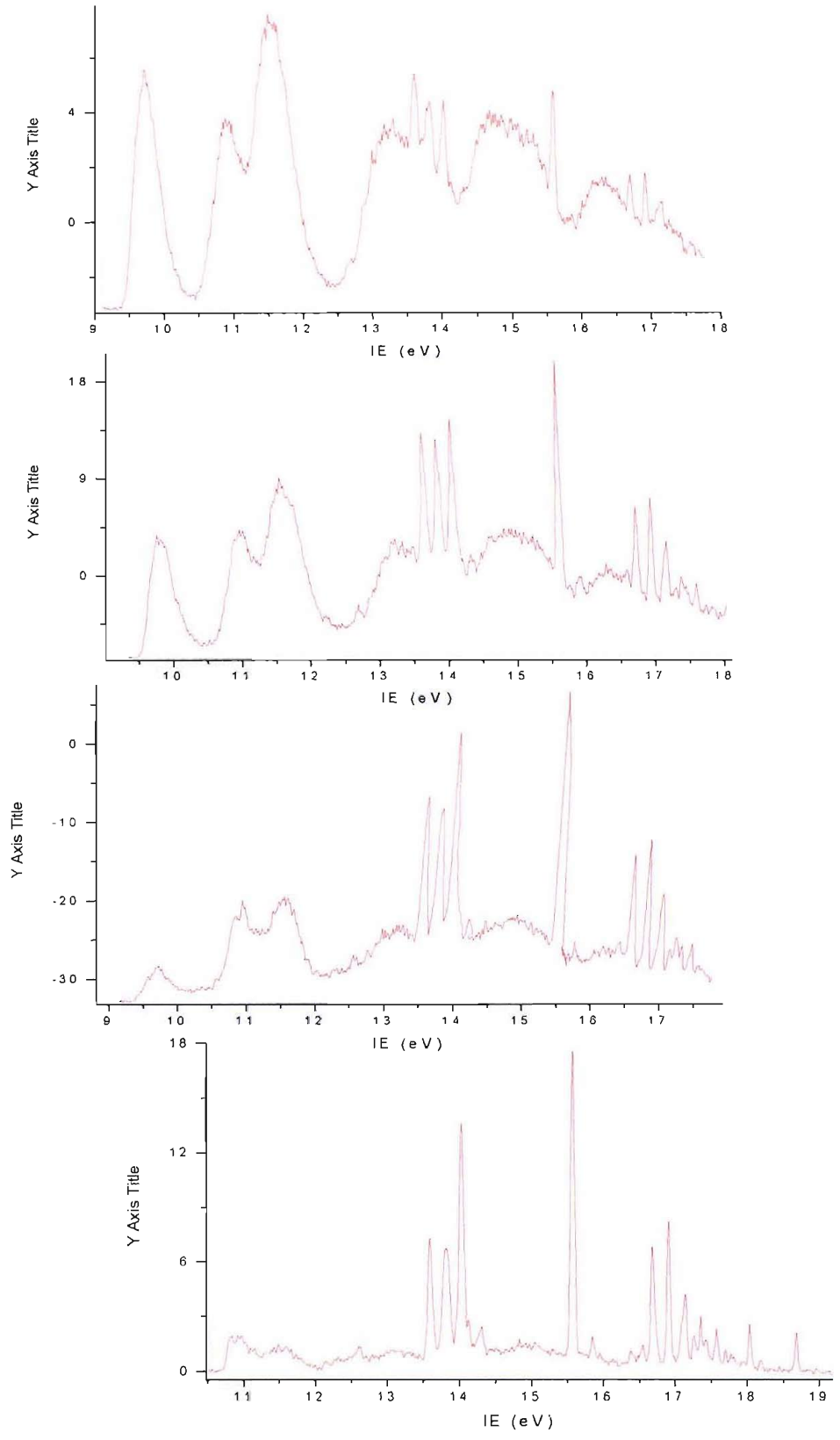

Figure 5.141- HeI-photoelectron spectra of methyl-azidoacetate heated at a) 200, b) 330, c) 400 and d) 460 °C

When the sample vapours are heated to increasing temperatures, the spectrum of the azide is modified according by the presence of products arising from its decomposition: a typical sequence of spectra is reported in Figure 5.141.

The first evidence of pyrolysis, like in all the organic azides, is the release of molecular nitrogen (sharp band at 15.58 eV, [8]), which in the case of methyl azidoacetate begins at approximately 190 °C. Around 200 °C, HCN is also produced (the vibrationally structured band with VIE at 13.60 eV, [8]). The decomposition looks largely incomplete up to a temperature of 350 °C; apart from the appearance of N_2 and HCN bands- whose intensities remain low-, the main evidence of the on-going pyrolysis is marked by the slight decrease in intensity of the azide first band. Only at temperatures around 380 °C this effect is more marked; the fact that the azide second and third bands do not appear to decrease by the same amount as the first band shows that these bands are overlapping with the bands of new products that are formed. Also, CO is observed, as can be seen from the increase of a band at the position of the third vibrational component of the first band of HCN, which overlaps with the carbon monoxide first band, VIE = 14.01 eV [8]. It is not clear if CO_2 is also formed: the appearance of vibrationally resolved bands in the 16-19 eV region supports this assumption, but no major broadening of the second vibrational component of HCN (overlapping with carbon monoxide first band, with VIE= 13.78 eV) is clearly observed.

In a very narrow temperature range, between 400 °C and 430 °C, the amount of azide reduces dramatically and at 440 °C it is totally decomposed, as estimated by the complete disappearance of the band at 9.78 eV VIE. A closer investigation of the product bands in the 10-13 eV region by means of a slower acquisition and a retarding voltage applied to the reaction cell shows that (Figure 5.142) there are different contributions to the PE spectrum: bands can be identified centred at 10.36, 10.84, 10.98, 11.15 and 11.54 eV.

Considering the structure of methyl azidoacetate, all these bands except that at 10.36 eV, have been attributed to methyl formate (first band AIE = 10.85 eV, VIE = 11.02 eV; second band VIE = 11.55 eV, [18]) or methanol (first band AIE = 10.85 eV, VIE = 10.96 eV; second band VIE = 12.68 eV, [18]). Apart from the VIE values, the shapes and the relative band intensities are also consistent with this assignment.

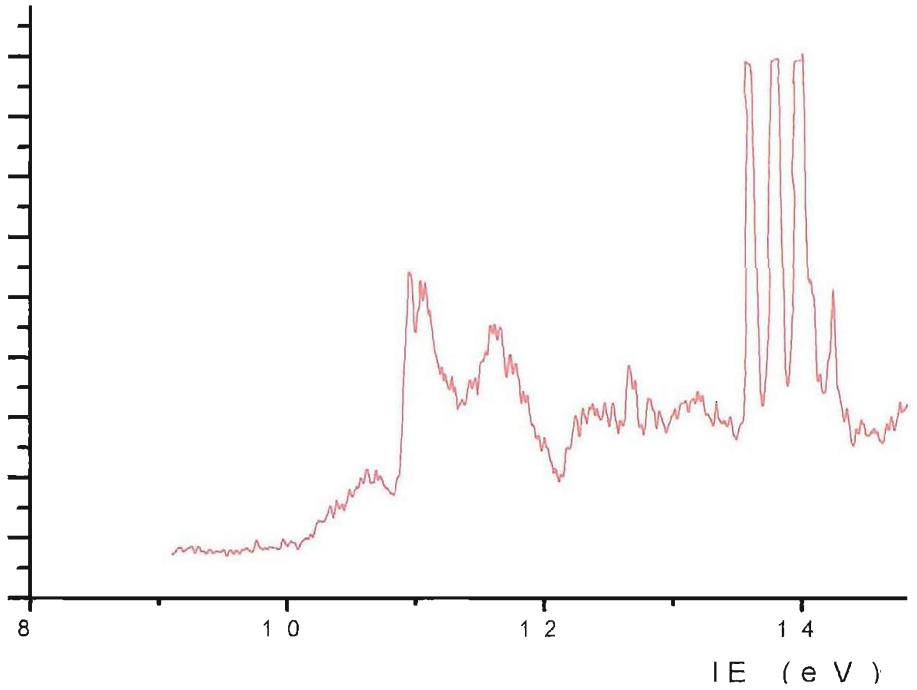

Figure 5.142- HeI-photoelectron of methyl-azidoacetate recorded at 440 °C with a voltage of 1V applied to the reaction cell

A mixture of CH_3OH and $HCOOCH_3$ has been studied to reproduce the results of the pyrolysis: the position and shape of the bands recorded for this mixture are in very good agreement with those obtained in the pyrolysis spectra, especially for ratios methanol/methyl formate (evaluated just by partial pressures in the ionization chamber and assuming equal photoionization cross sections) varying between 40/60 and 60/40, i.e. with an approximate 1:1 ratio. The broad band with VIE = 10.36 eV could be due a persisting imine intermediate. Beyond 400 °C the only effect is the strong increase of CO production compared to HCN. Separate pyrolysis experiments on methanol and methyl formate have been carried out, showing that methanol begins to release CO at approximately 380 °C and methyl formate releases CO at approximately 320 °C. Even if the amount of such decomposition in these separate experiments is quite low, the conditions in which these two molecules are produced in the pyrolysis of methyl azidoacetate (that is, at high temperatures and therefore with a high internal energy) are expected to increase their degree of decomposition. CO can therefore arise from thermal decomposition of the azide as well as from secondary decomposition of $HCOOCH_3$ (earlier) and CH_3OH (later). Beyond 500 °C the bands associated with methanol and methyl formate were markedly lower in intensity, as was the case for the band at 10.36 eV. The fact that they do not totally disappear leads to the conclusion that all the observed bands are due the relatively thermally stable compounds.

Assuming that the azide first releases nitrogen by decomposing to methyl nitreneacetamide following the reaction

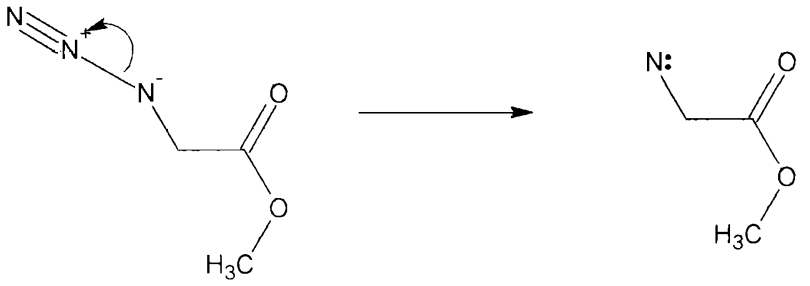

then the nitrene can undergo decomposition following the two usual decomposition schemes described so far as Type 1 or 2. When a Type 1 mechanism is followed, the 1,2-hydrogen shift operates on the nitrene producing methyl-iminoacetate ($HN{=}CHCOOCH_3$) following the scheme

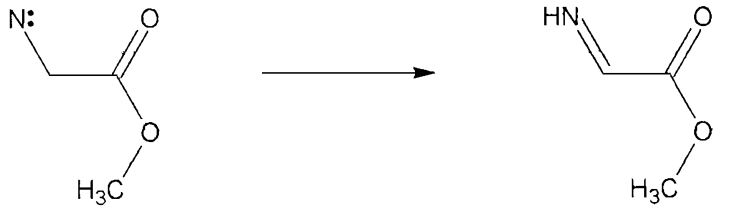

Methyl-iminoacetate can decompose in two alternative ways, one leading to methyl formate and HCN

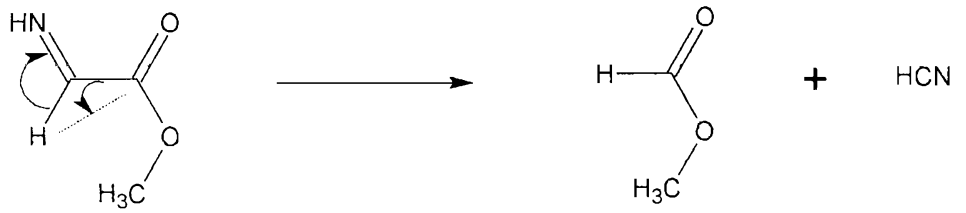

or via a concerted mechanism to HCN, CO and methanol

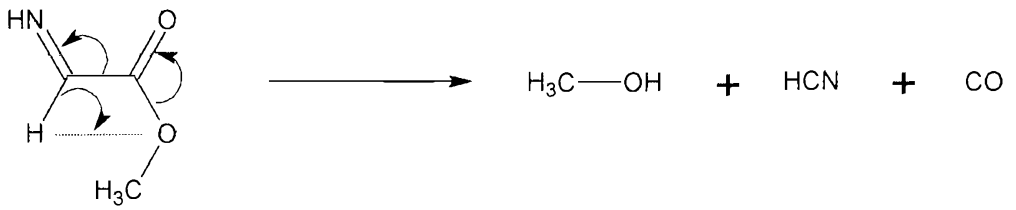

It must be underlined that methanol can also be produced by decomposition of methyl formate, according to the reaction $HCOOCH_3 \rightarrow CO + CH_3OH$. This assumption seems to be confirmed by the fact that the relative intensity of the CH_3OH signal increases relatively to the signal of $HCOOCH_3$ at increasing temperatures.

When the nitrene follows a Type 2 isomerization mechanism, the nitrogen atom on which the unpaired electrons are present attacks a remote site within the molecule: in this case the obvious target is the terminal methyl group. The decomposition then leads to a five-membered ring similar to 2-oxazolidone, encountered in the decomposition of ethyl-azidoformate

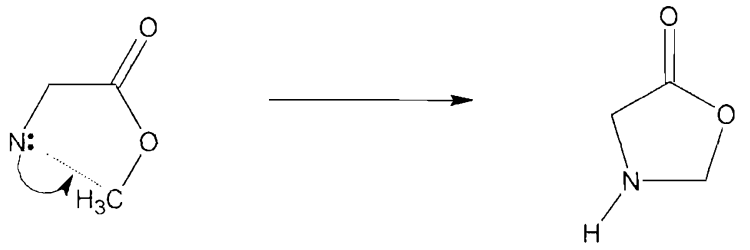

As for 2-oxazolidone, this cyclic compound is expected to be stable: *ab initio* calculations at the MP2/6-31G** level were performed to calculate its first VIE. Koopmans' theorem obtained this value to be 11.28 eV, which when scaled by the 0.92 factor becomes 10.38 eV; the ΔSCF method yelds a value of 10.45 eV for the VIE, while the adiabatic IE was calculated as 9.97 eV. These values are quite close to the experimental value of 10.36 eV calibrated for the unassigned broad band appearing when the azide is almost fully pyrolized: this, and the thermally stable behaviour of the band, allows an initial assignment of this band to the cyclic compound. Confirmation of this assumption can be based on the IR matrix isolation results and comparison with the vibrational frequencies obtained from the *ab initio* calculations: such a discussion is not presented here, as no IR spectra are available at the moment.
Finally, the presence of CO_2 can be due to decomposition of methyl-iminoacetate

$$HN{=}CHCOOCH_3 \rightarrow HCN + CO_2 + CH_4$$

which also produces methane, whose photoelectron spectrum is too broad and unresolved to allow its experimental detection. Also to establish the presence of methane, the contribution from IR matrix isolation spectra will be decisive.

5.8.2 3-methylazidopropionate ($N_3CH_2CH_2COOCH_3$)

3-methylazidopropionate was prepared using the same method used for the other aliphatic azides: 3-methylchloropropionate was added to an excess of sodium azide at a temperature of 60 °C, the aliphatic azide was then extracted in an organic phase, dried and distilled. It was characterized by 70 eV electron impact mass spectrometry, ^{1}H- and ^{13}C-NMR, and by IR spectroscopy in the liquid phase and in a nitrogen matrix. The samples used in the experiments proved to be of satisfactory purity.

3-methylazidopropionate is a colourless liquid with quite low volatility, but has too high vapour pressure at room temperature to allow placing the sample in small vials near the pyrolysis region (in this configuration, it was pumped away through the ionization chamber in only a few minutes after pumping down the spectrometer), so it was preferred to introduce it into the ionization chamber of the photoelectron spectrometer by directly connecting the flask containing the sample to the quartz inlet system via a needle valve, despite a low intensity of the PE bands obtained.

Figure 5.143 reports the UV-PE spectrum of 3-methylazidopropionate recorded at 30 °C, with the main bands labelled. Calibration was carried out averaging VIEs obtained from six spectra when methyl iodide and argon [18] were added in the ionization chamber of the spectrometer: the results of the calibration are listed in Table 5.99 and compared with the VIE values calculated from *ab initio* calculations on one of the possible conformers of 3-methylazidopropionate.

When the sample vapour is heated at increasing temperatures, the spectrum of the azide is modified according to the products arising from its decomposition: two spectra acquired at high temperatures (respectively 370 and 460 °C) are reported in Figure 5.144.

For 3-methylazidopropionate the release of nitrogen (sharp band at 15.58 eV) begins at approximately 150 °C, and HCN (the vibrationally structured band with VIE at 13.60 eV) is produced around 260 °C [8]. Until 360 °C the extent of the pyrolysis is mainly seen by the decrease in intensity of the azide first band as well as the presence of N_2 and HCN bands. As observed for methyl azidoacetate, the second and third azide bands do not decrease by the same amount as the first one, showing that these bands are overlapped with the bands of products being formed. Also another new weak, broad band is observed with VIE approximately 8.50 eV. At 420 °C the azide is almost totally decomposed, as estimated by the complete disappearance of the band at 9.67 eV VIE, and CO begins to be observed (sharp band at 14.01 eV, [8]). The broad band at 8.50 eV disappears at temperatures above 440 °C, showing typical behaviour for a pyrolysis intermediate, while the set of bands in the 10-12 eV IE region remain constant with temperature. A closer investigation of this region by means of a slower scan shows that there are different contributions to the PE spectrum: bands can be identified at 10.46, 10.74 and 11.17

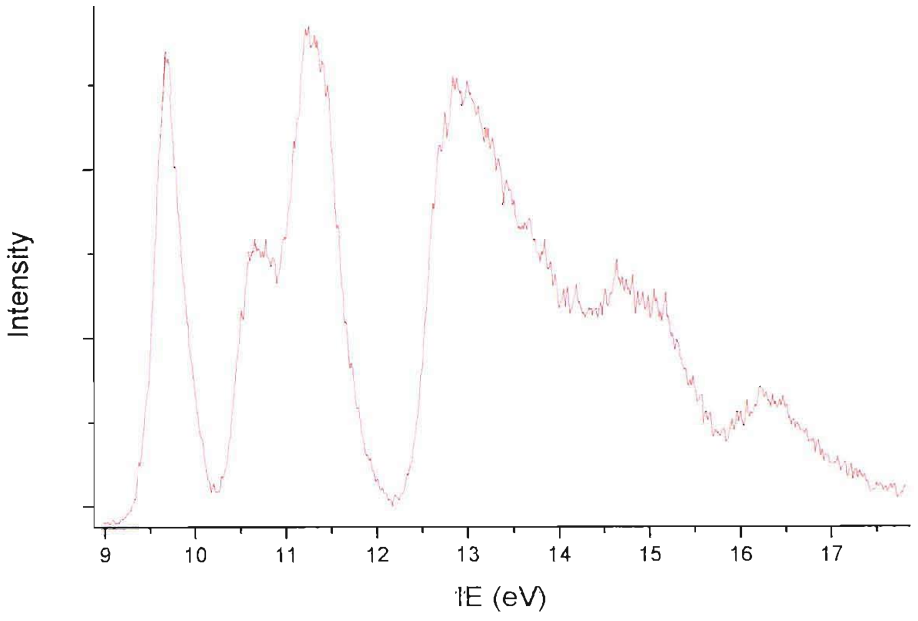

Figure 5.143- HeI-PE spectrum of 3-methylazidoporpionate at room temperature

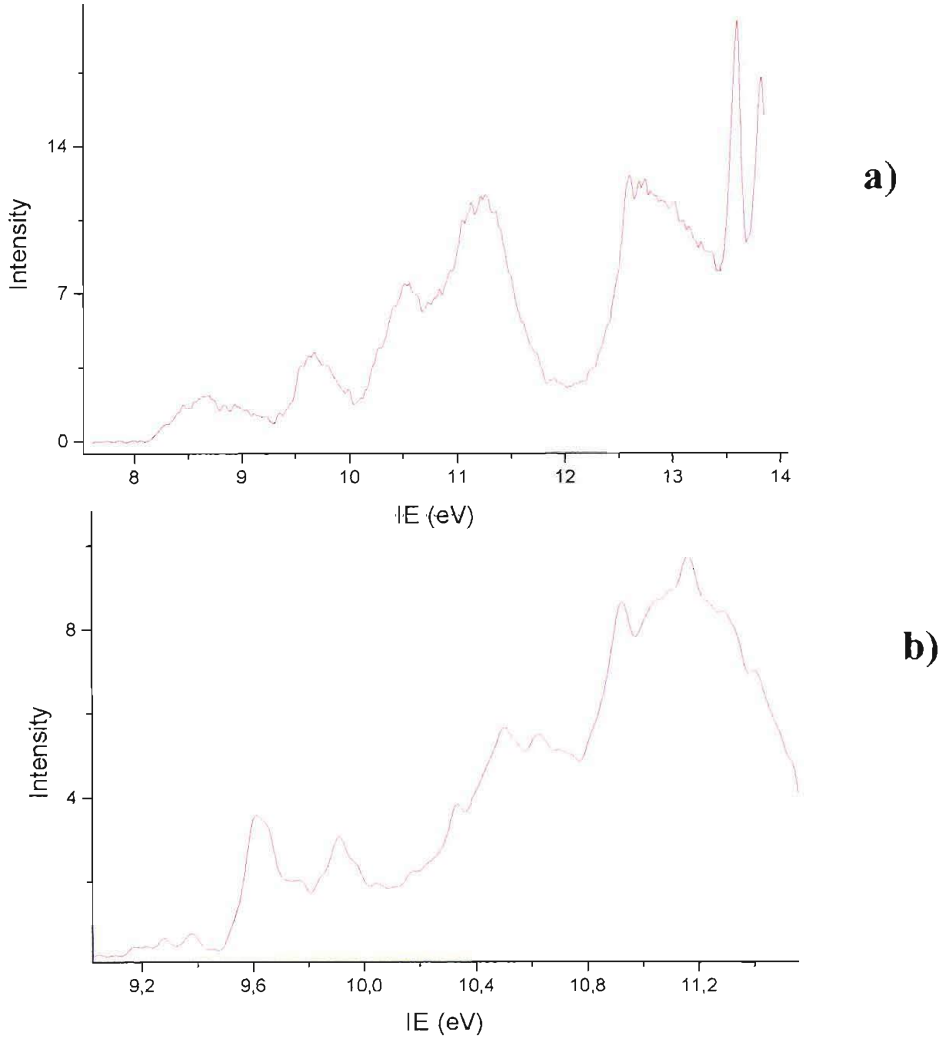

Figure 5.144- HeI-PE spectra of 3-methylazidoporpionate heated at a) 370 and b) 460 °C

eV. Considering the structure of 3-methylazidopropionate, these bands have been attributed to methyl acetate (first band AIE = 10.33 eV- almost invisible- VIE = 10.48 eV; second band VIE = 11.16 eV, [39]) and ethanol (first band VIE = 10.64 eV, [18]). The shapes and relative intensities of these components seem to confirm the assignment. There is also evidence of a very weak series of sharp bands in the 9.3-9.7 eV region: they are due to ketene, which displays a first vibrationally resolved band with VIE = 9.61 eV [8, 18]; they are visible only when the azide is fully pyrolyzed and the broad intermediate band has disappeared. Beyond 400 °C the only effect is the strong increase of CO production compared to HCN.

Matrix isolation infrared results confirm the presence of methyl acetate and ketene, and moreover suggest that methanol is being formed in later stages of the decomposition; the infrared spectra must be more fully interpreted, because in this case the main vibrational mode for CH_2=C=O [40] and CO [21] are very close in frequency, so it is difficult to distinguish the contribution of ketene from that of carbon monoxide at different temperatures. A typical series of IR matrix isolation spectra is reported in Figure 5.145.

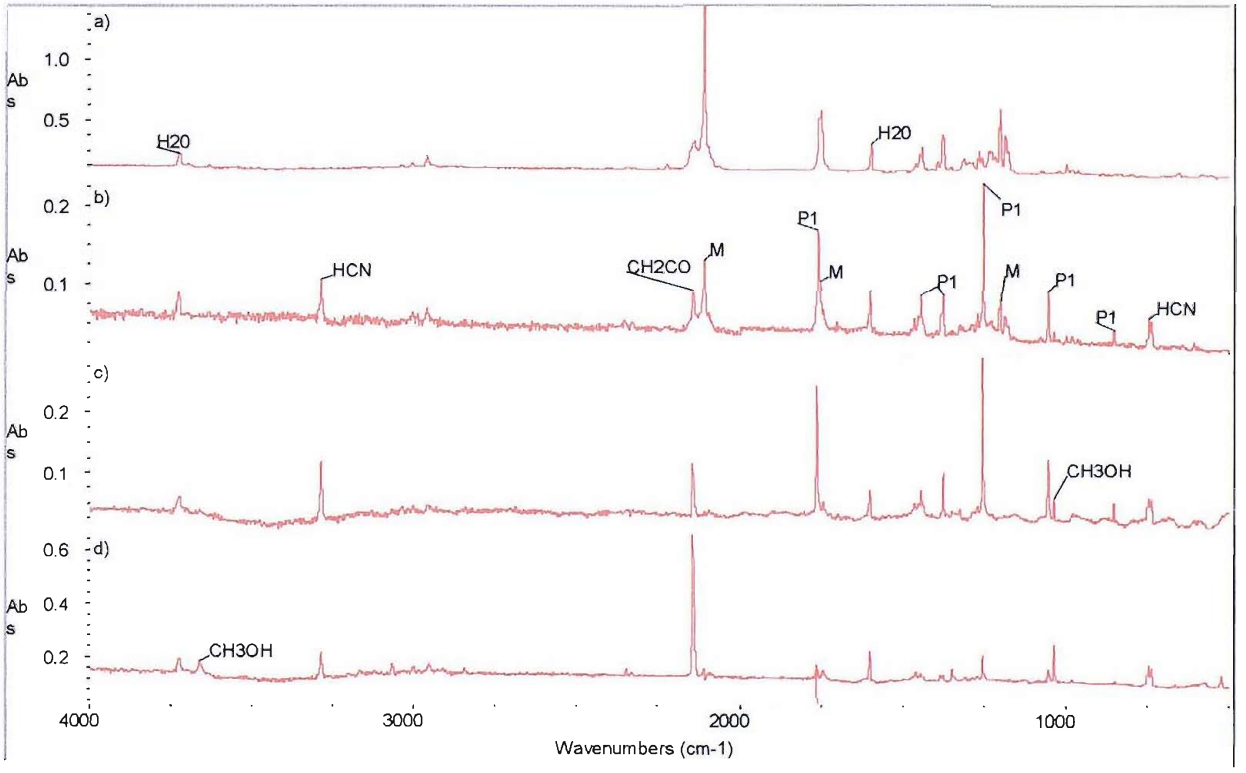

Figure 5.145- IR matrix isolation spectra of 3-methylazidopropionate heated at 30 °C, 260 °C, 330 °C and 605 °C

From these observations, multiple decomposition paths for 3-methylazidopropionate are shown to be open, both involving an intermediate and direct decomposition from the azide to the main products.
As in the other cases, it was supposed that the azide first decomposes to a nitrene as a consequence of nitrogen release; in this case 3-methylnitrenepropionitrile is formed following

The nitrene can decompose following a Type 1 mechanism, producing 3-methyliminopropionate following a 1,2-hydrogen shift

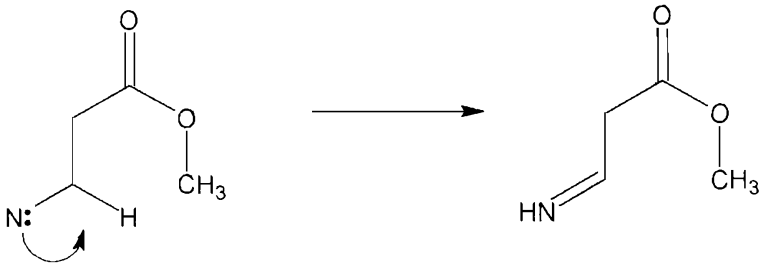

If a Type 2 mechanism is followed, the most likely attack site from the electron deficient nitrogen atom is the terminal methyl group, forming a six-membered ring according to the scheme

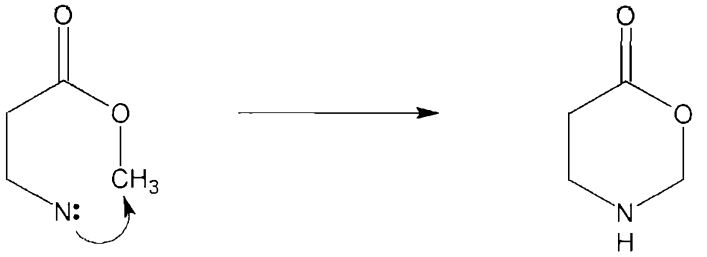

This cyclic structure is expected to be relatively stable, and therefore it can be associated with the band with VIE at 8.50 eV associated with a short lived molecule; from *ab initio* calculations at the MP2/6-31G** level, it was found that the six-membered ring is expected to have a first PE band with a VIE in good agreement with the experimental value (VIE with Koopmans' theorem = 8.24 eV).

Another alternative for a Type 2 mechanism is that the nitrogen attack causes the migration of the methyl group from the oxygen to the nitrogen atom. In this case $CH_3NHCH{=}CHCOOH$ is formed.

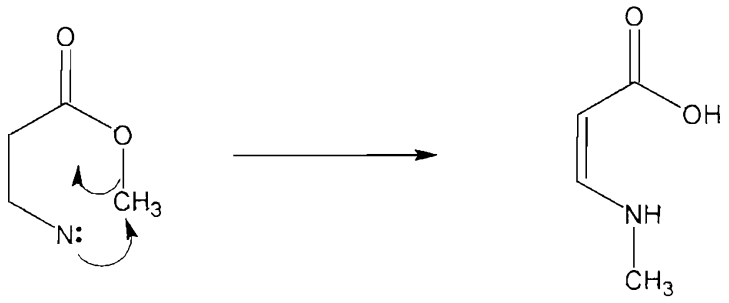

For $CH_3NHCH{=}CHCOOH$ the agreement between *ab initio* calculations at the MP2/6-31G** level and the experimental VIE is even better (VIE with Koopmans' theorem = 8.68 eV, with ΔSCF = 8.36 eV; AIE = 7.88 eV). At this stage, no clear preference as to which of these molecules is actually responsible for the band at 8.50 eV can be expressed.

The presence of other molecules produced in the pyrolysis of 3-methylazidopropionate is better explained starting from 3-methyliminopropionate. From this molecule, the formation of methyl acetate and cyanic acid is justified by the scheme

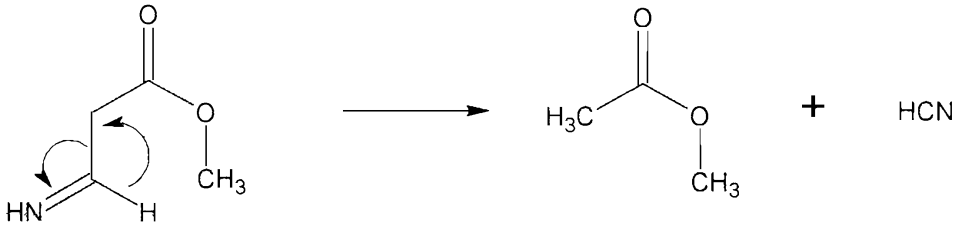

Ketene and methanol can be formed either from decomposition of CH_3COOCH_3 (and this confirms the evidence that the bands associated with these products become stronger with increasing temperature), or directly from the imine following the scheme

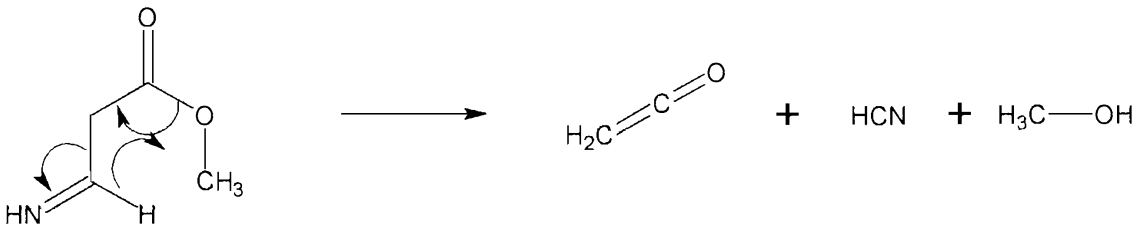

So far no valid explanation has been found to support the formation of carbon monoxide: if it arises from thermal decomposition of methyl acetate, ethanol or diethyl ether should be released too as consequence of this process, but none of them has been so far detected in the PE spectra.

5.8.3 2-methylazidopropionate ($N_3(CH_3)CHCOOCH_3$)

2-methylazidopropionate was prepared by the same procedure as used for the 3-methylazidopropionate isomer and characterized with the same techniques.

Upon thermal decomposition, bands associated with methyl formate, methanol, methyl cyanide, carbon monoxide and carbon dioxide were observed- along with nitrogen- by UV-photoelectron spectroscopy [8, 18].

From IR matrix isolation bands also associated with methane have also been detected. The bands associated with methyl formate lower in intensity with increasing temperature, while those associated with all the other compounds increase steadily, indicating a more stable thermal behaviour. A series of spectra acquired at increasing degree of pyrolysis is presented in Figure 5.146.

In the PE studies, two bands due to relatively stable reaction intermediates are still not assigned: a careful calibration of these bands, along with a deeper analysis of the IR matrix isolation data and supporting *ab initio* calculations, is necessary to make assignments of these intermediates.

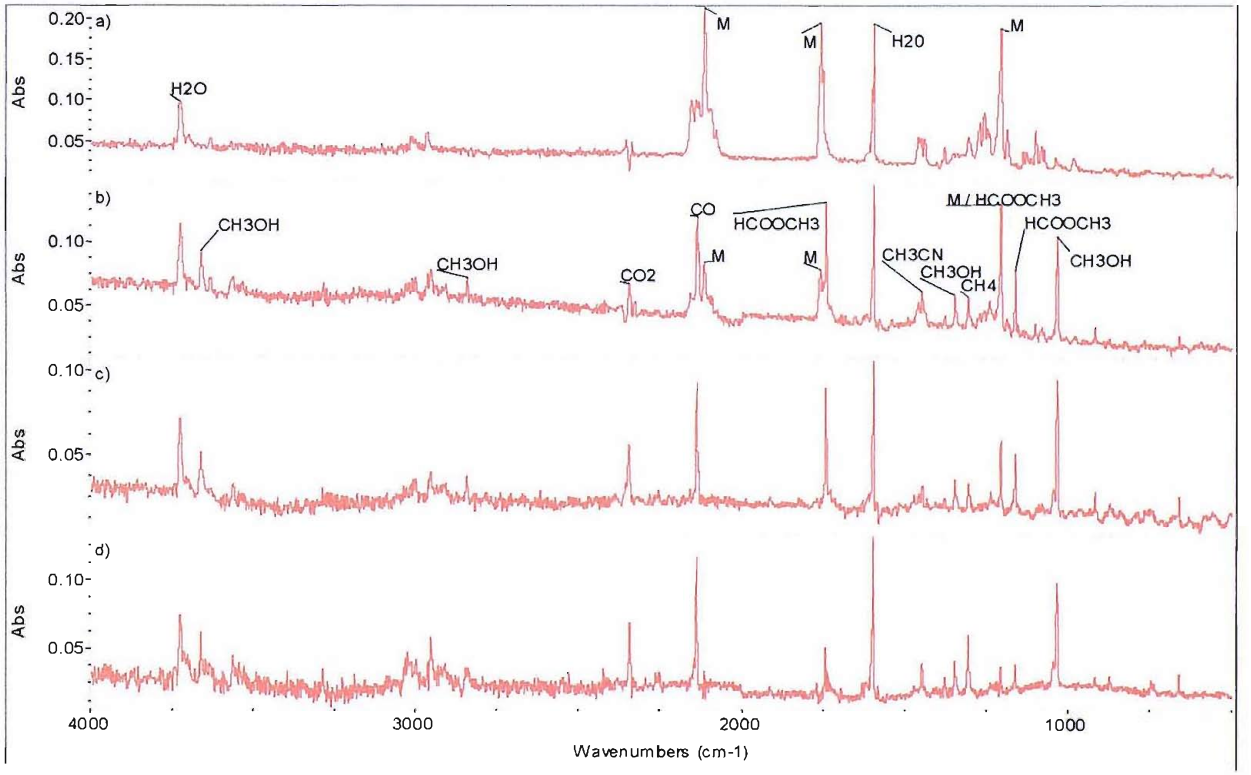

Figure 5.146- IR matrix isolation spectra of 2-methylazidopropionate heated at 30 °C, 250 °C, 320 °C and 470 °C

From the experimental results obtained so far, it is possible to rationalize the presence of the observed decomposition products on the basis of the decomposition of 2-methyliminopropionate obtained when nitrogen begins to be formed from the azide following the scheme

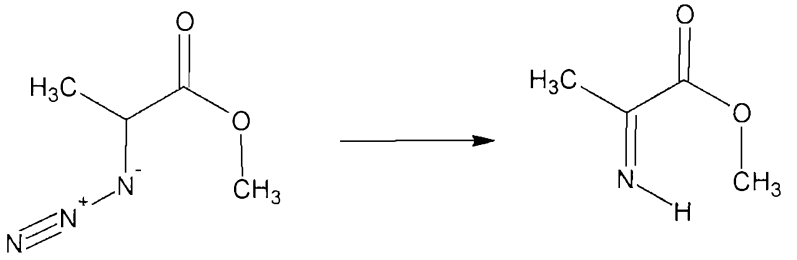

The formation of methyl cyanide and methyl formate can be visualized as

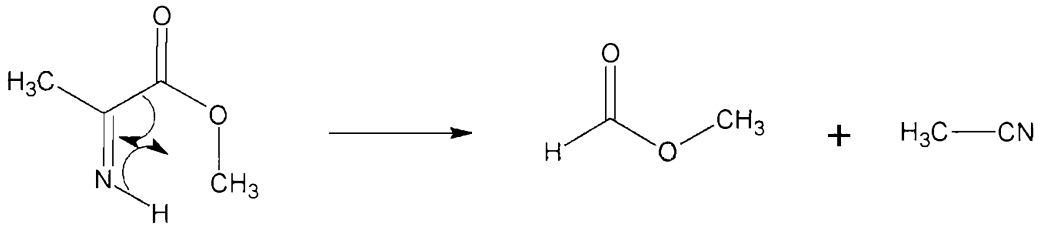

while carbon monoxide and methanol are formed following the scheme

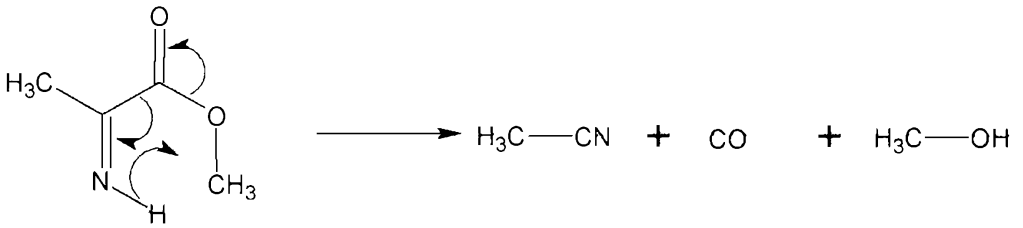

Finally, the scheme for the production of carbon monoxide and methane can be represented as

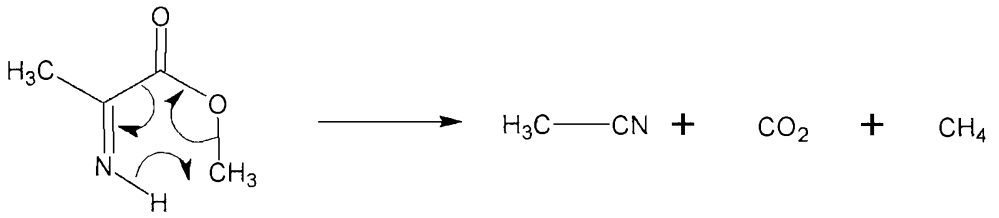

One obvious candidate for the unassigned band could be the five-membered cyclic structure arising from a Type 2 isomerization of the nitrene produced when the azide begins to decompose.

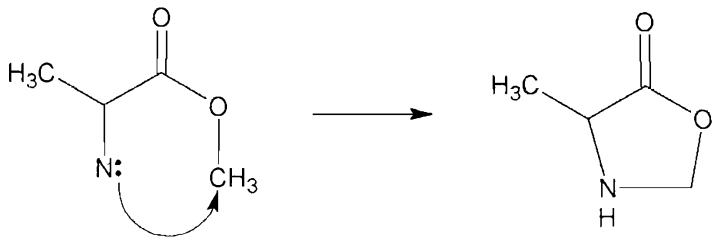

5.8.4 Azidoacetonitrile (N_3CH_2CN)

Azidoacetonitrile thermal decomposition has already been studied [4, 41], and PE spectra of partial and full degrees of pyrolysis have been already described in literature. In the present project azidoacetonitrile was studied mainly to compare its thermal behaviour with the behaviour displayed by 2- and 3-azidopropionitrile; also, IR matrix isolation spectra showed that cyanic acid produced as consequence of its pyrolysis is actually formed in the matrix as a $(HCN)_2$ dimer.
The UV-photoelectron spectroscopy spectra for degrees of pyrolysis varying from 0% to 100% are reported in Figure 5.147.

The overall decomposition scheme is then represented as

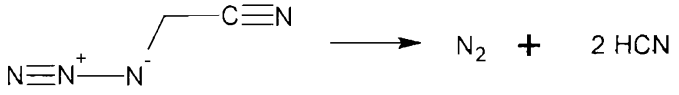

where some cyanic acid is produced as the dimer

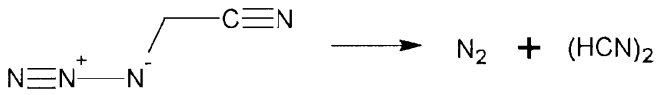

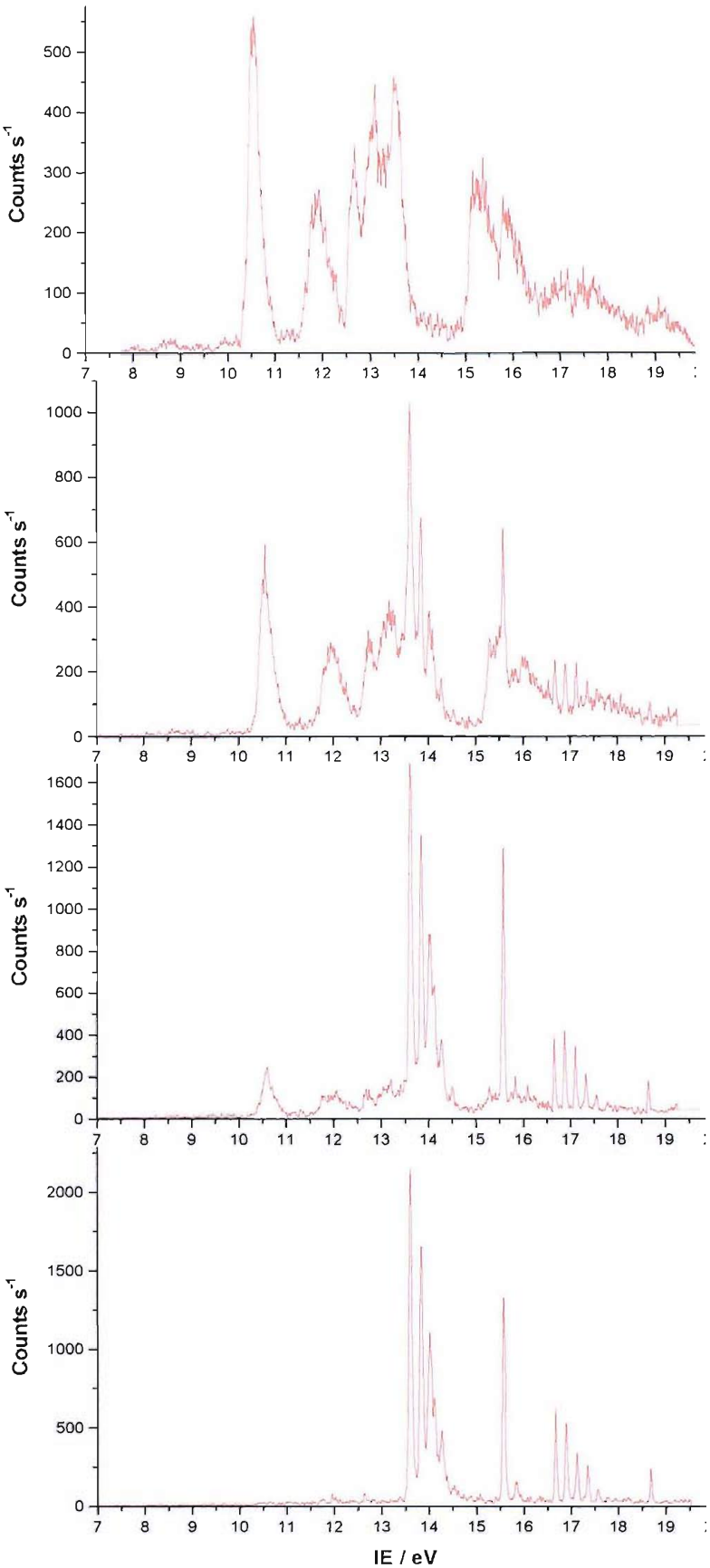

Figure 5.147- HeI-PE spectra of azidoacetonitrile vapours at increasing degrees of pyrolysis

5.9 A COMPARISON OF THE UV-PES SPECTRA OF THE ALIPHATIC AZIDES STUDIED IN THIS WORK

The azides considered in this project can be divided into two main groups, according to their structure. The first group is characterized by the presence of the cyano group: three azides of this group have been studied:

Azidoacetonitrile	N_3CH_2CN
2-azidopropionitrile	$N_3CH(CH_3)CN$
3-azidopropionitrile	$N_3CH_2CH_2CN$

The second group consists of azidoformates, azidoacetates and azidoacetamides. Azidoformates are characterized by adjacent azide and ester groups:

Methyl-azidoformate	N_3COOCH_3
Ethyl-azidoformate	$N_3COOCH_2CH_3$

while in azidoacetates a methylene group is inserted between the azide chain and the ester group:

Azidoacetic acid	N_3CH_2COOH
Methyl-azidoacetate	$N_3CH_2COOCH_3$
Ethyl-azidoacetate	$N_3CH_2COOCH_2CH_3$

The azidoacetamides studied are:

Azidoacetamide	$N_3CH_2CONH_2$	(isoelectronic with azidoacetic acid)
Dimethyl-azidoacetamide	$N_3CH_2CON(CH_3)_2$	(isolectronic with ethyl-azidoacetate)

The insertion of a second alkyl group between the azide and ester groups, producing azidopropionates, can be done in two ways, according to the number and position of the alkyl groups between the azide and the ester groups. For the methyl-azidopropionates, this leads to

2-methylazidopropionate	$N_3CH(CH_3)COOCH_3$
3-methylazidopropionate	$N_3CH_2CH_2COOCH_3$

In the case of azido-esters, the general structure of the molecules can be expressed as N_3RCOOR', and those studied in this project can be summarized in the following table

N_3RCOOR'	R'= H	**R'= CH_3**	**R'= CH_2CH_3**
R = —		N_3COOCH_3	$N_3COOCH_2CH_3$
R = CH_2	N_3CH_2COOH	$N_3CH_2COOCH_3$	$N_3CH_2COOCH_2CH_3$
R = $(CH_2)_2$ or $CH(CH_3)$		$N_3CH_2CH_2COOCH_3$ $N_3CH(CH_3)COOCH_3$	

Azido-amides are isoelectronic with azido-esters, as the –NHR group is isolectronic with the –OR group. The equivalents of the azido-esters presented in the previous table can be therefore presented as

$N_3RCONR'R''$	R', R''= H	**R'= H, R''= CH_3**	**R', R''= CH_3**	**R'= H, R''= CH_2CH_3**
R = --				
R = CH_2	$N_3CH_2CONH_2$		$N_3CH_2CON(CH_3)_2$	
R = $(CH_2)_2$ or $CH(CH_3)$				

Only the azides studied in this project (considering also those from previous investigations in Southampton and Lisbon, such as azidoacetic acid or ethyl azidoacetate) have been reported in the schemes: the blank cells represent azides not yet studied. In some cases this was due to synthetic problems: for example, it was found particularly difficult to obtain azido-amides with different R'' and R' groups. Among azido-esters, azidoformates are very reactive, and the synthesis of azidoformic acid (N_3COOH) looks extremely risky.

For an overview of the differences in UV-photoelectron spectra of these azides, Figure 5.148 reports all the spectra of the azides, whose comparison reflects the changes in their structure. The order of the spectra is chosen so that every azide is linked to the previous or the following one by the simple addition or removal of a methyl group, or by a isoelectronic relation.
The spectra in Figure 5.148 are:

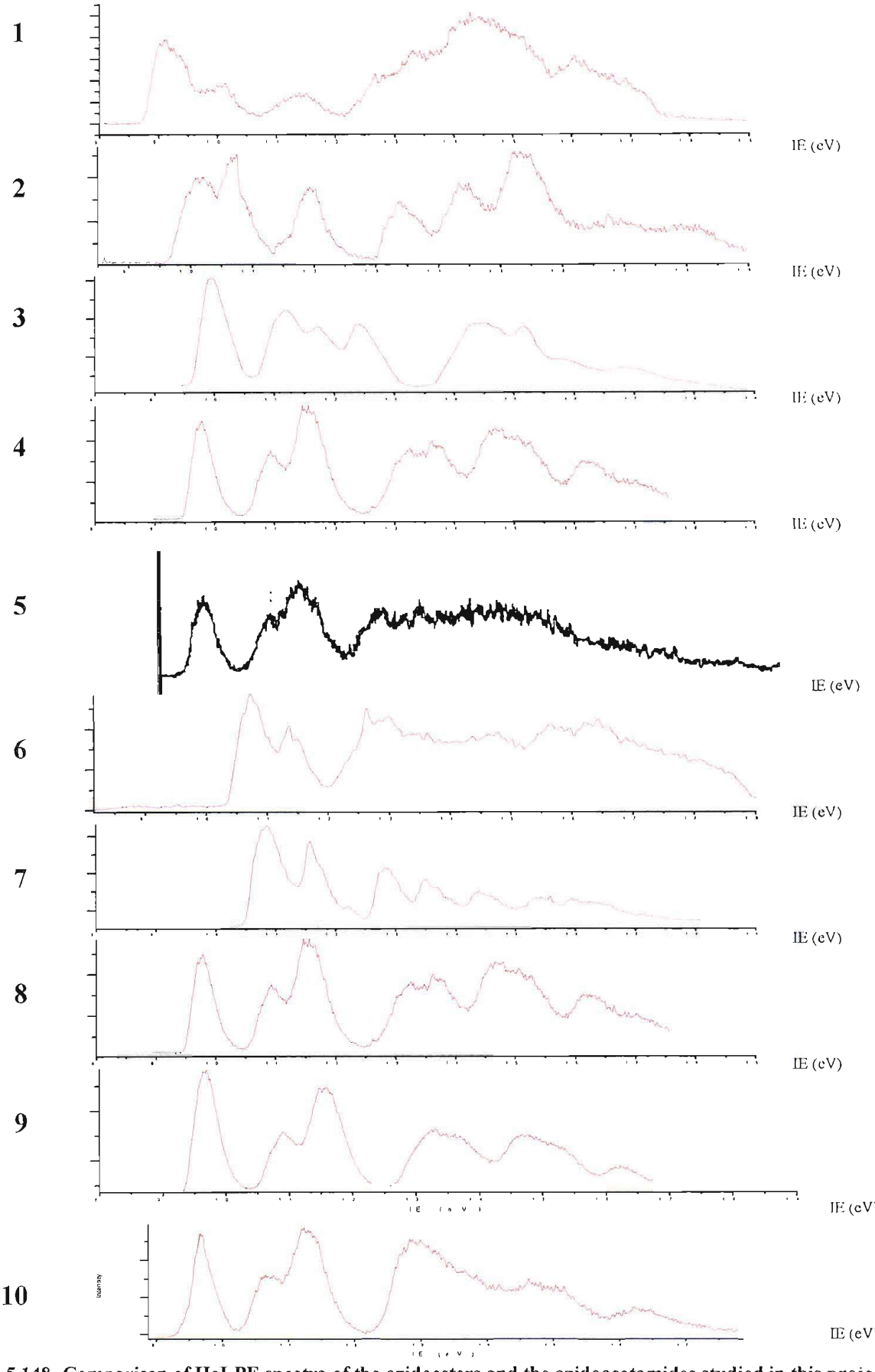

Figure 5.148- Comparison of HeI-PE spectra of the azidoesters and the azidoacetamides studied in this project

1) dimethylazidoacetamide
2) azidoacetamide (methyl groups removed from the amidic part)
3) azidoacetic acid (isoelectronic with azidoacetamide)
4) methyl azidoacetate (methyl group added to the ester part)
5) ethyl azidoacetate (methylene group added to the ester part)
6) ethyl azidoformate (methylene group removed from the azide part)
7) methyl azidoformate (methylene group removed from the ester part)
8) methyl azidoacetate (second time, methylene group added to the azide part)
9) 3-methylazidopropionate (methylene group added to the azide part)
10) 2-methylazidopropionate (diffferent disposition of the alkyl groups in the azide part)

In all the azides the first band is also the most intense one, or the second most intense one; also, very often the first band is well separated from the second band. This reproducible behaviour reflects what is found in *ab initio* calculations, that is that often this band is characterized by a marked contribution from the azide chain.

It is clear that when an ethyl group is attached to the ester group, the azide spectrum presents much broader bands than when a methyl group is attached to the ester group (cf. Spectra 4-5 and 6-7); the change is much less emphasized when a methyl group is substituted by a hydrogen atom (cfr. Spectra 3-4). Also in azidoacetamides the effect is clearly visible (cf. Spectra 1-2), although here a difference of two methyl groups is considered, and therefore it is impossible to state if the difference is due mostly to the introduction of the first or the second methyl group.

The effect is the opposite when the distribution of the bands is considered: ethyl- and methyl-azidoesters (or azidoamides) display almost the same pattern of bands with increasing energy (Spectra 1-2, 4-5 and 6-7), while methyl-azidoacetate clearly shows a different intensity distribution of the PE bands with respect to azidoacetic acid (Spectra 3-4).

The isoelectronic relation (azidoacetamide/azidoacetic acid, Spectra 2-3) does not imply particular similarities among the PE spectra. Azidoacetamide shows the first two bands quite close to each other, plus a well separated third one: azidoacetic acid shows an isolated first band with the three following ones almost overlapping.

When changes are introduced between the azide and the carbonyl groups, it can be seen that the change azidoacetates-azidopropionates introduces very few changes in the spectra (8-9-10), both in the band distribution and in their shape. In contrast, the change is dramatic when azidoformates are compared to

azidoacetates (Spectra 5-6 and 7-8): for example, the first bands of methyl azidoformate and methyl azidoacetate differ in VIE of around 1.0 eV, and a comparison between Spectra 7 and 8 clearly shows different band distributions.

In azidonitriles, the comparison scheme- reported in Figure 5.149- is much simpler because only azidoacetonitrile and the azidopropionitriles have been studied.

The azides show similar PE spectra, characterized by the two first bands being well isolated (the first in the 10.0-11.0 eV region, the second in the 11.5-12.0 region), then by a series of three sharp bands followed by broader bands at high energy. The main differences arise from the position of the first band, the separation of the series of bands and from the degree of overlap of the three sharp bands in the 12.0-13.5 eV region.

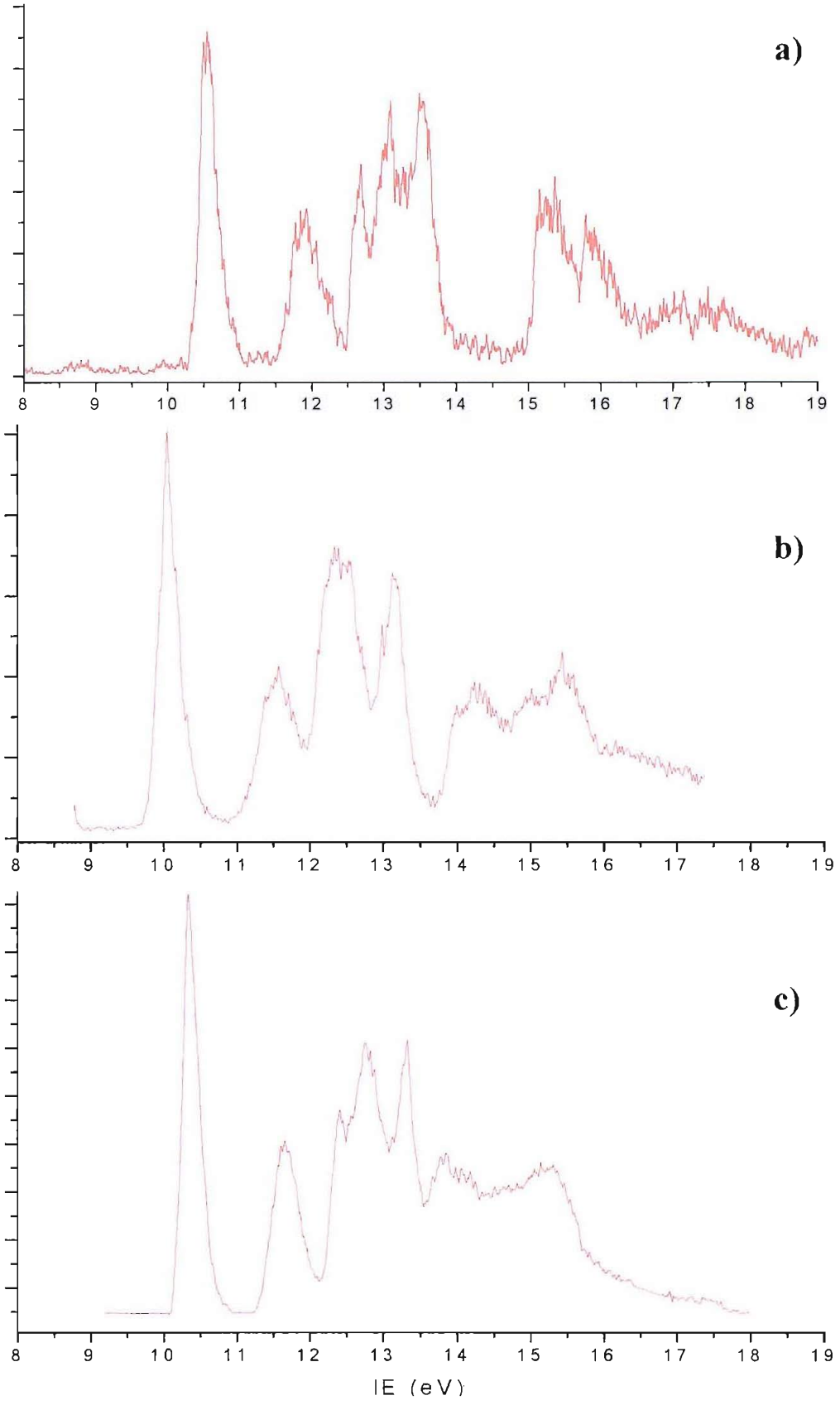

Figure 5.149- Sequence of HeI-PE spectra of a) azidoacetonitrile, b) 3-azidopropionitrile and c) 2-azidopropionitrile

5.10 CONCLUSIONS

Different azides have been studied by means of photoelectron spectroscopy and infrared matrix isolation spectroscopy, both to characterize the azide and to monitor its thermal decomposition behaviour.

As expected, all of them decompose releasing molecular nitrogen. The temperature of complete decomposition does not vary consistently among the classes of azides, being generally between 300 and 400 °C; the most stable were found to be azidoacetamide- which was also the only solid azide studied- and the two azidopropionitriles.

In all cases, it was not possible to detect the formation of nitrene intermediates: however, because of their well known instability this was an expected result, and it does not contradict the assumption that such radicals are formed in the first step of the azide decomposition. The alternative concerted mechanism is in fact less suited to explain all the products observed; the formation of nitrenes provides a better interpretation of the decomposition pathways.

Two main mechanisms have been found with which the nitrene can decompose to the experimentally detected products.

The first mechanism- called Type 1- is the one already proposed by Bock and Dammel [1-4], in which a hydrogen atom or a methyl group is transferred to the electron-deficient nitrogen atom of the nitrene from an adjacent carbon atom. This produces an imine, which in some cases (azidoacetamides) can be experimentally observed before it decomposes to smaller molecules. In other cases the imine is not detected and the nitrene directly eliminates the small molecules.

The second mechanism- called Type 2- involves an attack of the electron-deficient nitrogen atom of the nitrene radical at another remote site within the nitrene itself. This can lead to production of cyclic products- sometimes experimentally detected, such as 2-oxazolidone produced from ethyl azidoformate- or to major rearrangements in the molecule and subsequent elimination of smaller molecules, as in the azidopropionitriles.

The two mechanisms can be open at the same time, and which one dominates varies from azide to azide. Among the classes fully studied in this work, azidoacetamides clearly prefer a Type 1 mechanism, azidoformates decompose uniquely by a Type 2 mechanism, while in azidopropionitriles the two mechanisms seem to occur roughly to the same extent.

The nature of the decomposition products depends on the specific characteristic of the single azide: for example, both the azidoacetamides decompose producing iminoacetamides, but these imines are

subsequently decomposed in different ways because of their structural difference. The same happens in the azidopropionitriles, where a different disposition of the alkyl groups leads to different decomposition products.

The most urgent development of the work is the full interpretation of the pyrolysis spectra for the remaining azides, in order to describe their decomposition behaviour and confirm the thesis of the two alternative pathways.
For this, additional examples of different classes of azides should be studied, such as aromatic azides. Another decisive factor for the determination of the decomposition mechanism- especially if monitored by IR matrix isolation- would be the possibility of studying azides selectively deuterated. This work has just been started, and the most crucial aspect is related to the difficulty of synthesis of partially deuterated samples.

REFERENCES

[1] H. Bock, R. Dammel, *Angew. Chem. Int. Ed. Engl.*, **26**, 1987, 504

[2] H. Bock, R. Dammel, S.J.Aygen, *J. Am. Chem. Soc.*, **105**, *1983*, 7681

[3] H. Bock, R. Dammel, *J. Am. Chem. Soc.*, **110**, *1988*, 5261

[4] R. Dammel, *Reaktive Moleküle mit N-Mehrfachbindungen: azide, imine, nitrile*, Inaugural-Dissertation, University of Frankfurt am Main (1985)

[5] W. Jing, S. Zheng, Z. Xinjiang, Y. Xiaojun, G. Maofa, W. Dianxun, *Angew. Chem. Int. Ed. Engl.*, **40**, *2001*, 3055

[6] J.F. Arenas, J.I. Marcos, J.C. Otero, A. Sanchez-Galvez, J. Soto, *J. Chem. Phys.*, **111 (2)**, *1999*, 551

[7] D. Bulgin, J.M. Dyke, F. Goodfellow, N. Jonathan, E.P. Lee, A. Morris, *J. Elec. Spectr. and rel. Phen.*, **12**, *1977*, 67

[8] D.W. Turner, C. Baker, A.D. Baker, C. Brundle, *Molecular Photoelectron Spectroscopy*, Wiley Interscience, London, *1970*

[9] R.M. Silverstein, G.C. Bassler, T.C. Morrill, *Spectrometric identification of organic compounds*, Wiley-Interscience, New York, *1991*

[10] J.M. Dyke, A.P. Groves, A. Morris, J.S. Ogden, A.A. Dias, A.M.S. Oliveira, M.L. Costa, M.T. Barros, M.H. Cabral, A.M. Moutinho, J. Am. Chem. Soc., **119**, *1997*, 6883

[11] J.M. Dyke, A.P. Groves, A. Morris, J.S. Ogden, M.I. Catarino, A.A. Dias, A.M.S. Oliveira, M.L. Costa, M.T. Barros, M.H. Cabral, A.M. Moutinho, *J. Phys. Chem. A*, **103**, *1999*, 8239

[12] N. Hooper, L.J. Beeching, J.M. Dyke, A. Morris, J.S. Ogden, A.A. Dias, M.L. Costa, M.T. Barros, M.H. Cabral, A.M. Moutinho, *J. Phys. Chem. A*, **106**, *2002*, 9968

[13] J.A. Pople, A.P. Scott, M.W. Wong, L.Radom, *Isr. J. Chem.*, **33 (3)**, *1993*, 345

[14] A.P Scott, L. Radom, *J. Phys. Chem.*, **100**, *1996*, 16502

[15] R.F. Hout, B.A. Levi, W.J. Hehre, *J. Comput. Chem.*, **3**, *1982*, 234

[16] J.B. Peel, G.D.Willett, *J.C.S Faraday Trans. II*, **71**, *1975*, 1799

[17] J.H.D. Eland, *Phil. Trans. Roy. Soc. A*, **268**, *1970*, 87

[18] K. Kimura, S. Katsumata, Y. Achiba, T. Yamasaki, S. Iwata, *Handbook of He(I) Photoelectron spectra*, Japan Scientific Press, Tokyo, *1981*

[19] M. Pettersson, L. Khriatchtev, S. Jolkkonen, M. Rasanen, *J. Phys. Chem. A*, **103**, *1999*, 9154

[20] C.M. King, E.R. Nixon, *J. Chem. Phys.*, **48**, *1968*, 1685

[21] H. Dubost, L. Abouaf-Marguin, *Chem. Phys. Lett.*, **17**, *1972*, 269

[22] M.E. Jacox, D.E. Milligan, *J. Mol. Spectrosc.*,**56**, *1975*, 333

[23] J.A. Cugley, A.D.E. Pullen, *Spectrochim. Acta A*, **29**, *1973*, 1665

[24] M.N. Cordeiro, A.A. Dias, .M.L. Costa, A.N. Gomes, *J. Phys. Chem. A*, **105**, *2001*, 3140

[25] H. Bock, R. Dammel, L. Horner, *Chem. Ber.*, **114**, *1981*, 220

[26] W. Dianxun *et al.*, Chinese academy of Science, Beijing, unpublished results, 2001

[27] H. Basch, M.B. Robin, N.A. Kuebler, C. Baker, D.W. Turner, *J. Chem. Phys.*, **51**, *1969*, 52

[28] M.B. Robin, C.R. Brundle, N.A. Kuebler, G.B. Ellison, K.B. Wiberg, *J. Chem. Phys.*, **57**, *1972*, 1758

[29] J.S. Ogden, University of Southampton, *private communication*

[30] S.H. Gerson, S.D. Worley, N. Bodor, J.J. Kaminski, T.W. Fletchner, *J. Elec. Spectr. and rel. Phen.*, **13**, *1978*, 421

[31] L. Fredin, B. Nelander, G. Ribbegard, *J. Mol. Spectrosc.*, **53**, *1974*, 410

[32] I. Stolkin, T.K. Ha, Hs.H. Gunthard, *Chem. Phys.*, **21**, *1977*, 327

[33] H. Khoshkoo, E.R. Nixon, *Spectrochim. Acta*, **29A**, *1973*, 603

[34] W. Dianxun, Q. Ximei, J. Peng, *Chem. Phys. Lett*, **258**, *1996*, 149

[35] H.W. Kroto, G.Y. Matti, R.J. Suffolk, J.D. Watts, M. Rittby, R.J. Bartlett, *J. Am. Chem. Soc.*, **112**, *1990*, 3779

[36] M.E. Jacox, *Chem. Phys.*,**43**, *1979*, 157

[37] R.K. Thomas, E.C. Liesegang, H.W. Thompson, *Proc. R. Soc. London Ser. A*, **330**, *1972*, 15

[38] a) M. Rodler, R.D. Brown, P.D. Godfrey, L.M. Tack, *Chem. Phys. Lett.*, **110**, *1984*, 447

b) F. Ito, T. Nakanaga, K. Sugawara, H. Takeo, M. Sugie, C. Matsumura, *J. Mol. Spectr.*, **140**, *1990*, 177

[39] D.A. Sweigart, D.W. Turner, *J. Am. Chem. Soc.*, **94**, *1972*, 5592

[40] C.B. Moore, G.C. Pimentel, *J. Chem. Phys.*, **38**, *1963*, 2816

[41] R.A. Evans, P. Lorencak, T.-K. Ha, C. Wentrup, *J. Am. Chem. Soc.*, **113**, *1991*, 7261

CHAPTER 6

CONCLUSIONS AND SUGGESTIONS FOR FUTURE WORK

The present thesis was centred on two main topics, the study of the thermal decomposition of aliphatic azides and the study of the reaction between DMS and molecular chlorine. Both studies were conducted by means of photoelectron spectroscopy (PES) and infrared matrix isolation spectroscopy, with the support of *ab initio* calculations. The DMS + Cl_2 reaction was also monitored with FT-IR and FT-UV spectroscopic techniques carried out in Rutherford Appleton Laboratory. The necessity of supporting the experimental results with *ab initio* calculations was not only to facilitate the spectroscopic assignments, but also to provide significant insight to the mechanisms of the reactions under study. The aim of the work was not only the experimental determination of important parameters of the reactions (temperature of initial and total pyrolysis, molar ratios, mixing times) but also the mechanism through which they proceed, including the possible formation of reactive intermediates.

Chapter 4 described the results on the DMS + Cl_2 reaction, which has relevance to atmospheric chemistry, as DMS is the most important source of natural sulphur in the troposphere. The results from gas-phase PES indicate that the reaction proceeds initially via the formation of an intermediate, $(CH_3)_2SCl_2$ formed by direct co-ordination of the chlorine atoms onto the sulphur atom via the probable involvement of a third body

$$CH_3SCH_3 + Cl_2 + M \rightarrow (CH_3)_2SCl_2 + M$$

The intermediate, characterized by a pseudo-octahedral co-ordination around the sulphur atom, is geometrically equivalent to the $(CH_3)_2SeCl_2$ molecule already studied in the past by means of *ab initio* calculations [1]. In the present study, it was not possible to detect the formation of $(CH_3)_2SCl_2$ as a product of the co-deposition of DMS and Cl_2 in a matrix, because its most intense vibrational band is expected at a wavenumber too low for the detection window used in this work. However, the calculated frequency of this most intense band is in very good agreement with the frequency reported in literature- and left unassigned- for an analogous matrix co-deposition studied with a suitable detection window [2]. When DMS and Cl_2 are allowed to mix for a longer time, or when higher Cl_2: DMS pressure ratios are used, the dominant species become chlorinated DMS molecules, with the chlorine atom(s) attached to the carbon atom. The number of chlorine substitutions is dependent on the Cl_2: DMS ratio. For an

approximate 1:1 ratio- which is indicated to correctly reproduce the natural environment above the oceans at night-time [3]- the dominant species is CH_3SCH_2Cl (MDMS). Its formation can be interpreted with a stepwise mechanism proceeding via $(CH_3)_2SCl_2$,

$$CH_3SCH_3 + Cl_2 \rightarrow (CH_3)_2SCl_2 \rightarrow CH_3SCH_2Cl + HCl$$

because the activation barrier predicted for this mechanism is 10 kcal/mol lower than the barrier for the route which by-passes the intermediate. However, the calculated activation energy (4.5 kcal/mol at the MP2/aug-cc-pVDZ level) is still slightly too high to be compatible with a rate constant of $3.4 \cdot 10^{-14}$ $cm^3 \cdot molecule^{-1} \cdot s^{-1}$ [3]. This suggests that a more detailed investigation of the potential energy surface should be carried out with multi-reference methods and larger basis sets.

At higher Cl_2: DMS pressure ratios, it appears that the dominant species is not dichloro-DMS, but trichloro-DMS (TDMS). This means that the reaction

$$MDMS + Cl_2 \rightarrow TDMS + H_2$$

is faster than the stepwise reactions

$$MDMS + Cl_2 \rightarrow DDMS + HCl$$
$$DDMS + Cl_2 \rightarrow TDMS + HCl$$

The chlorination proceeds by replacing the protons of the same methyl group before the second methyl group is attacked: a chlorine atom is introduced on the second methyl group only after all three protons are replaced by chlorine on the first methyl group (therefore after TDMS is formed). Tetrachloro-DMS was observed in the matrix only at a very high Cl_2: DMS ratio.

Chapter 5 presented the results on the thermal decomposition of aliphatic azides: six azides have been studied in detail experimentally and computationally, while four more need further *ab initio* investigations on their decomposition mechanisms.

Two main mechanisms have been proposed to explain the experimental evidence and they can also successfully interpret results obtained in the past on other simpler aliphatic azides [4-10].

With PES and IR matrix isolation it is not possible to detect the formation of nitrene intermediates as a consequence of the liberation of molecular nitrogen once the azide is heated: however, the mechanisms have general validity, with or without nitrene formation.

The first one- called here Type 1- is the azide→imine→products mechanism already observed in the pyrolysis of alkyl azides [4-7]. It involves a 1,2-H shift on the nitrogen atom attached to the leaving N_2 group from an adjacent carbon atom.

It can be represented as:

$$R'R''CH\text{-}N_3 \rightarrow R'R''C{=}NH + N_2 \rightarrow \text{fragmentation}$$

The imine is not always detected, as it is formed with high internal energy and fragmentation can occur as soon as is formed. The nature of the fragmentation depends on the specific azides and the small molecules that can be formed.

The second general mechanism- called Type 2- is characterized by the attack of the nitrogen atom attached to the leaving N_2 group towards another site of the molecule. This can lead to a sudden fragmentation of the molecule, as happens in methyl azidoformate

$$N_3COOCH_3 \rightarrow N_2 + CO_2 + CH_2NH$$
$$N_3COOCH_3 \rightarrow N_2 + HNCO + HCHO$$

or to the formation of a cyclic molecule, which can be very stable as shown by 2-oxazolidone produced in the decomposition of ethyl azidoformate

$$N_3COOCH_2CH_3 \rightarrow N_2 + \text{cyc-}HNCH_2CH_2COO$$

In the case of the azides studied, the *ab initio* calculations indicate that the reactions proceed through very high activation energy barriers: the first step- the liberation of nitrogen- involves transition states that have been calculated to be of the order of 35-45 kcal/mol at the MP2/6-31G** level above the reactants. Such energy would require much higher decomposition temperatures than those observed in the experiments (the usual temperature of full pyrolysis is around 500 °C, and at 500 °C k_BT is ca. 0.90 kcal/mol). Even by assuming that these energy barriers would be slightly lowered if a more accurate calculation method is used, the decomposition reaction cannot be viewed as a pure gas-phase reaction, and surface decompositions need to be invoked to explain the observation of decomposition at the temperatures used.

The importance of surface effects has already been highlighted by Bock and Dammel [5]. The involvement of surfaces is also clear in the work of Dianxun *et al.*, when they detected the nitrene arising from pyrolysis of methyl azide when the heated inlet system of the PE spectrometer was filled with molecular sieve and the flowing sample was allowed to flow through the sieve [11].

As well as decomposition of aliphatic azides, the reaction between DMS and Cl_2 could also be studied on surfaces. For this, a possible method would be Reflection Absorption Infra Red Spectroscopy (RAIRS), where a molecule adsorbed on a surface is irradiated with IR radiation and the reflected radiation detected: only vibrations perpendicular to the surface can be observed, and this would give important insights on the method of adsorption of the molecule and therefore on the mechanism of the reaction of Cl_2 with DMS on the surface. As an alternative to RAIRS, high resolution High Resolution Electron Energy Loss Spectroscopy (HREELS) can also give information on the vibrations of molecules anchored to a surface.

An infrared characterization of the $(CH_3)_2SCl_2$ molecule is essential: experiments involving co-deposition of DMS and Cl_2 in a matrix should be performed with a matrix infrared spectroscopic apparatus with a window that allows detection of its most intense band at around 350 cm^{-1} and the measurement of the intensity of this band relative to the other IR bands of the molecule at higher wavenumbers (see Figure 4.43).

The fact that the reaction between DMS and Cl_2 produces MDMS means that from the atmospheric point of view it is necessary to study the reactivity of MDMS, in particular all the oxidation reactions that lead in the atmosphere to the production of SO_2. Photolysis is the first candidate among these reactions, but also reactions with OH and NO_3 radicals, O_3 and H_2O_2 should be investigated.

Also regarding atmospheric chemistry, the reactivity of DMS with molecular iodine is of interest, as I_2 is present in marine environments [12]: once a stable flow of I_2 vapours has been obtained, the same kind of characterization techniques adopted for the DMS + Cl_2 reaction could be conducted. In particular the formation of a $(CH_3)_2SI_2$ reactive species should be investigated and the reaction products established.

The $(CH_3)_2SeCl_2$ molecule has been studied by means of an X-ray diffraction study on single crystals and by means of *ab initio* calculations [1]: it would be useful to obtain its PE spectrum and make a comparison with that of $(CH_3)_2SCl_2$.

The necessity of taking into account surface effects for the azide thermal decompositions provides a first indication for future work: it would be of interest to study azides adsorbed on a surface, for example a metallic surface, and then their thermal decomposition. RAIRS or HREELS could be used in this case, as it would give information on the mechanism of easier release of N_2 from the azides.

For a more detailed mechanism of the surface effects on azide decomposition, it would be necessary to perform higher level *ab initio* calculations on the first steps of the reaction, both in the presence and absence of the surface, in order to have an accurate value for the activation energy in each case: apart

from the choice of different basis sets, single point calculations at the CCSD(T) level could be the first step to make, even if the size of the azides will require a significant computational effort. It is also necessary to include the metallic surface in the calculations and investigate its effect on the reaction barriers. In the literature it was found that CAS-SCF calculations on methyl azide [13] were able to underline the fact that the reaction proceeds via the formation of the nitrene: even if CAS-SCF calculations on the azides studied in this work would probably be very time consuming, it would be very valuable to have a combination of *ab initio* information of this type with a PE study with a similar experimental set-up as described by Dianxun *et al.* [11] in order to confirm the presence (or otherwise) of nitrene intermediate for the very larger azides studied in this work.

All the *ab initio* characterization of the azides presented in Section 5.8 must be performed: this includes geometry optimization of reactants, products and intermediates, and the study of the energy surface linking them. This is particularly important in those cases where still unassigned PE bands of intermediates are visible.

The scheme reported in Section 5.9 must be completed by studying the azides that are isoelectronic to those studied in the Southampton PES group: this would give completeness to the overview of the different characteristics of each azide, and would indicate more clearly the similarities and differences in decomposition mechanisms between the classes of azides under study. In this case, the crucial point would be to investigate the feasibility of their synthesis.

Also associated to synthetic problems is the possibility of studying selectively deuterated azides: in IR studies of the parent and decomposition products this would give an important contribution to the study of the decomposition mechanism.

Other azides could be studied, -for example aromatic or allyl azides: the presence of an aromatic ring adjacent or in the vicinity of the azide group could involve new decomposition mechanisms as well as the two found in this work.

The study of the decomposition of the azides described in this work could be combined with a technique like flash photolysis: this has already been applied to other types of azides, giving information about the possibility of forming nitrenes or other reactive intermediates [14].

Finally, a more detailed study of the azides and their decomposition products could be achieved by performing flash vacuum pyrolysis: this technique allows more resolved PE spectra to be recorded and it has been developed for studies of reactive intermediates [15, 16]. It can be combined with Laser Induced Fluoresence (LIF) [17] or Zero Kinetic Energy (ZEKE) photoelectron spectroscopy [18], so that additional information on the electronic structure and thermochemistry of the reactive intermediates can be obtained.

The fact that nitrene intermediates have been observed also as consequence of the photodissociation of simple alkyl azides [19] indicates that photodissociation could be conducted on the larger azides presented in this work: the combination of results from thermal decomposition and photodissociation could lead to a full understanding of the dissociation mechanisms.

REFERENCES

[1] a) S.M. Godfrey, C.A. McAuliffe, R.G. Pritchard, S. Sarwar, *J. Chem. Soc. Dalton Trans.*, *1997*, 1031

b) N. Kaltsoyannis, *J. Chem. Soc. Dalton Trans.*, *1997*, 4759

[2] N.P. Machara, B.S. Ault, *J. Phys. Chem.*, **91**, *1987*, 2046

[3] J.M. Dyke, M.V. Ghosh, D.J. Kinnison, G. Levita, A. Morris, D.E. Shallcross, *PCCP*, **1**, 2005, 868

[4] H. Bock, R. Dammel, *Angew. Chem. Int. Ed. Engl.*, **26**, 1987, 504

[5] H. Bock, R. Dammel, S.J.Aygen, *J. Am. Chem. Soc.*, **105**, *1983*, 7681

[6] H. Bock, R. Dammel, *J. Am. Chem. Soc.*, **110**, *1988*, 5261

[7] R. Dammel, *Reaktive Moleküle mit N-Mehrfachbindungen: azide, imine, nitrile*, Inaugural-Dissertation, University of Frankfurt am Main (1985)

[8] J.M. Dyke, A.P. Groves, A. Morris, J.S. Ogden, A.A. Dias, A.M.S. Oliveira, M.L. Costa, M.T. Barros, M.H. Cabral, A.M. Moutinho, J. Am. Chem. Soc., **119**, *1997*, 6883

[9] J.M. Dyke, A.P. Groves, A. Morris, J.S. Ogden, M.I. Catarino, A.A. Dias, A.M.S. Oliveira, M.L. Costa, M.T. Barros, M.H. Cabral, A.M. Moutinho, *J. Phys. Chem. A*, **103**, *1999*, 8239

[10] N. Hooper, L.J. Beeching, J.M. Dyke, A. Morris, J.S. Ogden, A.A. Dias, M.L. Costa, M.T. Barros, M.H. Cabral, A.M. Moutinho, *J. Phys. Chem. A*, **106**, *2002*, 9968

[11] W. Jing, S. Zheng, Z. Xinjiang, Y. Xiaojun, G. Maofa, W. Dianxun, *Angew. Chem. Int. Ed. Engl.*, **40**, *2001*, 3055

[12] a) A. Saiz-Lopez, J.M.C. Plane, Geophys. Res. Lett., **31**, 2004, L04112

b) C.D. O'Dowd, J.L. Jimenez, R. Bahreini, R.C. Flagan, J.H. Seinfeld, K. Hameri, L. Pirjola, M. Kulmala, S.G. Jennings, T. Hoffmann, *Nature,* **433**, *2005*, E13

[13] J.F. Arenas, J.I. Marcos, J.C. Otero, A. Sanchez-Galvez, J. Soto, *J. Chem. Phys.*, **111 (2)**, *1999*, 551

[14] A. Maltsev, T. Bally, M-L. Tsao, M.S. Platz, A. Kuhn, M. Vosswinkel, C. Wentrup, *J. Am. Chem. Soc.*, **126**, *2004*, 237

[15] P. Chen, *Unimolecular and bimolecular reaction dynamics*, Chapter 8, page 371, John Wiley & sons, 1994

[16] H-K. Kim, H-C. Kwon, J-H. Park, Y-S. Choi, J-H Choi, *Bull. Korean Chem. Soc.*, **20** (**12**), *1999*

[17] a) X.Q. Tan, T.G. Wright, T.A. Miller, Jet spectroscopy and molecular dynamics, Chapter 3, Blackie Academics, Ed. J.M. Hollas and D. Phillips, *1994*

b) H.R. Shang *et al., Chem. Phys. Lett.*, **267**, *1997*, 345

[18] a) E.W. Schlag, ZEKE spectroscopy, Cambridge University press, Cambridge, *1998*

b) K. Mueller-Detlefs, E.W. Schlag, *Ann. Rev. Phys. Chem.*, **42**, *1991*, 109

[19] L. Ying, Y. Xia, H. Shang, X. Zhao, Y. Tang, *J. Chem. Phys.*, **105**, *1996*, 5798